J. Astrophys. Astr. (1995) **16,** 1–36

The Radio Structure of 45 Quasars at $z < 1.5$

V. K. Kapahi *National Centre for Radio Astrophysics, Tata Institute of Fundamental Research, Poona University Campus, Pune 411007, India*

Received 1995 January 3; accepted 1995 January 11.

Abstract. Radio maps at 5 GHz with an angular resolution of 1 to 2 arcsec and a dynamic range $\gtrsim$200:1 are presented for a sample of 45 radio quasars at redshifts between 0.2 and 1.5. The sources were imaged from observations made with the Very Large Array with the aim of investigating the epoch dependence of misalignments and asymmetries in their extended radio structure. Maps of some of the larger radio sources are presented also at a frequency of 1.5 GHz with a typical angular resolution of ~ 4 arcsec. The radio structure of most of the quasars reported here has been delineated in considerably greater detail than available in the literature.

Key words: Quasars—active galactic nuclei—radio structure.

1. Introduction

Radio quasars are among the most distant and energetic extragalactic objects known in the Universe. In the three decades since their discovery, a variety of observational and theoretical studies of their radio emission has provided a considerable body of information and insight into the processes responsible for their workings. While the source of their enormous energy output is widely believed to result ultimately from the gravitational energy associated with the collapse of super massive black holes, the overall double radio structure with characteristic features such as hot spots, lobes and bridges or tails is attributed to the propagation of twin jets from the central engine and their interaction with the ambient interstellar and intergalactic medium surrounding the objects. Observations of radio quasars at different redshifts also provide an important source of information on the evolution with epoch in the physical conditions both inside and outside their parent galaxies.

Although the extended structure of most radio quasars is generally fairly symmetric, with the hot spots on the two sides being almost collinear with the radio core and roughly equidistant from it, a sizeable fraction of quasars are now known to show significant departures from symmetry and collinearity (e.g. Hintzen *et al.* 1983; Barthel *et al.* 1988). Several mechanisms have been invoked to explain such asymmetries and misalignments, such as: light travel time differences from the two hot spots; intrinsically asymmetric ejections; ejection only on one side at a time; motion of the quasar in a cluster; precession of the central engine; gravitational lensing effects; bending of jets by interstellar or intergalactic gas clouds etc. From a study of the misalignments at different cosmic epochs, it was reported by Barthel & Miley (1988) that the extended emission appeared much more bent and distorted at high redshifts ($z \geqslant 1.5$) than at lower redshifts. They considered the jet-cloud interaction to be the most plausible

explanation for the effect and regarded this as evidence for a clumpier intergalactic medium at earlier epochs.

In view of the cosmological significance of the above mentioned result, it is important to confirm the increase in misalignments with redshift and to rule out the possibility of any instrumental or observational selection effects being responsible for the effect. This is particularly important because the effect appears to become important mainly at $z \geqslant 1.5$, which was also the dividing redshift between two samples of quasars used by Barthel & Miley (1988) to investigate the epoch dependence of misalignments. While the structures of almost all the 80 objects in their high-z ($z > 1.5$) sample were determined by Barthel *et el.* (1988) using the Very Large Array with a high angular resolution of ~ 0.4 arcsec and a dynamic range generally exceeding ~ 200:1, the data for most of their comparison sample of about 40 quasars at $z < 1.5$ were taken from maps available in the literature that had been made with much poorer angular resolutions and dynamic ranges, mostly with the Cambridge 1mile array(e.g. Riley & Pooley 1975) or with the Westerbork Synthesis Radio Telescope (Miley & Hartsuijker 1978).

The observations reported in the present paper were undertaken primarily to map the extended structure of a larger sample of quasars at low redshifts ($z < 1.5$) with higher angular resolution and dynamic range than available in the literature in order to carry out a better comparison of the radio structures at different redshifts. A sample of 45 quasars was mapped using the VLA at a frequency of 5 GHz. The resulting radio images and the values of some derived parameters are presented here. The sample selection and observations are described in section 2 and the results presented in section 3.

Preliminary results of an investigation of the epoch dependence of misalignments based on the data presented here and available in the literature have been presented earlier (Kapahi 1990). A detailed analysis together with a comparison of the quasar data with similar data on samples of radio galaxies will be reported in a subsequent publication.

2. Sample selection and observations

While enlarging the low-z quasar sample it was important to keep in mind the criteria used to form the high-z sample in order to minimize the effect on the structures due to factors other than the redshift. The following criteria were employed to select the sources to be mapped with VLA.

i. $z < 1.5$

ii. Steep radio spectra, with spectral index $\alpha_{1.4\,\mathrm{GHz}}^{5\,\mathrm{GHz}} \geqslant 0.6$. (defined such that $S(\nu) \propto \nu^{-\alpha}$. This criterion was used by BM to form the high-z sample and ensures that the samples do not contain core-dominated quasars which may have their jet axes close to the observer's line of sight as suggested by quasar unification schemes based on the relativistic beaming effects in the nuclear jets (Kapahi *&* Saikia 1982; Orr & Browne 1982).

iii. Known to have extended radio structure with angular sizes $\geqslant 4$ arcsec. This was to ensure at least a few beam sizes over the radio extent in order to determine the misalignments with reasonable confidence.

iv. High radio luminosity; P(5GHz)> 10^{26}WHz^{-1} , assuming $q_{.0}$ = 0.5 and H_0 = 75kms^{-1} Mpc^{-1}. This is also the minimum luminosity in the high-z sample.

The sample of sources selected for observations was drawn up starting from the compilation of known extended steep-spectrum quasars (Singal 1988) and essentially picking all those that satisfied the criteria (i) to (iii) listed above and in addition had a flux density $\gtrsim 2$ Jy at 400 MHz (to ensure that criterion (iv) is also satisfied) and did not already have radio maps with high angular resolution (~ 1–2 arcsec) and dynamic range ($\geqslant 200$) available in the literature.

The 45 quasars selected by the above criteria for observations with the VLA had a median redshift of ~ 0.7 which is about 2.5 times smaller than the median z in the high-z sample of Barthel and Miley. Because the median angular size of radio quasars is known to decrease roughly linearly with increasing z (e.g. Kapahi 1987), a typical angular resolution of ~ 1 arcsec was necessary for the low-z sources to have a similar number of resolution elements across their total extent on average as was available for the maps of the high-z quasars which had an angular resolution of ~ 0.4 arcsec. It was therefore decided to map the 45 sources at a frequency of 5 GHz in the "B" configuration of VLA which provides a resolution of ~ 1 arcsec. As observations in this configuration are not very sensitive to structure on a scale $\gtrsim 30$ arcsec it was decided to observe some of the larger sources in the sample at the lower frequency of 1.5 GHz (in the same "B" configuration) as well.

The observations were made on 18 March 1989 during a continuous run of about 15 hours. Each source was observed for a duration of about 5 to 8 minutes at each of two hour angles. A phase calibrator was observed typically every 30 minutes. The flux calibration was carried out using 3C48. The observations in the 6 cm band had an effective bandwidth of 100 MHz centred at 4.86 GHz while those in the 20 cm band had a bandwidth of 100 MHz centred at 1.54 GHz.

3. Data reduction and results

The data were mostly processed at the Array Operations Centre of NRAO at Socorro, USA, using the standard AIPS software. After calibration and editing, the visibility data in the two IF channels were combined together and maps (generally of 512 × 512 pixels) made using the task 'MX'. The visibility phases were then self-calibrated using one or two iterations of the task 'SELFCAL' before making the final maps.

The final maps generally had an rms noise level of 0.1 to 0.2 mJy per beam at 6 cm λ in most cases. The dynamic range achieved in these maps (defined as the ratio of the peak intensity to the rms value) was generally in the range of ~ 200 to 1500.

The maps of all the 45 sources are presented in Fig. 1 and some observed parameters are summarised in Table 1, which is arranged as follows:

Column 1: Source name in the IAU designation.
Column 2: An alternative name from a radio survey.
Column 3: Redshift (taken from Veron & Veron 1989 or Hewitt & Burbidge 1993).
Column 4: The total flux density at 4.86 GHz. For sources mapped also at 21 cm λ, the total flux density at 1.5GHz is listed on the second line in this column. In the case of large sources (LAS $\gtrsim$ 30 arcsec) some extended flux may have been missed in the synthesis mapping for lack of short spacings, particularly at 6 cm λ. Flux density values for such sources are enclosed in parentheses.

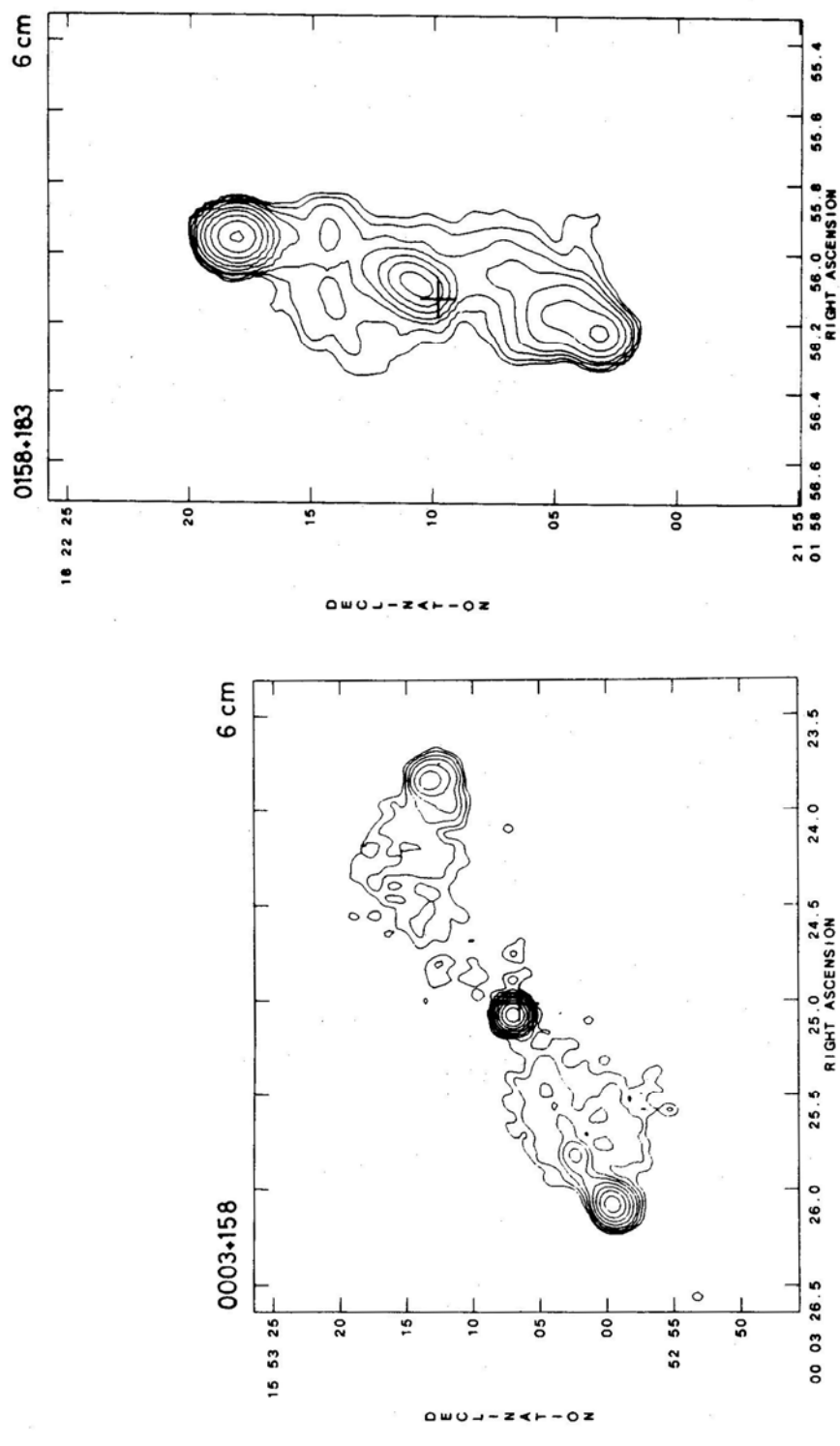

Figure 1. Contour plots of the radio images of 45 quasars. Optical positions of the quasars are indicated by the '+' signs. Negative contours are shown by dotted lines. The contours of total intensity are plotted at $C \times [-1, 1, 1.5, 2.5, 4, 8, 16, 32, 64, 128 \ldots]$ mJy per beam area. The values of 'C' and the details about the gaussian restoring beams used in the plots are listed in Table 2.

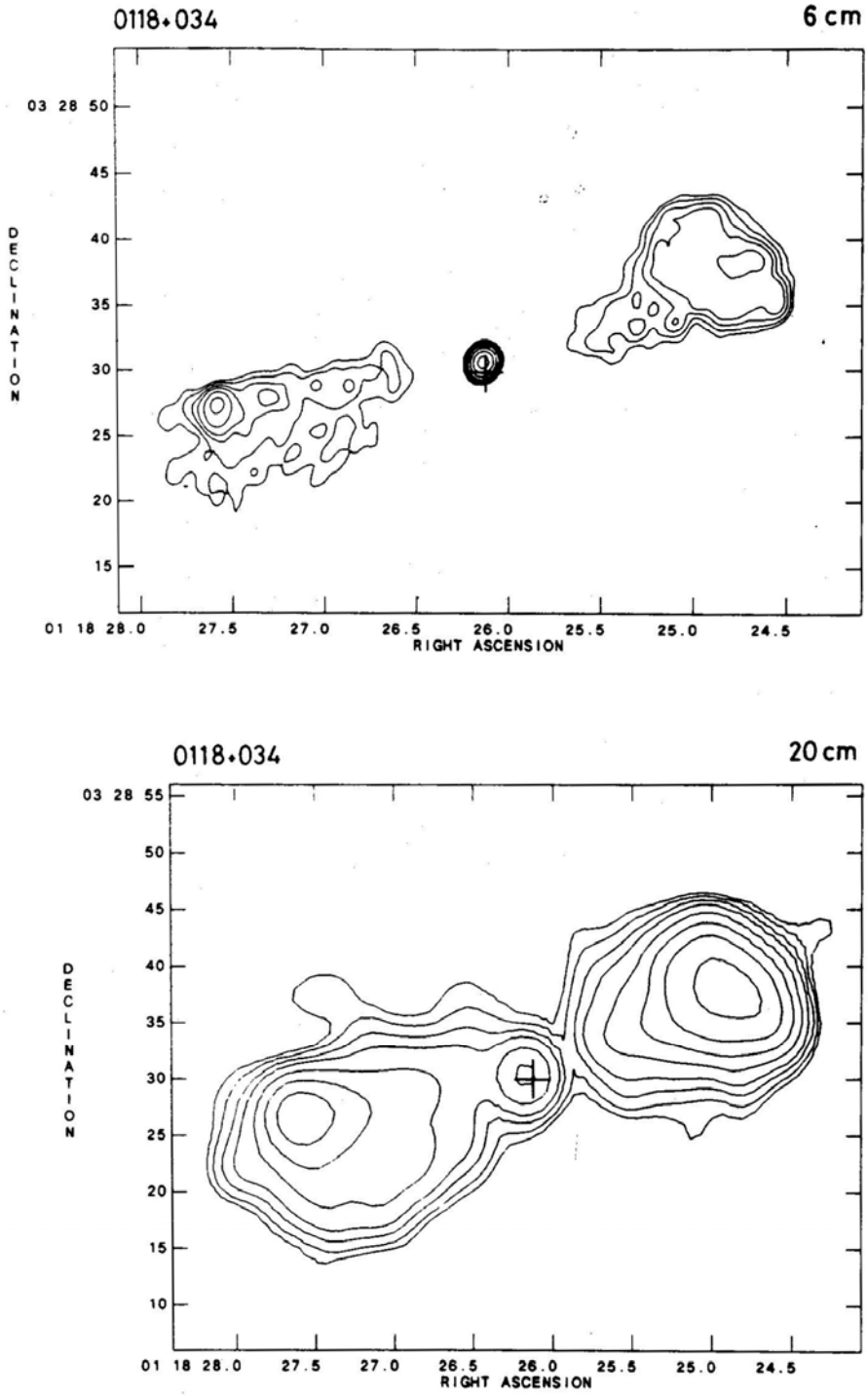
0118+034
6 cm
03 28 50
45
40
35
30
25
20
15
DECLINATION
01 18 28.0
27.5
27.0
26.5
26.0
25.5
25.0
24.5
RIGHT ASCENSION
0118+034
20 cm
03 28 55
50
45
40
35
30
25
20
15
10
DECLINATION
01 18 28.0
27.5
27.0
26.5
26.0
25.5
25.0
24.5
RIGHT ASCENSION

Figure 1(b).

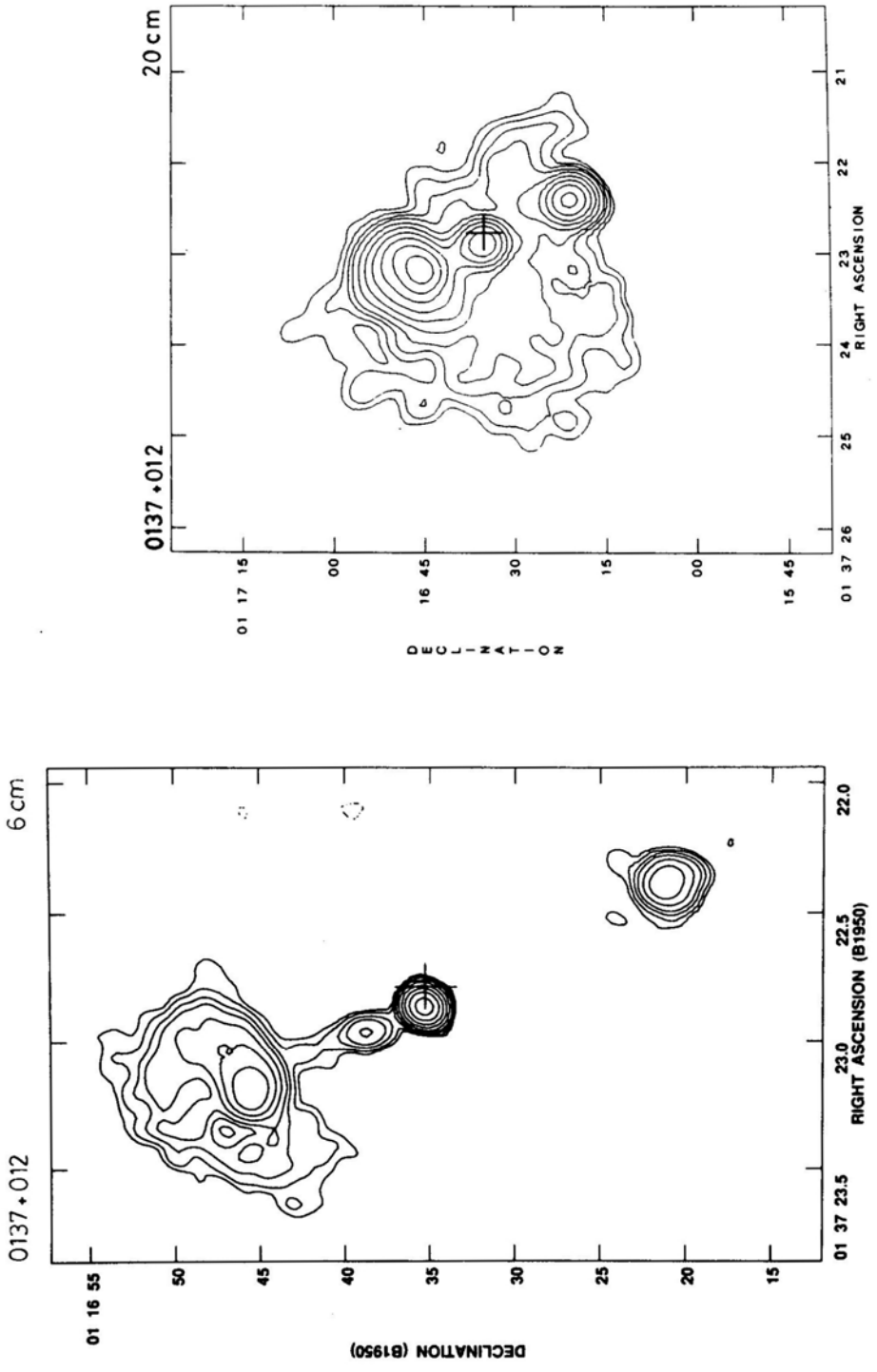
20 cm
0137+012
01 17 15
00
16 45
30
15
00
15 45
DECLINATION
25
24
23
22
21
RIGHT ASCENSION
01 37 26
6 cm
0137+012
01 16 55
50
45
40
35
30
25
20
15
DECLINATION (B1950)
01 37 23.5
23.0
22.5
22.0
RIGHT ASCENSION (B1950)

Figure 1(c).

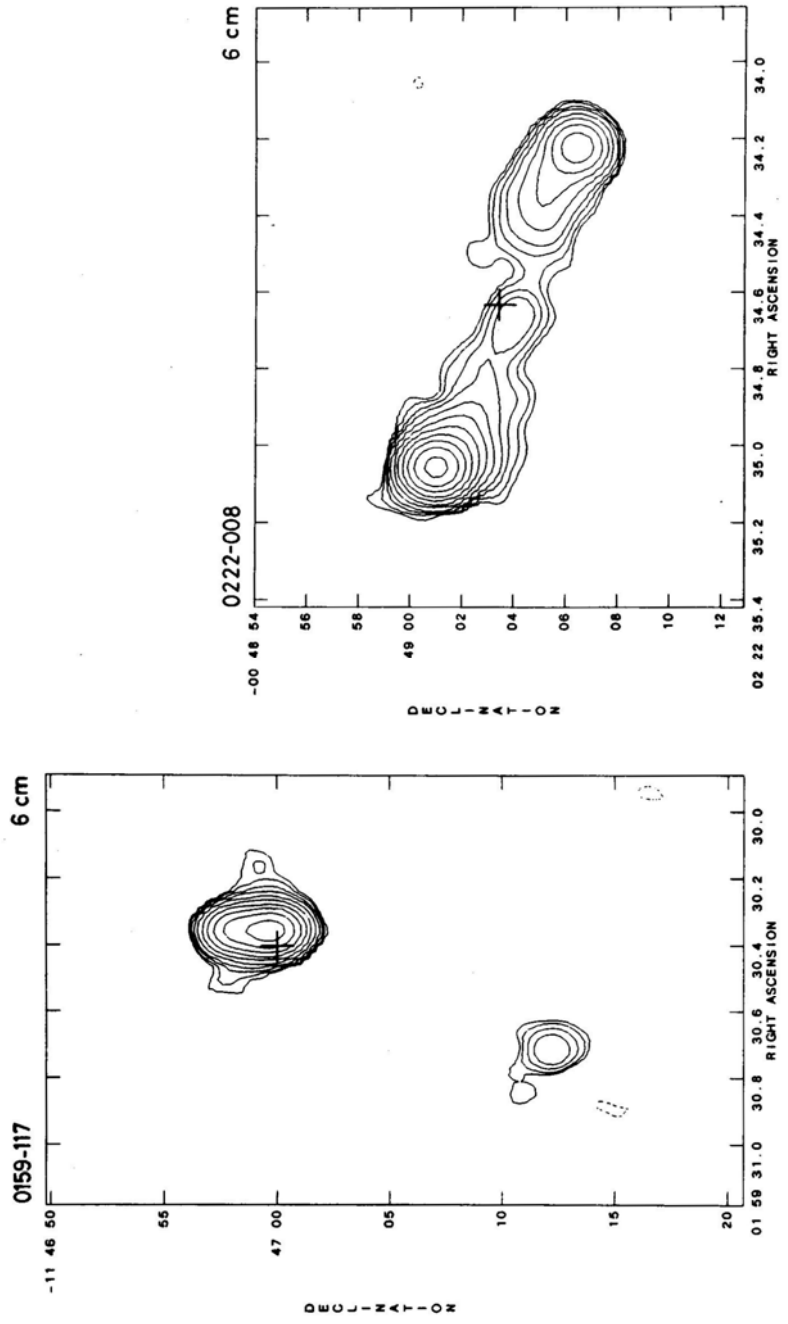
6 cm
0222-008
-00 48 54
56
58
49 00
02
04
06
08
10
12
02 22 35.4
35.2
35.0
34.8
34.6
34.4
34.2
34.0
RIGHT ASCENSION
DECLINATION
6 cm
0159-117
-11 46 50
55
47 00
05
10
15
20
01 59 31.0
30.8
30.6
30.4
30.2
30.0
RIGHT ASCENSION
DECLINATION

Figure 1(d).

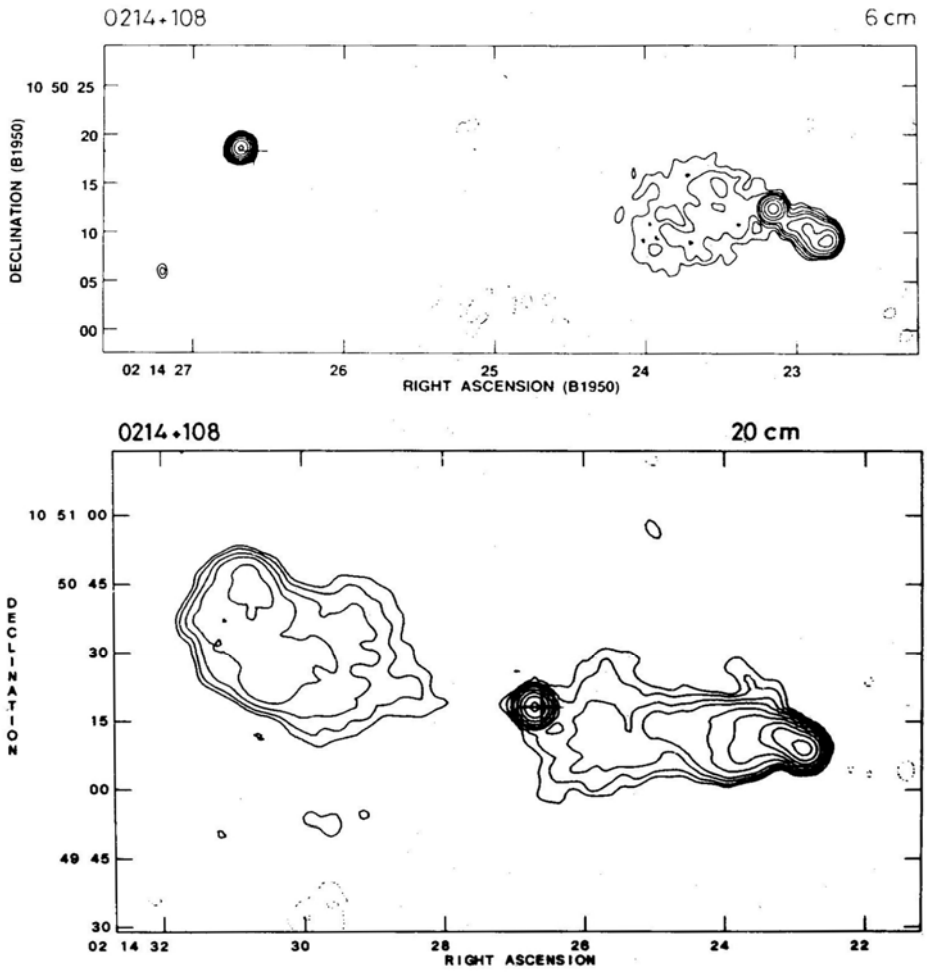

Figure 1(e).

Column 5: Flux density of the radio core component S_{core} at 4.84 GHz. The corresponding value at 1.5 GHz is listed on the second line in some cases.

Columns 6 & 7: The right ascension and declination (1950.0) of the radio core component. The accuracy in the position should generally be better than ± 0.5 arcsec.

Columns 8-10: The optical position of the quasar. Only the seconds of right ascension and arcseconds of the declination are listed in columns 8 and 9 respectively. The reference to the optical position is coded in column 10. The positions are generally accurate to better than ± 1 arcsec.

Column 11: The largest angular size (LAS) in seconds of arc. LAS is defined as the separation between the hotspots or the brightest features in the two lobes.

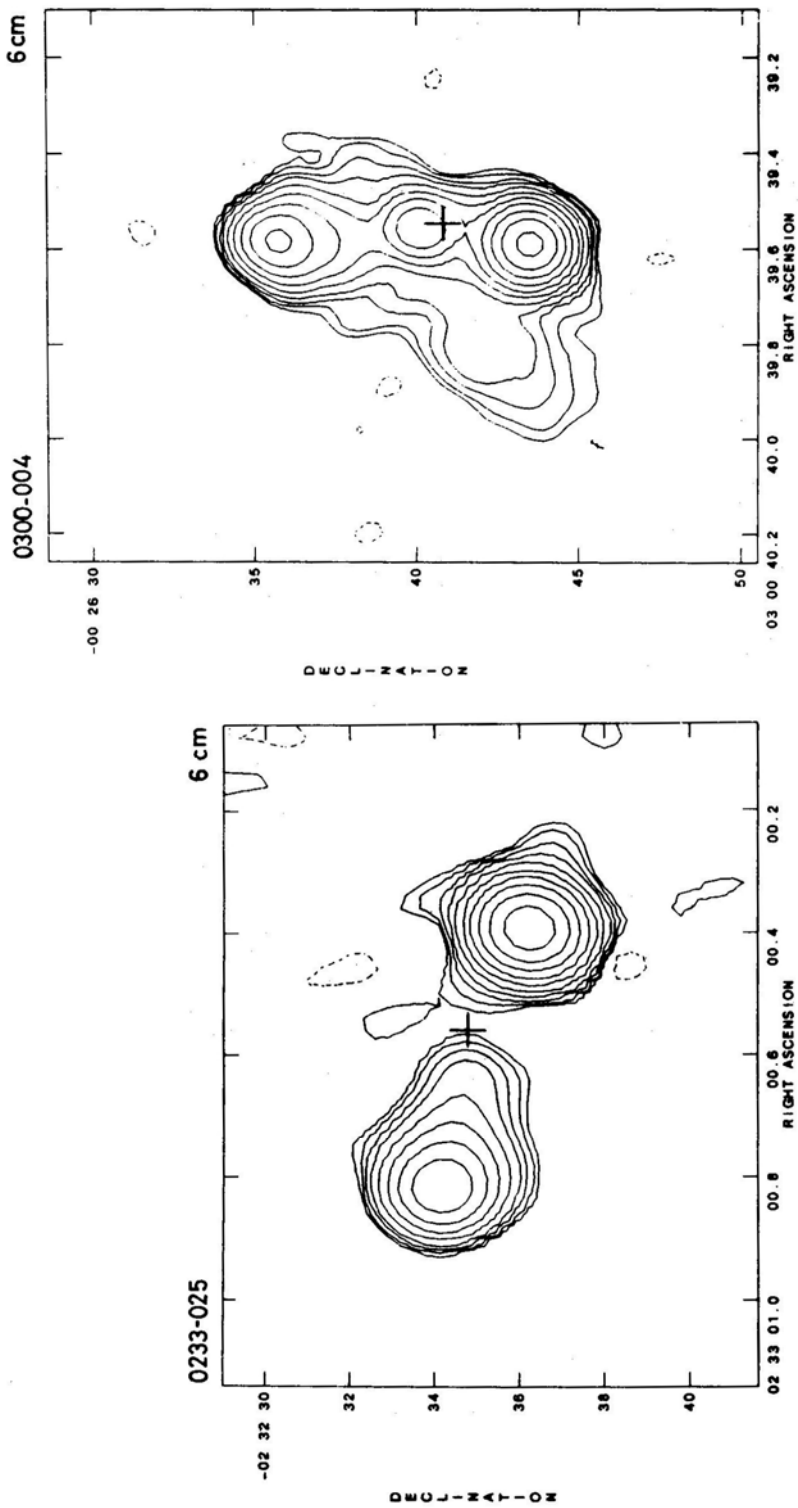
6 cm
0300-004
-00 26 30
35
40
45
50
03 00 40.2
40.0
39.8
39.6
39.4
39.2
RIGHT ASCENSION
DECLINATION
6 cm
0233-025
-02 32 30
32
34
36
38
40
02 33 01.0
00.8
00.6
00.4
00.2
RIGHT ASCENSION
DECLINATION

Figure 1(f).

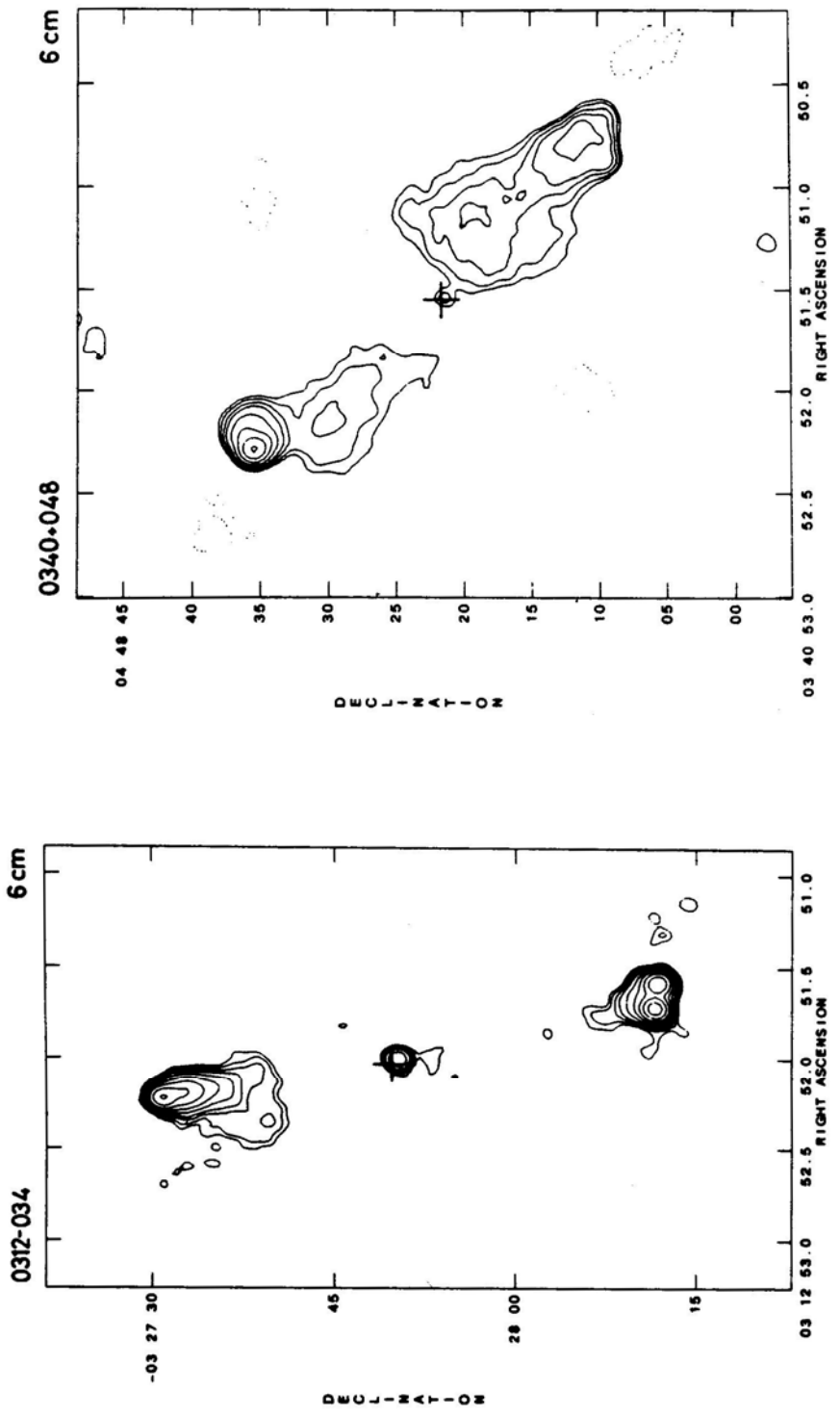
6 cm
0340+048
DECLINATION
04 48 45
40
35
30
25
20
15
10
05
00
03 40 53.0
52.5
52.0
51.5
51.0
50.5
RIGHT ASCENSION
6 cm
0312-034
DECLINATION
-03 27 30
45
28 00
15
03 12 53.0
52.5
52.0
51.5
51.0
RIGHT ASCENSION

Figure 1(g).

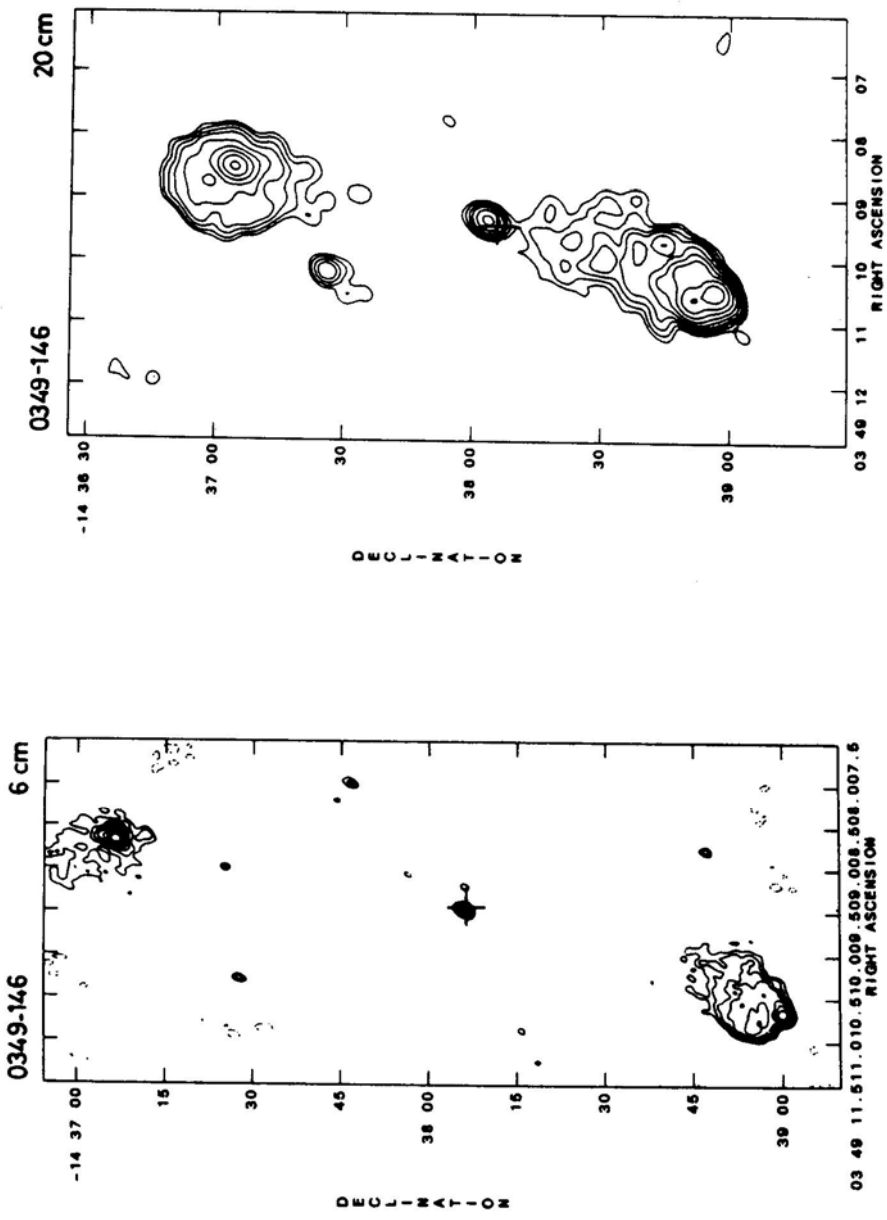
20 cm
0349-146
-14 36 30
37 00
30
38 00
30
39 00
03 49 12
11
10
09
08
07
RIGHT ASCENSION
DECLINATION
6 cm
0349-146
-14 37 00
15
30
45
38 00
15
30
45
39 00
03 49 11.511.010.510.009.509.008.508.007.5
RIGHT ASCENSION
DECLINATION

Figure 1(b).

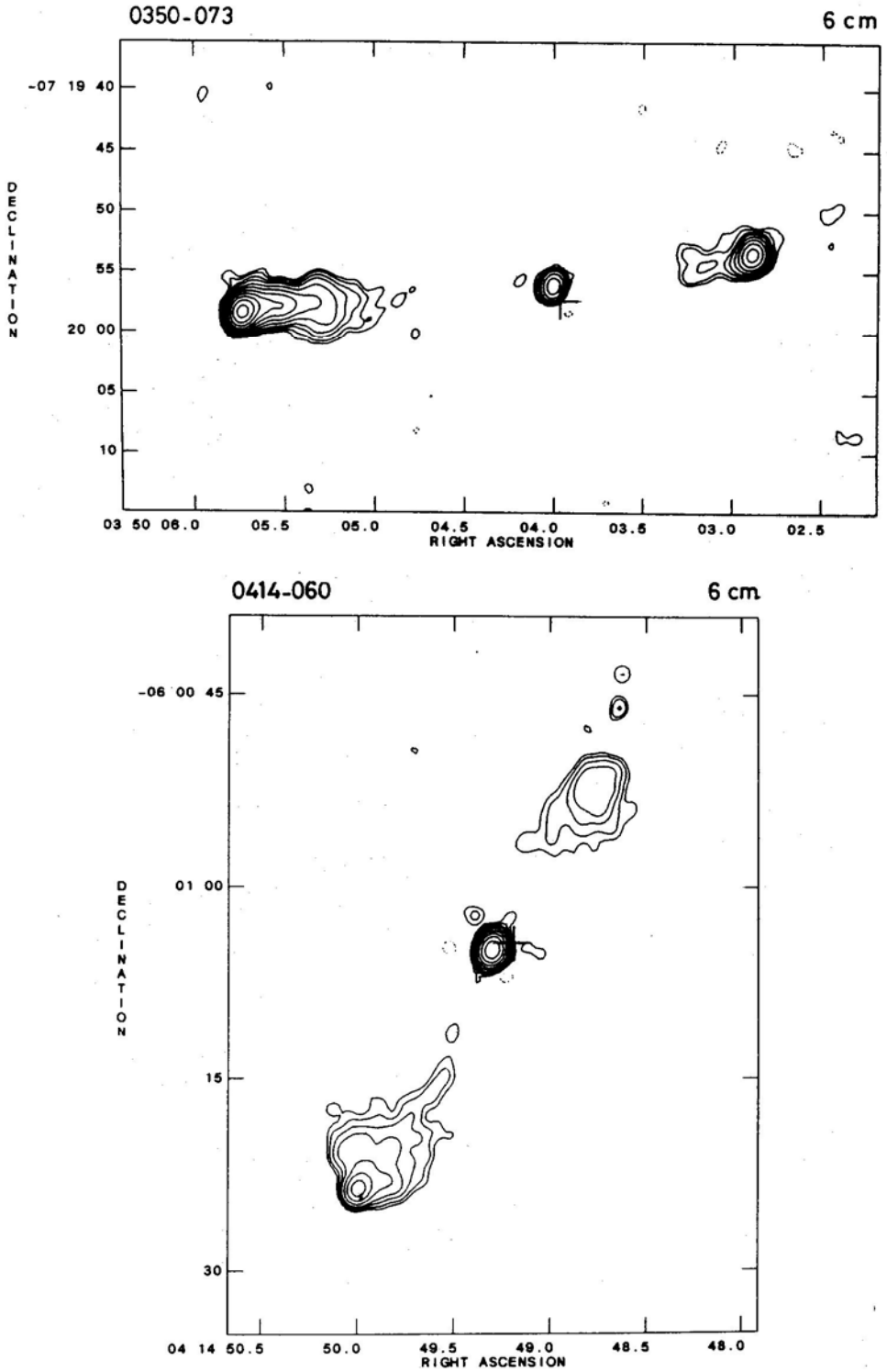
0350-073
6 cm
-07 19 40
45
50
55
20 00
05
10
DECLINATION
03 50 06.0
05.5
05.0
04.5
04.0
03.5
03.0
02.5
RIGHT ASCENSION
0414-060
6 cm
-06 00 45
01 00
15
30
DECLINATION
04 14 50.5
50.0
49.5
49.0
48.5
48.0
RIGHT ASCENSION

Figure 1(i).

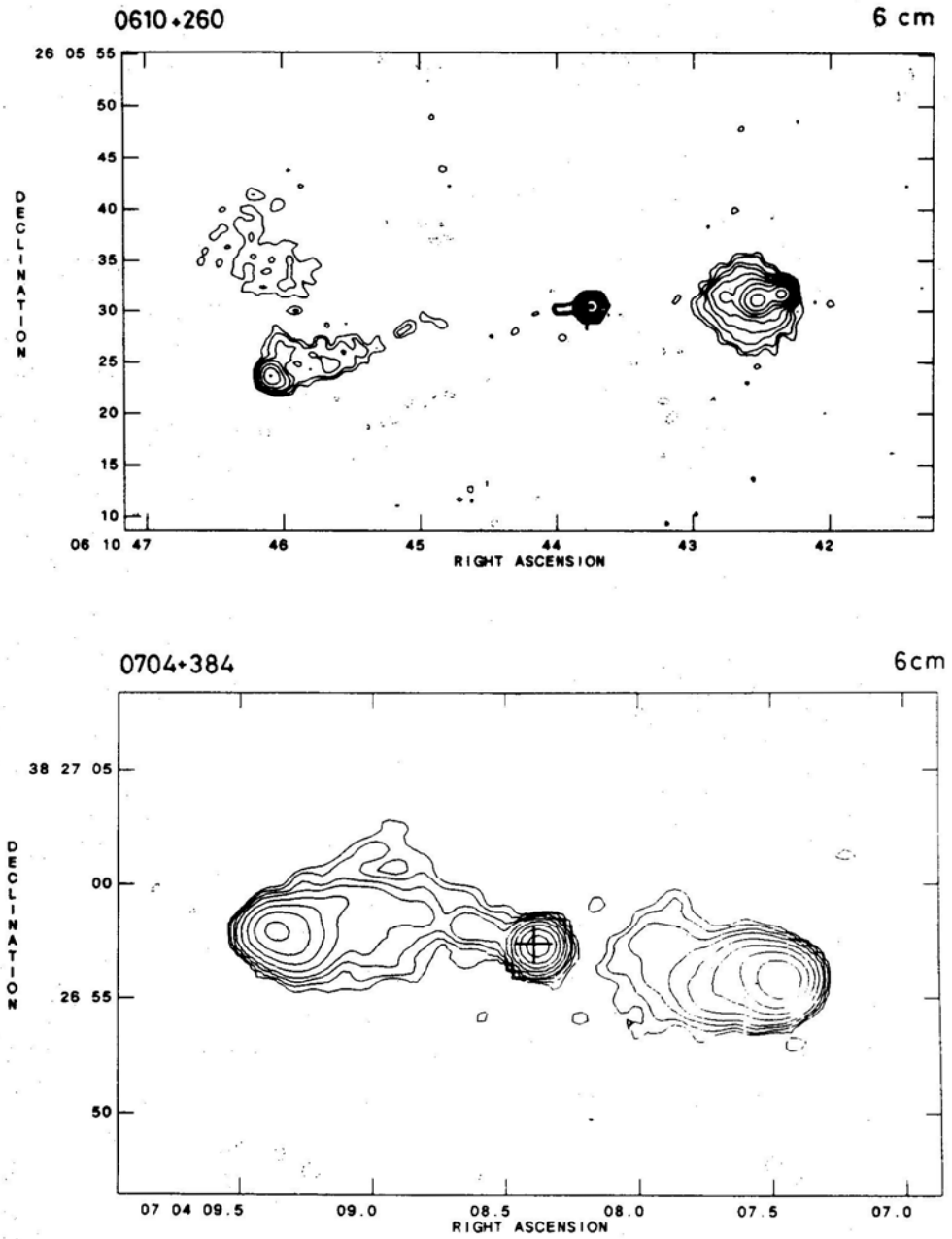

Figure 1(j).

Asterisks in the table refer to additional notes in the text on some objects at the end of this section.

Information on the contour values and the restoring beams used in the maps shown in Fig. 1 is summarised in Table 2. While the typical rms noise in each map is listed in column 2, the peak value of the flux density, in mJy is given incolumn3 and the value of

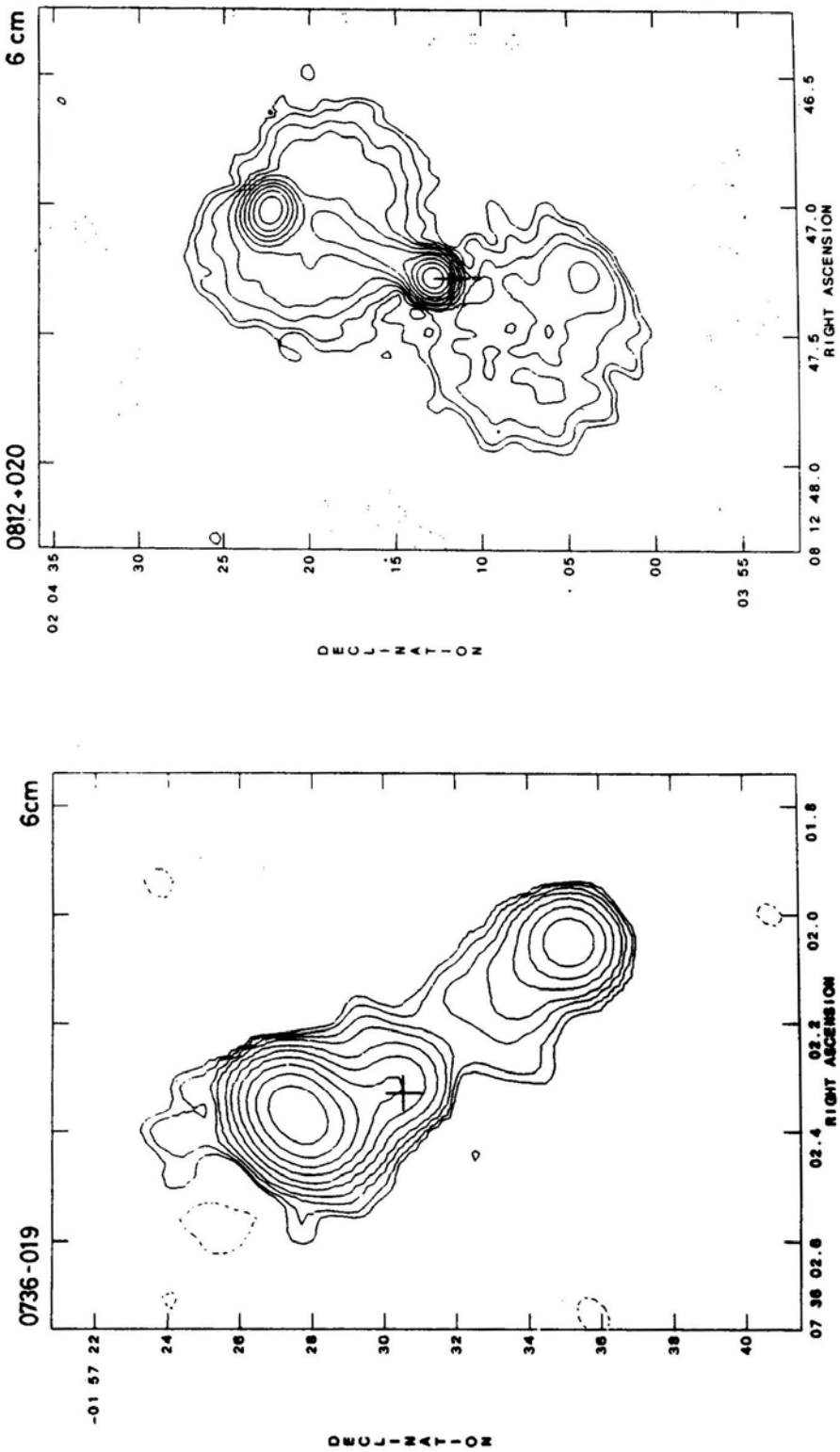
6 cm
0812+020
02 04 35
30
25
20
15
10
05
00
03 55
DECLINATION
08 12 48.0
47.5
47.0
46.5
RIGHT ASCENSION
6cm
0736-019
-01 57 22
24
26
28
30
32
34
36
38
40
DECLINATION
07 36 02.6
02.4
02.2
02.0
01.8
RIGHT ASCENSION

Figure 1(k).

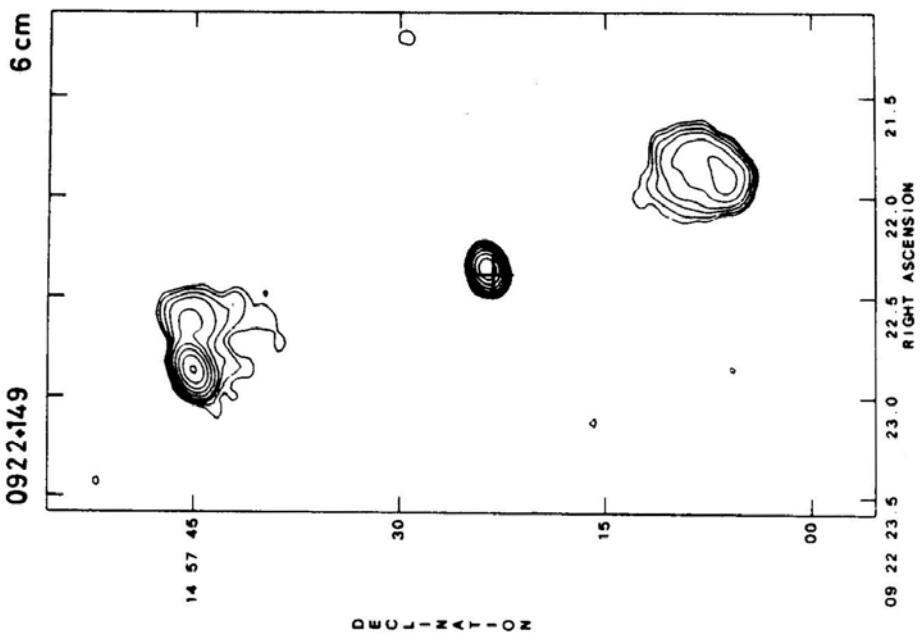
6 cm
0922+149
14 57 45
30
15
00
DECLINATION
09 22 23.5
23.0
22.5
22.0
21.5
RIGHT ASCENSION

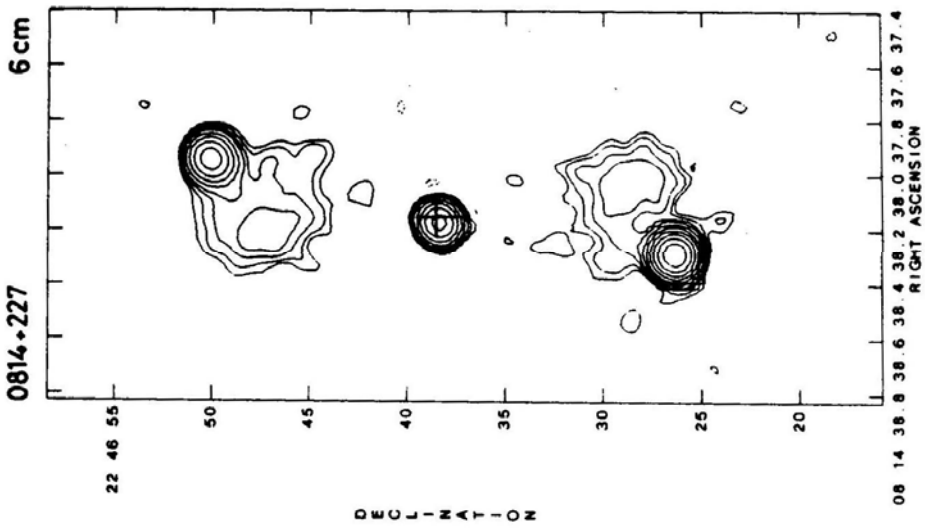
6 cm
0814+227
22 46 55
50
45
40
35
30
25
20
DECLINATION
08 14 38.8
38.6
38.4
38.2
38.0
37.8
37.6
37.4
RIGHT ASCENSION

Figure 1 (l).

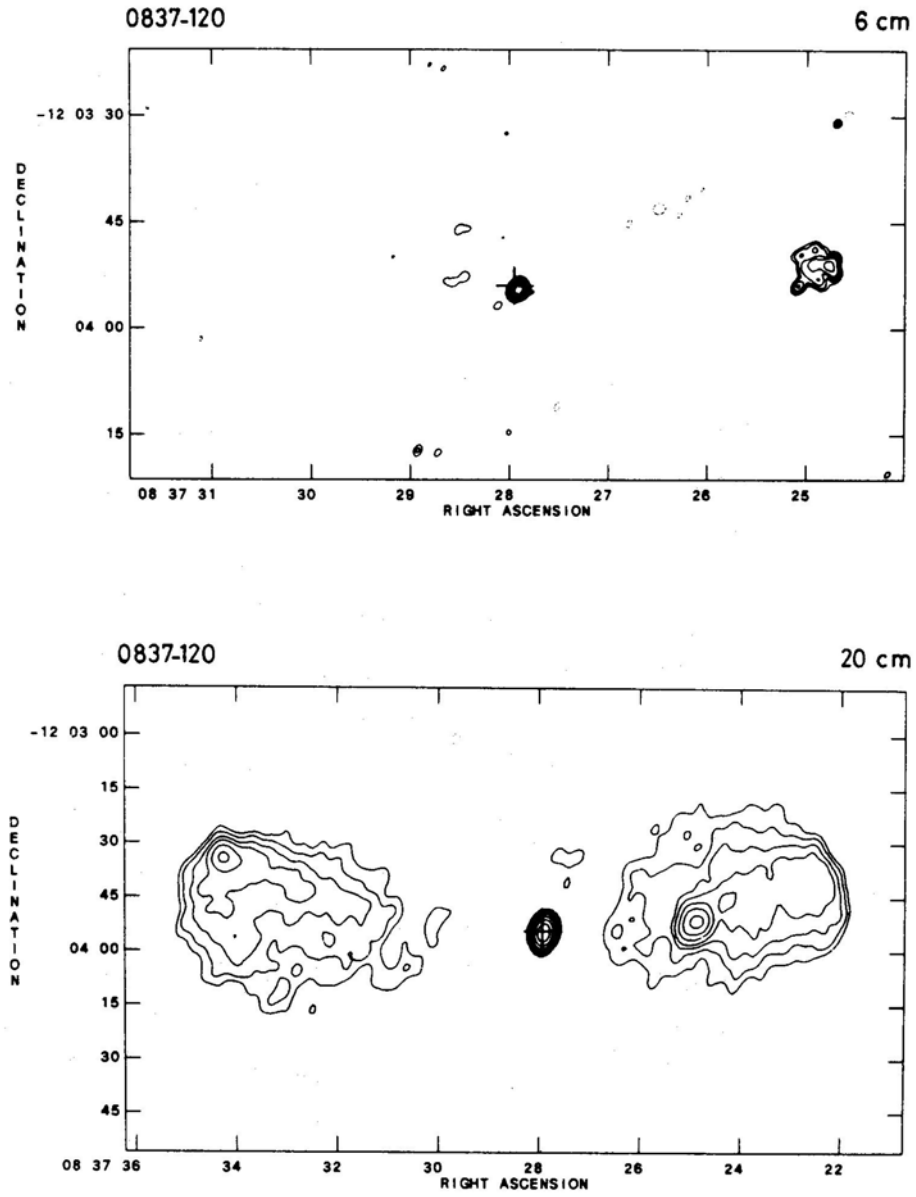

Figure 1(m).

the first positive contour (C), in mJy per beam area, is given in column 4. The contours plotted in the corresponding maps in Fig. 1 are at $C \times$ (-1, 1, 1.5, 2.5, 4, 8, 16, 32, 64, 128…)mJy/beam area.

The half power widths of the major and minor axes of the restoring Gaussian beam widths and the position angles of the major axes are listed in columns 5, 6 and

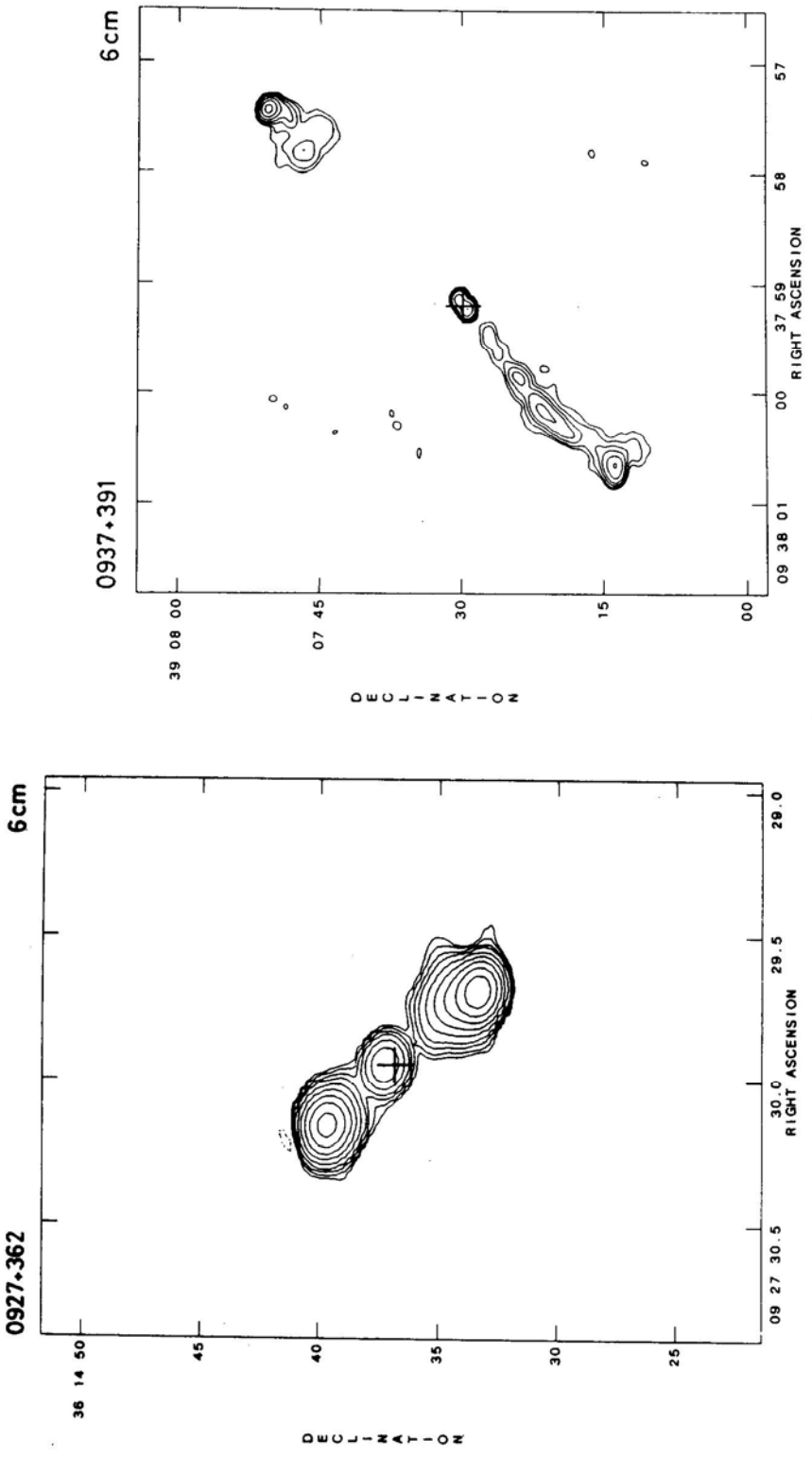
6cm
0937+391
39 08 00
07 45
30
15
00
DECLINATION
09 38 01
00
37 59
58
57
RIGHT ASCENSION
6cm
0927+362
36 14 50
45
40
35
30
25
DECLINATION
09 27 30.5
30.0
29.5
29.0
RIGHT ASCENSION

Figure 1(n).

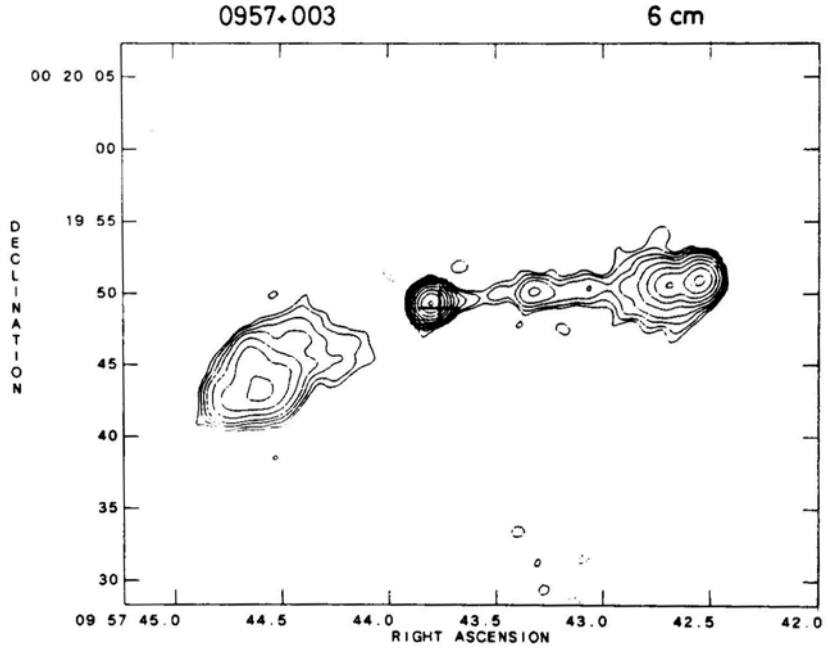
0957+003
6 cm
00 20 05
00
19 55
50
45
40
35
30
DECLINATION
09 57 45.0
44.5
44.0
43.5
43.0
42.5
42.0
RIGHT ASCENSION

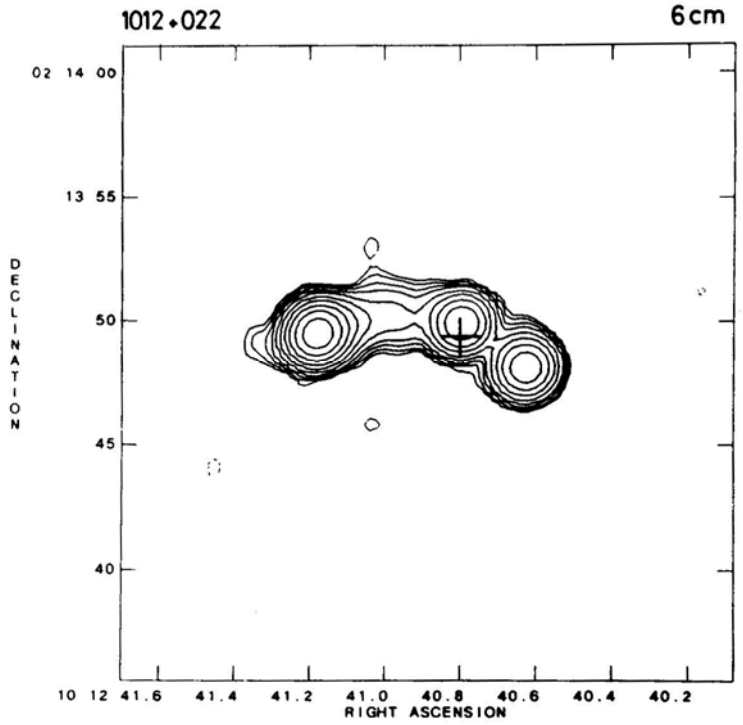
1012+022
6cm
02 14 00
13 55
50
45
40
DECLINATION
10 12 41.6
41.4
41.2
41.0
40.8
40.6
40.4
40.2
RIGHT ASCENSION

Figure 1(o).

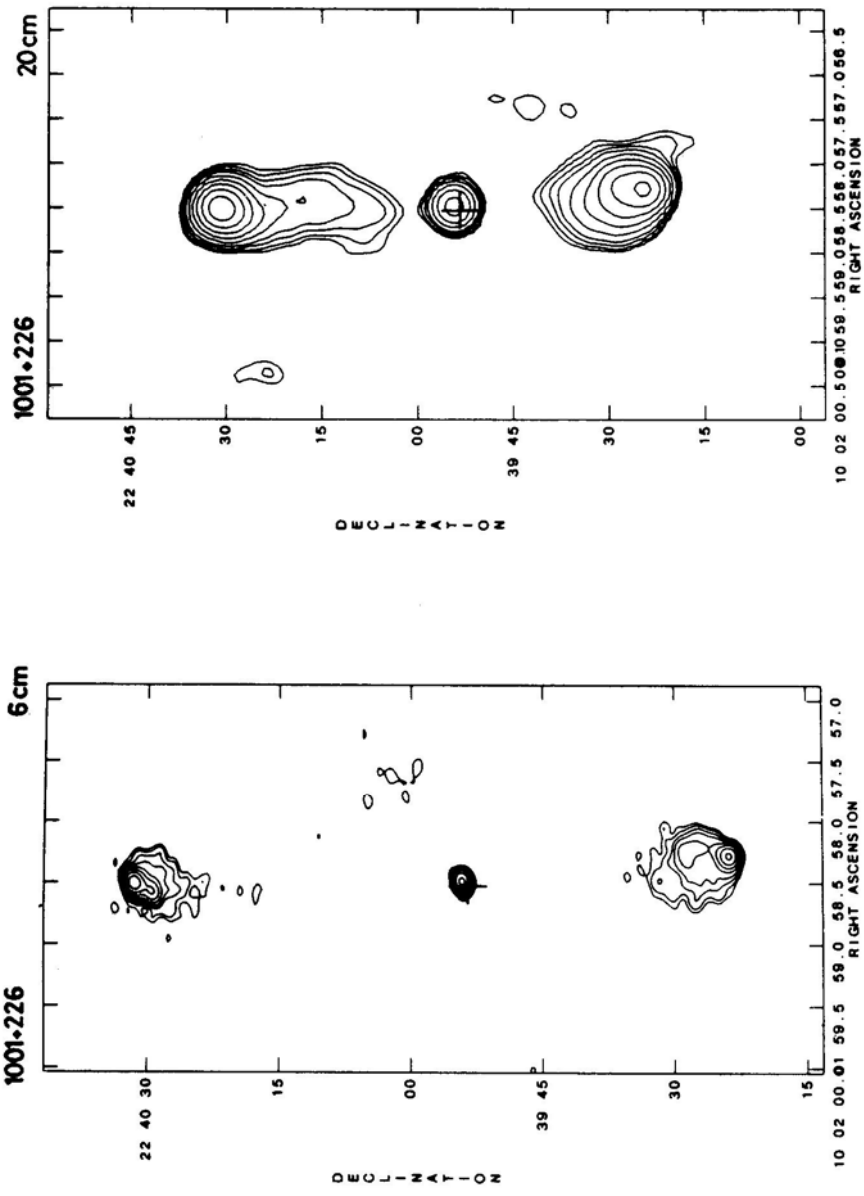
20cm
1001+226
22 40 45
30
15
00
39 45
30
15
00
10 02 00.5 00 59.5 59.0 58.5 58.0 57.5 57.0 56.5
RIGHT ASCENSION
DECLINATION
6cm
1001+226
22 40 30
15
00
39 45
30
15
10 02 00.0 01 59.5 59.0 58.5 58.0 57.5 57.0
RIGHT ASCENSION
DECLINATION

Figure 1(p).

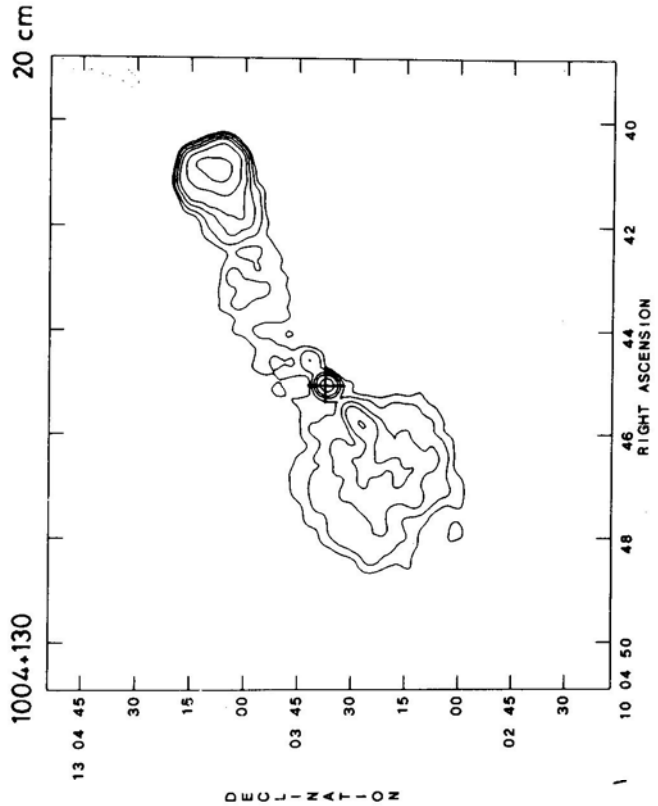
20 cm
1004+130
13 04 45
30
15
00
03 45
30
15
00
02 45
30
10 04 50
48
46
44
42
40
RIGHT ASCENSION
DECLINATION

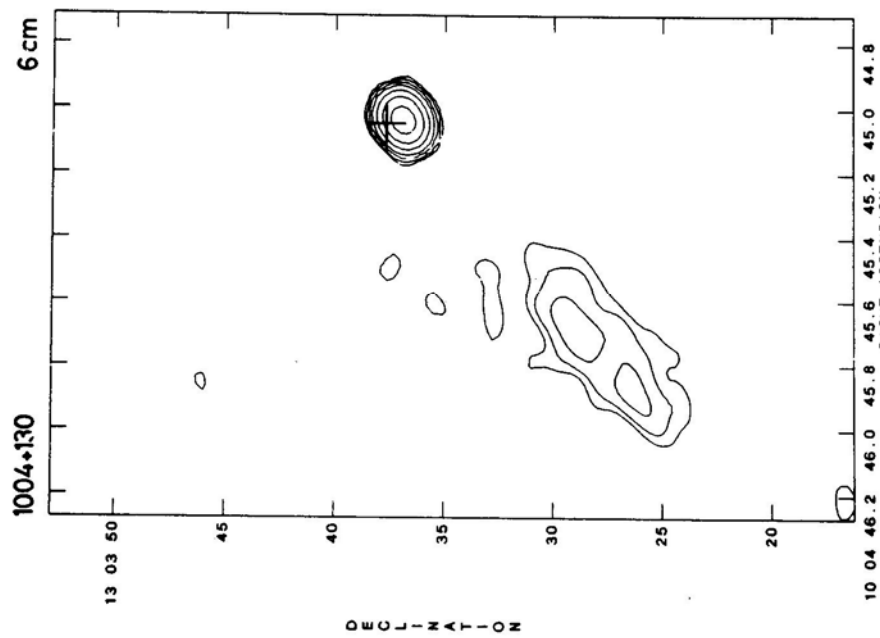
6 cm
1004+130
13 03 50
45
40
35
30
25
20
10 04 46.2
46.0
45.8
45.6
45.4
45.2
45.0
44.8
RIGHT ASCENSION
DECLINATION

Figure 1(q).

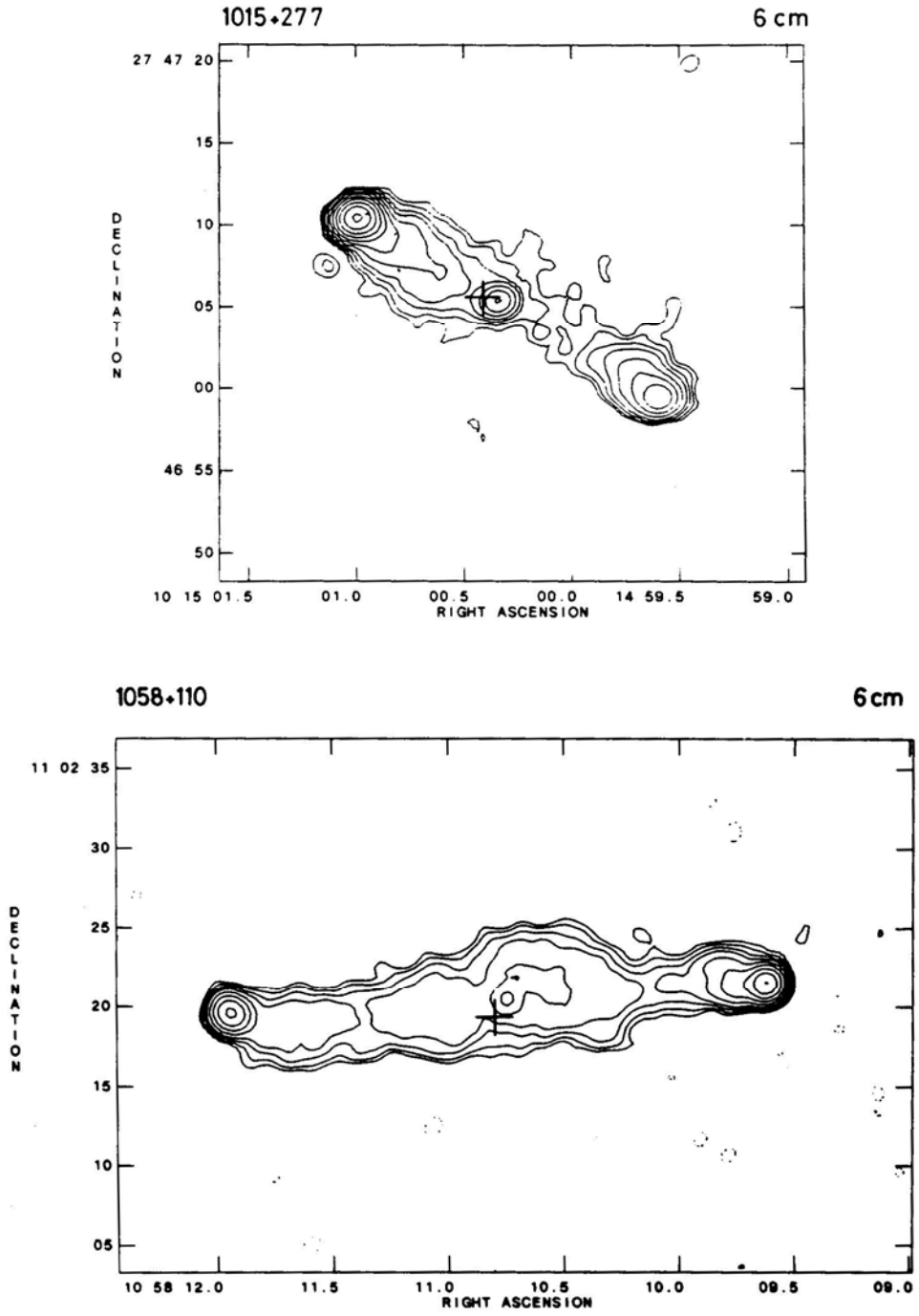
1015+277
6 cm
27 47 20
15
10
05
00
46 55
50
DECLINATION
10 15 01.5
01.0
00.5
00.0
14 59.5
59.0
RIGHT ASCENSION
1058+110
6cm
11 02 35
30
25
20
15
10
05
DECLINATION
10 58 12.0
11.5
11.0
10.5
10.0
09.5
09.0
RIGHT ASCENSION

Figure 1(r).

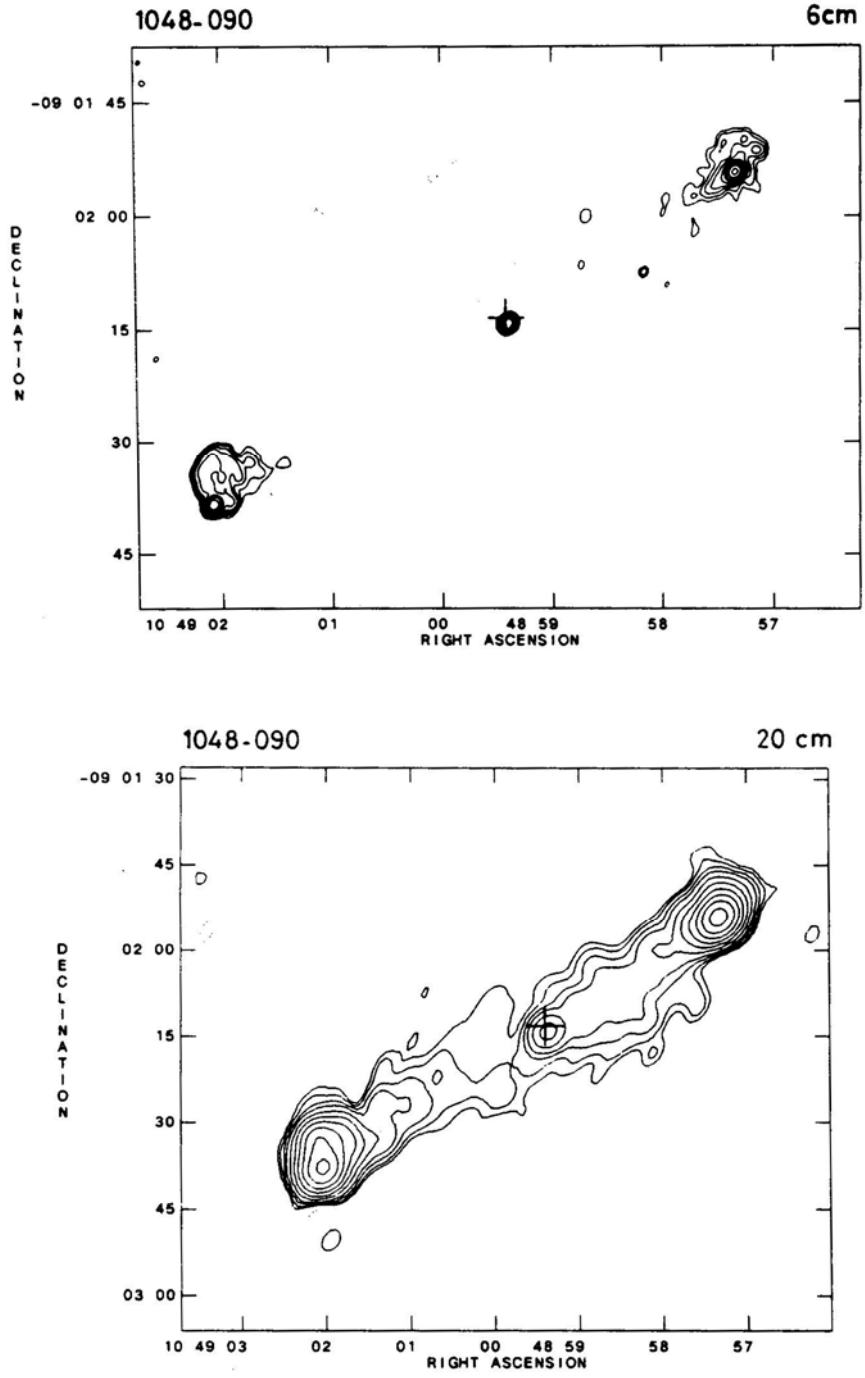
1048-090
6cm
-09 01 45
02 00
15
30
45
DECLINATION
10 49 02
01
00
48 59
58
57
RIGHT ASCENSION
1048-090
20 cm
-09 01 30
45
02 00
15
30
45
03 00
DECLINATION
10 49 03
02
01
00
48 59
58
57
RIGHT ASCENSION

Figure 1(s).

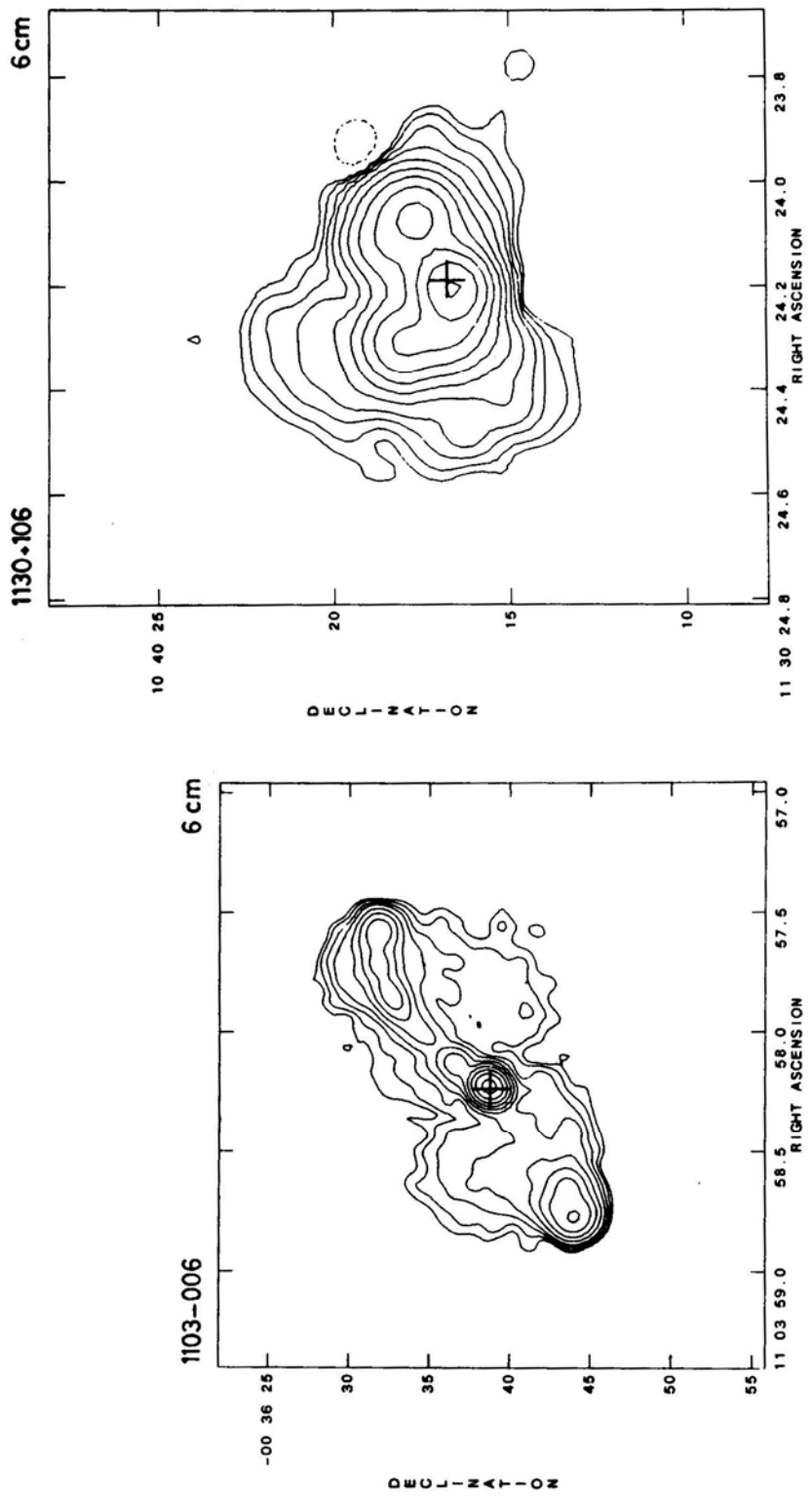
6 cm
1130+106
10 40 25
20
15
10
DECLINATION
11 30 24.8
24.6
24.4
24.2
24.0
23.8
RIGHT ASCENSION
6 cm
1103-006
-00 36 25
30
35
40
45
50
55
DECLINATION
11 03 59.0
58.5
58.0
57.5
57.0
RIGHT ASCENSION

Figure 1(t).

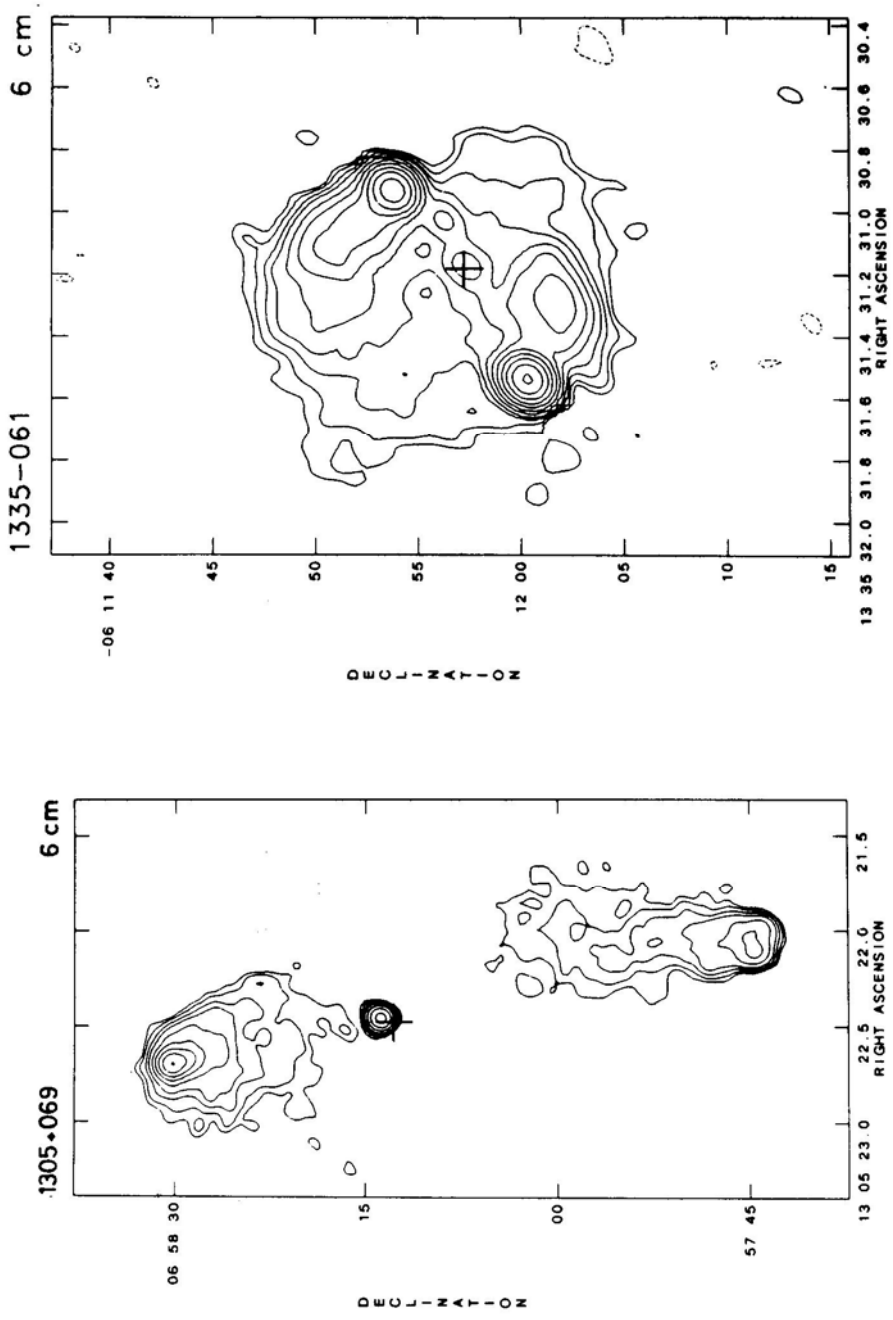
6 cm
1335−061
-06 11 40
45
50
55
12 00
05
10
15
DECLINATION
13 35 32.0 31.8 31.6 31.4 31.2 31.0 30.8 30.6 30.4
RIGHT ASCENSION
6 cm
1305+069
06 58 30
15
00
57 45
DECLINATION
13 05 23 0 22.5 22.0 21.5
RIGHT ASCENSION

Figure 1(u).

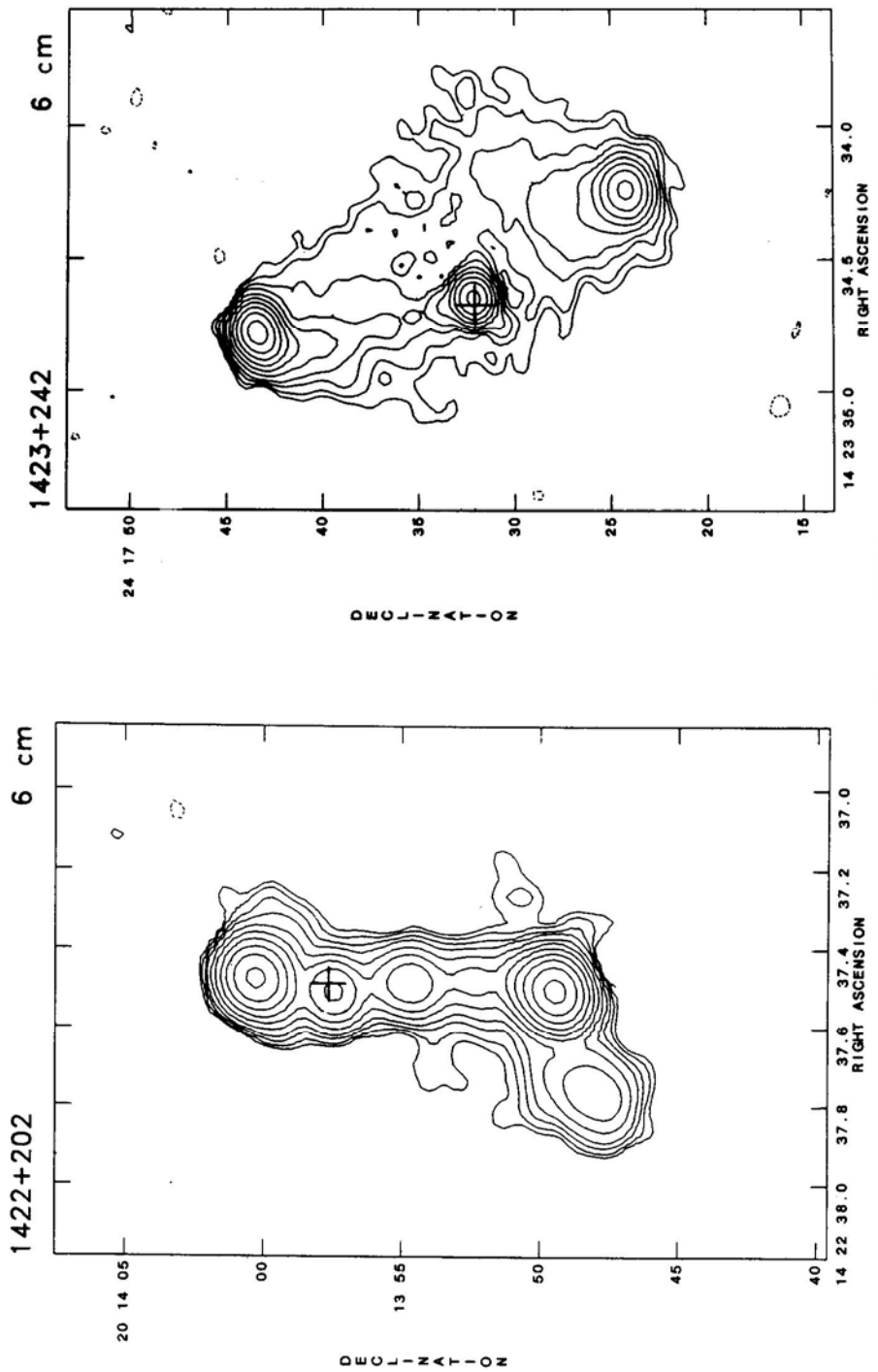
1423+242
6 cm
24 17 50
45
40
35
30
25
20
15
DECLINATION
14 23 35.0
34.5
34.0
RIGHT ASCENSION
1422+202
6 cm
20 14 05
00
13 55
50
45
40
DECLINATION
14 22 38.0
37.8
37.6
37.4
37.2
37.0
RIGHT ASCENSION

Figure 1(v).

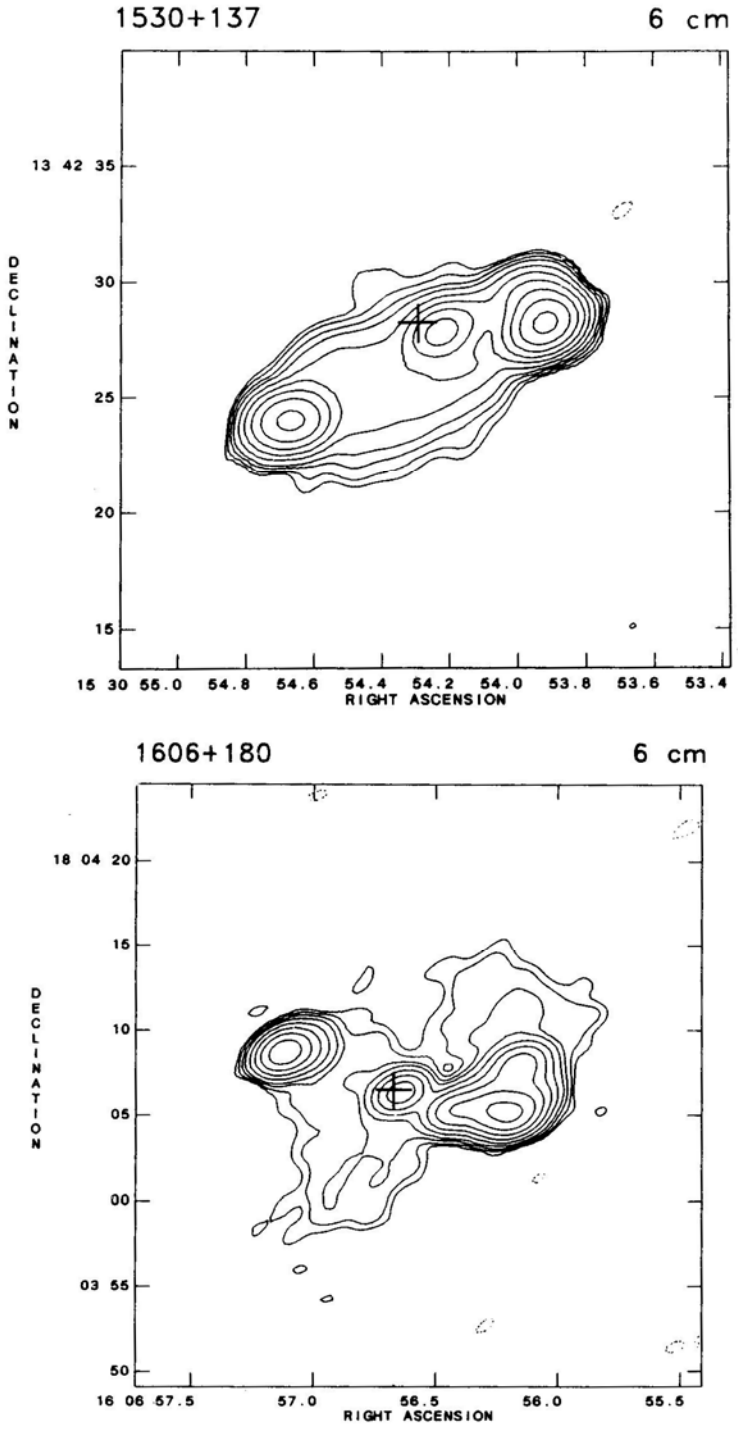
1530+137
6 cm
13 42 35
30
25
20
15
DECLINATION
15 30 55.0
54.8
54.6
54.4
54.2
54.0
53.8
53.6
53.4
RIGHT ASCENSION
1606+180
6 cm
18 04 20
15
10
05
00
03 55
50
DECLINATION
16 06 57.5
57.0
56.5
56.0
55.5
RIGHT ASCENSION

Figure 1(w).

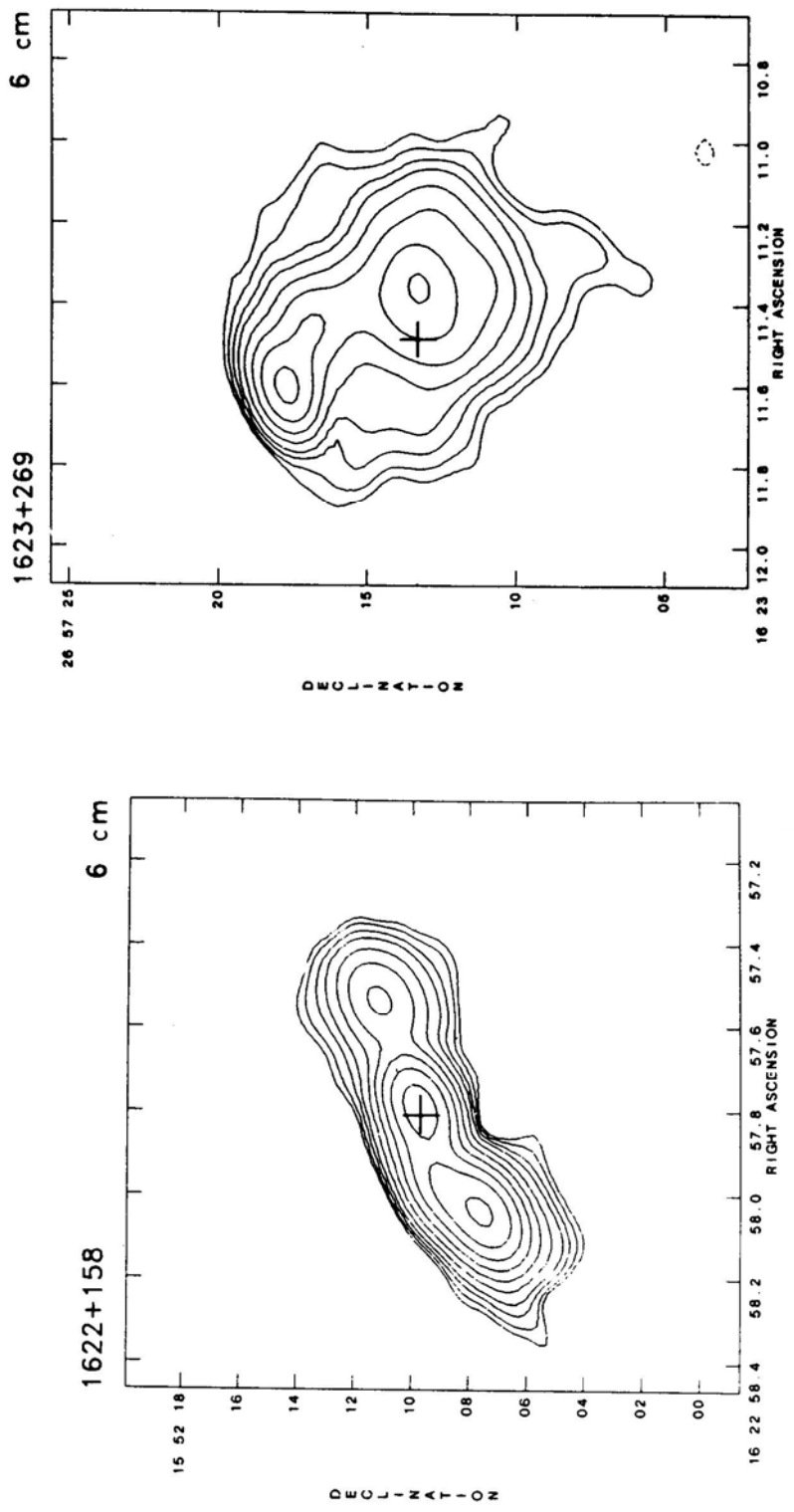
6 cm
1623+269
DECLINATION
RIGHT ASCENSION
6 cm
1622+158
DECLINATION
RIGHT ASCENSION

Figure 1(x).

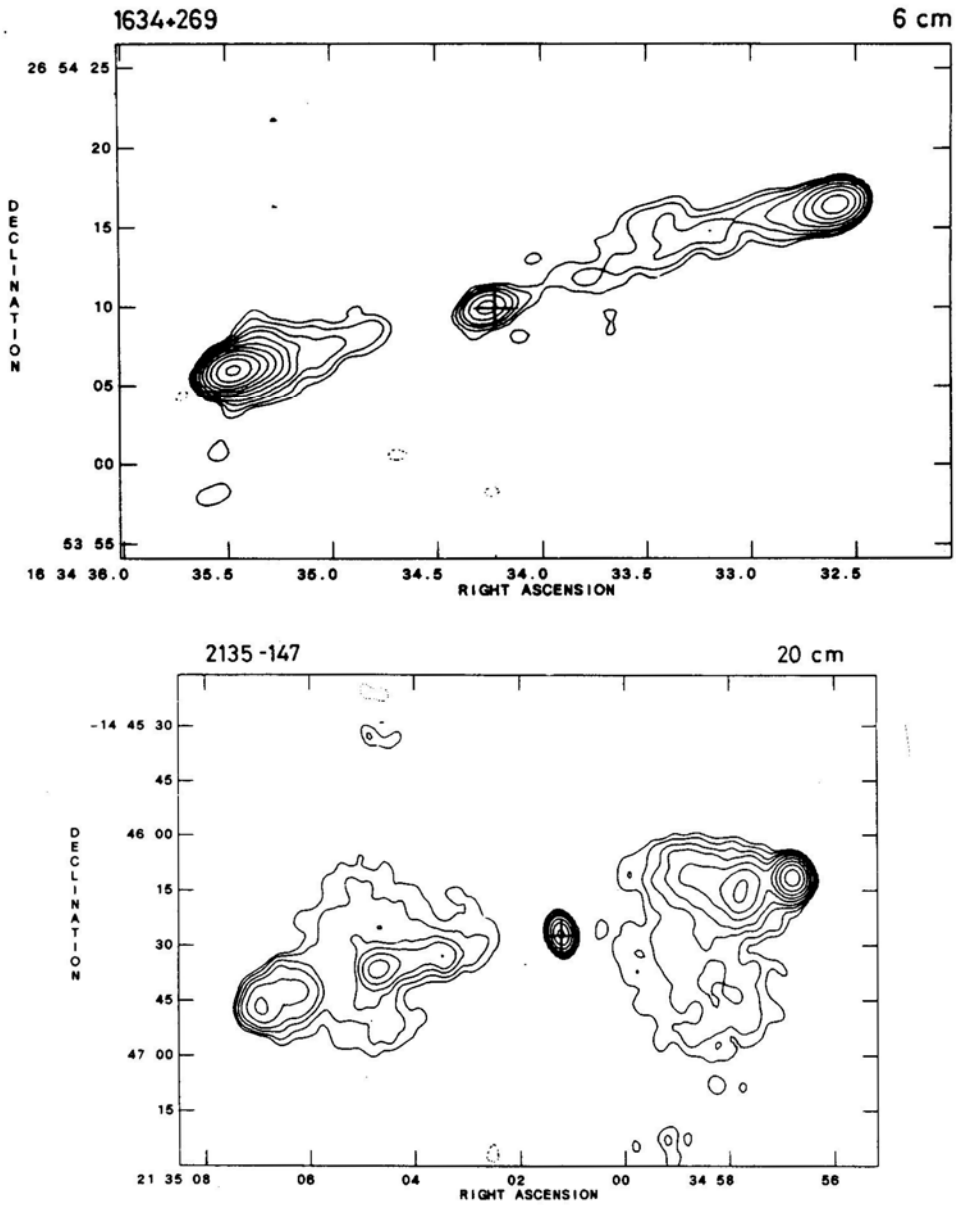

Figure 1(y).

7 respectively. As in Table 1, entries on the second line for any source refer to the source maps at 20 cm λ.

Notes on some individual sources

0137 + 012: Our 20 cm map shows considerably more extended emission surrounding the two lobes than seen in the earlier 20 cm map by Hintzen *et al.* (1983).

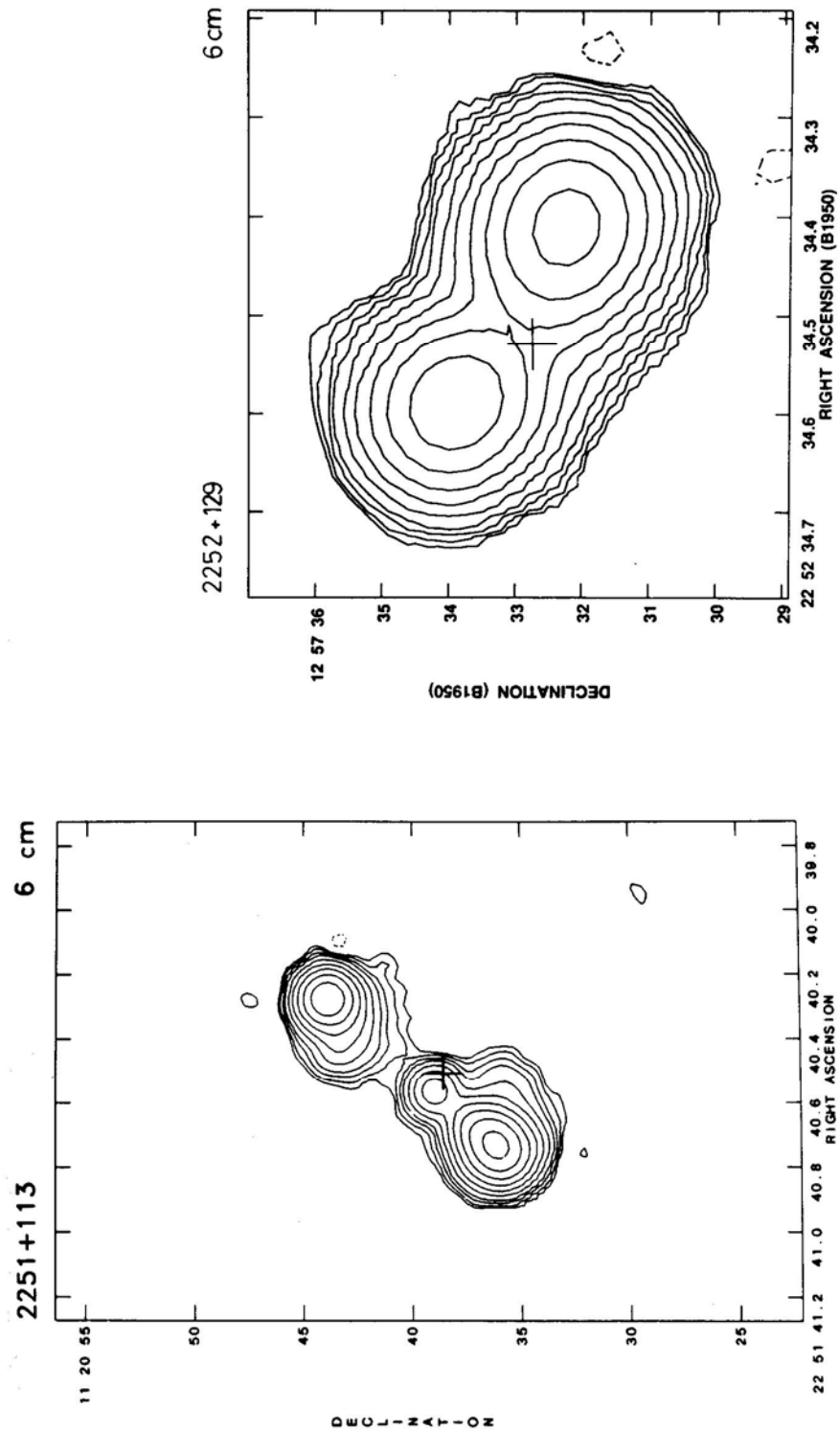
6 cm
2252+129
DECLINATION (B1950)
12 57 36
35
34
33
32
31
30
29
22 52 34.7
34.6
34.5
34.4
34.3
34.2
RIGHT ASCENSION (B1950)
6 cm
2251+113
DECLINATION
11 20 55
50
45
40
35
30
25
22 51 41.2
41.0
40.8
40.6
40.4
40.2
40.0
39.8
RIGHT ASCENSION

Figure 1(z).

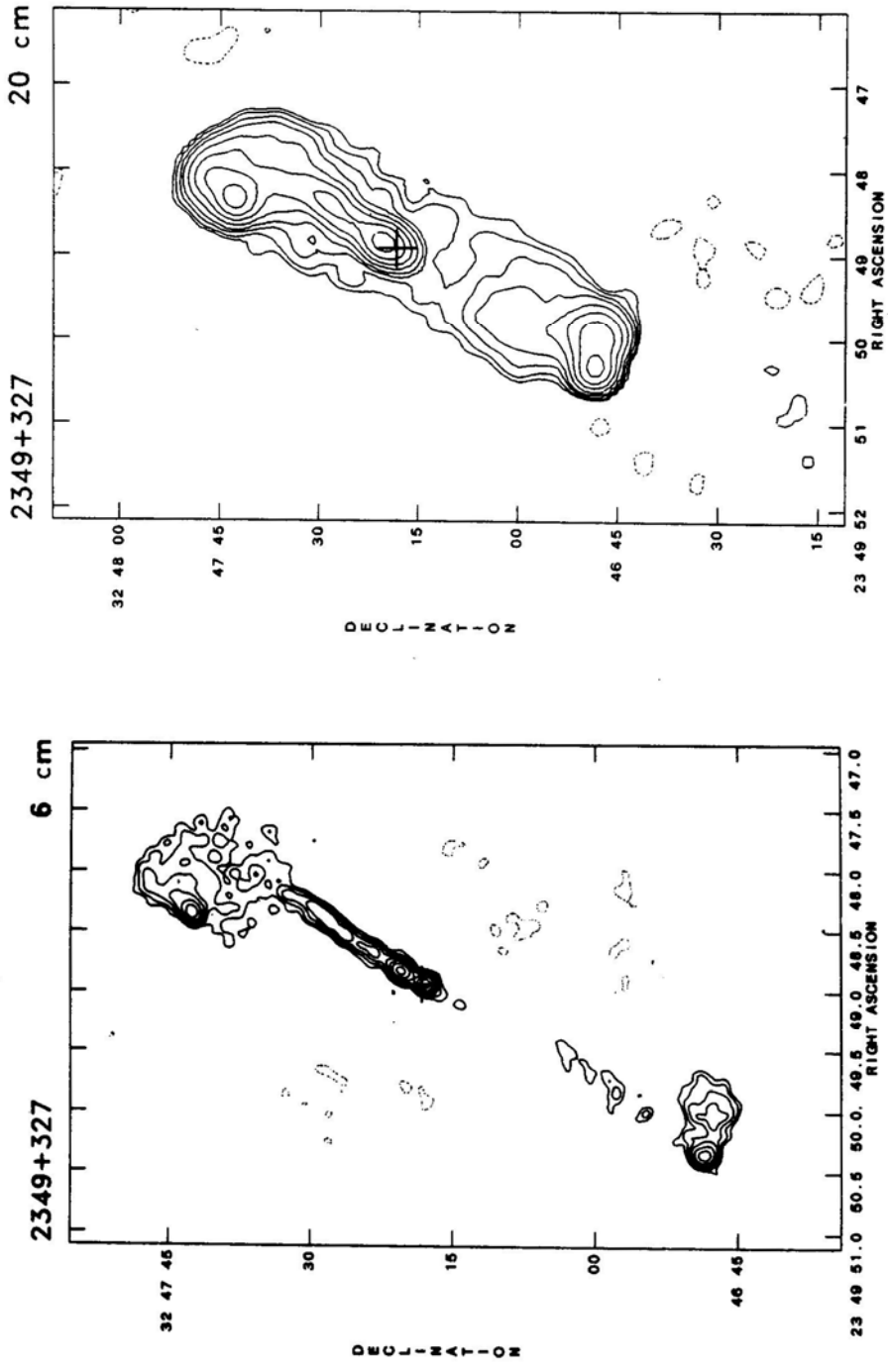
20 cm
2349+327
32 48 00
47 45
30
15
00
46 45
30
15
DECLINATION
23 49 52
51
50
49
48
47
RIGHT ASCENSION
6 cm
2349+327
32 47 45
30
15
00
46 45
DECLINATION
23 49 51.0
50.5
50.0
49.5
49.0
48.5
48.0
47.5
47.0
RIGHT ASCENSION

Figure 1(A).

0158 + 183: The core flux of 40 mJy includes a contribution from part of a nuclear jet.

0159 – 117: The weak component, 13.7arcsec SE of the optical quasar has a flux density of S_{6cm} = 20 mJy. It was not seen in the earlier 20 cm map of Hintzen *et al.* (1983). The radio structure thus appears to be quite asymmetric. The other lobe which is much stronger, appears to lie only about 1.5 arcsec north of the core and is not fully resolved with the present resolution. In a higher resolution map at 6 cm λ, published recently by Price *et al.* (1993), the northern component is clearly separated from the core and faint emission is seen also from the weaker SE lobe.

0214 + 108: The eastern lobe is totally resolved out in the 6 cm observations.

0233 – 025: This is one of the very few quasars in the sample in which a radio core component was not detected.

0300 – 004: There is considerable amount of off axis extended emission to the east and northeast of the southern hotspot.

0610 + 260: The eastern lobe has extended emission almost at right angles to the source axis.

0736 – 019: This source was earlier classified to be of D2 type radio structure by Hintzen *et al.* (1983), possibly because of an incorrect optical position of the quasar plotted on their VLA map. The present map shows a triple structure with the optical position of McEwan *et al.* (1975) close to a possible radio core.

0812 + 020: Hintzen *et al.* (1983) considered this source to have D2 type structure as the extended southeastern lobe was not seen in their 20 cm VLA map. This lobe is resolved out also in the higher resolution 6 cm map of Price *et al.* (1993).

0814 + 227: Both the lobes appear to be extended at large angles to and on opposite sides of the axis defined by the hotspots.

0837 – 120: The eastern lobe clearly seen in the 20 cm map has been resolved out in our 6 cm map.

0937 + 391: It is difficult to identify the radio core as there are two compact components close to the optical position. The total flux density of the two components at 6cm λ is 14 mJy. We have considered the northwest component to be the radio core because it is found to have a flatter spectral index between 20 cm and 6 cm as noted by Price *et al.* (1993). The southern lobe thus appears to consist of a long jet with several knots in it.

0957 + 003: The jet connecting the core to the western lobe, seen in our map is resolved out in the higher resolution map of Price *et al.* (1993).

1004 +130: Most of the extended structure in the lobes seen in our 20 cm map is resolved out at 6 cm λ.

1012 + 022: The lobes are strongly non collinear with respect to the radio core.

1130 +106: The higher resolution 6 cm map of Price *et al.* (1993) confirms that the radio peak close to the optical position is indeed the radio core. The lobes are thus strongly misaligned with the core.

1335 – 061: The two lobes have emission extended at large angles to the axis defined by the hotspots.

1422 + 202: There appears to be a sharp bend in the radio structure near the southern end.

Table 1. Radio structure of 45 quasars.

Source	Other name	Redshift	S_{total} (mJy)	S_{core} (mJy)	Radio Core Posn. (1950.0) h	m	s	°	′	″	Opt. posn. s	″	Ref. pos.	LAS (″ arc)
0003 + 158	4C15.01	0.45	315	109	00	03	25.07	15	53	07.0	25.01	06.6	1	35.1
0118 + 034	4C03.04	0.765	296	29	01	18	26.13	03	28	30.7	26.12	29.9	2	45.0
			945	37										
0137 + 012	4C01.04	0.260	515	150	01	37	22.86	01	16	35.3	22.78	35.2	1	27.5*
			1240	185										
0158 + 183	4C18.07	0.799	325	40*	01	58	56.09	18	22	10.7	56.13	09.8	3	15.0
0159 − 117	3C57	0.669	1195	*	01	59	30.36	−11	46	59.4*	30.40	00.0	4	15.5
0214 + 108	4C10.06	0.408	(297)	76	02	14	26.68	10	50	18.6	26.60	18.3	1	121.0*
			1163	82										
0222 − 008	PKS	0.687	405	5	02	22	34.68	−00	49	04.0	34.63	03.4	5	13.6
0233 − 025	PKS	1.322	315	*							00.56	34.8	1	6.5
0300 − 004	PKS	0.693	385	48	03	00	39.56	−00	26	40.1	39.55	40.9	6	7.8*
0312 − 034	PKS	1.072	335	7	03	12	52.00	−03	27	50.3	52.04	49.8	3	41.0
0340 + 048	3CR93	0.357	580	4	03	40	51.53	04	48	21.2	51.54	21.7	7	33.1
0349 − 146	3C95	0.614	(480)	46	03	49	09.47	−14	38	05.9	09.45	06.4	1	117.0
			2720	48										
0350 − 073	3C94	0.962	675	14	03	50	04.00	−07	19	56.1	03.97	57.4	1	42.1
0414 − 060	3C110	0.781	290	144	04	14	49.30	−06	01	04.9	49.18	04.3	8	36.4
0610 + 260	3CR154	0.580	1600	360	06	10	43.75	26	05	30.4	43.79	30.1	9	50.0*
0704 + 384	4C38.20	0.579	285	64	07	04	08.38	28	26	57.2	08.40	57.3	1	22.0
0736 − 019	3C185	1.033	346	40	07	36	02.34	−01	57	29.7	02.33	30.5	6	9.0*
0812 + 020	4C02.23	0.402	715	200	08	12	47.28	02	04	12.9	47.28	11.7	1	18.6*
0814 + 227	3C197	0.980	435	43	08	14	38.17	22	46	38.4	38.15	38.6	1	24.2*
0837 − 120	3C206	0.200	(245)	189	08	37	27.91	−12	03	54.4	27.96	53.9	1	174.0*
			1820	128										
0922 + 149	4C14.31	0.896	190	48	09	22	22.36	14	57	23.6	22.41	23.2	1	41.2
0927 + 362	3CR220.2	1.157	550	34	09	27	29.95	36	14	37.2	29.95	36.7	1	8.4
0937 + 391	4C39.27	0.618	130	8*	09	37	59.15	39	07	30.4	59.20	30.0	1	52.6*
0957 + 003	4C00.34	0.907	325	86	09	57	43.80	00	19	49.3	43.76	49.0	2	31.5*

1001 + 226	4C22.26	0.974	175	24	10	01	58.49	22	39	54.2	58.53	53.6	10	67.5
			571	35										
1004 + 130	4C13.41	0.240	(45)	24	10	04	45.04	13	03	36.9	45.05	37.7	1	100.0*
			915	33										
1012 + 022	4C02.30	1.374	245	43	10	12	40.80	02	13	49.9	40.80	49.3	3	8.5*
1015 + 277	3C240	0.469	405	15	10	15	00.34	27	47	05.4	00.42	05.6	11	21.7
1048 − 090	3C246	0.344	610	60	10	48	59.40	− 09	02	14.2	59.42	13.2	1	82.0
			1920	35										
1058 + 110	4C10.30	0.420	235	5	10	58	10.73	11	02	20.6	10.80	19.4	1	33.9
1103 − 006	PKS	0.426	480	150	11	03	58.23	− 00	36	38.7	58.24	38.8	8	21.6
1130 + 106	4C10.33	0.540	410	158	11	30	24.21	10	40	16.7	24.19	16.8	8	3.5*
1305 + 069	3C281	0.599	320	18	13	05	22.46	06	58	13.8	22.48	12.9	1	46.5
1335 − 061	PKS	0.625	995	22	13	35	31.17	− 06	11	57.4	31.18	57.1	1	11.3*
1422 + 202	4C20.33	0.871	590	30	14	22	37.51	20	13	57.5	37.49	57.5	12	11.0*
1423 + 242	4C24.31	0.649	510	65	14	23	34.65	24	17	32.2	34.66	31.9	1	22.5
1530 + 137	4C13.55	0.771	370	35	15	30	54.22	13	42	27.8	54.29	28.3	8	11.8
1606 + 180	4C18.47	0.346	240	15	16	06	56.64	18	04	06.3	56.67	06.5	13	15.6*
1622 + 158	4C15.55	1.409	365	94	16	22	57.81	15	52	09.7	57.81	09.7	5	8.1
1623 + 269	4C26.48	0.779	190	*							11.50	13.3	14	5.5*
1634 + 269	3C342	0.561	400	9	16	34	34.26	26	54	10.0	34.22	10.0	1	39.7
2135 − 147	PKS	0.200	590	126	21	35	01.17	− 14	46	27.8	01.21	27.3	1	151.0*
			3450	117										
2251 + 113	4C11.72	0.323	530	24	22	51	40.57	11	20	38.8	40.51	38.6	1	10.3
2252 + 129	3CR455	0.543	735								34.53	33.5	15	3.2
2349 + 327	4C32.69	0.659	(195)	24	23	49	48.93	32	47	17.9	48.94	18.3	10	60.0*
			735											

References to optical positions:

1. Miley & Hartsuijker (1978); **2.** Hintzen, Ulvestad & Owen (1983); **3.** Wills, D. (1979); **4.** Bolton *et al.* (1966); **5.** Wills, B. J. (1976); **6.** McEwan *et al.* (1975); **7.** Argue & Kenworthy (1972); **8.** Wills, Wills & Douglas (1973); **9.** Riley & Pooley (1975); **10.** Stannard & Neal (1977); **11.** Fanti *et al.* (1975); **12.** Argue, Kenworthy & Stewart (1973); **13.** Ghigho (1977); **14.** Potash & Wardle (1979); **15.** Wills (1978).

Table 2. Contour maps of 45 quasars

Source	Rms value (mJy)	Peak value (mJy)	C (mJy)	Restoring beam Maj. axis ″	Min. axis ″	PA °
0003 + 158	0.13	104.7	0.5	1.27	1.25	52
0118 + 034	0.15	26.5	0.6	1.36	1.24	− 27
	0.35	121.8	1.0	4.20	3.90	18
0137 + 012	0.25	144.5	0.75	1.38	1.26	− 25
	0.20	300.5	0.75	4.37	4.00	09
0158 + 183	0.10	145.6	0.5	1.19	1.13	− 07
0159 − 117	0.42	770.9	2.0	1.65	1.14	05
0214 + 108	0.16	74.0	0.5	1.28	1.17	− 03
	0.30	188.4	1.0	4.06	3.79	21
0222 − 008	0.1	269.3	0.4	1.37	1.21	00
0233 − 025	0.14	206.0	0.5	1.41	1.19	− 02
0300 − 004	0.10	186.4	0.3	1.37	1.22	− 08
0312 − 034	0.13	80.0	0.4	1.44	1.17	− 06
0340 + 048	0.37	104.6	1.5	1.29	1.18	− 14
0349 − 146	0.30	59.1	1.0	1.67	1.14	− 19
	0.50	447.0	2.0	4.80	3.80	− 30
0350 − 073	0.16	355.4	0.5	1.50	1.15	− 10
0414 − 060	0.16	142.0	0.6	1.45	1.19	− 15
0610 + 260	0.35	321.5	1.2	1.20	1.17	63
0704 + 384	0.11	62.6	0.3	1.17	1.12	− 84
0736 − 019	0.13	189.4	0.4	1.45	1.29	− 16
0812 + 020	0.13	187.8	0.4	1.31	1.27	− 39
0814 + 227	0.18	240.4	0.5	1.31	1.27	− 39
0837 − 120	0.21	172.3	0.75	1.31	1.16	− 37
	0.45	120.9	2.0	5.18	3.67	− 13
0922 + 149	0.12	54.1	0.4	1.65	1.27	− 72
0927 + 362	0.15	222.0	1.0	1.47	1.08	79
0937 + 391	0.13	20.0	0.5	1.41	1.09	71
0957 + 003	0.09	84.0	0.3	1.31	1.25	− 38
1001 + 226	0.10	32.2	0.3	1.57	1.23	− 78
	0.22	159.3	0.75	4.30	4.20	− 65
1004 + 130	0.17	23.6	0.5	1.70	1.40	− 62
	0.75	44.1	2.0	4.31	4.24	− 60
1012 + 022	0.09	133.7	0.3	1.29	1.26	− 40
1015 + 277	0.12	231.9	0.4	1.39	1.18	− 76
1048 − 090	0.26	159.4	1.0	1.41	1.20	− 33
	0.50	531.9	2.0	4.47	3.92	− 34
1058 + 110	0.09	39.4	0.3	1.28	1.24	− 31
1103 − 006	0.13	137.0	0.4	1.41	1.25	− 24
1130 + 106	0.09	166.2	0.3	1.29	1.24	− 34
1305 + 069	0.12	53.6	0.4	1.27	1.22	− 35

(*Continued*)

Table 2. (*Continued*)

Source	Rms value (mJy)	Peak value (mJy)	C (mJy)	Restoring beam Maj. axis ″	Min. axis ″	PA °
1335 – 061	0.18	285.7	0.5	1.36	1.20	– 33
1422 + 202	0.12	261.6	0.4	1.41	1.24	– 73
1423 + 242	0.12	153.0	0.4	1.39	1.20	– 83
1530 + 137	0.10	128.1	0.4	1.81	1.37	– 64
1606 + 180	0.10	50.5	0.3	2.04	1.36	– 66
1622 + 158	0.10	146.1	0.5	2.22	1.41	– 63
1623 + 269	0.14	32.0	0.4	1.87	1.22	– 74
1634 + 269	0.10	236.0	0.4	1.86	1.21	– 73
2135 – 147	0.50	114.4	1.5	1.76	1.14	13
	1.00	587.9	3.0	5.42	3.62	10
2251 + 113	0.14	166.9	0.5	1.49	1.42	51
2252 + 129	0.35	349.7	1.0	1.49	1.33	58
2349 + 327	0.18	23.7	0.5	1.17	1.09	05
	0.26	71.7	0.75	3.62	3.46	33

1606 + 180: Both the lobes appear to have tails oriented almost at right angles to the source axis.

1623 + 269: Higher angular resolution is necessary to identify the radio core unambiguously. The radio structure appears to be significantly distorted and bent.

2135 – 147: Our 20 cm map shows extended structure in the lobes (particularly the western lobe) oriented almost at right angles to the source axis.

2252 + 129: Higher resolution is required to detect any possible radio core.

2349 + 327: While there is a strong and almost continuous jet on the northwest side, part of a faint counter jet is seen on the southern side of the radio core.

Acknowledgement

I acknowledge the support of a US National Research Council – JPL Senior Research Associateship under which part of this research was carried out. The National Radio Astronomy Observatory and the VLA are operated by Associated Universities Inc., under contract with the National Science Foundation, USA.

References

Argue, A. N., Kenworthy, C. M. 1972, *Mon. Not. R.. astr. Soc ,* **160**, 197.

Argue, A. N., Kenworthy, C. M., Stewart, P. M. 1973, *Astrophys. Lett.,* **14**, 99.

Barthel, P. D., Miley, G. K. 1988, *Nature,* **333**, 319.

Barthel, P.D., Miley, G. K., Schilizzi, R.T., Lonsdale, C. J. 1988, *Astr. Astrophys. Suppl.,Ser.,* **73**, 515.

Bolton, J. G., Shimmins, A. J., Ekers, J., Kinman, T. D., Lamia, E., Wirtanen, C. A. 1966, *Astrophys. J.,* **144**, 1229.

Fanti, C., Fanti, R., Ficarra, A., Formaggini, L., Giovannini, G., Lari, G, Padrielli, L. 1975, *Astr. Astrophys. Suppl*, **19,** 143. 975.

Ghigho, F. 1977, *Astrophys. J. Suppl,* **35**, 359.

Hewitt, A., Burbidge, G. 1993, *Astrophy. J. Suppl Ser.,* **87**, 451.

Hintzen, P., Ulvestad, J., Owen, F. 1983, *Astr. J.,* **88**, 709.

Kapahi, V. K. 1987, in *Observational Cosmology,* Eds. A. Hewitt, G. Burbidge & L. Z. Fang (Dordrecht: D. Reidel) p. 252.

Kapahi, V.K. 1990, *Curr. Sci.,* **59**, 561.

Kapahi, V. K., Saikia, D. J. 1982, *J. Astrophys. Astr.,* **3**, 465.

McEwan, N. J., Browne, I. W. A., Crowther, J. H. 1975, *Mem. R. astr. Soc,* **80**, 1.

Miley, G. K., Hartsuijker, A. 1978, *Astr. Astrophys. Suppl. Ser.,* **34**, 129.

Orr, M. J. L, Browne, I. W. A. 1982, *Mon. Not. R. astr. Soc,* **200**, 1067.

Potash, R. I., Wardle, J. F. C. 1979, *Astr. J.,* **84**, 707.

Price, R., Gower, A. C, Hutchings, J. B., Talon, S., Duncan, D., Ross, G. 1993, *Astrophys. J. Suppl Ser.,* **86**, 365.

Riley, J., Pooley, G. 1975, *Mon. Not. R. astr. Soc,* **80**, 105.

Singal, A.K.1988, *Mon. Not. R. astr. Soc,* **233**, 870.

Stannard, D., Neal, D. 1977, *Mon. Not. R. astr. Soc,* **179**, 719.

Veron, M.P., Veron, P. 1989, *A Catalogue of Quasars end Active Nuclei* (4th Edition), ESO, Germany.

Wills, B. J. 1976, *Astr. J.,* **81**, 1031.

Wills, D. 1978, *Mon. Not. R. astr. Soc,* **184**, 559.

Wills, D. 1979, *Astrophys. J. Suppl,* **39**, 291.

Wills, B. J., Wills, D., Douglas, J. 1973, *Astr. J.,* **78**, 521.

J. Astrophys. Astr. (1995) **16,** 37–43

The Orbit of the Double-line Spectroscopic Binary System HR 7112

P. N. Appleton, J. J. Eitter & C. Uecker *Erwin W. Fick Observatory*, *Department of Physics and Astronomy*, *Iowa State University*.

Received 1993 September 27; accepted 199 5 January 11

Abstract. We present velocity observations, obtained with the E. W. Fick Observatory 0.6 m telescope, of the 7th magnitude *K*1 star HR 7112. Our observations show that HR 7112 is a double-line spectroscopic binary system composed of almost equal mass stars with a period of 215.6 days. The orbit has an eccentricity e = 0.142 and the stars orbit each other with a mean semi-major axis distance of approximately 0.4sin(i) AU. The masses of the stars are consistent with the classification as giant stars. Tidal effects are known to circularise the orbits of giant stars and this process is apparently underway in this system.

Key words: Spectroscopic binary stars—radial velocity.

1. Introduction

The star HR 7112 (= HD174881) has a visual magnitude V= 6.81 and is classified as spectral class *K*1 II-III (Yoss 1961). The star was not previously suspected as being a spectroscopic binary. There have been 9 previous radial observations of the star, 3 measurements by Harper (1934) yielding a mean velocity of – 23.3 ± 1.1 kms $^{-1}$ and 6 observations by Young (1942) yielding a mean velocity of – 20.8 ± 2.2kms $^{-1}$. The double-line nature of the system became clear when the system was systematically observed as part of the Fick Observatory Radial Velocity Survey of bright late-type stars (see for example Beavers & Eitter 1986).

2. Observations

The observations were made with a coude spectrometer attached to the 0.6 m Mather telescope of the Erwin W. Fick Observatory (Beavers & Eitter 1986). The high-dispersion spectrograph provides a dispersion of 2.619 Å mm $^{-1}$ and uses a mask-type cross-correlation technique to determine radial velocity of the star and is similar in design and concept to that used by R. Griffin at the Cambridge Observatory, UK (e.g. Griffin 1967). An example of a single 10 minute observatory of HR 7112 is shown in Fig. 1. The two dips in the cross-correlation function indicate the velocity of the two stars which are seen near their maximum separation in velocity.

A total of 70 usable observations were made of the system over a period of 4.2 years beginning in August 1988. The analysis of these data follows the earlier work of, for example Beavers & Salzer (1983), and will not be described in detail here. By plotting

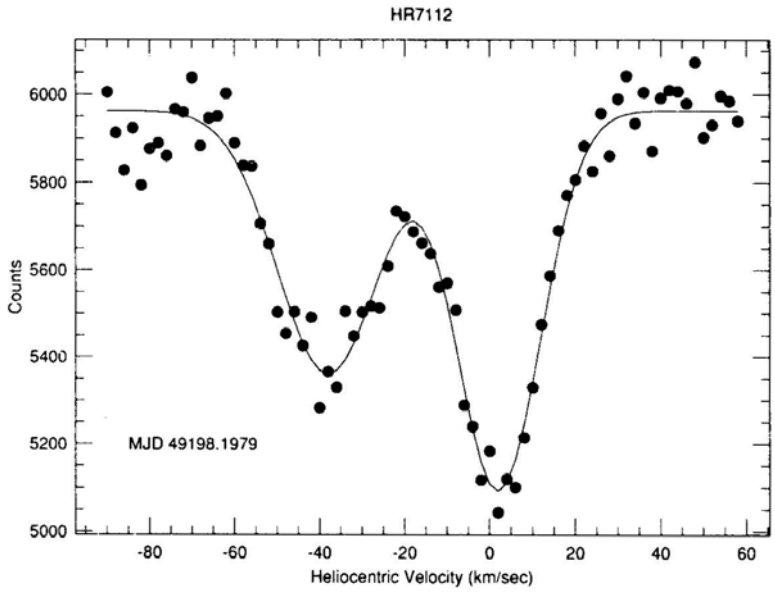

Figure 1. A typical ten minute observation of HR 7112 obtained when the stars are near maximum separation in velocity. The filled dots are the observations and the solid line is the model fit to the two separate binary components.

the velocities as a function of time, it was possible to identify the two components of the binary system which we will denote as HR 7112a and HR 7112b respectively (we have designated the "a" component to be the most massive star). In Table la and Table 1b we present the results of the individual observations for the two components. Column (1) gives the Mean Julian Date (MJD) of the observation (beginning MJD 2247364). Column (2)is the relative phase of the measurement based on the model fit to the period of the orbit, column (3) gives the observed heliocentric velocity and column (4) the observed minus calculated (O — C) heliocentric velocity (this is discussed later). Column (5) gives the statistical weight (defined in Beavers & Eitter 1986) assigned to each measurement.

The period of the binary system was obtained using a least-squares period fitting program independently for the two stellar components and the values obtained were found to agree within 0.2 days, which was well within the error. in the fit (± 0.7 days). The average period P was found to be 215.6 days and this was then fixed in the subsequent calculation of the orbital parameters. The orbit was determined for each component using a version of the program first presented by Wolfe, Horak & Storer (1967) and modified to run on a DecStation 5000 series workstation at ISU. The results of the analysis are presented in Table 2 and Fig. 2.

3. The orbit of the stars

We present in Table 2 the parameters of the orbit derived from the data presented in Fig. 2. It is clear from the observations that the two components of the binary have almost equal mass. Indeed if we designate M_a as the mass of the more massive

Table 1a. Radial velocity observations of HR 7112a.

MJD	Phase	V'Obs (km/sec)	O − C (km/sec)	Weight
47364.22	0.028	0.4	− 1.8	0.67
47364.22	0.028	1.8	− 0.4	0.67
47679.34	1.489	− 36.5	− 1.7	0.59
47694.26	1.559	− 40.5	− 1.9	0.68
47706.27	1.614	− 38.7	0.8	0.72
47720.23	1.679	− 38.8	− 2.4	0.57
47748.18	1.809	− 18.9	− 1.9	0.09
47749.15	1.813	− 17.9	− 1.7	0.10
47768.13	1.901	0.2	2.9	0.18
47784.09	1.975	0.1	− 2.1	0.67
47796.05	2.031	2.8	0.7	0.73
47813.04	2.109	− 0.6	0.8	0.67
48003.42	2.992	1.9	− 0.6	0.57
48017.37	3.057	0.2	− 1.1	0.71
48060.31	3.256	− 20.4	− 6.8	0.10
48065.32	3.279	− 19.4	− 3.5	0.10
48072.28	3.312	− 18.9	0.1	0.10
48078.25	3.339	− 18.4	3.2	0.10
48095.20	3.418	− 23.8	5.2	0.01
48109.16	3.483	− 36.0	− 1.7	0.53
48116.16	3.515	− 37.6	− 1.1	0.36
48122.13	3.543	− 38.4	− 0.4	0.72
48127.12	3.566	− 39.5	− 0.6	0.71
48131.10	3.585	− 39.4	− 0.1	0.67
48135.11	3.603	− 38.8	0.7	0.67
48143.08	3.640	− 39.3	− 0.5	0.76
48147.11	3.659	− 38.3	− 0.4	0.78
48150.08	3.673	− 36.5	0.5	0.67
48156.09	3.700	− 36.2	− 1.8	0.54
48160.04	3.719	− 32.4	− 0.3	0.35
48166.05	3.747	− 22.9	5.1	0.01
48175.02	3.788	− 17.8	3.0	0.10
48181.01	3.816	− 18.2	− 2.6	0.10
48194.99	3.881	− 0.6	4.5	0.22
48202.99	3.918	− 2.4	− 1.3	0.54
48209.98	3.950	1.2	0.0	0.64
48209.99	3.950	2.4	1.2	0.72
48439.27	5.014	1.5	− 1.0	0.65
48462.23	5.120	− 1.6	0.6	0.65
48469.18	5.153	− 4.3	0.2	0.31
48478.20	5.194	− 9.6	− 1.6	0.07
48503.10	5.310	− 18.8	0.0	0.10
48525.06	5.412	− 22.6	5.8	0.02
48532.04	5.444	− 27.2	4.0	0.14
48546.01	5.509	− 35.4	0.7	0.68
48546.02	5.509	− 35.9	0.2	0.71
48552.00	5.537	− 36.6	1.0	0.59
48552.01	5.537	− 38.5	− 0.8	0.64
48568.00	5.611	− 38.1	1.3	0.72
48792.33	6.651	− 39.6	− 1.3	0.64

(*Continued*)

Table 1a. (*Continued*)

MJD	Phase	V'Obs (km/sec)	O − C (km/sec)	Weight
48799.31	6.684	− 35.6	0.4	0.54
48820.26	6.781	− 17.5	4.6	0.10
48824.23	6.799	− 20.3	− 1.5	0.08
48845.19	6.896	− 2.8	0.4	0.50
48847.18	6.906	− 2.5	− 0.2	0.55
48850.16	6.919	− 1.1	− 0.2	0.76
48854.14	6.938	1.1	0.6	0.71
48868.13	7.003	4.2	1.7	0.86
48875.10	7.035	3.2	1.1	0.80
48884.06	7.077	2.3	1.9	0.73
48885.07	7.081	1.5	1.3	0.80

Table 1b. Radial velocity observations of HR 7112b.

MJD	Phase	V'Obs (km/sec)	O − C (km/sec)	Weight
47364.22	0.011	− 40.4	0.8	0.81
47364.22	0.011	− 41.1	0.1	0.77
47679.34	1.472	− 2.1	− 1.9	0.73
47694.26	1.542	1.7	− 0.5	0.80
47706.27	1.597	1.6	− 0.6	0.86
47720.23	1.662	− 2.7	− 2.0	0.68
47734.21	1.727	− 14.7	− 7.6	0.08
47748.18	1.792	− 18.9	− 2.2	0.09
47749.15	1.796	− 17.9	− 0.4	0.10
47768.13	1.884	− 31.1	0.8	0.25
47784.09	1.958	− 40.8	− 0.9	0.84
47796.05	2.014	− 41.4	− 0.2	0.81
47813.04	2.092	− 37.1	0.3	0.78
48003.42	2.975	− 41.0	− 0.3	0.72
48017.37	3.040	− 41.3	− 0.8	0.84
48060.31	3.239	− 20.4	1.4	0.10
48065.32	3.262	− 19.4	− 0.3	0.10
48072.28	3.295	− 18.9	− 3.4	0.10
48078.25	3.322	− 18.4	− 5.9	0.10
48095.20	3.401	− 2.9	2.3	0.71
48109.16	3.466	− 3.1	− 2.5	0.64
48116.16	3.498	− 0.6	− 1.5	0.48
48122.13	3.526	1.9	0.0	0.81
48127.12	3.549	4.0	1.6	0.78
48131.10	3.568	− 0.1	− 2.6	0.53
48135.11	3.586	2.2	− 0.2	0.81
48143.08	3.623	3.0	1.6	0.87
48147.11	3.642	2.4	1.8	0.84
48150.08	3.656	0.5	0.8	0.81
48156.09	3.683	− 1.8	0.6	0.61
48160.04	3.702	− 4.3	− 0.1	0.50

(*Continued*)

Table 1b. (*Continued*)

MJD	Phase	V'Obs (km/sec)	O – C (km/sec)	Weight
48166.05	3.730	– 3.4	4.1	0.36
48170.05	3.748	– 16.3	– 6.3	0.10
48175.02	3.771	– 17.8	– 4.3	0.10
48181.01	3.799	– 18.2	– 0.3	0.10
48188.00	3.831	– 19.5	3.9	0.10
48189.00	3.836	– 20.1	4.2	0.10
48190.00	3.841	– 20.4	4.7	0.11
48192.00	3.850	– 21.3	5.3	0.10
48194.99	3.864	– 25.1	3.8	0.03
48202.99	3.901	– 33.7	0.5	0.67
48209.98	3.933	– 37.1	0.8	0.83
48209.99	3.933	– 37.1	0.8	0.83
48439.27	4.997	– 41.2	0.0	0.78
48462.23	5.103	– 36.4	0.1	0.77
48469.18	5.135	– 35.2	– 1.8	0.41
48478.20	5.177	– 31.7	– 2.8	0.13
48482.17	5.196	– 22.4	4.4	0.10
48488.14	5.223	– 19.6	4.0	0.09
48493.13	5.247	– 19.8	1.1	0.10
48503.10	5.293	– 18.8	– 3.0	0.10
48525.06	5.395	– 4.3	1.3	0.61
48532.04	5.427	– 2.1	1.0	0.40
48546.01	5.492	1.7	1.0	0.81
48546.02	5.492	0.9	0.2	0.81
48552.00	5.520	2.0	0.3	0.65
48552.01	5.520	2.1	0.4	0.76
48568.00	5.594	2.8	0.5	0.83
48792.33	6.634	– 1.1	– 2.0	0.80
48799.31	6.667	– 0.4	0.6	0.73
48820.26	6.764	– 17.5	– 5.3	0.10
48824.23	6.782	– 20.3	– 5.1	0.08
48845.19	6.879	– 30.2	1.0	0.45
48847.18	6.889	– 34.0	– 1.4	0.71
48850.16	6.902	– 36.0	– 1.6	0.84
48854.14	6.921	– 37.7	– 1.0	0.86
48868.13	6.986	– 40.1	0.9	0.92
48875.10	7.018	– 40.9	0.3	0.87
48884.06	7.060	– 40.0	– 0.4	0.80
48885.07	7.064	– 39.0	0.4	0.89

component and M_b as the mass of the companion star, then Table 2 shows that $M_b / M_a = K_b / K_a = 0.96 \pm 0.01$. This follows from the relationships (see for example Batten 1989):

$$M_{1,2} \sin^3 (i) = 0.0385 \times 10^{-7} (1 - e^2)^{3/2} (K_1 + K_2)^2 K_{2,1} P M,$$

where subscripts 1 and 2 refer to the two stars, and the values for K are given in km s^{-1} and those for the period P are in days. The angle i is the inclination of the orbit relative to the line of sight. The largest source of error in the mass calculation comes from the

Table 2. Orbital elements of HR 7112a and b.

P	215.6 ± 0.0 days
T	47358.22 ± 2.5 MJD
K_a	20.99 ± 0.22 km/sec
K_b	21.87 ± 0.22 km/sec
γ	-18.02 ± 0.50 km/sec
ε	0.141 ± 0.012
ω_a	193 ± 5 degrees
$a_a \sin i$	60.19 ± 0.64 Gm
$a_b \sin i$	64.42 ± 0.63 Gm
$f_a(M)$	$0.1872 \pm 0.0060\, M_\odot$
$f_b(M)$	$0.2294 \pm 0.0070\, M_\odot$
rms residual 2.12 km/sec	

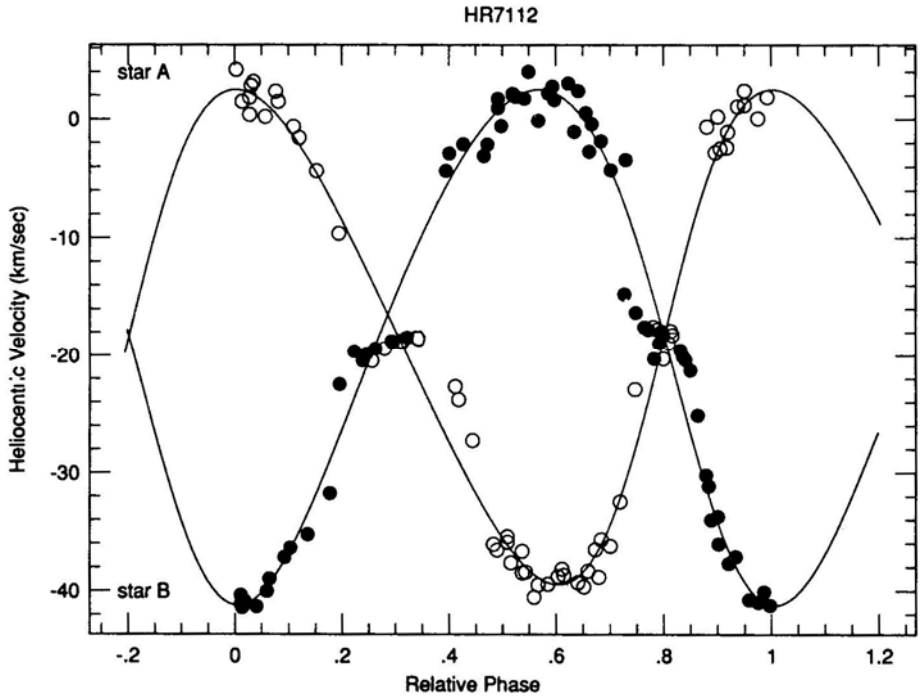

Figure 2. The velocity of each star as a function of orbital phase. The more massive star A is shown with open circles and the filled circles show the velocities associated with component B.

contribution from the uncertainty in the values of K_a and K_b. From this relation we can also determine the minimum mass of the two stars "a" and "b". These are $M_a \sin^3(i) = 0.873 \pm 0.030 M_\odot$ and $M_b \sin^3(i) = 0.838 \pm 0.028 M_\odot$. Corresponding values for the minimum semi-major axis distances are given by:

$$a_{a,b} \sin(i) = 13{,}751\,(1 - e2)^{1/2} K_{a,b} P \text{ km},$$

and these values are presented in Table 2. The stars "a" and "b" therefore have minimum semi-major axis sizes of a sin (i) = 0.414 AU and 0.428 AU respectively.

The spectroscopic classification of HR 7112 by Yoss (1961) combined with the similar strengths of the cross-correlation dips obtained when the stars were well separated in velocity suggests that both stars are *K* giants of approximately equal luminosity. According to Allen (1976) the average mass of a *K*1 giant is approximately 4 $M_{\odot}$ Although these mass relationships for giants are extremely uncertain, a mass of this order for each of the components of HD 7112 is quite conceivable if the orbital inclination was approximately 3637°.

4. Conclusions

We have discovered that the *K*1 II-III star HD 7112 is a double-line spectroscopic binary system with components in near circular orbits of nearly equal mass. The derived masses are consistent with the spectral classification of system as a pair of red giants if the orbital inclination is approximately 36-37°. In such a case, the stars are orbiting each other with a mean separation of 1.5 AU. It has been noted by Griffin (1990) and Griffin & Eitter (1992) that binaries containing giants appear to become circularised somewhere in the range of periods 118 to 260 days, and that there is a dearth of data in this region. HD 7112, which falls towards the high end of this data 'gap' with a period of 215.6 days, appears to have an orbit of relatively low eccentricity (e = 0.142) and may be still in the process of becoming more circular as a result of tidal effects.

Acknowledgements

The authors wish to thank the National Science Foundation for funding the Fick Observatory Radial Velocity project under NSF grant number AST-8819696. The authors also wish to thank Brian Adams for invaluable help with the installation of software on the DecStation 5000 workstation computer.

References

Allen, C.W.1976, *Astrophysical Quantities* (London: Athlone Press).
Beavers,W.I.,Salzer,J.J.1983, *Publ.Astr.Soc. Pacific*, **95**,79.
Beavers, W.I., Eitter, J.J.1986, *Astrophys. J.*, **62,147**
Batten, A. H. 1989, *Publ. Domin. Astr. Obs.,* **17**, 1
Griffin, R. F.1967, *Astrophys. J.*, **148**, 465.
Griffin, R.F.1990, *J. Astrophys. Astr.*, **11**,491.
Griffin, R. F., Eitter, J. J. 1992, *J. Astrophys. Astr.*, **13**,209.
Harper,W.E.1934, *Publ. Domin. Astr.Obs,***6**,151.
Wolfe, R. H., Horak, H. G., Storer, N. W. 1967, in *Modern Astrophysics: A Memorial to Otto Struve*, Ed. M. Hack (Paris: Gauthiers-Villars) p. 251.
Young, R. K. 1942, *Publ. David Dunlap Obs.*,**1**, 251.
Yoss 1961, *Astrophys. J.*, **134**, 809.

J. Astrophys. Astr. (1995) **16,** 45–52

Statistical Response of Randomly Excited Nonlinear Radial Oscillations in Polytropes*

Anunay K. Chaudhary & V. B. Bhatia *Department of Physics and Astrophysics*, *University of Delhi*, *Delhi 110007*, *India*.

M. K. Das *Department of Physics and Electronics*, *Sri Venkateswara College*, *University of Delhi*, *Dhaula Kuan*, *New Delhi 110 021*, *India*.

R. K. Tavakol *School of Mathematical Sciences*, *Queen Mary and Westfield College*, *Mile End Road*, *London El 4NS*, *U.K*.

Received 1993 June 15; accepted 1995 March 29

Abstract. The effect of internal noise on the response characteristics of nonlinear radial pulsation in polytropic model has been investigated using the equivalent linearization technique. The model of the noise is taken to be δ-correlated with zero mean. Both non-stationary and stationary response characteristics have been computed for various nonlinearity parameters in different polytropes.

Key words: Pulsation—radial, star—polytropes, noise.

1. Introduction

Recent developments in the theory of nonlinear dynamical system have proved to be of immense value for theoretical framework in understanding various intriguing observed features in variable stars (Buchler & Regev 1983; Perdang 1985; Tavakol & Das 1986; Kovacs & Kollath 1988; Buchler 1990). Stellar pulsation phenomenon, in general, is now considered to be a completely nonlinear one and various observed characteristics are being explained in terms of deterministic nonlinear equations in the dynamic variables of mean flow field. In view of the observed fact that, in general, only upto three modes are seen in radially pulsating stars, e.g., Cepheids, large amplitude δ-scuti variables etc., the theoretical modeling of these pulsators is, in general, a truncated one and considers only the modes which show up predominantly in the observations. The photometric data of most of the variable stars show the presence of significant irregular features which are inherently present due to unresolved degrees of freedom or scale of variations. It is known that a small scale turbulence or random perturbation is induced in the system due to these unresolved degrees of freedom or scales of variations and thereby affecting the evolution of the dynamical systems (Lindenberg & West 1984). Thus a stochastic forcing term must be incorporated in the above truncated descriptions and this necessitates the stochastic formulation of the radial pulsation phenomena. In section 2, we describe an equivalent linearization technique to study the

*This work is supported by UGC, New Delhi.

dynamical behaviour of a stochastically perturbed nonlinear radial pulsator. For illustrative purposes, the model of the nonlinear radial pulsator is taken to be that of a polytrope, pulsating only in the fundamental mode. In section 3, we discuss the results obtained for various polytropes.

2. Response statistics of nonlinear radial pulsation in polytropes

The equation governing nonlinear radial pulsation in fundamental mode of self gravitating gaseous masses with polytropic equations of state

$$p_0 = k\rho_0^{1+(1/n)},$$

$$\rho_0 = \rho_c \theta^n \text{ and}$$

$$r_0 = \left[\frac{k(n+1)\rho_c^{-1+(1/n)}}{4\pi G}\right]^{1/2} x \tag{1}$$

could be written as (Das *et al.* 1989).

$$\ddot{Q} + Q + AQ^2 + BQ^3 = f(t), \tag{2}$$

where

$$A = \frac{A_1}{\omega_1^2 (n+1) I_1},$$

$$B = \frac{A_2}{\omega_1^2 (n+1) I_1}, \tag{3}$$

together with

$$I_1 = \int_0^{x_1} \xi^2 \theta^n x^4 \, dx,$$

$$A_1 = \int_0^{x_1} x^3 [f_1(x)\xi^3 + (f_2(x) + f_4(x))\xi\xi'^2 + f_3(x)\xi'^3] \, dx,$$

$$A_2 = \int_0^{x_1} x^3 \xi [g_1(x)\xi^3 + g_2(x)\xi^2\xi' + g_3(x)\xi\xi'^2 + g_4(x)\xi\xi'\xi''$$
$$+ g_5(x)\xi'^2\xi'' + g_6(x)\xi^2\xi'' + g_7(x)\xi'^3] \, dx, \tag{4}$$

and due to the unresolved scales of motion, a zero-mean, δ-correlated random force $f(t)$ is introduced, such that, $E[f(t)]=0$ and $E[f(t)f(t+\tau)] = 2D\delta(\tau)$. Here ω_1 is the frequency of the fundamental mode, primes denote derivatives w.r.t. r and functions f_i and g_i are defined in Das *et al.* (1994). Defining a variable $q(t)$ such that $Q(t) = \lambda q(t)$ and adding a dissipation term, $\mu\dot{q}$, with μ as damping coefficient (cf. Kumar *et al.* 1988; Sorensen 1988), we write equation (2) as:

$$\ddot{q} + \mu\dot{q} + q + \lambda A q^2 + \lambda^2 B q^3 = f(t). \tag{5}$$

In terms of scaled parameters equation (5) may be written as:

$$\ddot{x} + \mu\dot{x} + x + A\varepsilon x^2 + B\varepsilon^2 x^3 = \sqrt{2\mu}F(t), \tag{6}$$

where $x = (q/\sigma_{qo})$ $\varepsilon = (\lambda/\sigma_{qo})$, $F(t)$ is the Gaussian white noise with zero mean and unit variance, and σ_{qo} is the standard deviation of the response of the linear system, i.e., when $\lambda = 0$. It may be noted that the presence of an asymmetric nonlinearity in the restoring term makes the response a non-zero mean random process. On writing the zero mean part of the response as $x_o(t)$ and the mean by $m_x(t)$, we may express the non-zero mean response $x(t)$ as:

$$x(t) = x_0(t) + m_x(t). \tag{7}$$

Substituting equation (7) in equation (6), we get equations for the zero mean response, x_0 and the mean m_x of $x(t)$ as:

$$\ddot{x}_0 + \mu\dot{x}_0 + x_0 + g(x_0 + m_x) = \sqrt{2\mu}F(t), \tag{8}$$

$$\ddot{m}_x + \mu\dot{m}_x + m_x + E\{A\varepsilon(x_0 + m_x)^2 + B\varepsilon^2(x_0 + m_x)^3\} = 0, \tag{9}$$

where

$$g(x_0 + m_x) = \varepsilon(x_0 + m_x)^2[A + \varepsilon B(x_0 + m_x)] - E\{\varepsilon(x_0 + m_x)^2[A + \varepsilon B(x_0 + m_x)]\}. \tag{10}$$

In the equivalent linearization technique (cf. Roberts & Spanos 1990), the nonlinear system (8) may be approximated by an equivalent linear system, as:

$$\ddot{x}_0 + \mu\dot{x}_0 + (1 + k_e)x_0 = F_0(t), \tag{11}$$

where

$$F_0(t) = \sqrt{2\mu}F(t)$$

$$k_e = 2A\varepsilon m_x + 3B\varepsilon^2[\sigma_{x_o}^2 + m_x^2]. \tag{12}$$

Equation (11) can also be written as a first order matrix equation in the state variable form as:

$$\dot{\mathbf{X}}(t) = \mathbf{G}(t)\mathbf{X}(t) + \mathbf{W}(t), \tag{13}$$

where

$$\mathbf{X}(t) = \begin{bmatrix} x_0 \\ \dot{x}_0 \end{bmatrix}, \quad \mathbf{W}(t) = \begin{bmatrix} 0 \\ F_0 \end{bmatrix} \quad \text{and} \quad \mathbf{G}(t) = \begin{bmatrix} 0 & 1 \\ -(1 + k_e) & -\mu \end{bmatrix}. \tag{14}$$

If $C(t)$ defines the covariance matrix of $X(t)$, i.e.,

$$\mathbf{C}(t) = E\{\mathbf{X}(t)\mathbf{X}^{\mathrm{T}}(t)\}, \tag{15}$$

then the differential equation for $C(t)$ could be written as (see Appendix):

$$\dot{\mathbf{C}} = \mathbf{G}(t)\mathbf{C}^{\mathrm{T}} + \mathbf{C}\mathbf{G}^{\mathrm{T}}(t) + 2\mu\mathbf{I}, \tag{16}$$

where I represents the Identity matrix. Equations (9) and (16) along with equation (12) describe the variation of different statistical parameters of the noisy nonlinear radial

pulsation equation (6) and could be written in the general form of coupled differential equation as:

$$\begin{aligned}
&\dot{m}_x = m_{\dot{x}},\\
&\dot{m}_{\dot{x}} = -\mu\dot{m}_x - m_x - A\varepsilon[\sigma_{x_o}^2 + m_x^2] - B\varepsilon^2 m_x[3\sigma_{x_o}^2 + m_x^2],\\
&\dot{c}_{11} = 2c_{12},\\
&\dot{c}_{12} = c_{21} = c_{22} - (1+k_e)c_{11} - \mu c_{12},\\
&\dot{c}_{22} = 2\mu - 2(1+k_e)c_{21} - 2\mu c_{22},
\end{aligned} \tag{17}$$

where we have defined

$$\begin{aligned}
&c_{11} = E\{x_0^2\} \equiv \sigma_{x_o}^2,\\
&c_{12} = c_{21} = E\{x_0\dot{x}_0\},\\
&c_{22} = E\{\dot{x}_0^2\}.
\end{aligned} \tag{18}$$

Numerical integration of equation (17) along with equations (12) and (18) has been carried out, using 4th order Runge-Kutta method for different values of nonlinearity parameter ε, damping parameter μ and polytropic index n. In the following section, we discuss the results of estimating various statistical parameters of the system.

3. Results and discussion

Determination of the time dependent statistical response of a nonlinear oscillator in the presence of a noise is fairly complicated as it involves the time dependent solution of Fokker-Planck equation (FPK), which is known only for simple systems (Cai & Lin 1988). It is in this regard that powerful approximate numerical techniques have been developed in recent years (cf. Roberts 1981a, b; Crandall 1985; Roberts & Spanos 1986). Method of equivalent linearization (ELT) is one of such techniques which has been found to give very satisfactory results for estimating the statistical response of the systems with complicated nonlinearity (cf. Spanos 1980). In the present analysis we used ELT to obtain the nonstationary and stationary response characteristics of noise driven nonlinear radial pulsator in polytropes oscillating only in the fundamental mode (cf. equation 6).

Results obtained from the numerical computation using ELT could be summarised as follows:

■ Figure 1 shows the variations of mean of response displacements and velocities for different polytropic index. It is evident that for a given nonlinearity parameter and damping coefficient the mean of the response displacement decreases with the increase in central condensation. Mean of the response velocity tends to become zero as the equilibrium is reached, for all the polytropes. For a given polytrope, numerical results obtained for different ε suggest that the mean of the response displacement increases with the increase in the nonlinearity in the system.

■ Figure 2 shows the plot of variance of the displacement with time in different polytropes. It is quite obvious that the time taken by the system to attain equilibrium

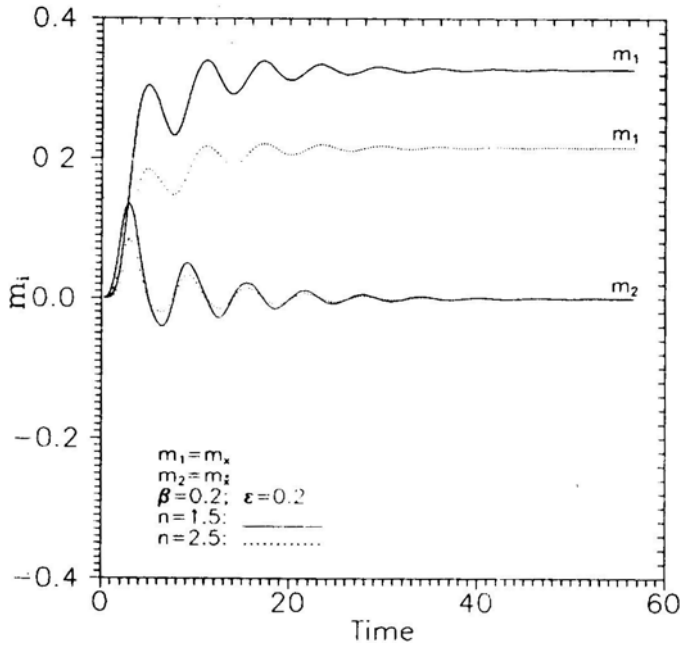

Figure 1. Mean of the displacements and velocities for two different polytropes.

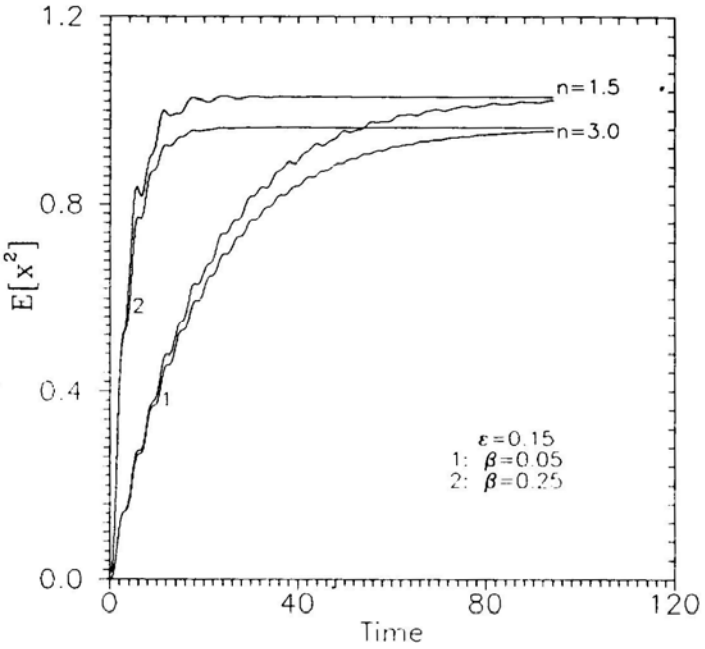

Figure 2. Variance of the displacements for two different polytropes and damping coefficients.

for a less damped system is more than that for a system with larger damping parameter μ. For a given ε, it may be inferred that the variance of response displacement is more in less centrally condensed polytrope.

■ The observed magnitude of amplitude variation ranges from 0.05 to 0.15 in classical Cepheids, from 0.01 to 0.08 in RR Lyrae and from 0.10 to 0.30 in W Virginis stars (cf. Stothers 1981; Buchler 1990; Das *et al.* 1994). In view of this, we have computed the stationary variance, $E[x_0^2]$, of the displacement profiles for different values of nonlinearity parameter, ε, in various polytropes using ELT (Fig. 3). In Fig. 3 we have also given the plot of $E[x_0^2]$ versus ε, obtained from the stationary solution of FPK for different ε. For polytropic index n = 1.5, 2.5 and 3.0, the maximum error for the case of ε = 0.25 is found to be 6%, 5% and 3%, respectively. It may be noted that in a given polytrope the stationary probability distribution function of the response becomes more asymmetric with increase in ε (Fig. 4). Even though the nonlinearity of the system results in non-Gaussian response of the system, the deviation from Gaussian characteristics becomes important only for large ε. The percentage small deviation in $E[x_0^2]$ using ELT for different polytropes is mainly due to this factor in the limit of large ε.

The foregoing analysis assumes the noise to be δ-correlated, i.e., white noise. However from physical consideration in real situation, we do expect the spectrum of noise/fluctuation to be different from that of white noise. In our subsequent communication, we plan to study the response characteristics of the nonlinear oscillator in the presence of noise with different correlation functions.

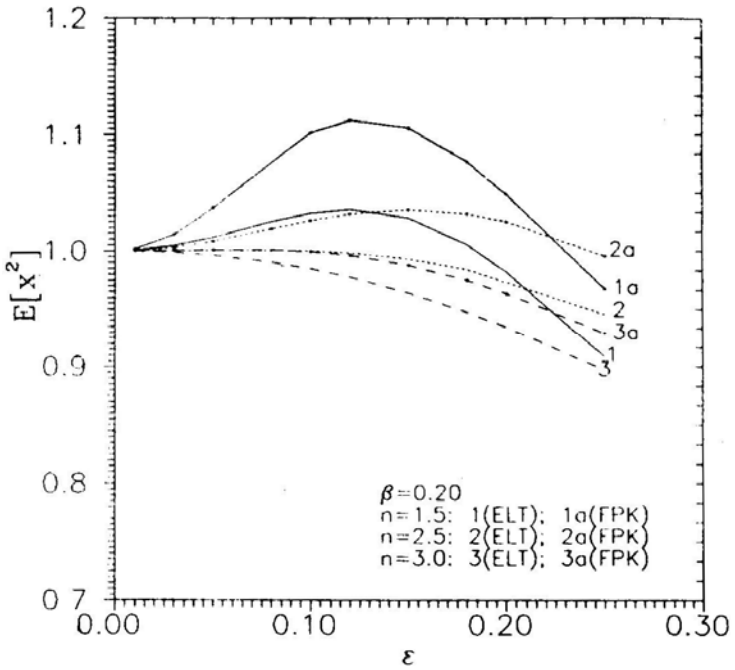

Figure3. Comparison of the stationary variance of the response displacements obtained from FPK and ELT.

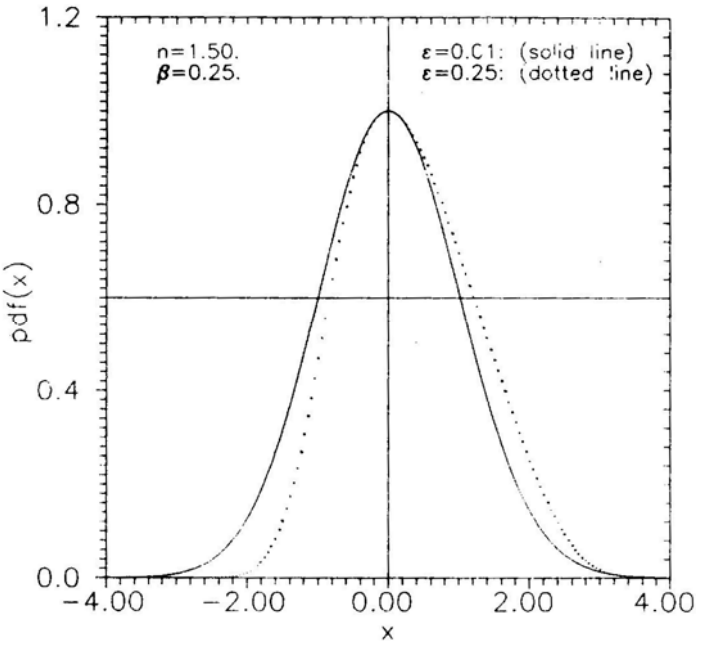

Figure 4. Normalised probability density functions derived from the solution of stationary Fokker Planck equation.

Appendix

To obtain the differential equation for covariance matrix C(t), we start with the relation for covariance matrix

$$\mathbf{C}(t) = E[\mathbf{X}\mathbf{X}^{\mathrm{T}}]. \tag{A. 1}$$

Differentiating equation (A.1) w.r.t. time, we get

$$\dot{\mathbf{C}} = E[\dot{\mathbf{X}}\mathbf{X}^{\mathrm{T}}] + E[\mathbf{X}\dot{\mathbf{X}}^{\mathrm{T}}]. \tag{A. 2}$$

Using equation (13) in equation (A.2), we obtain

$$\dot{\mathbf{C}}(t) = \mathbf{G}(t)\mathbf{C}^{\mathrm{T}}(t) + \mathbf{C}(t)\mathbf{G}^{\mathrm{T}}(t) + E[\mathbf{X}\mathbf{W}^{\mathrm{T}}] + E[\mathbf{X}^{\mathrm{T}}\mathbf{W}]. \tag{A. 3}$$

To determine $E[\mathbf{X}\mathbf{W}^{\mathrm{T}}]$, let us consider a homogeneous equation

$$\dot{\mathbf{Y}} = \mathbf{G}(t)\mathbf{Y}, \tag{A. 4}$$

with solution

$$\mathbf{Y}(t) = \exp\left(\int_0^t \mathbf{G}(\theta)\mathrm{d}\theta\right). \tag{A. 5}$$

Here the initial condition is taken as Y(0) = I, where I is the Identity matrix and θ is the dummy variable for time. The general solution of inhomogeneous equation (13) is given

by (cf. Reid 1983)

$$\mathbf{X}(t) = \mathbf{Y}(t)\mathbf{X}(0) + \mathbf{Y}(t)\int_0^t \mathbf{Y}^{-1}(\theta)\mathbf{W}(\theta)\mathrm{d}\theta, \tag{A. 6}$$

With this solution, we write

$$E[\mathbf{X}\mathbf{W}^{\mathrm{T}}] = \mathbf{Y}(t)E[\mathbf{X}(0)\mathbf{W}^{\mathrm{T}}]^{\cdot} + \mathbf{Y}(t)\int_0^t \mathbf{Y}^{-1}(\theta)E[\mathbf{W}(\theta)\mathbf{W}^{\mathrm{T}}(t)]\mathrm{d}\theta.$$

If we assume that the initial condition is uncorrelated to the fluctuating force, W(t), then

$$E[\mathbf{X}\mathbf{W}^{\mathrm{T}}] = \mathbf{Y}(t)\int_0^t \mathbf{Y}^{-1}(\theta)E[\mathbf{W}(\theta)\mathbf{W}^{\mathrm{T}}(t)]\mathrm{d}\theta. \tag{A. 7}$$

For a δ-correlated fluctuation

$$E[\mathbf{W}(\theta)\mathbf{W}^{\mathrm{T}}(t)] = 2\mu\delta(t-\theta). \tag{A. 8}$$

Substituting equation (A.8) in equation (A.7) and using the property of δ-function, we get

$$E[\mathbf{X}\mathbf{W}^{\mathrm{T}}] = \mu\mathbf{I}, \tag{A. 9}$$

and hence

$$\dot{\mathbf{C}}(t) = \mathbf{G}(t)\mathbf{C}^{\mathrm{T}}(t) + \mathbf{C}(t)\mathbf{G}^{\mathrm{T}}(t) + 2\mu\mathbf{I}. \tag{A.10}$$

References

Buchler, J. R. 1990, *Ann. N.Y Acad. Sci*., **617**, 17.

Buchler, J. R., Regev, O. 1983, *Astr. Astrophys*., **123**, 331.

Cai, G. Q., Lin, Y. K. 1988, *Int. J. Nonlinear Mech*., **23**, 215.

Crandall, S. H. 1985, *Int. J. Nonlinear Mech*., **20**, 1.

Das, M. K., Singh, H. P., Tandon, J. N. 1989, *Astrophys. J*., **346**, 289.

Das, M. K., Mollikutty, O. J., Tavakol, R. K. 1994, *Astrophys. J*., **433**, 786.

Kovacs, G., Kollath, Z. 1988, in *Multimode Stellar Pulsation*, Eds. G. Kovacs, L. Szabos & B. Szeidl, (Budapest: Konkoly Observatory) p. 33.

Kumar, P., Franklin, J., Goldreich, P.1988, *Astrophys. J*., **328**, 879.

Lindenberg, K., West, B. J. 1984, *J. Atmos.Sci*.,**41**,3021

Perdang, J. 1985, in *Chaos in Astrophysics*, Eds. J. R. Buchler, J. Perdang & E. A. Speigel (Dordrecht: Reidel), C191.

Reid, J. G. 1983, *Linear System Fundamentals: Continuous and Discrete*, *Classic and Modern*, (New York: McGraw-Hill).

Roberts, J. B. 1981a, *Shock Vibration Digest*, **13**, 17.

Roberts, J. B. 1981b, *Shock Vibration Digest*, **13**, 15.

Roberts, J. B., Spanos, P. D. 1986, *Int. J. Nonlinear Mech*.,**21**, 111.

Roberts, J. B., Spanos, P.D.1990, *Random Vibration and Statistical Linearization,* (John Wiley& Sons).

Spanos, P. D. 1980, *J. Appl. Mech*, *ASME*, 47,209.

Sorensen, J. M. 1988, *Proc. Symp. Seismology of the Sun and Sun-like Stars* (Spain), **41**, ESA SP286 p. 557.

Stothers, R. 1981, *Astrophys. J*., **247**, 941.

Tavakol, R. K., Das, M. K. 1986, *Mon. Not .R. astr. Soc.,* **221**, 625.

J. Astrophys. Astr. (1995) **16,** 53-67

Are Many Pulsars Processed in Binary Systems?

A. A. Deshpande, R. Ramachandran & G. Srinivasan *Raman Research Institute, Bangalore 560080, India*

Received 1995 May 5; accepted 1995 June 8

Abstract. A detailed statistical analysis of pulsar *current* is presented. The conclusions reached are the following: (1) The birthrate of pulsars is about one in 75 ± 15 years. (2) There is evidence for *injection* of pulsars into the population of solitary pulsars. Such an injection is particularly pronounced in the magnetic field range $12 < \log B < 12.6$. (3) This is interpreted as due to *recycled pulsars* being released into the population. (4) We tentatively conclude that as much as 10 – 15% of all pulsars may have been born and processed in binary systems.

Key words: Pulsars—stars: evolution—stars: magnetic, stars: stellar statistics.

1. Introduction

Ever since their discovery pulsars have been a subject of many statistical studies. There have been several attempts to estimate the birthrate and other statistical properties of the pulsar population, and over the past ten years many new suggestions/ models have emerged to carefully account for various selection effects which enable one to study more reliably the intrinsic properties of the pulsar population (e.g. Narayan 1987; Narayan & Ostriker 1990; Bhattacharya *et al*. 1992). The recent electron density model of Taylor & Cordes (1993) represents an important improvement and its use has led to significant revision of several earlier conclusions (see Lorimer *et al* 1993). In the light of this we feel it may be worthwhile to re-examine the properties of the pulsar population by studying the distribution of the *pulsar current*. Apart from attempting to obtain a more reliable estimate for the pulsar birthrate, we focus on possible evidences for *injection* of pulsars in various field ranges (Vivekanand & Narayan 1981). The motivation for this stems from the recent suggestion by Srinivasan *et al*. (1990) on the mechanism for the magnetic field decay. This mechanism involving the binary history of recycled pulsars predicts an apparent injection of pulsars processed in binaries close to the equilibrium period line (Srinivasan *et al*. 1990).

In the first part of this paper we present the results of our analysis based on the current of pulsars, where we have tried to carefully account for several observational selection effects. In the second part we address the following important question: *What fraction of pulsars comes from binary systems*? We also present evidence for the 'injection' of recycled pulsars from binary systems into the population of normal solitary pulsars.

1.1 *The pulsar current*

One of the important questions related to the pulsar population is the pulsar birthrate. There are many methods of estimating this. However, for the result to be reliable the method must allow for the possibility that the birthrate of pulsars with different magnetic fields may not be the same. One of the ways of taking this into account is by calculating the current of pulsars. The pulsar current in a period bin of width ΔP around a period (P) can be formally defined as (Phinney & Blandford 1981; Vivekanand & Narayan 1981),

$$J(P) = \frac{\sum_{i=1}^{n_{psr}} S_i \dot{P}_i}{f \Delta P}. \tag{1}$$

where $n_{\rm psr}$ is the number of known pulsars in the bin, f is the beaming fraction (which is assumed to be 0.2 throughout our analysis), $\dot{P}_i$ is the time derivative of the period and S_i is the scale factor (which corrects for the observational selection effects) for the ith pulsar. Provided the current in the bin considered has reached its maximum value – i.e. the initial periods of all pulsars are less than the period under consideration, and death of pulsars has not yet set in, then *this maximum value of the current represents the birth rate of pulsars* (Vivekanand & Narayan 1981). The procedure to compute the scale factors involves a detailed Monte Carlo simulation, which is described below.

1.2 *Selection effects*

The observed distribution of pulsars in the Galaxy differs systematically from the *true* distribution due to various observational selection effects. The detectability of a pulsar is affected by both its low luminosity and the pulsed nature of the emission. Effects such as interstellar scattering and dispersion cause broadening of the pulses, resulting in a reduction of the peak pulsed flux. A detailed treatment of modeling the various selection effects in the Galaxy can be found in Narayan (1987) and Narayan & Ostriker (1990). The parameters which go into the modelling of selection effects are (i) regions covered by the pulsar surveys, (ii) the time resolution used and sensitivities of the surveys, (iii) scattering and dispersion smearing of pulse profiles, and (iv) the assumed luminosity model for pulsars. In the discussion to follow, our sample of pulsars is restricted only to those which in principle could have been detected by any one of the following eight major surveys: (1) Jodrell Bank survey, (2) U. Mass-Arecibo survey, (3) Second Molonglo survey, (4) U. Mass-NRAO survey,(5)Princeton-NRAO Phase-I survey, (6) Princeton-NRAO Phase-II survey, (7) Princeton-Arecibo survey and (8) Jodrell Bank-1400 MHz survey. Of the 570 known pulsars to date, only 325 pulsars satisfy the above mentioned criterion. The globular cluster pulsars, extragalactic pulsars and millisecond pulsars are not included in this analysis.

The *detection probability* is the ratio of the observed number of pulsars to the *true* number. It can be defined for a given pulse period P and a luminosity L, at a given height z from the galactic plane as,

$$\text{Det. Prob.}(P, L, z) \equiv \frac{\iint_{\rm obs} \rho_R(R) R \, dR \, d\phi}{\iint \rho_R(R) R \, dR \, d\phi}. \tag{2}$$

Here, R and ϕ are the galactocentric radius, and the azimuthal angle, respectively. The function ρ describes the distribution of pulsars with respect to the corresponding variable inside the bracket. The integral in the denominator is over a volume of a slab of the galaxy at a height z from the galactic plane while that in the numerator is only over a subset of the above volume of the galaxy where a pulsar of period P and luminosity L can be detected by at least one of the eight surveys mentioned above. The *scale factor* $S(P, L, z)$ is defined to be the reciprocal of the detection probability.

We computed this scale factor for various luminosities, periods and z heights by a Monte Carlo simulation. A detailed description of such a procedure to estimate the scale factors can be found in Narayan (1987) (see also Narayan & Ostriker 1990; and Bhattacharya *et al.* 1992).

A model for the luminosity as a function of P and $\dot{P}$ then enables one to evaluate $S(P, \dot{P}, z)$ from $S(P, L, z)$ (see Prozynski and Przybycien 1984; Narayan & Ostriker 1990, for luminosity models). To account for the dispersion of luminosities around the model luminosity one finds two methods in the literature. The first method can be summarized by the following equation (Narayan 1987),

$$S(P, \dot{P}, z) = \int S(P, L, z)\rho_L[\log L - \log L_m(P, \dot{P})]\,\mathrm{d}\log L, \tag{3}$$

where the *scale factor* $S(P, L, z)$ is averaged with the luminosity spread function $\rho_L[\ ]$, giving a weighted harmonic mean of the detection probability ($S^{-1}(P, L, z)$). The second way is to average the detection probability (note that the scale factor is the reciprocal of the detection probability) with the luminosity spread function (Narayan & Ostriker 1990). According to this prescription,

$$\begin{aligned} S(P, \dot{P}, z) &= \left[\int \rho_L[\log L - \log L_m(P, \dot{P})](\text{det. prob.})\,\mathrm{d}\log L\right]^{-1} \\ &= \left[\int \frac{\rho_L[\log L - \log L_m(P, \dot{P})]}{S(P, L, z)}\,\mathrm{d}\log L\right]^{-1}. \end{aligned} \tag{4}$$

Noting that the spread function $\rho_L[\ ]$ is a *probability distribution function* and that the reciprocal of the scale factor gives the pulsar detection probability, it is clear that the procedure given in equation (4) is more appropriate. Hence we adopt the second method in the following analysis. The use of the first method (equation 3) leads to the overestimation of the scale factors.

The scale factors thus evaluated as a function of P and $\dot{P}$, can also be expressed as scale factors as a function of P and B viz., $S(P, B, z)$, where B is the surface magnetic field. This is done in a straight-forward way with the help of the simple relation $B^2 \propto P\dot{P}$.

2. The birthrate of pulsars

As explained in section 1 the pulsar current is a measure of the birthrate minus the deathrate. Figure 1 shows the pulsar current calculated by us, as a function of the rotation period. As may be seen from this histogram the current continues to rise till a period of ~0·6 sec. A straightforward interpretation of this is that not all pulsars are

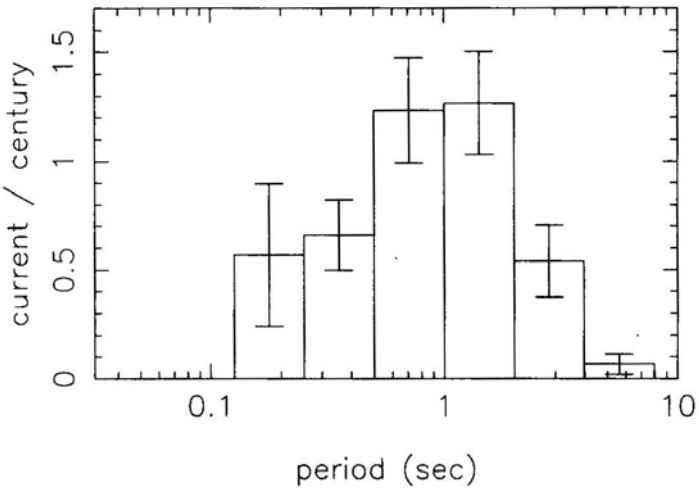

Figure 1. The current distribution as a function period. As may be seen, the current reaches its maximum value around a period of 0.5 s, and begins to decline at around 2 s. The maximum value of the current corresponds to a pulsar birth rate of about 1 in 75 years.

born spinning as rapidly as say, Crab pulsar. The current is roughly constant in the period range of 0·6–2 sec. Beyond a period of ~ 2 sec. the current decreases presumably because the death of pulsars becomes important. The maximum current attained implies a birthrate of pulsars of one in 75 ± 15 years (the error indicated is only the Statistical error). This should be compared with one in about 100 years derived by Narayan & Ostriker (1990) and one in 125250 years for a luminosity limited set of samples by Lorimer *et al.* (1993).

To understand the sensitivity of the derived birthrate to the assumed distance model (Taylor & Cordes 1993) as well as the luminosity model (Narayan & Ostriker 1990), we repeated the current analysis using luminosity model of Narayan (1987), and the distance model of Lyne *et al.* (1985). The corresponding birthrates are summarized in Table 1. In every case the spread of luminosities about the model value was taken into account in a manner given in equation (4).

As one can see, *the old luminosity model severely underestimates the birthrate*. This should be expected because this model does not allow for observational selection effects. The revision in the birthrate due to the change in the distance model is roughly by a factor of two.

Table 1. Galactic birthrate of pulsars obtained by old and new distance model and luminosity model.

	Old dist. model (per century)	New dist. model (per century)
Old lumin. model	0.32	0.15
New lumin. model	2.8	1.4

Refs. **1.** Narayan(1987), **2.** Narayan & Ostriker (1990), **3.** Lyne *et al.* (1985) and **4.** Taylor & Cordes (1993).

While the birthrate estimated by us is in good agreement with that of Narayan & Ostriker (1990), the estimate by Lorimer *et al.* (1993) is somewhat on the lower side. We wish to comment upon this briefly. As already mentioned, Lorimer *et al* consider only pulsars with radio luminosities greater than 10mJy kpc^2. The recent discovery of PSR J0108-1431 indicates that active pulsars with radio luminosities as low as 0-06 mJy kpc^2 may not be uncommon. Tauris *et al.* (1994) have argued that the number of pulsars in the Galaxy similar to J0108-1431 could be at least 5×10^5. The inclusion of such a population will increase the estimated birthrate substantially. A short field decay timescale ~ 5 Myr as assumed by Tauris *et al* (1994), will revise the birthrate upwards to one in 40 years. Even a more reasonable field decay time scale ~ 25 Myr will give a birthrate of about one in 120 years. We therefore conclude that there is no serious discrepancy between our birthrate and that derived by Lorimer *et al.* (1993).

The pulsar birthrate should ideally match the rate of Supernovae that results in the formation of neutron stars. The core-collapse supernova rate (Type Ib + II) inferred from the observations of external galaxies (van den Bergh 1991 and references therein) of morphology similar to ours is about 1.6 per century per $10^{10}L_{\odot}$(B) (about one in 60 years). Using the Initial Mass Function of Scalo (1986) and the Population-I star model of Ratnatunga & van den Bergh (1989), van den Bergh (1991) estimates the Galactic core-collapse supernova rate to be one in about 100 years. Given the uncertainties in the determination of the birthrate of pulsars as well as the frequency of Supernovae, we do not consider them to be discrepant.

3. Fraction of pulsars from binary systems

Although the number of known binary pulsars is still only a couple of dozens, there is no reason to conclude that the vast majority of the solitary pulsars may not have come from binaries. After all, one expects the majority of the binaries to disrupt during supernova explosions. The question is, *can one estimate the fraction of pulsars that comes from binaries*? Radhakrishnan & Srinivasan (1981) were the first to address this question. If the magnetic field of the first-born pulsar had decayed significantly in the time interval between its birth and the onset of mass transfer from the companion, then it will be spun up to relatively short periods and will stand out from the general population of pulsars like PSR 1913 + 16. Based on this criterion, PSR 1541-52 and PSR 1804-08 were tentatively identified by Radhakrishnan & Srinivasan (1981) as recycled pulsars. If on the other hand the magnetic field of the first-born pulsar had not decayed significantly, then even after it is spun up it will be deposited close to the spin-up line but this time inside the main island of pulsars. It now appears that the magnetic fields of solitary neutron stars do not decay significantly during their lifetime as pulsars. But there are strong reasons to believe that the magnetic fields of neutron stars born and processed in binary systems do decay (Srinivasan *et al.* 1990; Bhattacharya *et al.* 1992). In the model due to Srinivasan *et al.* (1990), the decay is related to the expulsion of flux from the interior as the neutron star is dramatically spun down during the main sequence phase of the companion. If one accepts this scenario, then there are three possibilities as showninFigure2. In the case of low mass binaries, which are presumably the progenitors of millisecond pulsars, the neutron stars are possibly spun down sufficiently for the field to decay to very low values ~ 10^8 G (Jahan Miri & Bhattacharya 1994). In intermediate mass and/or wide binaries, the spin-down and the consequent flux expulsion may be less pronounced as shown m the alternative

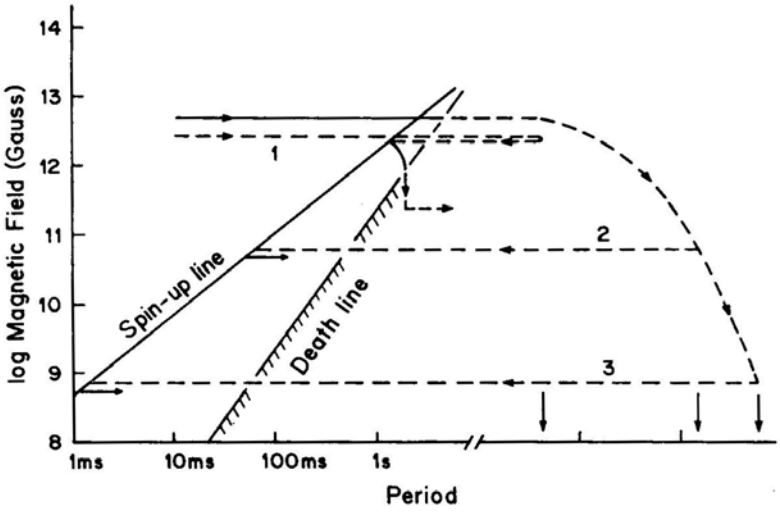

Figure 2. (From Srinivasan *et al.* 1990). Three possible evolutionary scenarios for recycled pulsars are shown here. Track 3 corresponds to the life history of the firstborn neutron star in low mass binary systems. In such systems the magnetic field of the neutron star presumably decays by many orders of magnitude and is spun up during accretion to a period of a few milliseconds. Track 2 represents the life history of recycled pulsars such as PSR 1913 + 16 and **PSR** 0655 + 44. The progenitors of such pulsars are thought to be intermediate mass binaries, and the decay of the magnetic field of the firstborn neutron star is still quite significant. In massive binary systems the first born neutron star may not be spun *down* significantly enough for a substantial fraction of the core field to be expelled. Consequently the magnetic fields of such pulsars will still be close to its original value when it is spun up during the mass transfer phase. These pulsars will consequently be injected into the normal population of high field solitary pulsars. This scenario is labelled as Track 1. The 'spin-up line' in this figure is the equilibrium period line corresponding to accretion at the Eddington rate.

(2) in the figure. In the case of massive and tight binaries the companion may evolve so quickly that there may not have been time for the flux to be expelled from the interior, let alone decay in the crust. This is scenario (1) in the figure. Keeping in mind these various possibilities we looked for *injection* of pulsars close to the spin-up line within the main population of pulsars.

3.1 *Evidence for injection in the low field range* 10^{10}–$10^{11.5}$ G

Let us first concentrate on the pulsars with fields less than about $10^{11.5}$ G (encircled in Fig. 3) and ask how these pulsars might have evolved to their present position in the log *B*-log *P* diagram. Let us first consider the possibility that they might have evolved to their present positions in the diagram from the *left.* This admits two alternative scenarios: (i) Their fields are relatively low because of rapid field decay, or (ii) they were born with low fields. The first alternative, i.e., they are old aged Crab or Vela pulsars is inconsistent with the present estimates of the field decay time scales. Infact, it may be appropriate to mention in this context that it is this scenario (i) that led one to erroneously conclude earlier that magnetic fields of neutron stars decay rapidly (Radhakrishnan & Srinivasan 1981; Radhakrishnan 1982). Such a conclusion is in

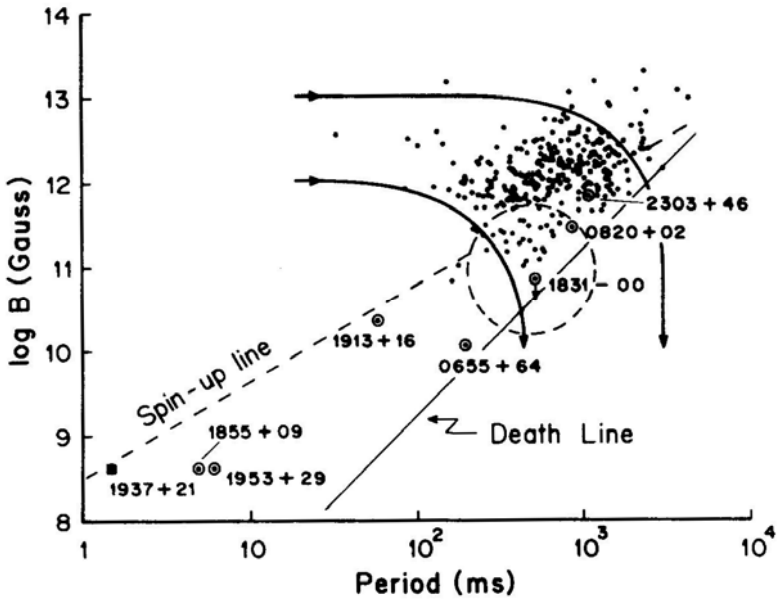

Figure 3. (From Srinivasan 1991). The distribution of observed pulsars. As argued in the text, it is quite likely that the low field pulsars inside the *dashed circle* did not evolve from the left of the diagram due to rapid field decay (as was suspected earlier), but were 'injected' close to the spin-up line. In other words, these are most likely *recycled pulsars.*

contradiction with what an analysis of pulsar statistics reveals. The second alternative viz., that they were born with short period and low magnetic field cannot be ruled out so easily. At first sight one would be tempted to say that the absence of a few pulsars with low magnetic fields and periods in the range of a few hundred milliseconds rules out this possibility. But this would not be a sound argument since one is dealing with a very low birthrate in this field range and the absence of low field pulsars to the left of the diagram may merely be a consequence of small number statistics (Fig. 4 suggests that one may be dealing with a birthrate as low as one in ~ 5000 yr). In addition the recently discovered pulsar PSR J0108-1431 with P = 0·8076 sec. and log B = 10·92 Gauss may be a counter example. Despite this we now wish to suggest that the pulsars with fields less than $\sim 10^{11.5}$ G might have evolved to their present position from the *right* of the diagram.

Figure 5 shows the distribution of *true* number of pulsars in the P – B plane. The *true* number of pulsars in any given bin of width ΔP around a period P and ΔB around field B is given by,

$$N_B(P) = \frac{1}{f} \sum_{i=1}^{n_{psr}} S(P_i, \dot{P}_i, z_i), \tag{5}$$

where f is the beaming factor and $S(P_i, \dot{P}_i, z_i)$ is the scale factor corresponding to the period P, period derivative $\dot{P}$ and the height z from the plane of the ith pulsar. One sees that the low field pulsars that we have been discussing appear to form a distinct island in the *true*-number distribution shown in Fig. 5, there appears to be a valley between

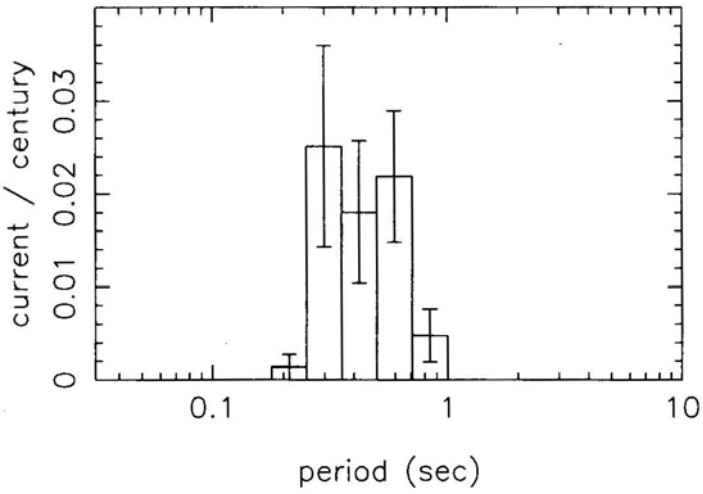

Figure 4. The current of pulsars in the field range log B = 10.5 –11.5. As may be seen, the birth rate of these pulsars is roughly 1 in 5000 years.

the two populations of pulsars. We have tried to test the statistical significance of this valley by doing a variety of tests. For example, a valley was defined in the field range 11.5 < log $B(G)$ < 11.6 and the period range from 0.1 second to the period at the deathline. Then the number of known pulsars in the valley was counted. This number was taken as a reference. Then (i) every pulsar was randomly assigned the luminosity of some other pulsar, (ii) every pulsar was randomly assigned the $\dot{P}$ of some other pulsar, (iii) the number of pulsars in the valley was counted. Steps (i) to (iii) were repeated a large number of times (~ 10000). From the distribution of the number of pulsars in the valley the significance of the reference number was found to be 98·37%.

Although the significance level is not extremely high we wish to advance the view that these pulsars form a distinct population. Their location close to the *spin-up line* suggests that they may, infact, be recycled pulsars. As we shall see later, additional support for this comes from the location of these pulsars with respect to the Galactic plane. The birthrate of these relatively low field pulsars suggests that they constitute roughly 3% of the total population.

3.2 *High field injection*

Let us now examine the pulsar population with larger magnetic fields (log B > 12) in the upper part of Fig. 3. If at all there is *injection* of firstborn pulsars (from massive binaries) into this population, then one expects to see a step in the current in the vicinity of the spin-up line. The integrated current of pulsars shown in Fig. 1 shows such a step at a period ~ 0.5 sec. If such an injection is not an artefact, and if it were due to recycled pulsars then one would expect pulsars contributing to that step to have magnetic fields in a narrow range defined by the spin-up line. To see if this is true or not we have plotted in Fig. 6 histograms of current in three different field ranges. As may be seen, only in the narrow field range 12 < log B < 12.6, there is a step in the current. It one takes the step in the

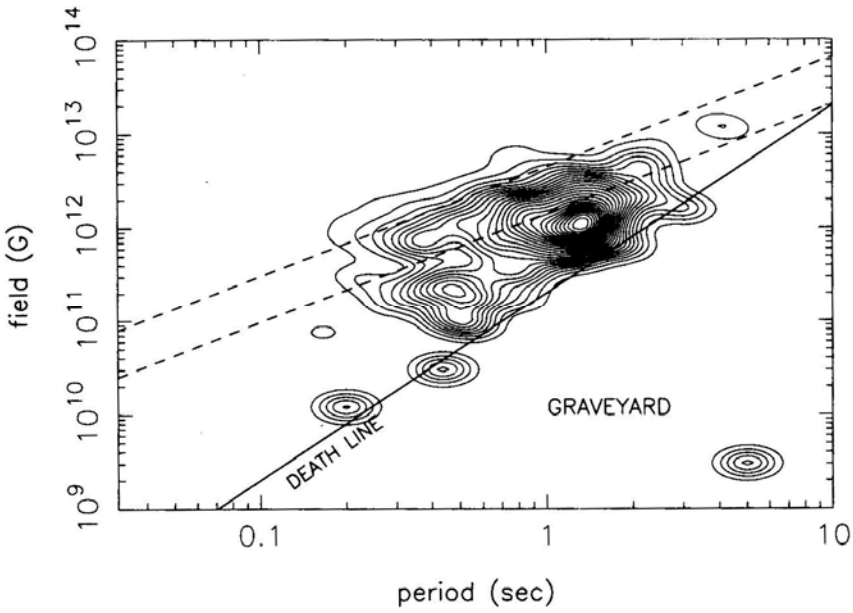

Figure 5. The *true* number distribution of pulsars as defined by equation 5. The contours have been smoothed with a function shown in the bottom right hand corner of the panel. It may be seen that pulsars in the field range log B = 10.5–11.5 appear to form a distinct island; there appears to be a *valley* between the distribution of these pulsars and the high field pulsars. As discussed in section 3, the statistical significance of this valley is 98.37%. The two 'dash' lines are equilibrium period lines; the lower one corresponds to accretion at the Eddington rate, and the upper one to accretion at 10 times the Eddington rate.

current seriously then there certainly appears to be a tight correlation between the magnetic field and the periods of the pulsars contributing to the step in the current, thus lending support to the suggestion that a reasonable number of recycled, but solitary pulsars are present in the pulsar population. It should be pointed out that an injection of pulsars at a period of ~0·5 sec. was originally pointed out by Vivekanand & Narayan (1981). More recently Narayan & Ostriker (1990) noted that injection occurs in a narrow field range (however their approach was very different from the present current analysis). The new suggestion we wish to make is to relate the injection to recycled pulsars.

The correlation between the rotation periods and the magnetic fields of the injected population may be seen better in Fig. 7 where we have plotted the current as a contour diagram in the B — P plane. This current is calculated using equation (1) in various magnetic field 'bins'. Concentrating for a moment in the field range $10^{12} < B < 3 \times 10^{12}$ Gauss, one can see that the current builds up rather continuously till a period of about 0.5 sec., at which there is a step or a cliff (as may be readily seen, the contour plot reveals many 'hills'. These are merely individual high $\dot{P}$ pulsars which appear as 'little hills' due to the fact that the current distribution has been smoothed with the function shown in the right hand bottom corner of the plot. Contrary to this, the step in current referred to above, and also discussed in the above paragraph, is a statistically significant feature since a fairly large number of pulsars contribute to it). Also shown in the figure are two equilibrium period lines corresponding to the Eddington accretion

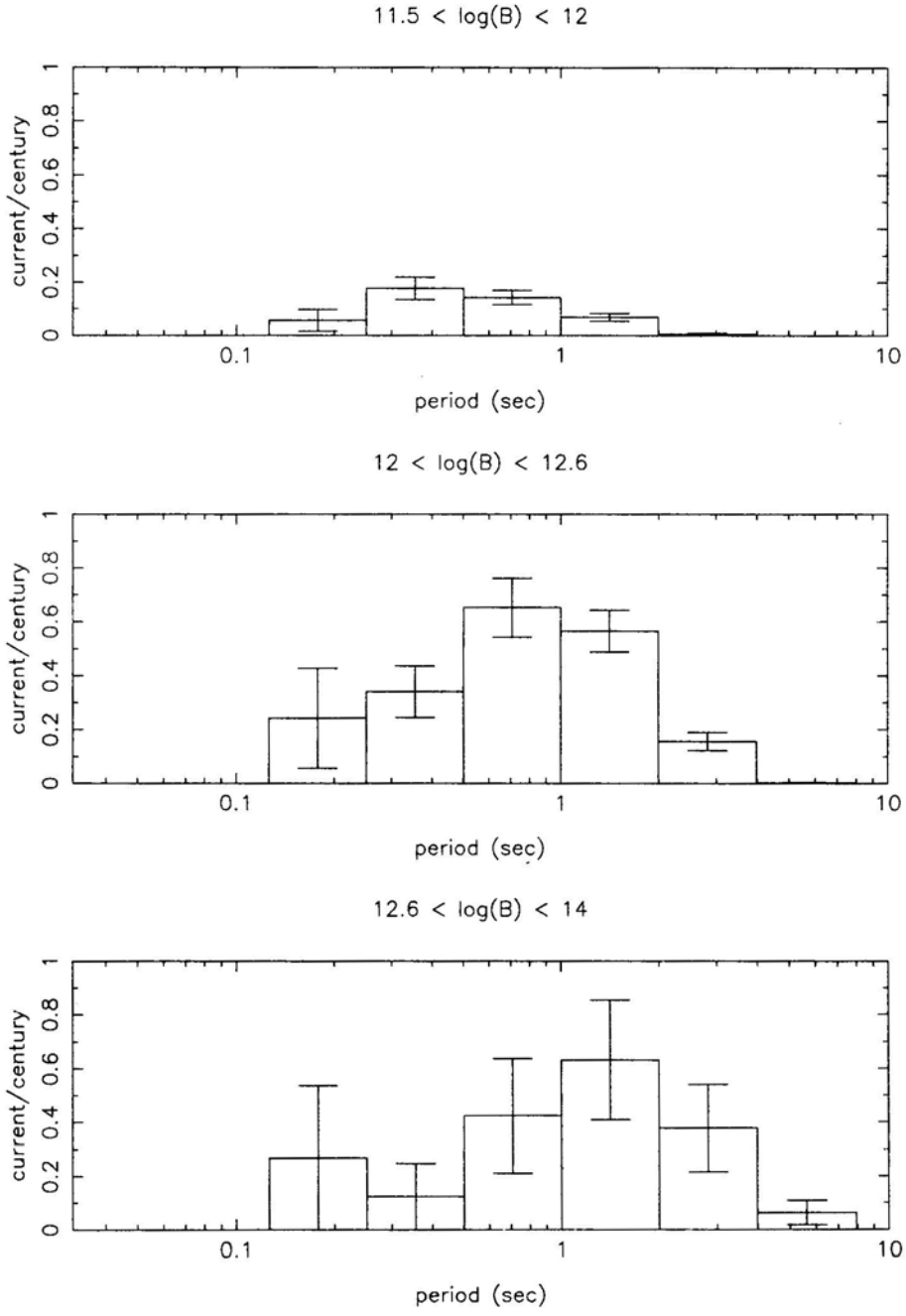

Figure 6. The current distribution shown in Fig. 1 has been binned into three magnetic field ranges. As may be seen, it is only in the central panel which corresponds to $12 < \log B < 12.6$ that one sees a *step* in the current at a period of about 0.5 s.

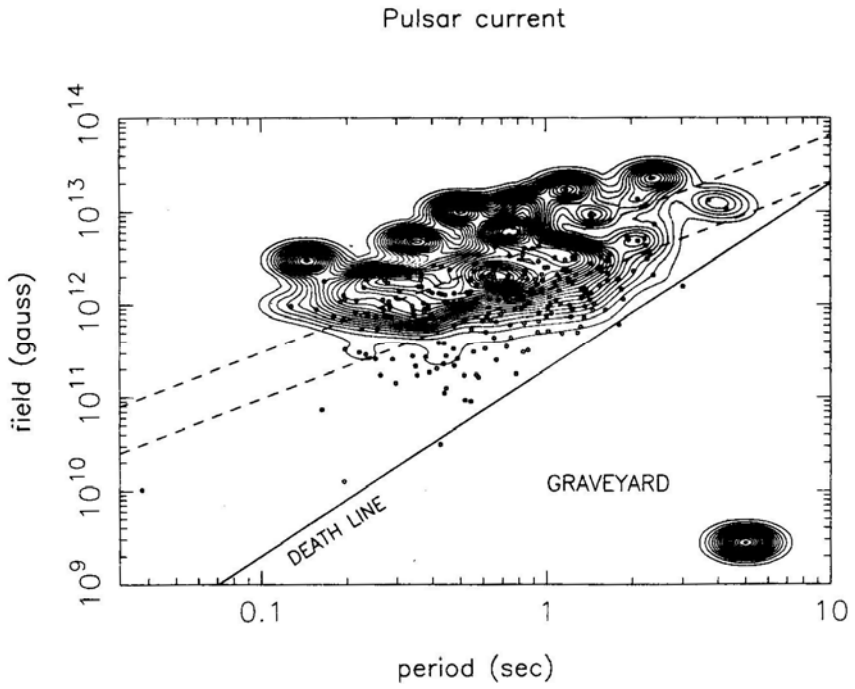

Figure 7. This shows the current distribution as a function of the period and magnetic field. This distribution has been smoothed with a function shown in the bottom right hand corner of the panel. Most of the 'hills' seen in this distribution correspond to individual high $\dot{P}$ pulsars (shown as open circles). But the distinct 'cliff' in the field range $10^{12} < B < 3 \times 10^{12}$G and a period around 0·5 s is a statistically significant feature since a fairly large number of pulsars contribute to it. It is this step in the current close to the upper spin-up line ($\dot{M} = 10\ \dot{M}_{\rm Edd}$) that we interpret an injection of recycled pulsars from massive binaries.

rate and ten times its value. Therefore, if the injection is interpreted as due to the recycled pulsars then it would imply that they experience accretion at super-Eddington rate. In our opinion this is quite likely to happen in massive binary systems.

3.3 *Birth places of injected pulsars*

Further support for the above conjecture namely that recycled pulsars may be injected into the main population of high field solitary pulsars comes from the distribution of pulsars with respect to the Galactic plane. Pulsar current as a function of characteristic age ($\tau_{\rm ch} = P/2\dot{P}$) and the distance z from the Galactic plane can be defined as

$$J_z(\tau_{\rm ch}(P,\dot{P})) = \frac{1}{f}\frac{\sum_{i=1}^{n_{\rm per}} S(P_i,\dot{P}_i,z_i)}{\Delta\tau_{\rm ch}}. \tag{6}$$

In Fig. 8a we show the current distribution in the z– $\tau_{\rm ch}$ plane for the entire field range $9 < \log B < 14$. This can easily be understood in terms of the majority of pulsars

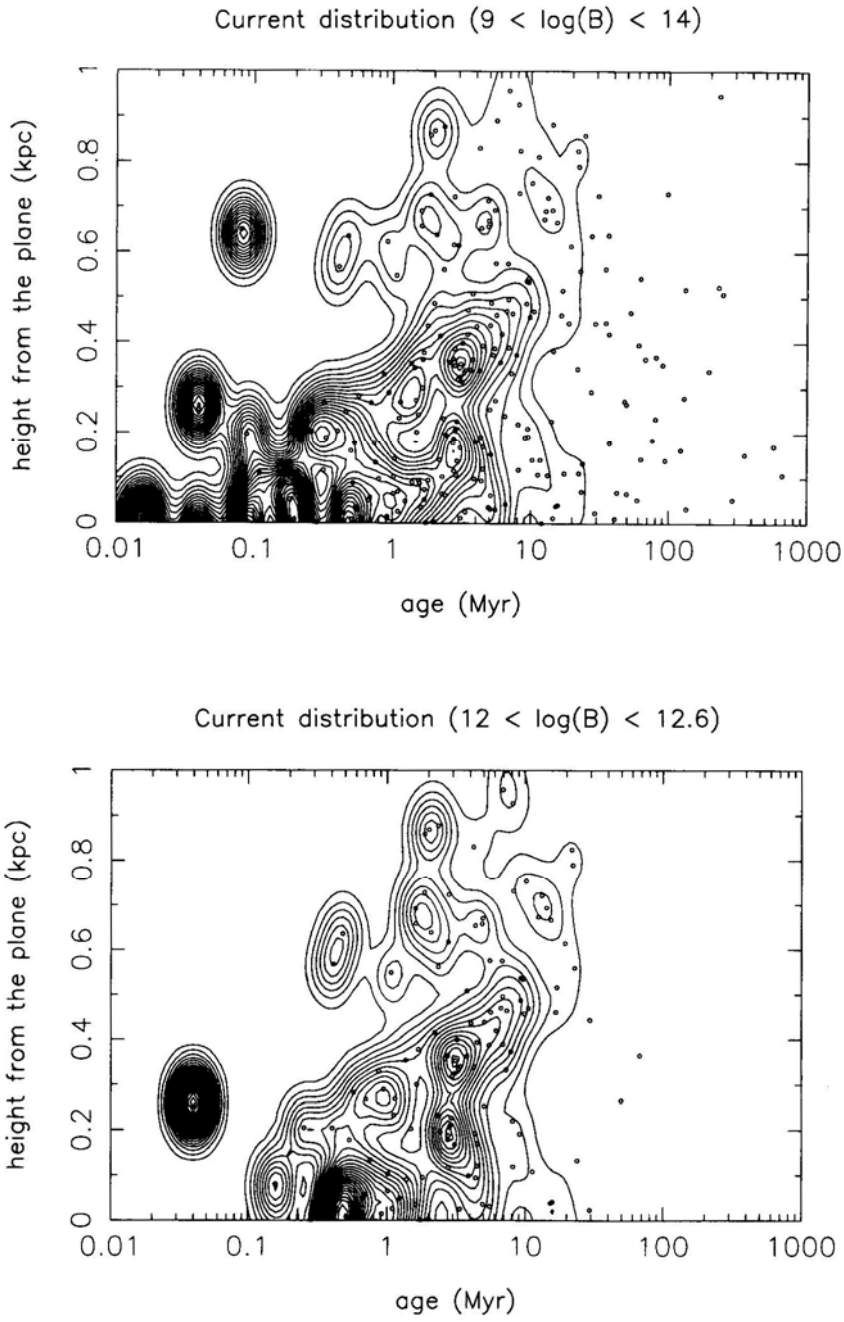

Figure 8. (a) The pulsar current as a function of the characteristic age and the height from the galactic plane. This distribution is easily understandable in terms of the majority of pulsars being born close to the galactic plane and migrating away from it due to velocities acquired at birth; **(b)** In this figure the current of pulsars in the magnetic field range $12 < \log B < 12.6$ alone is shown. We wish to suggest that this distribution is more consistent with pulsars not only being injected with a characteristic age of about 1 Myr but at a variety of distances from the galactic plane ranging all the way up to 800 pc.

being born with short periods and within a hundred parsec or so from the Galactic plane, and their subsequent migration from the plane due to velocities acquired at birth. If one now restricts oneself to pulsars with fields in the range $12 < \log B < 12.6$, then the corresponding current distribution (shown in Fig. 8b) is precisely what we would expect if there is an injection of pulsars with a characteristic age of about 1 Myr and injected at large distances (~ 800 pc) from the Galactic plane.

What could be the progenitors of these pulsars which explode at substantial distances from the galactic plane? The binary hypothesis offers a natural explanation. It is conceivable that a certain fraction of binaries acquires substantial centre of mass velocities during the first explosion, and a certain fraction of them floats away from the galactic plane. When they disrupt during the second supernova explosion two pulsars will be released. The firstborn will have the characteristics of a recycled pulsar, and the second one will have a short characteristic age at birth. This would offer a natural explanation for why some short characteristic age pulsars are seen to be moving towards the galactic plane (Harrison *et al.* 1993).

4. Discussion and summary

If the binary hypothesis for *injection* is correct then a plausible evolutionary scenario is as follows: Most massive binaries are presumably born fairly close to the galactic plane. After the primary evolves and explodes, the centre of mass of the binary system (in most cases the binary is unlikely to be disrupted in the first explosion) will acquire some velocity since the explosion is not symmetric with respect to the centre of mass of the system. A fraction of these binaries can in principle migrate to substantial heights from the galactic plane. The subsequent evolution of such binaries depends upon several factors, in particular their orbital periods. To be specific, we consider below only binaries in which the secondary is either a B-star or a Be-star since they will be much larger in number than binaries with O stars.

If the orbital period is greater than about a year then such systems after the spiral-in phase will become very tight binaries consisting of the firstborn neutron star and the helium core of the companion. If this core is massive enough then it will explode as a supernova and produce a second supernova. Most of such binaries will disrupt during the second explosion releasing two runaway pulsars: the firstborn recycled pulsar, and the second-born neuron star which will be indistinguishable from those born from solitary progenitors. On the other hand, if the binary is sufficiently close to begin with, (orbital periods significantly shorter than about a year) the common envelope formed during the spiral-in may not be expelled, and the first-born neutron star might actually spiral into the core of the companion. The eventual outcome of such systems will be single recycled pulsars (for a detailed review of these and other scenarios see (Bhattacharya & van den Heuvel 1991). Binaries with initially wide orbits which release two neutron stars can naturally account for some of the short characteristic age pulsars which are at considerable distance from the plane and which are moving *towards* the plane (Harrison *et al.* 1993).

Thus the binary hypothesis offers logically consistent explanation for several things; (i) the injection of pulsars into the population of solitary pulsars, (ii) the tight correlation between the rotation period of the injected pulsars and their magnetic field, and (iii) the large spread in their birth places with respect to the galactic plane.

Regarding the actual fraction of solitary pulsars which may be identified with recycled pulsars, one can only make a simpleminded estimate. In a sense, the magnitude of the *step* in the current at a period around 0.5 s will tell us the desired fraction. However, one must bear in mind that such an estimate of the fraction of pulsars from binaries is quite likely to be an overestimate since a part of the step may also be due to a spread in the distribution of initial periods. Faced with this difficulty we wish to tentatively suggest that about 10 –15% of the solitary pulsars might have been processed in binary systems. Given the total birthrate of pulsars this would roughly correspond to one recycled pulsar injected into the population every thousand years. Such a birthrate for recycled pulsars would imply a total number of wide binaries with a neutron star and a B/Be star companion to be roughly 10–1000 (corresponding to an average lifetime of such systems in the range 10^6 - 10^4yr). The recently discovered pulsar PSR B1259 – 63 is one such system. The estimated distance to this pulsar is about 4kpc. A simple-minded scaling suggests that there could be as many as 100 such systems in the Galaxy, which is certainly consistent with the expected numbers mentioned above.

Finally, we wish to summarize our main conclusions:

1. Our estimate for the birthrate of pulsars in the Galaxy is 1 in 75 ± 15 years.
2. We wish to suggest that pulsars with magnetic fields in the range 10^{10}–$10^{11.5}$ G are recycled pulsars from binary systems.
3. In addition, there may be a substantial number of solitary recycled pulsars which are injected into the normal population of pulsars born from single stars.

Acknowledgement

It is a pleasure to acknowledge many fruitful discussions with Ravi Sankrit during his stay at the Institute as a Summer Student.

References

Bhattacharya, D., van den Heuvel, E. P. J. 1991, *Phys. Rep.,* **203,** 1.

Bhattacharya, D., Wijers, R. A. M., Hartman, J. W., Verbunt, F.1992, *Astr. Astrophys*., **254**, 198.

Harrison, P. A., Lyne, A. G., Anderson, **B**. 1993, *Mon. Not. R. astr. Soc.,* **261,** 113.

Jahan Miri, Bhattacharya, D. 1994, *Mon. Not. R. astr. Soc.,* **269,** 455.

Lyne, A. G., Manchester, R. N., Taylor, J. H. 1985, *Mon. Not. R. astr. Soc.,* **213,** 613.

Lorimer, D. R., Bailes, M., Dewey, R. J., Harrison, P. A. 1993, *Mon. Not. R. astr. Soc.,* **263,** 403.

Lyne, A. G., Lorimer, D.R.1994, *Private communication.*

Narayan, R.1987, *Astrophys. J*., **319**,162.

Narayan, R., Ostriker, J. P. 1990, *Astrophys. J*., **352**, 222.

Phinney, E. S., Blandford, R. D. 1981, *Mon. Not. R. astr. Soc*., **194,**137.

Prozynski, M., Przybycien, D.1984, in *Millisecond Pulsars,* Eds. S. P. Reynolds & D. R. Stinebring, (NRAO) p. 151.

Radhakrishnan,V.,Srinivasan,G.1981, *Paper presented in the Second Asia-Pacific Regional Meeting in Astronomy, Bandung, proceedings* Eds. B. Hidayat & M. W. Feast, (Tira Pustaka, Jakarta (1984)) p. 423.

Radhakrishnan, V.1982, *Contemp. Phys.,* **23**, 207.

Ratnatunga, K. U., Sydney van den Bergh 1989, *Astrophys. J*., **343,** 713.

Scalo, J. M. 1986, *Fundam. Cosmic Phys.*, **11,** 1.
Srinivasan, G., Bhattacharya, D., Muslimov, A. G., Tsygan, A. I. 1990, *Curr. Sci.*, **59,** 31
Srinivasan, G. 1991, *Annals of the New York Academy of Sciences* **647,** 538
Tauris, T. M., Nicastro, L., Johnston, S., Manchester, R. N., Bailes, M., Lyne, A. G., Glowacki, J., Lorimer, D. R., D'Amico, N. 1994, *Astrophys. J.*, **428,** L53.
Taylor, J. H., Cordes, J. M. 1993, *Astrophys. J.*, **411,** 674.
van den Bergh, S. 1991, *Phys. Rep.*, **204,** 385.
Vivekanand, M., Narayan, R. 1981, *J. Astrophys. Astr.* **2,** 315.

Diamond Jubilee Symposium on Pulsars
14–17 March 1994
Raman Research Institute, Bangalore

J. Astrophys. Astr. (1995) **16,** 69–88

The Progenitors of Pulsars

A.A. Deshpande, R. Ramachandran, G. Srinivasan *Raman Research Institute, Bangalore 560 080, INDIA.*

1. Introduction

This is not only the Diamond Jubilee of the Indian Academy of Sciences but also the Diamond Jubilee of the publication of the prophetic paper by Baade and Zwicky (1934) in which they suggested a possible connection between the supernova phenomena and the formation of neutron stars. Sixty years later the mechanism suggested by them is still the most convincing one for the majority of supernovae. Since this is the only talk in this symposium focussing on the progenitors of pulsars some general remarks may be appropriate. Let us first recall the main conclusions in this regard from stellar evolution theory. These may be summarized as follows:

Stars with $M < 1.4M_{\odot}$ will definitely end their lives as white dwarfs. In recent years one has come to appreciate that stars as massive as $5 - 6M_{\odot}$ may also leave behind white dwarfs. Although the upper mass limit for the formation of white dwarfs is still not known with certainty, observations of white dwarfs in open clusters suggest that this mass limit may be as high as $6M_{\odot}$ (Tinsley, 1977).

According to prevalent opinion some years ago, stars in the mass range $5 - 8M_{\odot}$ will ignite carbon in a degenerate core resulting in a total disruption of the star. Indeed this was the popular model for Type I supernovae (Tinsley, 1977). Although considerable uncertainties still surround this scenario there is reasonable agreement that stars in the mass range $8 - 10M_{\odot}$ will collapse to form neutron star cores due to electron capture instability (van den Heuvel and Habets, 1985), Above, say, $10M_{\odot}$ stars are expected to form degenerate iron cores which will eventually reach the Chandrasekhar limiting mass for white dwarf configurations and consequently collapse. The result will be the formation of a neutron star and a supernova explosion just as envisaged by Baade and Zwicky. Although the details of how to effectively utilize the binding energy released in the formation of the neutron star to produce a supernova are still not clear, this is the moat favoured scenario for Type II supernovae.

Continuing with the theoretical expectations, as one goes to larger masses there must be a critical mass above which degeneracy never sets in however high the density may become. As shown by Chandrasekhar (1932) this happens when the radiation pressure exceeds 9.2% of the total pressure. To quote from

Chandrasekhar's paper:

> *For all stars of mass greater than a critical mass the perfect gas equation of state does not break down however high the density may become, and the matter does not become degenerate. An appeal to Fermi-Dirac statistics to avoid the central singularity cannot be made.*

Stars with masses above this critical mass will presumably find peace as black holes. Given the mass function of stars the majority of the progenitors of neutron stars will have masses close to the lower limit for the formation of neutron stars. One of the things that we wish to estimate is this lower mass limit.

2. Pulsar Birth Rate

The first step towards determining the lower limit to the mass of stars which will leave behind neutron stars is an estimation of the birth rate of pulsars. Before proceeding further let us once again remind ourselves about the observed population of pulars. Fig. 1 shows 560 pulsars with their measured periods and derived surface magnetic fields. One notices that the overwhelming majority of pulsars have fields in the range $10^{12} - 10^{13}$ G.

There are several ways of estimating the birth rate of pulsars. For example, if one is able to derive an *average lifetime* for pulsars then given their total number in the Galaxy one can estimate a mean birth rate. If the birth rate obtained this way has to be reliable it must explicitly allow for the possibility that the birth rate of pulsars with different magnetic fields may not be the same. One of the ways in which this can be allowed for is by calculating the *current* of pulsars (Phinney and Blandford 1981, Vivekanand and Narayan 1981). The current of pulsars along the period axis may be formally defined in analogy with the current of electrons in a wire. Let us consider a period window between P and $P + \Delta P$. The current of pulsars may be defined as follows:

$$J(P) = \frac{1}{\Delta P} \sum_{\mathrm{i}=1}^{N_{psr}} \dot{P}_{\mathrm{i}} \tag{1}$$

where the summation is performed over all the pulsars in the period bin. Provided the current in a bin so defined has reached its maximum value it would represent the birth rate of pulsars. (This will be the case if the initial periods of all the pulsars in the population are less than the period chosen and if the death of pulsars is not yet relevant.) Although the above statement is correct in principle one must remember that one has not allowed for the fact that the observed population of pulsars, is only a small fraction of the true galactic population. To calculate the true galactic birth rate one has to make two corrections: (1) one must allow for the fact that the radiation from pulsars is "beamed", and (2) one must also account for various *selection effects* which work against the detection of pulsars.

Consider a pulsar with period P and radiation luminosity L. One can compute the probability of detecting such a pulsar in one of the major surveys. Let us define the reciprocal of this detection probability as the scaling factor $S(P, L)$. And let

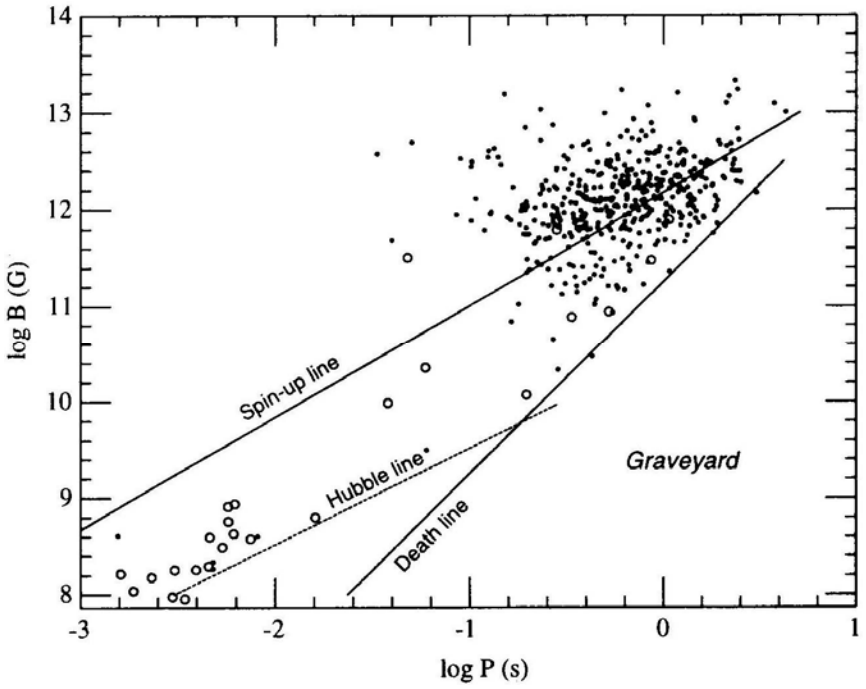

Figure 1: The measured periods and derived surface magnetic fields of 560 pulsars are shown. The pulsar parameters are taken from Taylor et al. (1993).

f be the beaming factor. One can now estimate the true current of pulsars as follows:

$$J(P) = \frac{1}{\Delta P} = \sum_{i=1}^{N_{psr}} \frac{1}{f}\, S(P_i, L_i)\, \dot{P}_i \qquad (2)$$

In practice what one really needs is the scaling factor as the function of P and $\dot{P}$ i.e., S(P, $\dot{P}$) rather than $S(P, L)$. At first sight this may seem like a simple change of variables but it is more subtle than that. One can of course assume an empirical relation between the period and period derivative of a pulsar and its radio luminosity. But one has to allow for the fact that there is a *distribution of luminosities* of a given combination of P and $\dot{P}$. Thus in going from the variables (P, L) to (P, $\dot{P}$) one has to average over the probability distribution of luminosities. Such an averaging procedure should not be done after deriving the scaling factor but rather at the level of the more basic quantity viz. the detection probability itself. Although this might seem like a very minor point the conclusions reached can depend upon how the averaging over the luminosities is done (Narayan, 1987; Narayan and Ostriker, 1990).

The current of pulsars calculated in a manner outlined above is shown as a histogram in Fig. 2. It will be seen that the current continues to rise till a period ~ 0.6 s. This clearly points to the fact that not all pulsars are born spinning very rapidly, but there is a broad distribution of initial periods. Beyond this period the

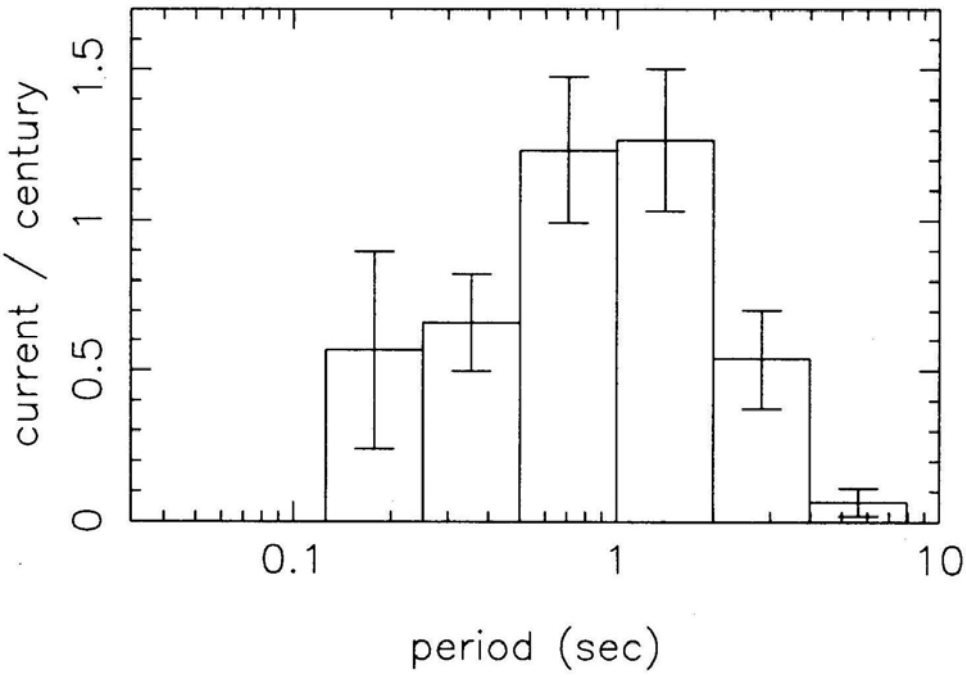

Figure 2: The current distribution as a function of period. As may be seen, the current reaches its maximum value around a period of 0.5 s, and begins to decline at around 2 s. The maximum value of the current corresponds to a pulsar birth rate of about 1 in 75 years.

current is roughly constant till a period ~ 2 s and then begins to decrease due to deaths of pulsars becoming significant. The maximum value of the current yields a pulsar birth rate of ~ 1 in 80 years. This number should be compared with a birth rate of 1 in 100 years derived by Narayan and Ostriker (1990), and also with the estimate of Lorimer et al. (1993) who got a birth rate of 1 in 125 to 250 years for a set of luminosity-limited samples. For a comparison of these birth rates under discussion we refer to Deshpande et al. (1995). It is appropriate to recall that the derived birth rate of pulsars is particularly sensitive to the distance scale to pulsars. In the present analysis we have used the latest distance model due to Taylor and Cordes (1993) for comparison. The previously preferred distance model due to Lyne, Manchester and Taylor (1985) yields a birth rate of 1 in 40 years.

Given a birth rate of pulsars one would of course like to compare it with the supernova rate, as well as the birth rate of supernova remnants. Such a comparison continues to be difficult as in the past. There is still no agreement on the estimated supernova rate in the Galaxy based upon the statistics of supernovae in external galaxies with morphology similar to ours. The estimate of Clark and Stephenson (1977) of 1 in ~ 30 years based upon the historical supernovae recorded in the last two millenia continues to be the only firm estimate.

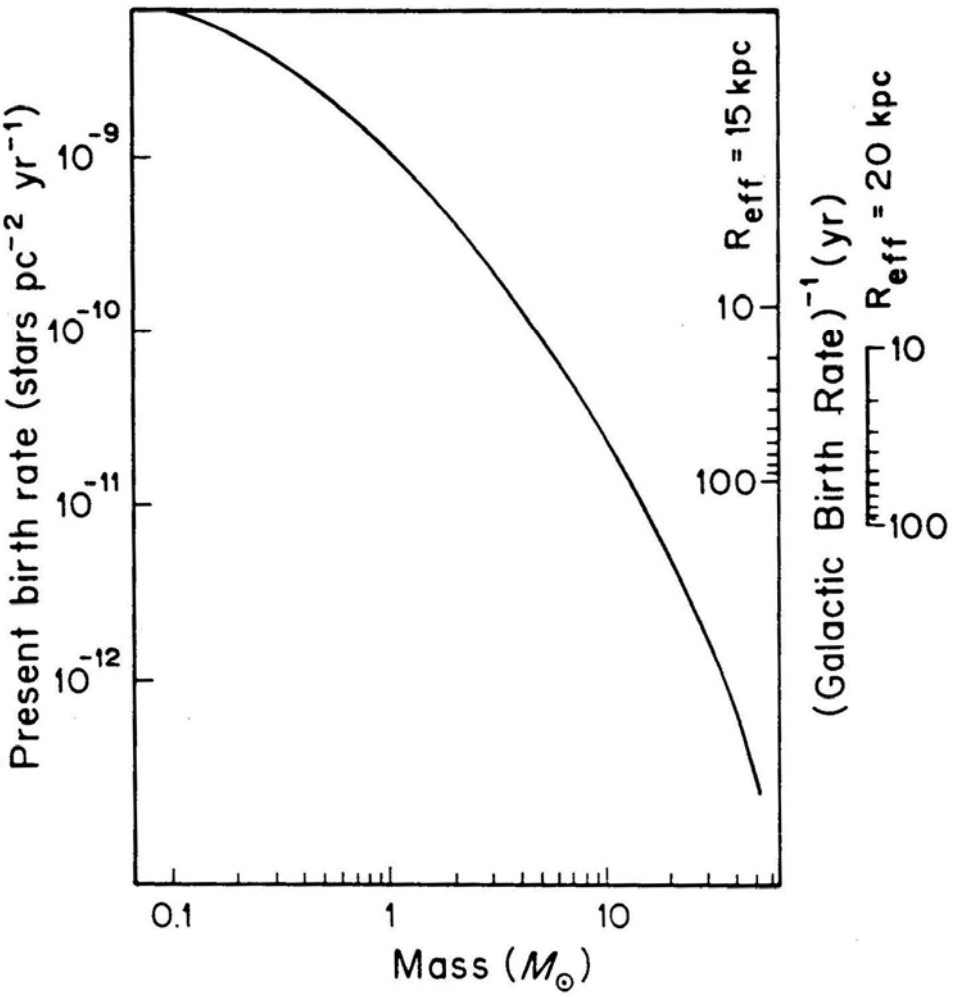

Figure 3: Integrated stellar birth rate as a function of Mass. This has been adapted from Wheeler et al. (1980). On the right hand side we have shown the galactic pulsar birth rate for two assumed effective radii for the Galaxy.

Turning to supernova remnants, an estimate of their birth rate depends critically on the assumed model of the interstellar medium into which they are expanding. In the standard model all supernova remnants are assumed to be in the Sedov or self-similar phase of expansion. If one accepts this for a moment then it yields a supernova birth rate ~ 1 in 120 years (Clark and Caswell, 1976). But this assumption needs to be questioned. The standard model is justifiable in the case of those remnants that have expanded for a long time in a relatively dense interstellar medium with a number density ~ 1 atom/cm^3. However, if the ambient density is much lower then the free expansion phase will last longer, and one would be grossly over-estimating the age of a given remnant if one used the

standard model. During the past decade there is growing observational evidence for a much more rarified component of the interstellar medium with a relatively large filling factor (McKee and Ostriker, 1977). If one allows for the possibility that a certain fraction of supernova remnants may be expanding in a rarer component of the interstellar medium then the estimated supernova remnant birth rate will be much higher than that suggested by the standard model. Given all these uncertainties it appears that the birth rate of supernova remnants may be telling us more about the properties of the interstellar medium rather than the supernova rate itself.

After this digression let us return to our discussion of the progenitors of pulsars. Given a reasonable estimate for the pulsar birth rate one should now attempt to define the mass range within which stars end their lives as neutron stars. To do this one must compare the birth rate of pulsars to the death rate of stars. For sufficiently massive stars ($M > 3M_{\odot}$) their birth rate may safely be assumed to be equal to their death rate. The birth rate of stars can be inferred from star counts and their theoretical lifetimes on the main sequence. But there are some uncertainties in the derived birth rate. For example, the distribution of O and B stars is patchy. Also, star counts are done as a function of spectral types which have to be converted to masses. In addition there is the following complication. The birth rate of pulsars one has derived is a galactic rate, while star counts yield a local rate. If the distribution of pulsars was uniform not only in the azimuthal coordinate but also as a function of galactocentric radius then using the estimated radius of the Galaxy one can convert the galactic pulsar rate to a local birth rate. But there is observational evidence for a gradient in the distribution of supernova remnants, HII regions, giant molecular clouds etc. as one goes away from the inner Galaxy. Therefore, to properly convert a galactic rate to a local rate one must assume a larger *effective radius* for the Galaxy than its actual dimensions. In Fig. 3 we have shown the integrated death rate of stars using the initial mass function due to Miller and Scalo (Wheeler et al., 1980). If one assumes an effective radius for the Galaxy of 20 kpc then a pulsar birth rate of 1 in 80 years implies that all stars with masses above $12 - 15M_{\odot}$ should produce neutron stars. On the other hand a pulsar birth rate of 1 in 40 years would require that all stars more massive than $7 - 8M_{\odot}$ should leave behind neutron stars.

3. Do pulsars trace spiral arms?

An interesting question related to the minimum mass for the formation of neutron stars is their possible spatial association with the spiral arms of the Galaxy. This question was first explicitly discussed by Blaauw (1985). He, too, was trying to estimate the minimum mass for the formation of neutron stars, but he directly tried to estimate the local birth rate of pulsars by restricting himself to the sample of pulsars whose distances projected on to the galactic plane were less than 0.5 kpc. From information on the scale height of pulsars, their measured proper motions and their mean lifetime he concluded that *the local population of pulsars must be replenished by local progenitors.* He went on to conclude that OB associations cannot by themselves account for the local population of pulsars, and that lower

mass field stars in the mass range 6 – $10M_{\odot}$ must make the major contribution to the pulsar birth rate. If this conclusion is correct then Blaauw argued that "*pulsars are on a galactic scale*, *tracers of regions of past spiral structure rather than of active spiral structures*". To elaborate on this beautiful point, if the progenitors of the majority of pulsars were the massive OB stars which delineate the spiral arms then one would expect pulsars also to be located close to the leading edge of the spiral arms since massive stars have relatively short lifetimes. But if the majority of progenitors are less massive then, say, $10M_{\odot}$ then one would expect them to explode at substantial distances from the leading edge of spiral arms. This is because of the relative motion between the spiral density waves and the matter in the Galaxy during the lifetime of the star. Consequently the location of the majority of pulsars should not have any strong correlation with the present spiral pattern.

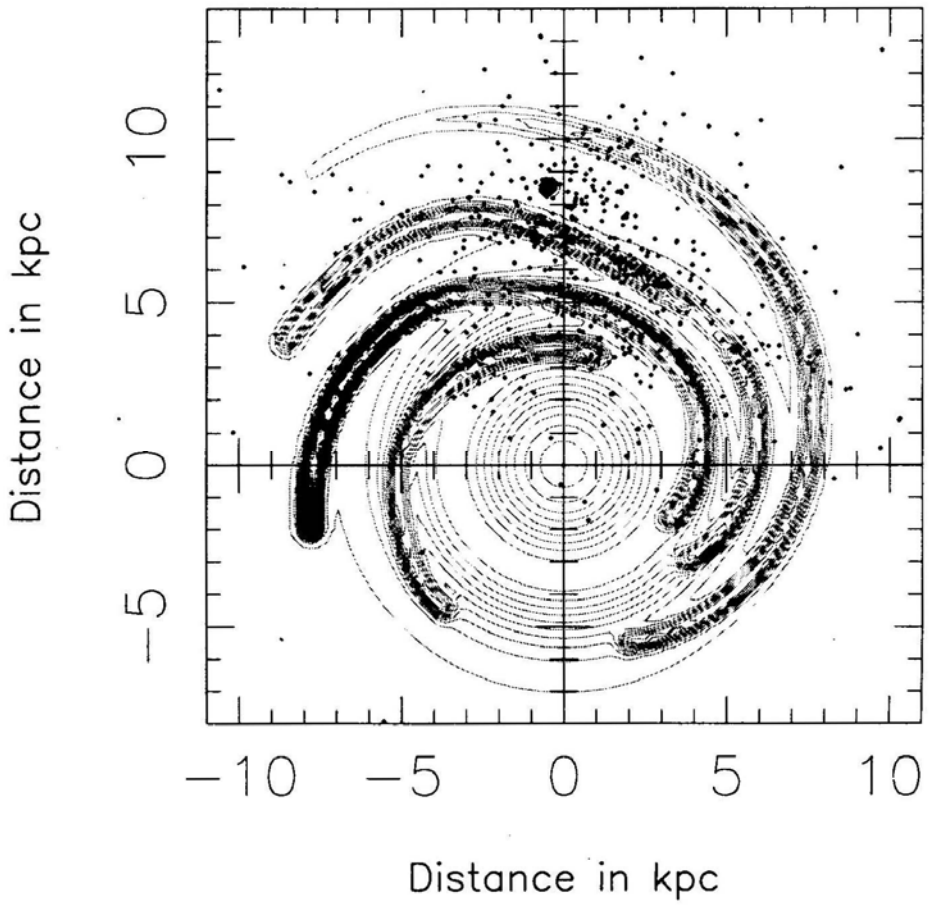

Figure 4: The electron density distribution derived by Taylor and Cordes (1993) is shown as a contour diagram. The *dots* indicate the location of the pulsars estimated from this model and projected on to the plane of the Galaxy.

Does the matter distribution lead the spiral pattern or lag behind it? This depends on the galacto-centric distance. Since the Galaxy is rotating differentially, and the spiral pattern rigidly, inside the *co-rotation radius* R_c the spiral pattern will lag behind the matter, and the converse will be true outside the co-rotation radius. From a detailed dynamical modelling of the gas distribution and their motions in our Galaxy it appears that the co-rotation radius is approximately 12 – 15 kpc (Burton, 1971). Since the majority of pulsars are inside the solar circle their circular velocities should be larger than that of the spiral pattern at the corresponding radius and consequently the present distribution of pulsars should be ahead of the present spiral pattern.

Recently an attempt was made to test this remarkable conjecture by Blaauw (Ramachandran and Deshpande, 1994), viz. one tried to look for a correlation between the present distribution of pulsars and the location of the spiral arms in the past. An essential ingredient in this analysis is the distance estimate to the known pulsars. Like in the birth rate analysis the recent electron density distribution due to Taylor and Cordes (1993) was used. The distribution of pulsars derived from this model and projected on to the plane of the Galaxy is shown in Pig. 4. The *dots* indicate the pulsars and the contours show the electron density distribution. As may be seen, the observed density of pulsars is systematically higher in the solar neighbourhood as might be expected from various selection effects. To be able to systematically correct for such a bias the sample of pulsars was restricted to those which, in principle, should have been detected by any one of the major eight surveys. The next step is to construct the true galactic distribution of pulsars from the observed distribution. Once again this involves the computation of scale factors. While deriving the current of pulsars we calculated the scale factor as a function of P and $\dot{P}$. In the present context one wants to ask a slightly different question, viz., given any location in the Galaxy where a pulsar has in fact been detected one wants to calculate the *probability* of detecting a pulsar at that location were it to have a different period or different magnetic field. This will enable one to calculate the scale factor as a function of position in the Galaxy. The procedure adopted was the following. In Fig. 5 we have shown the *true* number distribution of pulsars in the B-P plane. This distribution is derived from the observed B-P distribution by computing the scale factor in various "(B, P) bins" as described in Section 2. *The true distribution so derived is equivalent to a probability distribution for the occurrence of the observed periods and magnetic fields.* Thus, given a particular location in the Galaxy and given this probability distribution one can calculate the detection probability or the fraction of pulsars that are likely to be discovered at that particular location. From this one can derive the scale factors and the true galactic distribution of pulsars (Ramachandran and Deshpande, 1994).

As mentioned earlier there is a relative azimuthal angular motion between the spiral pattern and the matter in the Galaxy. Assuming a flat rotation curve for the Galaxy the relative angular rotation is given by

$$\beta(t, R) = V_{rot}\left(\frac{1}{R} - \frac{1}{R_c}\right)t \tag{3}$$

where V_{rot} is taken to be 225 km/s as recommended by the IAU (see Kerr and

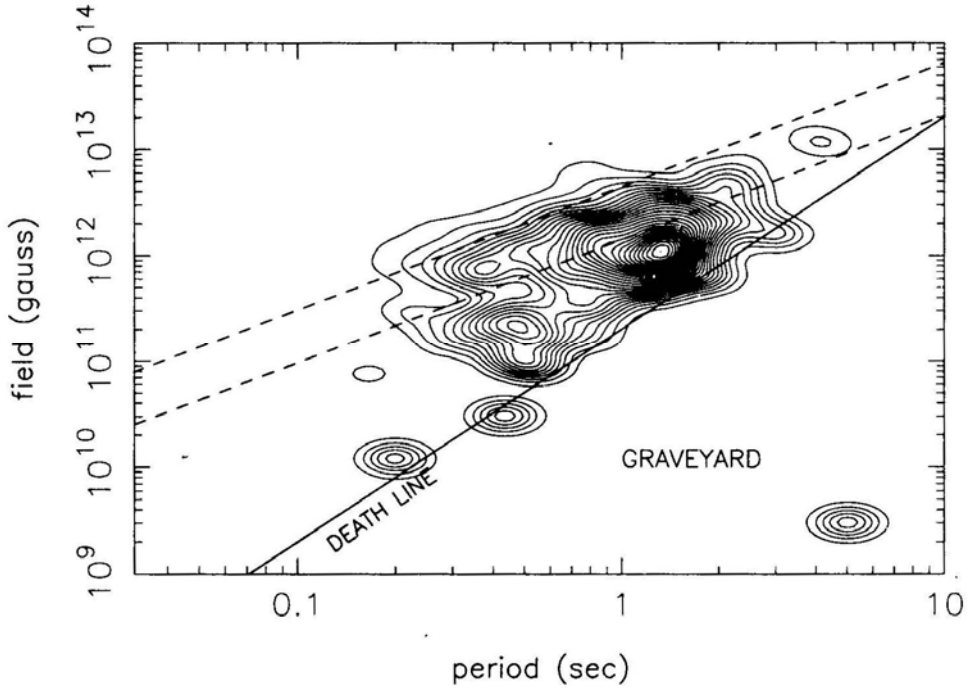

Figure 5: The *true* number distribution of pulsars. The contours have been smoothed with a function shown in the bottom right hand corner of the panel. It may be seen that pulsars in the field range log B = 10.5 – 11.5 appear to form a distinct island; there appears to be a *valley* between the distribution of these pulsars and the high field pulsars. As discussed in Section 4, the statistical significance of this valley is 98.37%. The two 'dash' lines are equilibrium period lines; the lower one corresponds to accretion at the Eddington rate, and the upper one to accretion at 10 times the Eddington rate.

Lynden-Bell 1986). Using this relation the pulsar distribution can be "rotated" as it were with respect to the spiral arms as delineated by the electron density distribution, and one can look for a correlation between the two at some past epoch. The expected correlation (Blaauw, 1985) can, in principle, be smeared due to three effects: (1) the spread in the birth places of the progenitors, (2) the motion of the progenitors between their birth and death, and (3) motion of the pulsars after their birth. The first two effects may not be significant, but the smearing due to the space velocities of the pulsars acquired at their birth could be important. If one finds a correlation despite this then one can turn it around to set limits on the space velocities of pulsars.

Before giving the results of the analysis it is worth recalling two assumptions that have been made in this analysis: (1) the "arm component" of the electron density in the Taylor-Cordes model adequately describes the mass distribution in the spiral structure. This is a reasonable assumption since the electron density model is based on the observations of giant HII regions. (2) In order to define the

circular velocity of the spiral pattern a value of 14 kpc has been assumed for the co-rotation radius. As mentioned before, this value is consistent with the detailed modelling of neutral hydrogen in the Galaxy.

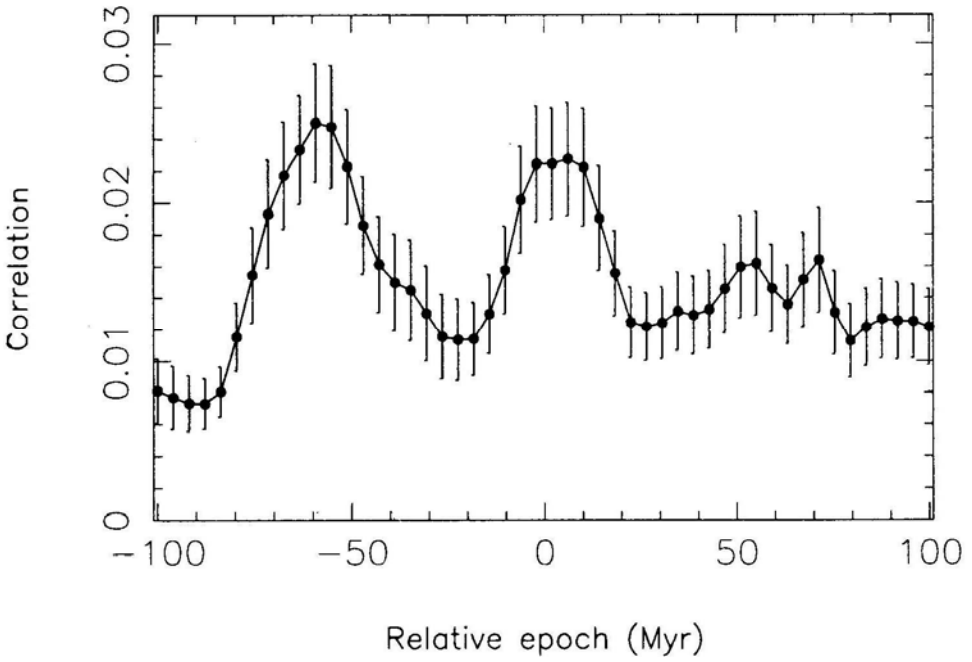

Figure 6: A plot of the correlation between the mass distribution in the spiral arms and the present pulsar distribution as a function of different past epochs. A co-rotation radius of 14 kpc has been assumed in this analysis. The error bars indicate 1σ deviation on either side. There are two strong features in this plot. It is argued in the text that the picture corresponding to the present epoch is most likely an artefact. The feature at –60 Myr has a very high statistical significance of 99.95%.

The conclusion arrived at by Ramachandran and Deshpande (1994) is shown in Fig. 6. Surprisingly there are two significant features, one corresponding to 60 Myr ago and the other to the present epoch. The correlation feature at the present epoch, viz., the correlation between the distribution of pulsars and the *present* spiral structure is most likely an artefact of the apparent clustering of pulsars in the "arm regions". This can happen, for example, if the spiral arm component of the electron density distribution is over-estimated relative to the smooth component. This can also happen if the location of the spiral arms in the model is in error. In the former case one would expect the effect to be more pronounced in the inner Galaxy. This is indeed the case. Pulsars which contribute the correlation at the present epoch are mostly between 5 to 7 kpc from the galactic centre.

Let us now turn to the other feature in Fig. 6 namely the one which corresponds to a correlation between the pulsar distribution and the spiral arms some 60 Myr

ago. The following tests were done to test the significance of this feature. The longitudes of the pulsars were scrambled and the whole analysis was repeated. Similarly, the distances to the pulsars were varied randomly by about 30% and the analysis was repeated. Based on many tens of thousands of simulations it was concluded that the correlation maximum at –60 Myr has a significance level of 99.95%. This should be compared with a significance level of about 93% for the other feature, which supports our earlier conjecture that it must be an artefact.

In our opinion the above analysis lends strong support to the prescient remarks of Blaauw that "pulsars are, on a galactic scale, tracers of regions of past spiral structure rather than of active spiral structure". Since the average lifetime of the pulsars in the sample is 10 ± 2 Myr, the above analysis leads one to the conclusion that the average lifetime of the progenitors of the pulsars must be about 50 Myr. This is roughly the lifetime of stars with masses ~ $7M_{\odot}$. This would suggest that a pulsar birth rate of 1 in 80 years derived earlier might be an under-estimate. The strong correlation found between the present distribution of pulsars and the location of spiral arms in the past argues against pulsars being high velocity objects. We feel that it may be hasty to conclude that the majority of pulsars are very high velocity objects.

4. On the fraction of pulsars from binary systems

We now turn to a completely different question. So far we have not been worried about whether the progenitors of pulsars are solitary stars or members of binary systems. This is obviously a very important question. Although the number of binary pulsars is still only a couple of dozen there is no reason to conclude that the vast majority of solitary pulsars may not have come from binaries. After all one expects the majority of binaries to disrupt at the time of the second supernova explosion. It would be of great interest if one could estimate the fraction of solitary pulsars which have come from binaries. It may be recalled that the Hulse-Taylor pulsar which is now understood in terms of it being born and recycled in the binary system has an anomalous combination of short rotation period and low magnetic field. If the magnetic field of the first-born pulsar had decayed significantly before being spun up then it will be spun up to relatively short periods and will stand out from the general population of solitary pulsars. On the other hand, if the magnetic field of the first-born pulsar had not decayed significantly then after being spun up it will be deposited inside the island of pulsars close to the spin-up line. Radhakrishnan and Srinivasan (1981) who were the first to address this question tentatively identified PSR 1541–52 and 1804–08 as recycled pulsars from binaries which were disrupted during the second supernova explosion (see Fig. 7).

Why should the magnetic fields of some first-born neutron stars decay more than in others? Although this question will be reviewed later by Bhattacharya (this volume) it is necessary for us to make a few remarks to motivate the discussion that follows. It now appears that the magnetic fields of solitary neutron stars do not decay significantly during their lifetime as pulsars. But there are strong reasons to believe that the magnetic fields of neutron stars born and processed in binary systems do decay. In the model due to Srinivasan et al. (1990) the decay

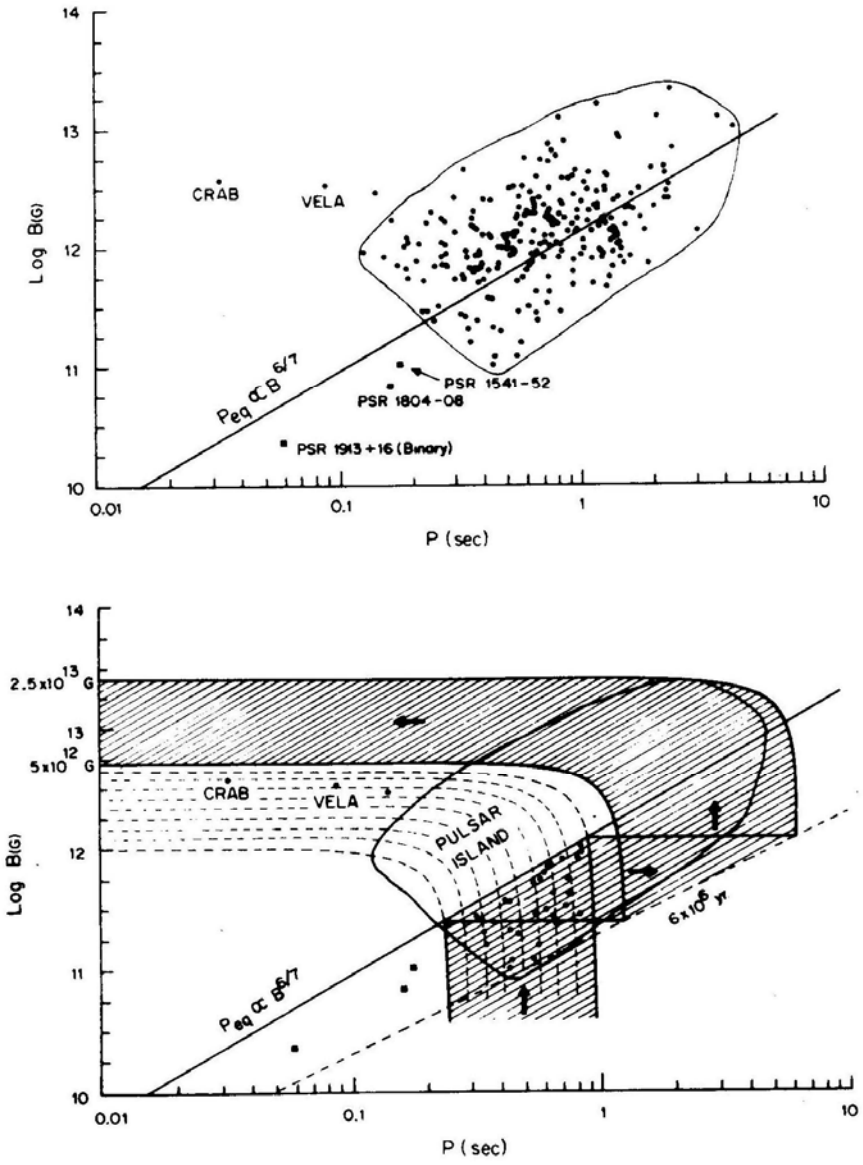

Figure 7: (from Radhakrishnan and Srinivasan, 1981) (a) This shows the population of solitary pulsars which form a distinct island. The binary pulsar PSR 1913+16 is believed to be the first-born pulsar in the binary whose field had decayed between its birth and the onset of mass accretion during which it was spun up to an *equilibrium period* determined by its magnetic field. PSR 1804–08 and PSR 1541–52 were tentatively identified as *recycled pulsars*, (b) It is conceivable that a fraction of solitary pulsars in the main population are such recycled pulsars. They are expected to be located to the *right* of the equilibrium period line. Two possible evolutionary scenarios are shown for the low field pulsars located in the bottom right hand corner of the island: The dashed lines show evolutionary tracks with rapid field decay, and the hatched track shows their evolution (traced backwards) in the recycling scenario.

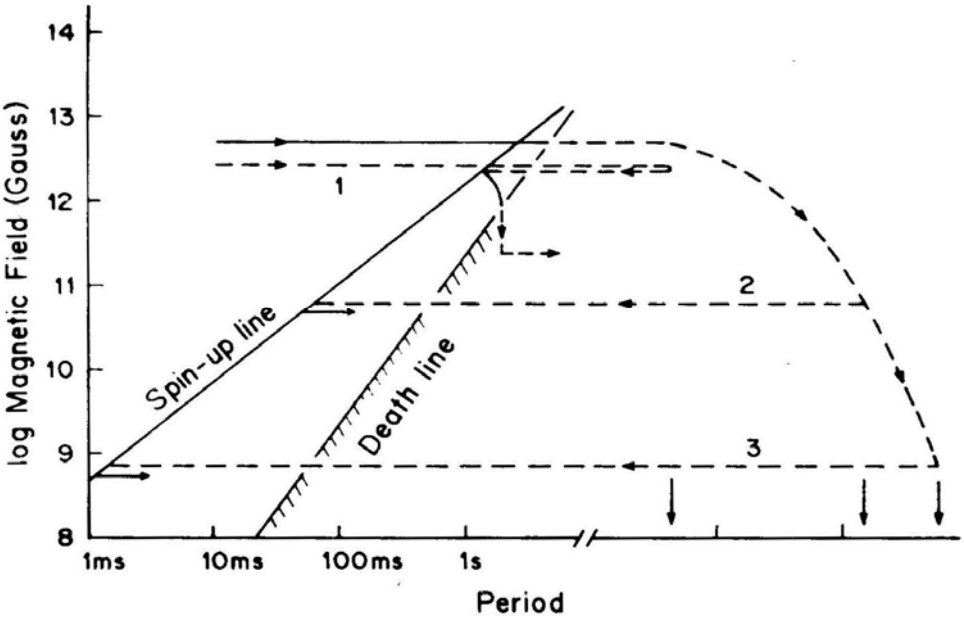

Figure 8: (from Srinivasan et al. 1990) Three possible evolutionary scenarios for recycled pulsars are shown here. Track 3 corresponds to the life history of the first-born neutron star in low mass binary systems. In such systems the magnetic field of the neutron star presumably decays by many orders of magnitude and is spun up during accretion to a period of a few milliseconds. Track 2 represents the life history of recycled pulsars such as PSR 1913 + 16 and PSR 0655 + 44. The progenitors of such pulsars are thought to be intermediate mass binaries, and the decay of the magnetic field of the first-born neutron star is still quite significant. In massive binary systems the first-born neutron star may not be spun *down* significantly enough for a substantial fraction of the core field to be expelled. Consequently the magnetic fields of such pulsars will still be close to its original value when it is spun up during the mass transfer phase. These pulsars will consequently be injected into the normal population of high field solitary pulsars. This scenario is labelled as Track 1. The "spin-up line" in this figure is the equilibrium period line corresponding to accretion at the Eddington rate.

is related to the expulsion of flux from the interior as the neutron star is dramatically spun down during the main sequence phase of the companion. If one accepts this scenario, then there are three possibilities as shown in Fig. 8. In the case of low mass binaries which are presumably the progenitors of millisecond pulsars the neutron stars are possibly spun down sufficiently and over a long time for the field to decay to very low values ($\sim 10^8$ G). In intermediate mass and/or wide binaries, the spin-down and the consequent flux expulsion may be less pronounced as shown in the alternative (2) in the figure. In the case of massive and tight binaries the companion may evolve so quickly that there may not have been time

for the flux to decay, even if it had been expelled from the interior to the crust. This is scenario (1) in the figure. Keeping in mind these various possibilities we looked for "injection" of pulsars close to the spin-up line inside the pulsar island. To illustrate our conclusions we will return to our earlier discussion of the pulsar current and the number distribution.

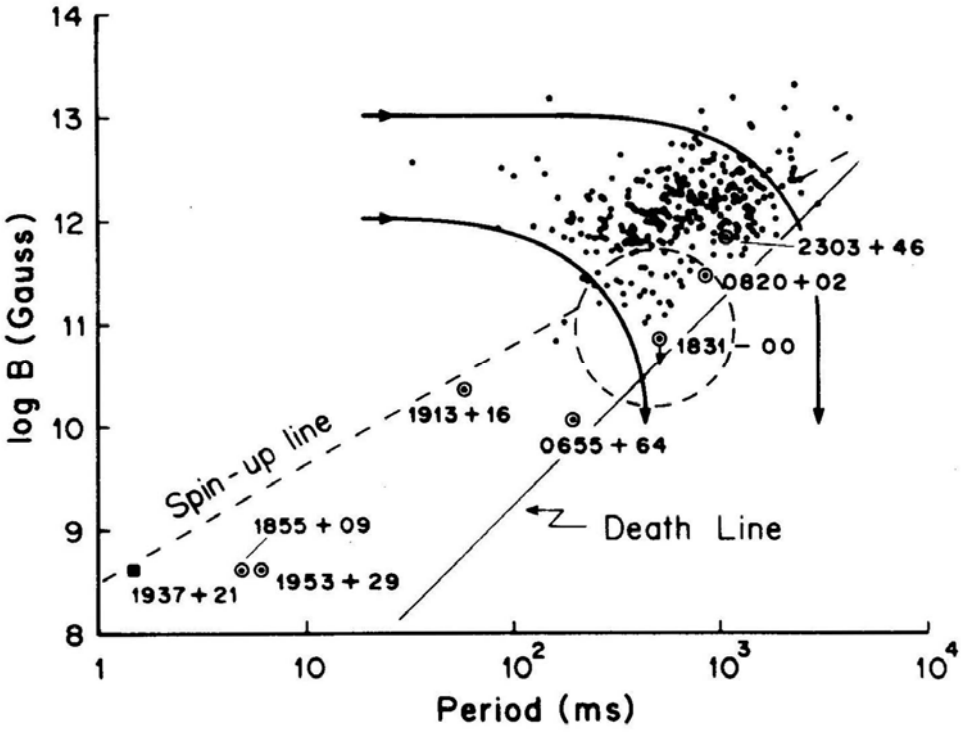

Figure 9: (from Srinivasan 1991) The distribution of observed pulsars. As argued in the text, it is quite likely that the low field pulsars inside the *dashed circle* did not evolve from the left of the diagram due to rapid field decay (as was suspected earlier), but were "injected" close to the spin-up line. In other words, these are most likely *recycled pulsars*.

Let us first concentrate on the encircled pulsars in Fig; 9 with fields less than $10^{11\,5}$ G. Let us ask how these pulsars would have evolved to their present position in the diagram. They could have evolved from the left. In this scenario there are two possibilities. If one entertains field decay with relatively short timescales, then their evolutionary track would be the curved line in the figure. Indeed one should say this in exactly the opposite manner! It is this argument that led to a field decay timescale of 3 – 4 Myr that was popular a few years ago. Such a short decay timescale is definitely not preferred now.

This leaves open the possibility that these pulsars evolved horizontally from the left. If this is the case one would expect to see at least a few pulsars with similar fields but shorter periods. Since such pulsars would have higher luminosities by virtue of their higher periods their absence cannot be easily attributed to selection

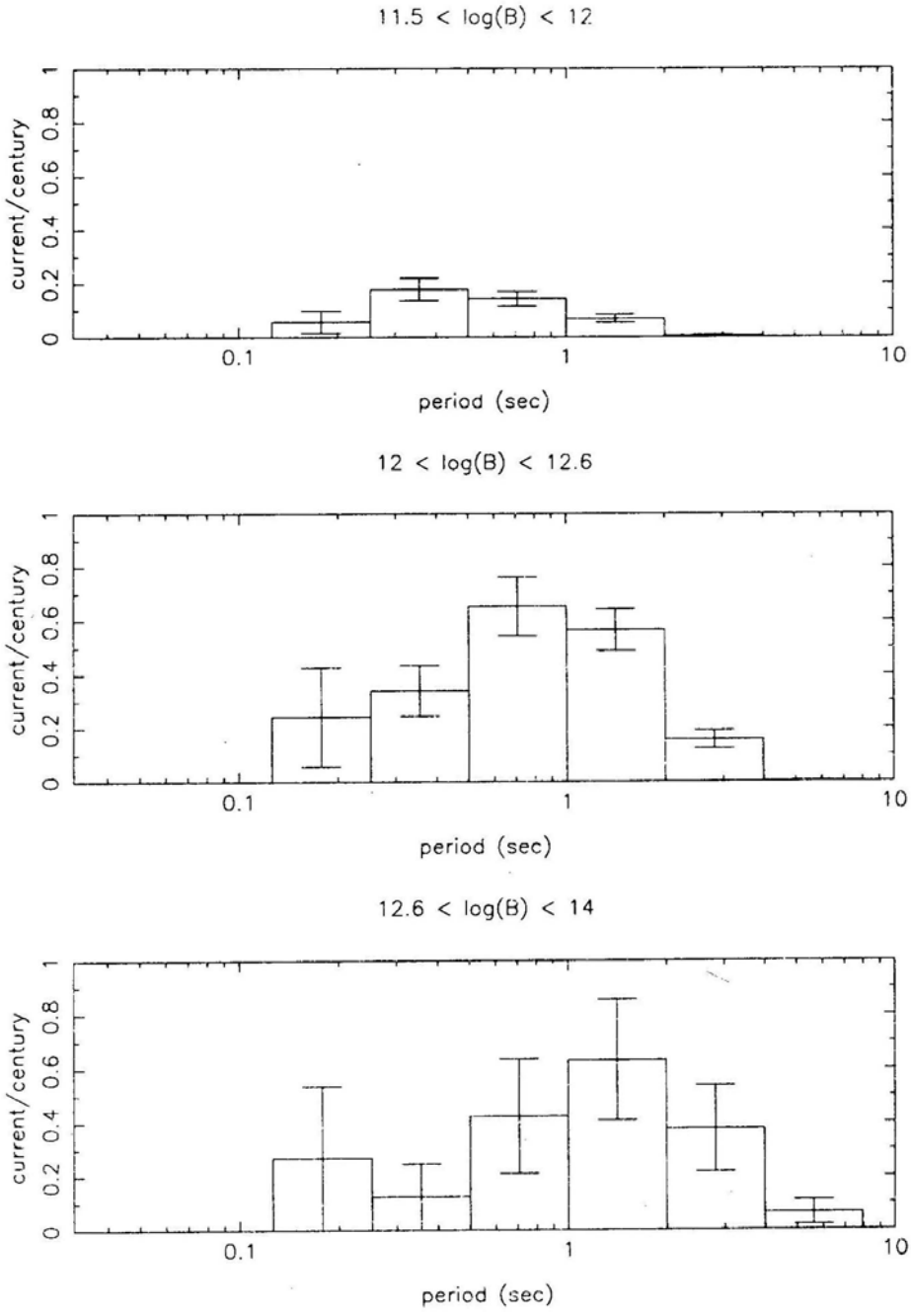

Figure 10: The current distribution shown in Fig. 2 has been binned into three magnetic field ranges. As may be seen, it is only in the central panel which corresponds to $12 < \log B < 12.6$ that one sees a *step* in the current at a period of about 0.5 s.

effects. But this could easily be due to their low birth rate. That their birth rate is low can be easily deduced from their contribution to the *current* Pulsars in this field range are born once in about 5000 years. Thus one cannot rule out the possibility that these low field solitary pulsars evolved from the left. But there is an argument which suggests that this might not have been the case. Let us return to the true number distribution of pulsars shown in Fig. 5. To recall, this distribution is obtained from the observed distribution by allowing for various selection effects. It may be seen in the figure that the low field pulsars that we have been discussing seem to form a distinct island. In other words, there appears to be a 'valley' between the population of high field and low field pulsars. To test the statistical significance of this valley we performed some simulations by scrambling the periods and magnetic fields of the pulsars in the distribution. (To be more precise, the *P*s were scrambled keeping the luminosity distribution unchanged.) From a large number of simulations we find that the valley in the number distribution of pulsars has a significance level 98.37%.

If one takes this seriously then one has to either invoke a bimodal distribution of magnetic fields at birth, or conclude that the low field pulsars possibly evolved to their present position from the *right* in the diagram. In other words, they might be recycled pulsars from binary systems.

Let us now move to the upper island of pulsars in Fig. 5 and ask whether there is any sign of injection of pulsars close to the spin-up line. A signature of such an injection of recycled pulsars into the island of solitary pulsars would be a *step* in the current close to the spin-up line. The integrated current of pulsars over the entire field range shown in Fig. 2 suggests a step in the current at a period around 0.5 s. In Fig. 10 we have once again shown the current distribution but this time binned into different field ranges. As may be seen, a step in the current is seen only in the field range 10^{12} – $10^{12.6}$ G. Admittedly the formal statistical significance of this feature is not very high. But the fact that there is a correlation between the period at which such an injection occurs and the magnetic fields of the injected pulsars suggests that one might take this seriously. Given this correlation between the rotation periods and magnetic fields one is led to the conclusion that this injection may be associated with recycled pulsars making their appearance close to the spin-up line. Narayan and Ostriker (1990) also found such a feature in their detailed statistical analysis (which was not based upon the current of pulsars).

The correlation between the rotation periods and the magnetic fields of the injected population may be seen better in Fig. 11. where we have plotted the current as a contour diagram in the B-P plane. This current is calculated using eqn. 1 in various magnetic field "bins". Concentrating for a moment in the field range $10^{12} < B < 3 \times 10^{12}$ G, one can see that the current builds up rather continuously till a period of about 0.5 s, at which there is a step or a cliff. (As may be readily seen, the contour plot reveals many "hills". These are merely individual high $\dot{P}$ pulsars which appear as "little hills" due to the fact that the current distribution has been smoothed with the function shown in the right hand bottom corner of the plot. Contrary to this, the step in the current referred to above, and also discussed in the above paragraph, is a statistically significant feature since a fairly large number of pulsars contribute to it.). Also shown in the figure are two equilibrium period lines corresponding to the Eddington accretion

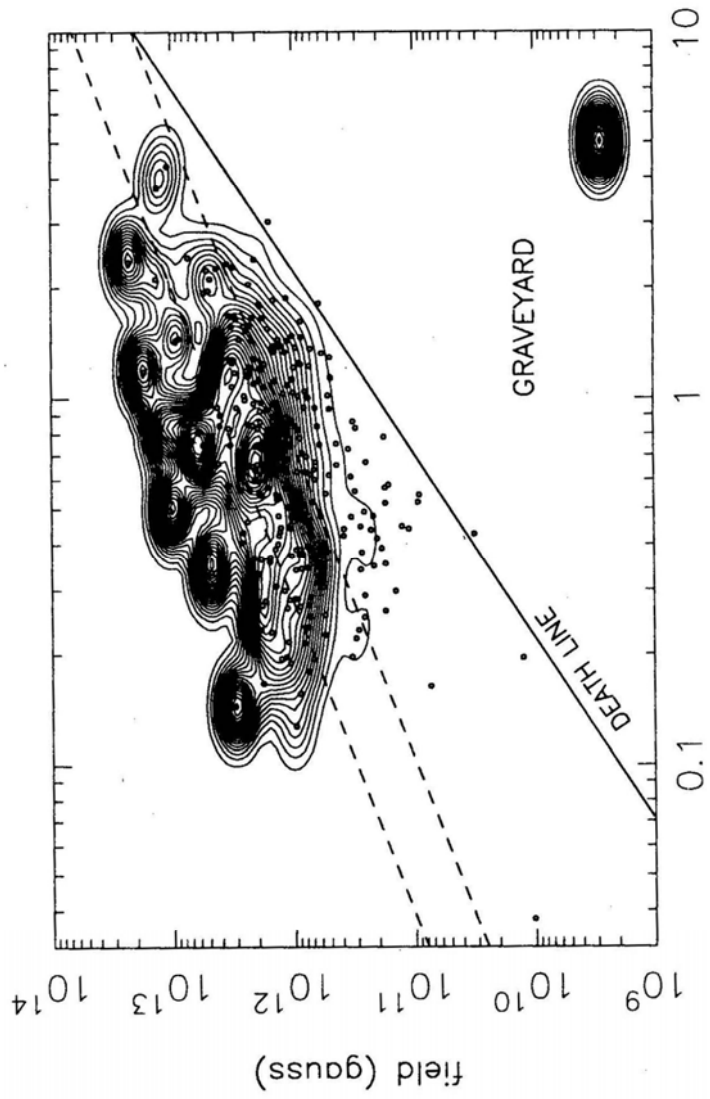

Figure 11: This shows the current distribution as a function of the period and magnetic field. This distribution has been smoothed with a function shown in the bottom right hand corner of the panel. Most of the "hills" seen in this distribution corresponds to individual high $\dot{P}$ pulsars. But the distinct "cliff" in the field range $10^{12} < B < 3 \times 10^{12}$ G and a period around 0.5 s is a statistically significant feature since a fairly large number of pulsars contribute to it. It is this step in the current close to the upper spin-up line ($\dot{M} = 10\dot{M}_{Edd}$) that we interpret an injection of recycled pulsars from massive binaries.

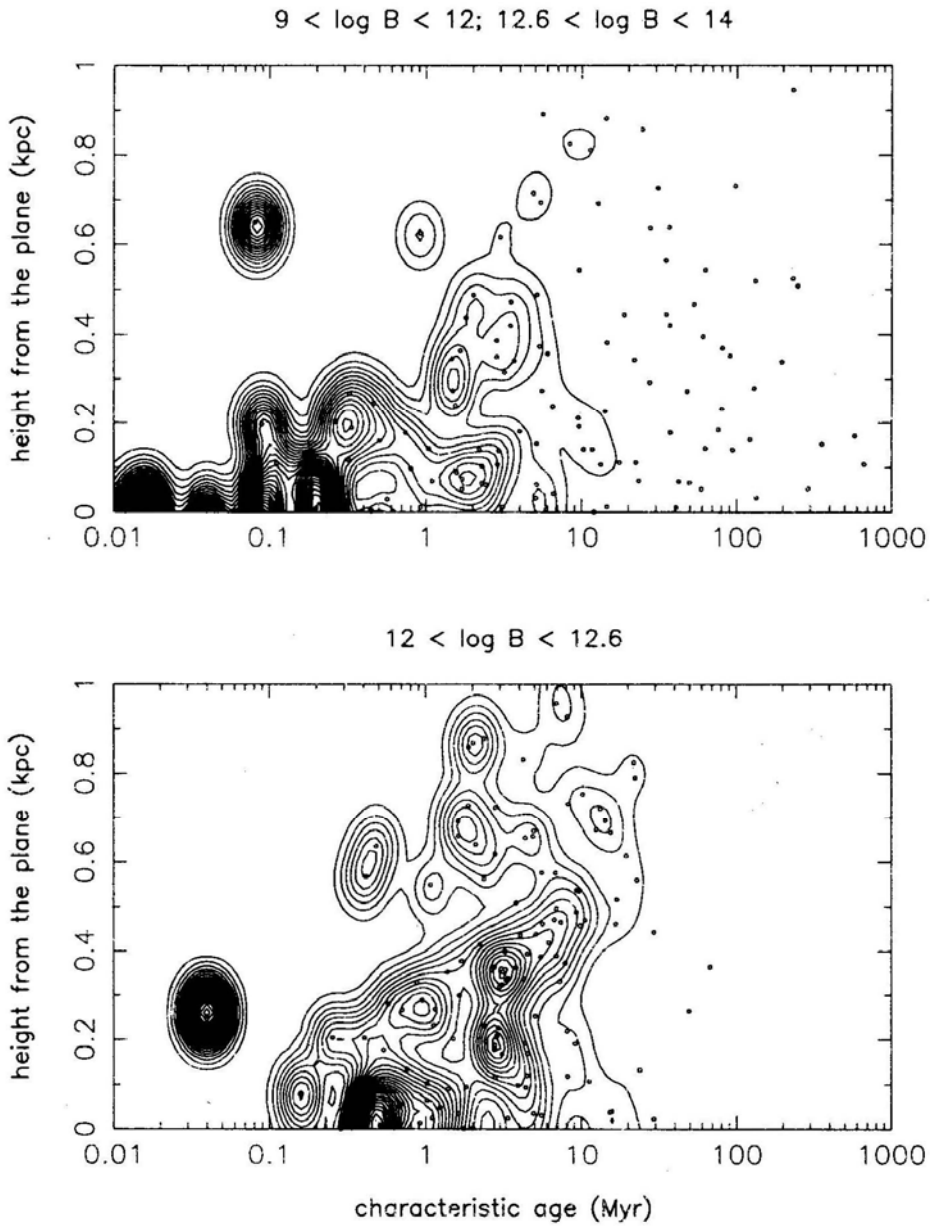

Figure 12: The pulsar current as a function of the characteristic age and the height z from the galactic plane. (a) In this panel we have deliberately *excluded* pulsars in the field range $12 < \log B < 12.6$ in which we believe there may be a substantial, fraction of recycled pulsars. The distribution shown is easily understood in terms of the majority of pulsars being born close to the galactic plane and migrating away from it due to velocities acquired at birth. (b) In this figure the current of pulsars in the magnetic field range $12 < \log B < 12.6$ alone is shown. We wish to suggest that this distribution is more consistent with pulsars not only being injected with a characterstic age of about 1 Myr but at a variety of distances from the galactic plane ranging all the way up to 800 pc.

rate and ten times its value. Therefore, if the injection is interpreted as due to recycled pulsars it would imply that they experienced accretion at a super-Eddington rate. In our opinion this is quite likely to happen in massive binary systems.

Further support for our conjecture that the injection of pulsars (at a period around 0.5 s and with magnetic fields in the range $12 < \log B < 12.6$) may be related to recycled pulsars comes from the distribution of these pulsars with respect to the galactic plane. Fig. 12 shows the pulsar current as a function of the characteristic age and the distance z from the galactic plane; the pulsars in the sample are shown as open circles. To bring out the point that something special may be happening in the field range mentioned above, we have shown the current distribution in two separate field ranges. In Fig. 12(a) we have *excluded* the field range $12 < \log B < 12.6$, and in Fig. 12(b) we have shown *only* those pulsars which have magnetic fields in this narrow range. Fig. 12(a) is consistent with majority of pulsars being born with relatively short periods and within a hundred parsec or so from the galactic plane, and their subsequent migration from the plane due to velocities acquired at birth. On the other hand, Fig. 12(b) looks very different. In our opinion this is more consistent with an injection of pulsars with characteristic ages of about 1 Myr and injected at a variety of distances from the galactic plane.

What could be the progenitors of these pulsars which explode at substantial distances from the galactic plane? It is conceivable that a certain fraction of binaries acquire substantial centre of mass velocities during the first explosion, and a certain fraction of them migrate *away* from the galactic plane. When such binaries disrupt during the second supernova explosion two pulsars will be released. The first-born will have the characterstics of a recycled pulsar, and the second one will have a short characterstic age at birth. In our opinion this offers a natural explanation for why some short characterstic age pulsars are seen to be moving *towards* the galactic plane (Harrison et al. 1993).

5. Summary

We wish to briefly summarize the main conclusions presented in this paper:

1. Our analysis of the current of pulsars yields a birth rate of 1 in 80 years.

2. There appears to be a strong correlation between the present distribution of pulsars and the location of the spiral arms of the Galaxy some 60 Myr ago.

3. If this correlation is confirmed, by future analyses using a larger population of pulsars then it would lead one to conclude that the majority of progenitors of pulsars must be relatively low mass field stars ($M \sim 7 - 10 M_{\odot}$) thus confirming the remarkable conjecture by Blaauw (1985).

4. Our analysis indicates that the population of solitary pulsars may include a certain fraction of recycled pulsars which were released from binaries that were disrupted during the second supernova explosion. Tentatively we would like to suggest that about 10% to 15% of solitary pulsars might have been processed in binary systems.

References

Baade, W., and Zwicky, F. 1934, *Phys. Rev*., **45,** 138.

Bhattacharya, D. 1994, i*n this volume.*

Blaauw, A. 1985, in *Birth and Evolution of Massive Stars and Stellar Groups*, Eds. W. Boland & H. van Woerden (Dordrecht: D. Reidel), p. 211.

Burton, W.B. 1971, *Astron. Astrophys*., **10,** 76.

Chandrasekhar, S. 1932, *Zeitschrift für Astrophysik*, **5** (5), 321.

Clark, D. H., and Caswell, J.L. 1976, *Mon. Not. R. Astr. Soc.,* **174,** 267.

Clark, D. H., and Stephenson, F.R. 1977, in *The Historical Supernovae*, Pergamon Press (Oxford).

Deshpande, A. A., Ramachandran, R., and Srinivasan, G. 1995, *J.Astrophys. Astr.,* **16,** 53.

Harrison, P.A., Lyne, A.G., and Anderson, B. 1993, *Mon. Not. R.Astr. Soc*., **261,** 113.

Kerr, F.J. and Lynden-Bell 1986, *Mon. Not. R.Astr. Soc*., **221,** 1023.

Lorimer, D.R., Bailes, M., Dewey, R.J., and Harrison, P.A. 1993, *Mon. Not. R.Astr. Soc*., **263,** 403.

Lyne, A.G., Manchester R.N., and Taylor, J.H. 1985, *Mon. Not. R.Astr. Soc*., **213,** 613.

McKee, C.F., and Ostriker, J.P. 1977, *Astrophys. J*., **218,** 148.

Narayan, R. 1987, *Astrophys. J*., **319**, 162.

Narayan, R., and Ostriker, J.P. 1990, *Astrophys. J*., **352,** 222.

Phinney, E.S., and Blandford, R.D. 1981, *Mon. Not. R.Astr. Soc*., **194,** 137.

Radhakrishnan, V., and Srinivasan, G. 1981, *Proc. of the 2nd Asia-Pacific Regional Meeting in Astronomy*, Bandung, Eds. B. Hidayat and M.W. Feast [Tira Pustaka, Jakarta (1984)], p. 423.

Ramachandran., R., and Deshpande, A.A. 1994, *J. Astrophys. Astr*., **15,** 69.

Srinivasan, G., Bhattacharya, D., Muslimov, A.G., and Tsygan, A.I. 1990, *Curr. Sci*., **59,** 31.

Taylor, J.H., and Cordes, J.M. 1993, *Astrophys. J*, **411,** 674.

Taylor, J.H., Manchester, R.N., and Lyne A.G. 1993, *Astrophys. J.Suppl. Series*, **88,** 529.

Tinsley, B.M. 1977, in *Supernovae*, ed. D.N. Schramm, D. Reidel Publishing Co. (Dordrecht–Holland)

van den Heuvel E.P.J., and Habets, G.M.H.J. 1985, in *Supernovae Their Progenitors and Remnants*, Supplement to *J.Astrophys. Astron*., 129.

Vivekanand, M., and Narayan, R. 1981, *J. Astrophys. Astron*., **2,** 315.

Wheeler, J.C., Miller, G.M., and Scalo, J.M. 1980, *Astron. Astrophys*., **82,** 152.

Diamond Jubilee Symposium on Pulsars
14–17 March 1994
Raman Research Institute, Bangalore

J. Astrophys. Astr. (1995) **16,** 89–95

New Pulsar/Supernova Remnant Associations

W.M. Goss, D.A. Frail *National Radio Astronomy Observatory, Socorro, NM, USA*

J. B. Z. Whiteoak *School of Physics, University of Sydney, Sydney, Australia*

1. Introduction

In recent years numerous claims have been made of new pulsar/supernova remnant associations. The list of potential associations has grown to the point where there are as many as perhaps 17. This is a far cry from the early decades of pulsar astronomy when only the Crab and Vela pulsars had associated remnants. Progress in this field is in large part due to advances in high frequency pulsar surveys (Clifton et al. 1992, Johnston et al. 1992) and low frequency radio imaging efforts (Cornwell 1993).

It is impossible to overstate the importance of these associations in studying the origin and evolution of neutron stars. Through the study of young pulsars and their supernova remnants we can gain information about the periods, magnetic fields, and velocities of pulsars at their birth. The supernova remnant provides an independent age and distance estimate for the system and acts as a probe of the ambient gas (density, filling factor, pressure, etc.) (Shull, Fesen & Saken 1989). In a recent paper Frail, Goss & Whiteoak (1994) presented evidence for three new pulsar/supernova remnant associations based on VLA observations and drew some general conclusions from a study of all associations with characteristic ages τ_c <60,000 yrs. The purpose of this paper is to summarize those results and to discuss the implications of their findings.

2. New Associations

2.1 *PSR 1643–43 and G341.2+0.9*

PSR1643–43 has a period P of 232 msec, a characteristic age τ_c of 32.6 kyrs and a dispersion measure based distance of 6.9 kpc (Johnston et al. 1994). A 20-cm image toward PSR 1643–43 (Fig. 1) shows that it lies in an extended (22′ × 16′) radio source which is assigned the galactic source name G 341.2+0.9. Comparison with data at 90 cm shows that G 341.2+0.9 is a non-thermal source and likely a

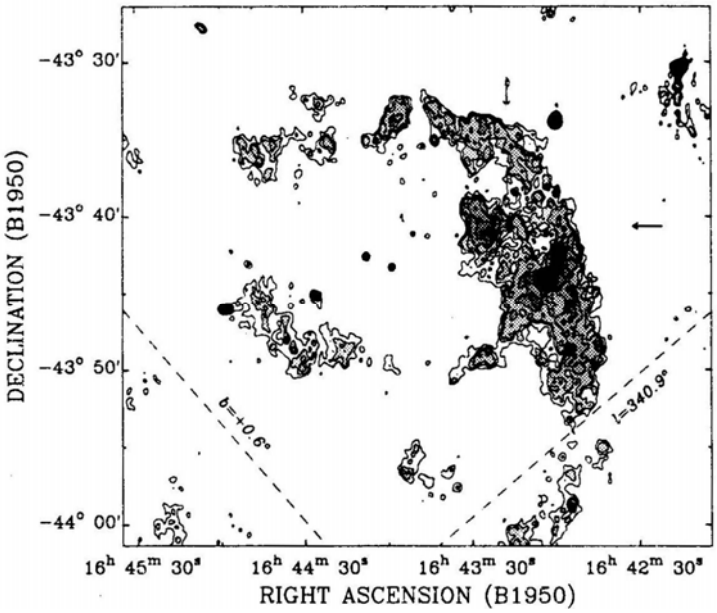

Figure 1: The PSR1643–43 and G 341.2+0.9 association. The position of the pulsar is indicated by the arrows.

supernova remnant with a Σ-D distance between 8.3-9.7 kpc (Milne 1979, Clark & Caswell 1976, Allakhverdiyev et al. 1983). In addition to the shell-type emission which brightens on the side closest to PSR1643–43, there is diffuse emission in the immediate vicinity of PSR 1643–43. This includes a 4′ nebulosity just east of the pulsar which is joined to the pulsar by a "bridge" of emission. The appearance of this structure is consistent with an implied westward motion of the pulsar.

Frail et al. (1994) argue that the similar distances of the pulsar and the supernova remnant and the morphological evidence, are strong indicators that a real physical association exists between this supernova remnant and the pulsar.

2.2 *PSR 1706–44 and G 343.1–2.3*

PSR 1706–44 has a period of 102 msec, a characteristic age of 17.5 kyrs and a dispersion measure based distance of 1.8 kpc (Johnston et al. 1994). McAdam, Osborne & Parkinson (1993) have claimed that a faint arc of radio emission, on which PSR 1706–44 is superimposed, is a supernova remnant and that the two objects were physically associated. New data by Frail et al. (1994) raise some questions about the validity of the association. PSR 1706–44 is indeed found on the edge of the non-thermal shell of G 343.1–2.3, 23′ south-east of the geometric center, but a higher resolution image at 20 cm (Fig. 2) shows a 4′ diameter radio

"halo" surrounding PSR 1706–44.

If the pulsar originated at the center of G 343.1–2.3 and traveled to its current position, then a cometary nebula pointing back to the center might be expected, much like that surrounding PSR 1757–23 outside G 5.4–1.2 (Frail & Kulkarni 1991). Furthermore there is no clear signs of an interaction between PSR 1706–44 and G 343.1–2.3. For these reasons Frail et al. (1994) considered the association between PSR 1706–44 and G 343.1–2.3 as unlikely but they could not could rule it out. Proper motion measurements should settle this issue.

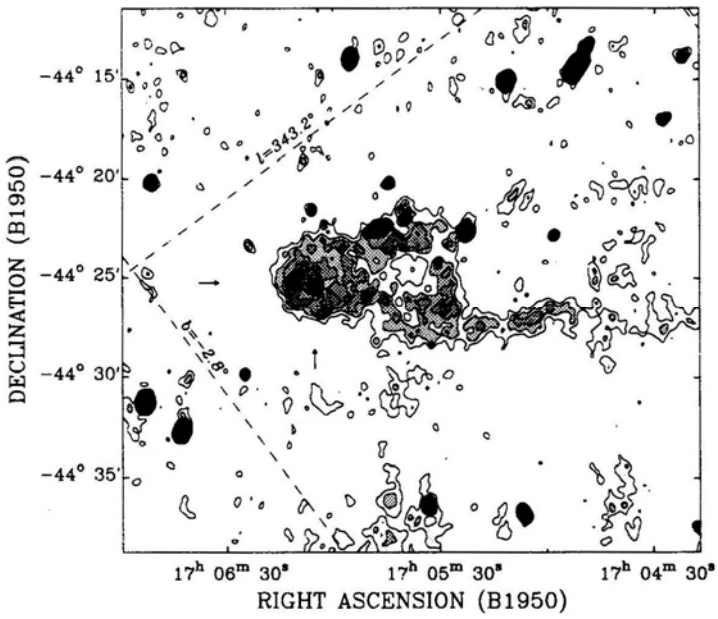

Figure 2: The PSR 1706–44 and G 343.1–2.3 association. The position of the pulsar is indicated by the arrows.

2.3 *PSR 1727–33 and G 354.1+0.I*

PSR 1727–33 has a period of 139 msec, a characteristic age of 26.0 kyrs and a dispersion measure based distance of 4.2 kpc (Johnston et al. 1994). The 20-cm image toward PSR 1727–33 shows a most unusual radio source. In addition to two bright HII regions G 354.486+0.085 and G 354.2–0.054 at a distance of 4.7-5.6 kpc there is a "contrail" of non-thermal emission that appears to originate from the pulsar. G 354.1+0.1 is not a typical shell-type or pulsar-powered SNR, but rather has the axisymmetric morphology of a rare class of non-thermal radio sources which includes G 357.7–0.1 (Shaver et al. 1985, Becker & Helfand 1985). Although it was once believed that the radio emission from these sources was

powered by an accreting binary (Helfand & Becker 1985), it is now more likely that it arises from the spindown energy of a young, high velocity pulsar (Predehl & Kulkarni 1994).

Frail et al. (1994) argue that PSR 1727–33 is at the same distance as the complex of HII regions and is physically associated with G 354.1+0.1.

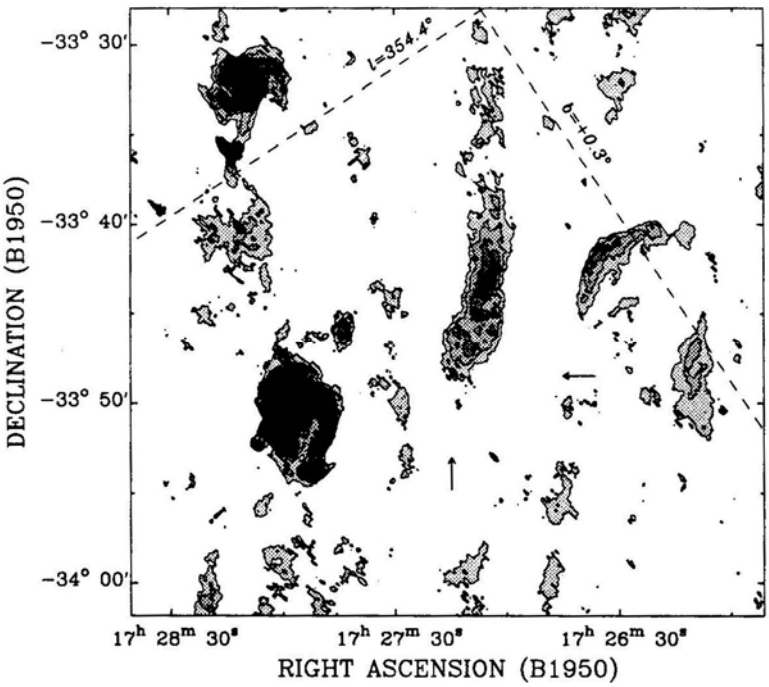

Figure 3: The PSR 1727–33 and G354.1+0.1 association. The position of the pulsar is indicated by the arrows.

3. Discussion

With the new association discussed above and a host of other associations that have been proposed in recent years (e.g Frail, Kulkarni & Vasisht 1993, Kaspi et al. 1992, Kassim & Weiler 1990, Kulkarni et al. 1993) it is worth taking a preliminary look at the data to draw some general conclusions on the current sample of pulsar/supernova remnant associations.

3.1 *The Mean Lifetimes of Supernova Remnants*

Earlier unsuccessful efforts (e.g Braun, Goss & Lyne 1989) to look for supernova remnants around young pulsars lead to the suggestion that the progenitors of pulsars exploded in low density environments ($n_o \simeq 0.01$ cm^{-3}), resulting in the

rapid expansion and dissipation of the remnant, which faded beyond detectability after $\simeq 10^4$ yrs (Bhattacharya 1990). Frail et al. (1994) re-examined this result and found that most remnants with associated pulsars were expanding into an ISM with a density of approximately 0.2 cm^{-3}. Furthermore, the radio lifetime of these supernova remnants is > 60, 000 years. Pulsars may play a role in extending these lifetimes (see below).

3.2 *The Distribution of Pulsar Velocities at Birth*

Proper motion studies (e.g. Harrison, Lyne & Anderson 1993) have established that pulsars are high velocity objects giving $\langle V_{PSR} \rangle \simeq 200$ km s^{-1}. However, there are well known selection effects in these samples (Cordes 1986, Helfand & Tademaru 1977) that limit our ability to measure the true distribution of pulsar velocities at birth.

Fortunately, an *inferred* velocity can be derived for the young pulsars associated with supernova remnants which is unaffected by this bias. The displacement of the pulsar from the geometric center of the remnant and the age of the pulsar gives a transverse pulsar velocity (Shull et al. 1989). Details of the method and the various difficulties and uncertainties are discussed more fully in Frail et al. (1994). The median value for V_{PSR} derived by this method is 480 km s^{-1}. Eliminating questionable associations does not significantly change the result. By correcting for the selection effect directly and using the newer Taylor & Cordes (1993) distance model Lyne & Lorimer (1994) have derived a mean pulsar birth velocity of 450±90 km s^{-1}.

3.2.1 The Distribution of Pulsars in the Galaxy

The implications of the existence of large numbers of high velocity pulsars is far-reaching; it has an impact on the mechanisms that give rise to pulsar velocities at birth, and it affects how they interact with their surroundings and what the final distribution of pulsars in the Galaxy will be. If this result holds up we will need to re-examine the birthrate of pulsars, their survival in binary systems and their escape from globular clusters and the Galaxy (Lyne & Lorimer 1994).

For example, if a significant population of high velocity pulsars exist then they could escape the disk, forming a halo population of old neutron stars. This extended halo population has been postulated to exist for many years in order to explain γ-ray bursts as a galactic phenomena (e.g. Li & Dermer 1992). While high velocity neutron stars no longer seem to be an "ad hoc" population, other problems remain if they are the progenitors of γ-ray bursts (Paczynski 1993). In order to not violate the high degree of angular isotropy seen by current γ-ray instruments, the high velocity pulsars must possess some special property (high B field?) that distinguish them from the low velocity objects and this is presumably related to the origin of the γ-ray bursts.

3.2.2 Interacting Composites

With $V_{PSR} \simeq 500$ km s^{-1} a pulsar catches up to its supernova remnant in only 40,000-70,000 years (Shull et al. 1989). Such pulsars will act as a "fountain

of youth" injecting fresh relativistic particles and field into the compressed shell of the aging remnant. Thus ambient density may not be the dominant factor influencing the radio lifetimes of supernova remnants. The distinction between shell-type remnants and pulsar-powered nebulae has been blurred, creating a new class of supernova remnants called "interacting composites". Examples may include a number of objects mentioned by Shull et al. (1989) like G 5.4-1.2, W28 and G 57.1+1.7 as well as G 114.3+0.3 (Kulkarni et al. 1993), G 308.8–0.1 (Kaspi et al. 1992), and MSH 15–52 (Caswell, Milne &·Wellington 1981).

4. Caveat Emptor

Some of the 17 pulsar/supernova associations that are currently known are less secure than others. Identifying those associations which are firmly established is an ongoing effort and a matter of active debate. Furthermore, some young pulsars seem to have no associated supernova remnant. Future efforts should concentrate on measuring proper motions to test the veracity of the associations. Both the magnitude and the direction of the velocity vector is useful in this regard. The former will test whether the high velocities are real and the latter will test the association (i.e. the pulsar must originate from the remnant). Instead of concentrating on the centers of supernova remnants, future searches for young pulsars would be well-advised to look both outside the remnant and in regions of the remnant where there is a local brightening, suggesting a possible pulsar/supernova remnant interaction.

Acknowledgements: The Very Large Array (VLA) is operated by Associated Universities, Inc. under cooperative agreement with the National Science Foundation.

References

Allakhrerdiyev, A. O., Amnuel, P. R., Guseinov, O. H. & Kasumov, F. K. 1983, Astrophy. & Sp. Sci., 97, 261

Becker, R. H. & Helfand, D. J. 1985, Nature, 313, 115

Bhattacharya, D. 1990, J. Astrophys. Astr., 11, 125

Braun, R., Goss, W. M. & Lyne, A, G. 1989, ApJ, 340, 355

Caswell, J. L., Milne, D. K. & Wellington, K. J. 1981, MNRAS, 195, 89

Clark, D. H. & Caswell, J. L. 1976, MNRAS, 174, 267

Clifton, T. R., Lyne, A. G., Jones, A. W., McKenna, J. & Ashworth, M. 1992, MNRAS, 254, 177

Cordes, J. M. 1986, ApJ, 311, 183

Cornwell, T. J. 1993, VLA Scientific Memorandum 164, National Radio Astronomy Observatory

Frail, D. A., Kulkarni, S. R., & Vasisht, G. 1993, Nature, 365, 136

Frail, D. A. & Kulkarni, S. R. 1991, Nature, 352, 785

Harrison, P. A., Lyne, A. G. & Anderson B. 1993, MNRAS, 261, 113

Helfand, D. J. & Becker, R. H. 1985, Nature, 313, 118

Helfand, D. J. & Tademaru, E. 1977, ApJ, 216, 842
Johnston, S., Manchester, R. N., Lyne, A. G, Kaspi, V. M. & D'Amico, N. 1994, A&A, in press.
Johnston, S., Lyne, A. G., Manchester, R. N., Kniffen, D. A., D'Amico, N., Lim, J. & Ashworth, M. 1992, MNRAS, 255, 401
Kaspi, V. M., Manchester, R. N., Johnston, S., Lyne, A. G. & D'Amico, N. 1992, ApJ, 399, L155
Kassim, N. E. & Weiler, K. W. 1990, Nature, 343, 146
Kulkarni, S. R., Predehl, P., Hasinger, G. &: Aschenbach, B. 1993, Nature, 362, 135
Li, H. & Dermer, C. D. 1992, Nature, 359, 514
Lyne, A. G., & Lorimer D. R. 1994, Nature, 369, 127
McAdam, W. B., Osborne, J. L. & Parkinson, M. L. 1993, Nature, 361, 516
Milne, D. K. 1979, Aus. J. Phys., 32, 83
Paczynski, B. 1993, in Compton Gamma Ray Observatory, eds M. Friedlander, N. Gehreis and D. J. Macomb (AIP: New York), p. 981
Predehl, P. & Kulkarni, S. R. 1994, Nature, submitted
Shaver, P. A., Salter, C. J., Patnaik, A. R., van Gorkum, J. H. & Hunt, G. C. 1985, Nature, 313, 113
Shull, J. M., Fesen, R. A., & Saken, J. M. 1989, ApJ, 346, 860
Taylor, J. H. & Cordes, J. M. 1993, ApJ, 411, 674

Diamond Jubilee Symposium on Pulsars
14–17 March 1994
Raman Research Institute, Bangalore

J. Astrophys. Astr. (1995) **16,** 97–106

Pulsar Velocities

A. G. Lyne and D. R. Lorimer *The University of Manchester, Nuffield Radio Astronomy Laboratories, Jodrell Bank, Macclesfield, Cheshire SK*11 9*DL*

Abstract. Radio pulsars have long been established as having high velocities that are probably produced in the violence of their formation in Supernovae (Gunn & Ostriker 1970; Lyne, Anderson & Salter 1982). Three recent developments have resulted in a reassessment of their velocities: the adoption of a new distance scale (Taylor & Cordes 1993), many new determinations of proper motion (Harrison, Lyne & Anderson 1993; Bailes et al. 1989; Fomalont et al. 1992) and the realisation (Harrison & Lyne 1993) that estimates of speeds derived from scintillation measurements were systematically low by about a factor of 2. Taking into account a strong selection effect that makes the observed velocities unrepresentative of those acquired at birth, it seems that the mean space velocity of pulsars at birth is 450 ± 90 km s^{-1} (Lyne and Lorimer 1994), about a factor of 3 greater than earlier estimates. The general migration from the Galactic plane is consistent with birth in the supernova of massive Population I stars. An outstanding question is how such velocities are produced in the kinetics of supernova collapse. This large increase in birth velocity is likely to have a major impact upon our understanding of the retention of neutron stars in binary systems, globular clusters and the Galaxy as it exceeds or is comparable with all their escape velocities. The rapid spatial separation of fast and slow pulsars will have a profound effect upon calculations of the galactic population and birth rate, both of which have been underestimated in the past. Furthermore, the distribution of dead neutron stars will be more isotropic and may better match the distribution of the gamma-ray burst sources. A small number of pulsars are at a large distance from the Galactic plane, but moving towards it. The most likely origin of these objects lies in OB runaway stars.

1. Introduction

The space velocities of pulsars are important indicators of their formation process and ages. They also have important implications for the evolution of the observed

population and the subsequent distribution of neutron stars in the Galaxy. Considerable technical effort over the past 20 years has now resulted in estimates of the transverse velocities of about 15% of the known pulsar population, mostly for bright and nearby objects. Since pulsars have no spectral features of known frequency their radiation, their radial velocities are unknown and individual 3-D space velocities cannot be obtained, although they can be studied in a statistical sense.

2. Velocity Measurement Techniques

The transverse velocities V_t of pulsars can be estimated using two methods, one based upon angular proper motion measurements, the other upon the measurement of the velocity of the interstellar scintillation pattern of the pulsar radiation. The first method is more accurate but requires a long series of precise observations using a high-resolution radio interferometer or accurate timing data, while the second can be carried out using a single telescope for perhaps an hour and can be applied to large numbers of pulsars.

The transverse speed of a pulsar may be calculated from its proper motion μ (mas yr^{-1}) and distance D (kpc):

$$V_{\rm pm} = 4.74 \mu D \ {\rm kms}^{-1}. \tag{1}$$

Measurements of proper motion from timing observations are prone to the effects of timing noise and, with the exception of millisecond pulsars, are usually less precise than direct astrometric techniques. Pulsar proper motions are now available from high-resolution interferometry for a total of 87 pulsars (Lyne, Anderson & Salter 1982; Bailes et al. 1989; Fomalont et al. 1992; Harrison, Lyne & Anderson 1993).

It was recognized soon after the discovery of pulsars that the interstellar scintillation properties of pulsar radiation (Scheuer 1968; Rickett 1970) might allow the transverse speed of a pulsar to be measured from the speed of the scintillation pattern as it moves across the Earth. Initially this was carried out using spaced receiver observations (Galt & Lyne 1972; Slee et al 1974), but later it was realized that it was possible to estimate the pattern speed from the fading time of the scintillation pattern, using a single telescope (Lyne & Smith 1982).

The speed of the interstellar scintillation pattern across the Earth, $V_{\rm iss}$, is usually (Lyne & Smith 1982; Cordes 1986) calculated from the characteristic bandwidth $\Delta\nu_{\rm iss}$ (MHz) and characteristic time-scale $\Delta\tau_{\rm iss}$ (s) observed at a radio frequency ν (GHz):

$$V_{\rm iss} = A \times (\Delta\nu_{\rm iss} D)^{0.5} / (\nu \, \Delta\tau_{\rm iss}) \ {\rm kms}^{-1}. \tag{2}$$

The constant A depends upon the spatial power spectrum of the irregularities and the distribution of scattering material along the line of sight between the pulsar and the Earth. It is estimated by Cordes (1986) to have a value of 1.27×10^4 for a Kolmogorov spectrum, provided that the scattering irregularities are uniformly distributed along the line of sight. In this case, the speed of the scintillation pattern relative to the scattering medium will be equal and opposite in direction to that of the pulsar, and the qualitative behaviour of the scintillation pattern

can be described by the thin-screen approximation (Scheuer 1968). Lyne & Smith (1982) used this method of speed determination and compared the results with those found by Lyne, Anderson & Salter (1982) from interferometric proper motion measurements. Although they noted some systematic departures, they confirmed that the scintillation method was valid and that it is largely the pulsar motion which determines the rate of scintillation, rather than instability in the pattern caused by shearing motions within the medium.

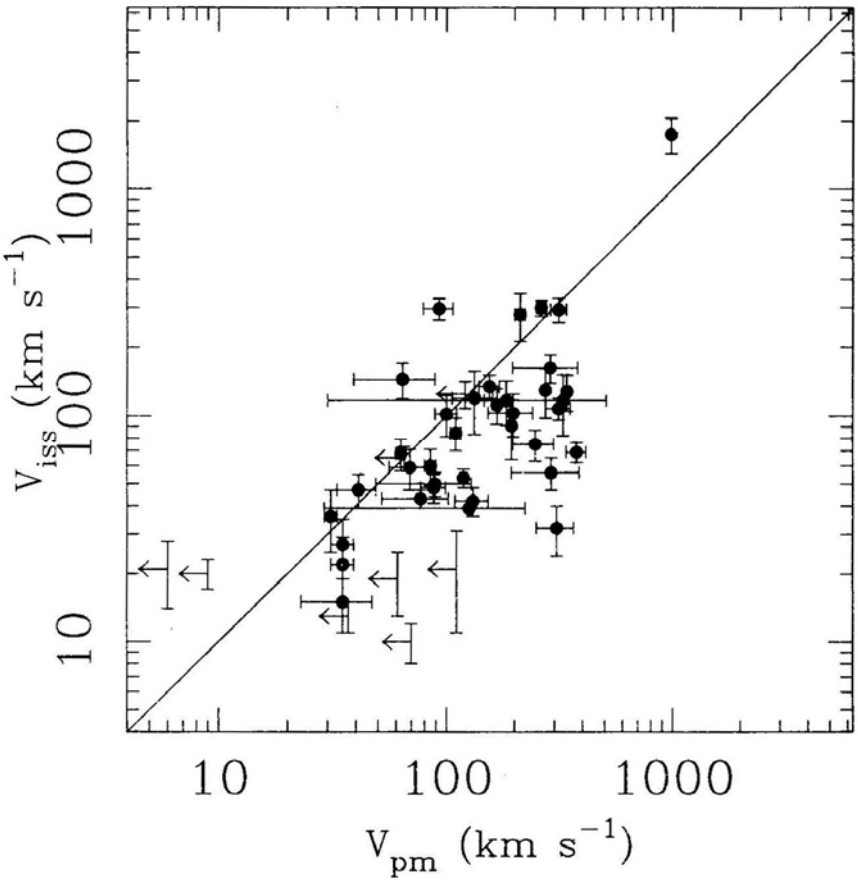

Figure 1: The transverse speeds of pulsars obtained from scintillation measurements V_{iss} plotted against those determined from proper motion V_{pm} (After Harrison & Lyne 1993).

The largest sample of scintillation speeds contains 71 pulsars and has been collected by Cordes (1986). Recent proper motion measurements using MERLIN on a sample of 44 pulsars (Harrison, Lyne & Anderson 1993) have permitted a reassessment of the method (Harrison & Lyne 1993). There are clear systematic differences between the two methods of velocity determination. In particular, Harrison & Lyne (1993) showed that the values of $V_{\rm iss}$ are smaller than $V_{\rm pm}$ by

about a factor of approximately 2 (Figure 1). Moreover, they found that the discrepancy was even greater for pulsars at large z-height from the galactic plane and smaller for those at small z-height. They noted that if most of the scattering occurs in a screen close to the Earth, then there will be a leverage effect, and the pattern speed will be less than the pulsar speed. It seems clear that the scintillation velocities were previously systematically underestimated because of a concentration of scattering material close to the Galactic plane with a scale-height of less than 100 pc. Once the velocities have been corrected for such systematic effects (Harrison & Lyne 1993), it is still found that the scintillation speeds differ from the proper motion ones by up to a factor of 2 in either direction in individual cases. These differences must be due to unmodelled variations in the position of scattering material along the line of sight and, to a lesser extent, due to errors in the distance which enters the velocity ratio as the square root.

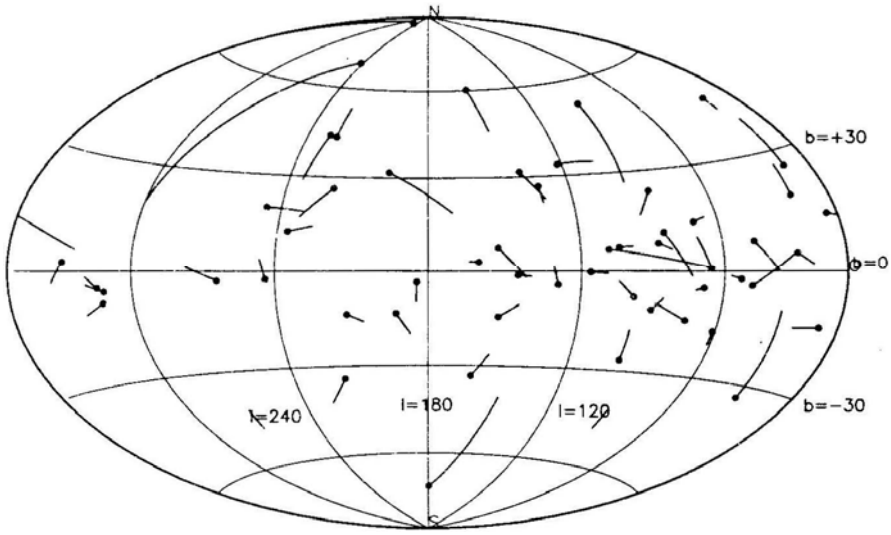

Figure 2: The galactic distribution of pulsars and their velocity vectors. The tails represent the approximate paths.travelled during the last million years (After Harrison, Lyne & Anderson 1993).

3. Pulsar Birth Velocities

The velocity vectors obtained from proper motion measurements are shown in figure 2 and demonstate a general migration from the galactic plane. These are mostly consistent with pulsar birth in a progenitor, population I, layer close to the plane, from which their velocities subsequently carry them away. Most of the pulsars which appear to be moving towards it are still within the progenitor layer, while some others at high latitude may in fact be moving away from the galactic

plane if they have a reasonable value of radial velocity. However, there are about 4 pulsars which are at large Z distance and are undoubtedly moving towards the plane (Harrison, Lyne & Anderson 1993). These objects may have their origin in the massive OB runaway stars.

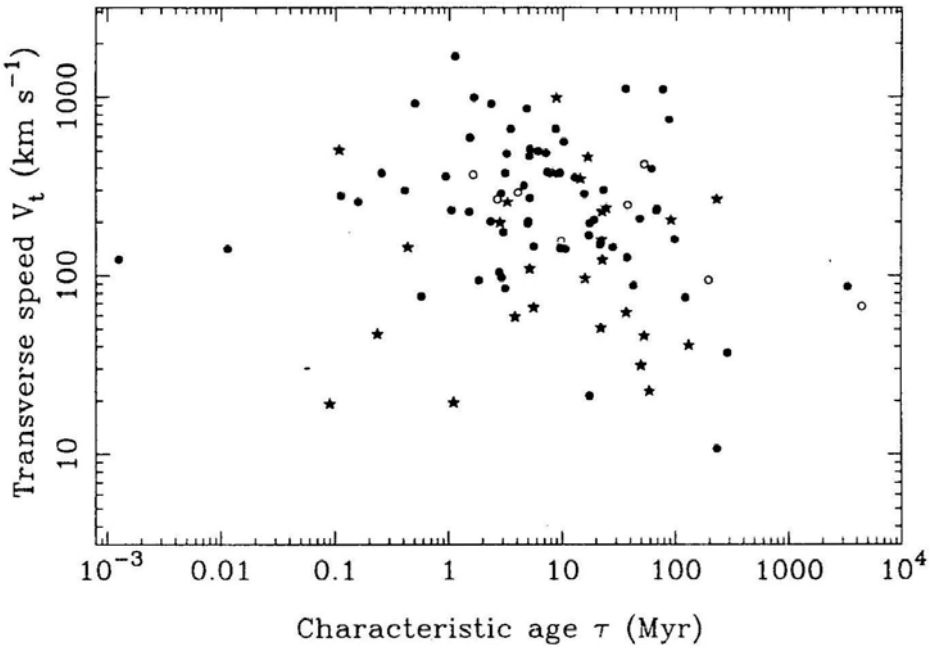

Figure 3: The transverse speed V_t of 99 pulsars plotted against characteristic age $\tau = P/2\dot{P}$, where P and $\dot{P}$ are the pulsar rotation period and time derivative. Pulsars with only upper limits to their transverse speed are represented by open circles at half the upper limits. Starred symbols represent transverse speeds obtained from scintillation data. The mean transverse speed for the 29 pulsars younger than 3 Myr is 345 km s^{-1}. In the unlikely circumstance that the two young pulsars in this group with upper limits have zero speed, this value would only be reduced by 6%.

Lyne & Lorimer (1994) have recently reassessed the velocities of normal, solitary pulsars and have used the 87 velocities derived from the proper motion data, apart from PSR B0736–40 which lies behind the Gum nebula and has an unknown distance in excess of 0.5 kpc. The distances D required to calculate the velocities were obtained from the new electron density model of Taylor and Cordes (1993) which is based upon a number of new independent distance measurements and which clearly shows that previous models had underestimated the distance to nearby pulsars. Because of the imprecision of the scintillation velocities, Lyne and Lorimer (1994) relied where possible upon the more direct proper motion measurements. However, for 14 pulsars which only have upper limits to their proper motion and a further 13 which do not have proper motion data, the scintillation data (Cordes 1986; Fruchter 1988) were used to estimate V_t. These scintillation speeds

have been calculated using the new distance model (Taylor & Cordes 1993) and the appropriate correction for the medium localisation (Harrison & Lyne 1993). Thus the sample contains 99 pulsars, of which only 8 have upper limits to V_t.

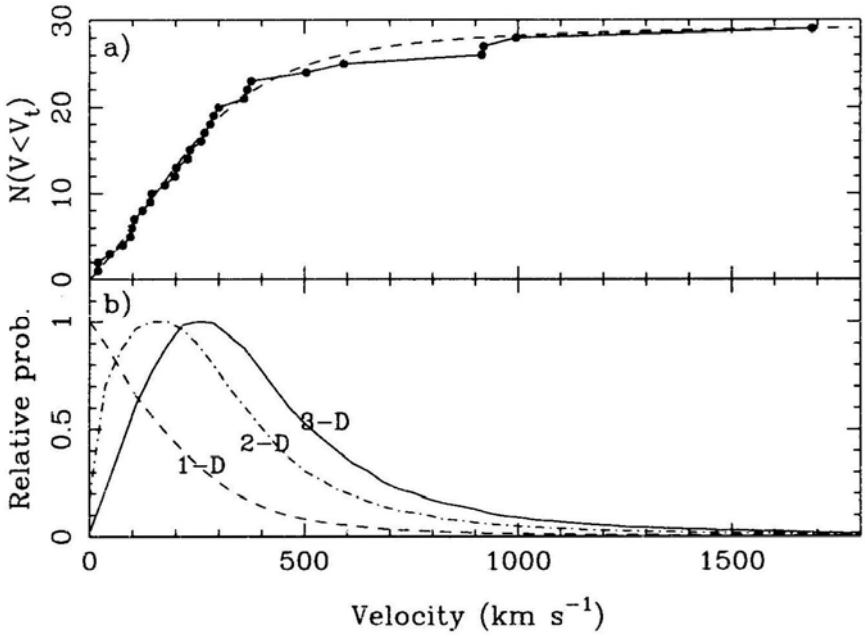

Figure 4: a) The cumulative distribution of transverse speeds V_t for the 29 pulsars younger than 3 Myr. For these pulsars, the selection effect against detecting high velocity pulsars is negligible and this is a good representation of the 2-D speed distribution at birth. The dashed curve is an analytic approximation to the data having the same mean and r.m.s. (see text), b) The 1-D, 2-D and 3-D velocity distributions corresponding to the analytic function in (a), obtained using an iterative Monte Carlo simulation. The 3-D distribution shows that pulsars have a mean space velocity of about 450 kms $^{-1}$.

This sample has a mean V_t of 300 ± 30 km s $^{-1}$, compared with 134 km s^{-1} obtained 12 years ago from 26 measurements (Lyne, Anderson & Salter 1982). The increase in value reflects the change in the adopted distance scale (Taylor & Cordes 1993), and also the greater number of young and higher velocity pulsars observed in the recent astrometric surveys (Harrison, Lyne & Anderson 1993; Bailes et al 1989; Fomalont et al. 1992). The much improved statistics also show that this velocity is not representative of the velocities at birth since we see that young pulsars on average have higher velocities than older ones (Harrison, Lyne & Anderson 1993). This can be seen in Fig. 1 in which the transverse speed of pulsars is plotted against characteristic age and surely does not arise because pulsars slow down significantly as they age. Rather, it is due primarily to a selection effect, first recognised by Cordes (1986): young pulsars are born from Population I stars, close to the galactic plane, and those pulsars with high

velocity mostly move rapidly away from the plane (1000 km $s^{-1} \approx 1$ kpc Myr^{-1}). After about 10 Myr, the mean distance of the fastest pulsars from an observer on the galactic plane is significantly greater compared with their mean distance at birth, reducing their likelihood of detection and hence lowering the apparent mean velocity. By this time, the pulsars remaining within detectable range are those with small velocity and a few high velocity ones moving roughly parallel to or towards the plane of the Galaxy (Harrison, Lyne & Anderson 1993).

During the first 3 million years, the strength of the above selection effect is minimal and the observed transverse speed distribution of the 29 pulsars younger than this should be a good representation of the true V_t distribution at birth. This distribution has a mean of 345 ± 70 km s^{-1} and an r.m.s. of 499 km s^{-1}. The mean velocity of only 105 ± 25 km s^{-1} for the 10 oldest pulsars illustrates the strength of the effect.

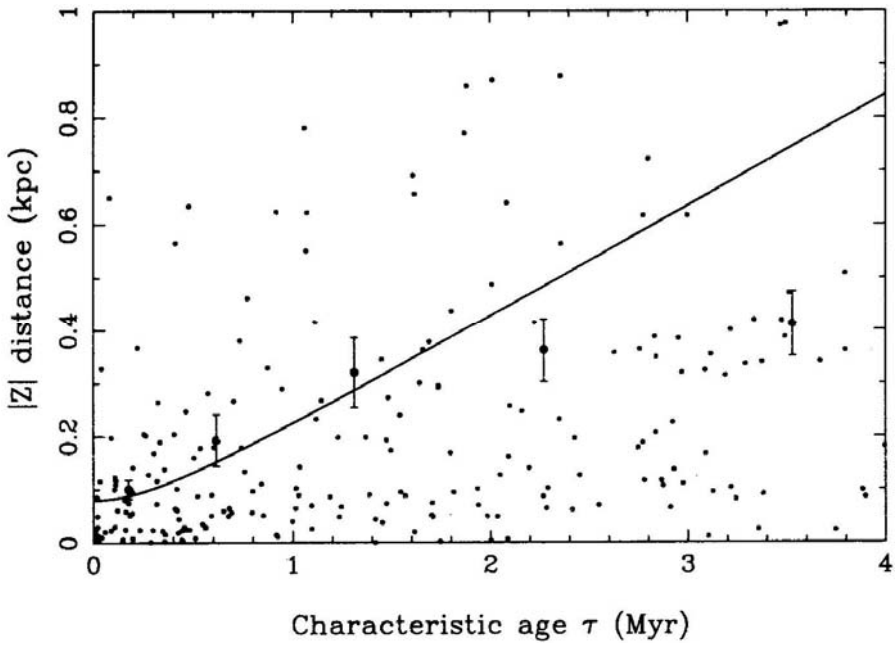

Figure 5: The distance of pulsars from the galactic plane $|Z|$ shown as a function of characteristic age τ for all the pulsars detected in the major pulsar surveye. The large symbols represent the means of groups of 40 pulsars. The line shows the variation expected from a simple dynamical model with the mean velocity derived from Fig. 4.

The 3-D space velocities must of course be somewhat greater than the observed 2-D transverse velocities, and we can estimate them statistically if we make the reasonable assumption that the velocities at birth are isotropic. Lyne & Lorimer (1994) used a simple, iterative Monte Carlo technique to determine the 1-D and 3-D velocity distributions required to give the observed 2-D transverse distribution. A cumulative plot of this observed distribution is compared with the model one

in Fig. 4a and the derived distributions are shown in Fig. 4b. From the 3-D distribution, it seems that the space velocity of pulsars at birth has a mean of 450 ± 90 km s^{-1} and an r.m.s. value of 535 km s^{-1}. This mean space velocity is a factor of three higher than the value of ~ 150 km s^{-1} deduced from the earlier sample (Lyne, Anderson & Salter 1982). The increase arises from the 3 main factors described above; namely a younger, faster sample (× 1.4), the new distance model (× 1.6) and the selection effect (× l.2).

There are two other indications that the birth velocities are large: firstly, such high birth velocities will give rise to a rapid migration from the galactic plane with a mean velocity V_z equal to 210 km s^{-1}, the mean of the 1-D distribution in Fig. 4b. This is clearly seen for the whole observed pulsar population in Fig. 5 as an increase in the mean distance Z of pulsars from the galactic plane with age. Assuming that pulsars are born in a progenitor Population I distribution with a width in Z of 80 pc, then pulsars of age τ will have a mean height given approximately by $Z = \sqrt{Z_0^2 + V_Z^2 \tau^2}$. This function is also shown in Fig. 5 and describes the data well for ages below about 2 Myr, confirming the large velocity dispersion. For older pulsars, the selection effect described earlier reduces the detected number of large Z pulsars and hence the mean Z of the observed population.

Secondly, the high transverse velocities found here are close to estimates of the velocities of young pulsars required by associations of pulsars with supernova remnants (Caraveo 1993). These associations are usually made on the basis of similarity of age, distance and position on the sky. Often the pulsar has moved significantly from the centre of the remnant since the supernova explosion, and the pulsar velocity can be determined from the ratio of the separation and the age. Taking 13 reasonably convincing associations, we find that the mean transverse pulsar velocity is about 530 ±180 km s^{-1}. Using the same form of velocity distribution as above, this implies a mean space velocity of 690 ± 230 km s^{-1}.

4. The Velocities of Binary and Millisecond and pulsars

The velocities of a handful of millisecond pulsars have been measured, mostly from measurements of proper motion from timing observations, made possible by the high rotational stability of these objects (e.g. Kaspi, Taylor & Ryba 1994; Bell et al. 1994; Nice & Taylor 1995). Some estimates have been made from scintillation measurements (e.g. Nicastro & Johnston 1995). The corresponding transverse velocities of these objects are almost without exception less than 100km s^{-1}, This is not surprising, as the large ages of such pulsars will result in any higher velocity ones occupying a much greater scale height above the galactic plane, making them more difficult to detect. In fact, a birth velocity distribution with a mean of 80 km s^{-1} or greater seems to be required to explain the wide observed Z distribution (Lorimer 1995). They probably do have much smaller velocities than normal pulsars since they have, or are believed to have had, stellar companions at some time since their formation. It seems likely that these objects represent the minority of neutron stars which were formed in binary systems with small velocity kicks, those with large velocities being disrupted. The binary systems which did survive the formation event will also be somewhat more massive than a single neutron

star, because of the presence of the companion, so reducing the systemic velocity kick even further.

5. Discussion

It is now clear that most pulsars are born with velocities of around 400-500 km s^{-1}. These large values indicate that their origin must lie in the kinetics of asymmetric supernova collapse rather than the disruption of binary systems (Dewey & Cordes 1987; Bailes 1989). The kinetic energy of the neutron stars so formed are an order of magnitude greater than previously thought. Although the mechanisms of such collapse are not well understood, the high degree of asymmetry now required might also be expected to show corresponding asymmetry in the gaseous supernova remnant in the opposite direction to the pulsar velocity.

While most recent statistical studies of the pulsar population and its evolution (Narayan & Ostriker 1990; Bhattacharya et al. 1992; Lorimer et al. 1993) have taken account of the spatial separation of fast and slow pulsars, this effect has been underestimated by a factor of 3 and they will need to be repeated. Similarly, the increase in birth velocity will clearly have a major effect upon our understanding of the number of pulsars that remain bound in binary systems, globular clusters and the Galaxy. While such high velocities make it easier to understand the small number of pulsars in binary systems (Bhattacharya & van den Heuvel 1991), the small proportion ($\sim$ 0.7%) with velocities below about 50 km s^{-1} make the large population of neutron stars in globular clusters surprising unless they are formed in a less violent scenario such as accretion induced collapse of a white dwarf (Bailyn & Grindlay 1990).

With mean birth velocities of 450 km s^{-1}, more than half of all pulsars will escape the galactic gravitational potential. Those that remain bound will form a much larger spherical halo of old neutron stars than previous models suggested (Paczy'nski 1990; Frei, Huang & Paczy'nski 1992; Blaes & Madau 1993). Such a distribution will more nearly match that required to produce the isotropic distribution of gamma-ray bursts observed by the Burst and Transient Source Experiment (Meegan et al. 1992). This provides some support for the possibility that old, high velocity pulsars are the source of the bursts (Hartmann, Epstein & Woosley 1990; Li & Dermer 1992), although it seems that only the high velocity tail of the distribution could provide a population of sufficient isotropy.

References

Bailes M., Manchester R. N., Kesteven M. J., Norris R. P., Reynolds J. E., 1989, ApJ, 343, L53

Bailes M., 1989, ApJ, 342, 917

Bailyn C. D., Grindlay J. E., 1990, ApJ, 353, 159

Bell J. F., Bailes M., Manchester R. N., Weisberg J. M., Lyne A. G., 1994, submitted to Ap. J.

Bhattacharya D., van den Heuvel E. P. J., 1991, Phys.Rep., 203, 1

Bhattacharya D., Wijers R. A. M. J., Hartman J. W., Verbunt F., 1992, AA, 254, 198
Blaes O., Madau P., 1993, ApJ, 403, 690
Caraveo P. A., 1993, ApJ, 415, L 111
Cordes J. M., 1986, ApJ, 311, 183
Dewey R. J., Cordes J. M., 1987, ApJ, 321, 780
Fomalont E. B., Goss W. M., Lyne A. G., Manchester R. N., Justtanont K., 1992, MNRAS, 258, 497
Frei Z., Huang X., Paczynski B., 1992, ApJ, 384, 105
Fruchter A. S., Taylor J. H., Backer D. C., Clifton T. R., Wolszczan A., 1988, Nat, 331, 53
Galt J. A., Lyne A. G., 1972, MNRAS, 158, 281
Gunn J. E., Ostriker J. P., 1970, ApJ, 160, 979
Harrison P. A., Lyne A. G., 1993, MNRAS, 265, 778
Harrison P. A., Lyne A. G., Anderson B., 1993, MNRAS, 261, 113
Hartmann D., Epstein R. I, Woosley S. E., 1990, ApJ, 3.48, 625
Kaspi V. M., Taylor J. H., Ryba M., 1994, ApJ, 428, 713
Li H., Dermer C. D., 1992, Nat, 359, 514
Lorimer D. R., Baues M., Dewey R. J., Harrison P. A., 1993, MNRAS, 263, 403
Lorimer D. R., 1995, MNRAS, in press
Lyne A. G., Lorimer D. R., 1994, Nat, 369, 127
Lyne A. G., Smith F. G., 1982, Nat, 298, 825
Lyne A. G., Anderson B., Salter M. J., 1982, MNRAS, 201, 503
Meegan C. A., Fishman G. J., Wilson R. B., Paciesas W. S., Pendleton G. N., Horack J. M., Brock M. N., Kouveliotou C, 1992, Nat, 355, 143
Narayan R., Ostriker J. P., 1990, ApJ, 352, 222
Nicastro L., Johnston S., 1995, MNRAS, in press
Nice D. J., Taylor J. H., 1995, ApJ, in press
Paczynski B., 1990, ApJ, 348, 485
Rickett B. J., 1970, MNRAS, 150, 67
Scheuer P. A. G., 1968, Nat, 218, 920
Slee O., Ables J. G., Batchelor R. A., Krishna-Mohan S., Venugopal V. R., Swarup G., 1974, MNRAS, 167, 31
Taylor J. H., Cordes J. M., 1993, ApJ, 411, 674

Diamond Jubilee Symposium on Pulsars
14–17 March 1994
Raman Research Institute, Bangalore

J.Astrophys. Astr. (1995) **16,** 107–117

The Shape of Pulsar Beams

R. N. Manchester *Australia Telescope National Facility, CSIRO, P. O. Box 76, Epping NSW 2121, Australia.*

Abstract. Observations of mean or average pulse profiles and their polarization give us much information on the shape of pulsar beams. The observed polarization variations, profile symmetry and frequency dependence of profile shape strongly suggest that the emission beam is conical and emitted from the vicinity of a magnetic pole. Central and outer parts of the beam have somewhat different properties, but the evidence is that they are emitted by the same basic mechanism. Recent observations suggest that the highly polarized pulse components seen in young pulsars may be emitted at a large angle to the magnetic axis.

1. Introduction

It is generally accepted that pulsars are rotating neutron stars. The fundamental frequency of the observed pulse train is then interpreted as the rotation frequency of the neutron star. One of the characteristic properties of pulsars is that, when an observed pulse train is folded at this fundamental frequency to form a mean or average pulse profile, this profile is (in most cases) extremely stable. Mean pulse profiles for different pulsars have some common properties, but differ in detail. For example, the pulsed emission is generally confined to a small portion (< 10%) of the pulse period, but some pulsars have one dominant component or peak, whereas others have several. Furthermore, the phase of this mean profile is very predictable – in fact, all precision timing of pulsars is based on observations of mean pulse profiles. This long-term stability implies that the mean profile is a cut through a radiation beam whose shape and orientation are fixed by relatively permanent features of the neutron star and its environs.

Another characteristic property of pulsar emission is that it is generally very highly polarized, with linear polarization dominating over circular. The form and phase of the polarization variations within mean profiles are also very stable. It is widely assumed that the polarization is determined by magnetic fields in or above the emission region, which are anchored to the solid neutron-star crust. Rapid swings of polarization position angle through the pulse, first observed in the Vela pulsar by Radhakrishnan et al. (1969), imply that the emission beam originates near a symmetry axis or vector which is fixed with respect to the neutron star.

For most pulsars, this 'rotating vector model' accounts very successfully for the observed position-angle variations (e.g. Rankin 1983; Lyne & Manchester 1988), at least when the presence of orthogonal modes (e.g. Stinebring et al. 1984) is recognized.

Again based on observations of the Vela pulsar, Radhakrishnan & Cooke (1969) proposed that the vector concerned was the dipole axis of the pulsar magnetic field. This interpretation, often known as the 'magnetic pole model', is supported by several of the observed characteristics of pulsar emission. The success of the rotating vector model in accounting for observed position-angle variations is certainly consistent with the magnetic pole model, but does not require it. Any vector fixed to the neutron star will do!

2. The Magnetic Pole Model

The magnetic pole model for pulsar beaming is popular, since many of the observed pulse properties can be readily accommodated within it. It also has theoretical backing (Sturrock 1971; Ruderman and Sutherland 1975; Arons 1983), although other theoretical ideas have been put forward (e.g. Michel 1987). As mentioned above, observed position-angle variations are generally consistent with the magnetic pole model. Other observational results which support the model are as follows.

Especially in pulsars of shorter period, a second pulse component is often observed midway, or very close to midway, between the main pulses. This interpulse may be interpreted as coming from the opposite pole of a dipole field.

Many mean pulse profiles have approximate time-reversal symmetry, that is, they are nearly symmetrical about the midpoint of the profile. Other properties, for example fluctuation characteristics or spectral properties, are also often symmetrical about the pulse centre. Figure 1 shows a good example. This symmetry implies, or at least is consistent with, a circular cross-section for the emission beam. A 'double' pulse structure with relatively strong outer components, usually with steep outer edges, such as that shown in Fig. 1, is common. Hence we are led to the idea of an annular or 'conal' beam. Especially in shorter-period pulsars and at lower frequencies, the profile is often dominated by a central component – the 'core' component. Core components are generally prominent only in pulsars where the 'impact parameter', or minimum angle between the symmetry (magnetic) axis and the observer's direction, is small.

For pulsars where the profile is dominated by conal emission, observations over a wide frequency range (e.g. Hankins et al. 1991; Phillips & Wolszczan 1992; Thorsett 1991) show that the component separation increases with decreasing frequency and, after removing the delays due to interstellar dispersion, the profile expands symmetrically about its central point. These observations are naturally explained in the magnetic pole model, with lower frequencies being emitted at greater distances from the neutron star surface where the opening angle of polar field lines is greater – the so-called 'radius-to-frequency mapping' (Cordes 1978).

Core components, that is, components located near the centre of the pulse profile have rather different properties to conal components (Rankin 1983; Lyne &

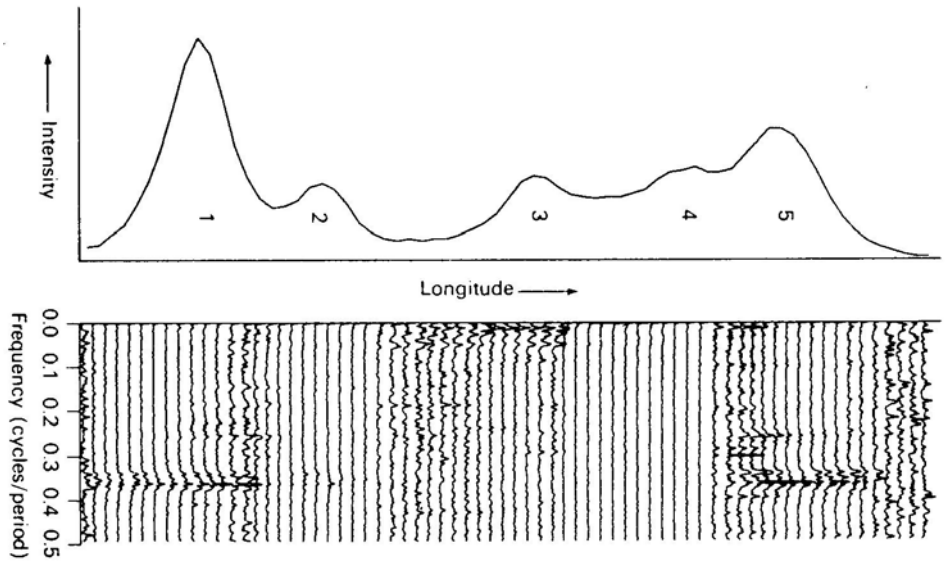

Figure 1: Mean pulse profile and phase-resolved pulse modulation spectra for PSR B1237+25 at 430 MHz (Backer 1973). Both the mean profile and the fluctuation characteristics are largely symmetric about the point midway between the outer edges of the profile.

Manchester 1988). For example, they generally have steeper spectra, especially in shorter-period pulsars. As illustrated in Fig. 1, fluctuation characteristics are often different. Drifting subpulses seem to be confined to the outer or conal parts of the emission beam. Rankin (1983, 1990) suggested that different emission processes are responsible for the core and conal parts of the beam and, in particular, that the core emission is generated close to the neutron-star surface from the entire polar cap. However, Lyne & Manchester argue that there is no fundamental difference between core and conal emission. Differences in properties result from differences in the location of the emission region with respect to the magnetic axis – core emission is generated close to the magnetic axis and conal emission from the outer parts of the open field-line bundle – and there is no need to invoke a different emission mechanism.

There are many similarities between the emission from the central and outer parts of pulse profiles. Despite varying pulse shapes and spectral indices, there is no great difference in the intensity of core and conal emission. If two emission mechanisms were involved, one might expect quite different emission intensities. Once allowance is made for orthogonal modes, polarization variations are normally continuous over the whole pulse profile; several examples are shown in Fig. 2. Orthogonal modes occur in both core and conal emission and variations in the

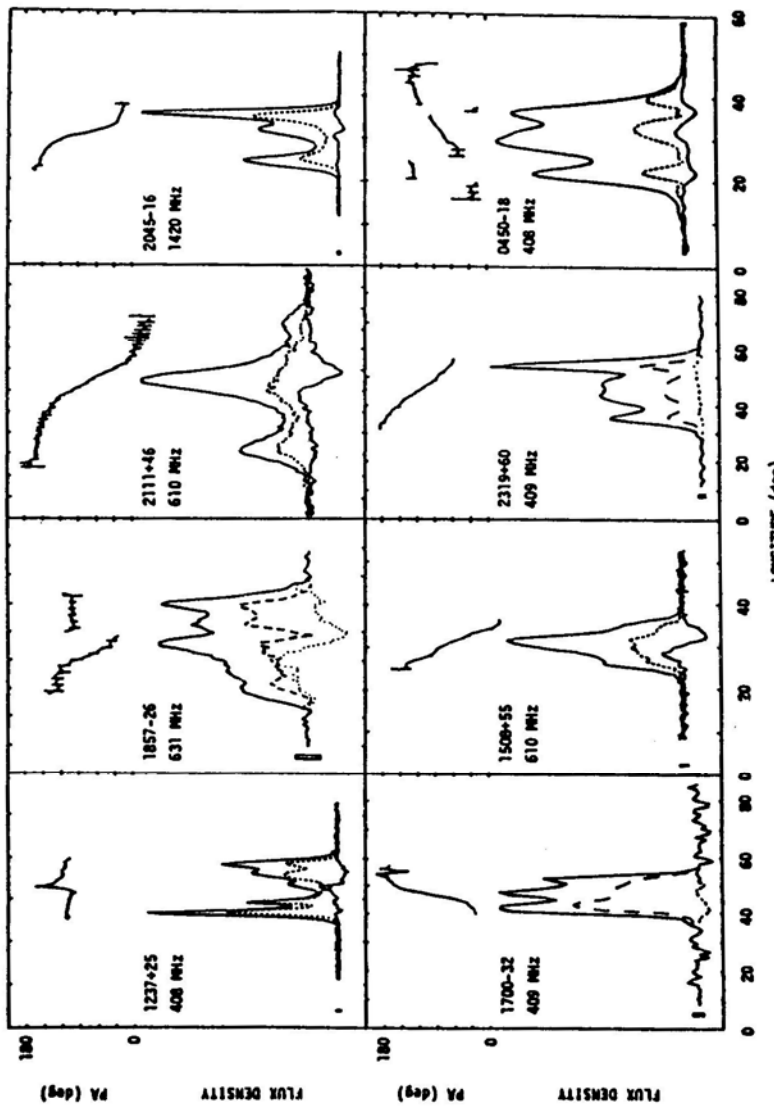

Figure 2: Mean pulse profiles and polarization parameters for pulsars showing both core and conal components (Lyne and Manchester 1988).

relative strength of the two modes occur smoothly across the profile. Subpulse widths are similar for core and conal emission (Taylor et al. 1975) and, although the sample is limited, micropulse properties seem similar for both core- and cone-dominated profiles (Cordes et al. 1990). Although spectral index differences are observed between core and conal components, these tend to be small or absent in longer-period pulsars, again suggesting that the same emission mechanism is involved.

For properties where there are clear differences between core and conal parts of the profile, these differences are related to location within the emission beam as a whole rather than to the actual core components. Figure 1 is a good illustration of this. The modulation patterns are symmetric about the mid-point of the profile (defined to be halfway between the outer edges) and are not related to the 'core' component which occurs at a significantly later phase. Spectral index differences are a function of radial distance from the beam axis, regardless of the presence or absence of components (Lyne & Manchester 1988). There is little spectral index variation across profiles for which the impact parameter is high, that is, where the observer sees emission from the outer parts of the cone. Furthermore, in wide double-pulse profiles in which there are no obvious core components, the central region often has a steeper spectrum than the outer regions.

Radio mean pulse profiles of pulsars are characterized by three components, two outer and one central. The relative strengths of these components vary with frequency and from pulsar to pulsar but they appear to be a common or generic feature of the emission beam. The central component often lags the centre of symmetry of the profile, defined to be midway between the outer edges of the outer components. Within this framework, each pulsar has its own character, often with lesser peaks apparently randomly distributed across the profile (Lyne & Manchester 1988). Rankin (1993) has suggested that a second pair of components, located inside the outer pair and corresponding to an 'inner cone', is also a characteristic feature. However, the evidence for this is weak. Inner components are not normally symmetrically located about the profile midpoint (e.g., Fig. 1). The characteristic separation of a few degrees of longitude between components simply reflects the fact that individual subpulses are a few degrees wide, and components more closely spaced than this are not resolved (or identified). Similarly, the observation that the number of components across profiles is usually five or less simply reflects the fact that the overall profile width is typically only a few times the subpulse width.

A model which represents the salient features of the radio pulse emission and beaming mechanism is illustrated in Fig. 3. Features which are common to all pulsars are represented by the window function, whereas the source function is unique to a given pulsar. The window function varies with radio frequency and pulsar period, and represents the basic or underlying form of the emission beam. The source function represents the emission pattern for a given pulsar and appears to be random in character. The window function is evidently determined by the dipole component of the pulsar magnetic field and the characteristics of the emission process, whereas the source function could, for example, be determined by the multipole structure of the magnetic field. Individual pulse observations suggest that the subpulse is a basic unit of emission. We therefore convolve the

source function with a 'subpulse beam', taken to be a two-dimensional Gaussian of half-intensity width equal to one sixth of the conal diameter. The final beam pattern is given by the product of the window and convolved source functions. The observed pulse profile is represented by a cut across this beam pattern, with the vertical position of the cut determined by the relative latitude of the magnetic axis and the observer's line of sight.

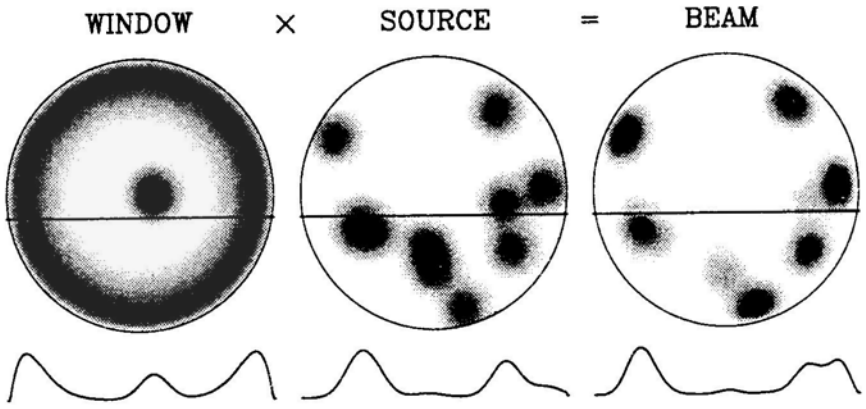

Figure 3: A model for the pulsar beam involving the product of a window function, common to all pulsars, and a source function, unique to each pulsar. Profiles under the beam patterns represent cuts through each pattern at the position of the horizontal lines.

It is well established that pulsars with shorter periods emit into a wider cone than longer-period pulsars, but the relationship between cone opening angle and period is somewhat uncertain. Lyne & Manchester (1988) found that the cone angular radius ρ is given by $\rho = 6.5° \; P^{-1/3}$, Rankin (1993) gives ρ $5.8° \; P^{-1/2}$, whereas Gould (1994) gives $\rho = 7.7° \; P^{-1/2}$. Observations of millisecond pulsars should help to tie down this relationship. The width of outer components of 'double' profiles (Fig. 4) and central components follow similar laws (Gould 1994). This suggests that the size of the bundle of emitting field lines relative to the size of the polar cap is independent of period. Fig. 4 also suggests that component width is independent of normalized impact parameter. This is consistent with the 'patchy cone' idea illustrated in Fig. 3, but not with complete cones; for complete cones, one would expect relatively wider components at higher impact parameters. Patchy cones are also implied by one-sided or partial conal profiles (Lyne & Manchester 1988; Qiao et al. 1994) and by secular variations in the mean pulse profile of PSR B1913+16 (Weisberg et al. 1989).

3. Interpulses

Interpulses are pulse components which lie close to midway between successive main pulses. As mentioned above, a natural interpretation is that interpulses originate from the other pole of a basically dipole magnetic field. This interpretation is supported by polarization data in several cases, e.g., PSR B1055–52 and PSR B1702–19 (Lyne & Manchester 1988) and PSR B1534+12 (Arzoumanian 1994). In many pulsars though, the separation of the main and interpulses is less than 180° of longitude. In some of these, for example, PSR B0950+08, polarization data suggest that the magnetic and rotation axes are nearly aligned and that all of the pulsed emission is from a single pole. A bridge of emission in the shorter gap between the main pulse and interpulse is a common feature of such profiles (Hankins & Fowler 1986).

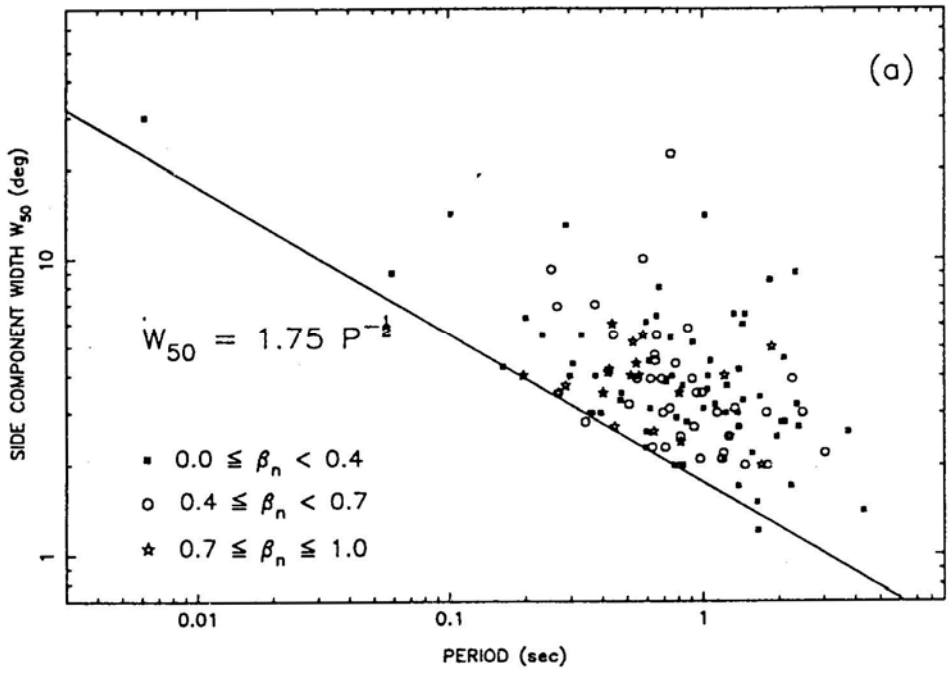

Figure 4: Half-power widths of outer or conal components as a function of pulsar period. Pulsars are divided into different classes depending on the 'normalized impact parameter', β_n , that is, the minimum angle between the observer's line of sight and the magnetic or symmetry axis normalized by the conal radius (from Gould 1994). If the observer's direction and the rotation axis are not orthogonal, the observed pulse width is greater than the emitted pulse width. The lower envelope of the points is therefore taken to represent the emitted pulse width.

Observed pulse profiles at optical, X-ray and γ-ray wavelengths for pulsars detected at these wavelengths also support a one-pole interpretation (Manchester

and Lyne 1977). As shown in Fig. 5, the low-energy γ-ray pulse profile for the Crab pulsar has a strong bridge between the two components and looks very similar in appearance to radio 'double' pulse profiles. Romani & Yadigaroglu (1994) have recently modelled the Crab and other high-energy pulse profiles with a one-pole outer-gap model. They show that, when the full retarded potentials are used to describe the magnetic field structure, both the high-energy pulse shape and the optical polarization data for the Crab pulsar are well represented by the model. If this one-pole interpretation for the Crab pulsar is accepted, the phase relationships with the radio main pulse and interpulse (Fig. 5) imply that these also originate from the same outer-gap regions. However, the so-called 'precursor' pulse, which leads the main pulse, seems to be of a different character (e.g. Smith 1986).

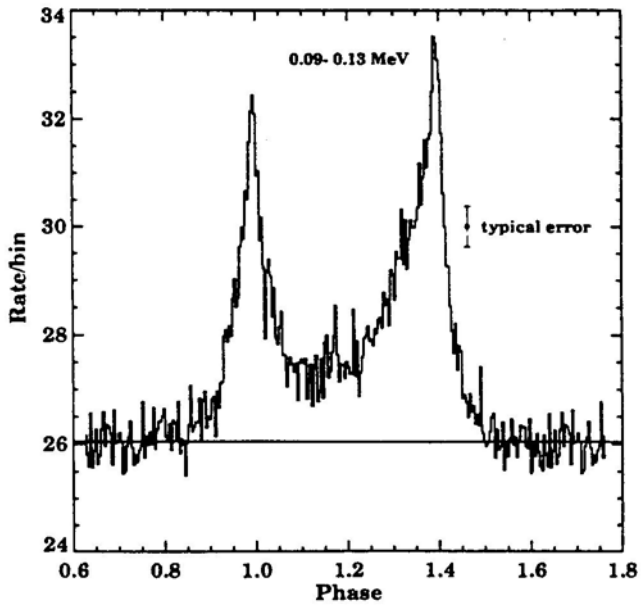

Figure 5: Low-energy γ-ray profile for the Crab pulsar from the OSSE experiment on the Compton Gamma Ray Observatory (Ulmer et al. 1994)

An extreme view would be that all pulsars emit from one pole only and that position-angle fits such as those for PSR B1534+12 are misleading us. Some observations seem to support such a view. An example is the remarkable mode-switching behaviour observed in PSR B1822-09 by Gil et al. (1994). The amplitude of the highly polarized precursor pulse, which leads the main pulse by about 15° of longitude, is anti-correlated with the amplitude of the interpulse, which is separated from the main pulse by 180° of longitude. Furthermore, the main pulse and interpulse amplitudes are correlated. These observations are difficult to understand on the standard two-pole model.

Recent observations of the eclipsing binary pulsar PSR B1259–63 have shown that the two pulse components are essentially 100% linearly polarized (Fig. 6).

In this respect they are similar to the precursor pulses of the Crab pulsar and PSR B1822–09 and to pulses from Vela and other young and short-period pulsars (Qiao et al. 1994). At 1520 MHz, the two components in PSR B1259–63 are separated by about 140°, but this separation is frequency dependent (Johnston et al. 1992). This strongly suggests that these two components emanate from a single pole. The wide separation of the components then implies that the emission is beamed at a correspondingly large angle to the magnetic axis. This has interesting implications for the Crab, Vela and other pulsars with these highly polarized components if they are emitted in the same way.

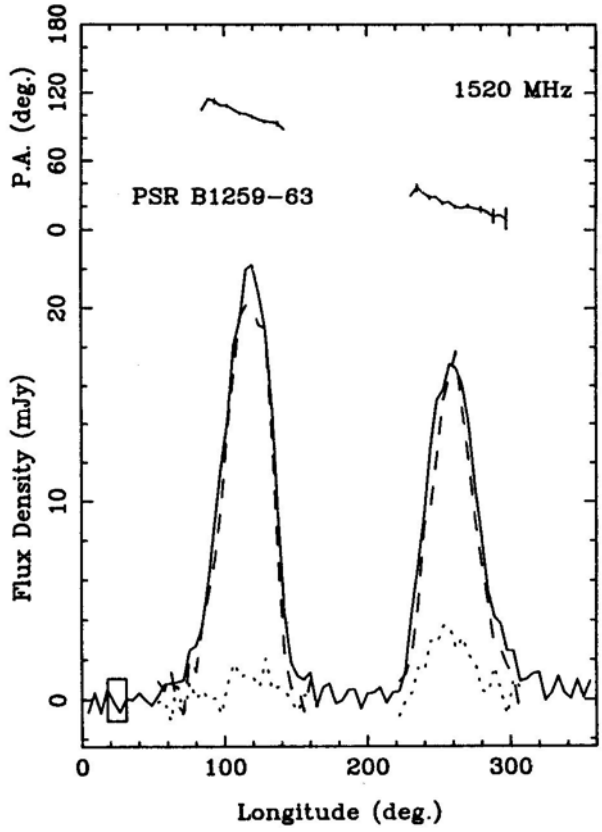

Figure 6: Mean pulse profile and polarization parameters for PSR B1259–63 at 1520 MHz (Manchester & Johnston, 1994). In the lower part of the figure the solid line represents the total intensity (Stokes parameter *I*), the dashed line the linearly polarized intensity and the dotted line the circularly polarized intensity (Stokes parameter *V*), The upper curve is the position angle of the linearly polarized part, plotted with $\pm 2\sigma$ error bars on every second point.

4. Conclusions

Observations of pulsar mean pulse profiles suggest that pulsar emission is in the form of a conical beam whose axis is the dipole axis of the neutron-star magnetic field. Although some properties such as radio-frequency spectral index and pulse-to-pulse fluctuations differ from central to outer parts of the observed pulse profile, it seems most likely that the same basic emission process is responsible for both parts of the profile. Observed pulse profiles can be represented by the product of a well-defined 'window function', which is determined by the dipole magnetic field structure and the characteristics of the emission process, and a random 'source function' which varies from pulsar to pulsar and may be determined by magnetic multipole structure.

High-energy pulse profiles suggest that, even in pulsars with interpulses, all of the observed emission originates. from a single pole on the star. This would make some observations, for example the correlated intensity fluctuations in the components of the PSR B1822–09 profile, easier to understand. Recent observations show that the two widely spaced components of PSR B1259–63 are highly linearly polarized and probably related to the similar highly polarized components observed mother young pulsars.

References

Arons, J. 1983, *Astrophys. J*, **266,** 215.

Arzoumanian, Z. 1994. Ph.D. thesis, Princeton University.

Backer, D. C. 1973, *Astrophys. J*, **182,** 245.

Cordes, J. M. 1978, *Asirophys. J*, **222,** 1006.

Cordes, J. M., Weisberg, J. M., & Hankins, T. H. 1990, *Astrophys. J.*, **100,** 1882.

Gil, J. A. et al.l994, *Astron. Astrophys.*, **282,** 45.

Gould, D. M. 1994. Ph.D. thesis, The University of Manchester.

Hankins, T. H. & Fowler, L. A. 1986,*Astrophys. J*, **304,** 256.

Hankins, T. H., Izvekova, V. A., Malofeev, V. M., Rankin, J. M., Shitov, Y. P., & Stinebring, D. R. 1991, *Astrophys. J. Lett*, **373,** L17.

Johnston, S., Manchester, R. N., Lyne, A. G., Bailes, M., Kaspi, V. M., Qiao, G., & D'Amico, N. 1992, *Astrophys. J. Lett.*, **387,** L37.

Lyne, A. G. & Manchester, R. N. 1988, *Mon. Not. R.astr. Soc*, **234,** 477.

Manchester, R. N. & Johnston, S. 1994, *Astrophys. J. Lett.*, submitted.

Manchester, R. N. & Lyne, A. G. 1977, *Mon. Not. R.astr. Soc*, **181,** 761.

McCulloch, P. M., Hamilton, P. A., Manchester, R. N., & Ables, J. G. 1978, *Mon. Not. R.astr. Soc*, **183,** 645.

Michel, F. C. 1987, *Astrophys. J,* **322,** 822.

Phillips, J. A. & Wolszczan, A. 1992, *Astrophys. J,* **385,** 273.

Qiao, G., Manchester, R. N., Lyne, A. G., & Gould, D. M. 1994, *Mon. Not. R. astr. Soc.*, submitted.

Radhakrishnan, V. & Cooke, D. J. 1969, *Astrophys. Lett.*, **3,** 225.

Radhakrishnan, V., Cooke, D. J., Komesaroff, M. M., & Morris, D. 1969, *Nature*, **221,** 443.
Rankin, J. M. 1983, *Astrophys. J*, **274,** 333.
Rankin, J. M. 1990, *Astrophys. J*, **352,** 247.
Rankin, J. M. 1993, *Astrophys. J*, **405,** 285.
Romani, R. W. & Yadigaroglu, I.A. 1994, *Astrophys. J*, **438,** 314
Ruderman, M. A. & Sutherland, P. G. 1975, *Astrophys. J*, **196,** 51.
Smith, F. G. 1986, *Mon. Not R . astr. Soc*, **219,** 729.
Stinebring, D. R., Cordes, J. M., Rankin, J. M., Weisberg, J. M., & BoriakofF, V. 1984, *Astrophys. J. Supp*., **55,** 247.
Sturrock, P. A. 1971, *Astrophys. J,* **164,** 529.
Taylor, J. H., Manchester, R. N., & Huguenin, G. R. 1975, *Astrophys. J*, **195,** 513.
Thorsett, S. E. 1991, *Astrophys. J*, **377,** 263.
Ulmer, M. P. et al. l994, *Astrophys. J*, **432,** 228.
Weisberg, J. M., Romani, R. W., & Taylor, J. H. 1989, *Astrophys. J*, **347,** 1030.

Diamond Jubilee Symposium on Pulsars
14-17 March 1994
Raman Research Institute, Bangalore
J. Astrophys. Astr. (1995) **16,** 119–135

Magnetospheric Models of Pulsars–Outstanding Questions

L. Mestel *Astronomy Centre, University of Sussex, Falmer, Brighton BN1 9QH, England*

Abstract. The difficulties of the pulsar magnetosphere problem are illustrated by two models for the axisymmetric magnetic rotator: (a) a classical model, in which the return current problem is linked with angular momentum dissipation' through incoherent gamma radiation beyond the light-cylinder; and (b) a quantum model, in which electron-positron pairs are produced near the star, and spin-down is primarily through the transport of angular momentum by an e_+-e_- wind. The first model has some pedagogic value, but it makes the embarrassing prediction that all the spin-down energy is emitted as gamma-radiation. In the second model a predicted small but significant emission in gamma- and X-rays is again linked with the return current problem, but the bulk of the energy emission is through the wind. The presence of both a high-γ primary electron beam and a moderate-γ pair plasma is as required by most models of coherent microwave emission. Problems persist in ensuring that the macroscopic conditions on the electric field are locally consistent with the microphysics. The most promising picture is of a spontaneous local hydromagnetic instability that yields a large effective resistivity. Some remarks are made on future extension of the theory to oblique geometry. For agreement with observations of the Crab nebula, the predicted dominance in the wind of the Poynting flux must be reversed in the far magnetosphere.

1. Introduction

The "outstanding question" of magnetospheric theory is that in spite of a great deal of effort, we still do not have an acceptable model, even for the superficially simplest case of the axisymmetric "non-pulsar", with the magnetic and rotation vectors aligned. Recall that the rate of energy loss from a rotating neutron star, inferred from the observed normal steady increase in the period, is orders of magnitude greater than that carried off by the pulsed emission in the radio waves, even after making generous allowance for beaming. Thus the radio noise is seen

to be a diagnostic of much more powerful energy loss processes, which a complete magnetospheric theory should elucidate. In trying to understand how a rotating magnetized neutron star comes to terms with its environment by settling into a state of steady spin-down, the theorist is responding to a challenge: it is just intolerable that such a well-defined problem in both classical or quantum physics should remain unanswered. A complete answer would include the location of the sources of the pulsed emission in radio, optical, u-v, gamma and X-radiation as well as in energetic particles; but as Don Melrose has pointed out, such a deductive approach to the problem of the emission mechanisms is not very promising.

Let me begin by going back to the early days of pulsar theory. The first model for the magnetosphere predated the actual discovery of pulsars: in a prophetic paper, Pacini (1967) adapted the solution constructed earlier by A.J.Deutsch for the electromagnetic field of an obliquely rotating star *in vacuo* with its magnetic dipole moment p inclined to the rotation axis k by the angle χ. Far from the star the dominant terms are those forming the wave field emitted by the perpendicular dipolar component $p\sin\chi$, rotating with the angular frequency $\alpha = 2\pi/P_1$ with P_1 the period in seconds. The energy transport per second is

$$(2p^2\alpha^4/3c^3)\sin^2\chi = (B_s^2R^6\alpha^4/6c^3)\sin^2\chi, \tag{1}$$

where R is the stellar radius and B_8 the polar field strength. If χ is assumed not very small, then the equating of (1) to the inferred energy loss $-I\dot{\alpha}\alpha = 4\pi^2 I\dot{P}_1/P_1^3$ from a star of moment of inertia I with the observed period increase P_1 yields the canonical value of $B_8 \approx 10^{12}$G (Gold 1969). A corollary is that the energy loss vanishes as $\chi \to 0$: the aligned model *in vacuo* is dead.

The enormous gravitational field of the neutron star ensures that for any reasonable temperature, the thermal scale height is so small that a thermally-supported atmosphere would exponentiate down to virtually zero density within a few centimetres, so apparently justifying treatment of the surroundings as not just a dynamical but also an electrodynamical vacuum. The axisymmetric model would then be like a dynamo on open circuit, with the rotation of the highly conducting neutron star crust generating enormous surface potential differences (of the order of $10^{17}/P_1$ Volts), but with no opportunity for currents to flow. The essence of the Goldreich-Julian ("GJ") critique (1969) is that the system will in fact build up its own conducting leads. The axisymmetric vacuum magnetosphere model, subject to finiteness at infinity and continuity at the star's surface of B_r and E_θ, has an external quadrupole electric field **E** with a component $\mathbf{E}_\parallel$ along **B** of the same order at the star's surface as the internal field $E = -(\alpha k \times r) \times \mathbf{B}/c$. The consequent normal discontinuity in **E** then requires a surface charge density, which is subject to very large outward-acting unbalanced electrical forces. Thus a charged magnetosphere is spontaneously built up, and if there is continuous current flow into and out of the star, the aligned model is no longer dead but suffers a steady loss of rotational energy and associated angular momentum. The argument applies also to the oblique case (Cohen and Toton 1971; Mestel 1971). In both the aligned and the oblique cases, the magnetospheric charge-current field acts as an extra source of the electromagnetic field, with the modification to the magnetic field becoming important as the light-cylinder is approached. The formidable the-

oretical problem is to describe in detail the mutually interacting electromagnetic and particle fields.

2. An illustrative classical model

It is instructive to begin by studying the problem within the limitations of classical physics. It is then difficult to understand why a "live" pulsar – i.e. one that is spinning down – does not manifest itself essentially as an efficient machine for the generation of gamma rays. The steps in the argument are as follows. The basic poloidal magnetic field is described by the flux function $P(\varpi, z)$:

$$\mathbf{B}_p = -\nabla \times (P\mathbf{t}/\varpi) = -\nabla P \times \mathbf{t}/\varpi, \tag{2}$$

where t is the unit azimuthal (toroidal) vector and (ϖ, ϕ, z) are cylindrical polar coordinates. For simplicity, P is for the moment given the dipolar form over the star's surface, so that if the star's surroundings were a strict electrodynamic vacuum,

$$P = -B_s R^3 \sin^2\theta/2r, \tag{3}$$

where (r, θ, ϕ) are spherical polar coordinates, and B_s is the polar field strength at the star's radius R. There will be a significant deviation from (3) as the 1-c is approached (*cf.* below). Nevertheless, we adopt (3) as a rough approximation: then the last field line to reach the 1-c defines the "polar cap" $0 < \theta < \theta_0$, with

$$\sin^2\theta_0 = (\alpha R/c) = 2 \times 10^{-4} R_6/\mathrm{P}_1, \tag{4}$$

where $R_6 = R/10^6$ and P_1 is the rotation period in seconds. The rigidly rotating pulsar crust is well approximated as a classical perfect conductor, with

$$-\nabla\phi = \mathbf{E} = -\alpha\varpi\mathbf{t} \times \mathbf{B}/c = \nabla(\alpha P/c), \tag{5}$$

so that the electric potential $\phi = -\alpha P/c +$ constant. From (3) and (4), the potential variation over the polar cap is

$$\Delta\phi = (\alpha B_s R^2/2c)(\alpha R/c) \simeq 6 \times 10^{12} (B_{12} R_6^3)/\mathrm{P}_1^2 \text{ Volts.} \tag{6}$$

(Over a whole quadrant, the potential variation is $\alpha B_s R^2/2c = 3 \times 10^{16} (\mathrm{B}_{12}\, \mathrm{R}_6^2/\mathrm{P}_1)$ Volts.) The field line defined by θ_0 is the separatrix between those field lines that close within the 1-c and those that cross it. Charges in the closed domain can corotate with the star without contradicting special relativity, and will acquire only modest energies. By contrast, charges emitted from the polar caps will flow across the 1-c and can acquire γ-values up to $\gamma_c \simeq \Delta\phi/mc^2 = 1.25 \times 10^7\, B_{12} R_6^3/P_1^2$; and particles of this energy will emit powerful gamma radiation.

Let us look at the problem more fully. In a steady state the curl-free electric field is conveniently written as

$$\mathbf{E} = -\alpha\varpi\mathbf{t} \times \mathbf{B}_p/c - \nabla\psi \tag{7}$$

so that the electric potential is

$$\phi = -\alpha P/c + \psi. \tag{8}$$

As noted, within the rigidly rotating, perfectly conducting stellar crust, the "non-corotational" part ψ of the potential is a constant. The simplest alternative to the untenable vacuum hypothesis for the surroundings is the original GJ proposal, by which charges originating in the star distribute themselves so as to short out the component $E_{\|}$, whence by (7), **B.** $\nabla\psi = 0$. If there are no vacuum gaps between the star and the point considered, the constant value of ψ with in the star is then propagated into the magnetosphere: the vacuum condition of zero charge-current density is replaced by the corotational electric field condition $\mathbf{E} = -\alpha\varpi t \times \mathbf{B}$ / c, B/c, maintained by the charge density

$$\rho_e = \nabla.\mathbf{E}/4\pi = -(\alpha/2\pi c)[B_z - \varpi(\nabla \times \mathbf{B})_\phi/2]. \tag{9}$$

Thus the GJ hypothesis converts the surroundings of the star into something like a classical perfect conductor. Much of the discussion of the different models in the literature centres around the domains of validity of the condition **E.B** = 0 and the consequences of its breakdown.

Prima facie, a classical magnetosphere built up and maintained by electrical forces rather than thermal pressure ought to be *charge-separated*, consisting of electrons where (9) yields $\rho_e < 0$ and ions where $\rho_e > 0$. Provided $E < B$, a charge subject to the orthogonal **E** and **B** fields performs the drift $c(\mathbf{E} \times \mathbf{B})/B^2$. If there were no poloidal current $\mathbf{j}_p$, the magnetic field remains purely poloidal, and this drift reduces to the corotation velocity $\alpha\varpi t$ for all charges within the light-cylinder ("l-c"). The simplest of such electrodynamically dead models (with $\mathbf{j}_p$ zero) has the corotating GJ charge density filling the whole domain within the l-c, and a vacuum beyond. The Ampere equation then yields for P within the l-c (*cf.* Michel 1991; Mestel and Wang 1979; Mestel and Pryce 1992)

$$\nabla^2 P[1 - (\alpha\varpi/c)^2] = 2\partial P/\varpi\partial\varpi. \tag{10}$$

The solution of (10), subject to a dipole singularity at the origin and with $B_z = 0$ at the l-c, illustrates how the magnetospheric currents distort the field significantly from the vacuum dipolar form as the l-c is approached. However, the discontinue-ities in E_{ϖ} and B_z across the l-c imply a surface charge-current distribution with corresponding unbalanced Maxwell stresses: like the original vacuum model, this dead model is again dynamically unacceptable (Mestel and Wang 1982). (Ax-isymmetric dead models have been constructed numerically by Krause-Polstorff and Michel (1985), satisfying the condition **E.B** = 0 within regions containing charge, but with large vacuum gaps. The models all have a large positive charge, and it is questionable whether they would in practice avoid conversion into live models following either discharging by the interstellar medium or electron-positron pair production under the strong $E_{\|}$fields in the gaps.)

As stated, it is the flow of poloidal current along the field lines crossing the l-c that is responsible for the spin-down of the star. We consider just the aligned rather than the counter-aligned case, so that the electric field is of the sign to draw

out electrons rather than ions; the steady outflow of electrons from each polar cap forms therefore a *convection current*, with the poloidal component j_p defined by the stream function S:

$$\mathbf{j}_p = \rho_e \mathbf{v}_p = -\nabla S \times \mathbf{t}/\varpi \tag{11}$$

with $\rho_e = \nabla.\mathbf{E}/4\pi$. Rather than making the GJ *ansatz* **E.B** = 0, it is preferable to retain inertial (and later dissipative) terms in the dynamical equations (though gravity is justifiably ignored); the validity of the GJ approximation in any domain can then be assessed. Thus for a cold, dissipation-free gas, the energy integral is

$$-e\phi + \gamma mc^2 = -e\phi^*(S) \tag{12}$$

and the angular momentum integral is

$$eP/c + \gamma m\Omega\varpi^2 = eP^*(S)/c, \tag{13}$$

where Ω is the local angular velocity. Equation (13) shows that electrons do not move strictly along the poloidal field but suffer an "inertial" drift: to increase its angular momentum $\gamma m\Omega\varpi^2$, an electron must have a component of poloidal velocity normal to $\mathbf{B}_p$ in order that the magnetic field exert the required torque. Together with the definition (8) of ψ, (12) and (13) combine into

$$\Gamma \equiv \{\gamma[1 - (\Omega\varpi/c)(\alpha\varpi/c)] - e\psi/mc^2\} = \Gamma(S). \tag{14}$$

The relativistic slingshot term $\gamma(\Omega\varpi / c)$ $(\alpha\varpi / c)$ is a consequence of the inertial drift, which takes the electrons to points with a higher corotational potential $-\alpha P / c$. The actual deviation from strict flow along $\mathbf{B}_p$ is of order $\gamma\Omega /(eB_p / mc)$ which remains very small until the gas becomes highly relativistic.

The current (11) generates by Ampere's law a toroidal field component $\mathbf{B}_t \equiv B_\phi \mathbf{t}$ given by

$$B_\phi = -4\pi S/c\varpi. \tag{15}$$

As in standard stellar wind theory, the sign of $B\phi$ ensures that the lines of $\mathbf{B}_p + \mathbf{B}_t$ are swept back with respect to the rotation axis **k**, so the outflowing gas sub-rotates, allowing smooth sub-relativistic flow which can penetrate the l-c. The condition that γ remain finite at the l-c fixes the velocity v^* with which electrons leave the star, typically at $\simeq c/2$. In this respect the model is similar to that in the classical GJ paper (1969). The crucial difference is that there is no surrounding collar containing outstreaming ions. The difficulty with the GJ model (pointed out by the authors) is that the positively charged ions would have to flow through a sea of electrons to ensure that the net charge density satisfies the GJ requirement (9). In order that the present model should not break down through a continual charging up of the star, the electron stream must cross field lines in some domain and return to the star.

The precise behaviour of the flow beyond the 1c depends on the detailed structure of the magnetic field lines, which strictly can only be determined simultaneously with the density-velocity fields of the particles. However, with virtually any plausible guess for the field structure, one finds that over much of the domain the quasi-mind flow breaks down somewhere beyond the l-c, with γ becoming

formally infinite when the electric field $\mathbf{E} = -\alpha\varpi\mathrm{t} \times \mathbf{B}_p/\mathrm{c}$ becomes equal in magnitude to the strength $(B_p^2 + B_t^2)^{1/2}$ of the total magnetic field, and simultaneously $\alpha\Omega\varpi^2/c^2 = 1$. In fact, when γ approaches the value $\gamma_c = (eB / mc)/\alpha$ (the ratio of the local non-relativistic gyro-frequency ω_g to .the stellar rotation), the inertial drift terms are no longer small, and simultaneously the non-corotational potential ψ, given by (14), becomes comparable wih the corotational part $-eP/c$. Near the l-c, $\gamma_c \simeq 2.6 \times 10^7(B^*/10^{12})(R/10^6)^3/P_1^2$, where the rough vacuum dipolar approximation has been used for the field strength. However, even in the slow pulsars with $P_1 \simeq 1$, particles with γ-values near γ_c will be emitting powerful incoherent gamma-radiation, strongly beamed in the direction of motion. If V is the radiated power per particle, the associated linear momentum loss is $(\mathcal{P}/\mathrm{c}^2)\mathrm{v}$, as is seen by making a Lorentz transformation from the particle rest frame to the inertial frame. The energy, angular momentum and Γ-integrals (12), (13) and (14) are now replaced by

$$\mathbf{v}.\nabla(\gamma mc^2 - e\phi) = -\mathcal{P}, \tag{16}$$

$$\mathbf{v}.\nabla(\gamma m\Omega\varpi^2 + eP/c) = -(\Omega\varpi^2/c^2)\mathcal{P}, \tag{17}$$

$$\mathbf{v}.\nabla\left\{\gamma\left[1 - \frac{\Omega\varpi}{c}\frac{\alpha\varpi}{c}\right] - \frac{e\psi}{mc^2}\right\} = -\frac{\mathcal{P}}{mc^2}\left[1 - \frac{\Omega\varpi}{c}\frac{\alpha\varpi}{c}\right]. \tag{18}$$

The first term on the right of (18) represents the direct loss of energy by radiation. The associated angular momentum loss in (17) implies a dissipative drift to field lines of higher corotational potential ($-\alpha P / c$), and so to a *gain* in energy, analogous to the inertial drift that yields the slingshot term in (14) and (18), In the present problem it is the radiation beyond the l-c of photons with high angular momentum that enables the electrons to pick up the energy available on field lines of higher potential, due ultimately to the rotation of the magnetic star. Clearly, this requires that the gain in energy due to the dissipative drift exceed the energy radiated. One can notionally integrate the equation (18) along a trajectory followed by an electron between emission from and return to the star (recall that Ψ is uniform over the star). Since $\mathcal{P}$ is essentially positive, it is clear that to avoid the nonsensical prediction of $\gamma < 1$ for a returning particle, $[1 - (\Omega\varpi / c)(a\varpi / c)]$ must be negative in the strongly dissipative regions: the dissipation must occur primarily beyond the l-c. This links up with a comment made by Gold (1980) and Holloway (1977). Since it is the star's rotational energy $I\alpha^2/2$ and the associated angular momentum $I\alpha$ that is powering the overall pulsar activity, on balance: (energy loss rate) = α (angular momentum loss rate). Photons emitted within the l-c, even if they are perfectly beamed in the toroidal direction, have too small a lever arm, requiring a compensating photon emission well beyond the l-c. The equation (18) shows there is an automatic "Gold-Holloway" condition not only for the system as a whole but for each trajectory.

Once particles begin to radiate, then a good approximation to the equation of motion ignores inertia and balances the Lorentz force against radiation drag – the "Stokes-Aristotle" approximation (Mestel *et al.* 1985):

$$-e(\mathbf{E} + \mathbf{v} \times \mathbf{B}/c) - (\mathcal{P}/c^2)\mathbf{v} = 0. \tag{19}$$

As long as $E < B$, the poloidal velocity v_p remains more nearly parallel to $\mathbf{B}_p$,

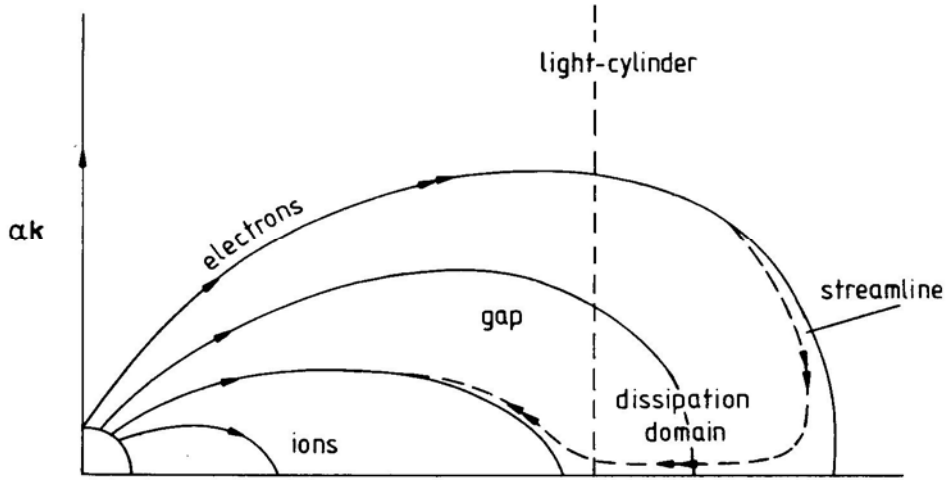

Figure 1: Classical model – schematic diagram

and in fact $\mathcal{P} \ll ecB$: the dissipation term is small compared with the Lorentz force, and so the perfect mhd condition $\mathbf{E} + \mathbf{v} \times \mathbf{B}/c = 0$ remains a good approximation, with $E_{\|} \ll E_{\perp}$. Once $E > B$, the flow more nearly follows **E**. Strong trans-field flow under the essentially quadrupolar E-field can be expected close to the equator, where $\mathbf{B}_t$ goes to zero by symmetry. The emitting electrons are kept at an energy $\simeq 7 \times 10^{12} / P_1^{1/4}$ eV, and the photons emitted are gamma-rays of energy $\simeq 5 \times 10^7 / P_1^{7/4}$ eV; the total power is of the same order as that from a vacuum oblique rotator, given by (1) with $\chi = O(1)$.

Some very approximate analytical and numerical work on this classical model (Fig. 1) is described in Fitzpatrick and Mestel I,II (1988). Besides the circulating electrons, there is a domain with non-circulating corotating electrons and a domain of non-circulating but sub-rotating ions, separated by a wedge-shaped gap, which is approximated as a vacuum and so has strong **E.B** components. (The returning electron current is forced to flow partly through the ion and gap domains, so these descriptions are only approximate). To keep the model working the whole system must have zero net charge, so that the electric field well beyond the l-c has the quadrupolar $1/r^4$ dependence. Since E must exceed B in the equatorial domain where the returning electrons have dominantly trans-$\mathbf{B}_p$ motions, the toroidal magnetospheric currents are required to yield a dipole moment equal and opposite to that on the star.

A crucial point of the model is the link-up of the spontaneous loss of energy and angular momentum with the return current requirement, for which dissipation is essential. In spite of some clear differences, brought out above, the theory is quite similar to that in a classical "centrifugal wind" problem. In particular, it is

the *perpendicular* component $\mathbf{E}_\perp$ that energizes the particles, through the sling-shot effect; but as long as inertial and dissipative drifts are small, the gas velocity is well described by the familiar mhd integrals, with the associated value of the non-corotational potential ψ given by the Γ-integral (14). The chain of causation is: $E_\perp \rightarrow \gamma \rightarrow E_{||}$.

This classical model illustrates how dissipation-free flow spontaneously establishes domains in which acceleration to high γ-values occurs, leading inevitably to dissipation. The trouble with the model is that it proves too much: for although observations are now showing that gamma-ray emission from some pulsars is a significant fraction (up to 10%) of the power, the bulk of the energy loss is in other modes. One can imagine a coherent radiation process occurring, with the γ-values kept much lower and the total power being again emitted as radiation but at much lower frequencies. However, with the overwhelming evidence that e.g. the Crab pulsar loses much of its spin-down energy in the form of a relativistic particle wind, it is best to look on the classical model as illustrative, with some of its features persisting into the more realistic picture described below.

3. Models with pair production

A crucial step in Section 2 is the requirement that the quasi-mhd flow extend through the l-c, which limits the speed with which the electrons leave the polar caps typically to $\simeq$ c/2. If the emission speeds v^* are somewhat higher, the particles will achieve high γ-values well within the l-c. Continuity of flow that is nearly parallel to $\mathbf{B}_p$ requires $\rho_e v_p / B_p$ = constant. The energy-angular momentum integral (14) can be read to show that the GJ approximation - which constructs ρ_e with neglect of ψ – remains excellent up to high γ-values: $\rho_e \propto -aB_z/2\pi c$, so $v_p \propto B/p_e \propto B/B_z$, and this increases outwards for field lines that curve away from the axis, as do all the lines, in the aligned case and most lines in moderately oblique cases. Thus if v^* is close to c, v_p is predicted to reach c on a surface S_i quite near to the star. Beyond S_i the flow will still follow the field lines closely, but now $v_p \simeq$ c, and continuity enforces $\rho_e \propto B$ instead of $\rho_e \propto B_z$. Thus the limitation imposed by special relativity shows that the neglect of $\nabla^2\psi$ in the construction of $\nabla.\mathbf{E}$ ceases to be valid near and beyond S_I. Equation (9) (with $(\nabla \times \mathbf{B})\phi$ still negligible) is replaced by

$$\nabla^2\psi \simeq (2\alpha B_z/c)[-1 + (B/B_z)/(B/B_z)_I], \tag{20}$$

so that beyond S_I, ψ is found to increase outwards in order to satisfy the Poisson-Maxwell equation. The integral (14) must now be read in reverse: because the geometry of the flow causes B/B_z and so also ψ to increase, there is simultaneously an increase in γ which is rapid, again because of the smallness of the ratio α/w_g.

Closer inspection shows that even within S_I the $\nabla^2\psi$ term is not strictly negligible. The GJ approximation holds in the mean, but superposed on the monotonic flow are stationary spatial oscillations in ψ , γ and v_p of scale $(\alpha/\omega_g)^{1/2}$ (c / α), the plasma wavelength corresponding to the local GJ density (Mestel, *et al.* 1985, Appendix B; Shibata 1991). As the gas flows across S_i, the solution with small-scale

oscillations in ψ and γ is replaced by one with rapid monotonic growth.

It should be noted that the model is different from those in the literature which appeal to a vacuum gap at the stellar surface. For some years it was thought that in the case of counter-aligned rotation and magnetic axes, the spontaneous emission of ions under the outward pointing vacuum electric field would be inhibited because of a quantum-mechanical work function. The 10^{12} Volt potential difference which builds up at the poles would then lead to spasmodic breakdown of the gap through electron-positron production (Ruderman and Sutherland 1975). Subsequent computations shed doubt on the previous work function estimates, and it is now generally assumed that the classical boundary condition $\mathbf{E.B} = 0$ is always a good approximation.

The present treatment of the aligned case shows that the curvature of the field lines away from the axis necessarily leads to "over-filling" of the flux tubes, in the sense that the relativistic limitation on v forces the density up beyond the GJ value, and it is the consequent $E_{||}$ which causes monotonic acceleration of the electrons to high γ-values. The discussion is fully consistent with that by Fawley et *al.* (1977), who show that no solutions exist for field lines curving away from the axis if the boundary condition $\mathbf{B}.\nabla\psi = 0$ is imposed not only at the star but also at the end of the acceleration domain.[1] A difference does arise in terminology: in the present treatment this upper boundary condition and so also the phrase "unfavourably curved" are inappropriate. The position and shape of the surface S_I is not prescribable locally but must emerge from a global solution.

Beyond *S1,* particles are accelerated rapidly to $\gamma \simeq 10_7$, at which value there is copious emission of gamma-rays of energy $h\nu \simeq 3\gamma^3\hbar c/2R_c$, where R_c is the radius of curvature of the field-streamline. The crucial new factor, noted first by Goldreich in a conference report and by Sturrock (1971), is that hard gamma-rays moving across a very strong magnetic field convert spontaneously into electron-positron ("e^+-e^-") pairs. The newly-created particles are themselves accelerated by the electric field until they radiate gamma-rays which again create pairs. This carcade is ultimately self-limiting, since the dense e^+-e^- plasma accompanying the high-γ primary electron current will short out the accelerating $E_{||}$ field. The basic picture has been applied to different models in many papers (Ruderman and Sutherland 1975; Arons and Scharlemann 1979; Arons 1981; Daugherty and Harding 1982; Jones 1980; Shibata 1991; Mestel and Shibata 1994; among others). Thus the originally pure high-γ electron gas is converted into a plasma consisting of primary electrons plus a high-density sea of pairs. The multiplicity $\boldsymbol{M}$ (the number of pairs per primary electron) is estimated to be from a few hundred for the slower pulsars to $\sim 10^4$ for the Crab pulsar. The pairs are estimated to have $\gamma \sim 10^2$ and the primary electrons $\sim 10^6$. The process will cut off if the potential difference across the polar cap is inadequate to produce primary electrons of high enough γ. This gives an upper limit of $P_1 \sim 1.5$. If the e^+-e^- cascade is essential for the generation of the coherent radio emission from pulsars, then as argued by Sturrock, Ruderman and Sutherland and others, there is a clear physical reason

[1]Beskin (1990) and Muslimov and Tsygan (1990, 1992) have shown that this conclusion no longer holds when general relativistic corrections are included. This result is of interest but in my view does not change radically the physics of pulsars, as it is the assumed outer boundary condition that needs to be changed.

for radio pulsars' shutting off as their periods lengthen beyond ≈ Is. As found earlier by Ruderman and Sutherland (1975), to get a cut-off line that is consistent with observation, the magnetic field has to possess higher multipole components so that the radius of curvature near the star is smaller and pair production correspondingly more efficient.

Beyond the pair production region $E_{||}$ is again small, and as long as inertial drifts are small the flow is again quasi-mhd, with

$$\mathbf{v} = \kappa\mathbf{B} + \tilde{\alpha}\varpi\mathbf{t}, \qquad \tilde{\alpha} = \alpha - cd\psi/dP, \tag{21}$$

$$\mathbf{E} = -\alpha\varpi\mathbf{t} \times \mathbf{B}/c - \nabla\psi = -\tilde{\alpha}\varpi\mathbf{t} \times \mathbf{B}/c, \tag{22}$$

and

$$j_p/B_p = \{j_p/B_p\}_{S_l} = -(\alpha/2\pi c)\{B_z/B_p\}_l. \tag{23}$$

It should be emphasized that the non-corotational potential $\psi(P)$ and the associated isorotation function $\tilde{\alpha}$ (P) are fixed by both the physics of the acceleration-plus-pair-production domain and the shape of S_l, and so are strictly determined as part of the global solution. It is anticipated that $\tilde{\alpha} < \alpha$ - subrotation of the field lines in the post-cascade plasma.

In the limit in which S_l is supposed. to be at the pulsar surface, then the model would look as if there were a discontinuity in ψ at the star, as in the Lebedev model (Beskin *et al.* 1993), which however postulates a vacuum gap (a double layer) at the star's surface. We recall that the Ruderman-Sutherland counter-aligned "anti-pulsar" model produced e^+-e^- pairs through the spontaneous breakdown of such a gap, but that model was based on what at that time seemed to be a correct estimate of the work-function for ion emission from the star. I agree with Don Melrose that without such a work function there is no clear reason why such a double layer should form or survive.

The Lebedev group write (in my notation)

$$\psi = \psi_0 + (\alpha/c)\beta P, \qquad \tilde{\alpha} = \alpha(1-\beta). \tag{24}$$

They assume also

$$\varpi B_\phi = i_0(\alpha/c)P, \qquad j_p = -i_0(\alpha/4\pi)B_p, \tag{25}$$

with the return current concentrated into a sheet along the separatrix between the domains with respectively open and closed field lines. They then use the balance between the $B\phi$ and ψ contributions to the Maxwell stresses, applied near the cusp on the separatrix, to derive the relation

$$\beta = 1 - (1 - .4i_0^2)^{1/2}. \tag{26}$$

But as pointed out by Lyubarskii (1992), this suppresses any contribution to the Maxwell stresses of a discontinuity in the poloidal field across the separatrix field line: there is in fact no automatic relation that requires a poloidal current to be associated with a potential jump at the star's surface

The flow described by (21) passes smoothly through the l-c, but –in partial analogy to the charge-separated flow in the classical model of Section 2 –

breakdown in the flow will occur when $E \rightarrow (B_p^2 + B_t^2)^{1/2}$, and simultaneously $\tilde{\alpha}\Omega\varpi^2/c^2 \rightarrow 1$ and $\gamma \rightarrow \infty$ through the slingshot term. The location of the points of breakdown is again to some extent model-dependent. As long as γ is moderate the inertial terms are small and so the poloidal field flux function P satisfies the *relativistic force-free* equation

$$\nabla^2 P(1 - \tilde{\alpha}^2 x^2) - 2\partial P/x\partial x + SdS/dP - \tilde{\alpha}(d\tilde{\alpha}/dP)x^2(\nabla P)^2 = 0, \qquad (27)$$

where P, S, $\tilde{\alpha}$, $x = \alpha\varpi / c$ are appropriate non-dimensional forms, with $\chi = 1$ representing the light-cylinder. If $\tilde{\alpha} = 1$ and $S = 0$, (27) reduces to (10) for the corotating magnetosphere. The two equations are similar in having each a singular surface on which the coefficient of $\nabla^2 P$ vanishes; it is therefore instructive to study first the simpler (10), even though corotation of the gas cannot hold beyond the l-c. Equation (10) is conveniently solved by Fourier transformation in z. Extrapolation across the l-c, *with no discontinuities in P or* $\partial P / \partial x$ yields a solution which blows up at $x = 2$. This is because only one of the two solutions of the Fourier transform equation is finite at $x = 1$, and without a discontinuous gradient at $x = 1$ one cannot extend the solution to infinity. One expects and finds similar behaviour with the realistic equation (27). In rapid rotators, α may be approximated by unity. Numerical integration with simple $S(P)$ functions shows that solutions of (27), smoothly continuous at $x = 1$, again diverge, typically when $x \simeq 1.4$, very close, to the point where the breakdown in the flow occurs, as discussed above.

The next generalization must take account of inertia. For even high γ-values the inertial drifts are small, and the flow is still well approximated by the quasi-mhd equations. The generalization of (27) now has the singular surface $(1 - \tilde{\alpha}^2 x^2 - \boldsymbol{M}_A^2) = 0$, where $\boldsymbol{M}_A$ is an Alfvenic Mach Number. It is perhaps possible that there now exist solutions which are both smoothly continuous and everywhere regular: conceivably the inertial term $\boldsymbol{M}_A^2$ could allow the singular surface to adjust its shape so as to yield such a solution. However, in the preliminary studies, it is postulated rather that there has to be a domain of *dissipative flow.* The tentative model is as follows (Fig, 2). The dissipation domain is taken to be a thin cylindrical layer, located at $x = \tilde{x}$, a little beyond the l-c. The reason for the choice of a cylindrical dissipation domain is in order that the convenient technique of Fourier transformation in z can again be applied, at least in the first iterative stages. Out to $x = \tilde{x}$ the field is taken to be corotating with the star, so that in non-dimensional form, $\mathbf{E} = -x\mathbf{t} \times \mathbf{B}$. (As noted above, the degree of isosubrotation associated with the relativistic acceleration beyond S_1 is in fact quite modest in a rapid rotator - $\tilde{\alpha} \simeq 1$). Beyond $x = \tilde{x}$, $E = -\beta(P)\, x\mathbf{t} \times \mathbf{B}$, where $\beta(P)$ is in fact approximated as a constant. Unless $\beta = 1$, there is a discontinuity in E_x at $\tilde{x}$, linked with the potential difference across the layer, which is in reality of finite thickness and of postulated high effective resistivity. Provided $\beta < 1$ – isosubrotation for $x > \tilde{x}$ – then the potential difference drives currents in the correct sense - inwards near the poles, outwards near the equator. For $x < \tilde{x}$, P is approximated by the solution of the force-free equation (27), with $S = -2P(1 - P/2\bar{P})$, where $\bar{P}$ is the field line along which j_p changes sign. For $x > \tilde{x}$, P satisfies the dissipation-free, quasi-mhd equation with inertial terms retained. Jump conditions at $\tilde{x}$ include radiation of

energy and angular momentum, and continuity of the (x, z) component of the total stress tensor.

The first numerical studies have adopted $\tilde{x} = 1.1$ as a standard value. The results yield β close to the value .9, implying a modest departure from corotation beyond the layer. The radiation loss in the layer is < 10% of the total energy flux. About 10% of the poloidal current closes in the layer. For the Crab pulsar, the wind has $\gamma \simeq 10_6$, carrying typically about .2 of the total energy flux, the rest being carried by the Poynting flux. About 2/3 of the magnetic flux crossing $x = \tilde{x}$ is open, and one third goes into an equatorial disc. It is suggested that the disc becomes periodically unstable, so that the gas flowing from the layer into the disc ultimately joins the wind.

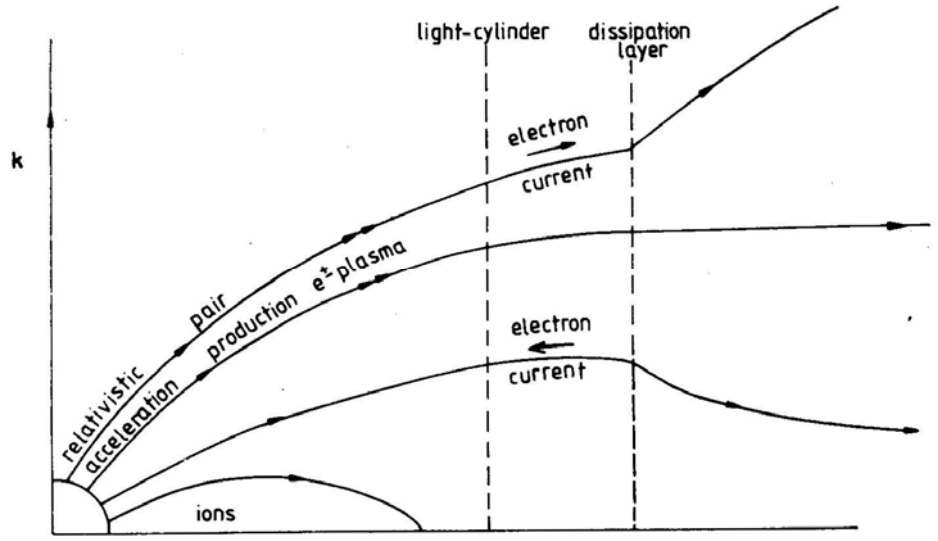

Figure 2: Model with pair production — schematic diagram

These numerical estimates emerge from approximate solution of the macroscopic equations with the appropriate boundary conditions. Just as in the classical problem, the same relativistic slingshot will force up the γ-values of the primary electrons from the value $\simeq 10^6$ pertaining at the end of the pair-production region, and again when γ reaches 10^7, strongly beamed incoherent gamma-radiation will occur. Within the layer, the parallel component of the electric force will maintain the γ-values at the level where the poloidal radiation drag force on the primary electrons is in balance with the electric force: again, the strong γ-dependence of incoherent radiative damping enables the primary particles to act as self-adjusting rheostats. The significant fraction of the power from a number of pulsars coming out as gamma-rays could have its origin as in this model. (However, other pro-

cesses for gamma-ray emission have been proposed. It is likely that the a viable model will include a *vacuum gap* region, in which again **E.B** differs markedly from zero (e.g. Fitzpatrick and Mestel I, II 1988). Cheng *et al.* (1986) have pointed out that e^+-e^- generation will occur in such a gap, with the created particles being accelerated in opposite directions to highly relativistic energies and so again emitting gamma-rays, especially by inverse-Compton scattering on infra-red photons).

The e^+-e^- pairs are also energized by the slingshot effect, the energy source being as usual the potential variation across the polar caps. The pair electrons will be further accelerated through the layer by $\mathbf{E}_{||}$, though their motion may be inertially- rather than dissipatively-limited; but the pair positrons are *de*celerated by the $\mathbf{E}||$ component. Recall that the existence of a dissipation layer – with a potential variation along each field line segment as it crosses the layer – has emerged from attempts to model the macroscopic structure of the magnetosphere. In a normal plasma problem, the $\boldsymbol{E}_{||}$ -component is determined locally from the balance of electric force against Ohmic resistance, due to the mutual scattering that inhibits the relative motion of the oppositely-signed charges that makes up the $j_{||}$. A *sufficiently high* resistivity would then determine a layer thickness well below a l-c radius. The ordinary micro-resistivity is far too small to be important. The highly supersonic relative motion of the e^+-e^- gases is subject to the two-stream instability. One can estimate an effective "anomalous" resistivity by replacing the binary collision frequency by the linear instability growth rate; however, this also does not appear to be large enough.

In the absence of any scattering, a positron could pass through the layer if it enters with a sufficiently high γ because of the slingshot effect. However, the total energy available is limited by the potential variation across the polar cap. Requiring a steady stream of positrons to cross against the adverse potential difference sets an upper limit on the multiplicity: $\boldsymbol{M} < 1/(1 - \beta)$. Thus if one were able to construct models with $\beta \approx .99$ rather than .9, a modest value $\boldsymbol{M} \approx 100$ might be acceptable within this no-scattering picture. However, a much more attractive alternative is that the system developes a more powerful effective resistivity, so that the outstreaming pairs are kept coupled as they cross the dissipative domain. It is significant that in the constructed model force-free fields, the toroidal component becomes large compared with the poloidal as the surface of breakdown is approached. This suggests that the poloidal currents are limited by a consequent hydromagnetic instability, which would yield a large effective macroresistivity (*cf.* Sect. 5, Mestel and Weiss 1987, Lyubarskii 1991, preprint).

Breakdown in the flow beyond the 1-c is found also by Beskin *et al.* (1993), even though they have postulated a potential jump at the star's surface. They argue that the electrons and positrons flow across the field lines in their boundary layer, the electrons equatorwards and the positrons polewards, with both species ultimately returning to the star. They suggest that the energy loss to infinity is via mhd waves, rather than through the escape to infinity of the e^+-e^- gas, as assumed by most other workers (e.g. Kennel et *al.* 1983, Shibata 1991, Camenzind 1993). In the classical model of Sect. 2, the return of electrons to the star (after dissipative drift across the field lines) is mandatory to avoid continual charging up of the star; and in any case the GJ number-density is so low that flow to infinity would in general require γ-values so large as to yield far too much radiation loss.

By contrast, in a model with pair production, once the bulk of the plasma has crossed the domain with finite $E_{||}$ it can then flow to infinity, dragging the field with it, provided $2M_{nGJ}\gamma_{c2} \gg B_2/8\pi$; so as long as the multiplicity M is large, only moderate γ-values are required. Charge balance may again be maintained by the return to the star of electrons at the (GJ) emission rate. Alternatively, pairs may be produced in outer magnetospheric gaps (Cheng *et al.* 1986), but a preferential loss of positrons may occur (Shibata, private communication).

4. Non-axisymmetric models

Most of the analysis in the literature has been carried out for the aligned rotator, the "non-pulsar", though Beskin *et al.* (1993) do apply their ideas to the oblique rotator. Any rigidly rotating, non-axisymmetric system that is "steady in the rotating frame" can be analysed using the operator-equivalence $\partial/\partial t = -\alpha\partial/\partial\Phi$, applied to scalars and e.g. to cylindrical and spherical polar scalar components of vectors, where Φ is the azimuthal angle about the rotation axis. One readily arrives at the generalization of the relativistic force-free equation (27) with $\tilde{\alpha} = 1$ (Endean 1974; Mestel 1973; Mestel *et al.* 1976):

$$\nabla \times \tilde{\mathbf{B}} = \kappa \mathbf{B}, \tag{28}$$

where

$$\tilde{\mathbf{B}} = [B_x(1 - x^2), B_\Phi, B_z(1 - x^2)]. \tag{29}$$

The corotating G-J charge density is responsible for the replacement of $\mathbf{B}$ by $\tilde{\mathbf{B}}$, and $\kappa\mathbf{B}$ represents the currents along $\mathbf{B}$. Results similar to the axisymmetric case can be expected, such as the inevitable breakdown of a continuous force-free model on a surface beyond the l-c. For example, in the case of the perpendicular rotator, asymptotic analysis applied to the simplest case, with $\kappa = 0$ - the analogue of (10) - shows that a continuous solution would again blow up at $x = 2$; and with $\kappa \neq 0$, one expects the breakdown surface to be somewhat nearer to the l-c.

In the aligned case, it was noted that quasi-mhd flow breaks down beyond the l-c, at points close to where the breakdown in (27) occurs. As pointed out by Kahn (1971), in the oblique problem one must distinguish between field lines that point forward with respect to the sense of rotation from those that point backwards. Particles moving out along forward-pointing lines will approach speed c near the l-c, and so are forced to deviate from the field line through an inertial or dissipative drift just before the l-c. Particles moving out along backward-pointing have no difficulty in passing through the l-c, but in general can again be expected to approach $\gamma = \infty$ some way beyond, and so will again drift across field lines. There are thus some qualitative similarities between the aligned and oblique cases. Construction of a reasonably accurate global model will clearly be more difficult than for the aligned case (even for the perpendicular rotator), but the experience gained from the axisymmetric problem should be valuable. One again anticipates a domain in which; the field is nearly force-free, beginning at the star and terminating near the l-c, and again separated by a dissipative domain from a non-force-free

but dissipation-free domain, extending to infinity.

5. The pulsar wind

Most workers picture the spin-down energy and angular momentum of an aligned or nearly aligned pulsar as being carried off by a magnetohydrodynamic wind. Michel (1970) and Goldreich and Julian (1970) pioneered the study of cold relativistic winds. Near the star, the transport is essentially all by the Poynting vector and the Maxwell stresses. A difficulty with the simple wind theory is that it predicts at infinity a dominant toroidal field component, and so also a Poynting flux that is still at least comparable with the particle energy flux. That this sets a difficulty emerged in early work by Rees and Gunn (1974). Their model for the Crab nebula combined a strong wave with a relativistic pulsar wind. The wind is decelerated by a strong shock at about 3×10^{17}cm from the pulsar. To make the post-shock speed decrease with radial distance, so as to match the observed 2000km/sec expansion speed of the outer Crab nebula, one needs rather that the ratio $\sigma \equiv$ (Poynting flux/kinetic energy flux)$\ll 1$ upstream -if instead $\sigma \gg 1$, the downstream flow is also Poynting dominated. Kennel and Coroniti (1984) came to a similar conclusion for their e^+-e^- wind: they require $\sigma_\infty = 3 \times 10^{-3}$, as compared with the value $\simeq 10^{4-5}$ yielded by most models. (The tentative Mestel-Shibata model referred to above has $\sigma \simeq 10$ after the dissipation layer, smaller but still too large).

The Poynting flux must be converted into kinetic energy but in the wind zone, well beyond the l-c, otherwise synchrotron losses would predict far too much X-ray and γ-ray emission near to the star. Lyubarskii and others suggest that the excess toroidal energy may ultimately be dissipated as a consequence of mhd instabilities that may set in when $|B_\Phi / B_p| \gg 1$, especially the kink instability (*cf.* the work of Tayler, Wright and others on instabilities of stellar magnetic fields). This is very plausible, though one has to extrapolate the linear instability theory into the unexplored non-linear domain. The oblique rotator offers other opportunities. Coroniti (1990) points out that the wind emitted by an oblique rotator will be magnetically "striped", with B of alternating sign. He therefore argues for the systematic mutual annihilation of opposite polarity stripes as the wind flows out, estimating that the initial Poynting flux is destroyed within about 8×10^6 l-c radii. It was noted in Mestel *et al.* 1976 that the extrapolation of the GJ *ansatz* **E.B** =0 to infinity led to unacceptable conclusions in the oblique problem. More recently, Melatos and Melrose (1994) have argued that it is in fact the breakdown in the ability of the charges to short out the displacement current that enforces efficient dissipation of the large toroidal fields.

6. Conclusion

The construction of fully self-consistent electromagnetic and particle fields remains still a formidable task for the future. It is noteworthy that although there are dif-

ferences on the presence or absence of a potential gap at the star's surface, there is agreement on the appearance beyond the l-c of a domain of breakdown of the force-free, quasi-mhd approximations. Further effort should be devoted to elucidate the physics of this domain, in particular to estimate its effective resistivity. Concentration on the axisymmetric model should not be decried, as success there is likely to be a useful guide to the oblique models; however, the time seems ripe for a return to a parallel study of quasi-steady, force-free models.

References

Arons, J., 1981. *Astrophys. J. ,* **248,** 1099.

Arons, J.& Scharlemann, E. T., 1979. *Astrophys. J.* , **231**, 854.

Beskin, V. S., 1990. *Sov. Astr. Lett.,* **16**, 286.

Beskin, V. S., Gurevich, A. V. & Istomin, Ya. N., 1993. *Physics of the Pulsar Magnetosphere,* Cambridge University Press.

Camenzind, M., 1993. *Astron. Astrophys.,* **270,** 71.

Cheng, K. S., Ho, C. & Ruderman, M., I & II, 1986. *Astrophys. J.* , **300,** 500 & 522.

Cohen, J. M. & Toton, E. T., 1971. *Astrophys. Lett.,* 7, 213.

Coroniti, F. V., 1990. *Astrophys. J.* , **349**, 538.

Daugherty, J. K. & Harding, A. K., 1982. *Astrophys. J.* , **252,** 337.

Endean, V. G., 1974. *Astrophys. J.* , **187**, 359.

Fawley, W. M., Arons, J. & Scharlemann, E. T., 1977. *Astrophys. J. ,* **217**, 227.

Fitzpatrick, R. & Mestel, L., I & II, 1988. *Mon. Not. R. astr. Soc.* , **232,** 277 & 303.

Gold, T., 1969. *Nature, Lond.,* **221,** 25.

Gold, T., 1980. In: *Ninth Texas Symposium on Relativistic Astrophysics*, p. 448, eds Ehlers, J., Perry, J. J. & Walker, M., New York Academy of Sciences.

Goldreich, P. & Julian, W. H., 1969. *Astrophys. J.* , **157**, 869.

Goldreich, P. & Julian, W. H., 1970. *Astrophys. J.* , **160,** 971.

Holloway, N. J., 1977. *Mon. Not. R. astr. Soc. ,* **181**, 9p.

Jones, P. B., 1980. *Mon. Not. R. astr. Soc. ,* **192,** 847.

Kahn, F. D., 1971. Paper read at Royal Astronomical Society.

Kennel, C. F. & Coroniti, F. V., 1984. *Astrophys. J.* , **283**, 694.

Kennel, C. F., Fujimura, F. S. & Okamoto, I., 1983. *Astrophys. Geophys. Fluid Dyn.,* **26**, 147.

Krause-Polstorff, J. & Michel, F. C, 1985. *Mon. Not. R. astr. Soc*. , **213**, 43.

Lyubarskii, Yu.E., 1992. In: *The Magnetospheric Structure and Emission Mechanisms of Radio Pulsars*, p.112, eds Hankins, T. M., Rankin, J. M. & Gil, J. A., Pedagogical Univ. Press, Zielona Gora, Poland.

Melatos, A. & Melrose, D. B., 1994. *Mon. Not. R. astr. Soc.* , submitted.

Mestel, L., 1971. *Nature Phys. Sci*., **233,** 149.

Mestel, L., 1973. *Astrophys. and Sp. Sc*., **24**, 289.

Mestel, L. & Pryce, M. H. L., 1992. *Mon. Not. R. astr. Soc.* , **254,** 355.
Mestel, L. & Shibata, S., 1994. *Mon. Not. R. astr. Soc.* , *in press.*
Mestel, L. & Wang, Y.-M., 1979. *Mon. Not. R. astr. Soc.* , **188,** 799.
Mestel, L. & Wang, Y.-M., 1982. *Mon. Not R. astr. Soc.* , **198,** 405.
Mestel, L. & Weiss, N. O., 1987. *Mon. Not. R. astr. Soc.* , **226,** 123.
Mestel, L., Westfold, K. C. & Wright, G. A. E., 1976. *Mon. Not. R. astr. Soc.*, **175,** 257.
Mestel, L., Robertson, J. A., Wang, Y.-M. & Westfold, K. C, 1985. *Mon. Not. R. astr. Soc.* , **217,** 443.
Michel, F. C, 1969. *Astrophys. J.* , **158,** 727.
Michel, F. C, 1991. *Theory of Neutron Star Magnetospheres,* Chicago University Press.
Muslimov, A.G. & Tsygan, A. I., 1990. *Astr. Zh.*, **67,** 263.
Muslimov, A.G. & Tsygan, A. I., 1992. *Mon. Not. R. astr. Soc.* , **255,** 61.
Pacini, F., 1967. *Nature, Lond*., **216,** 567.
Rees, M. J. & Gunn, J. E., 1974. *Mon. Not. R. astr. Soc.* , **167**, 1.
Ruderman, M. & Sutherland, P. G., 1975. *Astrophys. J.* , **196,** 51.
Shibata, S., 1991. *Astrophys. J.* , **378,** 239.
Sturrock, P. A., 1971. *Astrophys. J.* , **164,** 529.

Diamond Jubilee Symposium on Pulsars
14 –17 March 1994
Raman Research Institute, Bangalore

J. Astrophys. Astr. (1995) **16,** 137-164

The Models for Radio Emission from Pulsars – The Outstanding issues

D.B. Melrose *Research Centre for Theoretical Astrophysics, School of Physics, University of Sydney, NSW 2006, Australia*

Abstract. The theory of pulsar radio emission is reviewed critically, emphasizing reasons why there is no single, widely-accepted emission mechanism. The uncertainties in our understanding of how the magnetosphere is populated with plasma preclude predicting the properties of the emission from first principles. Some important observational features are incorporated into virtually all the proposed emission mechanisms, and other observational features are either controversial or fail to provide criteria that clearly favor one mechanism over others. It is suggested that the criterion that the emission mechanism apply to millisecond, fast young, and slow pulsars implies that it is insensitive to the magnetic field strength.

It is argued that coherent emission processes in all astrophysical and space plasmas consist of emission from many localized, transient subsources, that any theory requires both an emission mechanism and a statistical theory for the subsource, and, that this aspect of coherent emission has been largely ignored in treatments of pulsar radio emission. Several specific proposed emission mechanisms are discussed critically: coherent curvature emission by bunches, relativistic plasma emission, maser curvature emission, cyclotron instability and free electron maser emission. It is suggested that some form of relativistic plasma emission is the most plausible candidate although one form of maser curvature emission and free electron maser emission are not ruled out. Propagation effects are discussed, emphasizing the interpretation of jumps between orthogonal polarizations.

1. Introduction

The pulsar radio emission mechanism is still poorly understood. Reasons for our lack of success in identifying the emission mechanism unambiguously can be attributed to three aspects of the problem. The first aspect concerns the structure of the magnetosphere. In principle, if one understood the distribution of particles

and fields in the magnetosphere well enough, one could hope to predict the radio emission from first principles. However, the uncertainties in our knowledge make this impractical. The second aspect concerns the phenomenological interpretation of the radio data. Some general features clearly constrain the emission mechanism, specifically, the very high brightness temperature, the beaming, and the sweep of linear polarization. However, these features do not suffice to determine the emission mechanism uniquely. Furthermore, other properties of the observed emission (e.g., pulse profiles, microstructure, circular polarization, frequency-to-radius mapping, jumps between orthogonal modes) have not led to well-defined, widely-accepted criteria for selecting between different emission mechanisms. As remarked by Radhakrishnan (1992), "more and more detailed radio observations are NOT what is needed to help with theoretical modeling." Well-defined, observationally-based criteria that allow one to select between different mechanisms are required. The third aspect of the problem concerns the nature of coherent emission processes. It is argued below that coherent emission mechanisms are intrinsically more complicated than incoherent mechanisms, that existing treatments of such mechanisms are oversimplified and that expectations of what a successful theory should explain tend to be unrealistic. All of these three aspects are discussed in this paper, with emphasis on the nature of coherent emission processes. The effects of propagation of the escaping radiation through the pulsar magnetosphere are also discussed.

The very high brightness temperature of pulsar radio emission implies that some coherent emission mechanism is involved. It is clear that the pulsar emission mechanism is not the same as other forms of coherent emission that are known to occur in space and astrophysical plasmas. These are *plasma emission* in solar radio bursts and from planetary bow shocks and *electron cyclotron maser emission* from planetary magnetospheres, probably also in solar radio spike bursts and in the very bright emission from some flare stars (e.g., Melrose 1991). There is much more information on the plasma properties in some of these sources than there is for pulsars, but nevertheless, in no case is the theory better than semiquantitative. In these contexts, there is direct evidence that, at any given time, the coherent emission occurs in a very small fraction of the volume of the source, and it is argued here (section 4) that this is probably an intrinsic feature of every coherent emission process in an astrophysical plasma. This implies that any theory for such coherent emission needs two ingredients: the mechanism for emission from the localized regions and a statistical theory for the distribution of these localized regions within an envelope defined by the effective source. The statistical ingredient is neglected in most existing theories for pulsar radio emission, and needs to be taken into account to treat the emission even semiquantitatively.

The discussion of pulsar radio emission is set out as follows. The structure of the magnetosphere and how it impinges on theories for the radio emission is discussed in section 2. The phenomenological interpretation of the radio emission, and criteria on an acceptable emission mechanism are discussed in section 3. The foregoing general points on coherent emission are discussed in more detail in section 4, where existing models for pulsar radio emission are also reviewed. Propagation effects are discussed in section 5. The conclusions are summarized in section 6.

2. The Particle Populations in the Source Regions

Pulsar magnetospheres are thought to be populated by one-dimensional, relativistic pair plasmas that are created through a pair cascade in 'gaps' where there is a large parallel electric field. In most models, the radio emission is attributed to the pair plasma flowing outward along open magnetic field lines from the polar caps.

2.1 *Gaps and pair production*

Pulsar magnetospheres are assumed to consist of a magnetically closed region and two magnetically open regions. The closed region, or dead zone, is defined by those field lines that close within the light cylinder, of radius $r_{lc} = c/\Omega$, with $\Omega = |\mathbf{\Omega}|$, where $\mathbf{\Omega}$ is the angular velocity of rotation of the star. It is assumed that the dead zone is filled with sufficient plasma to provide the corotation electric field

$$\mathbf{E} = -(\mathbf{\Omega} \times \mathbf{x}) \times \mathbf{B}, \tag{2.1}$$

where x is the position vector relative to the center of the star, and **B** is the magnetic induction. The polar caps are the remaining regions where the magnetic field lines are open in the sense that they cross the light cylinder.

An inconsistency arises when one considers whether or not the open region is filled with plasma. On the one hand, if there were no plasma in the magnetosphere, then the electrodynamics implies (a) an electric field with component, $E_{||}$, parallel to the magnetic field, and (b) a large potential difference, Φ_{pc}, between the center and the edge of the polar cap region. For a dipolar field, with $B_p \sim 10_8$ T (10_{12} G) at the poles, the values at the stellar surface (radius $r = R$ with $R = 10$ km) are

$$(E_{\|})_{pc} \approx \left(\frac{\Omega R}{c}\right)^{3/2} cB_P, \tag{2.2}$$

$$\Phi_{pc} = \frac{\Omega^2 B_P R^3}{2c}$$

$$= 6.6 \times 10^{14} \left(\frac{B_P}{10^8\,\mathrm{T}}\right)\left(\frac{P}{0.1\,\mathrm{s}}\right)^{-2} \mathrm{V}, \tag{2.3}$$

where $P = 2\pi/\Omega$ is the period of the pulsar. In the superstrong magnetic field, a stray gamma ray with energy greater than twice the rest energy of the electron decays into a pair, $\gamma + B \rightarrow e^- + e^+ + B$. The components of this pair are accelerated to very high energy ($\lesssim e\Phi_{pc}$) by $E_{||}$. These *primary* particles emit gamma rays, through curvature emission and other processes, triggering a pair cascade (Sturrock 1971). As a result, a secondary pair plasma is created. The secondary pair plasma tends to shield out $E_{||}$, and to set up the corotation electric field (2.1), invalidating the original assumption that vacuum conditions apply.

On the other hand, if one assumes that that the. polar cap regions are filled with plasma, so that the corotation electric field (2.1) is set up everywhere, there is nothing to prevent the plasma from flowing outward along the open field lines and being lost through a pulsar wind. Hence, one requires a source of plasma to maintain the electric field (2.1) in the polar cap regions. The only acceptable

source of plasma is a pair plasma generated by the processes outlined above, but this requires $E_{||} \neq 0$ at least in the source region where the primary pairs are created.

A self-consistent model requires that that there be a source region (or several source regions) with $E_{||} \neq 0$. Such a region is referred to as a *gap*. Gaps must fil only a fraction of the volume, or be present only a fraction of the time. The pair plasma generated in the gaps populates the remainder of the open-field region, and supplies the particles that form the pulsar wind. There are several specific models for the gaps, including polar-cap, slot-gap and outer-gap models.

The open field lines cross the light cylinder and the magnetic field continues to influence the flow until the Maxwell (magnetic) stress decreases to below the ram pressure (γmnc^2) of the relativistic outflow. Without pair production, the outflow involves only the single-sign Goldreich-Julian density and balancing of the stresses implies Lorentz factors γ large enough for there to be strong gamma-ray emission, so that particles are no longer tied to the field (e.g., Mestel 1981). However, with a dense pair plasma generated through pair creation, more modest γ-values enable the flow to continue to infinity as a wind, dragging the field with it.

2.2 *Location of the source of the pairs*

In polar-gap models, the gap occurs immediately above the stellar surface in the polar cap. In the model of Ruderman & Sutherland (1975) this gap is attributed to the strong binding of nuclei to the stellar surface, preventing ions from being ripped off the surface. This model applies only to neutron stars with $\mathbf{\Omega} \cdot \mathbf{B} < 0$, in which case the sign of $(E_{||})_{\rm PC}$ is such that ions tend to be accelerate upward. (Neutron stars with $\mathbf{\Omega} \cdot \mathbf{B} > 0$ would not be pulsars in this model.) The binding energy was subsequently shown to be inadequate for this model to apply (e.g., Neuhauser, Koonin & Langanke 1987, Abraham & Shapiro 1991), at least for most pulsars. Despite the absence of a clear alternative physical basis for them, polar-gap models continue to be considered. For example, in the model of Beskin, Gurevich & Istomin (1988, 1993) the pair plasma is postulated to be created in a double layer near the stellar surface. However, why such a double layer should form near the surface is not clear to this author.

In a second class of model, it is assumed that plasma can flow freely from the surface, screening $E_{||}$ immediately above the stellar surface. This class includes the slot-gap model of Arons and coworkers (e.g., Fawley, Arons & Scharlemann 1977; Scharlemann, Arons & Fawley 1978; Arons 1981, 1983, 1992), and a modified form of the Ruderman & Sutherland model (Cheng & Ruderman 1980). A related "classical" model has been developed by Mestel and coworkers (e.g., Mestel 1981, 1993; Mestel et al 1985; Fitzpatrick & Mestel 1988a, b; Shibata 1991), as discussed elsewhere in these proceedings by L. Mestel. Although these models differ in details, the important feature that they have in common is that somewhere above the surface a large parallel electric field tends to build up. This arises from the incompatibility of two requirements. One is the requirement that the charge density, for $r \ll r_{\rm lc}$, be maintained at the Goldreich-Julian value (Goldreich &

Julian 1969)

$$n_{GJ} = -\frac{2\varepsilon_0 \boldsymbol{\Omega} \cdot \mathbf{B}}{e}. \tag{2.4}$$

This is necessary for the plasma to shield out the $E_{||}$ that would be present in vacuo. The other requirement is that, in the absence of any other source of charge, the outflowing current be conserved. As the cross-sectional area (α $1/B$) of a magnetic flux tube changes, the current density, $\boldsymbol{J} = en_{GJ}\upsilon_f$, must change to satisfy $J \alpha B$. Once the flow speed, υ_f, becomes relativistic, these requirements become, respectively, $n_{GJ} \alpha B_z$, where the z-axis is along the rotation axis, and $n_{GJ} \alpha B$, and they are obviously incompatible for any realistic magnetic structure. Hence, an $E_{||}$ builds up, and the two requirements can only be satisfied by this electric field leading to a source of pairs that can provide the required shielding. The upper limit on $E_{||}$ in such space-charge-limited flows is two to four orders of magnitude smaller than $(E_{||})_{pc}$.

The models based on space-charge-limited flows apply to neutron stars with $\boldsymbol{\Omega} \cdot \mathbf{B} > 0$, when electrons flow away from the stellar surface, and to neutron stars with $\boldsymbol{\Omega} \cdot \mathbf{B} < 0$, provided that the ions are not too tightly bound. One might expect there to be some qualitative difference between these two cases, that is, one might expect two classes of pulsars determined by the sign of $\boldsymbol{\Omega} \cdot \mathbf{B}$. However, there is no observational evidence for two such classes. This suggests that the two classes are indistinguishable from an observational viewpoint, or that one class is not observed at all. Assuming that the two classes are indistinguishable, one infers that the binding of the ions to the stellar surface and the inertia of the ions or electrons are unimportant in the processes leading to the production of the secondary pair plasma (cf. Beskin 1982).

A third type of model has outer gaps, associated with the field lines that pass through the surface where the Goldreich-Julian charge density changes sign (e.g., Holloway 1973; Holloway & Pryce 1981). Such outer gaps occur near the last closed field lines at the edge of the dead zone. Outer-gap models are favored for those pulsars that have pulsed gamma-ray emission (e.g., Cheng, Ho & Ruderman 1986a,b).

2.3 *Current closure*

A current flow, with current density ~ $en_{GJ}\,c$, is implied in polar-cap models and the question of how this current closes is an important ingredient in any acceptable model (e.g., Arons 1992). A current circuit that closes near the light cylinder is a feature of most closed-circuit models (e.g., Arons 1979, 1981, 1992; Rylov, 1979; Mestel 1981, 1993; Mestel et al 1985; Beskin et al 1986, 1993). However, the identification of the processes involved in closing the current circuit, so that the star does not charge up, remains one of the weak points of the theory (e.g., Michel 1982, 1991, 1992).

An interesting way of resolving the difficulties with current closure was suggested by Shibata (1991), who proposed a DC circuit with two sources of pair plasma, in an inner gap and in an outer gap. The closure of the current across field lines occurs in the wind zone where the $\mathbf{J} \times \mathbf{B}$ force is related to the acceleration of the wind. An important constraint on the model is that the angu-

lar momentum loss is in balance with the energy loss (Holloway 1977). Shibata (1991) found that for fast pulsars there are two possible regimes depending on the dominant component in the angular momentum loss: a wind-dominated regime in which the angular momentum is carried off primarily by the wind, and an outer-gap-dominated regime in which the angular momentum loss is dominated by high-energy photons from the outer gap. The former seems to apply to the Crab pulsar. For slower pulsars these two regimes merge.

An alternative approach to the current closure problem is to assume that the neutron star charges up, so that electrostatic forces cause a closed structure with zero current outflow (e.g., Jackson 1976; Michel 1979, 1982, 1991; Krause-Polstorff & Michel 1985a,b). Such models are not discussed in detail here.

2.4 *The secondary pair plasma*

The production of the secondary plasma is attributed to a pair cascade, which has been treated both numerically and analytically (e.g., Sturrock 1971; Arons & Scharlemann 1979; Daugherty & Harding 1982; Gurevich & Istomin 1985). The primary particles generate gamma rays, with energy $\varepsilon_{\rm Ph}$, through curvature emission, synchrotron emission and possibly other processes. The curvature photons are directed along the magnetic field lines but, due to the curvature of the field lines, the angle, θ, between their direction of propagation and **B** increases systematically. When the threshold

$$\varepsilon_{\rm ph} \sin\theta > 2m_e c^2 \tag{2.5}$$

is exceeded, a photon decays into a pair. (In a detailed calculation the polarization of the photons and the different thresholds for different polarizations need to be taken into account.) If this decay occurs in the gap, then the components of the pair are accelerated in opposite directions by $E_{||}$ and become primary particles. If the decay occurs outside the gap, then the pairs form a secondary pair plasma. The detailed distribution of secondary particles depends on how the value of $E_{||}$ varies through the region where the pairs are created, and the value of $E_{||}$ in turn depends on the distribution of the pairs that tend to shield it out.

Once produced, the pair plasma rapidly becomes one dimensional in the superstrong magnetic field, where superstrong corresponds to B being comparable to the critical magnetic field

$$B_{\rm crit} = m_e^2 c^2 / e\hbar = 4.4 \times 10^9 \ {\rm T}. \tag{2.6}$$

(The ratio $B/B_{\rm crit}$ is equal to the ratio of the cyclotron energy $\hbar\Omega_e$, where $\Omega_e = eB / m_e$ is the cyclotron frequency, to the rest energy, $m_e c^2$.) The perpendicular motion of a particle is simple harmonic motion, and hence is quantized as a simple harmonic oscillator. When the spin is included, the energy eigenvalues are

$$\varepsilon_n(p_{||}) = (m^2 c^4 + p_{||}^2 c^2 + 2neB\hbar c^2)^{1/2}, \tag{2.7}$$

with the ground state, $n = 0$, nondegenerate, and each excited state, $n = 1, 2, \ldots$, doubly degenerate. The states with different values of n are referred to as the Landau levels. Due to gyromagnetic emission, which is synchrotron emission for

$nB / B_{\rm crit} \gg 1$, particles jump to lower Landau levels sequentially. For $p_{||} = 0$, the rate of transitions from state n to state $n - 1$ is

$$R_{n\to n-1} = n\alpha \frac{4m_e c^2}{3\hbar} \left(\frac{B}{B_{\rm crit}}\right)^2, \tag{2.8}$$

where $\alpha \approx 1/137$ is the fine structure constant. The lifetime for the decay to the ground state is of order the inverse of the transition rate for the slowest transition, which is the transition $1 \to 0$. This gives a lifetime of order $3/B^2$ s, where B is in tesla. The lifetime is so short, $\sim 2 \times 10^{-17}(B/0{\cdot}1B_{\rm crit})^{-2}$ s in its rest frame (increased by a factor γ in the pulsar frame), that one expects all electrons and positrons to be in their ground state, corresponding to one-dimensional motion.

Another property of the secondary pair plasma concerns the multiplicity factor, which is the ratio of the number of secondaries to the number of primaries, and which is estimated to be in the range 10^3-10^5. The mean Lorentz factor of the secondaries is estimated to be $\gamma \sim 10^2$–10^3.

An effect that should be important in stronger fields, $B \gtrsim 0{\cdot}1B_{\rm crit}$, is the formation of positronium (e.g., Shabad & Usov 1984; Shabad 1992; Meszaros 1992). This effect should impede pair production, and reduce the effectiveness of the shielding of $E_{||}$. However, there is no obvious observational feature in the radio emission that has been associated with the threshold ($B \sim 4 \times 10^8$ T) for this effect to become important.

2.5 *Summary*

One may conclude that some features of pulsar electrodynamics are sufficiently well understood to indicate the general conditions under which pulsar radio emission is generated, but that the finer details are poorly understood.

1. The production of primary and secondary pairs probably occurs in the polar cap regions at some height above the surface of the neutron star.

2. The secondary plasma involves electrons and positrons flowing outward along the field lines in one-dimensional motion.

3. The multiplicity of the secondary pairs is estimated to be 10^3-10^5 and their Lorentz factors to be $\sim 10^2$, but neither number is well determined.

4. The detailed distribution functions of the secondary pairs is poorly determined, e.g., due to the dependence of the distribution of the partial shielding of $E_{||}$ near the edges of gaps.

These arguments suggest that radio emission mechanisms that involve pairs flowing outward along open, curved magnetic field lines in the polar cap regions are consistent with what is known of the electrodynamics. However, important details concerning the distribution functions of the secondary plasma are poorly determined. Clearly, a "bottom-up" approach, in which one attempts to identify the radio emission mechanism from first principles, is not realistic.

3. Criteria for an Acceptable Eumission Mechanism

Several general observational criteria (brightness temperature, beaming and linear polarization, microstructures) are incorporated into nearly all suggested pulsar emission mechanisms. However, other observational features (core or conal emission, frequency to radius mapping, circular polarization) lead to selection criteria that are either controversial or fail to distinguish between different specific emission mechanisms. One criterion that can be used to argue against some emission mechanisms is that the mechanism must apply to both weak-B (millisecond) and strong-B (young, fast) pulsars, that is, the mechanism must apply to a range of four to five orders of magnitude in B.

3.1 *The brightness temperature*

The brightness temperature of pulsar radio emission is very much higher than for any other radioastronomical sources. Its maximum value, estimated to be in the range $T_b \sim 10^{25}$–10^{30} K, is at least ten orders of magnitude greater than the next brightest sources, which are some flare stars (e.g., Dulk 1985). The very high T_b requires a coherent emission mechanism, and this requirement is built into all the emission mechanisms discussed here. Although it is clear that pulsar emission is due to some coherent emission mechanism, the required high T_b does not distinguish between possible coherent emission mechanisms in any obvious way.

3.2 *Beaming*

In all pulsar models, the pulsed nature of the emission is interpreted in terms of beamed radiation from the pulsar sweeping across the line of sight of the observer as the neutron star rotates. In polar cap models, the beaming is explained in terms of the relativistic beaming effect for relativistic particles propagating along the magnetic field lines, which implies that the radiation is confined to a cone with half-angle $\sim 1/\gamma$ about the direction of the magnetic field. This beaming is a feature of emission by relativistic particles and applies to all relevant emission mechanisms. It cannot be used as a criterion to distinguish between emission mechanisms that involve relativistic particles in one-dimensional motion along **B.**

3.3 *Linear polarization*

The most obvious features of the polarization of pulsars are the high degree of linear polarization, and the systematic sweep of the plane of polarization through a pulse. In young pulsars the polarization is typically 100% linear. Older (slower) pulsars tend to have a more complicated polarization structure, sometimes with a significant circular component.

The linear polarization is well explained in terms of the single-vector model of Radhakrishnan & Cooke (1969). This model applies to any mechanism that produces linear polarization, with the plane of polarization fixed by the direction of the magnetic field at the point of emission. This condition is satisfied by all

relevant emission mechanisms, and so cannot be used as a criterion to distinguish between mechanisms.

3.4 *Core and coned emission*

The structure of pulses from different pulsars have been classified in several different ways. Some pulsars, typically younger pulsars, have pulses with a single peak, and others have two or more peaks. Rankin (1983a, b, 1986, 1990) argued for two types of emission: 'core' emission and 'conal' emission, with the former near the center of the pulsar beam and the latter near its edge. The observed pulse profile depends on the relative level of these two components in the beam and on where the line of sight intersects the beam. In its simplest form, this model provides the following interpretation for multiple peaks. The core emission is assumed to dominate in pulsars with single-peak profiles and to give the central component in triple-peak profiles when the line of sight passes, close to the center of the beam. The conal emission is assumed to give the two peaks in double-peak profiles, when the line of sight misses the core component, and the outer peaks in triple-peak profiles. However, when random variation in the intensity is taken into account, more complicated interpretations need to be considered. For example, a double-peak profile at one frequency can be one edge of the conal emission and core emission, with the other edge of the conal emission missing at that frequency (but possibly present at other frequencies); also, the polarization can often allow one to distinguish between such truncated triple and truly double burst profiles.

Lyne & Manchester (1986) argued for a different interpretation in which the observed pulse profiles are interpreted in terms of favored regions for emission within a pulse envelope. Rankin's model could be regarded as a special case of Lyne & Manchester's model, with the favored regions corresponding to a core and a cone.

A controversial point is whether as Rankin argued, the core and conal component are qualitatively different, with different frequency dependencies, and coming from different heights (at a fixed frequency). Rankin's arguments have been interpreted by some authors in terms of intrinsically different core and conal emission mechanisms (e.g., Beskin et al 1993, p. 337). In the alternative model of Lyne & Manchester there is no implication that there is any such difference. In formulating criteria for distinguishing between proposed emission mechanisms, the case for favoring mechanisms that distinguish between core and conal emission is not well established. What is well established is that the beam has an envelope, which in many cases is in the form of a hollow cone, sometimes with a core component and sometimes with a more complicated structure. In the hollow-cone model this envelope is attributed to the magnetic flux tube defined by the set of open field lines, that is, of the field lines that extend beyond the light cylinder.

3.5 *Microstructure*

Another effect that may be related to beaming is the microstructure in pulsar radiation (e.g., Cordes 1975, 1979). Microstructure could be explained in terms of either spatial or temporal structures. An explanation in terms of spatial structures

involves subsources with narrow intrinsic beamwidth inside the pulsar beam, which defines an envelope for the narrow beams. As discussed in section 4, small spatial and temporal structures are to be expected in coherent emission mechanisms. Although study of microstructures in the emission may well provide useful information on microstructures in the distribution of particles, once again it does not provide an obvious criterion for distinguishing between different coherent emission mechanisms.

3.6 *Frequency to radius mapping*

There is indirect evidence for a frequency to radius mapping that favors emission from the polar cap regions well inside the light cylinder (e.g., Cordes 1978, 19 9, 1981, 1992; Phillips 1992). In particular, the narrowing of the separation between peaks with increasing frequency is interpreted in terms of emission at higher frequency coming from a lower height where the cone defined by the open field lines is narrower. However, whether this is to be interpreted as broad-band emission from a narrow range of heights, or narrow-band emission from a large range of heights is unclear (e.g., Barnard & Arons 1986). There is some direct evidence from scintillations on the size of the emission region (Wolszczan & Cordes 1987; Kuzmin 1992), which tends to support the suggestion that the emission region is located at $r \lesssim 0{\cdot}1\, r_{\rm lc}$ (Arons 1992).

The frequency to radius mapping suggests that pulsar emission has a characteristic frequency that decreases with increasing height. For all relevant emission mechanisms there is some typical frequency that decreases with height, and it is plausible that all could be made consistent with the data relevant to frequency to radius mapping.

3.7 *Circular polarization*

Some pulsars have significant circular polarization. Radhakrishnan & Rankin (1990) argued that there are two contributions to the circular polarization: an intrinsic contribution, which tends to reverse its sense near the center of the pulse beam, and a circular polarization that arises as a propagation effect. One model that accounts qualitatively for intrinsic circular polarization is based on curvature emission by bunches of particles (e.g., Gil & Snakowski 1990a,b; Gil 1992). However, as argued in section 4, this mechanism is not acceptable for other reasons. There is strong evidence for production of a circularly polarized component as a propagation effect in some pulsars. In particular, changes between orthogonal modes of polarization (e.g., Stinebring et al 1984a, b) may to be due to a propagation effect through a pulsar magnetosphere with elliptically polarized natural modes (e.g., Allen & Melrose 1982; Arons & Barnard 1986; Barnard & Arons 1986).

The arguments that some of the circular polarization is intrinsic to the emission mechanism do not appear strong enough to impose the criterion that the emission mechanism be intrinsically capable of producing partial circular polarization. Until the effects of propagation on the polarization are adequately understood, the possibility of explaining all circular polarization as a propagation effect remains

open.

3.8 *High-frequency emission*

Strong high-frequency radiation is observed from five radio pulsars: PSR 0531+21, PSR 0833-45, PSR 1509-58, PSR 1706-44 and PSR 0540-69 in the Large Magellanic Cloud. The main part of the radiation of all these pulsars falls in the X-ray and γ-ray ranges. The γ -ray pulsar Geminga is probably also a radio pulsar which is radio quiet (Harding, Ozernoy & Usov 1993). For the remaining five pulsars, their X-ray and γ -ray luminosities are very high. Assuming that the total energy flux carried by relativistic particles from the polar gaps into the pulsar magnetosphere is proportional to the potential across the polar gaps, the maximum luminosity expected in the modern polar gap models cannot account the observed X-ray and γ -ray luminosities. The high-frequency emission is attributed to an outer gap (Cheng et al 1986a,b). Thus, the study of the high-frequency radiation is unlikely to have direct implications on our understanding of the radio emission, because, in the presently favored interpretations, the one is related to the outer gap and the other to the polar gap. A possible exception is in models in which these gaps are related (e.g., Shibata 1991), allowing the possibility of feedback from one to the other.

3.9 *Millisecond pulsars*

The radio emission from millisecond pulsars is remarkably similar to that from most fast, young pulsars. From the pulse profile alone one could not distinguish between a millisecond pulsar and an ordinary pulsar. This suggests a criterion that may be applied to emission mechanisms: the emission mechanism must be capable of accounting for similar emission from slow pulsars and from millsecond pulsars. The parameter that is markedly different for these two classes of pulsars is the magnetic field, B. Hence, this criterion would argue against those mechanisms that are sensitive to the value of B.

3.10 *Summary*

A "top-down" approach based on criteria deduced from observations has some notable successes, but has failed to provide a unambiguous identification of the emission mechanism.

1. A coherent emission mechanism is required, and a mechanism that involves a one-dimensional distribution of relativistic particles streaming out along polar-cap field lines can account for the basic features of pulsar radio emission.

2. The interpretation of the pulse profile in terms of core and conal emission with different properties is controversial, and the evidence for more than one emission mechanism is not compelling.

3. Other observational properties, such as microstructure, frequency to radius mapping and partial circular polarization, do not lead to criteria that obviously favor one emission mechanism over others.

4. The criterion that the same emission mechanism apply to all pulsars excludes mechanism that are sensitive to the value of B, which varies over more than four orders of magnitude.

Despite the foregoing rather negative discussion, it should be emphasized that progress in understanding pulsar radio emission requires observationally-based selection criteria. The difficulties raised here concern identifying unambiguous, definitive criteria. There is no shortage of detailed data, but the piecemeal interpretation of each specific feature of the observations has not led to a consensus of which of them are crucial to the identification of the emission mechanism, and which may be ignored as minor details.

4. Specific Coherent Emission Mechanism

The bright radio luminosity of pulsars implies that the emission mechanism must be coherent. Three different types of coherent emission are possible in principle. It is argued here that only one of them, maser emission, should be considered in astrophysical applications. Several maser mechanisms remain possible candidates for the pulsar emission mechanism.

4.1 *Three types of coherent emission*

Coherent emission processes can be classified in three ways (e.g., Ginzburg & Zheleznyakov 1975; Melrose 1981, 1986a, 1991), referred to here as antenna mechanisms, reactive instabilities and maser mechanisms.

1. An antenna mechanism involves emission by bunches of particles with negligible velocity dispersion. The coherence is attributed to the particles radiating in phase with each other.

2. A reactive instability involves an intrinsically growing, phase-coherent wave whose growth rate exceeds the intrinsic bandwidth of the growing waves. The intrinsic bandwidth is due to the velocity dispersion of the particles, which is required to be very narrow so that all the particles remain in phase with the growing wave.

3. A maser mechanism involves negative absorption. Maser (or laser) emission is familiar in bound-state systems (atoms or molecules), in which the emission between two levels produces a narrow line. Negative absorption between two levels results from the higher-energy level being overpopulated relative to the lower-energy level, called an inverted population. In a plasma, maser emission can occur under a variety of condition where there is a continuum of states and a continuum of emission frequencies. The allowed transitions are subject to a resonance condition that depends on the specific emission process. The particle distribution needs to have some feature that corresponds

in a meaningful sense to an inverted energy population. In the case of a one-dimensional distribution of relativistic particles, this condition is $\partial f / \partial \gamma > 0$ over some range of γ. Maser emission applies in the random phase approximation, so that (unlike the other two types of coherent emission) the phas of the growing waves is irrelevant.

4.2 *Back-reaction to coherent emission*

In all cases the back reaction to the coherent emission tends to reduce the feature in the distribution of particles that is causing the coherent emission. The radiation reaction to an antenna mechanism tends to disperse the bunch, the back reaction to a reactive instability tends to increase the velocity dispersion, and the back reaction to a maser mechanism is the so-called quasilinear relaxation that tends to reduce the inverted energy population. The time scale on which the back reaction occurs is determined roughly by the time required for the energy density in the radiation to become comparable to the energy density in the radiating particles. This is fastest for an antenna mechanism and slowest for a maser mechanism.

4.3 *Why maser emission mechanisms should be favored*

There is a strong argument for considering only maser mechanisms in astrophysical applications. This argument is presented here in two parts.

On the one hand, in order for coherent emission to occur some process is required to set up the feature in the distribution function that causes the coherent emission. The time scale on which this feature must be set up needs to be at least as short as the time scale on which the back reaction would destroy this feature. For a maser, the process that sets up the effective inverted population is referred to as a pump. It is convenient to use the word 'pump' to describe the process that sets up the conditions for the other types of coherent emission, that is, for the creation of a bunch with negligible velocity dispersion required to allow an antenna mechanism to operate, or for the creation of an appropriate distribution with a very narrow velocity dispersion required to allow a reactive instability to develop. The requirements on the pump are most demanding for an antenna mechanism (extreme localization in coordinate space and velocity space) and are very demanding for a reactive instability (extreme localization in velocity space). The requirements on the pump are least demanding for a maser mechanism, and hence the simplest explanation of any coherent emission is in terms of a maser mechanism. In fact, there is no well-established case of a coherent emission in astrophysics that is not due to a maser mechanism.

On the other hand, because of the very rapid transfer of energy from particles to waves, all coherent emission mechanisms have short time and space scales. As a result, a Coherently emitting astrophysical source necessarily consists of a large number of very small, transient subsources. This is observed for coherent emission in cases where appropriate data are available, specifically for plasma emission in the solar wind (e.g., Melrose & Goldman 1987), for electron cyclotron maser emission in planetary magnetospheres (e.g., Melrose 1986b) and for solar spike bursts (e.g., Benz 1986). As a consequence, the overall source must be the

envelope of a large number of individual subsources. Thus, a model for coherent emission from an astrophysical source requires not only a specific mechanism but also a statistical theory for the distribution of these individual subsources. One can argue, at least in simple cases, that the only acceptable statistical theory is equivalent to quasilinear theory (e.g., Melrose & Cramer 1989). The localized back reaction to the maser growth tends to maintain the average growth at close to the threshold value, referred to as marginal stability, and the statistical properties can be introduced relatively simply through a stochastic growth theory (e.g., Robinson 1993). Due to the large number of localized, transient subsources the details of the coherent emission in each subsource is partly obscured by the averaging over many subsources. A random collection of coherently emitting sources should act like a single phase-random source, and it is appropriate to use a. maser-type theory to describe it.

4.4 *Emission by lunches*

The antenna mechanism proposed for pulsar radio emission is curvature emission by bunches (e.g., Sturrock 1971; Ruderman and Sutherland 1975; Buschauer & Benford 1976, 1983; Benford 1977; Benford & Buschauer 1977; Kirk 1980). The basic idea is that N particles in a volume less than a cubic wavelength radiate like a 'macrocharge' $Q = Ne$, and because the power radiated is proportional to Q^2, the power is N^2 times the power from an individual particle.

There are seemingly insurmountable difficulties with this theory (Melrose 1981, 1992, 1993a). For example, when one takes into account the highly anisotropic nature of curvature emission by relativistic particles, the bunch really needs to be a pancake with its normal within an angle $1/\gamma$ of the direction of the magnetic field. An obvious difficulty is to identify a pump (a bunching mechanism) that allows such an exotic bunch to form; none of the suggested pumps works (Melrose 1978). Moreover, even if such a bunch did form, the coherent emission would quickly be suppressed, both due to the bending of the field lines causing the normal to the bunch to deviate more than $1/\gamma$ away from the direction of the magnetic field (Melrose 1981), and due to the back reaction to the coherent emission dispersing the bunch through the ponderomotive force (Melrose 1978). For these and for the general reasons discussed above, coherent curvature emission by bunches is considered unacceptable by this author. A possible exception is the model of Michel (1992) in which the pair cascade occurs inward due to the electrostatic force, in a model in which the neutron star charges up, which type of emission is somewhat analogous to that suggested for terrestrial cosmic ray showers (e.g., Kahn & Lerche 1965).

4.5 *Relativistic plasma emission*

The currently most widely favored emission mechanism for pulsars is described here as relativistic plasma emission. Plasma emission is the mechanism that operates in solar radio bursts (e.g., Melrose 1986a, 1991). It involves two essential stages: generation of Langmuir waves through a streaming (or other) instability, and a nonlinear process that partially converts energy in Langmuir waves into energy in

escaping radiation. Langmuir waves are longitudinal waves with frequency close to the plasma frequency, $\omega \approx \omega_P$. Langmuir waves cannot escape to infinity, and to produce escaping radiation they must be partially converted into one or both of the modes that can escape, which are the o-mode and x-mode of magnetoionic theory. In plasma emission, the maser process is the streaming instability, and the feature in the distribution function that causes the instability is a "bump-in-tail" distribution with $\partial f / \partial v_z > 0$ over a range of velocity, v_Z, along the streaming direction. The pump is the overtaking of slower particles by faster particles tending to increase $\partial f / \partial v_z > 0$.

The overtaking of slower by faster particles may also be the pump in relativistic plasma emission. This may be understood in terms of a simple model. Suppose that all particles leave a source of small spatial extent (small range Δ_{Z0}) over a short time interval (small time interval Δt_0)· The orbit of each particle is $z = z_0 + v_z(t - t_0)$. At a fixed distant point, z , the fastest particles arrive first and the slower particles arrive later, and at any given time the particles present have a range of velocities $\Delta v_z / v_z \sim \Delta_{Z0} / Z_0$, $\Delta t_0 / t_0$. A fractionation tends to occur in the sense that the range of Δv_z of the particles present (at given z, t) decreases as the beam gets further from the source. This implies a peak in the velocity distribution, with $\partial f / \partial v_z > 0$ below the peak and $\partial f / \partial v_z < 0$ above the peak, and such that these gradients increase with increasing distance from the source The back reaction to the maser emission of Langmuir waves, called quasilinear relaxation, tends to reduce the gradient $\partial f / \partial v_z > 0$. In the relativistic case, the same effects occur due to an initial spread $\Delta\gamma$ in γ.

Relativistic plasma emission is analogous to plasma emission in the sense that it involves two essential stages: an instability that generates waves that cannot escape to infinity, and a nonlinear conversion process (e.g., Istomin 1988) that partially converts the energy in these waves into escaping radiation, that is, into wave modes that are free to propagate to infinity. However, in the application to pulsars all the details are different from the application to the solar corona. In a pulsar magnetosphere the wave properties are assumed to be those of a relativistic, streaming one-dimensional pair plasma (e.g., Melrose & Stoneham 1977; Melrose 1979; Volokitin, Krasnoselskikh & Machabeli 1985; Arons"& Barnard 1986; Beskin, Gurevich & Istomin 1986, 1988, 1993; Lominadze et al 1986; Kazbegi, Machabeli & Melikidze 1991; Asseo 1993; Luo, Machabeli & Melrose 1994). Such a plasma supports a Langmuir-like mode and an Alfvén-type mode at lower frequencies, and two high-frequency modes that are somewhat analogous to the o-mode and x-mode of magnetoionic theory. Thus, relativistic plasma emission involves some instability that generates Langmuir-like or Alfvén-type waves, and these are converted into the escaping waves (in one or both of the two high-frequency modes) through nonlinear processes in the relativistic plasma. There are many specific models that vary in the details of the instability, the waves that it generates and the details of the nonlinear or other conversion mechanism (e.g., Asséo Pellat & Rosado 1980; Asseo, Pelletier & Sol 1983, 1990; Kazbegi, Machabeli & Melikidze 1987).

The streaming instability, in the case of a one-dimensional ultrarelativistic distribution, requires a distribution with $\partial f / \partial \gamma > 0$ in the inertial frame in which the bulk motion of the plasma is zero. This could be due to the high energy beam

of positrons moving through the pair plasma, to a relative motion of the electrons and positrons in the pair plasma, or to other less obvious types of relative motion. However, the growth rates for most of these instabilities are too small: the pair plasma leaves the magnetosphere before it has given up significant energy (e.g., Larroche & Pellat 1987). A larger growth rate can result if the generation of the pair plasma fluctuates in time, producing a sequence of beams, with the faster particles in a following beam overtaking the slower particles in a preceding beam (Usov 1987; Ursov & Usov 1988).

The requirement for a pump to maintain $\partial f / \partial \gamma > 0$ has been given relatively little attention. In a pair cascade, one expects there to be few electrons or positrons at low energies, and for their number to rise to a peak at some characteristic energy. One then has $\partial f / \partial \gamma > 0$ below this peak and $\partial f / \partial \gamma < 0$ above it. The back reaction to the streaming instability reduces the gradient $\partial f / \partial \gamma > 0$ through quasilinear relaxation. In the absence of a pump to reestablish the peak, the instability would be confined to the near vicinity of the region where the pairs are produced. Such a model is very restrictive, both on location of the emission region and on the energy available for the maser emission, which is given by the energy in the pairs below the peak multiplied by a presumably small efficiency factor for the relativistic plasma emission. A model is which the production of pairs fluctuates or is appropriately spatially structured (Usov 1987; Ursov & Usov 1988; Lyubarskii 1992) can provide a pump that continues to operate away from the region where the pairs are produced.

Relativistic plasma emission is perhaps the most widely favored pulsar radio emission mechanism, and development of the theory continues. In the past, most treatments have concentrated on the growth rate of the instability, the properties of the waves that grow, and the partial conversion into escaping radiation. As emphasized above, there are other important effects that should be taken into account: the need for a continuous pump, and the implication that the coherent emission occurs in many localized, transient subsources. A continuous pump is present in some models (Usov 1987; Ursov & Usov 1988; Lyubarskii 1992), and microstructures are taken into account in one recent model (Asseo 1993).

4.6 *Maser curvature emission*

Curvature emission is like synchrotron radiation in that, in the simplest case, the absorption coefficient cannot be negative (Blandford 1975; Melrose 1978), so that maser emission cannot occur. However, maser emission is possible when one includes the curvature drift (Zheleznyakov & Shaposhnikov 1979; Chugunov & Shaposhnikov 1988; Luo & Melrose 1992a,b) or field-line distortion (Luo & Melrose 1994).

The curvature drift speed is

$$v_{\rm cd} = \frac{v^2\gamma}{\Omega_e R_{\rm c}}, \tag{4.1}$$

where v is the parallel velocity of the particle and $R_{\rm c}$ is the radius of curvature of the field line. The direction of the curvature drift (opposite for opposite signs of the charge) is such that the Lorentz force $q\mathrm{v}_{\rm cd} \times \mathbf{B}$ provides the centripetal

acceleration, toward the center of curvature of the field line, needed to make the particle follow the curved path. In the following discussion it is more convenient to introduce a drift angle,

$$\theta_{\rm cd} = v_{\rm cd}/v, \tag{4.2}$$

which is the angle between the momentum of the particle and **B**. The drift angle is proportional to the particle energy, and when the particle energy changes as a result of emission, the drift angle also changes. This dependence is the essential ingredient in curvature-drift induced maser emission in that it allows negative absorption to occur.

The total emissivity (summed over the two polarizations) in the presence of curvature drift is (Luo & Melrose 1992b)

$$\eta(\omega,\theta,\gamma) = \frac{q^2}{4\pi\epsilon_0}\frac{\omega^2 R_{\rm c}}{6\pi^3 c^2}\left[(\theta-\theta_{\rm cd})^2\left(\xi^{-1}{\rm K}_{1/3}(y)\right)^2 + \left(\xi^{-2}{\rm K}_{2/3}(y)\right)^2\right]. \tag{4.3}$$

with $\xi = [2(1 - N) + N(\gamma^{-2} + (\theta - \theta_{\rm cd})^2)]^{-1/2}$, $y = \omega/3n^{1/2}\omega_{\rm R}\xi^3$, where N is the refractive index, and with $\omega_{\rm R} = v/R_c$. The absorption coefficients per unit time for a one-dimensional distribution function is

$$\Gamma(\omega,\theta) = -\frac{(2\pi c)^3 n_0}{2\omega^2 mc^2}\int d\gamma\,\frac{df(\gamma)}{d\gamma}\,\eta(\omega,\theta,\gamma), \tag{4.4}$$

where n_0 is the particle number density, and where $f(\gamma)$ is normalized to unity. From (4.4) the conditions for negative absorption are

$$\frac{df(\gamma)}{d\gamma} > 0, \qquad \frac{d\eta}{d\gamma} < 0. \tag{4.5}$$

The original proof that maser action is not possible is based on the inequality $d\eta/d\gamma > 0$ (Blandford 1975; Melrose 1978), where n is the emissivity for $\theta_{\rm cd} = 0$. For $\theta_{\rm cd} = 0$ one has

$$\frac{d\eta}{d\gamma} = \frac{\partial\eta}{\partial\gamma} - \frac{\theta_{\rm cd}}{\gamma}\frac{\partial\eta}{\partial\theta}. \tag{4.6}$$

The term involving the θ-derivative allows negative absorption (Zheleznyakov & Shaposhnikov 1979; Luo & Melrose 1992b; Melrose 1993a).

Curvature emission from a single particle has a relatively broad frequency spectrum centered on $\omega \sim (c/R_c)\gamma^3$. Luo & Melrose (1992b) considered the possibility of maser action near, well below and well above this frequency, and found that the optical depth is small except for $\omega \lesssim (c/R_c)\gamma^3$. The maser emission then occurs at an angle $\Delta\theta_0$ to the magnetic field determined by

$$\gamma^2\theta_{\rm cd}\Delta\theta_0 > 1. \tag{4.7}$$

At angles where the curvature drift of electrons tends to cause maser emission, the curvature drift of positrons is opposite and tends to cause absorption, so that a

difference in the distribution functions for electrons and positrons is necessary in order for there to be net negative absorption.

Maser curvature emission can also occur due to a twist of the field lines, corresponding to curved field lines that are not confined to a plane (Luo & Melrose 1994). Unlike curvature-drift induced maser emission, this mechanism is not sensitive to the magnitude of the magnetic field B, and electrons and positrons contribute with the same sign. Although this version of curvature maser emission seems more favorable than the curvature-drift induced mechanism, it does require a highly non-dipolar magnetic structure at the surface of the star for the growth rate to be large enough to be of relevance.

Any form of maser curvature emission requires $df / d\gamma > 0$, cf. equation (4.5), and a pump is required to continually regenerate such a distribution. The requirement $df / d\gamma > 0$ is the same as for a relativistic streaming instability, and hence any process that operates as a pump for relativistic plasma emission may also act as a pump for maser curvature emission.

Another (reactive) form of curvature-drift induced instability was proposed by Beskin, Gurevich & Istomin (1993), who considered the limiting case $B \rightarrow \infty$. The curvature drift speed (4.1) vanishes in this limit, and the nature of this instability is unclear. It has been claimed that this instability is spurious (Nambu 1989; Machabeli 1991).

4.7 *Cyclotron instability*

A cyclotron instability that involves the anomalous Doppler resonance was proposed by Machabeli & Usov (1979), cf. also Kazbegi, Machabeli & Melikidze (1991). In this anomalous Doppler transition, particles make a transition from the state $n = 0$ to $n = 1$ in (2.7) on emitting a wave quantum. This implies that the perpendicular energy of the electron (or positron) increases on emission. (The parallel energy decreases to provide both the perpendicular energy gained by the particle as well as the energy carried off by the photon.) The emission tends to have an intrinsic circular polarization, and Kazbegi, Machabeli & Melikidze (1991) argued that it is a plausible candidate for "core" emission. The waves that grow in this instability have refractive index greater than unity, and so are in a mode that cannot escape directly. To produce escaping radiation the energy in these waves needs to be partially converted into energy in the high-frequency modes through a plasma-emission type process.

The source of free energy in this instability is the intrinsic anisotropy of a one-dimensional particle distribution. The effect of the instability, that is the back reaction on the particle distribution, is to tend to make the distribution more isotropic. The emission mechanism in its simplest form is subject to a strict constraint: each particle can make only one transition $n = 0$ to $n = 1$, and so can emit only one cyclotron photon. This implies that the maximum rate at which cyclotron photons are emitted is equal to the rate of particle escape from the magnetosphere. Hence, each particle (energy $\gamma m_e c^2$) loses at most an energy $\hbar\Omega_e / \gamma$, with $\Omega_e / \gamma \approx \omega$, where ω is the observed frequency. It follows that the ratio of the radio power to the total power lost by the pulsar is limited to $< \hbar\omega / \gamma m_e c^2 \sim 10^{-12}$, which is inconsistent with observations. Thus, this

mechanism needs a continuous pump, e.g., a mechanism that returns the particles to the state $n = 0$. Otherwise the foregoing energetic argument seems to make the mechanism untenable.

The emission is near the (relativistic) cyclotron frequency, and for this to be in the range of observed radio frequencies requires that the emission occur relatively far from the neutron star ($> 10^7$m for a typical pulsar).

4.8 *Free electron maser emission*

A form of linear acceleration emission was proposed for pulsars by Cocke (1973). The Larmor formula implies that an accelerated charge radiates, and the acceleration of a particle by a parallel electric field is assumed to cause linear acceleration emission. However, emission occurs only if the parallel electric field varies in space or time (Melrose 1978; Kroll & Mullin 1979), and then, for a one-dimensional distribution, maser action is possible only for $df/d\gamma > 0$. The characteristic frequency of the emission is $\omega \sim \omega_o\gamma^2$, where ω_0 is the greater of the typical frequency of the oscillating electric field, or the typical wavenumber times c. The oscillating electric field needs to be identified with a large amplitude wave in the plasma, and there are several possibilities (e.g., Rowe 1992a,b).

A detailed treatment of this mechanism (Rowe 1992a,b) shows that it exists in two regimes. One corresponds to a form of relativistic plasma emission, in which the energy in the emitted waves comes primarily from the energy in the oscillating electric field. The other corresponds to a form of free electron maser emission, in which the oscillating field acts as a wiggler field, and the energy in the emitted waves comes primarily from the energy in the particles. Thus linear acceleration emission may be either an extreme form of relativistic plasma emission, or a form of free electron maser emission. Although there is no strong argument against the mechanism, the case that it might be a realistic pulsar emission mechanism centers on the question as to whether or not the required oscillating $E_{||}$ is plausibly present.

4.9 *Which is the most plausible mechanism?*

In the opinion of this author, emission by bunches is unacceptable, and should not be considered further. Of the other emission mechanism discussed here, two are sensitive to B: maser curvature emission due to the curvature drift, and the cyclotron instability. For the curvature drift speed, (4.1) implies $v_{cd} \propto 1/B$, and as a consequence the growth rate for this form of maser curvature emission is a sensitive function of the magnetic field. The cyclotron mechanism is clearly strongly dependent on the value of B. Adopting the criterion discussed above that the emission mechanism should apply to millisecond pulsars to young, high-B pulsars and to slow pulsars, this dependence on B makes these mechanism unfavorable. The cyclotron mechanism also seems to be subject to a severe constraint (one radio photon per escaping particle) that would rule it out immediately.

Some form of relativistic plasma emission is perhaps the most plausible emission mechanism. However, free electron maser emission and maser curvature emission due to a twisted magnetic field are not ruled out.

5. Polarization and Propagation Effects

Propagation effects inside the light cylinder may account for jumps between orthogonal modes of polarization and possibly for the partial circular in some pulsars. Another expected propagation effect is induced Compton scattering by the relativistic particles in the wind zone of a pulsar. Besides being of interest in the interpretation of the radio emission, such effects offer the possibility of inferring some properties of the plasma environment through which the radio waves pass.

5.1 *Properties of the natural modes*

The properties of the natural modes in a pulsar magnetosphere (e.g., Melrose & Stoneham 1977; Melrose 1979; Allen & Melrose 1982; Volokitin, Krasnoselskikh & Machabeli 1985; Arons & Barnard 1986; Lominadze et al 1986; Beskin, Gurevich & Istomin 1987) depend strongly on whether one is in the low-frequency or high-frequency regime. The low-frequency regime is $\omega \ll \bar{\Omega} = \Omega_e/\bar{\gamma}$, where $\bar{\gamma}$ is a mean Lorentz factor, and the high-frequency regime is $\omega \gtrsim \bar{\Omega}$. In the low-frequency regime, the two natural modes are somewhat analogous of the hydromagnetic modes, with one being Alfvén-like and the other being magnetosonic-like. The waves are linearly polarized, except for a small range of angles near parallel (to **B**) propagation. At other angles of propagation, a small ellipticity in the polarization is also present if the electron and positron distributions are not identical. In the high-frequency regime, the wave properties are closer to those of the magnetoionic o-mode and x-mode waves. The waves have substantial circular polarization near the cyclotron resonance, which occurs in the high-frequency regime. In models in which the emission occurs well inside the light cylinder, the low-frequency approximation applies near the emission region.

A simple model for the waves properties involves three small parameters, a, b, g (Melrose 1979) and suffices for a description of the wave properties in the low-frequency regime. Let the two modes be labeled $\pm$. The squares of their refractive indices, $1 + \Delta N^2$, and the axial ratios, $T_\pm$, of their polarization ellipses ($T = \infty$ corresponds to transverse polarization orthogonal to **B**) are

$$\Delta N_\pm^2 = \frac{1}{2}(a+b) \pm \frac{1}{2}[(a-b)^2 + g^2]^{1/2}, \tag{5.1}$$

$$T_\pm = \{a - b \mp [(a-b)^2 + g^2]^{1/2}\}/2g. \tag{5.2}$$

The three parameters depend on the number densities n_α and distribution functions $f_\alpha(\gamma)$, with $\int_1^\infty d\gamma\, f_\alpha(\gamma) = 1$, where α labels electrons or positrons, through

$$a = -\sum_\alpha \frac{4\omega_{p\alpha}^2}{\omega^2} \int_1^\infty d\gamma\, f_\alpha(\gamma)\, \frac{\gamma\theta^2}{(1+\gamma^2\theta^2)^2} + \sum_\alpha \frac{\omega_{p\alpha}^2}{4\Omega_e^2} \int_1^\infty d\gamma\, f_\alpha(\gamma)\, \frac{(1-\gamma^2\theta^2)^2}{\gamma^3},$$

$$b = -\sum_\alpha \frac{\omega_{p\alpha}^2}{4\Omega_e^2} \int_1^\infty d\gamma\, f_\alpha(\gamma)\, \frac{(1+\gamma^2\theta^2)^2}{\gamma},$$

$$g = -\sum_{\alpha} \eta_{\alpha} \frac{\omega_{p\alpha}^2}{2\omega\Omega_e} \int_1^{\infty} d\gamma \, f_{\alpha}(\gamma) \frac{1-\gamma^2\theta^2}{\gamma^2}, \tag{5.4}$$

with $\omega_{p\alpha}^2 = e^2 n_{\alpha}/\varepsilon_0 m_e$, $\Omega_e = eB/m_e$, and where η_{α} is the sign of the charge and $\gamma \gg 1$ is assumed.

In the simplest approximation in the low-frequency regime, one has $|g|, |b| \ll |a|$, in (5.3) and the wave properties (5.1)–(5.2) simplify to $\Delta N^2 \approx a$, $\Delta N^2 \approx 0$, with $T \approx 0,\infty$, respectively. These are the *O*-mode and *X*-mode, respectively, in the notation of Arons & Barnard (1986). Note that, in this simple approximation, refraction affects the *O*-mode but not the *X*-mode. The counterpart of Langmuir waves occurs where *a* is of order unity.

5.2 *Circular polarization*

One can imagine four possible causes for circular polarization present in the radio emission from some slower, older pulsars: (a) the emission process has an intrinsically circular component (e.g., Gil & Snakowski 1990a,b; Gil 1992), (b) cyclotron absorption preferentially removes one circular component (e.g., Mikhailovskii et al 1982), (c) the wave mode into which the emission occurs is partially circularly polarized on leaving the source, and (d) linear polarization is partly converted into circular polarization due to generalized Faraday rotation. Apart from (a), all of these involve propagation effects. Explanation (a) invokes curvature emission by bunches, which is not considered acceptable here. One has no reason to expect that maser curvature emission, even if it does occur, has similar polarization properties to curvature emission by a single particle, and one does not expect relativistic plasma emission to have any characteristic circular polarization.

Process (c) requires elliptically polarized wave modes. For (5.2) to lead to significantly elliptical polarization requires that *g* be nonzero. This requires that the distributions of electrons and positrons be significantly different, with *g* a function of the difference between these distributions (Kazbegi, Machabeli & Melikidze 1991). However, it appears that the detailed conditions required for this explanation to be effective have yet to be explored thoroughly. Process (d) occurs in a medium with linearly polarized natural modes when incident radiation has linear polarization at an angle to that of the natural modes. (A familiar example is a quarter-wave plate, when the incident polarization is at 45°) In a pulsar magnetosphere this mechanism requires some extreme assumption to allow linear polarization at an angle different from that defined by the natural modes. For example,, it could occur if radiation passed through a vacuum gap: the change in orientation of **B** across the gap causes a change in the polarization of the natural modes between one side and the other, and radiation in one mode as it enters the gap would preserve its polarization across the gap.

All of these suggested explanations for the circular polarization encounter difficulties, and the actual explanation for the circular polarization remains unclear (e.g., Radhakrishnan & Rankin 1990; Radhakrishnan 1992).

5.3 *Jumps between orthogonal modes*

The jumps between orthogonal states of polarization that occur in some older, slower pulsars are probably due to propagation causing rays in the two modes to separate in angle (e.g., Melrose & Stoneham 1977; Melrose 1979; Stinebring et al 1984a,b; Barnard & Arons 1986). Stinebring et al (1984a,b) argued against such an interpretation of orthogonal modes on the grounds that the observed effect does not show an expected strong frequency dependence. However, Barnard & Arons (1986) pointed out that this argument applies only in the high-frequency regime, and that the frequency dependence of the refractive effects in the low-frequency regime is roughly consistent with the observations.

5.4 *Refraction in a striated plasma*

Consider a simple model which would allow a separation between the two modes to occur as a result of refraction. Refraction separates components in the two modes due to any gradients in the difference, ΔN, between their refractive indices. Suppose that the plasma in the inner magnetosphere is striated along the magnetic field lines, so that there are gradients in the plasma density perpendicular to the field lines. Let the z-axis be along the magnetic field and the x-axis along the gradient. Then refraction causes the ray to deviate at a rate $d\theta/dz = \partial\Delta N/\partial x$. The value of U$N$ is probably small ($\lesssim 0{\cdot}1$) in the emission region, but depends on the details of the emission process. Suppose the striations are of thickness Δx. Then a ray initially parallel to the field lines propagates a distance $\delta z \sim (\Delta x R_C)^{\frac{1}{2}}$ before leaving the striation, due to the curvature of the field line. Refraction causes the ray to deviate through an angle $\delta\theta \sim (\delta z/\Delta x)\Delta N \sim (R_c/\delta x)^{\frac{1}{2}}\ \Delta N$. An observationally significant angular change is $\delta\theta \sim 10^{-2}$.

This simple model suggests that a significant deviation of the two rays can occur without appealing to extreme properties of the striations, provided that ΔN is not too small. For example, for $\Delta N \sim 10^{-2}$ one would have $\delta\theta \sim 10^{-2}$ for $\Delta x \sim R_c$. An implication is that if it is accepted that jumps between orthogonal modes are due to refractive effects, then either ΔN is not too small, or there are extremely large local gradients in the plasma density ($\Delta x \ll R_c$). Ignoring the latter possibility, the interpretation of jumps in the orthogonal modes as a refractive effect favors some form of relativistic plasma emission, which leads naturally to emission in a regime where ΔN is not very small (a of order unity in (5.1)).

5.5 *Scintillations in a pulsar magnetosphere*

An alternative model for refractive effects. involves random deviations at many plasma inhomogeneities, rather than refraction in a single striation. Such a model corresponds to refractive scintillations.

Scintillations, due to inhomogeneities in an isotropic medium, cause an angular broadening of the source (e.g., Lee & Jokipii 1975). In an anisotropic medium there is an additional effect due to the difference $\Delta N_+ - \Delta N_-$ implying that refraction has a contribution that is opposite for the two modes. Thus, in an anisotropic medium, scintillations cause (a) an increase in the size of the image of a point source, and (b) a separation of the centroids of the images formed in the two

modes of the medium (e.g., Melrose 1993b,c). Note that, except for $a \approx b$ in (5.1), one has $|\Delta N_+^2 - \Delta N_-^2| \sim |\Delta N_+^2 + \Delta N_-^2|$, and this implies that any refraction causes rays in the two modes to separate by about the same angle as their mean deviates from the original ray direction. Let $\delta\theta_\pm$ be the angular deviation of the rays in the two modes. In the special case $\Delta N_-^2 = -\Delta N_-^2$ one has $\delta\theta_- = -\delta\theta_+$, and hence

$$\langle \delta\theta_-^2 \rangle = \langle \delta\theta_+^2 \rangle, \qquad \langle (\delta\theta_+ - \delta\theta_-)^2 \rangle = 4\langle \delta\theta_+^2 \rangle. \tag{5.4}$$

This implies that the images in the two modes separate at the same rate as they broaden.

Applied to a pulsar, (5.4) implies that once the broadening exceeds the intrinsic size of the source, the emission, projected onto the plane of the sky, separates into contiguous regions of opposite polarizations. This provides a natural explanation for the jumps between orthogonal modes, as the line of sight crosses the boundary between such regions. Although (5.4) is strictly valid only for $\Delta N_-^2 = -\Delta N_+^2$, which corresponds to $a + b = 0$ in (5.1), the conclusion that the images in the two modes separate at about the same rate as they broaden should be approximately valid for any scintillations in the low-frequency regime, that is, scintillations due to inhomogeneities well inside the light cylinder of a typical pulsar.

According to (5.2), the orthogonal modes are linearly polarized for $(a - b)^2 \gg g^2$, in which case the jump is between orthogonal linear polarizations; the polarizations are significantly elliptical only when the condition $(a - b)^2 \gg g^2$ is not well satisfied.

5.6 *Induced Compton scattering*

Induced Compton scattering can pump photons from higher to lower frequencies, distorting the low-frequency spectrum of any source for which the effect is important. Wilson & Rees (1978) discussed the effect on the escaping radiation of induced Compton scattering by relativistic electrons in a pulsar wind. They found that the effect should be important for parameters thought plausible for the wind from the Crab pulsar. However, the expected signatures of induce Compton scattering are not present, implying that the properties of the wind are different from those anticipated. Wilson & Rees (1978) argued that the absence of the predicted effects places a limit on the Lorentz factors, γ, of the particles in the wind. For the Crab pulsar this limit is $\gamma > 10^4$. This idea was discussed further by Sincell & Krolik (1992) who included the effect of an ambient magnetic field on the Compton scattering. The implications of induced Compton scattering need to be explored in more detail (cf. Coppi, Blandford & Rees 1993).

6. Discussion and Conclusions

The outstanding problem in models for pulsar radio emission is that we simply do not understand how the radio emission is generated. The reasons why we has so far failed to solve the problem include the following.

1. There is no widely accepted, self-consistent model for the magnetosphere, including the location of gaps (the assumed source of pair plasma) and the

details of how the secondary pair plasma is produced. As a result, it is impracticable to attempt to predict the details of the distributions of particles required to identify the relevant coherent emission process.

2. The identification of observationally-based criteria for an acceptable emission mechanism are inadequate to select between several different alternatives. One helpful criterion is that the mechanism not be strongly dependent on $\boldsymbol{B}$, so that it can be applied to old (slow) pulsars, to young (fast) pulsars and to millisecond pulsars.

3. In this author's opinion, there has been a misplaced emphasis on coherent curvature emission by bunches, which is unacceptable for a variety of reasons.

4. There is no obvious simple analog for the pulsar coherent emission process, which presumably involves coherent emission in a relativistic pair plasma. Established coherent emission process, specifically plasma emission and electron cyclotron emission, apply to nonrelativistic plasmas. Some form of relativistic plasma emission, of which there are several in the literature, is perhaps the most plausible mechanism.

5. Possible alternatives to relativistic plasma emission include maser curvature emission and linear acceleration emission, or free-electron maser emission.

6. Relatively little attention has been given to two important features of coherent emission: the need for a pump and the localization of the emission into many small transient subsources. One can expect only an average (over the many subsources) balance between the pump and the back reaction to the coherent emission that opposes it. A coherent emission mechanism needs to be complemented by a statistical theory that describes the ensemble of such subsources, e.g., a stochastic growth theory or a marginal stability theory.

7. A final point that has only been alluded to in the discussion here is that expectations of what a theory for coherent emission in an astrophysical source can explain tend to be unrealistic. For example, even in those cases (the Earth's auroral kilometric radiation and type III solar radio bursts in the solar wind) where spacecraft have probed the source region and measured some properties of the electrons that produce the coherent emission, there remain major uncertainties in treatments of the coherent emission. There is little hope that we will ever understand coherent emission from pulsars in the same sense that we understand incoherent emission in synchrotron and other radioastronomical sources.

In summary, the pulsar radio emission mechanism remains poorly understood, and from the slow progress in our understanding of coherent emission under less exotic conditions) future progress is likely to be slow.

Acknowledgments

I have had profitable discussions with Leon Mestel and Vladimir Usov on the physics of pulsar magnetospheres. I thank Simon Johnston, Qinghuan Luo and Stephen Hardy for helpful comments on the manuscript.

References

Abrahams, A.M. & Shapiro, S.L., 1991, *Astrophys. J.,* **374,** 652
Allen, M.C., & Melrose, D.B. 1982, *Proc. Astron. Soc. Australia,* 4, **365**
Arons, J. 1979, *Space Sci. Rev.,* **24,** 437
Arons, J. 1981, *Pulsars,* ed. W. Sieber & R. Wielebinski, D. Reidel, Dordrecht, 69
Arons, J. 1983, *Astrophys. J.,* **266,** 215
Arons, J. 1992, *The Magnetospheric Structure and Emission Mechanisms of Radio Pulsars,* ed. T.H. Hankins, J.M. Rankin & J.A. Gil, Pedagogical University Press, Zielona Gora, 56
Arons, J., & Barnard, J.J. 1986, *Astrophys.* J., **302,** 120
Arons, J., & Scharlemann, E.T. 1979, *Astrophys. J.,* **231,** 854
Asseo, E. 1993, *Mon. Nov. R. astr. Soc,* **264,** 940
Asseo, E., Pellat, R., & Rosado, M. 1980, *Astrophys. J.,* **239,** 661
Asseo, E., Pellat, R., & Sol, H. 1983, *Astrophys. J.,* **266,** 201
Asseo, E., Pelletier, G., & Sol, H. 1990, *Mon. Not. R. astr. Soc,* **247,** 529
Barnard, J.J., & Arons, J. 1986, *Astrophys. J.,* **302,** 138
Benford, G. 1977, *Mon. Not. R. astr. Soc,* **179,** 311
Benford, G., & Buschauer, R. 1977, *Mon. Not. R. astr. Soc,* 179, 189
Benz, A.O. 1986, *Solar Phys.,* **104,** 99
Beskin, V.S. 1982, *Sov. Astron. AJ,* **26,** 443
Beskin, V.S., Gurevich, A.V., & Istomin, Ya.N. 1986, *Sov. Phys. Usp.,* **29,** 946
Beskin, V.S., Gurevich, A.V., & Istomin, Ya.N. 1987, *Sov. Phys. JETP,* **65,** 715
Beskin, V.S., Gurevich, A.V., & Istomin, Ya.N. 1988, *Astrophys. Space Sci.,* **146,** 205
Beskin, V.S., Gurevich, A.V., & Istomin, Ya.N. 1993, *Physics of the Pulsar Magnetosphere,* Cambridge University Press
Blandford, R.D. 1975, *Mon. Not. R. astr. Soc,* **170,** 551
Buschauer, R., & Benford, G. 1976, *Mon. Not. R. astr. Soc,* **177**, 109
Buschauer, R., & Benford, G. 1983, *Astron. & Astrophy.,* **118,** 358
Cheng, A.F., & Ruderman, M.A. 1980, *Astrophys. J.,* **235,** 576
Cheng, K.S., Ho, C. & Ruderman, M.A. 1986, *Astrophys. J.,* **300,** 500 & 522
Chugunov, Yu.V., Shaposhnikov, V.E. 1988, *Astrophys.* J., **28,** 98
Cocke, W J . 1973, *Astrophys. J.,* **184,** 291
Coppi, P., Blandford, R.D., & Rees, M.J. 1993, *Mon. Not R. astr. Soc,* **262,** 603
Cordes, J.M. 1975, *Astrophys. J.,* **195,** 193
Cordes, J.M. 1978, *Astrophys. J.,* **222,** 1006

Cordes, J.M. 1979, *Space Sci. Rev.,* **24,** 567

Cordes, J.M. 1981, *Radio observational constraints on pulsar emission mechanisms, Pulsars,* ed. W. Sieber & R. Wielebinski, D. Reidel, Dordrecht, 115

Cordes, J.M. 1992, "Probing magnetospheres of rotation-driven neutron stars", in *The Magnetospheric Structure and Emission Mechanisms of Radio Pulsars,* ed. T.H. Hankins, J.M. Rankin & J.A. Gil, Pedagogical University Press, Zielona Gora, 253

Daugherty, J.K., & Harding, A.K. 1982, *Astrophys. J.,* **252**, 337

Dulk, G.A. 1985, *Ann. Rev. Astron. & Astrophys.,* **23,** 169

Fawley, W.M., Arons, J., *k* Scharlemann, E.T. 1977, *Astrophys. J.,* **217,** 227

Fitzpatrick, R.& Mestel, L. 1988, *Mon. Not. R. astr. Soc,* **232,** 277 & 303

Gil, J.A. 1992, "Curvature radiation and polarized emission from PSR 2303+30", in *The Magnetospheric Structure and Emission Mechanisms of Radio Pulsars,* ed. T.H. Hankins, J.M. Rankin *k* J.A. Gil, Pedagogical University Press, Zielona Gora, 394

Gil, J.A., & Snakowski, J.K. 1990, *Astron. & Astrophys.,* **234**, 237

Gil, J.A., & Snakowski, J.K. 1990, *Astro. & Astrophys.,* **234**, 269

Ginzburg, V.L., & Zheleznyakov, V.V. 1975, *Ann. Rev. Astrn. & Astrophys.,* **13**, 511

Goldreich, P., & Julian, W.H. 1969, *Astrophys. J.,* **157**, 869

Gurevich, A.V., & Istomin, Ya.N. 1985, *Sov. Phys. JETP,* **62**, 1

Harding, A., Ozernoy, L.M., and Usov, V.V. 1993, *Mon. Not. R. astr. Soc,* **265,** 921

Holloway, N.J. 1973, *Nature Phys. Sci,* **246,** 6

Holloway, N.J. 1977, *Mon. Not. R. astr. Soc,* **181**, 9

Holloway, N.J., & Pryce, M.H.L. 1981, *Mon. Not. R. astr. Soc,* **194**, 95

Istomin, Ya.N. 1988, *Sov. Phys. JETP,* **67**, 1380

Jackson, E.A. 1976, *Astrophys.* J., **206,** 831

Kahn, F.D., & Lerche, I. 1965, *Proc. Roy. Soc. London,* **A289,** 206

Kazbegi, A.Z., Machabeli, G.Z.,& Melikidze, G.I. 1987, *Australian J. Phys.,* 40, 755

Kazbegi, A.Z., Machabeli, G.Z., & Melikidze, G.I. 1991, *Mon. Not. R. astr. Soc.,* **253,** 377

Kirk, J.G. 1980, *Astron. & Astrophys.,* **82,** 262

Krause-Polstorff, J., & Michel, F.C. 1985, *Mon. Not. R. astr. Soc,* **213,** 43

Krause-Polstorff, J., & Michel, F.C. 1985, *Astron. & Astrophys.,* **144,** 72

Kroll, N.M., & McMullin, W.A. 1979, *Astrophys. J.,* **231,** 425

Kuz'min, O.A. 1992, "Resolution of the PSR 1919+21 magnetosphere emitting region", in *The Magnetospheric Structure and Emission Mechanisms of Radio Pulsars,* ed. T.H. Hankins, J.M. Rankin *k* J.A. Gil, Pedagogical University Press, Zielona Gora, 287

Larroche, O., & Pellat, R. 1987, *Phys. Rev. Lett.,* **59,** 1104

Lee, L.C., & Jokipii, J.R. 1975, *Astrophys. J.,* **196,** 695

Lominadze, D.G., Machabeli, G.Z., Melikidze, G.I., & Pataraya, A.D. 1986, *Sov. J. Plasma Phys.,* **12,** 712

Luo, Q., & Melrose, D.B. 1992, *Proc. Astron. Soc. Australia,* **10,** 45

Luo, Q., & Melrose, D.B. 1992, *Mon. Not R. astr. Soc,* **258,** 616

Luo, Q., & Melrose, D.B. 1994, *Mon. Not. R. astr. Soc,* (submitted)

Luo, Q., Melrose, D.B., & Machabeli, G.Z. 1994, *Mon. Not. R. astr. Soc,* **268,** 159

Lyne, A.G., & Manchester, R.N. 1988, *Mon. Not. R. astr. Soc,* **234** 477

Lyubarskii, Yu. E. 1992, *Astron. & Astrophys.,* **261,** 544

Machabeli, G.Z. 1991, *Plasma Phys. Gontr. Fusion,* **33,** 1227

Machabeli, G.Z., & Usov, V.V. 1979, *Sov. Astron. Lett,* **5** 238

Melrose, D.B. 1978, *Astrophys. J.,* **225,** 557

Melrose, D.B. 1978, *Australian J. Phys.,* **32,** 61

Melrose, D.B. 1981, "Maser pulse emission mechanisms", in *Pulsars* ed. W. Sieber & R. Wielebinski, D. Reidel, Dordrecht, 133

Melrose, D.B. 1986, *Instabilities in Space and Laboratory Plasmas,* Cambridge University Press

Melrose, D.B. 1986, J. *Geophys. Res.,* **91**, 7970

Melrose, D.B. 1991, *Ann. Rev. Astron. & Astrophys.,* **29**, 31

Melrose, D.B. 1992, "Coherent radio emission mechanisms for pulsars", in *The Magnetospheric Structure and Emission Mechanisms of Radio Pulsars,* ed. T.H. Hankins, J.M. Rankin & J.A. Gil, Pedagogical University Press, Zielona Gora, 306

Melrose, D.B. 1993, "Coherent radio emission from pulsars", in *Pulsars as Physics Laboratories ed.* R.D. Blandford, A. Hewish & L. Mestel, Oxford University Press, 105

Melrose, D.B. 1993, *J. Plasma Phys.,* **50,** 267

Melrose, D.B. 1993, *J. Plasma Phys.,* **50,** 283

Melrose, D. B., & Cramer, N.F. 1989, *Solar Phys.,* **123,** 343

Melrose, D.B., & Goldman, M.V. 1987, *Solar Phys.,* **107,** 329

Melrose, D.B., & Stoneham, R.J. 1977, *Proc. Astron. Soc Australia* **3,** 120

Mestel, L. 1981, "Structure of the pulsar magnetosphere", in *Pulsars,* ed. W. Sieber & R. Wielebinski, Dordrecht, 9

Mestel, L. 1993, "Pulsar magnetospheres" in *Pulsars as Physics Laboratories,* ed. R.D. Blandford, A. Hewish & L. Mestel, Oxford University Press, 93

Mestel, L., Robertson, J.A., Wang, Y. M., & Westfold, K.C. 1985, *Mon. Not R. astr. Soc,* **217,** 443

Meszaros, P. 1992, *High-energy radiation from magnetized neutron stars,* Chicago University Press

Michel, F.C. 1979, *Astrophys. J.,* **227,** 579

Michel, F.C. 1982, *Rev. Mod. Phys.,* **54,** 1

Michel, F.C. 1991, *Theory of neutron star magnetospheres,* University of Chicage Press

Michel, F.C. 1992, "Pair-production avalanches revisited", in *The Magnetospheric Structure and Emission Mechanisms of Radio Pulsars,* ed. T.H. Hankins, J.M. Rankin & J.A. Gil, Pedagogical University Press, Zielona Gora, 236

Mikhailovskii, A.B., Onlschenko, O.G., Suramlishvili, G.I., & Sharapov, S.E. 1982, *Sov. Asiron. Lett,* **8**, 369

Nambu, M. 1989, *Plasma Phys. Contr. Fusion,* **31**, 143

Neuhauser, D., Koonin, S.E., & Langanke, K. 1987, *Phys. Rev.,* A**36**, 4163

Phillips, J.A. 1992, *Astrophys. J*., **385**, 282

Radhakrishnan, V. 1992, "The polarization of pulsar radio emission", in *The Magnetospheric Structure and Emission Mechanisms of Radio Pulsars,* ed. T.H. Hankins, J.M. Rankin & J.A. Gil, Pedagogical University Press, Zielona Gora, 367

Radhakrishnan, V., & Cooke, D.J. 1969, *Astrophys. Lett.,* **3**, 225

Radhakrishnan, V., *k* Rankin, J.M. 1990, *Astrophys. J.,* **352,** 258

Rankin, J.M. 1983, *Astrophys. J.,* **274,** 333

Rankin, J.M. 1983, *Astrophys. J.,* **274,** 359

Rankin, J.M. 1986, *Astrophys. J.,* **301,** 901

Rankin, J.M. 1990, *Astrophys.* J., **352,** 247

Robinson, P.A. 1993 *Solar Phys.,* **146,** 357

Rowe, E.T. 1992, *Australian J. Phys.,* **45,** 1

Rowe, E.T. 1992, *Australian J, Phys.,* **45,** 21

Ruderman, M.A., & Sutherland, P.G. 1975, *Astrophys. J,* **196**, 51

Rylov, Y.A. 1979. it Astrophys. Space Sci., **66,** 401

Scharlemann, E.T., Arons, J., & Fawley, W.M. 1978, *Astrophys. J.,* 2**22**, 297

Shabad, A.Ye. 1992, *Polarization of the Vacuum and a Quantum Relativistic Gas in an External Field* Nova Science Publishers, New York

Shabad, A.E., *k* Usov, V.V. 1984, *Astrophys. Space Sci.,* **102,** 327

Shibata, S. 1991, *Astrophys. J.,* **378,** 239

Sincell, M.W.& Krolik, J.H. 1992, *Astrophys. J*., **395,** 553

Stinebring. D.R., Cordes, J.M., Rankin, J.M.. Weisberg, J.M., & Boriakoff, V. 1984. *Astrophys. J.S,* **55,** 247

Stinebring, D.R., Cordes, J.M., Rankin, J.M., Weisberg, J.M., & Boriakoff, V. 1984, *Astrophys.* J.*S.*, **55,** 279

Sturrock, P.A. 1971, *Astrophys. J.,* **164,** 529

Ursov, V.N., & Usov, V.V. 1988, *Astrophys. Space Sci.,* **140,** 325

Usov, V.V. 1987. *Astrophys. J.,* **320,** 333

Volokitin, A.S., Krasnoselskikh, V.V., & Machabeli, G.Z. 1985, *Sov. J. Plasma Phys.,* **11,** 531

Wilson, D.B., & Rees, M. J. 1978, *Mon, Not. R. astr. Soc.,* **185,** 297

Wolszczan, A., & Cordes J .M. 1987, *Astrophys. J.,* **320,** L35

Zheleznyakov, V.V., & Shaposhnikov, V.E. 1979, *Australian J. Phys.,* **32,** 49

Diamond Jubilee Symposium on Pulsars
14–17 March 1994
Raman Research Institute, Bangalore

J. Astrophys. Astr. (1995) **16,** 165–171

Millisecond Pulsar Radiation Properties

D. C. Backer *Astronomy Department, University of California, Berkeley, CA 94720*

Abstract. Two investigations of millisecond pulsar radiation are discussed: average total intensity pulse morphology and individual pulse to pulse fluctuations. The average emission profiles of millisecond pulsars are compared with those of slower pulsars in the context of polar cap models. In general the full.widths of pulsar emission regions continue to widen inversely with period P as $P^{-(0.30-0.5)}$ as expected for dipole polar cap models. Many pulse components are very narrow. The period scaling of pulsar profiles – separations and widths – can tell us about the angular distribution of radiating currents. An investigation of individual pulses from two millisecond pulsars at 430 MHz shows erratic pulse to pulse variations similar to that seen in slow pulsars. PSR B1937+21 displays occasional strong pulses that are located in the trailing edge of the average profile with relative flux densities in the range of 100 to 400. These are similar to the giant pulses seen in the Crab pulsar.

1. Introduction

Why are some neutron stars pulsating radio sources? While no one knows the answer with any degree of certainty, many observations and theoretical inquiries are consistent with the neutron star polar cap model. In this model radiation, which is created in currents driven outward along field lines that connect to the interstellar medium, is relativistically beamed, along those field lines. The radiation is linearly polarized with a position angle parallel (or perpendicular) to the projection of the curved field lines. The Radhakrishnan & Cooke (1969) explanation of the monotonic sweep of linear polarization across the Vela pulsar's average pulse profile in terms of this polar cap model provided the cornerstone upon which most subsequent work has been based.

As a pulsar spins faster the separation between tangents to the outermost field lines which connect to the interstellar medium spreads in proportion to $P^{-0.5}$ for a simple dipole geometry when measured at the *same* altitude. If pulsar radiation fills a fixed fraction of this 'open' field zone, then we could expect a similar scaling of observed pulse width, measured in angle not time, with period. A dependency

of emission altitude on period can, of course, alter this relation. While the pulse width–period relation has been studied by many scientists since the early days of the pulsar discovery, the most convincing demonstration that this simple dependence is present comes only when objects with similar sight line / dipole axis / spin axis geometry are compared (*e.g.,* Backer 1976, 1984; Lyne & Manchester 1988 (LM88); Rankin 1990 (R90)). These studies proceed with the assumption that in any pulsar we observe a random cross section of a common pulsar two-dimensional beam pattern. We can piece together what this looks like with a statistical study.

The frequency dependence of pulse profiles is slight for slow pulsars, but does aid in the identification of pulse morphology. Pulse components have individual spectra, and component widths and separations generally decrease with increasing frequency with logarithmic index of around -0.25 (*e.g.,* Rankin 1983; Hankins & Rickett 1987; Thorsett 1991). The interpretation of this frequency dependence as the result of radius to frequency mapping of the altitude of emission in polar cap models is more controversial than the polar cap model itself.

What emerges from these studies is that the central component of the beam has a steep spectrum, and typically displays sign reversal of circular polarization. This is surrounded by a hollow cone of emission, or something approximating this morphology. The perimeter of the conal emission is probably circular (LM88). The sizes of the emitting cone and the core are 6.5° (LM88) and 2.5° (R90), respectively, for a period of 1 s. These values as well as conal component widths grow with $P^{-0.33 \text{ to } -0.5}$. Conal component widths are roughly a fraction 0.15-0.4 of the cone width, or about 2° at 1 s.

That millisecond pulsars, with rotation periods 100-1000 times smaller than the slow pulsars, pulse with any similarity to the slower pulsars is remarkable. Evidently, the radio emission mechanism in all neutron stars depends mostly on processes in the relativistic current structure *in the rotating frame*, and not on the speed of rotation itself. Of course, we believe that it is the rotation and oblique orientation of dipole field that are responsible for inducing the emf that drives this strong polar current. We would like to relate the polarization properties, the period dependence of pulse morphology, and the frequency dependence of pulse morphology of millisecond pulsars to polar cap models, or other models of the magnetospheric radiating current structure (Chen & Ruderman 1993). However, at this time observations are sparse (*e.g.,* Thorsett & Stinebring 1990), and often have poor resolution and/or low snr. In section 2 I report on my understanding of the pulse width – period relation in comparison to the 'expected' $P^{-0.33 \text{ to } -0.5}$ scaling discussed above. Multi-frequency polarization observations in the future will be particularly important to aid in assessing the relationship between millisecond pulsar pulse morphology and the simple ideas we currently have for polar cap models. In section 3 I will discuss the results of an individual pulse study of millisecond pulsars with attention given primarily to the strong pulses seen in radiation from PSR B1937+21.

2. Pulse Width – Period Relation

In my 1984 summary of the pulse width – period relation for pulsars I showed that pulse widths of single peaked pulse profiles and double peaked profiles follow an inverse period relation down to periods of 6 ms with a dependence of approximately $P^{-0.35}$, somewhat flatter than the constant altitude dipole model would predict. These two categories are roughly identifiable with Rankin's conal and core emission, respectively. LM88 include a few millisecond period pulsars in their study of a large body of slow pulsar data, and find a similar relation; Manchester (1990) again comes to the same conclusion with the addition of a few more millisecond pulsars. However the millisecond pulsar profiles are difficult to interpret. There are often many components which are spread widely across the period. As stated earlier, interpretation in terms of core and conal morphology is difficult to impossible owing to the limited frequency coverage and the absence of polarization data.

At present levels of resolution and sensitivity there seem to be unusually narrow components in millisecond pulsars (Fig.1) with full widths at half intensity of 10-20°. For example, the three shortest period pulsars in Figure 1 have components with widths, in angle, at least as narrow as those in the two longest period objects when account of scattering and instrumental effects (see caption) are considered. These narrow components were labeled 'cusp' emission in my 1984 paper. This study pointed out that the components of B1937+21 are remarkably narrow, and perhaps linked to the equally remarkably narrow main and inter pulse of the Crab pulsar which are only 4° wide. We can hope to learn more about the distribution of radiating currents in the polar cap by extending comprehensive pulse morphology statistical studies to millisecond pulsars.

Of the 16 millisecond (field) pulsars considered, six showed prominent interpulses or possible interpulses (B1821-24, B1855+09, B1937+21, B1957+20, J2019+2425, J2322+2057), although, as stated, more complete studies are required for firm identification. Several millisecond pulsars display simple double pulse morphology which one might associate with conal emission scaled to larger opening angles (J0751+18, B1953+29, J2235+1506, J2317+1439). These have larger component widths and separations that corroborate the period scaling, but they are too few in number to make a firm estimate on the exact power law index. This is particularly so owing to the strong selection of objects, and exclusion of what does not fit the paradigm. The three components in PSRs J0613-02 and B1821-24 shown in Figure 1 suggest a possible identification with core/cone emission. However, the central components in both of these as well as PSR B1957+20 (Fruchter *et al.* 1990) have relatively flat spectra in contrast to the reverse for standard core/cone components.

3. Strong Pulses from PSR B1937+21

Investigations of slow pulsars, starting with strip chart recordings of the very first pulsar B1919+21, revealed the erratic behavior of individual pulse emissions which stands in sharp contrast to the extremely stable average pulse profiles required for precise timing of neutron star rotations. The origin of pulse to pulse fluctuations

is no better understood than the origin of any radio emission although no one is surprised that the extreme conditions required for coherent radio emission are not steady from one instant to the next. Given the large ratio of periods between the slow pulsars, whose pulse to pulse fluctuations were extensively studied in the 1970's, and the millisecond pulsars, Shauna Sallmen and I were interested in

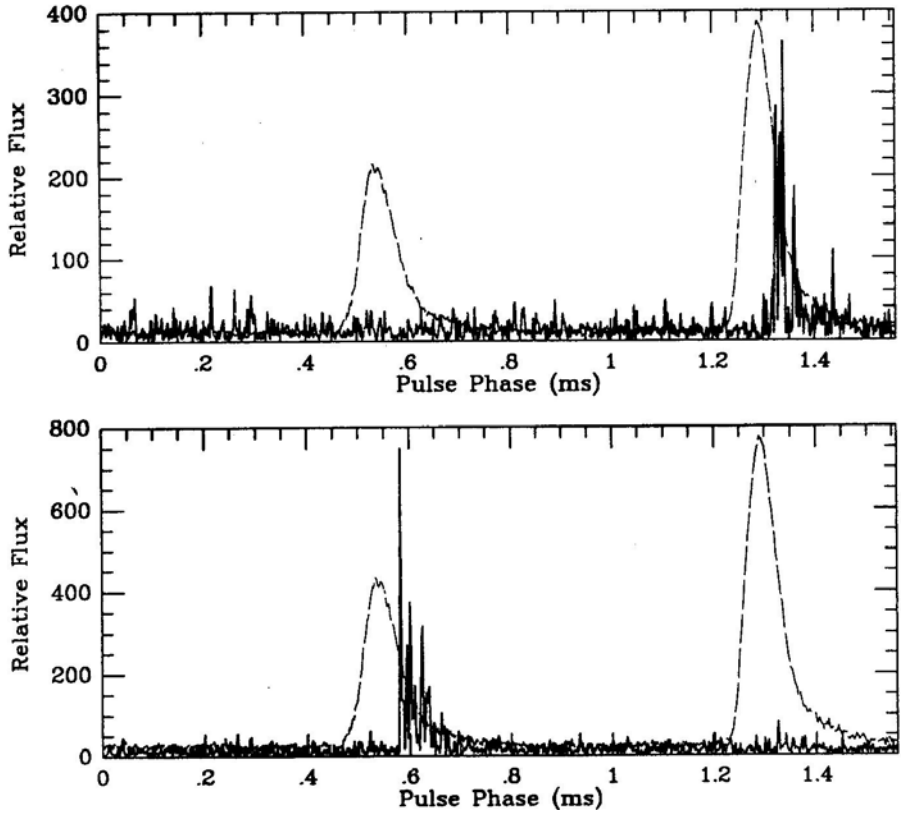

Figure 1: Average pulse profiles from pulsar timing array observations at the NRAO 42m telescope near 800 MHz. Ordinates are pulse phase in ms, and abscissas are flux in Jy. Typical bandwidth is 20 MHz and integration times range from 2-40 h. Resolution is typically 0.009 P except for B1937+21 where it is 0.016. Interstellar scattering contributes to the width of narrow components in B1821-24. Pulsar B1257+12 has a sharp component within the central pulse which is particularly prominent in 430 MHz data.

studying the statistics of individual pulses of millisecond pulsars to see if there were similarities in time scales or angle scales as well as the general level of modulation. Some Information was provided by Wolszczan (1984) who reported on the strongest pulses from B1937+21. More recently Johnston *et al.* (1993) presented a string of pulses from the very strong, nearby pulsar J0437-4715.

Our data were obtained at the Arecibo Observatory in November 1992 as part

of a low frequency dispersion measure monitoring project. The present study has focused on 430 MHz observations of B1534+12 and B1937+21. Complex voltages in a 250 kHz band from othogonally polarized feeds were recorded with sampling at 500 kHz. For B1534+12 data was recorded for a window centered on the pulse while for the 1.6ms pulsar B1937+21 data was recorded for 8 pulse periods and then 3 pulse periods were skipped. The data was analyzed with software dedispersion in predetection and postdedection algorithms. Histograms of pulse energies were formed to explore the level of modulation. The B1534+12 data was extremely strong, and the histogram showed a high level of modulation. There is similarity between the form of this histogram and that seen for the relatively short period pulsar B0950+08.

The B1937+21 data did not have as high a snr, but its histogram revealed a handful of pulse energies that were above 10 times the mean energy. Separate histograms for the two peaks in the pulse profile – the main pulse and interpulse – showed strong pulses in both. These seemed to form a distinct population reminiscent of the giant pulses of the Crab pulsar. Evidently these were typical of the pulses that Wolszczan (1984) had located. We went back to the raw data and extracted the pulses with full time resolution. Figure 2 displays two of the strong pulses, one at location of each pulse component. Surprisingly all the strong pulses are located on the trailing edge of the average pulse components. This makes their pulse energies 100-400 times that of the average.

One striking feature of both the average pulse and the strong pulses is that they are stretched out by interstellar scattering. In the single screen model of interstellar scattering the impulse response of the interstellar medium is an exponential. Any true pulse structure will be seen convolved by this temporal filter. Most curiously the strong pulses are located in just the part of the average pulse that is stretched out by the interstellar impulse response convolution, But we can't ascribe the strong pulses to scattering since the time scale for the diffraction pattern to change, which occurs as the earth-pulsar line of sight moves through an isoplanatic patch, is many seconds at 430 MHz while the strong pulses are there in one pulse and not in the next pulse or even the intervening interpulse. Furthermore, while we await 1400 MHz data for detailed analysis, we can conclude from the work of Wolszczan (1984) that the presence of strong pulses at both 1400 and 430 MHz would also argue against an interstellar propagation mechanism.

The data in Figure 1 show several spikes whose significance must be judged against the low number of degrees of freedom summed in construction the plot. What is expected for the narrow band impulse response of the interstellar medium has not been studied. We expect to see noise with the number of degrees of freedom being defined by the time-bandwidth product and an envelope given approximately by the exponential function. This is roughly what we see. Thus, what was emitted by the pulsar could be even stronger and as sharp as a microsecond. Higher frequency observations are required to escape the distortion of interstellar propagation. The instantaneous impulse response of the interstellar medium may not be a simple exponential, but rather individual paths may be turned on with a range of delays and a range of amplitudes of scattered radition. This would lead to non noise like fluctuations in these individual pulses. We are exploring these possibilities.

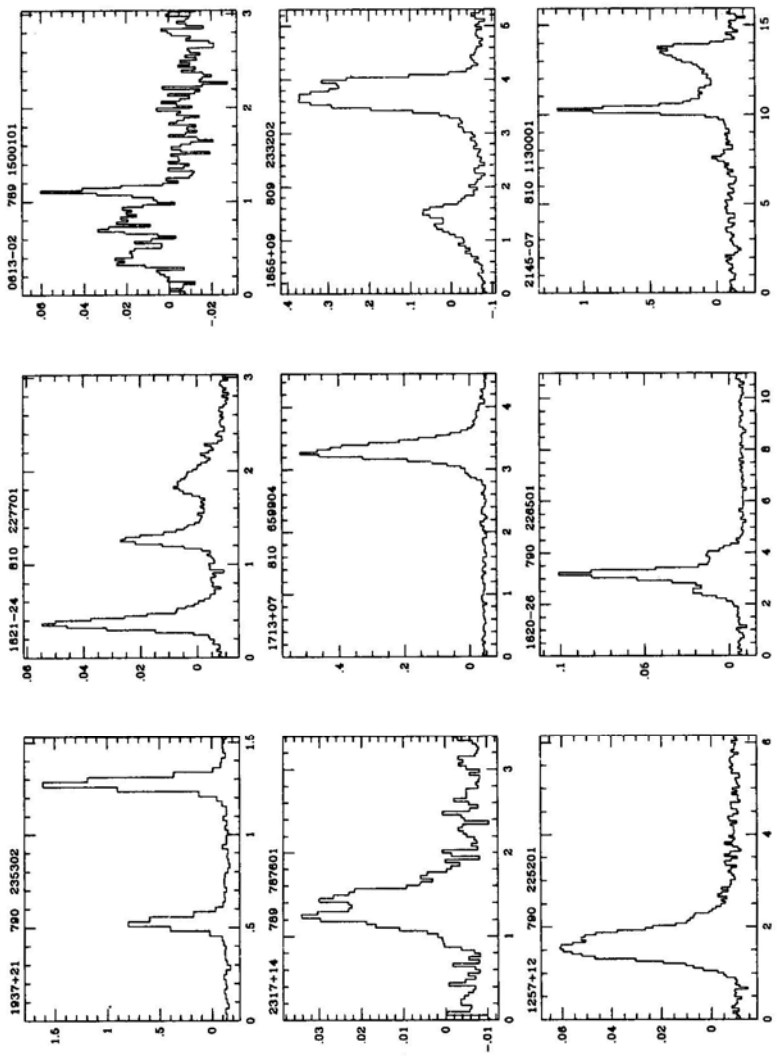

Figure 2: Two strong pulses from PSR B1937+21 at 430 MHz from observations at the Arecibo Observatory with 250 kHz bandwidth. Dashed line gives the average pulse profile from a total of four minutes of data. The stretching of main and inter pulses is the result of interstellar scattering. All strong pulses are observed to follow the peak flux of average pulse profile by about one pulse width. The fluctuations of these individual pulses is dominated by statistical noise. The individual pulses appear to have an envelope which is also scattered as expected.

The delay of the strong pulses from the average may provide a clue to their special origin. The delay of strong pulses after the average, which is of order 25 microseconds, corresponds to a few km of vacuum light travel time which is somewhat smaller than a stellar radius. Is this scale comparable to the size of the emission region? Perhaps some feedback condition in the emission region sets up a high gain, in the sense of a maser, oblique path which fires off an extra intense microwave beam.

Certainly it has been a special pleasure to bring this curiosity of 'light' in nature to the Raman Research Institute wherein many such curiosities have been unraveled by its distinguished directors and colleagues. I trust that there will be many more to come.

References

Backer, D. C. 1976, *Astrophyhs. J.* , **209,** 895
Backer, D. C. 1984, *J. Astrophys. Astron.,* **5,** 187
Chen, K., & Ruderman, M. 1993, *Astrophys. J.*, 408, 179
Fruchter, A. S., *et al.* 1990, *Astrophys. J.,* **351**, 642
Hankins, T. H., & Rickett, B. J. 1987, *Ap. J.,* **311** 684
Johnston, S., *et al.* 1993, *Nature,* 361, 613
Lyne, A. G., & Manchester, R. N. 1988, *Mon.Not.R.astr.Soc.,* **234**, 477
Manchester, R. N. 1990, *Proc. of IAU Coll. 128,* ed. T. Hankins & J. Gil, [xx : xx], p. 204
Radhakrishnan, V., & Cooke, D. J. 1969, *Astrophs. Lett.,* **3**, 225
Rankin, J. M. 1983, *Astrophys. J.*, **274**, 359
Rankin, J. M. 1990, *Astrophys. J.,* **352**, 247
Thorsett, S. E., & Stinebring, D. R. 1990, *Astrophys. J.*, **361**, 644
Thorsett, S. E. 1991, *Astrophys. J.*, **377**, 263
Wolszczan, A. 1984, *Millisecond Pulsars Workshop,* ed. S. Reynolds & D. Stinebring, [NRAO : Green Bank], p. 63

Diamond Jubilee Symposium on Pulsars
14–17 March 1994
Raman Research Institute, Bangalore

J. Astrophys. Astr. (1995) **16,** 173–178

Gamma-Ray Pulsars

Malvin Ruderman *Department of Physics, Columbia University, 538 West 120th Street, New York, NY 10027, USA.*

Abstract. Various observations of γ-ray pulsars are summarized briefly and related to outer-magnetosphere accelerator models.

1. Introduction

The charged particles on the closed magnetic field lines of a pulsar magnetosphere are expected to be "charge separated" (Michel 1991): because of gravitational and inertial forces the charge density needed to maintain $\boldsymbol{E} \cdot \hat{\boldsymbol{B}} \sim 0$ in the corotating magnetosphere (Goldreich and Julian 1969) consists in any region exclusively of positively charged particles or of negatively charged ones, but not a mixture of both. Relativistic current along open $\boldsymbol{B}$-field lines results in charge deficient regions where $\boldsymbol{E} \cdot \hat{\boldsymbol{B}} \neq 0$ if the current is carried by the flow of charge separated plasma (Scharlemann *et al.* 1978). In such regions e^- / e^+ would be accelerated to large relativistic energies and become powerful sources of high energy γ-rays. The materialization of some or all of that γ-ray emission could produce enough $e^{\pm}$ pairs to supply the charge needed to sustain magnetospheric current flow and quench further accelerator growth. These accelerators and the γ-ray emission which they power may be relatively close to the surface of a neutron star ("polar cap accelerators" (Sturrock 1971; Ruderman and Sutherland 1975; Michel 1991), "slot-gap" accelerators (Arons and Scharlemann 1979), or very far from the surface at a good fraction of the way to the corotation speed-of-light-cylinder ("outer-gap" accelerators (Cheng, Ho and Ruderman 1986a, Chiang and Romani 1992), or at both locations. The mechanism for $e^{\pm}$ pair production by the accelerator is quite different in the two locations. When the local magnetic field is as strong as that found near the stellar surface, γ-rays can be converted to pairs by the field itself (Sturrock 1971; Ruderman and Sutherland 1975; Daugherty and Harding 1982, 1983, 1989). In the outer-magnetosphere the local magnetic field is much too weak for such a mechanism to be effective and local $e^{\pm}$ pair production would have to be maintained by collisions of energetic γ-rays on X-rays or other γ-rays (Cheng, Ho and Ruderman 1986b); (or conceivably even on electron-volt photons if the initial γ-ray energies were high enough).

Seven solitary pulsars with strong energetic non-thermal emission have now been observed (Table 1). Many of the long known but still unidentified "COS-

	Pulsar	L_γ (erg s^{-1})	$I\Omega\dot{\Omega}$ (erg s^{-1})
	Crab	$3 \cdot 10^{35}$	$3 \cdot 10^{38}$
A	1509	$\sim 1 \cdot 10^{35}$	$2 \cdot 10^{37}$
	0540	?	$2 \cdot 10^{38}$
	Vela	$4 \cdot 10^{34}$	$7 \cdot 10^{36}$
B	1706	$3 \cdot 10^{34}$	$3 \cdot 10^{36}$
	Geminga	$2 \cdot 10^{34}$	$3 \cdot 10^{34}$
	1055	$1 \cdot 10^{34}$	$3 \cdot 10^{34}$

Table 1: Spin-down power ($I\Omega\dot{\Omega}$) and approximate luminosity of γ-ray pulsars (Thompson *et al.* 1994). PSR 1509 has not been detected much above several MeV. PSR 0540 in the LMC so far has been observed only at optical and X-ray energies. The assumed Geminga distance is 500 pc (Halpern and Ruderman 1993; Helfand 1993).

B sources" may also be γ-ray Pulsars. In several cases, and plausibly in all, the accelerators which power this radiation seem to be far from the neutron star surface (in the outer-magnetosphere) e.g., the very large ratio of γ-ray accelerator power to total spin-down power (unless there is very narrow beaming (Dermer and Sturner 1994) in PSR 1055 (and probably in Geminga) cannot be sustained if the accelerator magnetic field exceeds about 10^9 G; similarly it is difficult to find an origin for the Crab pulsar's powerful optical radiation other than ynchrotron emission e^- / e^+ in the relatively weak field ($B < 10^8$ G) of the Crab pulsar's outer-magnetosphere.

The pulsars of Table 1 fall into two groups. The pulsars of group A all have strong non-thermal X-ray emission and very much larger spin-down power. A model which was developed to describe the 1 – 10^9 eV Crab pulsar emissions (Cheng, Ho and Ruderman 1986a,b) also seems able to accommodate the other Group A spectra and pulse geometries (Chiang and Romani 1992). In this kind of outer-magnetosphere accelerator model, e^- / e^+ passing in opposite directions through the accelerator lose almost all of their energy to curvature radiation with $E_\gamma \sim$ several GeV. However almost all of these γ -rays are converted to $e^\pm$ pairs in the intense local X-ray flux (synchrotron radiation by the pairs created in this way just outside of the accelerator). The observed emission is the synchrotron and inverse Compton radiation from these same $e^\pm$ pairs. In such models, the observed L_γ power (mainly inverse Compton) is reduced relative to L_x (synchrotron emission with $E_x \lesssim 1$ MeV) as the accelerator magnetic field is increased (Cheng and Ruderman 1994). PSR 1509 is the most strongly magnetized radiopulsar known. The Crab pulsar and PSR 0540 have strong outer-magnetosphere fields because their outer-magnetospheres are closer to the star. In the group A γ-ray pulsars the very energetic primary curvature γ-rays from the accelerator itself are absorbed and unobserved.

The group B pulsars of Table 1 have more distant outer-magnetospheres than those of group A pulsars (except, in some cases, for PSR 1509). Because of the consequently very much weaker fields magnetic fields around group B outer-

magnetosphere accelerators, their secondary $e^{\pm}$ pairs do not give enough local synchrotron X-ray emission to sustain an outer-magnetosphere accelerator which works in this Crab-like mode. An alternative long ago proposed for Vela-like magnetospheres (Cheng, Ho and Ruderman 1986b) has difficulties in describing Vela's spectral break at γ-ray energies near or above 10 MeV, may predict too much 10^{12} eV γ-ray flux (Nel et *al* 1993), and seems to give too much optical-UV radiation from Geminga (Usov 1994). An outer-magnetosphere accelerator model for group B γ-ray pulsars, outlined below, which crucially utilizes the observed surface thermal X-ray emission from the group B pulsars, seems much more promising.

2. Soft Thermal X-rays and Group B. γ-ray Pulsars

Despite a variation in spin-down power by more than a factor of 10^2, the group B pulsars are roughly similar in 10^2 MeV – several GeV γ-ray spectra and power. It has been proposed that they all have essentially the same accelerators, (i.e., very similar potential drops, current flows and distances from their neutron stars) but differ among themselves mainly in their magnetic dipole inclination angles (Ruderman *et al.* 1993). They are also similar to the total soft thermal X-ray emission shown in Table 2, which includes, for comparison, two pulsars *not* observed as γ-ray pulsars. The soft thermal X-rays of Table 2, presumably from the heated neutron star surface, should also illuminate and pass through an outer-magnetosphere accelerator. Although they are not abundant and energetic enough to absorb many of the accelerator produced curvature γ-rays, they can materialize enough of the highest energy γ-rays to supply the new $e^{\pm}$ pairs needed to self-sustain the accelerator current. The group B γ-ray pulsars' primary curvature γ-ray emission should be directly observable, unlike that from the group A pulsar outer-magnetosphere accelerators. Therefore, the non-thermal part of the emission from the group B γ-ray pulsars should consist of (a) directly observable curvature γ-rays from e^{-} / e^{+} inside of outer-magnetosphere accelerators ($E_{\gamma} \sim 10^2$ MeV – 10 GeV); (b) inverse Compton scattering by the same e^{-} / e^{+} of radio-photons from any of the low frequency canonical radioemission which passes through the accelerator ($E_{\gamma} \lesssim 10^2$ MeV). Preliminary work on such a model (Cheng and Ruderman 1994) supports optimism for matching observed spectra. Independently, there are provocative questions about the origin of the soft quasi-thermal X-rays upon which the model depends.

3. Thermal X-rays and $e^{\pm}$ Annihilation from γ-ray Pulsars

Because the effective emission areas for group B γ-ray pulsars' soft X-ray emissions (Table 2) are near the stars' total surface areas rather than those of their stellar polar caps, it may indeed be the case that these emissions are just those from normal stellar cooling (Ögelman and Finley 1993; Ögelman, Finley and Zimmermann 1993). Moreover, the observed thermal L_x are suggestively close to that expected from an outer-magnetosphere accelerator heating its parent neutron star (Helfand 1993) and, at least for Geminga, 10% of the flux is otherwise too hot. The extreme relativistic e^{-} (or e^{+}) from the starward end of the accelerator will flow down onto

	Pulsar	log Age (yrs)	L_x (erg s^{-1})	$T(K)$
B	PSR 1706	4.2	$8 \cdot 10^{32}$	
	Vela	4.1	$4 \cdot 10^{32}$	$1 \cdot 10^6$
	Geminga	5.5	$3 \cdot 10^{32}$	$5 \cdot 10^5(90\%); 3 \cdot 10^6(10\%)$
	PSR 1055	5.7	$3 \cdot 10^{32}$	$7 \cdot 10^5$
	PSR 1929	6.5	$\sim 7 \cdot 10^{29}$	
	PSR 0950	7.2	$\sim 7 \cdot 10^{29}$	

Table 2: Very soft (thermal) emission from group B pulsars (Halpern and Ruderman 1993; Halpern and Holt 1992; Ögelman and Finley 1993; Ögelman, Finley and Zimmermann 1993) and two radiopulsars which have not been detected in γ-rays (Helfand 1993). As in Table 1 the Geminga distance is taken as 500 pc (Halpern and Ruderman 1993; Helfand 1993). The distance to PSR 1055 is uncertain and may be up to twice that used here.

the star's polar caps. On the way they will synchrotron radiate away any kinetic energy perpendicular to $\boldsymbol{B}$. The particle flow through Geminga's or PSR 1055's outer-magnetosphere accelerators must be near the maximum possible open field line flow to give such a high $L_\gamma / I\Omega\dot{\Omega}$(minus losses to synchrotron radiation after leaving the accelerator)Then the power brought down to Geminga's stellar surface should be $\sim 3 \cdot 10^{32}$ erg s^{-1} (Halpern and Ruderman 1993). However, instead of such radiation coming back out from small hot ($6 \cdot 10^6$ **K**) polar caps, most of this power seems to come from a large fraction of the surface area of the B group pulsars. One possible cause of this is the large density of $e^{\pm}$ pairs near these neutron stars. Their effectiveness in reflecting KeV X-rays from a hot polar cap is enormously increased wherever their cyclotron resonance frequency in the circumstellar magnetic field matches the X-ray frequency. The scattering cross section

$$\sigma = \sigma_T(\hat{e} \cdot \hat{\boldsymbol{B}})^2 + \frac{2\pi^2 e^2}{mc} \mid \hat{e} \times \hat{\boldsymbol{B}} \mid^2 \delta(\omega_B - \omega),$$

where σ_T is the Thomson cross section, ω_B the resonance frequency, $\hat{e}$ the X-ray polarization and $\hat{\boldsymbol{B}}$ the magnetic field direction. An $e^{\pm}$ density exceeding 10^{13} cm^{-3} at $r \sim 3R$ would make an optically thick cyclotron-resonant backscattering layer there. Local pair densities greatly in excess of this seem plausible from the conversion of some of the Geminga-family inward directed curvature γ–rays from particles within the outer-magnetosphere accelerator and, especially, from its starward directed extreme relativistic particle flow. Gamma-rays which pass near these stars will make pairs which backscatter most hot polar cap X-rays to the stellar surface where they will be reradiated, but at lower energies and from larger areas. For the Crab pulsar a strong, narrow, gravitationally red-shifted $e^{\pm}$ annihilation line should be marginally observable (Massaro *et al.* 1991).

4. Comments

An outer-magnetosphere accelerator seems a plausible ultimate power source for a γ-ray pulsar's main emission and, perhaps, also its soft X-rays. Both are needed for the accelerator current to be self-sustained. Such bootstrapped accelerators would grow in size (i.e., in the fraction of the open $\boldsymbol{B}$-field lines which they subtend) until they are self-sustained, but no larger since more $e^{\pm}$ pair production within the accelerator would begin to quench the needed $\boldsymbol{E} \cdot \hat{\boldsymbol{B}}$ there. These accelerators might indeed be expected to be rather similar among γ-ray pulsars, as is observed for group B and implied for group A. But what happens when even spanning all available open field lines is insufficient to give accelerated e^{-} / e^{+} enough energy for curvature radiation γ–rays to reach the needed multi-GeV? Equivalently, what happens when pulsar spin-down power ($-I\Omega\dot{\Omega}$)drops below the L_{γ} of Table 1? Does the pulsar turn off as a strong γ-ray source or does it manage to continue with an $L_{\gamma} \sim -I\Omega\dot{\Omega}$? At present the answer is unclear.

Most of the difficulty in constructing a quantitative model for outer magnetosphere accelerators arises from the lack of a reliable description of just how the corotating magnetosphere with mainly dipolar $\boldsymbol{B}$, almost certainly an adequate model for the relevant part of the magnetosphere which begins many radii from the neutron star, changes as the light cylinder is approached. Since much, and perhaps most, of an outer-magnetosphere accelerator probably lies in this region, this lack is crucial. For example, the accelerator magnetic field structure is uncertain there in shape and orientation because it is so heavily loaded with relativistic plasma (e.g., the accelerated $e^{\pm}$ which it has created) whose energy density can be comparable to that of the magnetic field which would otherwise control the plasma flow. Some models assume the accelerator is still close enough to the star that $\boldsymbol{B}$ can be approximated as the non-retarded one of a rotating dipole (Cheng, Ho and Ruderman 1986a,b). Others assume that the accelerator is nearer the light cylinder, but that the exact retarded magnetic field in an empty magnetosphere is still an adequate approximation (Chiang and Romani 1992). Both seem capable of giving pulse shapes which resemble those observed – especially the prevalence of those consisting of a pulse and a widely separated interpulse with comparable intensity.

References

Arons, J., Scharlemann, E. 1979, *Astrophys. J.,* **231**, 854,
Cheng, K, S., Ho, C., Ruderman, M. 1986a, *Astrophys.* J., **300,** 500.
Cheng, K. S., Ho, C, Ruderman M. 1986b, *Astrophys. J.,* **300**, 532.
Cheng, K. S., Ruderman, M. 1994 (in preparation).
Chiang, J., Romani, R. 1992, *Astrophys. J.,* **400**, 629.
Daugherty, J., Harding, A. 1982, *Astrophys. J.,* **252**, 337; 1983, *Astrophys. J.*, **273**, 761; and 1989, *Astrophys. J.*, **336**, 861.
Dermer, C, Sturner, S. 1994, *Astrophys. J.* (*Lett.*), in press.
Goldreich, P., Julian, W., 1969, *Astrophys. J.,* **157**, 869.
Halpern, J., Holt, S. 1992, *Nature,* **357**, 222.

Halpern, J., Ruderman, M. 1993, "Soft X-ray Properties of the Geminga Pulsar" *Astrophys. J.,* **415**, 286.
Helfand D., June 1993, private communication.
Ho, C. 1989, *Astrophys. J.,* **342**, 396 (especially Fig. 8).
Massaro, E. *et al.* 1991, *Astrophys. J.,* **376**, L11.
Michel, F. C. 1991, *Theory of Neutron Star Magnetospheres:* Univ. of Chicago Press, Chicago, and references therein.
Nel, H., De Jager, O., Raubenheimer, B., Brink, C., Meintjes, P., North, A. 1993, *Astrophys. J.,* in press.
Ögelman, H., Finley, J. 1993, "ROSAT Observations of Pulsed Soft X-ray Emission from PSR 1055–52", Univ. of Wisconsin Preprint.
Ögelman, H., Finley, J., Zimmermann, H. 1993, *Nature,* **361**, 136.
Ruderman, M., Sutherland, P. 1975, *Astrophys. J.,* **196**, 51.
Ruderman, M., Chen, K., Cheng, K.S., Halpern, J. 1993, *Proc. of 1992 Compton Observatory Symposium,* St. Louis, (ed) N. Gehrels.
Scharlemann, E., Arons, J., Fawley, W. 1978, *Astrophys. J.,* **222**, 297.
Sturrock, P. 1971, *Astrophys. J.,* **164**, 529.
Thompson, D., *et al.* 1994, "Spin Powered Gamma-Ray Pulsars", NASA Preprint,
Usov, V. 1994, "Radiation from Vela-like Pulsars Near the Death Line", *Astrophys. J.,* in press.

Diamond Jubilee Symposium on Pulsars
14–17 March 1994
Raman Research Institute, Bangalore

J. Astrophys. Astr. (1995) **16,** 179–190

Timing Noise and Glitches

A.G.Lyne, R.S.Pritchard & S.L.Shemar *The University of Manchester*, *Nuffield Radio Astronomy Laboratories*, *Jodrell Bank*, *Macclesfield*, *Cheshire SK*11 *9DL*

Abstract. One of the most remarkable properties of radio pulsars is their rotational stability which allows many uses as clocks, For instance they enable us to determine the shapes and sizes of binary orbits, to study general relativistic effects in strong gravitational fields, to demonstrate the existance of gravitational radiation from binary systems, to permit the detection of extra solar planets, and also to put limits on the long period gravitational wave background. However, some display timing imperfections which tell us about the insides of neutron stars. This review describes the basic physics of slowdown and how period instabilities seem to be related to the rate of slowdown and the presence of internal superfluid liquid. Careful studies of glitches and the subsequent rotational behaviour of the pulsars can provide valuable information on the internal structure of neutron stars.

1. Regular Slowdown

Pulsars slow down through the loss of kinetic energy in the form of low frequency electromagnetic waves or high energy particles and radiation. We first of all discuss the process of the regular slowdown and its observation, before discussion departures from this monotonic behaviour.

In a general slowdown, the braking torque is proportional to the rotational frequency Ω to some power n, the braking index, which depends upon the physics of the braking mechanism:

$$\dot{\Omega} = -k\Omega^n. \tag{1}$$

For magnetic braking by a dipolar field, the rate of spin-down is determined by the component of magnetic dipole moment M normal to the rotation axis and moment of inertia I of the neutron star according to the equation:

$$Torque = -2 \times M^2\Omega^3/3c^3 = I\dot{\Omega} \tag{2}$$

Comparing this with equation (1), we see that n=3. For particle loss from a completely aligned rotator, n also has an expected value of 3 (Goldreich & Julian 1969). We can express M in terms of the magnetic field $B_0 = M / R^3$ at the surface of the star of radius R and obtain B_0 in terms of the period, $P = 2\pi / \Omega$:

$$B_0 = \sqrt{3Ic^3 P\dot{P}/8\pi^2 R^6} = 3.3 \times 10^{19}(P\dot{P})^{1/2} \; gauss \tag{3}$$

where we have taken the neutron star to have ε radius R = 10 km and moment of inertia $I = 10^{45}$ gm cm^2. Integration of the general spindown equation (1) gives a time interval since the spin rate had an initial value Ω_i:

$$t = -\frac{\Omega}{(n-1)\dot{\Omega}}\left[1 - \left(\frac{\Omega}{\Omega_i}\right)^{n-1}\right] \tag{4}$$

In the case where the initial rotation rate was very high, i e. $\Omega_i \gg \Omega$, then

$$t = -\frac{\Omega}{(n-1)\dot{\Omega}} = +\frac{P}{(n-1)\dot{P}} = +\frac{P}{2\dot{P}}, \text{ for magnetic dipole braking (n = 3).} \tag{5}$$

The latter estimate is commonly known as the characteristic age of the pulsar. For the Crab pulsar the characteristic age is 1250 years, in reasonable agreement with the known age of 940 years. Since the initial period must have been finite, the characteristic age is usually regarded as an upper limit to the true age. Any decay in the magnetic field will also serve to make it an overestimate of the true age.

In principal we can check on the value of n by differentiation of the spindown equation (1), giving

$$n = \Omega\ddot{\Omega}/\dot{\Omega}^2. \tag{6}$$

A stable value of η has been measured in this way for only 3 pulsars as shown in Table 1.

These values are all somewhat less than 3 and probably result from the non-dipolar nature of the magnetic field or the presence of particles in the magnetosphere. For older pulsars, timing noise dominates the measured value of $\dddot{\Omega}$ (see section 3) and the value of n is variable and is not related to the braking mechanism. Conversely, note also that the youngest pulsars such as the Crab may show significant higher-order derivatives due to the slow-down process which may be mistaken for timing noise.

Table 1: The breking indices of pulsars

Pulsar	Braking Index, n	Reference
0531+21	2.509±0.001	Lyne,Pritchard & Smith (1988)
0540-69	2.01 ±0.02	Manchester & Peterson (1989)
1509-58	2.838±0.001	Kaspi et al. (1994)

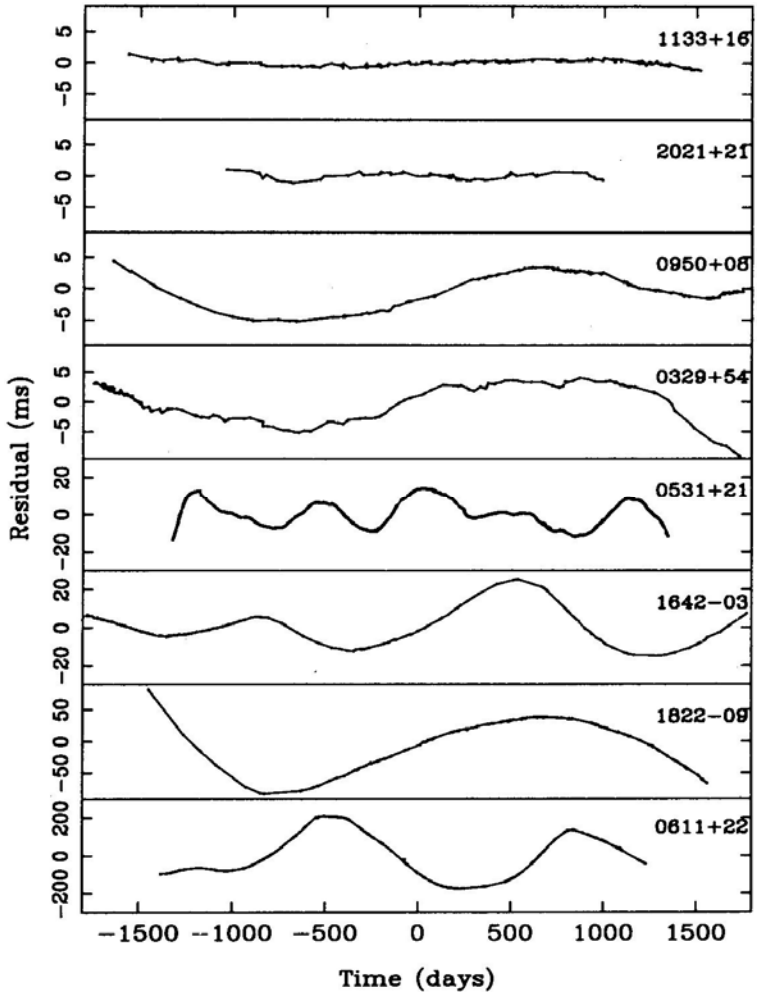

Figure 1: Examples of timing noise in 8 pulsars over about a 10 year period, showing increasing amounts of activity from the top to bottom.

2. Irregular Slowdown

This normal slowdown described above is steady and predictable. However some pulsars show unpredictable behaviour of two types: timing noise and glitches. Both are apparently associated with the transfer of angular momentum from the fluid interior (Lyne 1992) as the pulsar slows down and we discuss each of these in turn.

3. Timing Noise

Timing noise is characterised by a continuous, unpredictable, phase wandering of the pulses relative to a simple slow down model. It is seen most prominently in the Crab and other pulsars with large period derivatives (Cordes and Helfand 1980). Some examples of timing noise in a number of pulsars are shown in Fig. 1 where the unpredictability of the period in these pulsars is clear. The amount of this timing noise can be quantified by measuring the residuals relative to a simple slow-down model as described above. Fig. 2 shows the activity parameter, a logarithmic measure of the timing noise, as a function of the period derivative for a number of pulsars (Cordes and Downs 1985). The millisecond pulsars with very small period derivatives are found to be very stable, as indeed might be expected from the extrapolation of the trend in this diagram to their position in this diagram (Arzoumanian et al. 1994).

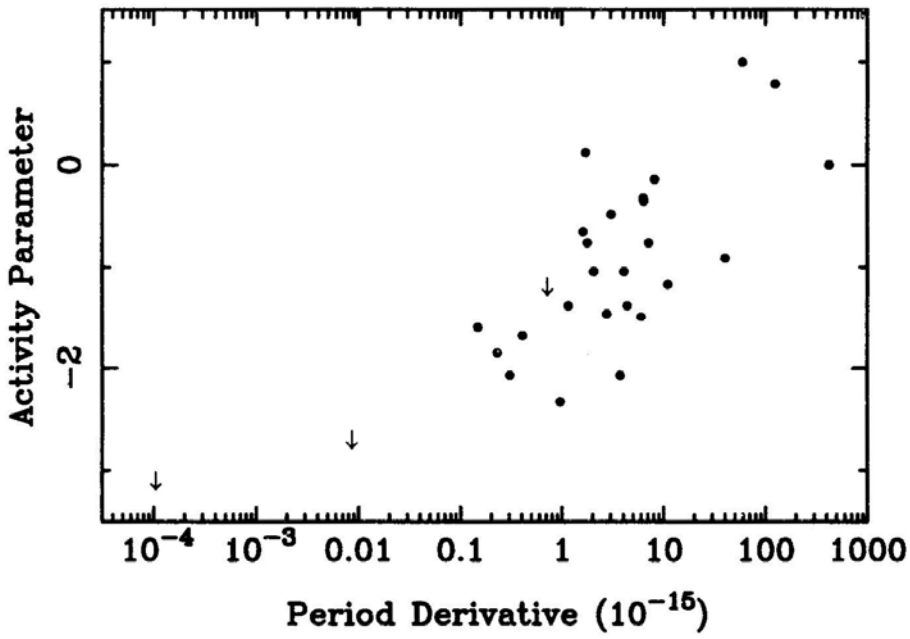

Figure 2: The timing activity parameter plotted as a function of period derivative

The most natural explanation is that timing noise is due to an irregular flow of angular momentum from a fluid component in the interior of the star for which direct evidence is provided by the glitches described in the next section.

4. Glitches

These are seen as sudden increases in the rotation rate $\nu = \Omega / 2\pi$, usually followed by an exponential recovery or relaxation back towards the pre-glitch period. For example, the slowdown of the Vela pulsar is shown in Fig. 3 over a 11-year period: during this interval, 4 glitches can be easily seen, each resulting in a fractional increase in rotation rate of about 2 parts in 10^6.

This behaviour can be explained by the presence of a fluid component in the interior of the neutron star which is loosely coupled to the rigid crust whose rotation we observe (Baym et al. 1969) through the emission beam which is tied to it. This simple model gives rise to the "glitch function" which describes the exponential recovery: $\Delta\nu(t) = \Delta\nu_0 \times [1 - Q\ (1 - e^{-t/\tau})]$. Here, $\Delta\nu_0$ is the initial rotational frequency increase and Q is the fraction of this which recovers on a timescale τ.

There are two main aspects of glitches which may or may not be related: firstly, the cause of the glitch, which might result from either a starquake or superfluid unpinning, and secondly, the post glitch relaxation, which gives information on the amount of fluid in the star and the physics of the angular momentum transfer from the core. First we discuss the possible causes of the glitches and then the possible implications of the recovery.

A starquake might arise from changing ellipticity of the crust of the neutron star as it slows down. The oblateness of an equilibrium spheroid will decrease as the rotation rate decreases. Stresses build up in the rigid crust as the departure from the equilibrium shape increases, until it cracks and assumes a shape closer to the equilibrium spheroid. The moment of inertia I decreases and conservation of angular momentum results in a spin-up given approximately in terms of the change in oblateness:

$$\Delta\epsilon = \Delta I/I = -\Delta\Omega/\Omega \tag{7}$$

For the Crab pulsar $\Delta\epsilon = -10^{-7}$ every 10 years and the current value of ϵ is about 10^{-3}. Clearly the time scale on which ϵ will decay due to this glitch activity is much greater than the age of the pulsar and this is quite satisfactory. However for the Vela pulsar $\Delta\epsilon = 2\times10^{-6}$ every 3 years and $\epsilon = 10^{-4}$. Clearly in this case ϵ would disappear in only about 100 years which is only about 1% of the age of the pulsar (Pines, Shaham &· Ruderman 1972). The current rate of glitching cannot be sustained, and another source of the discrete spin-ups is necessary.

It was suggested that superfluid neutrons probably exist in the inner part of the crust (Baym, Pethik & Pines 1969) and that these may be responsible for the glitches in the following way. The rotation rate of the superfluid is determined by the density of vortices and hence slowdown corresponds to an outward drift of vortices. However it is possible that the vortices pin to lattice nuclei in the inner part of the crust, so preventing them from drifting outwards (Anderson & Itoh 1975). The stress which drives the outward motion (the magnus force) builds up

until the strength of the pinning is exceeded. There is then a sudden catastrophic unpinning and a subsequent outward flow which causes an increase in the angular momentum of the crust. This is then probably followed by a re-pinning of the vortices and outward drift is reduced again. It is possible that, as the magnus force builds up, high temperature can permit vortex drift to occur, so relieving the pressure and reducing the rate of glitching (McKenna & Lyne 1990).

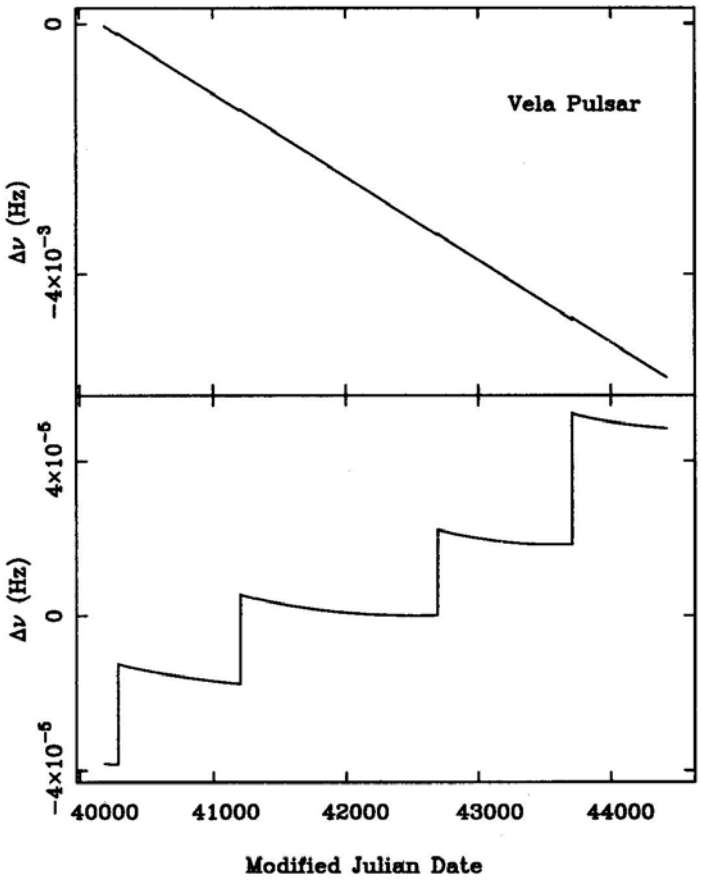

Figure 3: The change in the rotation rate of the Vela pulsar, PSR 0833-45, over an 11-year period. In the upper diagram, the steady slow-down is interrupted at intervals of a few years by the glitches, seen as sudden small increases in rotation rate. The lower diagram shows the same data after the removal of a constant, arbitrary value of frequency derivative in order to reveal the detail of the glitches and the recovery.

Glitches have a large range of amplitudes, of recovery timescales and of recovery amplitudes. As discussed earlier, the Vela pulsar is a frequent glitcher and 9 glitches have been observed over a 24 year period, the average fractional increase in rotation rate being about 2×10^{-6}. Recovery timescales seen in this pulsar are a few hundred days and less than a few days and the amount of recovery

in rotational frequency is only about 20% of the glitch amplitude. Alpar et al. (1993) have interpreted the recovery from these glitches in terms of both linear and non-linear relaxation in a number of regions within the crust.

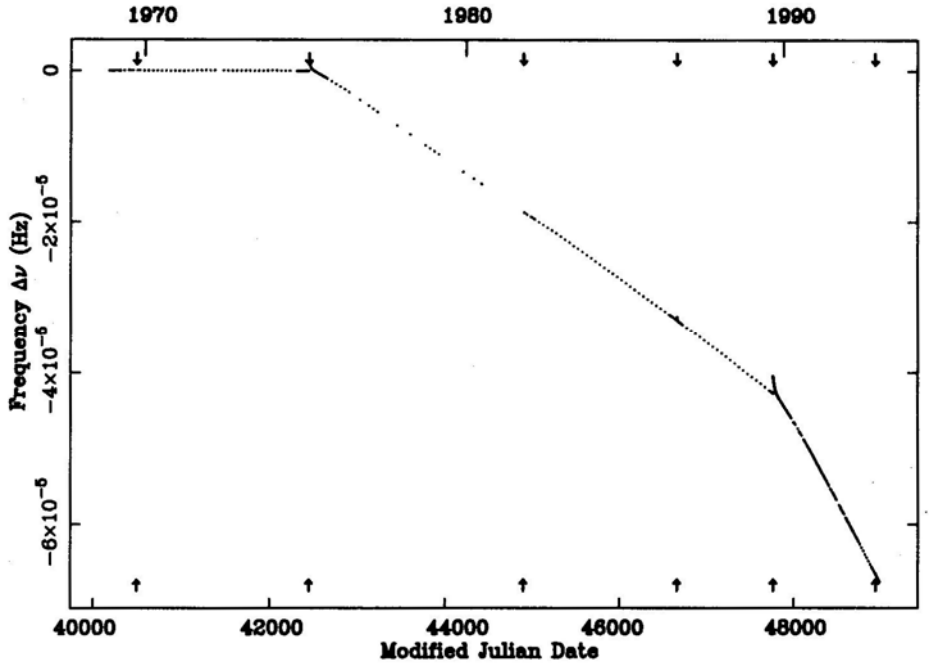

Figure 4: The rotation frequency of the Crab pulsar, PSR 0531+21, over a 23-year period, relative to a slow-down model fitted to the first few years of data. Two major glitches and their transient recoveries can be seen as small excursions in 1975 and 1989. However, their major effect was a permanent change in slowdown rate, seen as a sudden change in slope.

The Crab pulsar behaves rather differently (Lyne, Pritchard & Graham-Smith 1993) and has shown a series of glitches of magnitude 10^{-8} to 10^{-7}, which can be seen in figure 4 as changes in the rotation rate relative to a simple slow-down model fitted to the earliest data. The main effect of these glitches seems to be a persistent increase in slowdown rate amounting to about 0.1 % in total over a period of 23 years. How can this arise? Since the slowdown rate is primarily determined by B_0 and I (equation 3), there are 2 main possibilities. Firstly, the value of B_0 could have increased or its configuration could have changed. So far there is no observational evidence that this has occurred. The second possibility is that I has decreased. Now this cannot be due to a change in ellipsoid since the current moment of inertia is no more than 0.01% different from its value if it were rotating slowly. One possibility is that the decrease in I is due to an increase in vortex pinning as the star cools. Over the lifetime of the star this rate of pinning implies that more than 5% of the moment of inertia must now be tied up in the form of pinned superfluid neutrons.

5. The Frequency of Glitches

Until recently the study of glitches has been limited by their small number. Excluding Vela, only about 10 glitches were observed in about 20 years up to 1987. This was mainly due to the lack of known young pulsars. The small number arises both from the fact that pulsars do not stay young for very long, and also that there are strong selection effects against the discovery of young pulsars in most searches. Their short periods made them difficult to detect in the early surveys and their low z-distances give rise to a high sky background temperature, high dispersion, and high scattering at low frequencies, all of which were detrimental to their detection. To combat such effects, two surveys have been conducted at low latitude and high radio frequency. The survey at Jodrell Bank (Clifton & Lyne 1986) discovered 40 new pulsars in a sample which has a mean characteristic age of only 0.8 million years compared with 6 million years for all pulsars found in previous surveys (Clifton et al. 1992). Already 12 glitches have occurred in 5 years in 6 of these pulsars (Shemar & Lyne 1995). The subsequent high frequency Parkes survey of the southern galactic plane has shown a similar success rate Johnston et al. 1992a; Johnston et al. 1995).

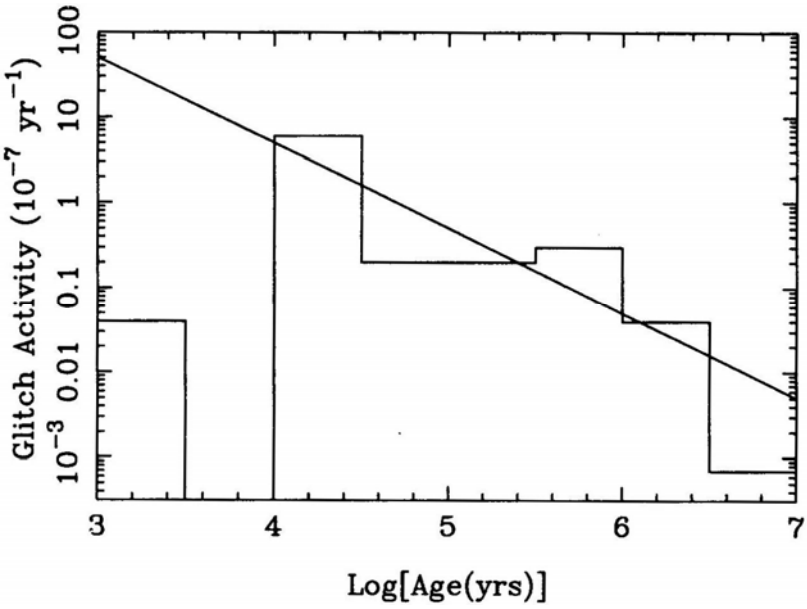

Figure 5: The glitch activity parameter, the fractional increase in rotation rate due to glitches/year, averaged over all observed pulsars in semi-decade ranges of characteristic age.

Table 2 provides a summary of the 20 pulsars which have glitched, together with the number of glitches, the fractional increase in rotational frequency at each glitch and the observational references. These data show that glitches occur

predominently in young pulsars which account for only about 3% of the known population. The rest of this section describes the frequency of glitches and their recovery as a function of the pulsar spin-down parameters.

TABLE 2: Known Glitching pulsars

Pulsar	N_{glitch}	$\Delta\Omega/\Omega \times 10^6$	References
0355+54	2	0.006, 4.4	A
0525+21	2	0.0013, 0.0003(?)	B
0531+21	4	0.01, 0.04, 0.01, 0.08	C,D,E,F
0833-45	9	2.3, 2.0, 2.0, 3.1, 1.1, 2.0, 1.3, 1.8, 2.7	G,H,I,J,K,L,M,N,O
1325-43	1	0.12	P
1338-62	3	1.5, 0.03, 1.0	Q
1508+55	1	0.0002(?)	R
1535-56	1	2.8	S
1641-45	1	0.2	T
1706-44	1	2.1	S
1727-33	1	3.1	S
1736-29	1	0.003	U
1737-30	6	0.42, 0.03, 0.007, 0.03, 0.60, 0.70	V
1758-23	3	0.20, 0.23, 0.35	W
1800-21	1	4.1	U
1823-13	2	2.7, 3.1	U
1830-08	1	1.9	U
1859+07	1	0.03	U
1907+00	1	0.0007(?)	X
2224+65	1	1.7	Y

REFERENCE KEYS:
A:Lyne (1987) B:Downes (1982) C:Boynton et al. (1972) D:Lohsen (1975) E:Lyne & Pritchard (1987) F:Lyne, Pritchard & Graham-Smith (1992) G:Radhakrishnan and Manchester (1969) H:Reichley & Downes (1971) I:Manchester, Goss & Hamilton (1976) J:Manchester et al. (1983) K:McKulloch et al. (1983) L:Cordes, Downes & Krause-Polstorff (1988) M:McKulloch et al. (1987) N:Flanagan (1989) O:Flanagan (1991) P:Newton, Manchester & Cooke (1981) Q:Kaspi et al. (1992) R:Manchester & Taylor (1974) S:Johnston et al. (1992b) T:Manchester et al. (1978) U:Shemar & Lyne (1995) V.McKenna & Lyne (1990) W:Kaspi et al. (1993) X:Gullahorn et al. (1976) Y:Backus, Taylor & Damashek (1992)

Apart from the youngest pulsars, most pulsars which have glitched have done so only once. The implication here is that the intervals between glitches in these objects and in similar ones is much greater than the observational timespan and, given enough time, they will all display glitch activity. For this reason, in order to understand the frequency of glitches, we have to consider the length of time that pulsars of similar characteristics have been observed. Dividing the number of glitches by the total observation time gives a rate of glitch activity (Shemar & Lyne 1995). Figure 5 shows the pulsar glitch activity as a function of age. We clearly

see that the glitch activity is greatest for pulsars with ages between about 10,000 and 30,000 years. For greater ages, it seems that the activity falls off roughly as the frequency derivative, presumably as the flow of angular momentum from the interior decreases. To first order, this can be understood in terms of glitches undoing of a fixed fraction of the normal rotational slow-down. This fraction amounts to about 0.03, suggesting that about 3% of the angular momentum in these pulsars is carried by superfluid neutrons whose outward flow to the crust is held up by vortex pinning and only moves in a stepwise manner. Since there is no significant recovery between glitches (see next section), this implies that there is little drift occurring in these vortices.

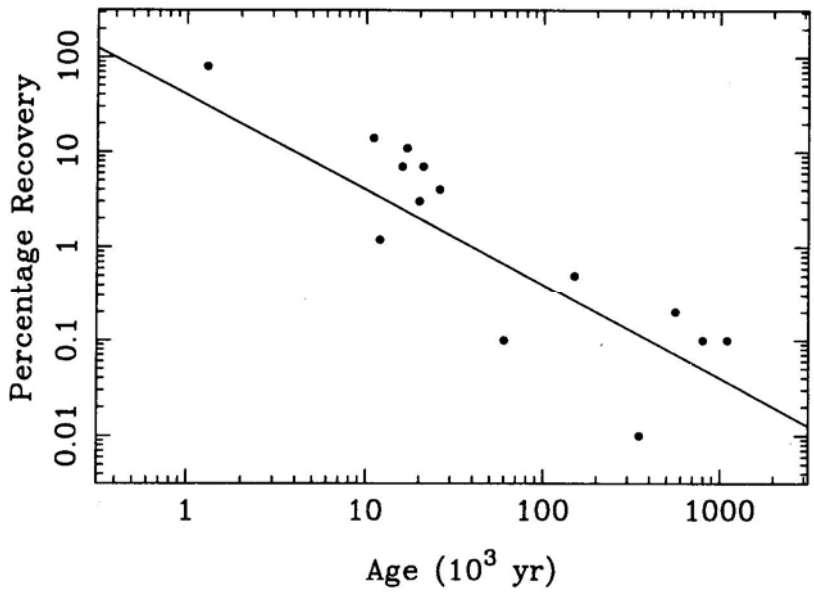

Figure 6: The percentage recovery of the initial frequency step, Q, as a function of pulsar characteristic age.

Somewhat surprising is the low level of glitch activity in the youngest pulsars such as the Crab pulsar, PSR 1509-58 and PSR 0540-69. Although these pulsars have very large slow-down rates, the angular momentum flow seems to be reasonably continuous. One possible reason for this is the youth of these pulsars and their corresponding high internal temperature, which may allow the stresses on the pinned vortices to be relieved by thermal drift of the vortices from one pinning site to another in a gradual fashion (McKenna & Lyne 1990).

6. The Recovery from Glitches

There is a wide range of recovery from glitches and again this seems to be related approximately to the age of the pulsar (figure 6). For glitches in the younger

pulsars, both the frequency and frequency derivative steps of the glitch recover substantially over the following months. In those glitches which have been observed closely following the event, exponential recoveries on up to 3 timescales are often recorded (McKulloch et al. 1990). For the older pulsars, the main effect of a glitch is a large step in frequency and there is very little recovery in this over the following years. In fact the small amount of frequency recovery depends inversely upon the characteristic age, suggesting that, as discussed above, in older pulsars the vortex pinning is strong and little vortex drift occurs.

7. Conclusion

The trends described above are only recently becoming quantifiable and are still somewhat preliminary. However, as more glitches are observed in the newly discovered young pulsars, the study of neutron star interiors will become more detailed and may impose limits upon the equation of state of matter at the super nuclear densities within these objects (Pines 1991).

References

Alpar M. A., Chau H. F., Cheng K. S., Pines D., 1993, ApJ, 409, 345
Anderson P. W., Itoh N., 1975, Nat, 256, 25
Arzoumanian Z., Nice D. J., Taylor J. H., Thorsett S. E., 1994, ApJ, 422, 671
Backus P. R., Taylor J. H., Damashek M., 1982, ApJ, 255, L63
Baym G., Pethick C, Pines D., 1969, Nat, 224, 673
Baym G., Pethick C, Pines D., Ruderman M., 1969, Nat, 224, 872
Boynton P. E., Groth E. J., Hutchinson D. P., Nanos G. P., Partridge R. B., Wilkinson D. T., 1972, ApJ, 175, 217
Clifton T. R., Lyne A. G., 1986, Nat, 320, 43
Clifton T. R., Lyne A. G., Jones A. W., McKenna J., Ashworth M., 1992, MNRAS, 254, 177
Cordes J. M., Downs G. S., 1985, ApJS, 59, 343
Cordes J. M., Helfand D. J., 1980, ApJ , 239, 640
Cordes J. M., Downs G. S., Krause-Polstorff J., 1988, ApJ, 330, 847
Downs G. S., 1982, ApJ, 257, L67
Flanagan C. S., 1989. LAU Circ. No. 4695
Flanagan C. S., 1991. IAU Circ. No. 5311
Goldreich P., Julian W. H., 1969, ApJ, 157, 869
Gullahorn G. E.., Payne R. R., Rankin. J. M., Richards D. W., 1976, ApJ, 205, L151
Johnston S., Lyne A. G., Manchester R. N., Kniffen D. A., D'Amico N., Lim J., Ashworth M., 1992a, MNRAS, 255, 401
Johnston S., Manchester R. N., Lyne A. G., Bailes M., Kaspi V. M., Qiao G., D'Amico N., 1992b, ApJ, 387, L37

Kaspi V. M., Manchester R. N., Johnston S., Lyne A. G., D'Amico N., 1992, ApJ, 399, L155
Kaspi V. M., Lyne A. G., Manchester R. N., Johnston S., D'Amico N., Shemar S. L., 1993, ApJ, 409, L57
Kaspi V. M., Manchester R. N., Siegman B., Johnston S., Lyne A. G., 1994, ApJ, 422, L83
Lohsen E., 1975, Nat, 258, 688
Lyne A. G., Pritchard R. S., 1987, MNRAS, 229, 223
Lyne A. G., Pritchard R. S., Graham-Smith F., 1992, Nat, 359, 706
Lyne A. G., Pritchard R. S., Graham-Smith F., 1993, MNRAS, 265, 1003
Lyne A. G., Pritchard R. S., Smith F. G., 1988, MNRAS, 233, 667
Lyne A. G., 1987, Nat, 326, 569
Lyne A. G., 1992, Phil. Trans. Roy. Soc. A, 341, 29
Manchester R. N., Peterson B. A., 1989, ApJ, 342, L23
Manchester R. N., Taylor J. H., 1974, ApJ, 191, L63
Manchester R. N., Goss W. M., Hamilton P. A., 1976, Nat, 259, 291
Manchester R. N., Newton L. M., Goss W. M., Hamilton P. A., 1978, MNRAS, 184, 35P
Manchester R. N., Newton L. M., Hamilton P. A., Goss W. M., 1983, MNRAS, 202, 269
McCulloch P. M., Hamilton P. A., Royle G. W. R., Manchester R. N., 1983, Nat, 302, 319
McCulloch P. M., Klekociuk A. R., Hamilton P. A., Royle G. W. R., 1987, Aust. J. Phys., 40, 725
McCulloch P. M., Hamilton P. A., McConnell D., King E. A., 1990, Nat, 346, 822 McKenna J., Lyne A. G., 1990, Nat, 343, 349
Newton L. M., Manchester R. N., Cooke D. J., 1981, MNRAS, 194, 841
Pines D., Shaham J., Ruderman M. A., 1972, Nature Phys. Sci., 237, 83
Pines D., 1991, in Ventura J., Pines D., eds, Neutron Stars: Theory and Observation. Kluwer Academic Publishers, p. 57
Radhakrishnan V., Manchester R. N., 1969, Nat, 222, 228
Reichley P. E., Downs G. S., 1971, Nature Phys. Sci., 234, 48
Shemar S. L., Lyne A. G. 1995. in preparation

Diamond Jubilee Symposium on Pulsars
14–17 March 1994
Raman Research Institute, Bangalore

J. Astrophys. Astr. (1995) **16,** 191–206

Lense-Thirring Precession of Radio Pulsars

R. D. Blandford *130–33 Caltech, Pasadena, CA 91125, USA.*

Abstract. It is shown that if neutron stars contain dynamically decoupled components, most plausibly discrete superfluid zones, then it is possible for the spin axes of these components o become slightly misaligned with respect to the crustal spin following a series of glitches. The crust will then undergo Lense-Thirring precession about the total angular moment with a period of $\sim 6 - 7.5P$ (assuming a crustal superfluid) and $\sim 3 - 6P$ (if the core superfluid is not tightly coupled to the crust). The precise precessional period is diagnostic of the mass distribution within each component. The implications of recent observational inferences concerning glitching pulsars are discussed. The conditions necessary for precession to be observable are analysed phenomenologically and a search of pulse-timing data for evidence of a Lense-Thirring modulation within the period range $\sim 3 - 8P$ is proposed.

1. Introduction

In this talk I will present a summary of a quite speculative possibility that Paolo Coppi and I have thought about over the past five years. To be specific, we suggest that neutron star interiors contain dynamical components which are quite weakly coupled to the crust and which can become misaligned following glitches. If this really can happen, (and we concede that most expert opinion is that it cannot), then the interior and the exterior undergo mutual Lense-Thirring precession which may be detectable as a tiny, periodic modulation of the pulsed signal. As the cost of attempting to measure this precession using a satellite orbiting the Earth may be five orders of magnitude more expensive than a pulsar experiment, I contend that a modest search for this effect in suitable pulsars is worth a try even if the odds are long. A fuller discussion of these ideas is contained in Blandford & Coppi (1994, in preparation).

Let me begin with a phenomenological approach to describing pulsar glitches that eschews microscopic theory. What we observe is that pulsars slow down in a more or less regular fashion, except that, occasionally, they undergo glitches - sudden increases in angular frequency. In young pulsars at least, these are also followed by a significant, though temporary, increase in the rate at which they slow

down. Beyond this, the details vary in a rather confusing manner from pulsar to pulsar and glitch to glitch, although, as we have heard here from Andrew Lyne, some systematics are starting to emerge. Now pulsars are neutron stars with moments of inertia $I \sim 10^{45}$ g cm ^{2} and it seems highly unlikely that an external torque (which would have to be several orders of magnitude larger than the steady decelerating electromagnetic torque and always have the same sign) can be responsible for glitches. For this reason, internal changes in the angular momentum are now universally invoked to explain large glitches.

There appear to be two generic models that can account for observed glitches. I shall call them the "Spin-exchange" model and the "Starquake" model. In the simplest version of the spin-exchange model, the neutron star has two separate components each with a fixed moment of inertia. One component, which I call "crust", is rigidly attached to the external magnetic field which causes it to decelerate and its angular frequency, $\Omega(t)$, is what radio astronomers measure. The second component, which I name "superfluid" is weakly coupled to the crust so its angular frequency Ω_2 is somewhat larger than Ω. (It is not necessary that it be an actual superfluid, but this is by far the most likely possibility based upon our understanding of neutron star structure.) During a glitch, the coupling between these two components becomes very strong for a short while and there is a rapid transfer of spin angular momentum from the superfluid to the crust, which consequently speeds up. After the glitch, the difference in angular velocity between the two components is reduced, along with the weak torque that couples them. The crust therefore decelerates more rapidly under the action of the electromagnetic torque until the lag in angular frequency recovers sufficiently to re-establish an equilibrium where both components decelerate at the same rate or another glitch takes place. During this whole process, the change in total angular momentum is the integral over time of the external torque and just what it would have been had there had been no glitch.

In the elementary starquake model, there are again crustal and superfluid components but this time the crustal moment of inertia is rot constant and during a glitch, it suddenly decreases causing the crust to start spinning a little faster. This then activates a crust-superfluid torque which causes the crust to decelerate more rapidly, simultaneously accelerating the superfluid until, once more, it shares a common rotation with the crust or another glitch occurs. Again the variation of the total angular momentum is unaffected, but the average angular velocity will increase following a glitch because the total moment of inertia decreases.

Now, for both of these models it has been generally assumed that when the angular velocities of the crust and one or more superfluid components differ, they do so only in magnitude, not in direction. However it would seem very strange if either the application of a sudden braking torque or the rearrangement of the superfluid were strictly axisymmetric with respect to the angular velocity and surely, this is not going to be the case. Therefore the assumption that all angular frequencies are parallel is really equivalent to assuming that, if we decompose the immediate post-glitch torque into three components, one aligning, one precessing and one decelerating, then the first does its job very quickly, making the second irrelevant and leaving us only the effects of the third torque to observe. It has never been clear to me why spin alignment has to be this rapid and so the question

that I now address is "What happens if the post-glitch angular velocities become misaligned?"

2. Lense-Thirring Precession

Neutron stars are relativistic objects and when they rotate, they "drag" local inertial frames with them - the Lense-Thirring effect. In the post-Newtonian limit, this effect can be thought of as an additional non-Newtonian, gravitational torque acting in a flat space. It is convenient to make the gravitoelectric/gravitomagnetic decomposition of the post-Newtonian equations of motion (*e.g.*Thorne, Price & MacDonald 1986). A spinning ring of matter with mass current density ρv acts as a source for a "gravitational vector potential" β,

$$\nabla^2\boldsymbol{\beta} = \frac{16\pi G}{c}\rho\mathbf{v}. \tag{1}$$

This vector potential is related in the usual manner to the gravitomagnetic field h= $\nabla \times \beta$. For simplicity, just confine attention to a spherically symmetric distribution of matter $\rho_1(r_1)$ spinning with uniform angular velocity Ω_1 about the z axis. (We can think of component. 1 as being the crust and label the superfluid with the subscript 2.) The vector potential at a point labelled using a radial coordinate r_2 and a polar angle θ_2 measured from the same z axis is given by

$$\beta_\phi(r_2,\theta_2) = -\frac{16\pi G}{3c}\Omega_1 \sin\theta_2 \int dr_1 r_1^3 \rho_1(r_1)\frac{\min[r_1,r_2]}{\max[r_1^2,r_2^2]} \tag{2}$$

Now add a second component, also labelled 2 and which also has a spherically symmetric mass distribution. These components may interpenetrate one another. The total torque that body 1 exerts upon it is obtained by taking a moment of the "Lorentz force"

$$\begin{aligned}\mathbf{G}_{12} &= \int d^3r_2\rho_2(r_2)\mathbf{r}_2 \times \left[\frac{\mathbf{v}_2(\mathbf{r}_2)}{c} \times \mathbf{h}(\mathbf{r}_2)\right] \\ &= \int d^3r_2\rho_2(r_2)[\mathbf{r}_2 \cdot \mathbf{h}(\mathbf{r}_2)]\frac{\mathbf{v}_1(\mathbf{r}_2)}{c}.\end{aligned} \tag{3}$$

After substituting for h and some further manipulation, this can be cast in the form

$$\mathbf{G}_{12} = K_{\rm LT}\frac{G}{c^2}\frac{\mathbf{S}_2 \times \mathbf{S}_1}{R^3} \tag{4}$$

where R is the total stellar radius and $K_{\rm LT}$ is a dimensionless structure constant given by

$$K_{\rm LT} = \frac{2R^3 \int_0^R dr_1 r_1^3 \rho_1(r_1) \int_0^R dr_2 r_2^3 \rho_2(r_2) \left[\frac{\min[r_1,r_2]}{\max[r_1^2,r_2^2]}\right]}{\int_0^R dr_1 r_1^4 \rho_1(r_1) \int_0^R dr_2 r_2^4 \rho_2(r_2)}. \tag{5}$$

Note that $G_{12} = -G_{21}$, consistent with Newton's third law and that both components undergo a mutual Lense-Thirring precession about the total angular momentum **J**, given by

$$\boldsymbol{\Omega}_{\rm LT} = K_{\rm LT}\frac{G}{c^2R^3}\mathbf{J} \tag{6}$$

Note also that, for a given star, the predicted precessional period $P_{\rm LT}$ is a fixed multiple of the spin period P

Coppi and I have computed this structure constant for a variety of assumptions about the internal structure of the neutron star and a variety of equations of state. If we assume that component 2 is a crustal superfluid and the total stellar mass is 1.4 $M_\odot$ with radius in the interval 7 km< R < 16 km, then

$$5.9P \lesssim P_{\rm LT} \lesssim 7.4P \tag{7}$$

where the variation is mostly attributable to the variation of the total mass distribution. Alternatively, if component 2 is a core superfluid, then

$$3.2P \lesssim P_{\rm LT} \lesssim 6.1P \tag{7}$$

These two cases ought to be distinguishable.

Before continuing, I should list some uncertainties in the technical calculation, even granted its premise. Firstly, the post-Newtonian approximation is only marginally valid and a fully relativistic calculation may change the answer by as much as 30 percent if the equation of state is soft. Secondly, there is a genuinely Newtonian contribution to the precession in addition to the Lense-Thirring term. This is caused by the Newtonian gravitational attraction of the misaligned rotational bulges of the two components. This can actually be computed and the result is

$$\Omega_{\rm N} = K_{\rm N}\frac{T_{\rm rot}}{|W|}\Omega_2 \tag{9}$$

where $T_{\rm rot}$ is the rotational kinetic energy and $|W|$ is the total gravitational potential energy. Typically $K_{\rm N} \sim K_{\rm LT} \sim 2$ and, to order of magnitude, $P_N / P_{\rm LT} \sim (P/P_{\rm min})^2$ where $P_{\rm min}$ is the shortest possible pulsar period. This contribution need only be considered further for millisecond pulsars and its small size emphasizes that we are truly in a regime where general relativistic effects are important. Thirdly, there is ample evidence that there are more than two components (*e.g.*Lyne, Graham-Smith & Pritchard 1992 and below). This multiplies the dynamical possibilities (*cf.*Hamilton & Sarazin 1982) but does not change the general principles.

3. The Interpretation of Glitching Pulsars

3.1 *Observations of Glitches*

Glitching pulsars have been carefully monitored ever since the first example was discovered in the Vela pulsar in 1969 (Radhakrishnan & Manchester 1969, Reichley & Downes 1969). For completeness, let me summarise the salient points of the observations which are discussed more comprehensively here by Lyne. The largest glitches involve relative frequency jumps $\Delta\Omega/\Omega \sim 4 \times 10^{-6}$ (Lyne 1987) and associated relative frequency derivative changes that can be as large as $\Delta\dot{\Omega}/\dot{\Omega} \sim 0.4$ (Chau *et al.*1993). Glitches seem to happen very quickly, in one instance, in less than two minutes (McCulloch *et al.*1990). As far as can be measured, post-glitch recoveries can be described by the superposition of simple exponential functions

with time constants that vary from ~ 10 hr. to much longer than the inter-glitch interval. (Sometimes a quadratic fit is adopted for long recoveries, but for our purposes, it is simpler to replace this with an incomplete exponential recovery.) Up to five distinct components may be involved in a single glitch. The fraction of the relative frequency jump that is recovered after a glitch, known as Q, is quite small in old pulsars, though it can approach, or even exceed, unity in young pulsars such as the Crab pulsar. A recent discovery (Lyne, these proceedings) is that, although young pulsars provide the most spectacular examples of period changes, it is their middle-aged counterparts that are *relatively* most active. On statistical grounds, it appears that over a long time interval the accumulated period *increase* attributable to large glitches is roughly two percent in magnitude of the total period *decrease* associated with the external electromagnetic torque. In the case of the Vela pulsar, this translates to one glitch, with $\Delta\Omega/\Omega \sim 3 \times 10^{-6}$, every ~ 3 yr. which is roughly what has been observed over the past ~ 25 yr.

3.2 *The spin exchange model*

3.2.1 Dynamics

A natural phenomenological interpretation of the observed exponential recovery is that the relative frictional torque between two components varies in direct proportion to their relative angular velocity (*cf.*Michel, Bland-Hawthorn & Lyne 1990). Let us suppose that there are only two components, a crust and a superfluid, that are related in this manner. Let the crust have a moment of inertia that is a fraction f of the total stellar moment of inertia. The equations of motion for the two components can be cast in the form

$$f\dot{\Omega} = \dot{\Omega}_e + \frac{f(1-f)\omega}{\tau} \tag{10}$$

$$(1-f)\dot{\Omega}_2 = -\frac{f(1-f)\omega}{\tau}; \quad t > 0 \tag{11}$$

where we drop the subscript 1 for the crustal component and $\omega \equiv \Omega_2 - \Omega$ is the angular velocity lag. (In this section I assume that all spins are parallel.) Combining these two equations, we identify the constant $\dot{\Omega}_e < 0$ with the steady spin down rate when $\dot{\omega} = 0$. Equivalently, it is the steady electromagnetic torque divided by the total stellar moment of inertia. (This quantity is actually time-dependent but, for present purposes, it is not necessary to include this refinement.) The solutions of these differential equations for the observable $\Omega(t)$ and the unobserved $\omega(t)$ are

$$\Omega = \Omega_- + \Delta\Omega + \dot{\Omega}_e t - Q\Delta\Omega\left(1 - e^{-\frac{t}{\tau}}\right) \tag{12}$$

$$\omega = \frac{-\dot{\Omega}_e \tau}{f} - \frac{Q\Delta\Omega}{(1-f)} e^{-\frac{t}{\tau}} \tag{13}$$

where $\Delta\Omega$ is the observed frequency jump and

$$Q = \frac{(\dot{\Omega}_e - \dot{\Omega}_0)\tau}{\Delta\Omega}, \tag{14}$$

the frequency recovery, appears as a constant of integration. The definition of Q involves $\dot{\Omega}_e$, which is not directly observed in an individual glitch and Ω_0 the angular frequency derivative measured immediately after the glitch. It differs from the conventional definition when glitches do not recover completely (see below) but is equivalent to the normal definition when glitches do recover and $\dot{\Omega}_e \equiv \dot{\Omega}_-$. Now we also observe the crust angular frequency just prior to the glitch, Ω_- and if we assume that angular momentum is conserved during the glitch, with no change in the moments of inertia, then the unobserved angular velocity lags just before (ω_-) and immediately after (ω_0) the glitch are related by

$$\omega_- = \omega_0 + \frac{\Delta\Omega}{(1-f)} \tag{15}$$

We can use these equations to express the angular velocity lag observed before, immediately after the glitch and long after its recovery ω_+ (if this happens before another glitch), in terms of the fractional moment of inertia of the superfiuid component.

$$\omega_- = -\frac{\dot{\Omega}_e \tau}{f} + \frac{(1-Q)\Delta\Omega}{(1-f)} \tag{16}$$

$$\omega_0 = -\frac{\dot{\Omega}_e \tau}{f} - \frac{Q\Delta\Omega}{(1-f)} \tag{17}$$

$$\omega_+ = -\frac{\dot{\Omega}_e \tau}{f} \tag{18}$$

The relative decrease in the angular velocity lag between the two components over a fully-recovered glitch is then given by

$$\frac{\omega_- - \omega_+}{\omega_+} = \left(\frac{1-Q}{Q}\right)\left(\frac{f}{1-f}\right)\left(\frac{\Delta\dot{\Omega}}{\dot{\Omega}}\right) \tag{19}$$

3.2.2 Application to the Vela pulsar

Now let us apply this analysis to the observations of the Vela pulsar (Cordes, Downes & Krause-Polstorff 1988, Chau *et al.*1993). (A similar application has been made to the frequently glitching pulsar PSR 1737–30 by Michel *et al.* 1990.) Nine glitches have been observed with varying precision and we are due for a tenth. For illustration purposes, let me take the eighth glitch which occured on December 24 1988 (Flanagan 1990, McCulloch *et* α*l.*1990, Alpar Pines & Cheng 1990) as this has received most scrutiny and has had a long recovery. It also seems to be typical in its recovery. (It should be emphasised that different groups derive significantly different timing models when analysing the same glitch, at least partly due to the insidious influence of timing noise Cordes *et al.*1988, Alpar *et* α*l.*1992. However the qualitative conclusions that I shall draw are not influenced by these differences.)

Flanagan's model for the eighth glitch resolves the initial frequency jump of $\Delta\Omega/\Omega = 1.8 \times 10^{-6}$ into three superposed frequency jumps, each of which recovers exponentially with a separate time constant. If we try to apply the two-component,

Spin-exchange model and assume complete recovery between glitches, then we should focus on the largest and slowest component, for which $\Delta\dot{\Omega}/\dot{\Omega} = 0.0029$, $Q = 0.018$, $\tau \equiv \tau_3 = 96$ d, and treat the other two jumps as perturbations. Adopting, the preglitch parameters of $\Omega_- = 70.4$ rad s^{-1}, $\dot{\Omega}_- = -9.8 \times 10^{-11}$ rad s^{-2}, Eq.(19) gives

$$\frac{\omega_- - \omega_+}{\omega_+} = 0.16\left(\frac{f}{1-f}\right) \tag{20}$$

Now Vela macroglitches recur, on average every 2.8 yr, and the present slowing down timescale is $-\Omega/\dot{\Omega} = 2.3 \times 10^4$ yr. If this glitching behaviour is to recur for a third of the slowing down timescale, say, then we require $(\omega_- - \omega_+)/\omega_+ \lesssim 4 \times 10^{-4}$ or $f \lesssim 2 \times 10^{-3}$. One physical way in which this condition may arise is if glitches only happen when ω exceeds a critical value that varies smoothly with Ω. However, the condition is really more general than this. Using Eq.(20), the crust, together with all of the star to which it is coupled, would have $f \lesssim 2\times 10^{-3}$, a very small fraction of the total stellar moment of inertia.

We can see why this is required in a quite direct manner. Immediately prior to the first observed glitch in 1969, when the star was (by hypothesis) dynamically relaxed, the frequency was $\Omega_1 = 70.43196$ rad s^{-1}. Just before glitch eight, when the star should also have been relaxed, $\Omega_8 = 70.37177$ rad s^{-1}, $\dot{\Omega}_8 = -9.79066 \times 10^{-11}$ rad s^{-1}, $\bar{\Omega}_8 = 2.6 \times 10^{-21}$ rad s^{-2}. The interval between these two glitches is $t_8 - t_1 = 6.3 \times 10^8$ s. Now suppose, still by hypothesis, that the total moment of inertia of the star, $I = 10^{45}\, I_{45}$ g cm^2, does not change and the torque $N(t)$ is unaffected by the glitches. We can estimate the rotational impulse due to the external torque by Taylor expanding about glitch 8.

$$\int_{t_1}^{t_8} dtN = [\dot{\Omega}_8(t_8 - t_1) - 0.5\ddot{\Omega}_8(t_8 - t_1)^2]I = -6.17 \times 10^{43} I_{45} \text{g cm}^2\text{s}^{-1} \tag{21}$$

This ought to equal the decrease in the total stellar angular momentum. The actual decrease is given by

$$\Delta J = (\Omega_8 - \Omega_1)I = -6.02 \times 10^{43}\, I_{45} \text{g cm}^2\text{s}^{-1} \tag{22}$$

Even if we make a generous allowance for the uncertainty in the long term timing model, we find that the star has somehow recovered a fraction 0.021 ± 0.005 of the spin angular momentum extracted by the electromagnetic torque. Therefore, one of our assumptions must be wrong.

We can locate the probable source of the problem by noticing that $\ddot{\Omega}$ is still unexpectedly large just before glitches. This suggests that there is a longer time scale coupling than τ_3 which does not proceed to completion. This invalidates the assumption that we made in deriving Eq.(18) namely that $\dot{\omega} \to 0$ before the next glitch. So, let us now treat the 96 d recovery as a perturbation and remove it as well and try to model the incomplete recovery which we treat as exponential with time constant τ_2 Operationally we can estimate τ_2 by measuring the best value of $\ddot{\Omega}$ for the long term recovery from Chau. *et al.*(1993) and correcting for the expected rate of change of Ω_e, to obtain $\ddot{\Omega} \simeq 3 \times 10^{-21}$ rad s^{-3}. The recovery

time is then given by differentiating Eq. (10), (11).

$$\tau_2 = \frac{\dot{\Omega}_e - \dot{\Omega}_0}{\ddot{\Omega}} \simeq 20\mathrm{yr} \tag{23}$$

where $\dot{\Omega}_e$ can be estimated from the total change of Ω over a long interval, *i.e.*

$$\dot{\Omega}_e \simeq \frac{\Omega_8 - \Omega_1}{t_8 - t_1} \simeq -9.63 \times 10^{-11}\mathrm{rad\ s^{-2}} \tag{24}$$

and $\dot{\Omega}_0 = -9.84 \times 10^{-11}$ rad s^{-2}, (Flanagan 1990)

We can now determine when the angular velocity lag will recover to its pre-glitch value using Eq.(13),(14), to obtain a time interval

$$t = \tau_2 \ln\left(\frac{\dot{\Omega}_s - \dot{\Omega}_0}{\dot{\Omega}_e - \dot{\Omega}_-}\right) \simeq 6\mathrm{yr} \tag{25}$$

This is about twice the actual time that elapsed, but considering the crudity of the assumptions is not discouraging. What this calculation does make clear is that, if the recovery is incomplete, then it is physically possible under the spin exchange model for glitches to recur over the whole lifetime of the pulsar. A global re-analysis of the whole Vela data set is probably necessary to see if this interpretation makes sense. In the limiting case that the superfluid decouples completely from the crust and $\tau_2 \to \infty$, then the lag will obviously recover in a time interval $\Delta\Omega/(\dot{\Omega}_e - \dot{\Omega}_0)$.

To what extent does adopting this model constrain the crustal moment of inertia? Unfortunately, not much. This can be seen directly from Eq.(10) which allows us to compute the crustal moment of inertia for different assumed values of ω_0. If the frictional torque is ignorably small, then $f \sim 0.98$. However, a difference as large as $\omega_0 = 0.7$ rad s^{-1} gives $f \sim 0.1$. In conclusion, unless we make some additional assumption about the dynamics, changes in the inferred crustal moment of inertia are indistinguishable from changes in the crust-superfiuid frictional torque under the spin-exchange model with incomplete recovery and we cannot deduce f directly from the observations, only an upper bound ~ 0.98 (*cf.*Alpar *et al.*1993).

3.2.3 Relaxation of secondary components

As an aside, we can go back and try to interpret the three small recoveries from the eighth Vela glitch on the assumption that each one is associated with the coupling of these additional components to the crust of additional superfluid components with a small fractional moment of inertia f_i, i= 3,4,5 to the crust; the coupling to superfluid component 2 is assumed, for simplicity, to be negligible. Now the dynamics is dominated by the exchange of spin between the crust and component 2. The perturbations associated with the interaction with component i is given by

$$\delta(\Delta\dot{\Omega})_i = -\frac{f_i}{f}\frac{\Delta\Omega}{\tau_i} \tag{26}$$

¿From this we infer that

$$\frac{f_i}{f} = Q_i \tag{27}$$

For component 3 with τ_3 = 96 d, I obtain $f_3/f \sim Q_3 \sim 0.02$ and find that the total angular frequency jump in the glitch is ~ 0.16 times the equilibrium angular frequency difference between component 3 and the crust. For component 4, with $\tau_4 \sim 4$ d, $f_4 \sim 0.004f$ and the crust changes during the glitch from trailing behind component 4 by $\sim 3 \times 10^{-5}$ rad s^{-1} to leading by $\sim 10^{-4}$ rad s^{-1} For component 5, which recovers in ~ 10 hr, $f_5 \sim 0.005f$ and the frequency jump, is ~ 40 times the equilibrium lag. The combined moment of inertia of these three additional superfluid components is only ~ 3 percent of the total crustal moment of inertia. (It is also possible that there are only two additional components and one of the three recoveries involves a separate frictional interaction with component 2.)

3.2.4 Physical interpretation of the spin-exchange model

The most popular microphysical interpretation of the spin exchange model (*e.g.*Alpar *et al.*1992) involves a crustal superfluid weakly coupled to the remainder of the star. (The core neutron superfluid is believed on theoretical grounds to be strongly coupled to the superconducting protons which in turn are argued to be coupled magnetically to the crust *e.g.*Sauls 1989). Now the velocity of a superfluid is proportional to the gradient of its Bose-condensed wave function and it is therefore curl-free. This means that the vorticity associated with the observed angular velocity has to be concentrated in a series of quantised vortex lines of normal fluid, each of which has carries a single quantum of vorticity of magnitude $h/2m_n$ so that the number of vortex lines per unit area is $n = 4m_n\Omega/h$ (*e.g.*Feynman 1972). The typical separation of vortex lines in the case of the Vela pulsar is $\sim n^{-1/2} \sim 40\mu$. These vortex lines are believed to be be pinned onto lattice sites in the solid crust so that there has to be a potential flow of genuine superfluid around them. This flow exerts an outwardly directed Coriolis plus Magnus force acting on the vortex lines which, in turn acts upon the lattice of $f = -\rho_s(2\Omega + \xi) \times (\omega \times r)/n$ per unit length of vortex line, (where ρ_s is the superfluid density and ξ is the vorticity measured in the frame of the crust). This is equivalent to a force density acting upon the lattice of $F = -2\rho_s\ \Omega_2 \times (\omega \times r)$ averaging over many vortex lines if the fluid is uniformly rotating. However, the force is transmitted to the lattice primarily at lattice points where the stress can be far greater than the average value. When this stress becomes large enough, there is supposed to be a catastrophic failure and a large number of vortex lines move radially outward, despinning the superfluid and transferring angular momentum to the lattice.

There are various opinions concerning the strength of the pinning interaction and the nature of the failure. The interaction is variously characterized as essentially rigid (*e.g.*Ruderman 1993), of intermediate strength (*e.g.*Alpar *et al.*1993) and negligible (*e.g.*Jones 1991). (It is possible for each of these interpretations to be correct for some component of some pulsar.) Ruderman (1993) attributes glitches to mechanical failure of the solid crust when subjected to strains $\gtrsim 10^{-4}$. Following a glitch, the whole crust is forced bodily outward through $\delta r \sim R\Delta\Omega_2/\Omega \sim$ several meters, releasing a strain $\sim \delta r/R \sim 10^{-4}$, which will be re-established

in time for the next glitch. There must be a compensatory upwelling near the rotational poles and subduction near the equator. In the limiting case when the superfiuid spins down only at glitches, $f \sim 0.98$. although some apparent recovery associated with an increase in the moment of inertia of the crust as it is re-stressed is permitted. This model is consistent with the reported statistical rate of glitches in older pulsars.

Alpar *et al.*(1992) argue that that there is a catastrophic unpinning of vortex lines from the crust, again over a large area, so that the vortex lines move outward through the crust. The kinematic consequences are broadly similar to those in Ruderman's model. In between glitches, the vortex lines creep steadily through at least some of the crust in response to the applied stress rather like dislocations which can be trapped on impurities. This creep is associated with the partial recovery and will happen far more readily at higher temperatures. This is qualitatively consistent with the observation that younger and presumably hotter pulsars like the Crab pulsar exhibit smaller, fractional glitching activity and greater post-glitch recoveries. For older pulsars, like PSR 0355+54 (Lyne 1987) the recovery is quite small.

An additional complication is associated with the interior magnetic field, that is also quantised and whose dynamical evolution has proved to be no less controversial than that of the vorticity. Bhattacharya *et al.*(1992) have argued that magnetic and vortex lines cannot intercommute. If magnetic flux is rigidly pinned to the outer crust and if vortexfield crossing is strictly forbidden then this would also require that the core and crust be tightly coupled; otherwise the magnetic field strength in the core will double in a time $\sim \omega_+^{-1}$ s. In addition, the core magnetic field must be expelled as the crust decelerates. Alternatively, a weak resistance to flux - vortex line crossing could be responsible for dynamical relaxation.

3.2.5 Precession of pinned superfluid

I have reported a divergence of published opinion as to whether or not the vortex lines associated with a superfluid component are pinned to the crustal lattice. If the pinning interaction is ignorable, then the fluid will behave purely classically and the vorticity will be Lie-transported by the fluid in the normal manner familiar from geophysical applications. However, there is a relativistic complication in that the wave function is defined relative to locally non-rotating inertial reference frames and these are dragged differentially by the spinning crust, leading to considerable stretching of the vortex lines. I suspect that the end result will be to damp out all but the component of vorticity parallel to the crust spin axis on a relatively short timescale. This needs further study. Obviously, if the vortex lines are loosely pinned, then there will be strong dissipation of both the parallel and the perpendicular components of ω. Observationally this appears not to be the case.

However, if pinning is strong, the vorticity will be Lie-transported by the crust. For the moment, let us ignore all relativistic effects including the Lense-Thirring precession. If we transform into the frame of the crust which rotates which rotates with a uniform angular velocity Ω with respect to an inertial frame. Let the velocity of the superfluid in this frame be u(r) and the residual vorticity in this frame

(after subtracting off 2Ω from the vorticity measured in the inertial frame) be $\xi(r)$. The secondary flow can then be determined (under the Boussinesq approximation) by solving

$$\nabla \times u = \xi, \tag{29}$$
$$\nabla \cdot u = 0. \tag{29}$$

Now we can, in principle, solve the differential equation for the secondary flow u, given a particular vorticity source by introducing a vector potential w, where $u = \nabla \times w$ and a gauge condition $\nabla \cdot w = 0$, so that $\nabla^2 w = -\xi$. This could then be solved subject to boundary conditions such as vanishing of the radial velocity component on the spherical boundaries of the superfluid zone. It does not matter if ξ is not parallel to Ω. For the simple case of uniform rotation, $u = \xi \times r/2$. However, as we expect the vorticity to evolve in a quite irregular manner, the flow is likely to be more complicated. Given a stationary velocity field, we can then solve for the density variations. The normal equation of motion for fluid in a rotating frame must now be augmented with the force density that the lattice exerts on the fluid which cancels the Coriolis plus Magnus force and which allows the vorticity to be constant in the frame of the crust. This leaves

$$\nabla\left(P + \frac{1}{2}u^2\right) = g\left(\frac{\delta\rho}{\bar{\rho}}\right) \tag{30}$$

where g is the gravitational plus centrifugal acceleration and $\bar{\rho}\ \nabla P$ is the true pressure gradient minus $\bar{\rho}g$ (*e.g.*Hide 1978). By combining with the equation of state of the superfluid, it is possible to solve for the self-consistent density and pressure fluctuations in a given vorticity field. Finally, having derived this flow, it is principle possible to repeat the exercise of section 2 and obtain the slower, mutual, Lense-Thirring precession. I would make the conjecture that the precession angular frequency is most sensitive to the radial location of the superfluid and the overall stellar structure and relatively insensitive to the details of the vorticity distribution and consequently the estimates of section 2 will still be valid. However more detailed calculations are needed to study this. Furthermore, whatever the nature of the superfluid-crust coupling, and there are many intriguing possibilities including creep, electron scattering and Eckman pumping, (*e.g.*Bildsten & Epstein 1989, Epstein, Baym & Link 1993, Reisenegger 1993), I believe that it will diminish the perpendicular and parallel angular velocity differences from steady deceleration on similar timescales.

3.3 *The starquake model*

3.3.1 Dynamics

Now let us see if these glitches can be interpreted adopting the starquake model. As an abrupt spin up is observed, the crust must undergo the catastrophic change in its moment of inertia, $\Delta f = -f\Delta\Omega/\Omega$. Again, let us make a two component model (*cf.*Baym *et al.*1969). The post glitch relaxation will proceed according to Eq.(10), (11) but with different initial conditions. Adopting the same notation,

for the completely relaxed, simple two component model, we obtain

$$\Omega = \Omega_- + \Delta\Omega + \dot{\Omega}_e t - (1-f)\Delta\Omega\left(1 - e^{-\frac{t}{\tau}}\right) \tag{31}$$

$$\omega \simeq \omega_- - \Delta\Omega e^{-\frac{t}{\tau}}; \qquad t > 0 \tag{32}$$

where $\omega_+ = \omega_- = -\dot{\Omega}_- \tau/f$. We see immediately that, unlike with the completely relaxed, spin-exchange model, the frequency difference between the two components does not have to decrease through the glitch and the recovery is $Q = 1 - f$. Note also that the equilibrium frequency difference ω_+ is indeterminate. When the coupling is strong, $(\omega_+ < \Delta\Omega)$, the crust will spin faster than the superfluid temporarily when it is weak the lag can be quite large.

For an incompletely relaxed starquake, if we continue to adopt a linear coupling and denote the interglitch interval by Δt, then we see that the preglitch. Angular frequency lag will adjust to an average value

$$\omega_+ = \omega_- = \frac{-N\tau}{f} - \frac{\Delta\Omega}{e^{\frac{\Delta t}{\tau}} - 1} \tag{33}$$

In the limiting case, $\tau >> \Delta t$, the superfluid will be almost completely decoupled from the crust and will follow a quite independent history.

3.3.2 Application to the Vela pulsar

Let me repeat the exercise of tentatively applying this model to the eighth Vela glitch. Again, I consider two subcases. If I adopt = τ_3 = 96 d as the relaxation time and regard the longer timescale partial relaxation as a sort of crustal rebound, then the "crustal" fraction of the moment of inertia has to be $f \sim 0.98$. This requires the core to be tightly coupled to the crust, consistent with theoretical dogma. The pre-glitch angular frequency lag between the crust-core and what is presumably a crustal superfluid is $\omega_= - \Omega_- \tau_3 / f = 6 \times 10^{-4}$ rad s^{-1}. Furthermore, we can adapt the argument we have just given to consider the angular momentum budget over 20 yr to compare the initial spin with the final spin corrected by the angular momentum extracted electromagnetically to estimate that the permanent reduction in the crust-core moment of inertia is

$$\frac{\Delta f}{f} = -2.14 \times 10^{-5} \tag{34}$$

Assuming a partial recovery, I again adopt $\tau_2 \sim 4$ yr and $Q_2 \sim 0.41$ to deduce that $f \sim 0.6$ for the crust and $1 - f \sim 0.4$ for the superfluid. In addition, the pre-glitch angular velocity difference is now $\omega_- = 0.02$ rad s^{-1}, much larger than the observed frequency jumps.

Taking the long term view, I calculate the angular momentum just prior to the eighth glitch allowing for the angular velocity difference of the two components to be $S_7 = 7.096 \times 10^{44} I_{7,45}$g cm^2 s^{-1}. Just prior to the first glitch, it was $S_1 = 7.102 \times 10^{44} I_{1,45}$ g cm^2 s^{-1}. The rotational impulse will, again, be given by Eq.(21) and so, in this case, the fractional change in the crustal moment of inertia over the ~ 20 yr interval is

$$\frac{\Delta f}{f} = -2.4 \times 10^{-5} \tag{35}$$

similar to before. Therefore, in either case, the crustal moment of inertia appears to change at a fractional rate $\sim 10^{-6}$ per year. If this has happened for a time $\sim \Omega/3\dot{\Omega}$ then there must have been a total fractional reduction $\sim 10^{-2}$ in the crustal moment of inertia over the pulsar lifetime. The interpretation of the secondary jumps should be broadly similar to that described under the spin-exchange model.

3.3.3 Physical interpretation of the starquake model

It has long been appreciated that the frequency of giant glitches in the Vela pulsar precludes attributing the structural changes to intermittent relaxation of the rotational bulge as the star decelerates. This is because the moment of inertia of the crust of the rotational bulge can only diminish at a rate $f / f \sim R^3\Omega\dot{\Omega}/GM \sim -10^{-9}$ yr^{-1}, some three orders of magnitude smaller than required. On these grounds, the starquake interpretation has been generally rejected. However, this seems unwarranted as there are alternative explanations of mechanical disequilibrium. For example, we can suppose that there is a large magnetic field within the core. The composition of the inner crust remains a source of mystery (*e.g.*Baym 1993, Pethick & Ravenhall 1992), but the shear modulus there might be as large as $\sim 10^{32}$ dyne cm^{-2}. The yield strain is equally uncertain, but adopting a value of ~ 0.01, we find that an anisotropic magnetic stress below the neutron star surface of $\sim 10^{30}$ dyne cm^{-2} $\sim 10^{-4}$ of the total pressure and therefore able to support a non-axisymmetric mass distribution giving $\Delta f/f \sim 10^{-4}$, enough for ~ 100 Vela glitches. If the magnetic field changes its configuration very few hundred years, then starquakes large enough to sustain even Vela glitches might result.

An alternative appeal to our ignorance of the actual conditions within neutron star cores is to posit that they have solid phases which can crack, independent of magnetic and rotational stresses *cf.*Pines *et al.*1972).

4. Observability of Lense-Thirring Precession

The purpose of the foregoing analysis of glitches was to determine the conditions under which a significant component of spin might become misaligned with the total angular momentum and undergo Lense-Thirring precession. On *phenomenological* grounds, I have argued that if a pulsar like Vela glitches according to the spin-exchange model, then a completely relaxed recurrent glitching behaviour requires the superfluid to possess the major fraction of the moment of inertia of the star, but that if the glitches do not heal to give a constant lag, then as much as 98 percent (in the case of Vela) of the moment of inertia is associated with the core. On the starquake model, complete recovery suggests a superfluid moment of inertia ~ 2 percent of the total, whereas partial recovery is consistent with a more even partition of the mass between the two phases.

By comparison, *theory* asserts quite confidently that there should be distinct superfluids in the core and the crust and slightly more hesistantly that the core superfluid is strongly coupled to the crust. Both of these statements are in need of observational test and I would argue that observations of glitching pulsars, while naturally interpretable in these terms, do not yet provide such a test. Theory also goes on to speculate about the nature of vortex line pinning, unpinning,

and creeping and crust cracking but here the details remain controversial. The problems are genuinely hard and their laboratory analogues have proved difficult to analyse.

¿From a phenomenological perspective, all of these models allow the parallel component of angular velocity of the major superfluid components to be significantly different from that of the crust. On either the spin-exchange or the starquake model, I expect that the angular velocity jumps will in general not be parallel to the total angular momentum and that the linear, frictional coupling I have invoked will produce a torque that is antiparallel to the difference in the vector angular velocity just as effective in diminishing the perpendicular component of ω as the parallel component. (On theoretical grounds, I have speculated that the parallel component will dissipated very quickly if the vortex lines are unpinned.) Consequently, if glitches fully recover, the mean square precession angle for the crustal angular momentum can be estimated by $< \alpha^2 > \sim < (\Delta\Omega/\Omega)^2 >$, immediately after the glitch and this will diminish to zero on a timescale τ. Under these circumstances, Lense-Thirring precession will be extremely hard to observe.

However, when the glitches do not heal on the inter-glitch timescale, as the observations suggest may actually be the case, then α can build up. If it increases stochastically, then in a steady state.

$$< \alpha^2 >= R\tau \left\langle \left(\frac{\Delta\Omega}{\Omega} \right)^2 \right\rangle \tag{36}$$

where R is the glitch rate. Typically $10^{-5} \lesssim \alpha \lesssim 3 \times 10^{-4}$. However, glitching need not be stochastic. For example, under the starquake model, a large density anomaly might relax through a series of glitches that always displace the angular velocity away from J. In this case, even larger precessional angles might be possible. In the limiting case of complete decoupling, the precessional angle will reflect conditions soon after the birth of the star and is essentially inestimable.

How small a precessional angle are we likely to be able to observe? In the absence of a detailed theory of pulsar emission, it is not possible to answer this question. However, some indication is given by examining the average variation of the emission with longitude, the pulse profile. That such a profile exists and has long-term stability suggests very strongly that the permanent field geometry will also imprint itself on the latitudinal variation of the radio emission. If we just consider a pulsar precessing uniformly about J, and introduce Euler angles in the notation of Landau & Lifshitz (1969), then, to first order in α, we identify the observed angular frequency Ω with $\phi + \psi$ and the precessional frequency Ω_{LT} with ϕ. The observed pulsar latitude b and longitude l are then given by

$$b = b_0 + \alpha \sin \Omega_{LT} t \tag{37}$$

$$l = -\Omega t + \alpha \tan b_0 \cos \Omega_{LT} t \tag{38}$$

where b_0 is the mean latitude observed. Both are modulated at the precessional frequency.

Suppose that a single measurement of a pulse arrival time of a non-precessing pulsar can be made with a standard deviation of δt by recording pulses over a

single interval $\Delta t >> P$ and comparing with a mean pulse profile. (We assume that we know the pulsar period and its derivative.) Now, suppose that we seek a precessional modulation with an unknown but stable period in a frequency band of width $\sim 0.03\Omega$, corresponding to $7P \lesssim P_{\rm LT} \lesssim 8P$. We can search for $\sim 0.03\Omega\Delta t$ discrete precessional periods in a discrete block. Typically this might be several hundred to a thousand. As a consequence, we estimate that it will take at least a $\sim 10\sigma$ detection of any individual period for it to have any statistical significance. One reasonable way to proceed, at least conceptually, is to gate the observations with trial precessional periods and to seek differences in arrival time or pulse shape. I would guess that the accuracy with which we can measure pulse longitude is comparable to the accuracy with which we can measure latitude in a precessing pulsar. (This would be true, to give one simple example, if there were a single sharp pulse for which the rate of change of longitude with respect to latitude.) If, finally, we observe for an interval t so that we have $\sim (t / \Delta t)$ independent measurements of this period, we find that we should be able to measure a modulation with angular amplitude

$$\alpha \sim 10\Omega\delta t \left(\frac{\Delta t}{t}\right)^{\frac{1}{2}}. \tag{39}$$

For illustration purposes, let us again turn to the Vela pulsar (though this may be too young to be the most promising candidate for the reasons outlined above). McCulloch *et al.*(1990) used $\Delta t = 120$ s to obtain an accuracy $\delta t = 50\mu s$ at 950 MHz. Flanagan (1990) achieved $\delta t \sim 15\mu s$ using $\Delta t = 45$ s at 1.6 and 2.3 GHz. I therefore estimate that it should be possible to measure $\alpha \sim 3 \times 10^{-4}$ with ~ 10 d of accumulated data using McCulloch *et al.*'s equipment and an accuracy $a \sim 10^{-4}$ d observing with Flanagan's system for a comparable time. Obviously the period immediately following a giant glitch would be most propitious. Comparable time scales are predicted for some of the older pulsars which are well timed. Although the reliability of these estimates is probably not high, they probably do demonstrate that a scrutiny of pulsar records for periodic modulation may be worthwhile. If it is detected, and we develop confidence in the view that neutron stars have masses close to 1.4 $M_\odot$, then it will provide a unique, quantitative diagnostic of the structure of cold nuclear matter.

Acknowledgements

I am indebted to my collaborator Paolo Coppi for many discussions, to D. Pines for a helpful correspondence and to several colleagues at this meeting for constructive criticism. I thank G. Srinivasan and V. Radhakrishnan for their hospitality in Bangalore. I also thank I. Shapiro for hospitality at CFA where this research was begun and R. Fosbury and R. Giacconi for the same in Garching where it was completed. Finally, I acknowledge financial support under NSF grant AST 89-17765, 92-23370

References

Alpar, M. A., Chau, H. F., Cheng, K. S., Pines, D. 1993, *Astrophys, J.*, **409,** 345
Alpar, M. A., Pines, D., Cheng, K. S. 1990, *Nature*, **348,** 707
Baym, G. 1993, *Isolated Pulsars*, ed. K. A. Van Riper, R. Epstein & C. Ho, Cambridge: Cambridge University Press p. 1
Baym, G., Pethick, C., Pines, D., Ruderman, M. 1969, *Nature*, **224,** 872
Bildsten, L., Epstein, R. I. 1989, *Astrophys. J.*, **342,** 951
Cordes, J. M., Downes, G. S., Krause-Polstorff, J. 1988, *Astrophys. J.*, **330,** 847
Chau, H. F., McCulloch, P. M., Nandkumar, R., Pines, D. 1993, Astrophys. J., **413** L113
Epstein, R . , Baym, G., Link, B. 1993, *Isolated Pulsars*, ed. K. A. Riper, R. Epstein & C. Ho Cambridge: Cambridge University Press p. 10
Feynman, R. P. 1972, *Statistical Mechanics*, New York:Benjamin
Flanagan, C. S. 1990, *Nature*, **345,** 416
Hamilton, A. J. S., Sarazin, C. L. 1982, *Monthly Notices Roy. Astron. Soc.*, **198,** 59
Hide, R. 1978, *Rotating Flows in Geophysics*, ed. P. H. Roberts and A. M. Soward London: Academic Press p. 3
Jones, P. B. 1991, *Astrophys. J.*, **373,** 208
Lyne, A. G. 1987, *Nature*, **326,** 569
Lyne, A. G., Graham-Smith, F., Pritchard, R. S. 1992, *Nature*, **359,** 706
McCulloch, P. M., Hamilton, P. A,, McConnell, D., King, E. A. 1990, *Nature*, **346,** 822
Michel, F. C., Bland-Hawthorn, J., Lyne, A. G. 1990, *Monthly Notices Roy. Astron. Soc.*, **246,** 624
Pethick, C. J., Ravenhall, D. G. 1992, *Phil Trans. R. Soc. A.*, **341**, 17
Pines, D., Shaham, J., Ruderman, M. 1972, *Nature Phys. Sci.*, **237,** 83
Radhakrishnan, V., Manchester, R. N. 1969, *Nature*, **222**, 228
Reichley, P. E., Downs, P. S. 1969, *Nature*, **222**, 229
Reisenegger, A. 1993, *J Low Temp Phys*, **92,** 77
Ruderman, M. 1993, *Isolated Pulsars*, ed. K. A. Van Riper, R. Epstein & C. Ho Cambridge: Cambridge University Press p. 66
Sauls, J. A. 1989, *Timing Neutron Stars*, ed. H. Ogelman & E. P. J. van den Heuvel Dordrecht: Kluwer p. 457
Thorne, K. S., Price, R. M., MacDonald, D. 1986, *Black Holes- The Membrane Paradigm*, New Haven: Yale University Press

Diamond Jubilee Symposium on Pulsars
14–17 March 1994
Raman Research Institute, Bangalore

J. Astrophys. Astr. (1995) **16,** 207–216

Spin-Driven Changes in Neutron Star Magnetic Fields

Malvin Ruderman *Department of Physics, Columbia University, 538 West 120th Street, New York, NY 10027, USA.*

Abstract. Interactions among a neutron star's superfluid neutrons, superconducting protons, and solid crust cause predictable spin-down and spin-up driven crustal motion and magnetic field changes. Applications and unsolved problems are discussed for millisecond pulsar evolution and properties, glitches and post-glitch responses, and transcient gamma-ray emission.

1. Crust Motion and Magnetic Field Evolution

Several years ago Sauls (1989) and Srinivasan *et al.* (1990) noted that nuclear interactions between neutron superfluid vortex lines and proton superconductor magnetic flux tubes within a neutron star's core could give a coupling between the star's magnetic field and its spin ($\boldsymbol{\Omega}$). This argument was later strengthened by including the effect of a neutron vortex line's own strong magnetic field (Ruderman 1991a,b). The core flux is no longer quantized into flux tubes as it passes out of the star through the crust. (Crustal nuclei are themselves superconductors but because their radii are less than their magnetic penetration depth (London length) they are not very effective in channeling $\boldsymbol{B}$ through the crustal lattice.) The almost rigid strongly conducting stellar crust does not permit the exterior surface field to adjust to the core flux motion beneath it unless either the crust's yield strength is exceeded or the time scale for changes is so long that finite crust conductivity allows diffusion. The latter is probably unimportant in young (age $\lesssim 10^6$ years) neutron stars and perhaps in all. If we ignore it, the stress on the crust from the core's moving flux tubes (whose ends are anchored in the crust base) would continue to grow as the core vortex line-flux tube complex moves out (in) during spin-down (spin-up). Then either the crust stress will ultimately exceed the yield strength, or the core's vortex lines will be forced to cut through the core's flux tubes. Estimates of the crust's yield strength indicate that the former should preempt the latter: the crust breaks to allow those regions which carry most of the flux through it (polar caps) to follow the core flux tube motions below them. More weakly magnetized or unmagnetized crust regions would be forced to move in an opposite direction to give a compensating crustal backflow

if stratification suppresses crustal radial flow. Crustal stresses from the crust's own pinned neutron superfluid vortex lines (Alpar *et al.* 1984; Ruderman 1976; Anderson and Itoh 1975) can add to those from core flux tube pull to move crustal "plates" (Ruderman 1991a,b,c).

The surface fields of a spinning-up neutron star should then evolve as indicated in Figs. 1, 2 and 3. Corresponding changes in the neutron star's dipole moment are shown in Fig. 4. Comparisons between the descriptions of Figs. 1–4 and observations support the indicated evolution and the following details:

(a) In the early spinning-down segment $\overline{01}$ for a young radio pulsar, the dipole B of Fig. 2 can grow (Ruderman 1991b) so that the spin-down index $n(\dot{\Omega} \propto -\Omega^n)$ satisfies $2 \lesssim n \lesssim 3$. This indeed is the case for the young pulsars PSR 1509 (n = 2.8), PSR 0540 (n = 2), and the Crab (n = 2.5). The values of n should increase for older pulsars but not above about 5.

(b) In all cases of accretion induced spinup, $\overline{37}$, $\overline{46}$, $\overline{345}$, the polar caps get pushed to the spin axis. Consequently the small accretion heated polar caps, if visible, would not have their thermal X-ray emission eclipsed as the star spins. This is consistent with the failure of Ginga to observe spin modulation of X-rays in LMXB's (believed to contain strongly spun-up neutron stars).

(c) The "sunspot" configuration of Fig. 2 allows maximum spin-up since the magnetic dipole continues to decrease (as $\Omega^{-1/2}$) until the accretion spin-up line is reached. For near Eddington limit accretion, the spin-up P and dipole B are then just those of the fastest millisecond pulsars, e.g., PSR 1937.

(d) The remarkable radioemission properties of the fastest pulsars, PSR 1937, shown in Fig. 5 and PSR 1957, are precisely those expected from the limiting field configuration of Fig. 6 (Chen and Ruderman 1993). A crucial feature is gravitational bending of "core" emission beams through closed field line parts of the magnetosphere and the effect of the magnetosphere on the radio beams which pass through it.

(e) Accretion induced spin-up of neutron stars with Fig. 1, or with Fig. 3 type field geometry with small S_1 (evolution paths between $3 \rightarrow 7$ and the reversal $3 \rightarrow 2$ in Fig. 4), will lead to canonical large dipole moment pulsars with periods P ~ 0.1 – 1 s. That there is an even larger population of such spun-up stars than of millisecond pulsars is suggested by analysis of the genesis of the binaries PSR 1831–00 and PSR 1718–19 (van den Heuvel, these Proceedings).

All of the above comparisons with observations, especially (d), support confidence that the spin-up induced crust motion and magnetic field evolution of Figs. 1–4 are a generally correct description. Then it should be possible to use the model's predictions as a tool to discriminate between millisecond pulsars which have been spun-up and those which may have been born as millisecond pulsars. There seems to be no apparent reason for the magnetic field geometry of the latter to resemble any of the limiting ones of Figs. 1–3.

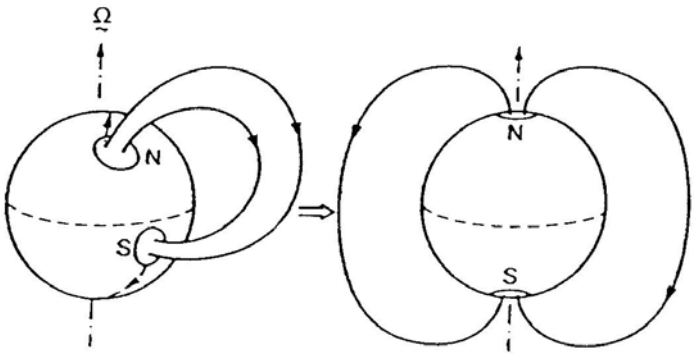

Figure 1: Evolution of the surface magnetic field of a spinning-up short-period neutron star when flux lines initially connect the two spin hemispheres.

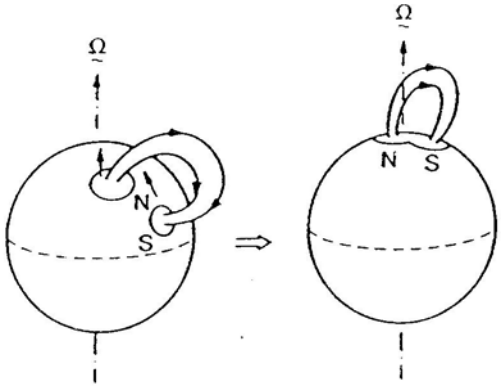

Figure 2: Evolution of the magnetic field of a spinning-up short-period neutron star when all flux leaving a hemisphere reenters the same hemisphere ("sunspot" configuration).

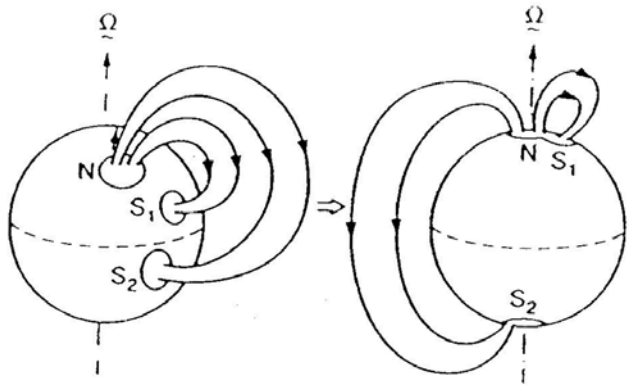

Figure 3: Evolution of the magnetic field of a spinning-up short-period neutron star with an initial flux configuration which is intermediate between that of Figs. 1 and 2.

2. Modelling the Radioemission Beam Geometry of Spun-Up Millisecond Pulsars

The fastest pulsar, PSR 1937, appears to be especially simple for two reasons: (a) its spun-up field geometry seems well described by Fig. 6; (b) the observed emission seems to have only "core components" whose source is close to the stellar surface (Rankin 1990). The absent "conal components" would have to be emitted from much further from the stellar surface, where they would not be gravitationally bent into a fan beam (Chen and Ruderman 1993) and thus might be more easily missed than the fan-beamed core component. A conal component would, however, be seen by an observer nearly perpendicular to the spin axis. Such a geometry is implied for PSR 1957 (P = 1.6 ms) by the observed eclipse by its secondary and for it a conal component is indeed also present (Fig. 7). For stronger field, longer period millisecond pulsars we expect the additional complication that these pulsars have been less spun-up because their field configurations resemble that of Fig. 3. The magnetic flux between N and S_2 gives a dipole moment component that cannot be diminished by further spin-up; this is why such a star reaches the accretion limit spin-up line with larger B and, thus, longer P than PSR 1937. The expected radioemission pulse geometry from a Fig. 3 configuration can be explored analytically for a two-dimensional model. When the dipole moment component parallel to $\boldsymbol{\Omega}(d_{||})$ is less than $2/\pi$ times $d_{\perp}$ (the perpendicular component), the two open field line bundles (which determine the radiation beaming) attach to the star as indicated in Fig. 8a. The field geometry is similar to that of Fig. 6, and two gravitationally bent core-emission fan beams can be formed as in that case.

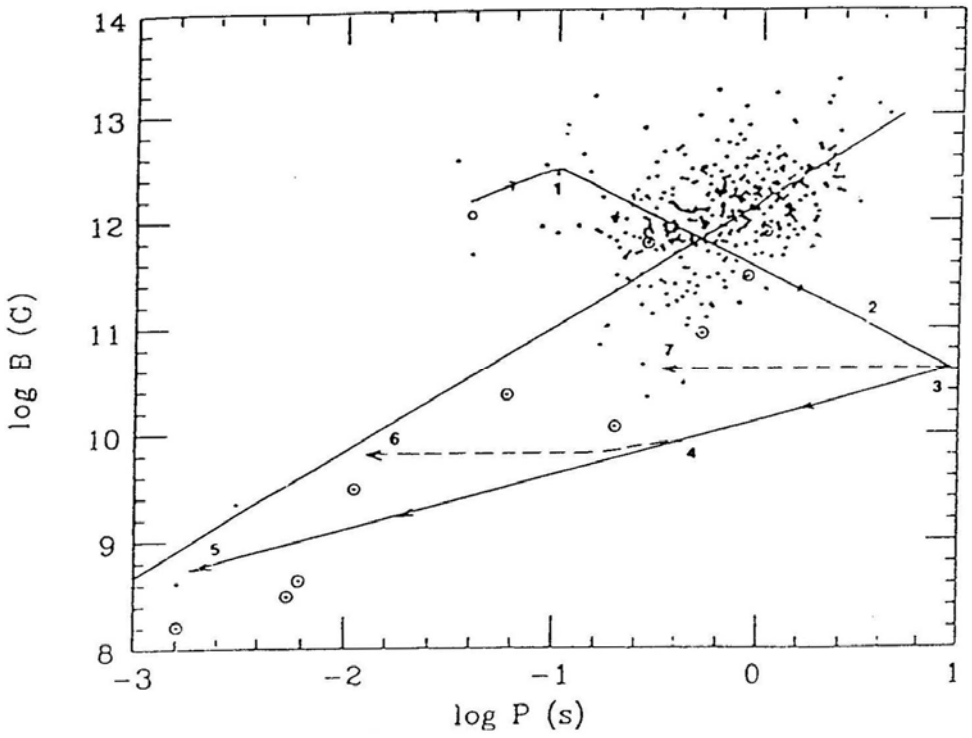

Figure 4: Evolution of dipole magnetic fields. Solitary radio pulsar spin-down would reach 2. Segment $\overline{12}$: $B \propto \Omega$ as crust plates move toward the equator where pole reconnection takes place. Some further spin-down to 3 is assumed if in an accreting binary. Spin-down below 3 would not be effective in reducing B, because the crust would no longer be stressed above its yield strength. Subsequent accretion induced spin-up would return the neutron star to 3, after which its evolution depends upon the magnetic field configuration. Segment $\overline{345}$ (solid line) is that for a sunspot-like configuration of Fig. 2. Segment $\overline{37}$ (dashed line) is that for a configuration of Fig. 1. Fig. 3 would give $\overline{346}$, intermediate between these two. The dots are for solitary radiopulsars; the circled dots are radiopulsars in binaries.

However, when $d_{||} \geq 2d_{\perp}/\pi$ the South pole open field line bundle jumps from S_1 to S_2 as in Fig. 8b. Gravitational bending of any core component emission would, if it exists, now give two fan beams with opposite polar angle spread. No one observer would any longer be likely to see two 180° separated core components with anything like comparable intensities. This qualitative conclusion seems robust enough to be valid in a three-dimensional model, but much needs to be explored quantitatively in three dimensions about the expected radioemission properties for field geometries like those of Fig. 3 which give less than the maximum millisecond pulsar spin-up.

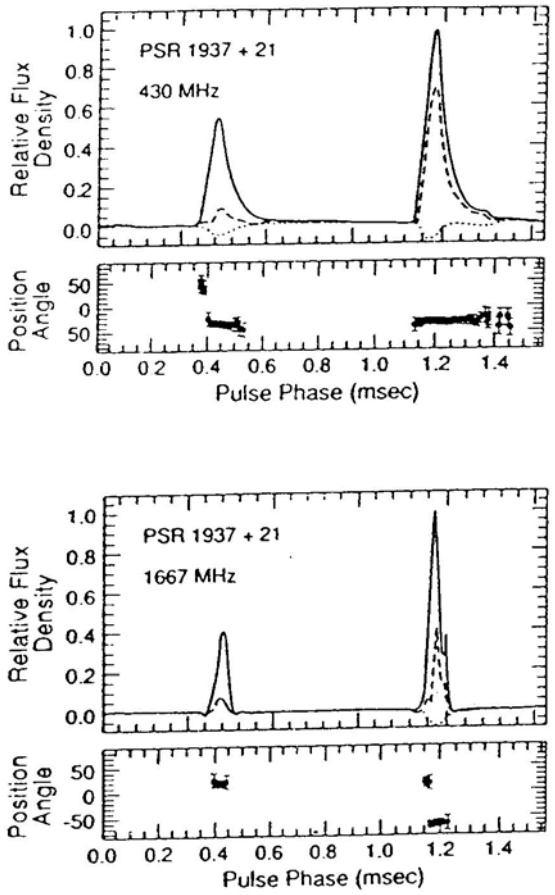

Figure 5: Pulse shape and polarization for PSR 1937+214 at 430 and 1667 MHz, respectively. The dashed line is the linearly polarized intensity; its position angle is shown below (Thorsett 1990).

3. Distinguishing Spun-Up Millisecond Pulsars from Pulsars Born with High Spin

As discussed above this now seems possible if the spin-period $P \sim 1.6$ ms as in PSRs 1937 and 1957, but not yet for significantly larger P. However, strongly spun-up pulsars would always have very small angular spread of open field lines at one of the poles (N in Figs. 8a, 8b) on the stellar surface, and further consequences of this should be explored. With a greater sample of pulsars with $P \lesssim 3$ ms (?) it may even now be possible to test whether globular cluster millisecond pulsars are spun-up by accretion (as seems confirmed for the disc population PSR 1937) or are born spinning rapidly (e.g., accretion induced collapse of White Dwarfs, fusion

of orbiting collapsed stars, capture of collapsed stars by Red Giant cores, etc.). Improved pulse shape resolution for globular cluster millisecond pulsars will be important. A first analysis for 47 Tuc, based upon poorly resolved data, suggested that the fastest of those globular cluster millisecond pulsars may indeed have been born with their fast spins (Chen and Ruderman 1993) but better time resolution is needed.

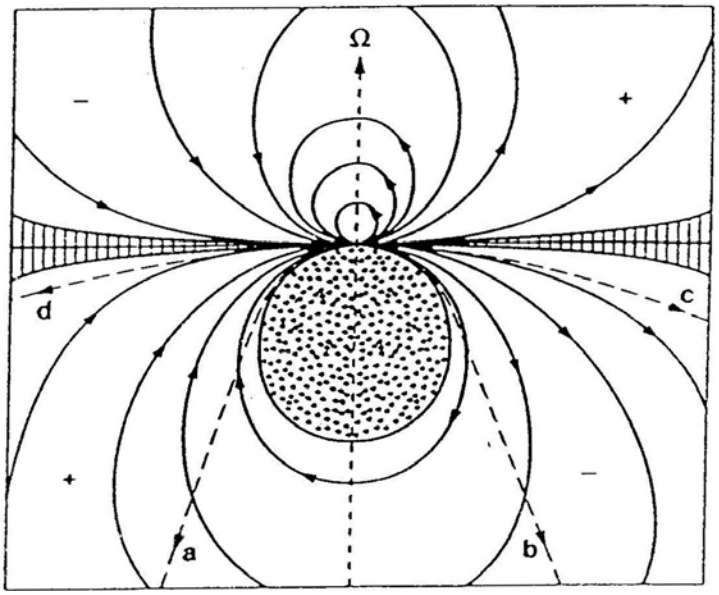

Figure 6: Magnetosphere of a strongly spun-up diamagnetic (because of core proton superconductivity) neutron star with the initial field geometry of Fig. 2 (from Chen and Ruderman 1993). One fan beam (cb) passes through electron filled magnetosphere, the other (da) through ions.

4. Magnetic Flux Tube Motion and Post-Glitch Responses in Neutron Star Cores

Much important microphysics on how vortex lines move flux tubes, under what circumstances they cut through them, moving flux tubes' drag, and just how the crust yields to flux tube stress, remain to be explored more quantitatively. Especially important is the flow of the core's electron plus superconducting-proton plasma through a moving flux tube array. This would be almost impossible if the protons were not superconducting. In that event the electron-proton plasma would move as if attached to the flux tubes just as a more conventional magnetic field distribution is frozen into an almost perfectly conducting classical fluid. However,

within the superconductor, the total (e + p) current density ($\boldsymbol{j}$) satisfies

$$4\pi \boldsymbol{j} = \Lambda^2 \nabla^2 \boldsymbol{j}_p,$$

where $\boldsymbol{j}_p$ is the proton superconductor's current and Λ is its London penetration length (c/plasma frequency). The screening current seems to allow flux tubes to move independently through e – p fluid (and possibly to bunch when pushed by neutron vortex lines). This is essential in understanding why the core's flux tubes move with its moving vortex lines rather than remaining immobile and being cut through by them. K.S. Cheng and M.R. have found that even the drag on a single moving flux tube is greatly reduced from previous estimates by this diamagnetic screening.

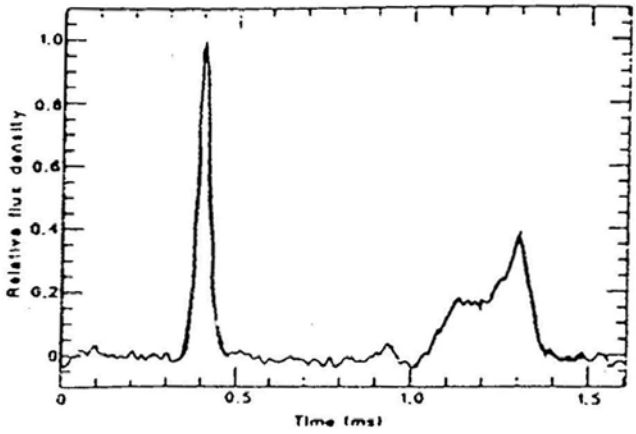

Figure 7: A pulse profile of PSR 1957+20.

Another important consequence of the flux tube – vortex line coupling is to the glitch and post-glitch response of a pulsar's core neutrons. Present models presume that all of a core's superfluid neutrons extremely rapidly adjust their rotation velocity to a suddenly changed one of core electrons and protons ($\lesssim 10^2$ s) (Alpar *et al.* 1984; Alpar *et al.* 1993). However, the neutron vortex – proton flux tube interaction could greatly affect this and it must be examined more closely and quantitatively. Preliminary theoretical estimates and observations both suggest a resulting "sluggishness" in neutron vortex response is observable in Crab glitches.

5. Crust Movement and Glitches

It has been argued (Ruderman 1991c; Ruderman 1976) that if spin-down induced crustal stresses are relieved by large scale crust cracking the resulting sudden jumps in pulsar spin-rate have a magnitude and repetition rate similar to those of the large glitches observed in the Vela family of radio pulsars (PSRs 0833, 1737, 1800, 1758, and 1823). Large crust cracking should also give a permanent change in magnetic dipole and thus part (of order 10^{-4}) of a glitch associated

$\Lambda\dot{\Omega}/\dot{\Omega}$ should not "heal". In addition to large glitches in the Vela-like family and some older pulsars there are very much smaller ones in the Crab pulsar, numerous microglitches in Vela, and timing "noise" quite generally. The glitch variety may, in part at least, be related to the complications of breaking phenomena in the highly structured neutron star crust. For example, the various crustal layers have lattices composed of different nuclei which may change rather discontinuously at layer boundaries. This would give rise to jumps there in lattice properties (and vortex pinning strengths) which complicate the description of how and where a lattice cracks. If slippage along layer boundaries is easier than other crustal breaks a variety of glitch responses may exist because sudden cracking can occur separately in layers with very different properties (e.g., the moment of inertia of the superfluid they contain). Crust cracking complexities, as well as temperature differences, may contribute to the variety of observed glitch-like changes in pulsar periods and period derivatives.

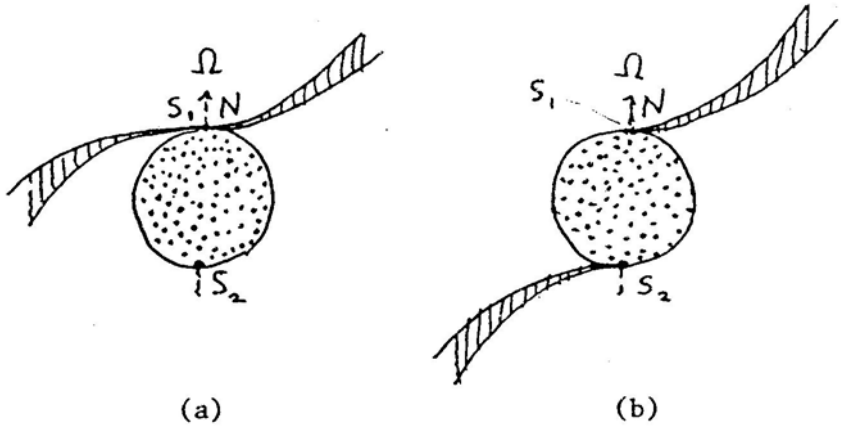

Figure 8: Open field line bundles for two-dimensional stars with Fig. 3 geometries. a) $d_\perp > (\pi/2)d_\parallel$, b) $d_\perp < (\pi/2)d_\parallel$.

6. Gamma-Ray Transients (Soft Gamma-Ray Repeaters)

One consequence of neutron vortex line – proton flux tube coupling is that extraordinarily large crust-cracking events (followed by a series of smaller ones) would be expected in a spinning-down neutron star whenever spin-down expels enough flux from the stellar core into the equatorial regions of the lower crust. Although this sort of event should occur less than once a millenium for a Vela-like pulsar, it should happen every few decades in a 10^4 year old pulsar with a magnetic field of several times 10^{14} G. Such a strongly magnetized pulsar, although still in an observable supernova remnant, would have spun-down to a 2 – 10 s period. The

possibility that Soft Gamma-Ray Repeaters are very strongly magnetized neutron stars has already been proposed by Duncan and Thompson (1992, 1993) and is being explored further by M.R. and M. Tavani. The energy release in the initial huge cracking event, powered by the sudden field reconnection, depends upon the yield strength of the crust. That from the "after-shocks" is of order the amount of elastic energy which can be stored in crustal strain and suddenly released. Theoretical estimates of both (10^{45} ergs and 10^{41} ergs respectively) give values very suggestive of those of the well known "March 5" gamma-ray burst and its series of after-bursts. The periodic modulation of its burst X-rays strongly supports an origin in a neutron star with an 8 sec. spin period. The apparent burst location in an LMC supernova remnant implies a burst energy above 10^{44} ergs, almost as great as the *total* spin energy of the star. However, the magnetic field energy within the stellar core (bunched into hugely magnetized quantized flux tubes) is about $B_{14}10^{47}$ ergs, enough for a neutron star with an external dipole field of $B \sim 3\cdot 10^{14}$ G to power several thousand such bursts and nearly a million of the much weaker "after-bursts". Thus the needed energy is available in such a star's magnetic field if there is a mechanism to push the field out of the star's superconducting core. Spin-down induced flux tube motion by moving neutron vortex lines may supply it.

References

Alpar, A., Anderson, P., Pines, D., Shaham, J., 1984, *Astrophys. J.*, **382,** 791.

Alpar, A., Chau, H., Cheng, K.S., Pines, D., 1993, *Astrophys. J.*, **409,** 345.

Anderson, P., Itoh, N., 1975 *Nature*, **256,** 25.

Chen, K., Ruderman, M., 1993, *Astrophys. J.*, **408,** 179.

Duncan, R., Thompson, C., 1993, "Astrophysics of Very Strongly Magnetized Neutron Stars: A Model for the Soft Gamma Repeaters", CITA preprint; 1992, *Astrophys. J.*, **392,** L9.

Rankin, J., 1990, *Astrophys. J.*, **352,** 247.

Ruderman, M., 1976 *Astrophys. J.*, **203,** 213.

Ruderman, M., 1991a, *Astrophys. J.*, **366,** 261.

Ruderman, M., 1991b, *Astrophys. J.,* **382,** 576.

Ruderman, M., 1991c, *Astrophys. J.*, **382,** 587.

Sauls, J., 1989, in *Timing Neutron Stars*, eds. H.Ögelman and E. J. P. van den Heuvel (Dordrecht: Kluwer).

Srinivasan, G., Bhattacharya, D., Muslimov, A., Tsygan, A. 1990, *Curr. Sci.* **59,** 31.

Thorsett, G., 1991, Ph.D. Thesis, Princeton University; see also Thorsett, G. and Stinebring, D. 1990, *Astrophys. J.*, **361,** 344.

van den Heuvel, E. P. J, (these Proceedings)

Diamond Jubilee Symposium on Pulsars
14–17 March 1994
Raman Research Institute, Bangalore

J. Astrophys. Astr. (1995) **16,** 217–232

The Evolution of the Magnetic Fields of Neutron Stars

Dipankar Bhattacharya *Raman Research Institute, Bangalore 560 080*

Abstract. Observational evidence, and theoretical models of the magnetic field evolution of neutron stars is discussed. Observational data indicates that the magnetic field of a neutron star decays significantly only if it has been a member of a close interacting binary. Theoretically, the magnetic field evolution has been related to the processing of a neutron star in a binary system through the spin evolution of the neutron star, and also through the accretion of matter on the neutron star surface. I describe two specific models, one in which magnetic flux is expelled from the superconducting core during spin-down, via a copuling between Abrikosov fluxoids and Onsager-Feynman vortices; and another in which the compression and heating of the stellar crust by the accreted mass drastically reduces the ohmic decay time scale of a magnetic field configuration confined entirely to the crust. General remarks about the behaviour of the crustal field under ohmic diffusion are also made.

Key words: Neutron Stars – Pulsara – Magnetic Field

1. Introduction

The evolution of the magnetic field influences practically all aspects of neutron star evolution, such as the active life times of radio pulsars and the distribution of their periods and luminosities, the rate of cooling of the star, spin-up and spin-down processes in accreting neutron stars and so on. In particular, the evolutionary link between young neutron stars similar to the majority of radio pulsars, and X-ray binaries and recycled binary pulsars is critically dependent on the magnetic field evolution.

Soon after the discovery of pulsars, Gunn and Ostriker (1970) suggested a very simple picture of the magnetic field evolution – an exponential decay with the time constant of a few million years, due to ohmic dissipation of currents in the stellar

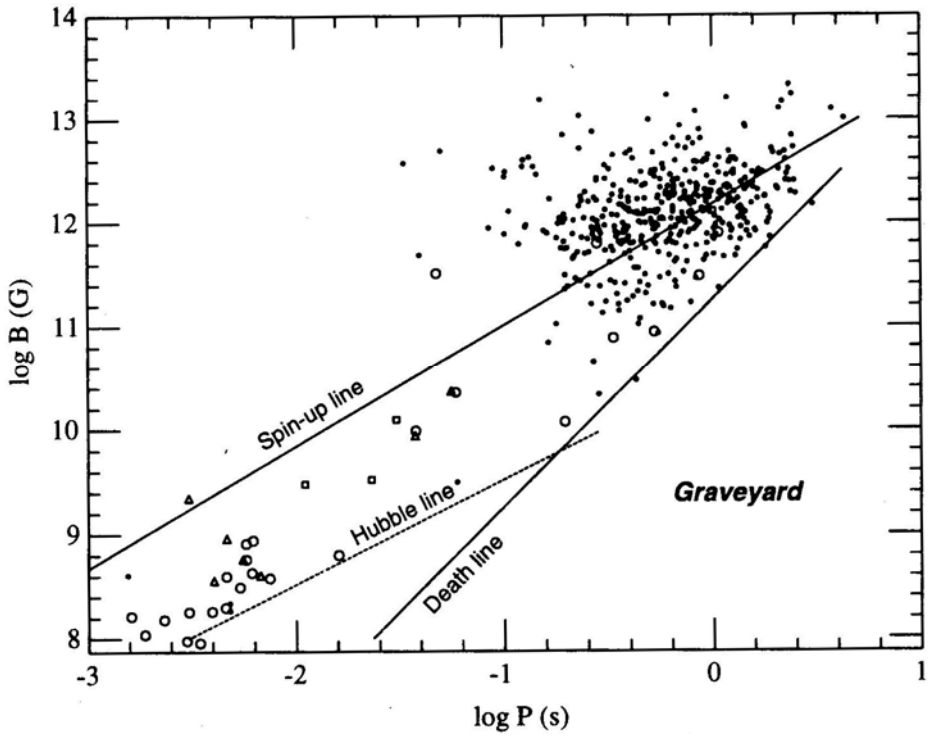

Figure 1: The magnetic fields and periods of known pulsars. Filled dots indicate isolated pulsars and open circles binaries, both in the galactic disk. Isolated pulsars in globular clusters are shown as triangles and binaries in globular clusters as squares. The spin-up line shows the minimum period to which a neutron star can be spun-up in an Eddington-limited accretion. Pulsar activity ceases to the right of the death line, and the spindown age of a pulsar equals 10^{10} yr on the Hubble line.

crust. Opinion has, however, substantially diverged from this view over the past decade with the accumulation of new observational data.

In this lecture I shall first briefly review the available facts on which the current picture of magnetic field evolution is based (section 2) and then describe a few theoretical models currently under development (sections 3 and 4).

2. Observational facts

Conclusions regarding the evolution of magnetic fields of neutron stars are based primarily on the following facts (see Bhattacharya 1994; Bhattacharya and Srinivasan 1995 for more detailed discussions):

- Most isolated pulsars have magnetic fields $B \sim 10^{12}$ G, with a dispersion of about an order of magnitude.

- Most pulsars in binaries have lower field strength, going down to $\sim 10^8$ G (see fig. 1).

- Recycled pulsars processed in low-mass binary systems (i.e. pulsars with low-mass white dwarf companions in circular orbits) have, in general, lower field strengths than those processed in massive binaries (i.e. those with heavy white dwarf or neutron star companions).

- Most pulsars in globular clusters have field strengths $\lesssim 10^{10}$ G.

- Massive X-ray binaries tend to have neutron stars with strong fields, in some cases cyclotron lines have been observed indicating local field strengths of order 10^{12} G.

- Low-mass X-ray binaries do not show X-ray pulsations, but exhibit thermonuclear bursts instead. This is attributed to low surface magnetic fields of the neutron stars in them.

- Several pulsars with white dwarf companions argue for a long-term stability of their fields at levels ranging from $\sim 10^8$ G to $\sim 10^{11}$ G.

One of the classical arguments for spontaneous decay of the magnetic fields of isolated pulsars, the so-called kinetic age–characteristic age relation (Lyne, Anderson and Salter 1982) has come under criticism of late, and it appears that given the uncertainties in the estimation of the kinetic age, and the selection effects involved in the detection of pulsars this relation is consistent with no decay of the magnetic fields of isolated pulsars (Bailes 1989, Lorimer 1994).

Statistical studies of the isolated pulsar population have often claimed the evidence of magnetic field decay in time scales of a few million years (see, e.g. Narayan and Ostriker 1990) . This has, however, not been an unanimous conclusion: several authors obtained results to the contrary (e.g. Krishnarnohan 1987, Srinivasan 1991, Michel 1992). The latest detailed studies in this regard appear to consistently argue that no appreciable magnetic field decay occurs during tha active life times of isolated radio pulsars (Bhattacharya et al 1992, Wakatsuki et al 1992, Lorimer 1994). Further, the "asymmetric drift" in the galactic plane displayed by pulsars (Phinney, this meeting) also argues for their magnetic fields being long-lived.

Two key points emerge from the above discussion: (*a*) that there is a large preponderance of binaries among low-field pulsars (fig. 1), and (*b*) that the magnetic fields of isolated pulsars, as well as those of binary pulsars well after recycling, appear to be long-lived and stable. These two points have been synthesised in a new hypothesis regarding the evolution of neutron star fields: that a significant field decay occurs only as a result of the interaction of the neutron star with its binary companion (Bailes 1989). This view is now rapidly gaining ground.

In the rest of this article I shall describe attempts to physically relate the evolution of the magnetic field with the interaction of the neutron star and a close binary companion.

3. Magnetic field in the neutron star interior

The neutron star is believed to consist of a core composed of superfluid neutrons and superconducting protons, covered by a crust of varying composition – the boundary between the two being at a density $\sim 2.4 \times 10^{14}$ g cm^{-3} (see e.g., Pines 1987). While the total stellar radius is ~ 10 km, the extent of crust is ~ 1 km.

While we know that a neutron star is strongly magnetized, we have little indication of where in the stellar interior this field may reside. In the literature, therefore, two classes of models are being considered — one in which the initial magnetic field is spread through the star more or less uniformly, and hence most of it penetrates the core region, while in the other the initial magnetic field is confined to the thin outer layers of the crust. The former is likely to be appropriate if the magnetic field is a fossil remnant of that in the neutron star progenitor, while the latter would be the case if the magnetic field is generated by processes such as thermomagnetic instabilities (Urpin and Yakovlev 1980; Blandford et al 1983) after the formation of the neutron star.

The structure of the interior field would be very different in these two cases. If the field penetrates the superconducting core, the field would be carried by Abrikosov fluxoids in the proton superconductor (see Sauls 1989 and Bhattacharya and Srinivasan 1995 for detailed reviews). These fluxoids have cores of size $\sim 10^{-12}$ cm consisting of normal proton fluid, through which the magnetic field passes. Outside the core superconducting currents screen out the field over the London length, $\sim 10^{-11}$cm. The field strength at the core of these fluxoids reach the lower critical field of the superconductor, $\sim 10^{15}$ G. The total number of such fluxoids in the core of the neutron star is $\sim 10^{31} B_{12}$, where B_{12} is the strength of the average magnetic field in units of 10^{12} G.

If the field is crustal, the accompanying currents are assumed to be wholly confined to the region where protons are in a normal state, and most of the initial field is considered to be anchored at densities below the neutron drip (see Blandford et al 1983, Romani 1990, Urpin and Muslimov 1992).

4. Models for magnetic field decay

Proposed physical models that relate the decay of the magnetic field of a neutron star with the evolution of the star in a binary systems can be broadly classified into two categories: one in which the field evolution is tied to the evolution of the spin of the neutron star and the, other in which the accreted mass causes a reduction in the field. In the former category fall models involving the interpinning of the Abrikosov fluxoids and the Onsager-Feynman vortices which carry the angular momentum of the neutron superfluid (Srinivasan et al 1990), and the models involving plate tectonics of the neutron star crust (Ruderman 1991). The latter category includes models involving screening of the neutron star field by the diamagnetic accreted plasma (Bisnovatyi-Kogan and Komberg 1974), an inverse thermoelectric battery (Blondin & Freese 1986), dragging and reconnection of the field by the incoming matter flow (Romani 1990), and enhanced ohmic decay due to the compression and heating of the crustal material as a result of mass accretion (Geppert and Urpin 1994, S. Konar and D. Bhattacharya, in preparation).

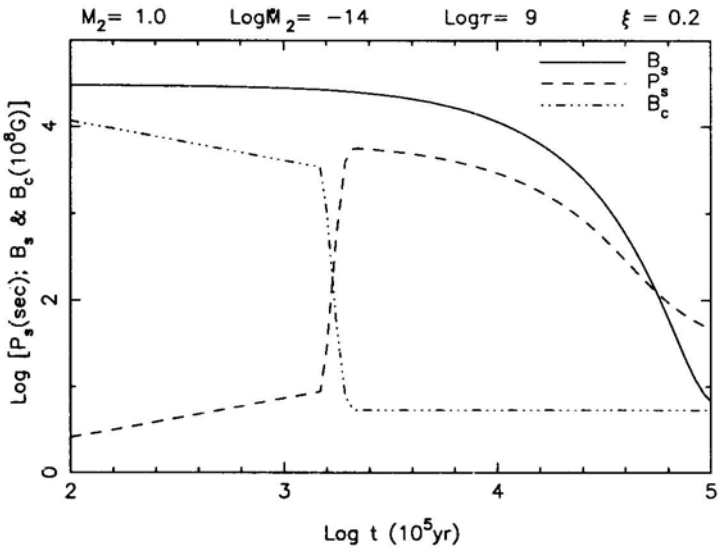

Figure 2: The evolution of the spin period P_s, core magnetic field B_c and surface field B_s of a neutron star in a low-mass binary, according to the spindown-induced flux expulsion scenario. M_2 is the secondary mass in solar masses, $\dot{M}_2$ is the wind rate of the secondary in $M_\odot$ /yr, τ is the ohmic decay time scale in the crust in yr and ξ is an efficiency factor that determines the degree of angular momentum transfer in the interaction between the wind matter and the neutron star magnetosphere. From Jahan Miri and Bhattacharya (1994).

In what follows I shall discuss only two of the above models, namely the decay of the core field due to vortex-fluxoid interpinning and the enhanced ohmic decay of crustal field due to accretion. The reader is referred to more extended reviews (e.g., Bhattacharya and Srinivasan 1995) for discussion on other models.

4.1 *Spindown-induced decay of the core magnetic field*

In this section we shall assume that the initial magnetic field of the neutron star passes through the superfluid-superconducting core and is carried by Abrikosov fluxoids in the proton superconductor. As mentioned above, in the core neutron superfluid and proton superconductor coexists, and the angular momentum of this superfluid is carried by quantized Onsager-Feynman vortices. It was pointed out by Sauls (1989) that a strong interpinning may exist between the vortices and the fluxoids due to many-body effects. In addition, there is also a strong magnetic interaction between the vortices and fluxoids (Ruderman 1991, Bhattacharya and Srinivasan 1991, Ding et al 1993). As the neutron star spins down, the vortices reduce in number by moving out, and in the process carry the fluxoids crustward. Once the field is deposited in the crust, it can undergo ohmic decay (Srinivasan et al 1990). As pointed out by Srinivasan et al (1990), a neutron star in a close binary system is spun down to a very long period (several hundred sec) in the wind-

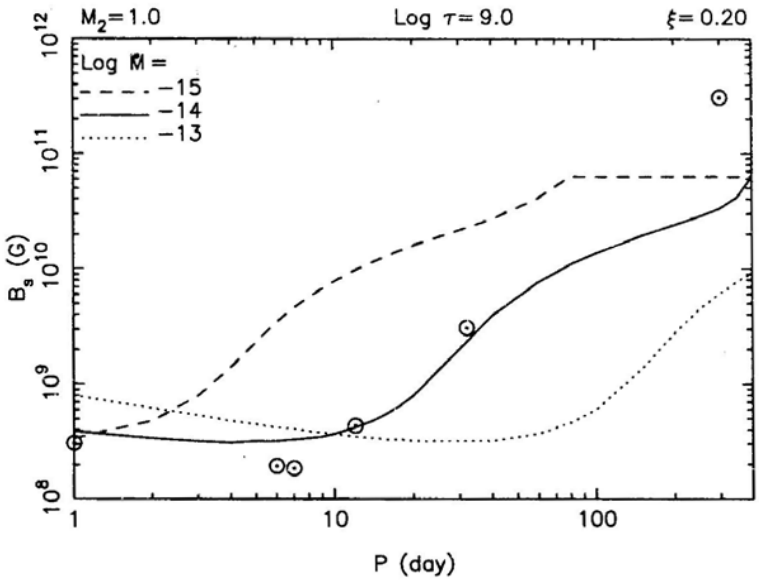

Figure 3: The final field strengths of the neutron stars in wide low-mass binaries as a function of the initial orbital period, according to the spindown-induced flux expulsion model. Results for three different mass loss rates of the secondary have been shown. The circles represent observed binary radio pulsars that are descendants of wide low-mass binaries, for which initial orbital periods can be estimated. See the caption of fig. 2 for explanation of legends. From Jahan Miri and Bhattacharya (1994).

interaction phase preceding the Roche Lobe overflow. Major flux expulsion from the superconducting interior takes place during this phase, and the expelled field eventually undergoes ohmic decay. It is to be noted that Ding et al (1993) obtained similar flux expulsion by dipole torques on isolated neutron stars, assuming the initial spin period of the neutron star to be $\lesssim 1$ ms. It is very doubtful, however, whether in the initial stages of the neutron star evolution, when the neutron star is very hot, the vortex-coupled flux movement can occur as effectively as Ding et al (1993) assume (Bhattacharya 1994). In addition, it is not at all clear whether many neutron stars are in fact born with such short spin periods. Indications to the contrary have been obtained in many statistical analyses (Vivekanand and Narayan 1983, Srinivasan et al 1984, Stokes et al 1986, Chevalier and Emmering 1986, Narayan 1987, Narayan and Ostriker 1990). In our view, field reduction by more than a factor of 5–10 can only be obtained by spindown due to interaction with a binary companion.

Spin-down to long periods due to interaction with the companion's stellar wind is indeed seen in massive X-ray binaries, where neutron star periods as long as 835 s have been observed (Nagase 1989). Since these objects show X-ray pulsations, it is clear, however, that their surface magnetic fields are not yet very low. This indicates that if spindown-induced flux expulsion is operative, then the field takes

a considerable time to decay after the expulsion. This is only to be expected, since the conductivity of the inner crust is likely to be rather large. On the other hand, the recycled pulsars with the lowest magnetic fields, namely the millisecond pulsars, are believed to have descended from low-mass X-ray binaries, systems in which the wind accretion phase has never been observed. Could neutron stars in LMXBs have spun down to sufficiently long periods to explain the present field strengths of millisecond pulsars?

To address this issue, Jahan Miri and Bhattacharya (1994) consider coupled spin and magnetic field evolution of neutron stars in wide low-mass binary systems for a variety of assumed ohmic decay time scales of the expelled flux. The evolutionary calculations pertain to the main sequence phase of the secondary, during which the binary is detached. The mass of the secondary is assumed to be $1M_{\odot}$, and its wind rate is assumed to lie between 10^{-16} to 10^{-13} $M_{\odot}$/yr. The neutron star goes through, successively, the dipole, ejector and accretor phases (Davis and Pringle 1981). In the dipole phase the wind matter is unable to penetrate the magnetosphere and the spin-down occurs as in an isolated neutron star. In the ejector phase the wind matter interacts with the magnetosphere of the neutron star, extracting angular momentum and causing rapid spin-down. This also causes most of the flux expulsion from the core. As this expelled flux undergoes ohmic dissipation, causing the surface magnetic field to drop, wind matter begins to accrete on the neutron star surface and causes a slow spin-up. Once the spin-down phase is over, no further magnetic flux is expelled, and since new vortices are now introduced into the core the remaining flux is trapped for ever.

Fig. 2 demonstrates the typical evolution of one such system: the evolution of the spin period P_s, core magnetic field B_c and the surface field B_a as a function of time are shown. From the model computations for many such systems with a wide variety of initial conditions, it is found that to obtain final field strengths as low as ~ 10^8 G, an ohmic decay time scale in the range $10^{8.5}$–$10^{9.5}$ yr is required. For such values of ohmic times, these computations also find a definite correlation between the initial orbital period of the system and the final long-lived component of the surface field, which follow a trend very similar to that observed (fig. 3).

This work also finds that the transport of flux across the crust-core boundary plays a significant role in determining the final surface field strengths of neutron stars. The results quoted in the previous paragraph correspond to the case when flux moves across the interface without any hindrance, i.e. the flux expulsion occurs instantaneously in response to an increase in the spin period. It has, however, been pointed out by Jones (1987) that once the flux density in the solid crust reaches a value close to the lower critical field of the proton superconductor, further transport of flux across the boundary may be hindered, and a layer of high fluxoid density may build up just below the border. From then on flux would be released into the crust in the same time scale in which flux transport occurs in the solid – by ohmic diffusion, Hall transport or plastic flow. If the time scale for flux release is assumed to be that of the ohmic diffusion in the crust, then to explain observations the required ohmic time scales would be an order of magnitude less than those obtained for free flux flow (Jahan Miri and Bhattacharya 1994).

Ohmic time scales of order 10^8–10^9 yr are, however, much shorter than that computed for pure matter in the inner crust (Sang and Chanmugam 1987). But

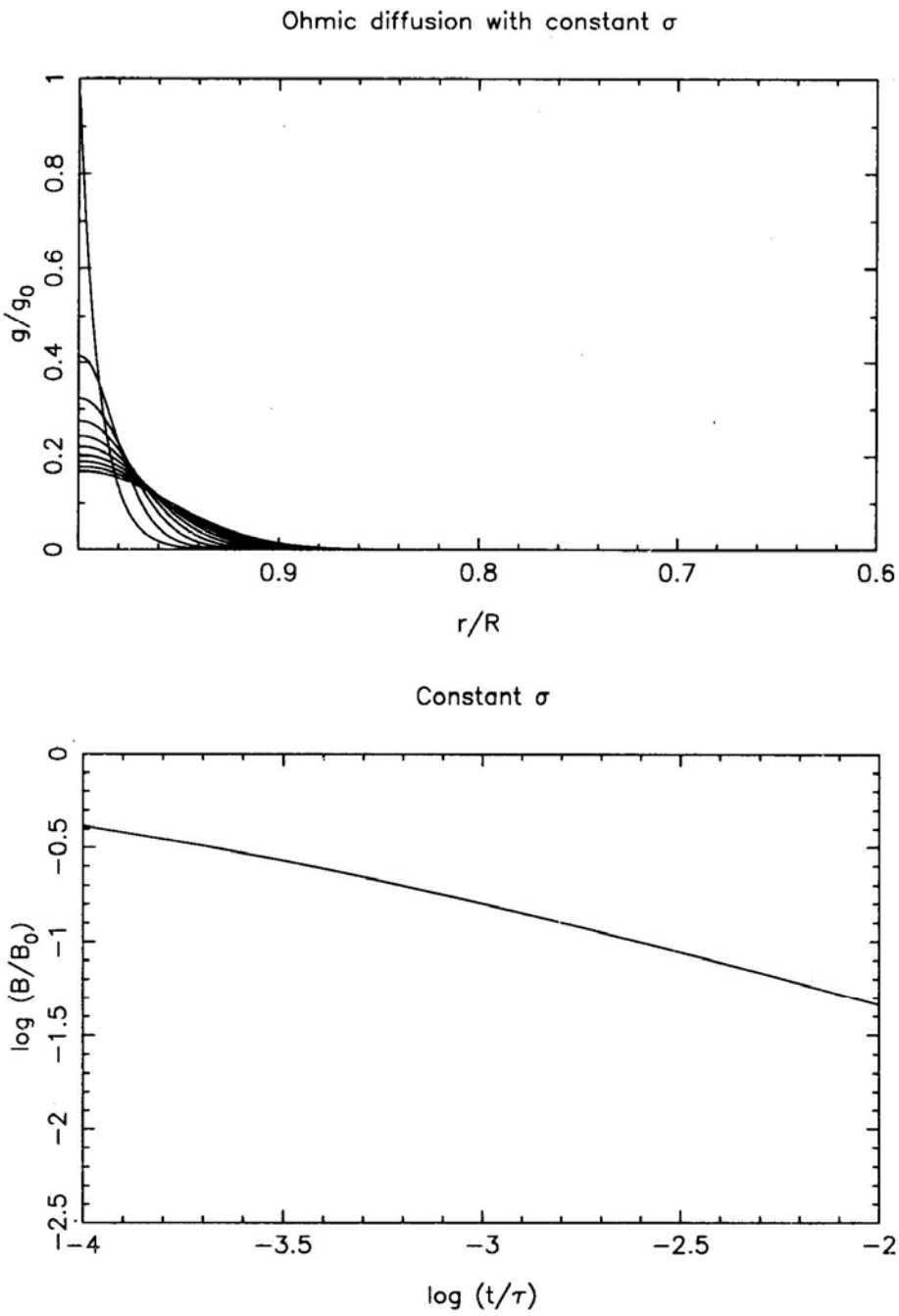

Figure 4: Ohmic diffusion of crustal magnetic field, assuming a constant electrical conductivity in the crust. The upper panel shows the evolution of the *g*-profile and the bottom panel the evolution of the field strength at the surface. See text for details.

it has been shown that even a small amount of impurities and dislocations can drastically reduce the ohmic time scale (Yakovlev and Urpin 1980, Urpin and Muslimov 1992). For the impurity parameter Q in the range 0.1–0.01 ($Q \equiv \{\Sigma_k\ n_k(Z - Z_k)^2\}/n_i$, where the dominant background ion species has density n_i and charge Z, and n_k, Z_k are the density and charge of the k-th interloper species), a range usually considered reasonable in the literature (e.g. Urpin and Muslimov 1992), computations show that the ohmic dissipation time of the expelled flux indeed lies in the range 10^8–10^9 yr (B. Datta and D. Bhattacharya, in preparation). Furthermore, the expelled field may undergo a turbulent cascade, reducing the scale length and hence the ohmic time (Goldreich and Reisenegger 1992).

4.2 *Ohmic evolution of crustal magnetic fields*

We shall now turn to the discussion of magnetic fields which are initially confined entirely to the crust. Most studies of this nature assume the initial field to be resident in the very outer layers of the crust, at densities below that of the neutron drip (i.e. 4×10^{11} g cm^{-3}) (cf. Urpin et al 1986). Ohmic evolution of this field is then computed as follows. The field is assumed to be dipolar, and to treat this a vector potential $\vec{A} = (0, 0, A_\phi)$ is introduced, with the form $A_\phi = g(r/R, t) \sin\theta/r$, where (r, θ, ϕ) are spherical polar coordinates with origin at the centre of the star, and R is the stellar radius. The field components can then be expressed in terms of the quantity $g(r/R, t)$ as

$$B_r = \frac{2g}{r^2}\cos\theta, \quad B_\theta = -\frac{\sin\theta}{r}\frac{\partial g}{\partial r}$$

The maximum field strength at the stellar surface is the polar value of B_r:

$$B_s(t) = 2g(1,t)/R^2$$

Using this description of the field, the equation for ohmic diffusion, namely,

$$\frac{\partial \vec{B}}{\partial t} = -\nabla \times \left(\frac{c^2}{4\pi\sigma}\nabla \times \vec{B}\right)$$

can be written as

$$\frac{\partial g}{\partial t} = \frac{c^2}{4\pi\sigma R^2}\left(\frac{\partial^2 g}{\partial x^2} - \frac{2g}{x^2}\right)$$

where $x = r/R$. In the above $\sigma(r, t)$)is the electrical conductivity. Following the ohmic evolution then just becomes a matter of solving the above one-dimensional second order partial differential equation, with the boundary conditions

$$\frac{\partial g}{\partial x} + g = 0 \quad \text{at } x = 1 \quad \text{(condition for dipole configuration)},$$

and

$g = 0$ at $x = x_c$, below which the field is assumed not to penetrate

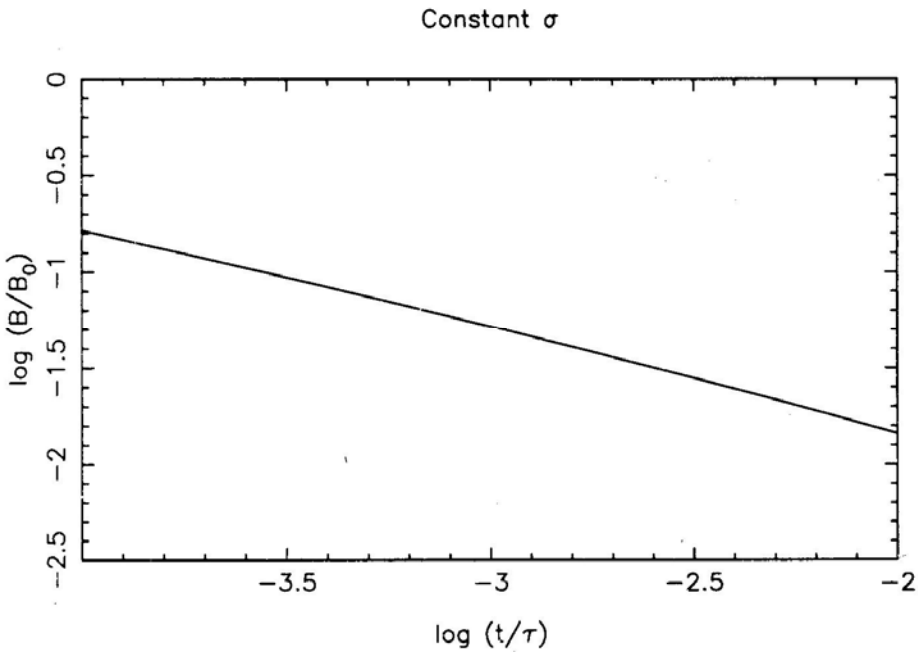

Figure 5; Evolution of the surface field strength if the initial g-distribution is assumed to be narrower by a factor of $\sqrt{10}$ compared to that in fig. 4.

(Wendell et al 1987, Sang and Chanmugam 1987, Urpin and Muslimov 1992). Two choices of x_c have been commonly used: zero, and that at the bottom of the crust. For fields initially confined to the outer crust, and a superconducting interior, the latter is possibly a better choice.

Clearly, two major parameters determine the ohmic evolution of the crustal field. One is the electrical conductivity, which is a function of the density, temperature and impurity concentration in the stellar interior, and since the stellar temperature is a function of time, the conductivity also acquires an implicit time dependence. The second is the scale length of the initial field distribution. The narrower the distribution, the faster is the decay.

In order to visualise the general trends in the basic evolution, we have constructed a series of evolutionary models with the electrical conductivity assumed to be *constant* from $x = x_c$ to $x = 1$, and infinite for $x < x_c$. The conductivity can then be absorbed into a time scale $\tau \equiv c^2/4\pi R^2\sigma$, all times be rescaled into those in units of τ, and computations restricted to $x > x_c$. Fig. 4 shows the evolution under such assumptions, with x_c (arbitrarily) set to 0.6. The initial g distribution is taken to be an exponential (the topmost curve in the upper panel) with a scale length $\Delta x = 0.01$. The top panel shows the evolution of the g-profile, in steps of 10^{-4} in t/τ, for the first 10 steps. The g-profile is seen to evolve towards wider and wider gaussians, a characteristic of the diffusion process. The bottom panel

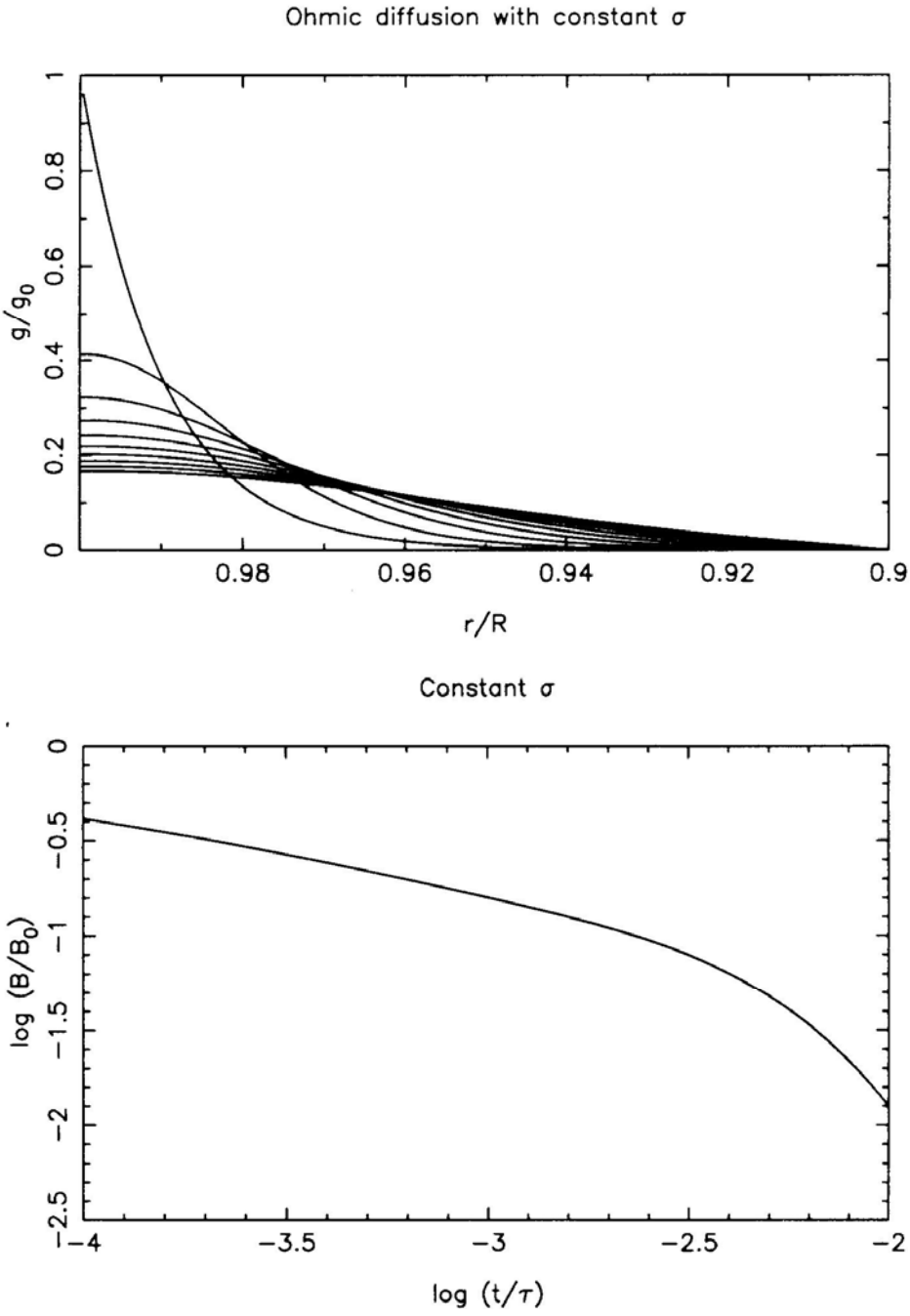

Figure 6: Same as fig. 4, but with the inner boundary set to 0.9*R* instead of 0.6*R*.

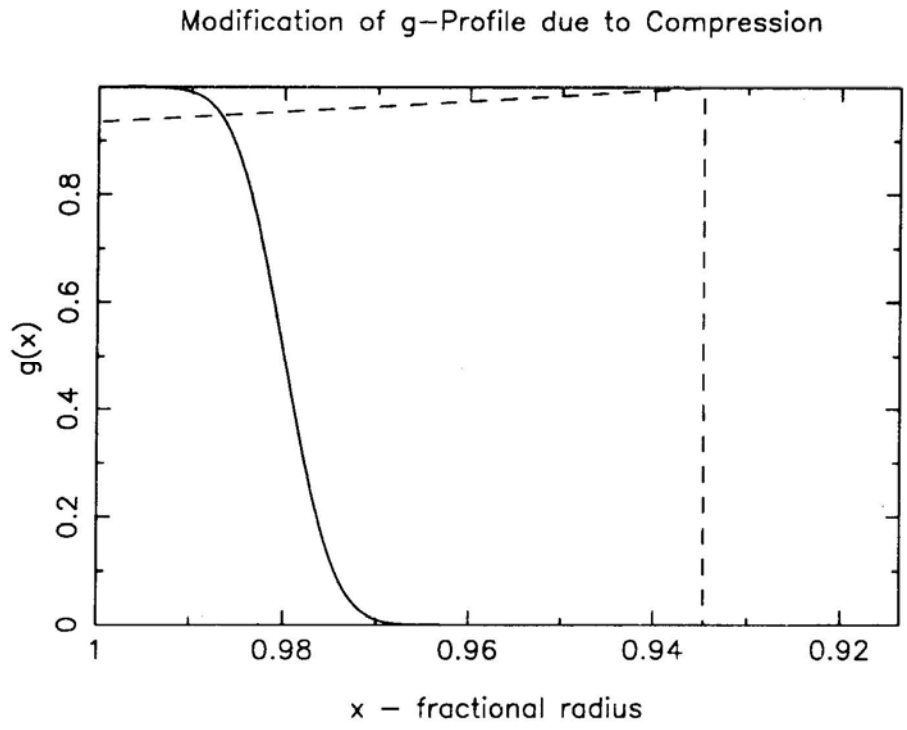

Figure 7: Modification of *g*-profile due to mass accretion on the surface of the neutron star. Solid line shows the initial profile, and the dashed line that after the accretion of $10^{-2}\,M_\odot$ of matter on a $1{\cdot}4M_\odot$ neutron star. No ohmic diffusion is assumed.

shows the evolution of the surface field strength. As can be seen, the evolution of the surface field strength is very close to a power law, a feature consistently obtained in late-time evolution of this kind of field in more realistic computations (e.g. Urpin and Muslimov 1992). In fig. 5 is shown a similar evolution, with all parameters other than the scale length of the original field kept the same as for fig. 4. The scale length has been reduced by a factor$\sqrt{10}$. The power-law nature of the evolution is seen again, but clearly the amount of decay at a given time is larger, by about the same factor by which the scale length has been reduced. Moreover, both in fig. 4 (bottom) and fig. 5 the power law index is close to –1/2, so the time required for the field to decay down to a given fraction of its original strength has been reduced by the square of the length scale reduction factor.

Why does the process of ohmic decay, which is commonly believed to behave exponentially, show a power-law behaviour in this case? It has been argued that the power-law arises due to the diffusion of the field into regions of higher conductivity (greater depth), which slows down the decay (Sang and Chanmugam 1987, Urpin and Muslimov 1992). The results presented above demonstrate that this is in fact not the major reason, for the power-law behaviour shows up even when the conductivity is assumed to be uniform. The real reason lies in the fact that

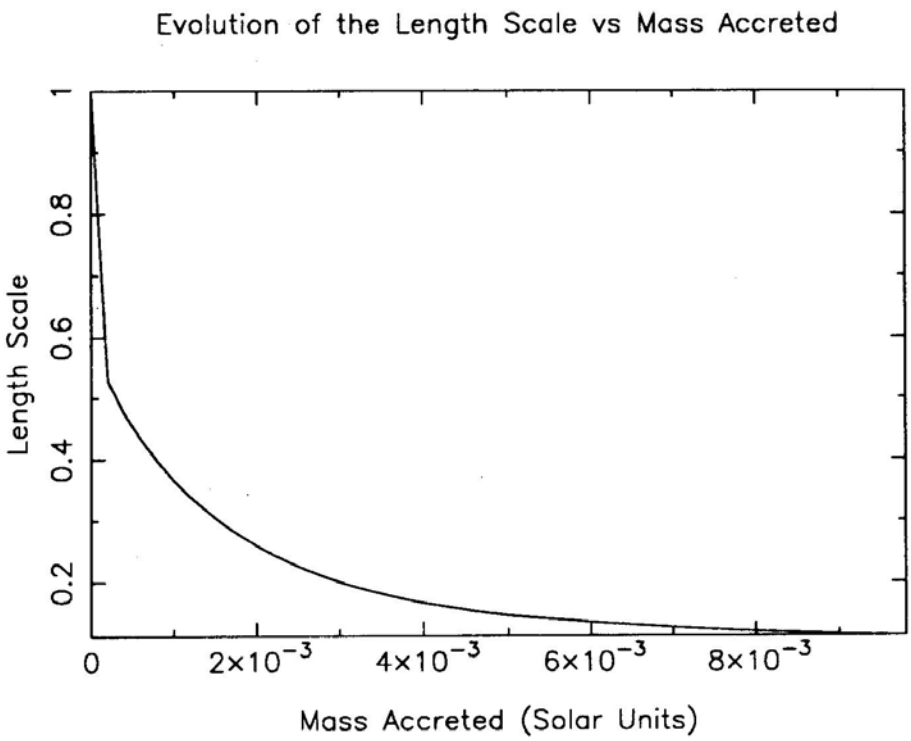

Figure 8: The evolution of the scale length of the *g*-distribution as a function of the accreted mass.

the original field occupies a very small fraction of the space in which it can later diffuse into. Described in fourier space, the original field distribution has a large amount of power in components of high order. Components of each order decay exponentially with a time scale appropriate for that order. Ohmic decay rate of the high-order components is much larger than that of components of lower order. As time progresses, the population of high-order components is depleted (the *g*-profile widening as a result), and the relevant decay time increases, resulting in a power-law behaviour. Once the field distribution occupies nearly all of the available space, the behaviour turns into an exponential, since no further reduction in the order number of the fourier components is possible. This transition can be easily seen in the evolution of an original *g*-distribution identical to that in fig. 4, but with $x_c = 0.9$, below which the field is now not allowed to diffuse. The evolution of the surface field strength in this case in shown in fig. 6, where the later part of the decay is very nearly an exponential.

The above discussion clearly demonstrates the very important role played by the scale length of the magnetic field distribution in determining the decay rate. It is to be noted at this point that mass accretion on the surface of the neutron star can drastically modify the scale length of the *g*-distribution. If the original profile is confined to the outer regions of the crust, the weight of the accreted matter

pushes this region into those of much higher density, compressing the whole layer in the process, the radial extent occupied by this slice of matter is thus enormously reduced, and so is the scale length of the *g*-distribution frozen into this. Fig. 7 compares the *g*-profile before (solid line) and after (dashed line) the accretion of $10^{-2}\ M_{\odot}$ on a neutron star of mass $1{\cdot}4M_{\odot}$ constructed with the equation of state of Wiringa, Fiks and Fabrocini (1988). It is clearly seen that the final profile is much sharper than the initial one. Fig. 8 shows the evolution of the scale length as a function of the mass accreted. No ohmic diffusion *during* the accretion process is assumed, and the accreted mass is assumed to settle uniformly over the neutron star surface. This huge compression in the length scale during accretion is likely to lead to a mass accretion-induced decay of the magnetic field, similar to the empirical suggestions by Taam and van den Heuvel (1986) and Shibazaki et al (1989). In reality the effect of compression will be reduced by the current distribution moving to regions of higher density and hence higher conductivity. However, the accretion process is also likely to raise the temperature of the crust and reduce the electrical conductivity as a result. Investigation of the evolution taking into account all these aspects is currently in progress (Geppert and Urpin 1994; S. Konar and D. Bha ttacharya, in preparation).

5. Summary

To summarize, it appears fr om recent observations and analyses of pulsar data that the decay of the magnetic field of a neutron star may be closely linked to the interaction of the star with a binary companion. Different physical models have been suggested for such evolution. If the original magnetic field resides in the core, the model of pinning between fluxoids in superconducting protons and vortices in the neutron superfluid predicts that during the interaction with the companion's stellar wind, the neutron star would spin down to long periods, expelling much of the core flux into the bottom of the crust. Good match with the observations can be obtained in this model if this expelled magnetic flux undergoes ohmic decay in a time scale of order 10^8–10^9 yr. Calculations of ohmic evolution of the expelled flux shows that time scales in this range can be easily obtained, for very reasonable impurity concentrations in the inner crust. On the other hand, if the original magnetic field resides entirely in the crust, and not decay appreciably in an isolated neutron star, then accretion of matter on the neutron star can vastly hasten the ohmic decay, due to the reduction of the scale length of the original field distribution caused by compression, and the reduction in conductivity resulting from heating. Other models of accretion-induced field reduction, involving inverse thermoelectric battery and reconnections caused by hydrodynamic flow, have also been suggested in the literature.

Acknowledgements

The work described above has been possible through collaborations and discussions with many of my colleagues. I thank them all, and in particular G. Srinivasan, Bhaskar Datta, M. Jahan Miri, Vadim Urpin and Sushan Konar. Thanks are due to Sushan Konar for providing figures 7 and 8 in advance of publication.

References

Bailes, M., 1989, *Astrophys. J.*, **342**, 917.

Bhattacharya, D., 1994, In Alpar, M. A. et al, editors, *Lives of the Neutron Stars*, Kluwer Academic Publishers, Dordrecht, in press.

Bhattacharya, D. and Srinivasan, G., 1991, In Ventura, J. and Pines, D., editors, *Neutron Stars: Theory and Observation*, page 219, Kluwer Academic Publishers, Dordrecht.

Bhattacharya, D. and Srinivasan, G., 1995, In W. H. G. Lewin, J. A. van Paradijs and E. P. J. van den Heuvel, editors, *X-ray Binaries*, Cambridge University Press, in press.

Bhattacharya, D., Wijers, R. A. M. J., Hartman, J. W., and Verbunt, F., 1992, *Astron. Astrophys.*, **254**, 198.

Bisnovatyi-Kogan, G. S. and Komberg, B. V., 1974, *Sov. Astr.*, **18**, 217.

Blandford, R. D., Applegate, J. H., and Hernquist, L., 1983, *Mon. Not. R. Astr. Soc.*, **204**, 1025.

Blondin, J. M. and Freese, K., 1986, *Nature*, **323**, 786.

Chevalier, R. and Emmering, R. T., 1986, *Astrophys. J.*, **304**, 140.

Davis, R. E. and Pringle, J. E., 1981, *Mon. Not. R. Astr. Soc.*, **196**, 209.

Ding, K. Y., Cheng, K. S., and Chau, H. F., 1993, *Astrophys. J.*, **408**, 167.

Geppert, U. and Urpin, V., 1994, *Mon. Not. R. Astr. Soc*, **271**, 490.

Goldreich, P. and Reisenegger, A., 1992, *Astrophys. J.*, **395**, 250.

Gunn, J. E. and Ostriker, J. P., 1970, *Astrophys. J.*, **160**, 979.

Jahan Miri, M. and Bhattacharya, D., 1994, *Mon. Not. R. Astr. Soc*, **269**, 455.

Jones, P. B., 1987, *Mon. Not. R. Astr. Soc.*, **228**, 513.

Krishnamohan, S., 1987, In Helfand, D. J. and Huang, J. H., editors, *IAU Symp 125: Origin and Evolution of Neutron Stars*, page 377, D. Reidel, Dordrecht.

Lorimer, D. R., 1994, *The Galactic Population of Millisecond and Normal Pulsars*, Ph. D. thesis, University of Manchester, U.K.

Lyne, A. G., Anderson, B., and Salter, M. J., 1982, *Mon. Not. R. Astr. Soc.*, **201,** 503.

Michel, F. C, 1992, In T. H. Hankins, J. M. Rankin and Gil, J. A., editors, *The Magnetospheric Structure and Emission Mechanisms of Radio Pulsars*, page 35, Pedagogical University Press, Zielona Góra, Poland.

Nagase, F., 1989, *Publ. Astr. Soc. Japan*, **41**, 1.

Narayan, R., 1987, *Astrophys. J.*, **319**, 162.

Narayan, R. and Ostriker, J. P., 1990, *Astrophys. J.*, **352**, 222.

Pines, D., 1987, In Pacini, F., editor, *High-Energy Phenomena around Collapsed Stars*, page 193, D. Reidel, Dordrecht.

Romani, R. W., 1990, *Nature*, **347**, 741.

Ruderman, M., 1991, *Astrophys. J.*, **366**, 261.

Sang, Y. and Chanmugam, G., 1987, *Astrophys.* J., **323**, L61.

Sauls, J., 1989, In Ögelman, H. and van den Heuvel, E. P. J., editors, *Timing Neutron Stars,* page 457, Kluwer, Dordrecht.

Shibazaki, N., Murakami, T., Shaham, J., and Nomoto, K., 1989, *Nature*, **342**, 656.

Srinivasan, G., 1991, *Ann. N. Y. Acad. Sci*., **647**, 538.

Srinivasan, G., Bhattacharya, D., and Dwarakanath, K. S., 1984, *J. Astrophys. Astron*., **5**, 403.

Srinivasan, G., Bhattacharya, D., Muslimov, A. G., and Tsygan, A. I., 1990, *Curr. Sci*., **59**, 31.

Stokes, G. H., Segelstein, D. J., Taylor, J. H., and Dewey, R. J., 1986, *Astrophys. J*., **311**, 694.

Taam, R. E. and van den Heuvel, E. P. J., 1986, *Astrophys. J*., **305**, 235

Urpin, V. A., Levshakov, S. A., and Yakovlev, D. G., 1986, *Mon. Not. R. Astr. Soc*., **219**, 703.

Urpin, V. A. and Muslimov, A. G, 1992, *Mon. Not R. Astr. Soc*, **256**, 261

Vivekanand, M. and Narayan, R., 1981, *J. Astrophys. Astron*., **2**, 315

Wakatsuki, S., Hikita, A., Sato N and Itoh, N., 1992, *Astrophys. J*., **392**, 628

Wendell, C.E., van Horn, H. M., and Sargent, D., 1983, *Astrophys. J*., **270**, 678.

Wiringa, R. B., Fiks, V., and Fabrocini, A., 1988, *Phys. Rev*., **C38**, 1010.

Yakovlev, D. G. and Urpin, V., 1980, *Sov. Astr*., **24**,303.

Diamond Jubilee Symposium on Pulsars
14–17 March 1994
Raman Research Institute, Bangalore

J. Astrophys. Astr. (1995) **16,** 233–244

The Population of Binary and Millisecond Pulsars

R. N. Manchester *Australia Telescope National Facility, CSIRO, P. O. Box 76, Epping NSW 2121, Australia.*

Abstract. Recent searches for millisecond and binary pulsars are reviewed, with particular emphasis on the nearly complete Parkes southern survey. Correlations between several of the major parameters of these systems are discussed.

1. Introduction

One of the most exciting developments in astronomy in recent years has been the discovery of binary and millisecond pulsars. The first binary pulsar discovered was the famous double-neutron-star system, PSR B1913+16, found by Hulse & Taylor (1975) at Arecibo. The first millisecond pulsar, PSR B1937+21, with its spin period of 1.55 ms, still the fastest known pulsar, was discovered by Backer et al. (1982), also at Arecibo. There are now a total of 39 binary pulsars and 45 millisecond pulsars (defined to be those with period less than 25 ms) known. Of these, 27 have both a millisecond period and a binary companion, so the connection between the two classes is very close. It is generally believed that millisecond pulsars acquire their very short periods by accreting mass and angular momentum from a binary companion; see Bhattacharya & van den Heuvel (1991) for a review. The cores of dense globular clusters are a favourable environment for formation of such binary systems, and just over half of the known millisecond pulsars, 24 to be exact, are found within globular clusters.

These pulsars have proven to be a rich harvest. They provide much information on the formation and evolution of binary systems and especially binary X-ray sources, the evolution of globular cluster systems and the internal structure of neutron stars. The extraordinary stability of pulsar periods, especially in these millisecond pulsars, has made possible a wide range of significant studies. Most prominent are the verification of Einstein's general relativity and the associated detection of the effects of gravitational radiation in the PSR B1913+16 and similar systems by Taylor and his co-workers (Taylor & Weisberg 1989; Taylor et al. 1992). Another important result is the first detection of an extra-solar planetary system (Wolszczan & Frail 1992; Wolszczan 1994). Studies of millisecond pulsars have the potential to establish a long-term standard for terrestrial time, to improve

our knowledge of solar-system dynamics and to detect a primordial background of gravitational radiation.

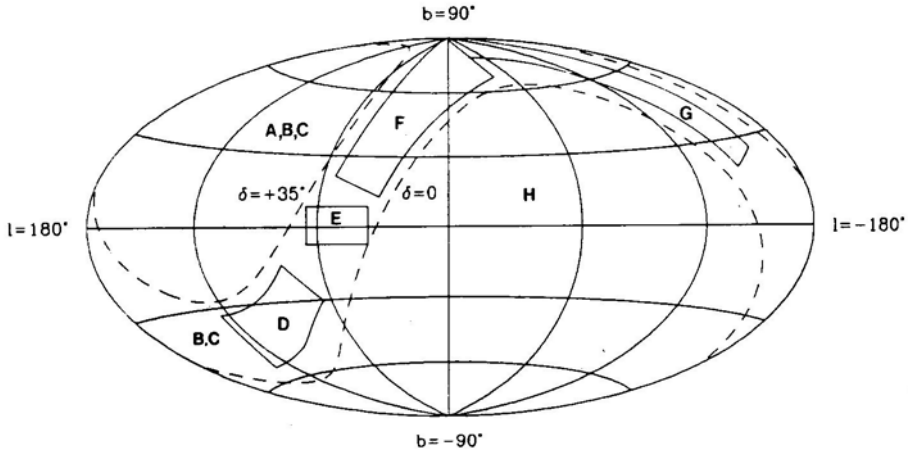

Figure 1: Sky coverage of the principal surveys sensitive to millisecond pulsars in Galactic coordinates. The dashed lines at declinations 0 and +35° delineate the approximate boundaries of the region visible to the Arecibo telescope.

2. Searches

To achieve these aims and make further progress on other studies we require a large sample of millisecond and binary pulsars which are well distributed across the celestial sphere. Over the past few years a number of very successful pulsar searches have been carried out. All of these searches have been at radio wavelengths and, since millisecond pulsars are relatively weak sources, have used large instruments, particularly the Arecibo and Parkes radio telescopes. The searches are of two types: those directed at globular clusters and those covering large areas of sky, searching for pulsars in the Galactic disc. Figure 1 shows the sky coverage of the main large-area surveys currently under way or recently completed. All of these surveys use sampling intervals close to 0.3 ms, and so are sensitive to pulsars with periods of a few milliseconds or more. Codes for the different surveys marked in Figure 1 are as follows:

- A – Jodrell Bank northern survey, 408 MHz, $\delta > +35°$
- B – Princeton/NRAO Green Bank survey, 370 MHz, $\delta > 0°$
- C – Princeton Cambridge survey, 80 MHz, $\delta > 0°$
- D – Princeton Arecibo survey, 430 MHz

Table 1. Millisecond pulsars discovered in recent searches (except the Parkes southern survey)

PSR J	Pulse Period (ms)	Binary Period (d)	Min. Comp. Mass ($M_\odot$)	Survey	Ref.
0024−72N	3.05	–	–	–	1
0218+4232	2.32	2.03	0.16	–	2
0751+18	3.48	0.26	0.12	–	3
1015+53	5.26	0.60	0.11	A	4
1640+22	3.16	175	0.30	F	5
1713+0747	4.57	67.82	0.28	F	6
2019+2425	3.93	76.51	0.32	E	7
2229+2643	2.98	93.02	0.12	D	8
2317+1439	3.44	2.46	0.18	D	9
2322+2057	4.81	–	–	D	7

Refs. 1. Robinson et al. (Submitted to MNRAS, 1994) 2. Navarro (1994) 3. Lundgren et al. (1993), Lundgren (1994) 4. Lyne (Unpublished, 1994) 5. Wolszczan (Unpublished 1994) 6. Foster et al. (1993) 7. Nice et al. (1993) 8. Camilo (Unpublished, 1994) 9. Camilo et al. (1993)

- E – Princeton Arecibo low-latitude survey, 430 MHz
- F – Penn State/ NRL Arecibo survey, 430 MHz
- G – Caltech Arecibo survey, 430 MHz
- H – ATNF/Jodrell Bank/Bologna Parkes survey, 436 MHz, $\delta < 0°$

The Jodrell Bank northern survey, using the Lovell 76-m telescope, started about a year ago and, as shown in Table 1, has discovered one millisecond pulsar so far. Parameters of the survey are similar to those of the Parkes southern survey, with a limiting flux density of approximately 3 mJy at long periods. The Princeton group is undertaking two surveys covering the whole northern sky; both started about a year ago. The first uses the 43-m telescope at Green Bank, while the second uses the 80-MHz Cambridge array with a somewhat more sophisticated data analysis system than was used to find the original pulsars. So far these two surveys have yet to yield positive results. The sky visible to Arecibo has been divided into several sections, with different groups searching each section. Because of the huge collecting area of Arecibo, these searches have very good sensitivity, with a minimum detectable flux density of < 1 mJy, but they take a long time to cover a given area of sky because of the small beam area. They have been very successful, so far discovering six millisecond pulsars, as listed in Table 1.

Three pulsars in Table 1 were not discovered in large- area surveys. PSR J0024– 72N was discovered in our continuing observations of the globular cluster 47 Tucanae (cf. Manchester et al. 1991) and is the 11th pulsar known in the cluster. It is not a member of a binary system. PSR J0218+4232 was discovered by the Caltech, Leiden and Jodrell Bank groups, based on observations at Westerbork

at 327 and 1400 MHz which revealed a highly polarized and steep-spectrum point source. It is notable that this is only the third pulsar discovered in this way, despite several intensive searches following the discovery of the first millisecond pulsar, PSR B1937+21, by this method. (The second was the millisecond pulsar in M 28; Lyne et al. 1987) Finally, PSR J0751+18 was discovered at Arecibo in a search of error boxes of unidentified gamma-ray point sources from the EGRET survey. As with the other Arecibo searches, this search was at 430 MHz, but it was somewhat more sensitive with a limiting flux density of about 0.5 may. It now seems unlikely that this pulsar is associated with a gamma-ray source (D. J. Thompson, private communication).

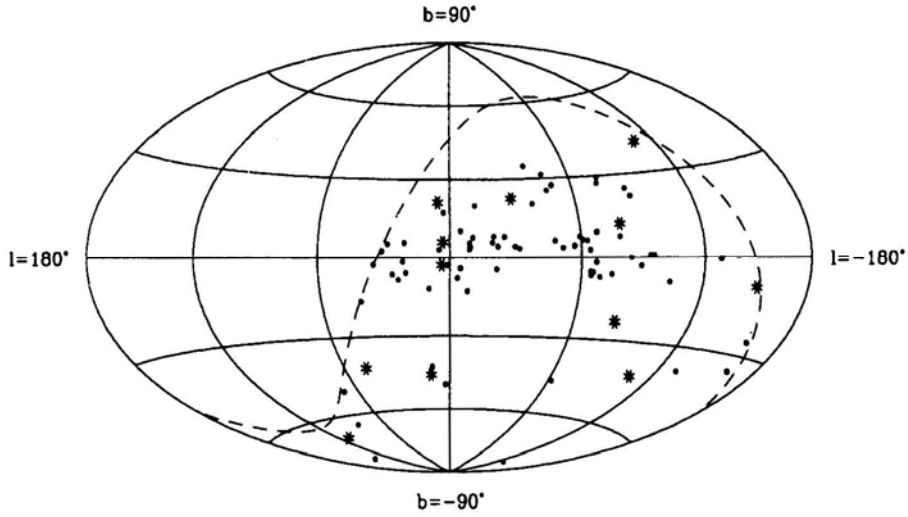

Figure 2: Positions in Galactic coordinates of pulsars discovered so far in the Parkes southern pulsar survey. The dashed line is declination 0^0, the northern limit of the survey. Millisecond pulsars are marked with an asterisk, others with a filled circle.

In May 1991, observations for a major survey of the southern sky for millisecond and low-luminosity pulsars began at the Parkes 64-m telescope. This survey is a collaboration between groups at the Australia Telescope National Facility, the University of Manchester, Jodrell Bank, and the Istituto di Radioastronomia del CNR, Bologna. The observing frequency is 436 MHz, and there are a total of 44,000 beam positions in the survey. Each point is observed for 2.5 minutes giving a limiting sensitivity of about 3 mJy. Currently, the survey is about 80% complete and a total of 12 millisecond pulsars and 82 ‘ordinary’ pulsars have been discovered. Table 2 lists the millisecond pulsars, showing that eight of the 12 are members of low-mass binary systems. Perhaps the most notable is PSR J0437–4715, which is by far the strongest and closest millisecond pulsar known. It has a white dwarf companion which has been optically identified and also an associated Hα bow-

shock nebula (Bell et al. 1993). One of the slower pulsars, PSR J0108–1431, is probably the closest known neutron star (Tauris et al. 1994).

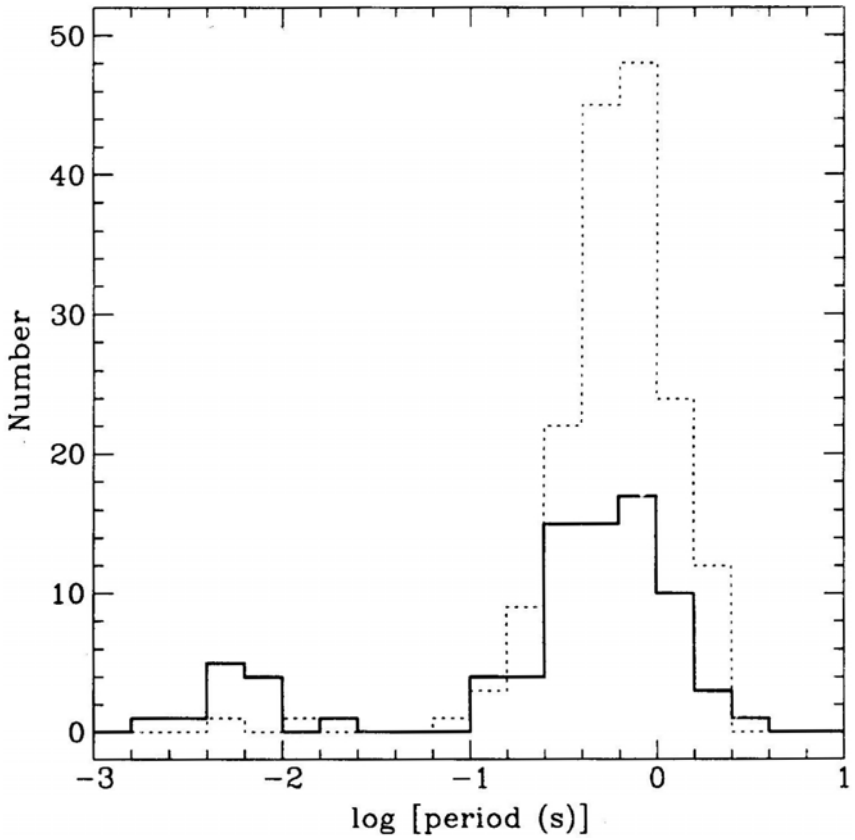

Figure 3: Period distribution for pulsars detected in the Parkes southern survey; thick line – new discoveries, dashed line – previously known pulsars.

The distribution on the sky of the pulsars discovered so far in the Parkes southern survey is shown in Figure 2. Ordinary pulsars are concentrated near the Galactic equator, but the distribution of the millisecond pulsars is essentially isotropic. Most are relatively close to the Sun, within 1 kpc. For both populations the Galactic *z*-distribution has a scale height of about 600 pc, although, especially for the millisecond pulsars, this is likely to be reduced by flux density selection.

Figure 3 shows the distribution in period of both the newly discovered pulsars and the previously known pulsars detected in the survey. This distribution is clearly bimodal. It is worth noting that the ratio of millisecond to ordinary pulsars is much greater for the new pulsars than for the old.

After considering the selection effects inherent in these surveys, Lorimer et al. (1994) estimate that there are at least 40,000 millisecond pulsars with radio luminosity greater than 2.5 mJy kpc^2 in the Galaxy. The known sample is therefore a very small part of the total.

Table 2. Millisecond Pulsars discovered in the parkes southern survey

PSR J	Pulse Period (ms)	Binary Period (d)	Min. Comp. Mass ($M_\odot$)	Ref.
0034−0534	1.88	1.58	0.14	1
0437−4715	5.75	5.74	0.14	2
0613−0200	3.06	1.20	0.13	3
0712−68	5.49	–	–	4
1025−07	5.16	–	–	4
1045−4509	7.47	4.1	0.16	1
1455−3330	7.97	78.1	0.26	3
1643−1224	4.62	149.3	0.12	3
1730−2304	8.12	–	–	3
1804−27	9.34	11.1	0.20	4
2124−33	4.93	–	–	4
2145−0750	16.05	6.83	0.43	1

Refs. 1. Bailes et al. (1994). 2. Johnston et al. (1993). 3. Lorimer et al. (1994) 4. Unpublished

Table 3. Globular cluster pulsars

Cluster	–	PSR B	Nr of Pulsars	Nr of MSPs	Nr of Binaries
M 28	–	1821−24	1	1	–
M 4	–	1620−26	1	1	1
M 15	–	2127+11	8	4	1
M 13	–	1639+36	2	2	1
M 53	–	1310+18	1	–	1
M 5	–	1516+02	2	2	1
47 Tuc	–	0021−72	11	11	4+
NGC 6440	–	1745−20	1	–	–
Terzan 5	–	1744−24	1	1	1
NGC 6624	–	1820−30	2	1	–
NGC 6539	–	1802−07	1	1	1
NGC 6760	–	1908+00	1	1	1
NGC 6342	–	1718−19	1	–	1

As mentioned in the Introduction, just over half of the known millisecond pulsars are found within globular clusters. Well over half of these are found in just

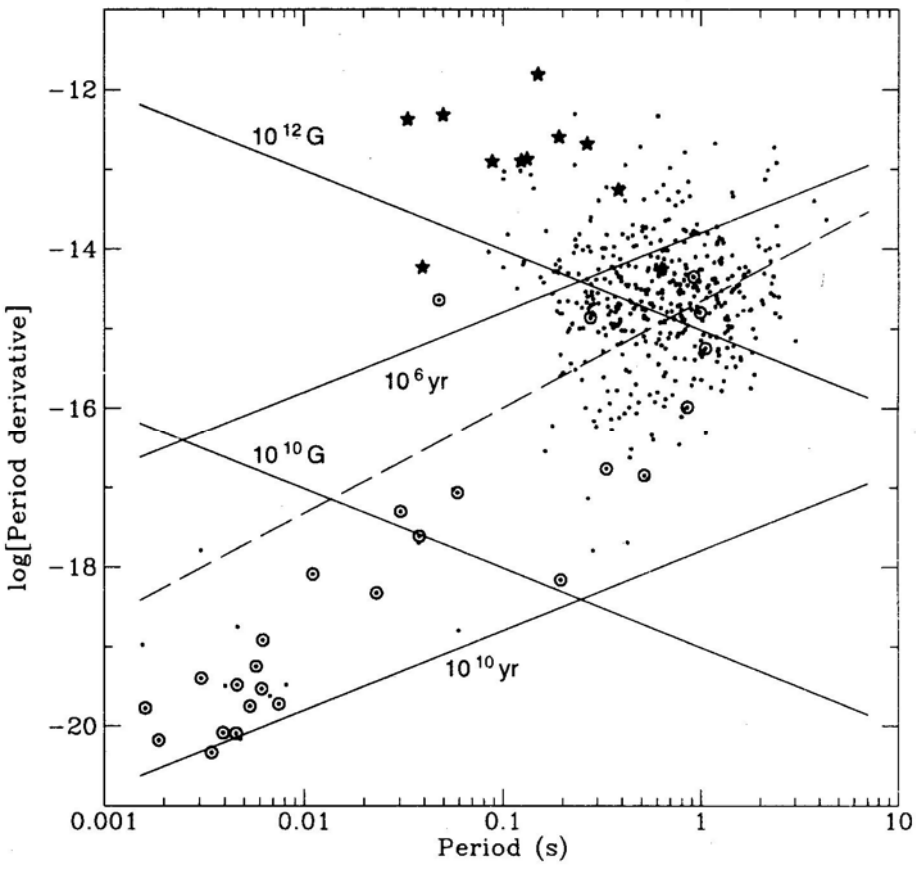

Figure 4: Plot of pulsar period derivative versus pulse period. Pulsars associated with supernova remnants are marked with a ⋆ and those which are members of a binary system are marked with an ⊙. Lines of constant surface magnetic field and constant characteristic age are marked. The dashed line is the so-called 'spin-up' line, which is the limiting period for pulsars being spun up by accretion from a binary companion.

two clusters, M 15 and 47 Tucanae. References to these discoveries are given in the Taylor et al. (1993) pulsar catalogue. Table 3 lists the known globular cluster pulsars, showing the number of millisecond and binary pulsars in each cluster. This table illustrates the fact that, although M 15 and 47 Tucanae are similar in harbouring a large number of detectable pulsars, the characteristics of these pulsars are quite different.

3. Properties

Millisecond pulsars are not only characterized by their short period. As shown in Figure 4, the rate at which this period is changing, the period derivative ($\dot{P}$), is typically five orders of magnitude smaller than that for ordinary pulsars. Since a pulsar's 'characteristic age', $\tau_c = P/(2\dot{P})$, is an upper limit to the true age, this implies that millisecond pulsars may be very old. Optical observations of white dwarf companions (Kulkarni 1986; Bell et al. 1993) confirm that at least some millisecond pulsars have ages in excess of 1 Gyr. The small period derivative also implies that the magnetic field at the surface of the neutron star, which is proportional to$(P\dot{P})^{1/2}$, is very small, typically 10^8 G compared to 10^{12} G for an ordinary pulsar.

The pulsars associated with supernova remnants are grouped in the top-left corner of the diagram and are therefore young. If they evolve with constant magnetic field (as is believed to be the case) they will move down to join the pulsar 'pool' centred at about $P = 0.6$ s and $\dot{P} = 10^{-15}$. The millisecond pulsars clearly do not form by simple ageing of young pulsars. Intervention by some agency is required to give them their short period (and probably also their weak magnetic field; Shibazaki et al. 1989). The fact that most of these pulsars are binary and also that almost all of them lie below and not too far from the spin-up line strongly suggests that they are spun up by accretion from a binary companion. It is notable that most of the millisecond pulsars with periods shorter than 10 ms lie closer to the 10^{10} yr line (also known as the Hubble line) than to the spin-up line. This suggests that they were born with spin periods not too different from those they presently have. This conclusion is reinforced by the fact that a significant fraction of the observed period derivative may be kinematic in origin (Camilo et al. 1994), making the pulsar characteristic ages even greater. The intermediate period pulsars (period between 10 and 100 ms) lie closer to the spin-up line. This group includes the neutron star – neutron star binaries such as PSR B1913+16, which have a lifetime limited by gravitational decay of their orbits.

Three binary pulsars lie above the spin-up line. Two of them (PSR B1259–63, $P = 47$ ms, $\dot{P} = 2.3 \times 15^{15}$, and PSR J0045–7319, $P = 926$ ms, $\dot{P} = 4.5 \times 10^{15}$) are in eccentric orbits with massive main-sequence companions (Johnston et al. 1994; Kaspi et al. 1994) and are almost certainly in a pre-spin-up phase. The other, PSR B1820–11 ($P = 279$ ms, $\dot{P} = 1.4 \times 10^{15}$) also has an eccentric orbit, but has a companion of lower mass (Lyne & McKenna 1989). The nature of the companion and the evolutionary history of the system are unclear.

Figure 5 shows binary period versus pulsar period for all known binary pulsars with established orbital parameters; this figure is analogous to that plotted by Corbet (1984) for X-ray binary pulsars. Several different groupings of pulsars are apparent in this diagram. Those with elliptical orbits tend to have longer pulse periods but cover a wide range of orbital period. The existence of an elliptical orbit implies substantial mass loss and/or a kick to the neutron star at birth and also the absence of an orbit circularization phase in subsequent evolution. Systems with neutron-star companions are quite tightly bunched at low orbital periods – they have evolved from high-mass binary systems and their evolution is reasonably well understood (Bhattacharya & van den Heuvel 1991). The two systems with

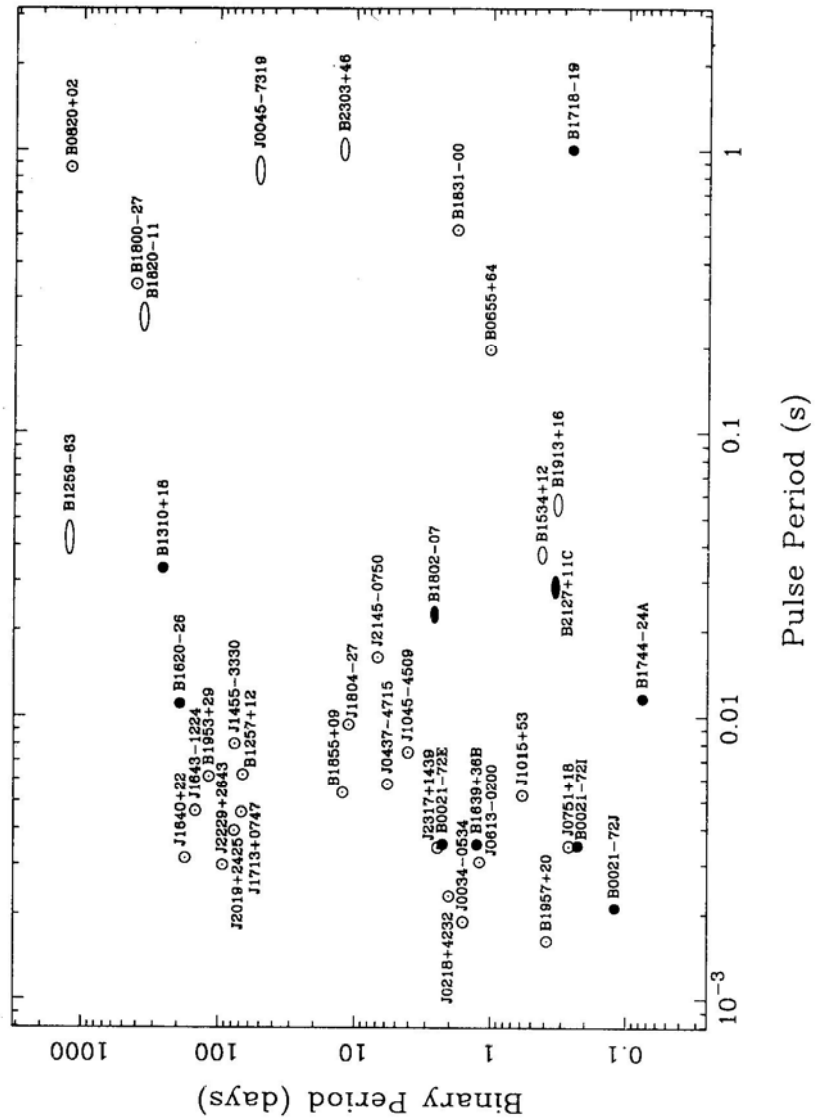

Figure 5: Plot of binary period versus pulsar period for all known binary sytems. Systems with near-circular orbits ($e < 0.05$) are plotted with a circle and those with more elliptical orbits are represented by an ellipse of the appropriate eccentricity. For systems associated with a globular cluster, the symbol is filled.

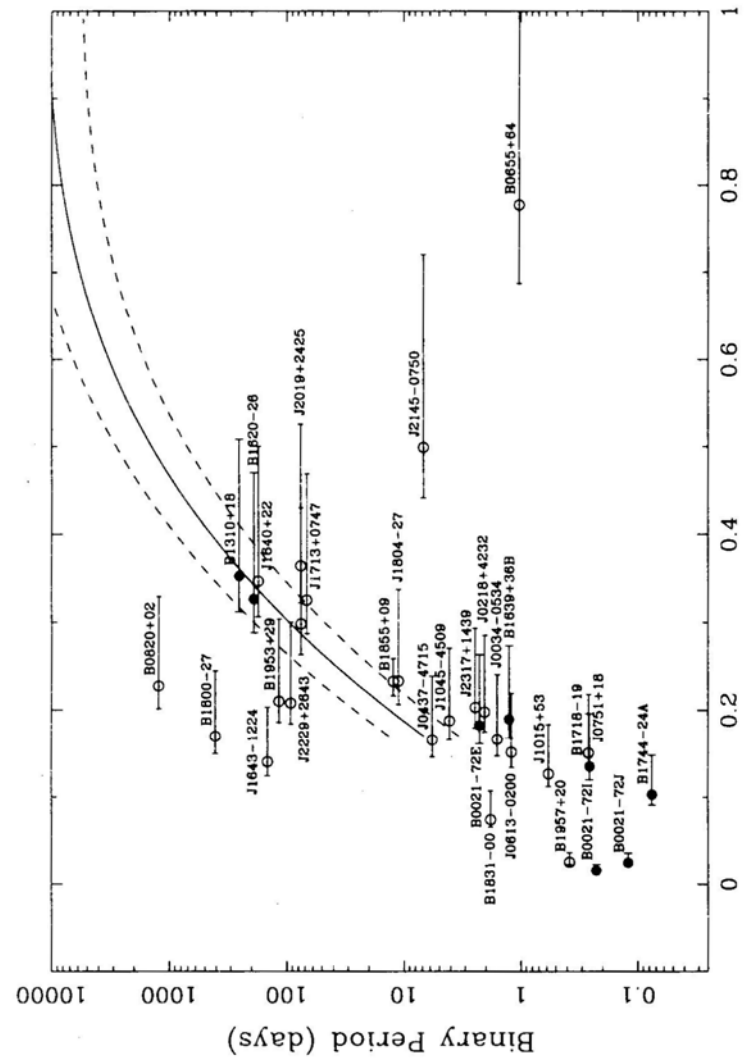

Figure 6: Orbital period versus companion mass for binary pulsars with near-circular orbits ($e < 0.05$). Systems associated with globular clusters are marked with a filled circle. For all except PSR B1855+09 (Ryba & Taylor 1991), the mass limits are plotted for $1 - \cos i = 0.2$ and 0.8, that is, the points where the probability of an inclination less than i is 20% and 80% respectively.

Main-sequence companions have long orbital periods and high eccentricity. PSR B1259–63 is eclipsed at periastron and so similar systems with shorter and more circular orbits would be hard to detect, but this is not true for PSR J0045–7319.

Systems with circular orbits generally have low-mass companions and are believed to have been circularized during a spin-up or accretion phase. If this accretion is due to Roche-lobe overflow from a companion, one expects a correlation between orbital and pulsar period as the accretion phase is shorter for wide systems. Such a correlation is seen, at least for orbital periods of less than 30 days or so, supporting the idea that these pulsars are old neutron stars which have been 'recycled' by the accretion process. It is not clear if this correlation extends to the very long period systems such as PSR B0820+02. There is now also a substantial group at orbital periods of about 100 days, above the so-called 'period gap' (Camilo 1994) and these also may evolve differently. Collapse of a high-mass white dwarf as a result of accretion (e.g. Helfand et al. 1983) provides an alternative formation mechanism for these systems.

Another plot relevant to the discussion of evolution of millisecond pulsars is shown in Figure 6. As first pointed out by Joss et al. (1987), if these systems evolve by Roche-lobe overflow, then a relation is expected between the final orbital period and companion mass. Since the size .of the companion's Roche lobe is dependent on its mass, the orbital period must decrease as the companion mass decreases to maintain the system in Roche lobe overflow. With a few exceptions, the observed companion masses are broadly in agreement with the theoretical relation. Joss et al. modelled stars to 0.17 $M_{\odot}$ only, but in fact the relation appears to extrapolate quite well to lower masses. PSRs J2145–0750 and B0655+64 clearly do not lie on the expected curve, suggesting that these two systems evolved in a different way. For example, van den Heuvel & Taam (1984) suggest that the neutron star in such systems spirals into the envelope of a giant star, ejecting the envelope and terminating the accretion phase. Several of the low-mass, long-period systems such as PSR B1800–27 appear to be significantly off the theoretical line. These systems may be formed in some other way (e.g. accretion-induced collapse) or may spiral out farther than predicted by the standard models.

References

Backer D. C, Kulkarni S. R., Heiles C, Davis M. M., Goss W. M., 1982, *Nature*, **300**,615

Bailes M. et al., 1994, *Ap. J.*, **425**, L41

Bell J.F., Bailes M., Bessell M. S., 1993, *Nature*, **364**, 603

Bhattacharya D., van den Heuvel E. P. J., 1991, *Phys. Reports*, **203**, 1

Camilo F., Nice D. J., Taylor J. H., 1993, *Ap. J.*, **412**, L37

Camilo F., Thorsett S. E., Kulkarni S. R., 1994, *Ap. J.*, **421**, L15

Camilo F., 1994, in Alpar M. A., van Paradijs J., eds, Lives of the Neutron Stars. Kluwer, Dordrecht, in press

Corbet R. H. D., 1984, *Astro. & Astrophys.*, **141**, 91

Foster R. S., Wolszczan A., Camilo F., 1993, *Ap. J*, **410**, L91

Helfand D. J., Ruderman M. A., Shaham J., 1983, *Nature*, **304**, 423
Hulse, R. A., Taylor, J. H., 1975, *Ap. J.*, **195**, L51
Johnston S. et al., 1993, *Nature*, **361**, 613
Johnston S., Manchester R. N., Lyne A. G., Nicastro L., Spyromilio J,, 1994, *MNRAS*, **268**, 430
Joss P. C, Rappaport S., Lewis W., 1987, *Ap. J.*, **319**, 180
Kaspi V. M., Johnston S., Bell J. F., Manchester R. N., Bailes M., Bessell M., Lyne A. G., D'Amico N., 1994, *Ap. J.*, **423**, L43
Kulkarni S. R., 1986, *Ap. J.*, **306**, L85
Lorirner D. R. et al., 1994, *Ap. J.*, in press
Lundgren S. C, Zepka A. F., Cordes J. M., 1993. IAU Circ. No. 5878
Lundgren S. C, 1994, PhD thesis, Cornell University
Lyne, A. G., Brinklow, A., Middleditch, J., Kulkarni, S. R., Backer, D. C, Clifton, T. R., 1987, *Nature*, **328**, 399
Lyne A. G., McKenna J., 1989, *Nature*, **340**, 367
Manchester R. N., Lyne A. G., Robinson C., D'Amico N. D., Bailes M., Lim J., 1991, *Nature*, **352**, 219
Navarro J., 1994, PhD thesis, Caltech
Nice D. J., Taylor J. H., Fruchter A. S., 1993, *Ap.J.*, **402**, L49
Robinson, C, Lyne, A. G., Manchester, R. N., Bailes, M., D'Amico, N., Johnston, S., 1994, *MNRAS,* submitted
Ryba M. F., Taylor J. H., 1991, *Ap. J.*, **371**, 739
Shibazaki N., Murakami T., Shaham J., Nomoto K., 1989, *Nature*, **342**, 656
Tauris T. M. et al., 1994, *Ap. J.*, **428**, L53
Taylor J. H., Weisberg J. M., 1989, *Ap*, *J.*, **345**, 434
Taylor J. H., Wolszczan A., Damour T., Weisberg J. M., 1992, *Nature*, **355**, 132
Taylor J. H. , Manchester R. N., Lyne A. G., 1993, *Ap. J. Suppl.*, **88**, 529
van den Heuvel E. P. J., Taam R. E., 1984, *Nature*, **309**, 235
Wolszczan A., Frail D. A., 1992, *Nature,* **355**, 145
Wolszczan A., 1994, *Science,* **264**, 538

Diamond Jubilee Symposium on Pulsars
14–17 March 1994
Raman Research Institute, Bangalore

J. Astrophys. Astr. (1995) **16,** 245–253

Deep Radio Observations of the Rich Globular Clusters Terzan 5 and Liller 1

A. S. Fruchter *Space Telescope Science Institute, 3700 San Martin Drive, Baltimore, MD 21210*

W. M. Goss *NRAO, P.O. Box 0,. Socorro, NM 87801*

Abstract. We have obtained deep 6, 20 and 90 cm observation of two of the richest globular clusters in the galaxy, Terzan 5 and Liller 1. In addition to the well known eclipsing pulsar, PSR1744-24A, our 20 cm image of Terzan 5 displays numerous point sources within 30″, or 4 core radii of the cluster center. The density of these objects rises rapidly toward the core, where an elongated region of emission is found. This feature may be due to the presence of a higher density of point sources than can be resolved by the 1″ resolution of our data. Observations at 6 and 90 cm show that the brightest individual sources, as well as the extended emission, possess the steep spectra expected of pulsars. Furthermore, we find that the strength of the sources in the 20 cm image agrees well with the standard pulsar luminosity function. The total luminosity and number of objects observed in Terzan 5 suggest that this cluster may contain 100 pulsars – probably more than any other Galactic cluster. Although we do not resolve individual sources in Liller 1, comparison of our images with other observations suggests that we are again observing the sum of emission from a number of objects. The 90 cm flux densities of Terzan 5 and Liller 1 are 35 and 9 mJy, respectively, implying that a number of bright pulsars in these clusters have been hidden from pulsed searches, perhaps by a combination of dispersion smearing, scattering and doppler broadening.

1. Introduction

The study of millisecond pulsars has recently undergone a renaissance, in large part because of the discovery of tens of pulsars in globular clusters (see the review by Dick Manchester in this proceedings). A few years ago, however, globular cluster pulsars were harder to come by. We, therefore, began a project to study the distribution and numbers of globular cluster pulsars by searching for steep-spectrum sources using the VLA. Rather than using the high-resolution A configuration to

search for individual point sources as previous pulsar searchers had done (Hamilton, Helfand, ansd Becker 1985), we chose to observe in the C array, so that the significant flux density expected from numerous weak pulsars would contribute to the total cluster signal (Fruchter and Goss 1992). This strategy proved productive; six new cluster radio sources were detected, four of which have subsequently been detected as radio pulsars (Biggs et al. 1994; D'Amico et al. 1993, Lyne et al. 1990; Manchester et al. 1989). These observations allowed us to put strong limits on the numbers and distribution of pulsars in globular clusters. We estimated that the total number of pulsars in the Galactic globular cluster system is between 500 and 2000, and that the true distribution of pulsars among clusters lies in-between the standard model which produced all pulsars through collision induced binaries (Verbunt, Lewin, and van Paradijs 1989) and one which distributed pulsars equally among clusters. However, in either the preferred model or in the collision model, one would have expected Terzan 5 and Liller 1 to be the two clusters in the galaxy richest in globular clusters. Our observations agreed well in the case of Terzan 5 – it was our brightest source (though the only *identified* pulsar in the cluster lies outside the cluster core, well away from the central radio emission, Lyne *et al*. 1990). Liller 1, however, displayed no detectable emission. This surprising result was made even more inexplicable when Johnston, Kulkarni and Goss (1991) obtained A array 20 cm observations of Liller 1 which were several times deeper than our survey and still failed to detect any radio emission. In this talk, we report on further radio observations which provide significantly more insight into the nature and number of sources in Terzan 5 and Liller 1.

2. Observations and Results

2.1 *Terzan 5*

The globular cluster Terzan 5 was observed at 20 cm in the A, BnA, B and CnB configurations of the Very Large Array (VLA)[1]. In each case, approximately four hours of data were obtained. All observations were done in continuum mode, using two 50 MHz bandpasses, centered on the sky frequencies of 1465 and 1515 MHz. Both right and left circular polarizations were observed. Terzan 5 was also observed at 6 cm in the B and C arrays. In both cases the observations were done in continuum mode, employing two orthogonal polarizations in each of two 50 MHz bandpasses, centered at the sky frequencies of 4835 and 4885 MHz. Here we discuss the 6 cm C array data as its beamsize closely approximates that which we used to measure the extended emission observed at 20 cm. Approximately six hours of data were taken in in the C array during two four hour observing sessions separated by about one week. Finally, Terzan 5 was reobserved on three successive days in the A/B array. During these observing session we rapidly switched between 20 cm and 90 cm. The 20 cm observations were done as described above. At 90 cm we observed across two 3.125 MHz bandpasses centered at 327.5 and 333 MHz. Both linear polarizations were observed. These dual frequency observations were

[1]The A configuration of the VLA is its largest. Each successive array (B, C, D) is approximately a factor of three smaller than its predecessor. Hybrid configurations (*e.g.* BnA), have the northern arm in the larger configuration, to provide a more circular beam for southern sources.

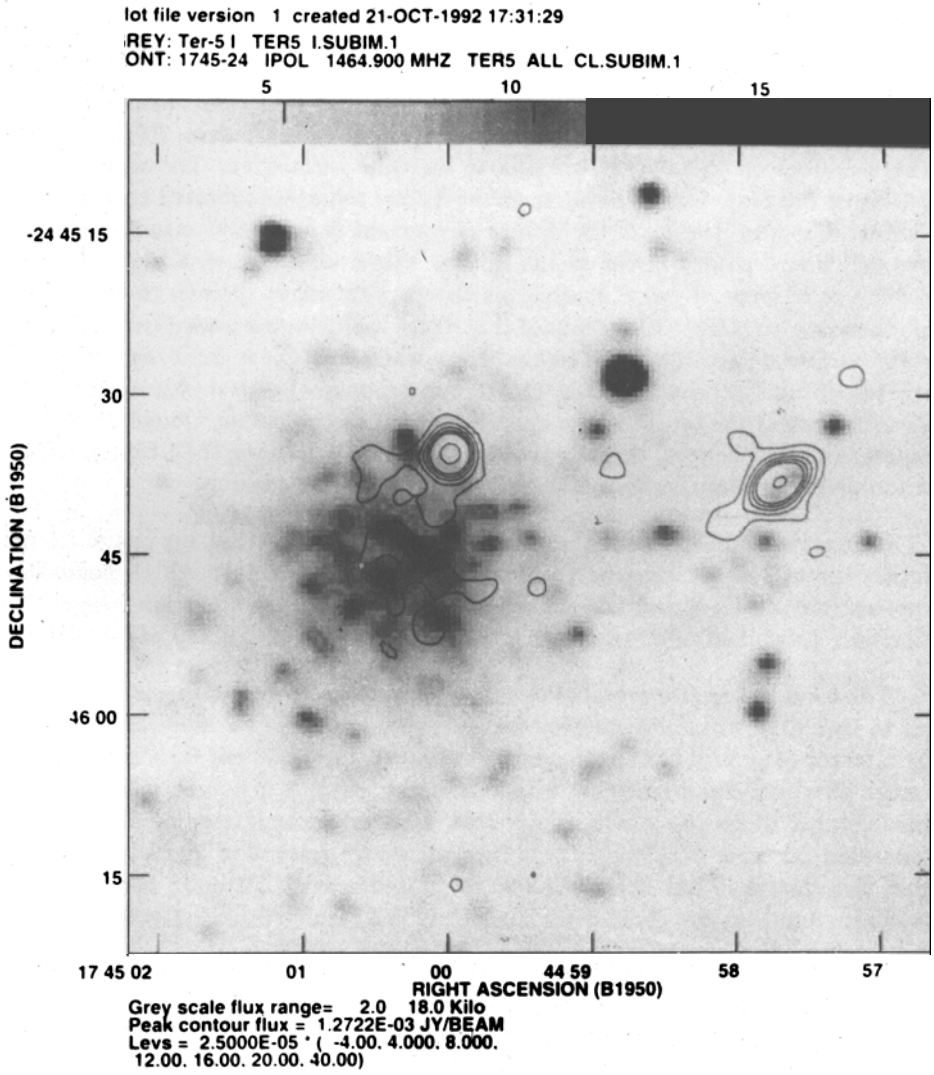

Figure 1: Radio contours are shown superposed on an I band image of the rich cluster Terzan 5. The 20 cm radio image has a beamsize of $3'' \times 3''$.

designed to allow us to study both the emission from the center of the cluster as well as the the low-frequency eclipse behavior of the 11 ms pulsar 1744-24A.

Figure I shows the contours of the 20 cm image of Terzan 5 superposed on an I band image of the cluster taken by Taft Armandroff with the CTIO 1-m telescope. The VLA image was made using uniform weighting and a 40 kilolambda taper. This weighting produces a small beam size (3″ × 3″) which sharpens the details of the image with the loss of some sensitivity to extended structure. The bright radio source about 30″ to the west of the cluster is the eclipsing pulsar, PSR 1744-24A. The sidelobes on this source are due to its time variability. The most striking feature of the radio image, however, is the diffuse radiation centered on the optical cluster. The flux density of the diffuse component is ≈ 2 mJy: stronger than the two prominent point sources in the image. When observed on a high resolution display, a number of point sources which are difficult to discern in the contour plot become apparent. We estimate that there are as many as a dozen individual point sources detectable in the image. Even when only the highest resolution data is retained and an image with a l″ beam is produced (with a consequent loss of signal-to-noise) the center of the cluster remains a continuous, elongated resolved source. If, as we believe, the source of this emission is pulsars, their central density is too great for them to be individually resolved in our data.

Comparison of the 20 cm and 6 cm observations shows that the the ≈ 1.5 mJy source about ten arc seconds to the northwest of the cluster center possesses a spectral index of –2 and the central diffuse emission has an index below –1.4. The only astrophysical sources likely to possess spectra this steep are pulsars.

The 6 cm image also reveals the ~ 200 μJy source to the south-east of the cluster to be highly variable source (undectable in one image its flux density increased by a factor of several in the other). Furthermore, in the 20 cm BnA configuration image obtained simultaneously with our 90 cm data, this source has brightened considerably to become a ~ 1 mJy source. Because these latter observations were separated from our previous 20 cm observations by more than 2 years, we suspect that this change in flux density is due to refractive scintillation in the interstellar medium, and that the rapid 6 cm variability is a result of diffractive scintillation.

Both the northern and southern point sources show up strongly in our 90 cm image. Each contributes about ~ 13 mJy to the total flux density of the cluster, with another ~ 10 mJy apparently due to the cluster as a whole. As our 90 cm beamsize is 9″ across, the division of the flux density into these components must be regarded as highly approximate. Unfortunately, a beamsize this large was required in order to make the necessary 3-D imaging of the 90 cm data computationally feasible. In Figure II, we display the 90 cm radio contours superposed on a greyscale image of the 20 cm data displayed in Figure I. The r.m.s. noise in the 90 cm image is approximately 1.3 mJy. Note that the only 20 cm source not also observed at 90 cm is the one identified pulsar in the cluster, PSR 1744-24A. Our data provides strong evidence that this pulsar is continuously enshrouded by material lost from the companion. We will discuss this aspect of our observations in detail in another publication.

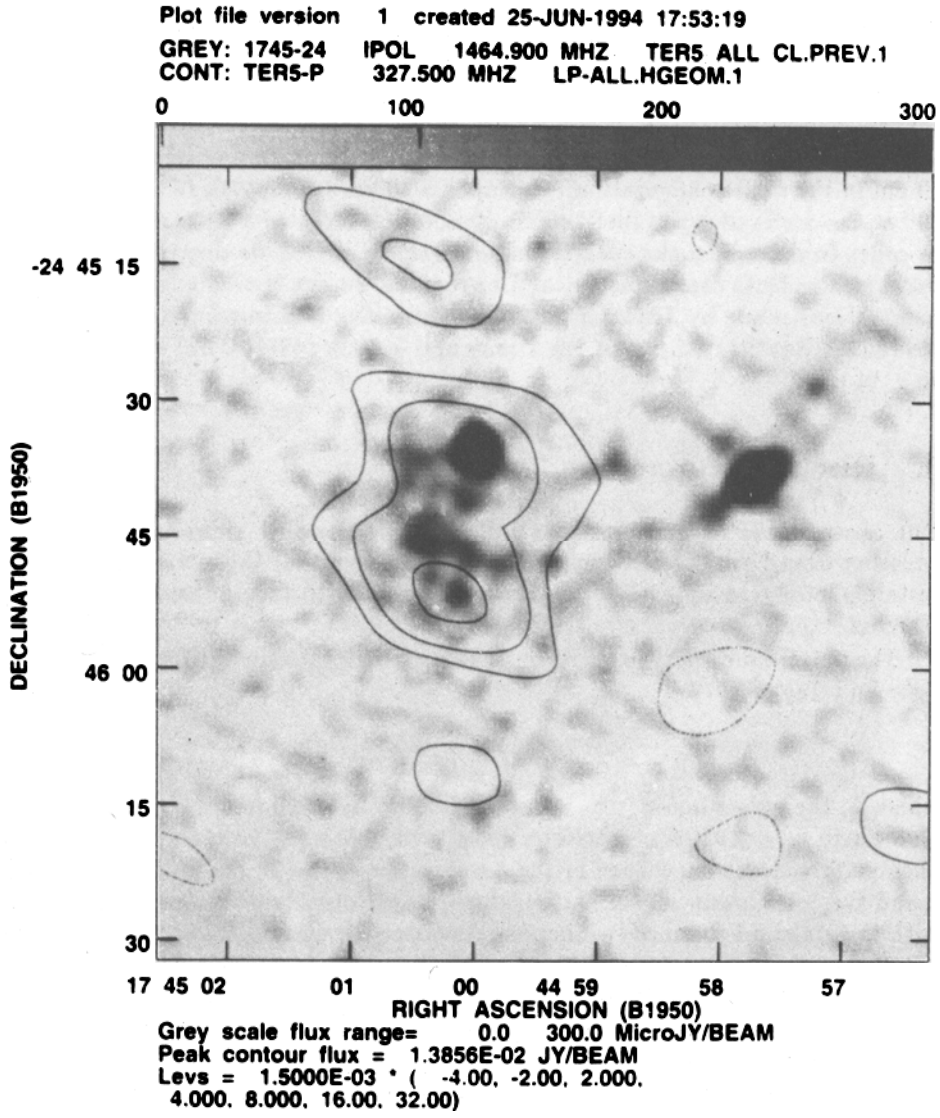

Figure 2: 90 cm radio contours are shown superposed on a 20 cm image of the cluster Terzan 5. While the central emission displays a steep spectral index characteristic of pulsars, the one identified pulsar in the field, PSR 1744-24A is not visible, even though it was strong a strong source in the simultaneous 20 cm observations. This pulsar appears to be continuously eclipsed at 90 cm.

2.2 *Liller 1*

The strong central emission observed in Terzan 5 made the non-detection of the nearly equally dense and equadistant cluster Liller 1 seem particularily surprising. While the observations of Johnston, Kulkarni and Goss (1991) were deep – their 20 cm 4σ limit was 180 μJy –, the data were taken in A configuration which has a beamsize of ~ 1.5″, and thus greatly over-resolve the ~ 7″ core radius of the cluster (Djorgovski 1993). If the cluster were to contain a number of sources, a lower resolution image would be more sensitive. We therefore observed Liller 1 at 20 cm in the CnB configuration, which has a 20 cm beamwidth of approximately 10″ at the declination of Liller 1. This observation revealed a 280 ± 50 μJy source. In order to determine the spectral index of this emission we observed Liller 1 at 6 cm in the DnC configuration, and re-reduced 90 cm B configuration archival observations made by Johnston and Kulkarni using 3D imaging. We find a 90 cm (330 MHz) flux density of 9 ± 1 mJy and a 6 cm (4885 MHz) flux density of 95 ± 14 μJy.

3. Discussion

Our observations of Terzan 5 and Liller 1 have revealed steep-spectrum radio emission from both clusters. In this section we show that this emission is almost certainly produced by a large population of pulsars so far undetected by pulsed searches.

The pulsar luminosity function is usually approximated by the formula (Manchester and Taylor 1977)

$$n(L) = \frac{1}{L^{\alpha}} dL,$$

where L, the pulsar luminosity, is bounded below by a minimum luminosity, L_{min} and where α = 2.0. We, therefore, have used a Monte Carlo simulation to determine, given our knowledge of the luminosities of the 20 cm sources in Terzan 5 and the total luminosity of the cluster, whether our observations are consistent with the standard luminosity function. As expected, we find that ability to fit the data is largely independent of the assumed L_{min}, but is strongly dependent on α We find that the 90% confidence interval for α given our Terzan 5 observations is –1.6 > α > –2.4, with the best fit at α = –1.85. Although we cannot α *priori* rule out another steep spectrum source mimicking this luminosity function, our analysis makes it appear highly probable that all of the radio emission observed from Terzan 5 is produced by pulsars.

Our observations of Liller 1, however, are much less informative. All of our detections are with beamsizes *larger* than the cluster core radius. Thus our inability to resolve the emission and study its luminosity function is not surprising. Nonetheless the signal to noise of our detections is good enough to allow us to obtain an accurate radio position in spite of our large beam. In the table below, we compare the position of the radio emission with that of the optical cluster and the x-ray source in Liller 1. All radio positions agree; therefore we have reported only the 6 cm position, which has the smallest error ellipse.

LILLER 1 SOURCE POSITIONS

Band	α_{2000}	error	δ_{2000}	error
Radio	$17^h\,33^m\,24^s.56$	$0^s.03$	$-33°\,23'\,19''.8$	$0''.5$
Optical	$17^h\,33^m\,24^s.47$	$0^s.08$	$-33°\,23'\,20''.2$	$1''.0$
X-ray	$17^h\,33^m\,24^s.09$	$0^s.08$	$-33°\,23'\,16''.4$	$1''.0$

While the rapid X-ray burster in Liller 1 would be an obvious possible source of variable radio emission, its position (Grindlay et al. 1984) is offset from the radio position by about 8 arcseconds. The agreement between the radio and optical positions of the cluster appears to be quite a bit better, although the position of the optical center of the cluster is somewhat controversial. Grindlay et *al.* report a position which disagrees by several arcseconds with the cluster discovery position of Liller (Liller 1977). However, Grindlay et *al.* used U band plates for their work whereas Liller worked in the R and I bands. As the visual extinction to this object is estimated at ~ 10 magnitudes (Djorgovski 1993), we have used Liller's position in the table.

While the position offset and steep spectrum of the radio source make it appear unlikely that it is the counterpart to the rapid X-ray burster, we cannot easily identify the total number of sources responsible for the radio emission. Nonetheless, it is improbable that a single pulsar is responsible for all the emission we see. Figure III plots the flux density of the radio source in Liller 1 versus frequency. Note that the 20 cm flux density reported here is a factor of two below what one would expect based on a spectral index determined by the 90 and 6 cm observations. As pulsar spectra are usually steeper at shorter rather than longer wavelengths (Manchester and Taylor 1977), it would appear that the source may have been low when we observed it at 20 cm. Yet our 20 cm flux density is 100 μJy greater than the 4σ A configuration limit of Johnston, Kulkarni and Goss (1991). Were the greater flux density caused by variability rather than the fact that the larger beam incorporates more objects, then the intensity at the time of the A configuration observations would have to be doubly suppressed.

Given that our Terzan 5 observations confirm that the standard field pulsar luminosity function can be applied to cluster millisecond pulsars, we can use our Monte Carlo simulations to estimate the number of pulsars in these clusters. Assuming that the minimum 20 cm pulsar luminosity is 0.3 mJy kpc^2 (see Fruchter and Goss 1992 for a discussion of this assumption), we estimate that there are between 60 and 200 pulsars in Terzan 5. Similarly we can use the fact that for an L^{-2} luminosity function, the expected number of pulsars N_{puls} given a total luminosity, L_{tot} is

$$N_{puls} = \frac{L_{tot}}{L_{min} \ln\left(\frac{L_{tot}}{L_{min}}\right)},$$

or in the case of Liller 1, about 15 pulsars (again see Fruchter and Goss 1992 for the derivation of this formula). While the reader may be justifiably suspicious of our assumed minimum luminosity, it should be noted that the relative expected

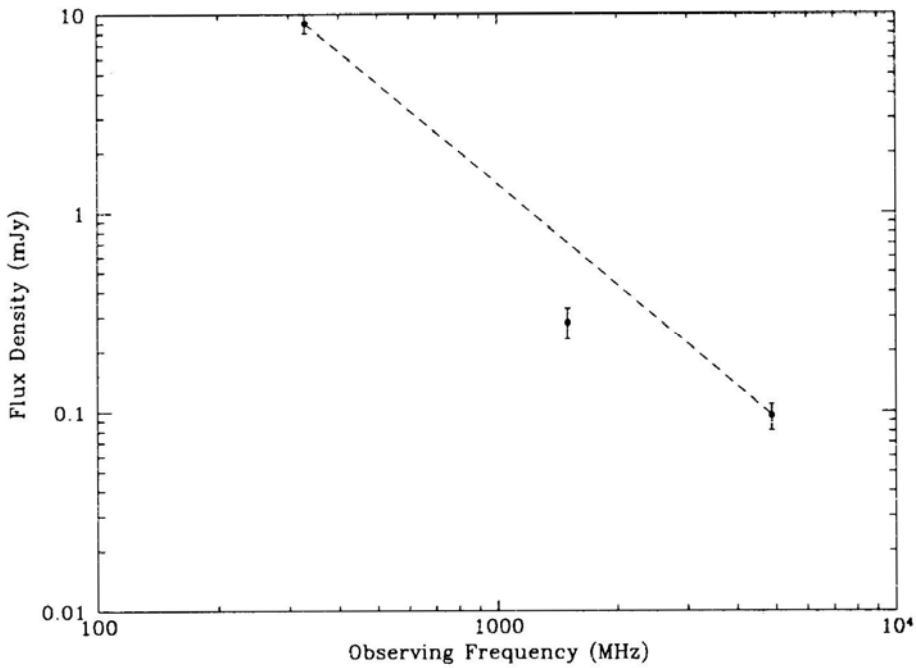

Figure 3: The flux density of the source radio source in Liller 1 as a function of observing frequency.

number of pulsars in different clusters is independent of the assumed L_{min}. Therefore, it seems highly likely that Terzan 5 is indeed several times richer than its apparent cousin Liller 1. Furthermore, when one extends this comparison to include other clusters (a point which will be taken up at greater length in another publication) one finds that Terzan 5 almost certainly contains more pulsars than any other cluster yet studied.

Both Terzan 5 and Liller 1 have been observed by pulsed searches described at this conference by Dick Manchester. Indeed, we have been told that acceleration searches have also been applied to the Terzan 5 data in an attempt to detect the bright central point sources reported here (M Bailes, private communication). The reason for the non-detection of these pulsars is unfortunately unclear. Little interstellar scattering is detected in observations of PSR 1744-24A (Nice and Thorsett 1992), and the expected dispersion measures of 200 to 400 cm^{-3} pc should be accessible to 20 cm searches. Nevertheless, when a new generation of large radio telescopes, such as the GMRT, are complete and these clusters can be searched with shorter integrations and narrower bandwidths at higher frequencies, we expect these objects to be revealed as troves of pulsar treasure.

Acknowledgements

We would like to thank Tim Cornwell, whose programs and assistance were invaluable to our 90 cm imaging. These observations were done at the Very Large Array of the National Astronomy Observatory, which is operated by Associated Universities, Inc., under cooperative agreement with the National Science Foundation. ASF was supported during much of this work by a Hubble Fellowhip, which was awarded by NASA through the Space Telescope Science Institute,

References

Biggs, J., Bailes, M., Lyne, A. G., Goss, W. M., and Fruchter, A. S. 1994, *Mon. Not. R. Astr. Soc.* 125–128.

D'Amico, N., Bailes, M., Lyne, A. G,, Manchester, R. N., Johnston, S., Fruchter, A. S., and Goss, W. M. 1993, *Mon. Not R. Astr. Soc*, **260**, L7L10.

Djorgovski, S. 1993, 373.

Fruchter, A. S. and Goss, W. M. 1992, *Astrophys. J.*, **384**, L47–L51.

Grindlay, J. E., Hertz, P., Steiner, J. E., Murray, S. S., and Lightman, A. P. 1984, *Astrophys.* J., **282**, L13–L16.

Hamilton, T. T., Helfand, D. J., and Becker, R. H. 1985, *Astron. J.*, **90**, 606–608.

Johnston, H, Kulkarni, S., and Goss, W. M. 1991, *Astrophys. J. Lett.*, **382**, L89–L92.

Liller, W. 1977, *Astrophys. J.*, **213**, L13–L15.

Lyne, A. G. et *al.* 1990, *Nature*, **347**, 650–652.

Manchester, R. N., Lyne, A. G., Johnston, S., D'Amico, N., Lim, J., Kniffen, D. A., Fruchter, A. S., and Goss, W. M. 1989. IAU circular 4905.

Manchester, R. N. and Taylor, J. H. 1977, *Pulsars*, (San Francisco: Freeman).

Nice, D. J. and Thorsett, S. E. 1992, *Astrophys. J.*, **397**, 249–259.

Verbunt, F., Lewin, W. H. G., and van Paradijs, J. 1989, *Mon. Not. R. Astr. Soc*, **241**, 5157.

Diamond Jubilee Symposium on Pulsars
14–17 March 1994
Raman Research Institute, Bangalore

J. Astrophys. Astr. (1995) **16,** 255–288

Scenarios for the formation of binary and millisecond pulsars - A critical assessment

E.P.J. van den Heuvel *Astronomical Institute 'Anton Pannekoek', University of Amsterdam & Center for High-Energy Astrophysics, Amsterdam, The Netherlands*

Abstract. The evolution of high-and low-mass X-ray binaries (HMXB and LMXB) into different types of binary radio pulsars, the 'high-mass binary pulsars'(HMBP) and 'low-mass binary pulsars' (LMBP) is discussed. The HMXB evolve either into Thorne-Zytkow objects or into short-period binaries consisting of a helium star plus a neutron star (or a black hole), resembling Cygnus X-3. The latter systems evolve (with or without a second common-envelope phase) into close binary pulsars, in which the companion of the pulsar may be a massive white dwarf, a neutron star or a black hole (some final systems may also consist of two black holes). A considerable fraction of the systems may also be disrupted in the second supernova explosion. We discuss the possible reasons why the observed numbers of double neutron stars and of systems like Cyg X-3 are several orders of magnitude lower than theoretically predicted. It is argued that the observed systems form the tip of an iceberg of much larger populations of unobserved systems, some of which may become observable in the future. As to the LMBP, we consider in some detail the origins of systems with orbital periods in the range 1 - 20 days. We show that to explain their existence, losses of orbital angular momentum (e.g., by magnetic braking) and in a number of cases: also of mass, have to be taken into account. The masses of the low-mass white dwarf companions in these systems can be predicted accurately. We notice a clear correlation between spin period and orbital period for these systems, as well as a clear correlation between pulsar magnetic field strength and orbital period. These relations strongly suggest that increased amounts of mass accreted by the neutron stars lead to increased decay of their magnetic fields: we suggest a simple way to understand the observed value of the 'bottom' field strengths of a few times 10^8 G. Furthermore, we find that the LMBP-systems in which the pulsar has a strong magnetic field ($> 10^{11}$ G) have an about two orders of magnitude larger birth rate (i.e., about 4×10^{-4} yr^{-1} in the Galaxy) than the systems with millisecond pulsars (which have $B < 10^9$ G). Using the observational fact

that neutron stars receive a velocity kick of ~450 km/s at birth, we find that some 90% of the potential progenitor systems of the strong-field LMBP must have been disrupted in the Supernovae in which their neutron stars were formed. Hence, the formation rate of the progenitors of the strong-field LMBP is of the same order as the galactic supernova rate (4×10^{-3} yr^{-1}). This implies that a large fraction of all Supernovae take place in binaries with a close low-mass (< 2.3 $M_\odot$) companion.

1. Introduction

A brief historical overview of the development of ideas on the recycling of neutron stars seems well in place here, as so much as these ideas originated in the Raman Research Institute. The first suggestion that the pulsating X-ray sources in X-ray binaries may later in life become radiopulsars, after their companion stars have exploded as a supernova or otherwise disappeared, was made by Bisnovatyi - Kogan and Komberg (1974). This was a quite natural suggestion as it had become clear around that time that some of the pulsating X-ray sources in binaries, such as SMC X-l (P = 0.71 sec) and Cen X-3 (P = 4.84 sec), are rapidly spinning up on a timescale of only a few thousand years, and have spinperiods in the range observed for radiopulsars. So, after disappearance of the companion such neutronstars are expected to become normal radiopulsars.

In 1974 the Hulse-Taylor binary pulsar PSR 1913+16 was discovered, which appeared to have very abnormal characteristics for a radio pulsar: its magnetic field strength is only 2.10^{10} G, some two orders of magnitude lower than that of the other pulsars then known, and its spinperiod (0.059 sec) is abnormally short which, at the time, made it the second-fastest pulsar known, after the Crab pulsar (P = 0.033 sec). In these days magnetic fields of neutron stars were thought to decay spontaneously on a relatively short timescale, of order 5.10^6 yr. The abnormal characteristics of PSR 1913+16 therefore led Smarr and Blandford (1976) to suggest that this pulsar is the oldest of the two neutronstars in the system which, after a long episode of field decay, was spun-up by accretion in a binary system in which, subsequently, the other star exploded.

Srinivasan and I in 1978. elaborated further on this idea. We showed that the Smarr-Blandford model, in fact, is the *only* explanation possible for the peculiar combination of rapid spin and weak magnetic field observed in PSR 1913+16 since, with normal exponential field decay on a timescale $\sim (2 — 10) \times 10^6$yrs, this combination of spin period and field strength can never be reached by any known pulsar: in the B vs. P diagram the 'progenitor'-region for such pulsars is empty. We therefore concluded that PSR 1913+16 was spun-up by accretion in a binary. This then immediately implies that its companion must also be a neutron star. This is because during the accretion and spin-up phase the orbit of the system must have been completely circularized by tidal and/or frictional forces, as the orbit was already very narrow. The only way to then, subsequently obtain the presently observed very large orbital eccentricity of the system is: if a second supernova explosion took place. This then implies that the companion of

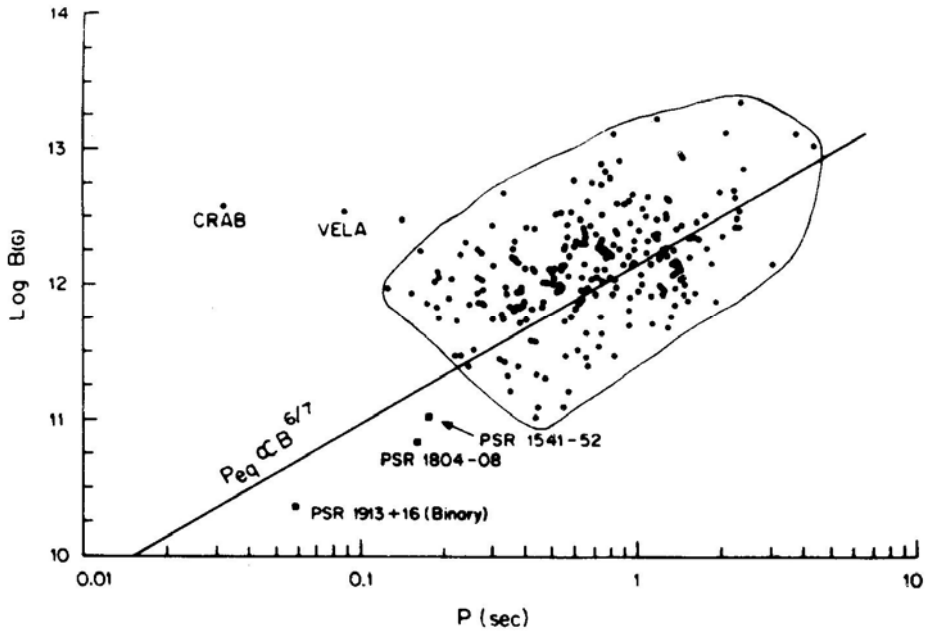

Figure 1: The introduction of the 'spin-up line' in the magnetic field strength (B) versus Period diagrams of pulsars, by Radhakrishnan and Srinivasan in 1981 at the 2nd Asian-Pacific Regional Meeting of the IAU (published in 1984 - see text). The three pulsars indicated as squares located outside the 'pulsar island' could never have reached their present B-P combinations without recycling. Further explanation in the text.

PSR 1913+16 must itself also be a neutron star: the youngest one of the two.

We presented this result orally at the 1978 Texas Symposium in München and wrote it down in a paper submitted to Astronomy and Astrophysics in 1980, which was immediately accepted, but published only in 1982 as the manuscript had been lost at the printers (Springer Verlag) for two years (Srinivasan and Van den Heuvel 1982). The reason why one does not observe the second-born pulsars in PSR 1913+16 and PSR 1534+12 is nowadays also quite obvious: that pulsar has not been recycled and therefore will be a normal strong-field pulsar which spins down rapidly and disappears into the graveyard within a few million years after its formation. On the other hand, the recycled pulsars in these systems have spindown timescales $\geq 10_8$ yrs - since it is no longer believed that the magnetic fields of non-accreting neutronstars decay spontaneously - and therefore remain observable some twenty or more times longer than their newborn companions. Therefore, the probability of observing the recycled pulsars in these systems is much higher than that of observing the newborn ones, which explains why in both these systems we see only the recycled pulsar (cf. Van den Heuvel and Taam 1984).

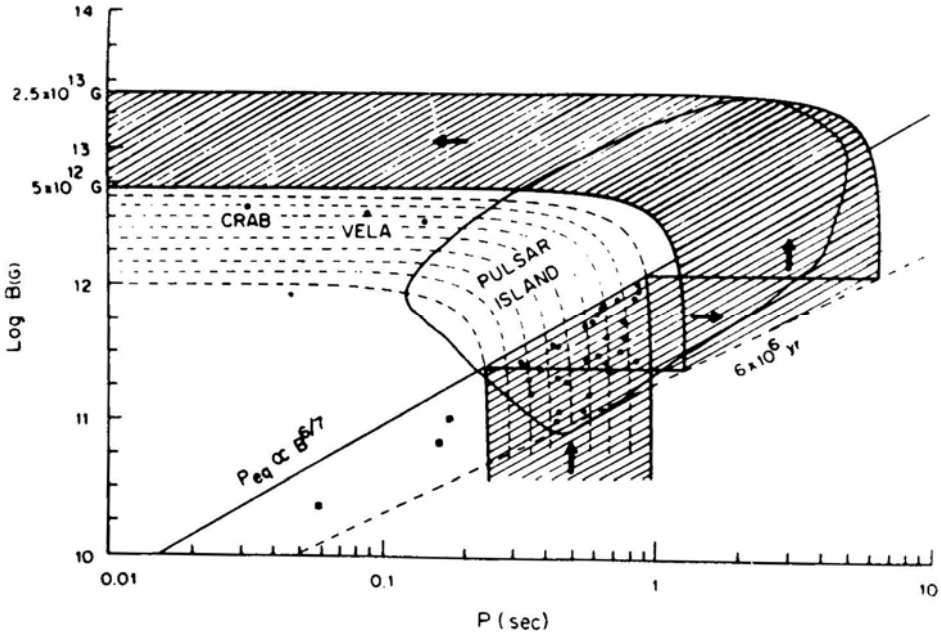

Figure 2: The possible location of recycled pulsars within the 'pulsar island'. The twenty-nine pulsars below the spin-up line in this island, could have reached their positions either by normal pulsar evolution with field decay (dashed tracks) or by recycling (full tracks). The three pulsars indicated as squares can *only* have reached their present positions by recycling (from Radhakrishnan and Srinivasan's 1981 presentation mentioned in the caption[x] of figure 1.)

The spin-up line was put forward for the first time in 1981 in a paper by Radhakrishnan and Srinivasan presented at the 2nd Asian-Pacific Regional Meeting of the IAU in Bandung, Indonesia (this paper came out in print in 1984 in Jakarta: Radhakrishnan and Srinivasan, 1984).Figure 1 shows this 1981 figure with the spin-up line. Radhakrishanan and Srinivasan argued in this paper that there is an entire class of 'recycled' pulsars (this word was invented in this paper), and with certainty identified two pulsars below the spin-up line as such. Like PSR 1913+16 with normal field-decay evolutionary tracks these pulsars could never have reached their present combination of rapid spin and weak field, as their progenitor region in the B-P diagram is empty. This is the more so if fields do not decay spontaneously.

As to the other pulsars in their diagram below the spin-up line: the authors showed that these might either have originated by field decay from the normal 'pulsar-island' in the B-P diagram, or they might have been recycled as well. They probably are a mixture of both types (see figure 2).

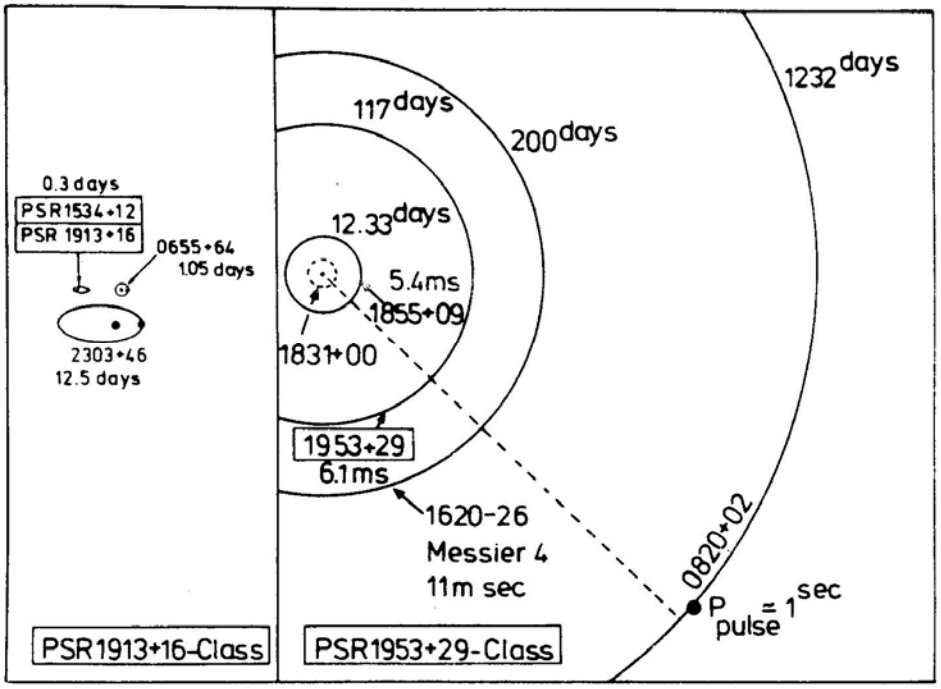

Figure 3: The two classes of binary radio pulsars (explanation in the text)

Then, in the fall of 1982, Don Backer and collegues dropped a bombshell in the pulsar community by announcing the discovery of the 1.55 millisecond pulsar PSR 1937+21, spinning *twenty* times faster than the fastest pulsar then known (the Crab pulsar), and with a magnetic field strength two orders of magnitude below that of PSR 1913+16. Independently Radhakrishnan and Srinivasan (1982) and Alpar et al. (1982) suggested that this pulsar originated in a binary system and had been spun-up by heavy accretion ($\geq 0.15 M_{\odot}$).

At that time I thought that this was a quite ludicrous idea: the only pulsar for which we then had clear evidence of recycling was PSR 1913+16, but the suggestion that the millisecond pulsar was recycled meant extrapolation of the recycling idea by *a factor forty* in spin period and a *factor hundred* in magnetic field strength. And, on top of this, one also had to get rid of the companion, since PSR 1937+21 is single.

This all combined I found a bit too much to believe. But history quickly proved these authors to be right: less than half a year later Boriakoff et al. (1983) discovered a millisecond pulsar in a binary system with a low-mass white dwarf companion: PSR 1953+29, which at once proved that millisecond pulsars can,

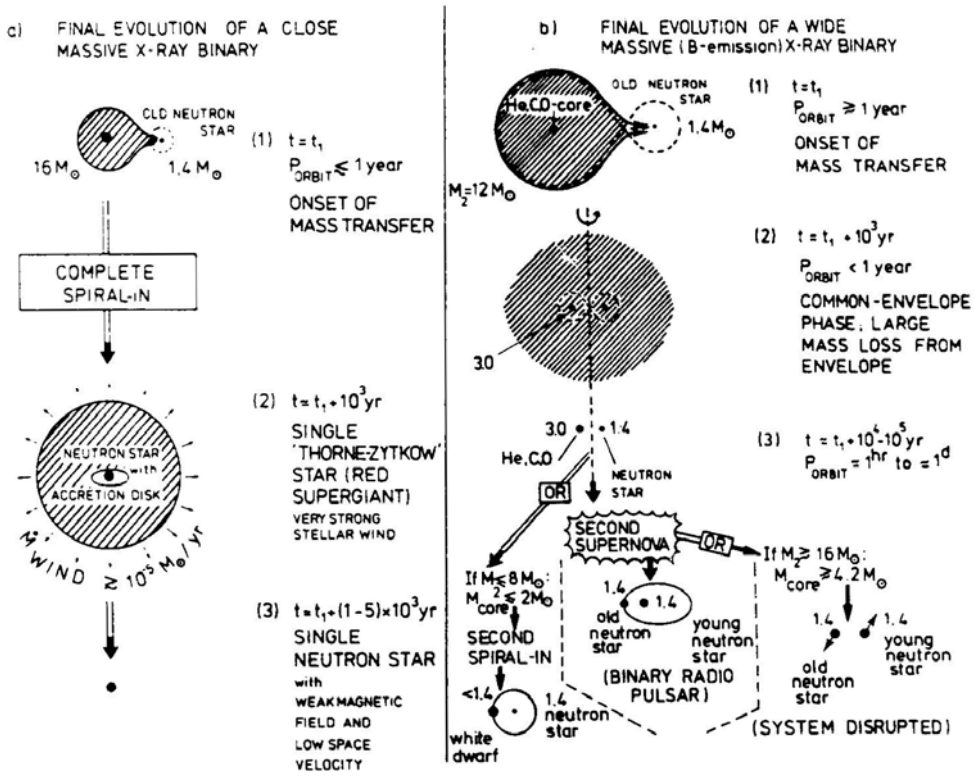

Figure 4: The various possibilities for the Anal evolution of a high mass X-ray binary. In all cases the onset of thermal-timescale Roche-lobe overflow leads to deep spiral in, probably due to the formation of a common envelope. In close systems (left) there is most probably not enough energy available in the orbit to eject the envelope of the massive star, and the neutron star spirals down into the core of its companion, producing a Thorne-Zytkow star. The envelope of this star is slowly ejected in the form of a strong stellar wind. In wider systems, the envelope of the massive star is ejected during spiral in and a close binary is left, consisting of the neutron star and the core (consisting of helium and heavier elements) of the companion. When this heavy-element core terminates its evolution, it may either leave a neutron star (in an eccentric bound orbit, or in a hyperbolic orbit), or a massive white dwarf. These three possiblities are indicated.

indeed, be formed by recycling in binary systems. The evolutionary history of this system was immediately understood, as the existence of such wide and circular binary systems had just been *predicted* in two papers which then were in print (Webbink et al. 1983; Taam 1983): they are a later evolutionary phase of low-mass X-ray binaries that started out with orbital periods longer than about one day (cf. Savonije 1983, Joss and Rappaport 1983; Paczynski 1983): in such systems the mass transfer is driven by the interior nuclear evolution of the low-mass donor, which is a (sub)giant with a small degenerate helium core. Figure 5 (after Joss

and Rappaport 1983) depicts the evolution of such a system.

After this brief historical introduction, I would now like to discuss some - in our view - key issues regarding the evolution of the two known types of binary radio pulsars, depicted in figure 3. These are the PSR 1913+16 - class, which presumably originate from High-Mass X-ray Binaries (HMXB), and the PSR 1953+29 class, which are thought to originate from relatively wide Low-Mass X-ray Binaries (LMXB).

The first group, which we will call HMBP, is discussed in section 3, and the second group, the LMBP, in section 4. Before this we briefly outline, in section 2, the current ideas on the origins of the two classes of binary pulsars. In section 3 and 4 we particularly consider some problems concerning the birthrates of the systems, and the relation between field decay and accretion that can be derived from the observations of LMBP systems. For more extensive reviews we refer to Bhattacharya and Van den Heuvel (1991); Canal et al. (1990) and Verbunt (1993).

2. From X-ray binaries to Binary Pulsars

The HMBP systems, depicted in the left-hand panel of Fig. 3 (the 'PSR 1913+16 class'), tend to have very narrow and highly eccentric orbits, and the companions of these pulsars have masses in the range 0.8 to 1.45 $M_\odot$: they are neutron stars or massive white dwarfs. On the other hand, the systems in the second class have in general much wider orbits which always are practically circular, and their companions are low-mass white dwarfs, in the mass range 0.2 to 0.45 $M_\odot$. The evolutionary history of these two classes of systems is thought to be quite well understood in terms of the later evolution of HMXB and fairly wide LMXB, respectively (Van den Heuvel & Taam 1984; Bhattacharya & Van den Heuvel 1991), as depicted in Fig. 4 and 5, respectively. Fig. 4 depicts the various possibilities for the later evolution of HMXB in which the compact star is a neutron star. Our early calculations (Van den Heuvel & De Loore 1973) showed that once thermal-timescale Roche-lobe overflow ensues in such systems, they will evolve with large losses of mass and angular momentum, and will end as ultra-short-period binaries consisting of a helium star (the helium core of the massive star) together with the neutron star, as depicted in stage 3 in Fig. 4b. More recent works, in which this evolution is considered in terms of common-envelope (CE) evolution, lead to a similar outcome (Taam *et al.* 1978; Taam & Bodenheimer 1992). Only if the drop in orbital binding energy during spiral-in is sufficiently large to overcome the binding energy of the envelope, a short-period binary will remain. This probably requires that the initial orbital period of the HMXB be quite long: longer than of order 50 -100 days. For short-period systems, there may not be enough orbital binding energy available to eject the envelope: in that case the neutron star will spiral down completely into the center of the companion and a single so-called Thorne-Zytkow star is expected to be formed: a massive star with a neutron star in its center. This is depicted in Fig. 4a. For the formation of binary pulsars only Fig. 4b is of interest. If the helium star is sufficiently massive (>2.5 $M_\odot$, cf. Habets 1985, 1986) it will later explode as a supernova and leave a second neutron star, either in a highly eccentric orbit (due to the explosive mass ejection, possibly

in combination with kicks) or in a hyperbolic orbit, in which case two runaway pulsars result (Flannery & Van den Heuvel 1975; De Loore *et al.* 1975). If the mass of the helium star was < 2.0 - 2.5 $M_\odot$ (initial mass of the donor in the HMXB < 8 – 10 $M_\odot$) a second spiral-in phase will ensue, in which the envelope of the helium star is removed and its degenerate CO-core stays behind as a massive white dwarf, in a close circular orbit with the neutron star. PSR 0655+64 is thought to be the result of such evolution (Van den Heuvel & Taam 1984). [The second spiral-in also occurs for more massive helium stars, up to about 3.5 $M_\odot$, but for M_{He} > 2.5 $M_\odot$ the remnant core will be sufficiently massive to still collapse to a neutron star.]

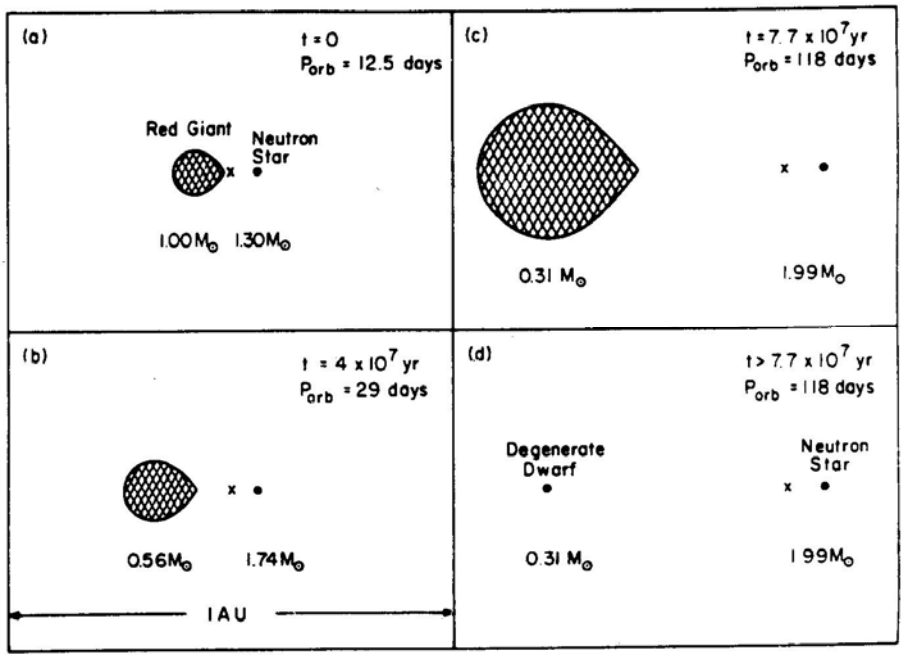

Figure 5: The evolution of a wide low-mass X-ray binary (LMXB), starting out as a 1 $M_\odot$ red (sub-)giant and a 1.3 $M_\odot$ neutron star, with an initial orbital period of 12.5 days. At the end of its evolution the system (frame (d)) consists of a 0.31 $M_\odot$ helium white dwarf and a 1.99 $M_\odot$ neutron star in a circular orbit with P = 118 days, closely resembling the binary pulsar PSR 1953+29 (after Joss & Rappaport 1983).

Concerning the origins of the LMBP systems depicted in the right-hand panel of Fig. 3: they are simply the later evolutionary products of fairly wide LMXB, initially consisting of a low-mass donor star (< 1.4 $M_\odot$) and a neutron star. The donor overflows its Roche lobe after it has terminated core-hydrogen burning, as described already in the introduction, and has developed a degenerate helium core. Energy generation in such stars occurs by hydrogen-shell burning around the core. As the core mass grows, the outer envelope gradually expands. Since, once the

star overflows its Roche lobe, mass transfer takes place from the lower-mass to the more massive component, the orbit will expand, such that this mass transfer is self-stabilizing. Thus the mass transfer and orbital expansion take place on a semi-nuclear time scale of the donor star. Fig. 5 depicts such evolution for a system initially consisting of a 1 $M_\odot$ donor and a 1.3 $M_\odot$ neutron star, with an initial orbital period of 12.5 days, as calculated by Joss & Rappaport (1983). After ~80 million years of mass transfer, the envelope mass of the donor has been exhausted and the 0.31 $M_\odot$ degenerate helium core of this star stays behind as a helium white dwarf in a 117 days orbit. Since during the entire mass-transfer phase the donor was filling its Roche lobe, tidal forces in its convective envelope will have been strong and have circularized the orbit. This evolution explains the low companion masses and circular orbits of these systems, even though they very probably started out with large orbital eccentricities just after the supernova explosion in which the neutron star was formed.

3. Some Key Problems concerning the Origins of the HMBP

3.1 *Cygnus X-3: a missing link*

In 1973 it was suggested that a possible identification of a close helium star plus neutron star system, resulting from spiral-in evolution as depicted in Fig. 4b would be the system Cygnus X-3 (Van den Heuvel & De Loore 1973). This is a very peculiar 4.8 hour period X-ray binary, which from time to time shows gigantic radio synchrotron outbursts, indicating mass ejection with relativistic speeds. (It has been called a. 'mini-quasar', as its radio emission during outbursts can be remarkably well represented by the 'Van der Laan model' of an expanding bubble of relativistic electrons and magnetic fields, that was constructed to explain the radio spectra of quasars). It is right in the galactic plane, at a distance of about 10 kpc, behind three 21cm neutral-hydrogen spiral arms. Interstellar extinction makes its optical identification impossible, but recently, infrared spectroscopic observations have shown that its companion is a Wolf-Rayet star of WN-type, which means: a massive helium star (Van Kerkwijk *et al.* 1992; Van Kerkwijk 1993). Its spectrum, dominated by strong emission lines of He I and He II, is shown in Fig. 6.

Wolf-Rayet stars are known to be the helium core remnants of massive stars that have lost practically their entire hydrogen-rich envelopes (cf. Abbott & Conti 1987; Van der Hucht 1992). The known WR stars have masses larger than about $6M_\odot$, which implies that their progenitors had masses > 22 $M_\odot$. The defining characteristic of Wolf-Rayet stars is, apart from the strong emission lines of He, the presence of strong emission lines of C and N, in various stages of ionization, with a half-width of 1000 to 2500 km/s. This indicates the presence of a very strong stellar wind with outflow velocities of this order, and implies a mass-loss rate of order 10^5 to 10^4 $M_\odot$ yr^{-1}. The fact that the WR-stars in binaries typically have M > 6 $M_\odot$, indicates that this type of strong stellar-wind mass loss apparently is restricted to helium stars with masses in excess of this value. Thus, the conclusion from Fig. 6 is that the Cyg X3 system consists of a helium star of mass > 6 $M_\odot$ and a compact object, most probably a neutron star. The X-ray

source is powered by the accretion from the strong stellar wind, and the peculiar rounded shape of the X-ray light curve - without eclipses - is due to the various degrees of extinction that the X-rays experience in this wind, as a function of orbital phase. Thus, thanks to Van Kerkwijk *et al.*' s work we now know that Cyg X-3 is the first identified 'missing link' between the HMXB and the close double neutron star systems.

In view of the high mass loss rate ($> 10^{-5} M_{\odot} yr^{-1}$), the WR-component of the Cyg X-3 system may well have reduced its mass below 4 $M_{\odot}$ before it explodes as a supernova; in that case the system needs not be disrupted by that explosion. Important as the discovery of the WR-character of Cyg X-3 may be, this does by no means imply that all problems with the origins of the double neutron stars have been solved. We will now discuss problems that still remain.

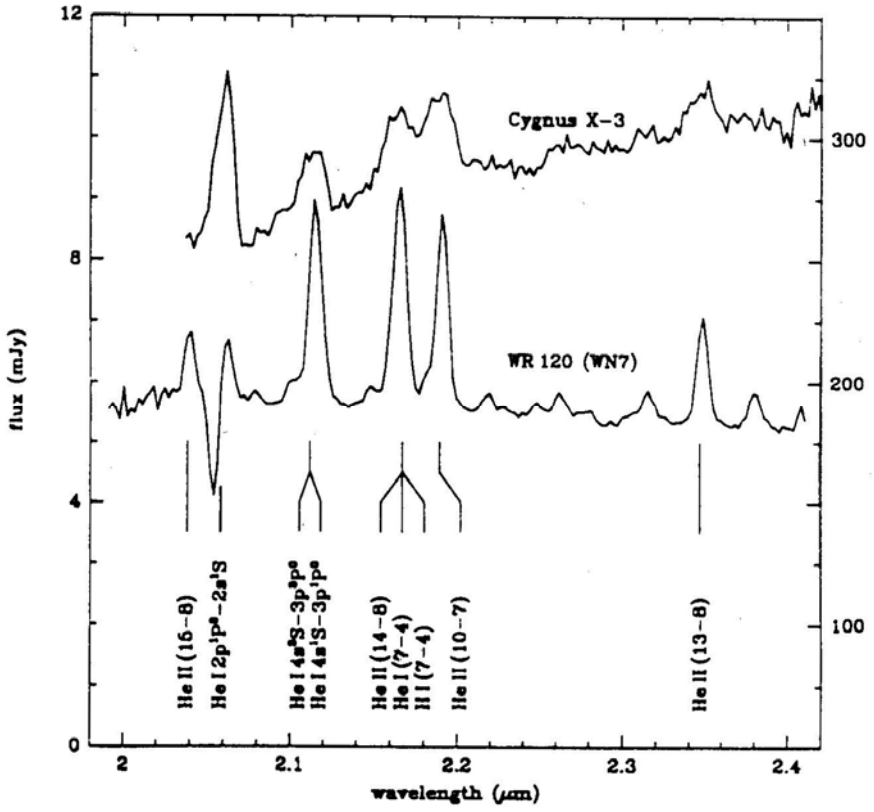

Figure 6: The infrared spectrum of Cygnus X-3 is dominated by emission lines of He I and II and closely resembles that of the WN 7-type Wolf-Rayet Star WR 120 (after Van Kerkwijk *et al.* 1992).

3.2 *The birth rate problems of close helium star plus neutron star binaries and of double neutron stars*

3.2.1 Introduction

Studies of the evolution of stellar populations that contain a realistic fraction of binaries, with realistic distributions of mass ratios and orbital separations (as derived from the observations), carried out by various groups (e.g., Lipunov 1992; Tutukov & Yungelson 1993; Meurs & Van den Heuvel 1989) predict for the Galaxy the presence of about (1 - 2) × 10^4 helium star plus neutron star systems with MHe >2.5$M_\odot$ (the lower limit for exploding as a supernova and leaving a neutron star behind). Also, these simulations predict a formation rate of close double neutron stars in the galaxy of order 10^{-4} yr^{-1}, whereas the formation rate derived from the known systems PSR 1913+16, PSR 1534+12 and PSR 2303+46 in the galactic disk is rather of order 7 × 10^{-6} yr^{-1} (Phinney 1991; Narayan *et al.* 1991), a discrepancy of about one to two orders of magnitude (see also Table I).

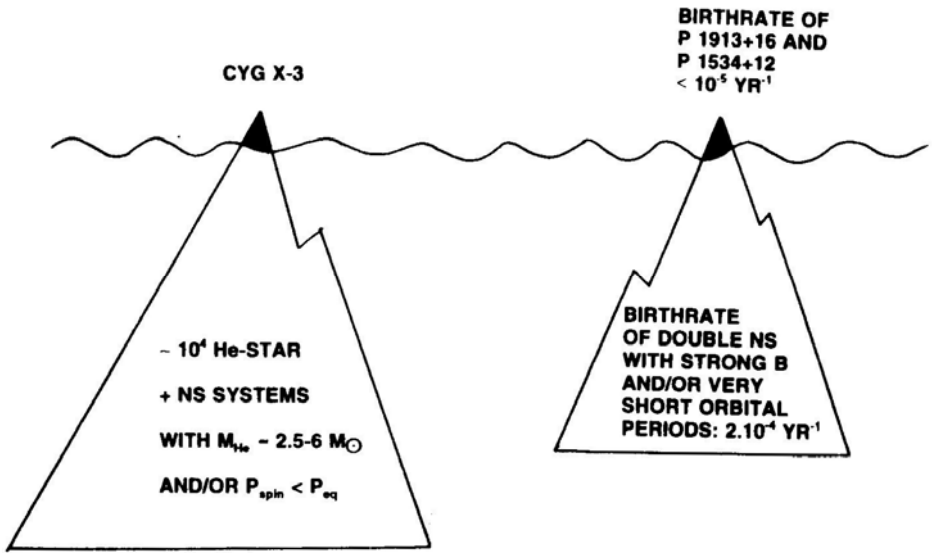

Figure 7: Cygnus X-3 and the close double neutron star systems PSR 1913+16 and PSR 1534+12 probably are just 'tips of icebergs' of much larger populations of helium star plus neutron star systems and double neutron star binaries, respectively (explanation in the text).

The question arises: why do we see only one Cyg X-3 system in the Galaxy? If there were more, we would easily have seen them, because of their enormous X-ray luminosity, about equal to the Eddington limit of a 1.4 $M_\odot$ object.

We will argue, in what follows, that both Cyg X-3 and the three observed double neutron star systems form samples that are highly biased by observational selection effects, and that they are just the 'tips' of huge 'icebergs' of much larger

populations of helium star plus compact star systems, and of double neutron star systems, respectively, as schematically depicted in Fig. 7. We will now discuss the selection effects that we expect to play a role in the detection of these two types of systems.

3.2.2 Factors that may reduce the observable number of helium star plus neutron star systems

(i) The first factor is that, as mentioned above, the lower mass limit for becoming a Wolf-Rayet star with a strong wind is about 6 $M_\odot$, while the lower mass limit for helium stars to terminate life with a supernova is about 2.0 to 2.5 $M_\odot$ (Habets 1985, 1986). The mass function for helium stars ϕ (M_{He}) results directly from that of main-sequence stars, and will therefore have about the same form, i.e.,

$$\phi(M_{\rm He}) \propto M_{\rm He}^{-5.5} \tag{1}$$

Consequently, only the fraction $f_1 = (2.5/6)^{4.5} = 1/60$ of the relevant helium star plus neutron star systems will have $M_{He} > 6\ M_\odot$, and may resemble Cyg X-3.

(ii) The second factor is, that during the spiral-in phase the mass-accretion rate onto the neutron star will be very large, and probably super-Eddington. As a result, the neutron star will be spun up to a very short spin period, which may well be located to the left of the spin-up line. When the spiral-in phase is over, the accretion rate will decrease dramatically, which will cause the Alfvén radius to increase, such that the neutron star will spin faster than the equilibrium spin rate corresponding to its decreased accretion rate M, in combination with its magnetic field strength B. This implies that no accretion can take place, and the object will be unobservable as an X-ray source, as was first pointed out by Lipunov (1994). Thus, a considerable fraction of the potential Cyg X-3 - like systems may not show up as accreting X-ray sources. A precise estimate of this fraction cannot be given, but it seems not unlikely that it may be 90% or higher, which would reduce the observable number of systems by another factor of ten, leading to a reduction factor $f_2 = 0.1$.

(iii) In view of the large kick velocities (450 ± 90 km/s) that neutron stars appear to receive at birth (Lyne & Lorimer 1994), a considerable fraction of the massive systems may be disrupted in the first supernova explosion. This fraction is expected to be of order 50% for the shorter-period systems, with P < 15 - 20 days (with randomly directed kicks), and may be as high as 90 percent for the wider systems, which form the bulk of the massive systems. The resulting reduction factor f_3 is therefore expected to be about 0.2, but might well be as low as 0.05 (cf. Van den Heuvel 1994, for a more extensive discussion).

Due to these three effects the number of helium star plus neutron star systems that is observable as Cyg X-3 type X-ray binaries reduces to of order $f_1\ f_2\ f_3(1 - 2) \times 10^4 = 3$ to 6. Taking the uncertainties, in all these correction factors into account, this small number can probably be reconciled with the fact that we see only one Cyg X-3 system in the Galaxy.

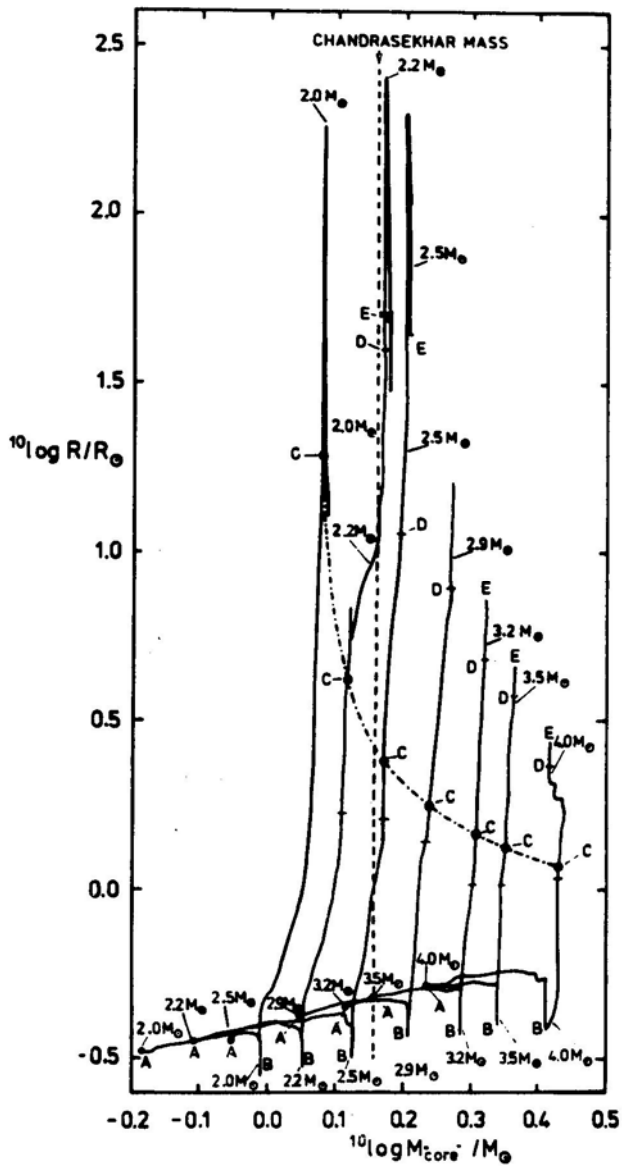

Figure 8: Evolution of the radii of helium stars of different masses is depicted here in a radius versus core-mass diagram. The core mass before core-helium exhaustion is defined as the mass of the convective core plus adjacent semi-convective regions. After core-helium exhaustion it is the mass inside the helium burning shell. Letter C indicates central or off-center carbon ignition, D is neon-ignition. Notice that helium stars with masses < 3.5 $M_{\odot}$ still evolve to large radii (after Habets 1985, 1986).

3.2.3 The birth rate of double neutron star systems: the incidence of strong-field or ultrashort-period systems

Concerning the predicted birth rate of double neutron star systems of about 10^{-4} yr^{-1} versus an observed birth rate of 7×10^6 yr^1 in the Galaxy: also here the observed two systems on which this 'observed' birth rate is based, may not at all be representative for the bulk of the double neutron star systems. They may be a highly biased sample, for example because of their abnormally weak magnetic fields (10^{10} and 2×10^{10} G in the cases of PSR 1534+12 and PSR 1913+16, respectively). These fields make them abnormally long-lived as pulsars (2×10^8 yr and 10^8 yr, respectively). If the 'average' pulsar in a double neutron star system is born with a more 'standard' magnetic field strength, of order a few times 10^{12} G, it will spindown rapidly and disappear into the graveyard within a few million years after its birth. Thus, such systems may have a birth rate that is one to two orders of magnitude larger than that of systems like PSR 1913+16 and PSR 1534+12, without them having been detected so far.

Table 1: Birth rates of observed binary pulsars (double neutron star) systems and of hypothetical systems that may result from common envelope evolution of Be/X-ray binaries

	PSR name	τ_{sd}(yr)	τ_{gw}(yr)	Galactic birthrate (yr^{-1})	Number in Galaxy active pulsars	Number in Galaxy turned-off pulsars
Observed Systems	1913+16	10^8	3×10^8	5×10^{-6}	500	1000
	1534+12	2.5×10^8	1.5×10^9	2×10^{-6}	500	2500
	2303+46	3×10^7	∞	1.7×10^{-5}	500	3×10^5
Hypothetical Systems	strong-field close binary pulsar	5×10^6	5×10^8	$< 10^{-4}$	< 500	$< 5 \times 10^4$
	strong-field wide systems	5×10^6	∞	$< 10^{-4}$	< 500	1.5×10^6
	ultra-close systems	5×10^6(?)	5×10^6(?)	$< 10^{-4}$	< 500	---

There is another factor that may render a considerable fraction of the systems unobservable. Helium star plus neutron star systems with $M_{He} < 3.5\ M_\odot$ might undergo a second phase of spiral-in (CE evolution) during helium-shell burning, since later in life the envelopes of such helium stars expand to large radii (cf. Delgado & Thomas 1978; Habets 1985,1986; see Fig. 8). This was pointed out by Phinney (1991) and the effects on the production of double neutron stars were worked out by Van den Heuvel (1992) and Tutukov & Yungelson (1993). During this second spiral-in phase, the orbital periods of these systems might shrink by another factor of 5 to 10 (Van den Heuvel 1992). As the orbital periods after the first spiral-in phase are expected to be of the order of a few hours (PSR 1913+16 had P = 1.5 h just before the second supernova explosion), those after the second spiral-in will be of the order of 10 to 20 minutes. After the second supernova the

Table 2: The 24 binary pulsars with nearly circular orbits and low mass companions

Pulsar name PSR	P (ms)	$\dot{P}$ (10^{-19})	B_s (G)	P_{orb} (d)	e	M_{cf} ($M_\odot$)	ΔM_t ($M_\odot$)	ΔM ($M_\odot$)	Ref.
B0021-72E°	3.536			2.22	0.05	0.19*	>0.7	>0.7	1
B0021-72I°	3.48			0.23	0.0	0.02*	>0.7?	>0.7?	2
B0021-72J°	2.101			0.1207	0.00	0.03*	>0.7?	>0.7?	1
J0034-05	1.887	0.067	1.1×10^{8}	1.589	$<10^{-4}$	0.17*	>0.7	>0.7	3
J0214+42	2.32			2.029	0.0	0.20*	>0.7	>0.7	4
J0437-4715	5.7575	0.4	4.9×10^{8}	5.7410	1.8×10^{-5}	0.23*	>0.77	>0.77	1
B0820+02	864.872	1.04×10^{-3}	3.0×10^{11}	1232.47	1.19×10^{-2}	0.45	0.55	0.04	1
J1045-45	7.45		3.8×10^{8}	4.09	1.9×10^{-5}	0.19*	>0.7	>0.7	3
B1310+18°	33.16			255.8	0.00	0.36*	0.56	0.34	1
J1620-26°	11.08	8.16	3.0×10^{9b}	191.4428	0.025	0.33*	0.57	0.45	1
J1639+36B°	3.528			1.2591	<0.001	0.19*	>0.7	>0.7	1
J1713+074	4.57014	0.085	2.0×10^{8}	67.8	7.5×10^{-5}	0.28	0.72	0.65	5
B1718-19°	1004.0	1.59×10^{4}	1.28×10^{12}	0.258	0.000	0.14*	>0.7	>0.7	1
B1744-24A[a,o]	11.56	-1.9×10^{-1}	?	0.0756	0.000	0.10*	>0.7	>0.7	1
B1800-27	334.415	1.73×10^{2}	7.7×10^{10}	406.781	5.07×10^{-4}	0.36	0.64	0.18	1
B1831-00	520.95	1.43×10^{2}	8.7×10^{10}	1.8111	0.000(4)	0.20	0.80	0.80	1
B1855+09	5.362	0.1784	3.1×10^{8}	12.237	2.17×10^{-5}	0.25	0.75	0.75	1
B1908+00°	3.6185			0.141	$<10^{-2}$	0.02*	>0.7	0.7	2
B1953+29	6.1331	0.295	4.3×10^{8}	117.349	3.3×10^{-4}	0.31	0.69	0.59	1
B1957+20[a]	1.6074	0.168	1.66×10^{8}	0.382	$\leq5\times10^{-6}$	<0.06	?	?	1
J2019+24	3.9345	0.083	1.82×10^{8}	76.51163	1.11×10^{-4}	0.29	0.71	0.65	1
J2146-07	16.05			6.839	2.1×10^{-5}	0.51*	?	?	3
J2229+26	2.98			93.016	2.56×10^{-4}	0.30*	0.7	0.7	2
J2317+14	3.445	0.046	1.27×10^{8}	2.45	1.2×10^{-6}	0.21*	0.79	0.79	6

a='evaporating' companion; *b*=upper limit to B_s derived from spin-up line is 7×10^{9}G; o=Globular Cluster. B and J indicate 1950.0 and 2000.0 coordinates respectively. The companion masses M_{cf} are consistent with the observed mass functions of the systems. Values without an asterisk ($\star$) were estimated on the basis of evolutionary computations for Low Mass X-ray binaries (LMXBs), as described in the text. Values with an asterisk are 50% probability estimates, derived from the mass function. The transferred amounts of mass ΔM_t and the amount ΔM accreted by the neutron stars were derived from evolutionary computations, assuming an initial companion mass of $1M_\odot$ for the systems in the Galactic disk and $0.9M_\odot$ for systems in globular clusters. For systems with $P_{orb} < 0.7^d$, M_{cf} is expected to be $<0.2M_\odot$, but no precise estimate of its value can be given. In the calculations of ΔM it was assumed that the neutron star was present from the start of the mass-transfer phase. *References:* 1. Taylor et al. (1993), and references therein; 2. F. Camilo (private communication); 3. Bailes et al. (1994); 4. De Bruin (private communication); 5. Foster et al. (1993); 6. Nice et al. (1993).

resulting binary periods of the very elliptic double neutron star binaries will be about 30 to 60 minutes. The orbits of such systems will decay very rapidly by gravitational radiation losses, on a timescale of order 5×10^6 yrs or less. With a lifetime of 5×10^6 yrs for the bulk of the double neutron stars, a birth rate of 10^{-4} yr^{-1} in the Galaxy will result in a steady-state population of such systems of only 500 at any time. As the observable galactic pulsar population has been estimated to be of order 3×10^5, of which at present about 600 have been discovered, we presently observe about one out of 500 of the entire galactic pulsar population. Thus, if the population of strong-field and/or ultrashort-orbital period neutron star binaries is < 500, it is not at all surprising that so far we have not seen any of these. If the birth rate of close double neutron stars is indeed 10^{-4} yr^{-1}, as predicted by the population-synthesis models, it is, in view of the above, to be expected that in future pulsar searches, within a few years one or two such ultrashort period systems may be discovered.

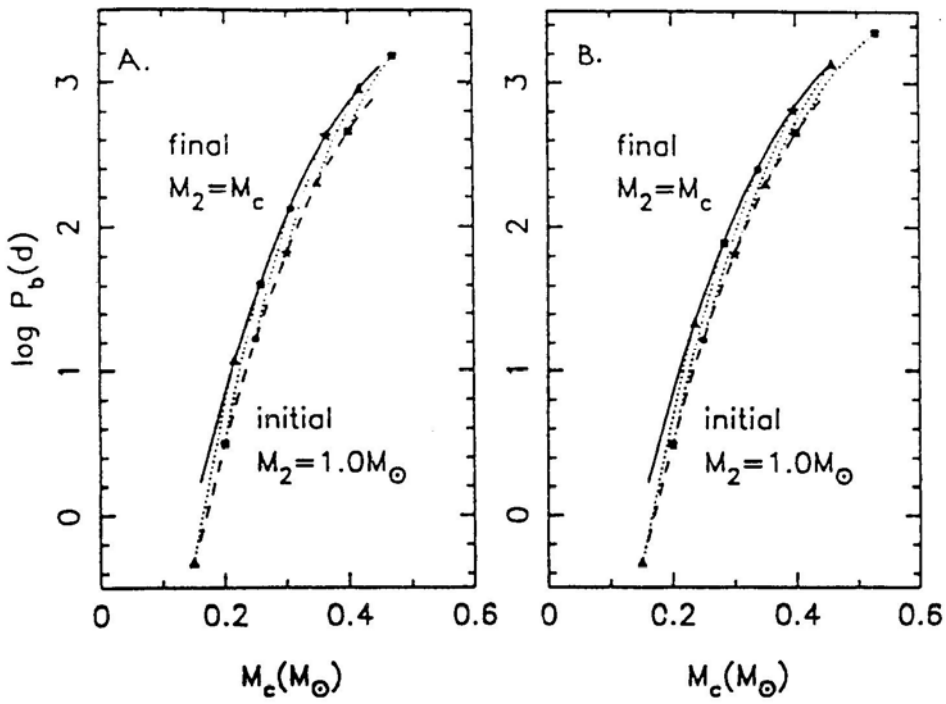

Figure 9: Orbital-period evolution of low-mass X-ray binaries in which the mass transfer is driven by the evolutionary expansion of an evolved companion, in this case a low-mass giant of one solar mass (M_2-initial). In the left-hand picture the accreting star is a 1.4 $M_\odot$ neutron star, in the right-hand picture a 7 $M_\odot$black hole. The dashed lines are the orbital periods at the onset of the mass transfer, the fully drawn curves give the final orbital periods. Dotted lines indicate the evolution of the orbital periods for six different systems. Assumed is Z – 0.02 (after Verbunt, unpublished).

Table I (after Van den Heuvel 1994) summarizes the birth rates of observed and of potentially observable types of double neutron star systems in the Galaxy. It may be that the above quoted numbers are a factor of five too large as very recent estimates of the galactic pulsar birthrate suggest a total galactic number of 'living' pulsars of only 6.10^4, instead of the above used number of 3.10^5 (M. Bailes, priv. comm.). In that case the birthrates and numbers of the hypothetical systems in table I should be reduced by a factor of five.

4. Low-mass Binary Radio Pulsars

4.1 *Introduction*

In the presently known literature there are 24 systems of this class, listed in Table II, of which a number are depicted in the right hand frame of Fig. 3. As mentioned in Section 2, the evolutionary history of the wider systems among them (P > 30 - 40d) was immediately understood at the time of their discovery: they are the products of the later evolution of fairly wide LMXB, in which the donor star did not fill its Roche lobe before it had terminated core-hydrogen burning. In such stars, if M < 2.3 $M_\odot$, the helium core is degenerate and energy is generated by hydrogen burning in a shell around this core. For such stars there is a simple relation between the outer radius R and the mass M_c of the degenerate helium core (Refsdal & Weigert 1971), regardless of the mass of the hydrogen-rich envelope. Thus, when such a low-mass (sub-)giant star evolves, its outer radius gradually increases, due to the gradual growth of the mass of the helium core. When these stars are donor stars in accreting binary systems, and are less massive than the neutron star, the mass transfer will make the orbit expand, such that the orbital evolution can - at any time - remain in pace with the evolution of the donor star. The evolution ends when the entire hydrogen-rich envelope of the donor has been transferred. The final orbital period is uniquely determined by the mass M_c of the final helium white dwarf remnant (Joss *et al*. 1987; Verbunt 1990, 1993). This is obvious, since still a few hundredth of a solar mass of hydrogen is present around this core, its radius R is still determined by M_c : $R = R(M_C)$. As this radius equals that of the Roche lobe R_L, and the ratio R_L/a is a function only of the mass ratio M_c/M_n (e.g., Paczynski 1971):

$$R_L/a = 0.46[M_c/(M_c + M_n)]^{1/3} \quad (2)$$

one will have that, through RL = $R(M_C)$ - the final orbital separation a and orbital period P will depend only on M_C (for a given neutron star mass). This relation is listed, for example, by Joss *et al.* (1987). Because of the above, for a given initial donor mass and initial orbital period, the final orbital period is uniquely determined. Fig. 9 shows for example such relations for $M_d = M_\odot$, $M_n = 1.4M_\odot$, after Verbunt (priv. comm.). The figure shows that even for , P_O as short as 0.5 d, the final orbital periods predicted by such models are still > 15 d. However, as Fig. 3 and 12 show, many of the LMBP in the galactic disk (and also in globular clusters) with circular orbits and low-mass helium white-dwarf companions have orbital periods between 1 and 15 days. How can these short periods for the galactic disk systems be explained? (In globular clusters it

is possible that the evolution has been modified by collisions with other stars, but in the galactic disk this is not possible.) The answer is that systems with short initial periods, in the range 0.5 d to 2 d will not simply evolve with conservation of orbital angular momentum, as suggested in Fig. 9, since these slowly evolving short-period systems will also suffer losses of orbital angular momentum by a magnetically coupled stellar wind, so-called 'magnetic braking' (MB), cf. Verbunt & Zwaan (1981). [For still shorter initial orbital periods, the systems will also lose angular momentum by gravitational waves; due to these combined angular-momentum losses such systems will always evolve to shorter orbital periods. For a review, see Verbunt (1993)]. Therefore, for Po $\lesssim$ 0.5 to 2 d, the orbital evolution picture of Fig. 9 is too simplified.

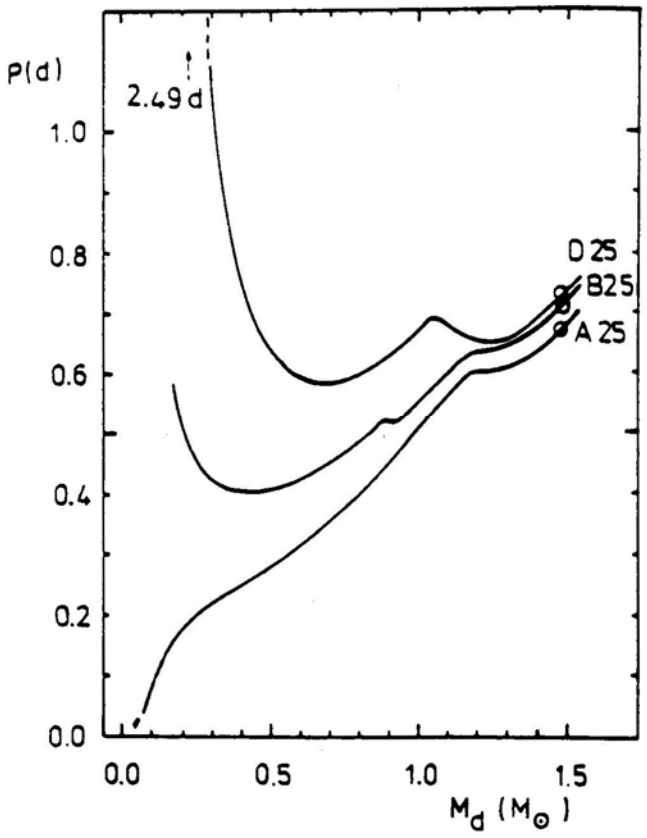

Figure 10: Evolution of the orbital period during mass exchange, as a function of decreasing donor star mass for three systems with initial donor mass 1.50 $M_\odot$; effects of magnetic braking and interior nuclear evolution of the donor are included. The systems A25) B25 and D25 have initial orbital periods of 0.7045, 0.7460 and 0.7609 days respect tively. The latter two periods are just above the bifurcation period, the first one is below it. After Pylyser & Savonye (1988) (further explanation in the text).

Table 3: The relation between initial and final orbital period (P_i and P_f, respectively) and between final orbital period and final white dwarf companion mass, for binary millisecond pulsars with helium white dwarf companions, as calculated by the authors (see figures 11, 12). The initial companion mass was $1M_\odot$ and the initial neutron star mass $1.4M_\odot$. Magnetic braking was included in the calculations.

P_i(d)	P_f(d)	$M_{wd}(M_\odot)$
0.783	1.154	0.187
0.890	3.101	0.217
1.130	8.508	0.243
1.914	18.86	0.267

4.2 *Evolution of systems with initial orbital periods shorter than a few days*

The first calculations of evolution of such systems in which the effects of MB angular momentum losses were included, were carried out by Pylyser & Savonije (1988, 1989). They showed that, for any given set of initial values of the masses (M_d, M_a), and an adopted MB-law, there is a bifurcation initial orbital period $P_O(b)$, such that for $P_O > P_O(b)$ the systems in the end evolve towards longer orbital periods (though less rapidly than if only the interior evolution of the donor played a role), whereas for $P_O < P_O(b)$ the angular-momentum loss effects dominate over the tendency of the interior evolution to make the orbit expand, and the systems evolve to shorter and shorter orbital periods. As an example, Fig. 10 shows the evolution of systems with $M_d(0) = 1.5\ M_\odot$, $M_a = M_\odot$. The figure shows that the bifurcation period $P_O(b)$ is about 0.75 d in this case. Notice that for P_O slightly above $P_O(b)$ final orbital periods as short as $P_f = 0.6$ d ($M_c = 0.17\ M_\odot$), and $P_f = 2.69$ d ($M_c = 0.21\ M_\odot$) are reached, i.e., much shorter than 15 d, and in the range where a number of systems in Fig. 3b are located. Fig. 11 and 12 similarly show the evolution of four systems with initial component masses $M_d = M_\odot$, $M_a = 1.4\ M_\odot$, for four different initial orbital periods, calculated by Van den Heuvel & Bitzaraki (1994). Fig. 11 shows the evolutionary tracks of the donor stars in the HR diagram, and Fig. 12 shows the evolution of their orbital periods as a function of the (decreasing) donor mass. One clearly observes here the relation between final donor mass and final orbital period, described in Section 4.1. The relation obtained here is given in Table III. By interpolation between these values, one can precisely predict the masses of the white-dwarf companions for the LMBP with orbital periods in the range 1 d to 15 d. For example, for PSR 1855+09 we obtain $M_c = 0.25\ M_\odot$ and for PSR 1831–00 $M_c = 0.20\ M_\odot$.

4.3 *The birth rate problems for LMBP*

4.3.1 Do we know all the types of progenitors?

As pointed out in Section 4.1, the core-mass versus radius relation $R(M_c)$ is independent of the envelope mass for stars in the mass range $< 2.3\ M_\odot$. Thus, for the

LMBP there is no way to infer, from their presently observed orbital period and corresponding M_c, what the initial mass of the donor has been. It may have been a star of 0.9 $M_\odot$ as well as one of almost 2.3 $M_\odot$. In the case M_d = $M_\odot$, as the donor is less massive than the neutron star (which has M = 1.2-1.4 $M_\odot$), the mass transfer is stable and takes place on a nuclear timescale, i.e., is long-lasting (of order 10^8 yr if the initial orbital period is <10 d). Thus, in this case a long-lived LMXB phase occurs before the system becomes a LMBP. As the mass-transfer rate in systems with final periods P_f < 150 – 200 d was always < M_{Edd}, most of the matter transferred in the system will have been accreted by the neutron star, such that this star can easily be spun up to periods of order of milliseconds. [The suggestions that the X-ray phase may last much shorter than 10^8 years, due to short-lasting heating-induced rapid expansion phases of the donor, during which $\dot{M}$ is very high, alternated by long-lasting detached phases (Harpaz & Rappaport 1991; Podsiadlowski 1991) are quite debatable. New calculations with one-sided heating, by Hameury & Lasota (1993) do not support these models: with one-sided heating there is negligible energy transfer from the heated side to the dark side, in view of the very short radiative cooling times of the outer layers, and it seems impossible to make the entire star swell up, as in the older above-mentioned calculations, where the heating was assumed to be all around the star. So, there are not expected to be short-lasting bloated phases of the companion, interrupted by long-lasting off-phases: the X-ray phase is continuous and long-lasting, as in the cases where heating was ignored.]

Thus, the end product of the evolution of the wider LMXB is likely to be a LMBP with a spin period in the millisecond range. However, there is no reason why the reverse should also be true: also systems in which the donor star has a mass $\lesssim$ 2 $M_\odot$ will produce LMBP, but in such systems a long-lasting X-ray phase may be absent, because, since $M_d > M_a$, the mass transfer occurs on a (short) thermal timescale:

$$\tau_{th} = \frac{3 \times 10^7 \text{ yrs}}{(M/M_\odot)^2} \tag{3}$$

which results in a mass transfer rate

$$\dot{M}_{th} = \frac{0.8(M/M_\odot)^3}{3 \times 10^7} (M_\odot/\text{yr}) \tag{4}$$

For M_d = 2$M_\odot$ this rate is 2×10^{-7} $M_\odot$ y^{-1} = 10 $\dot{M}_{Edd}$. This thermal-timescale mass transfer phase is preceded by a short-lasting phase of 'beginning Roche-lobe overflow' during which $\dot{M}$ is still < $\dot{M}_{Edd}$, and the system appears as an X-ray source. For $M_d \simeq 2M_\odot$ this phase may last only of order a few times 10^5 yrs (Savonije 1983). The only known X-ray binary of this type in the Galaxy is Hercules X-l. Assuming the X-ray lifetime of the ordinary LMXB with M_d = $M_\odot$ to be of order 10^8 yrs, one observes that the ratio of the birth rates of Her X-l type systems and of these LMXB is roughly given by:

$$\frac{r_{HerX-1}}{r_{LMXB}} = \frac{N_{HerX-1}}{N_{LMXB}} \times \frac{t_{LMXB}}{t_{HerX-1}} \tag{5}$$

where N_{HerX-1} and N_{LMXB} denote the galactic numbers of Her X-l type systems and LMXB, respectively, and t indicates their respective lifetimes. Thus, since

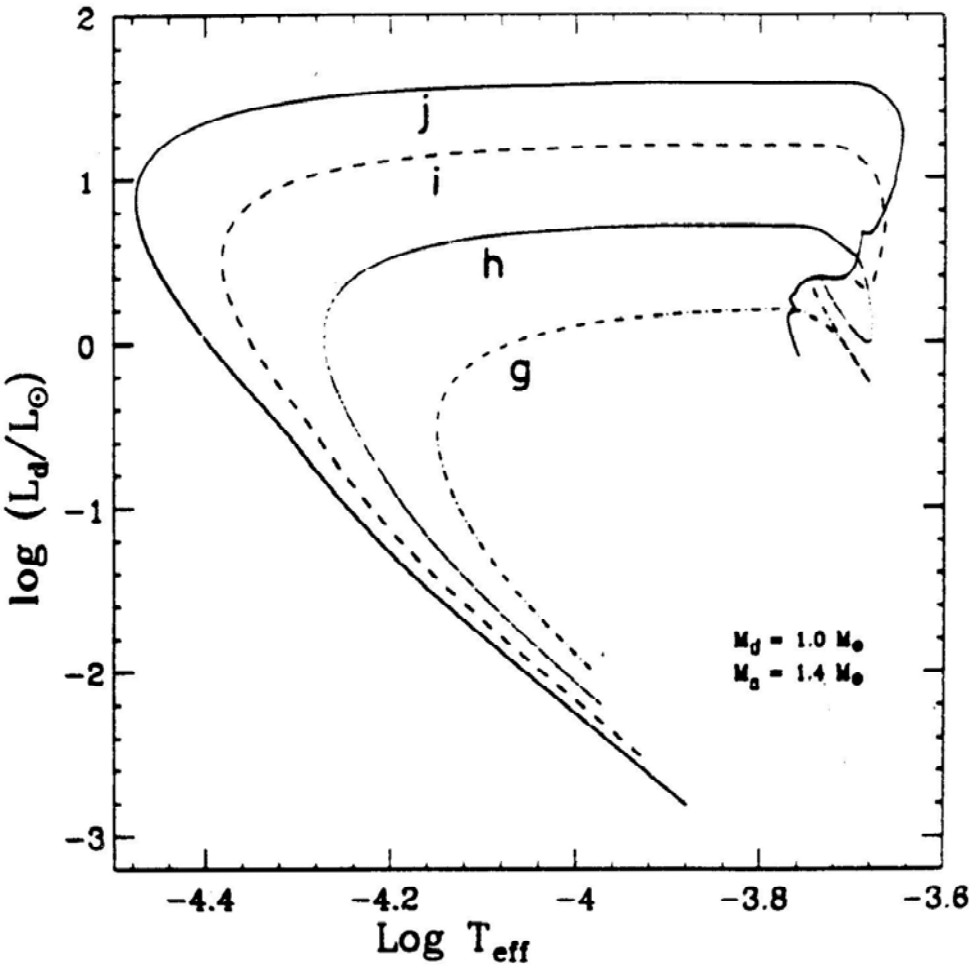

Figure 11: Evolutionary tracks in the Hertzsprung-Russel diagram of the donor stars in four LMXBs in which the mass transfer started after the donor left the main-sequence, and the effects of magnetic braking were included. All systems started out with a donor mass of $M_{\odot}$ and an accretor of 1.4 $M_{\odot}$. the mass transfer is assumed to be conservative (calculation by Van den Heuvel & Bitazaraki 1994). The intial and final orbital periods of the systems are given in Table III. The donor stars all end as helium white dwarfs.

Her X-l is the only system of its type known in the Galaxy, and the number of LMXB is estimated to be 1.3×10^2, one has, with $t_{\mathrm{HerX\text{-}1}} = 3 \times 10^5$ yrs, that, roughly:

$$\frac{\tau_{\mathrm{HerX-1}}}{\tau_{\mathrm{LMXB}}} = 3 \tag{6}$$

Consequently, even though Her X-1 systems are extremely rare, their short X-ray lifetimes imply that they may well make a three times larger contribution

to the LMBP birth rate than the ordinary LMXB. This is quite important since only a fraction of the ~ 130 LMXB in the Galaxy have orbital periods such (i.e. > 0.7 d) that later in life they will produce a LMBP. This fraction is probably not larger than 0.3 or 0.4 (cf. Van Paradijs 1994). So, this additional reservoir of LMBP progenitors is very welcome (see next section). It should be further pointed out here that systems like Her X-l, after the phase of rapid thermal-timescale mass transfer, in which about 1 $M_\odot$ is transferred in a few million years, may go through a long-lasting phase of slow mass transfer, on a nuclear timescale, in which they will resemble wider LMXB such as Cygnus X-2 (cf. Van den Heuvel 1981a,b, and the Appendix). Most of the mass transferred during the rapid-transfer phase will be lost from the system. The amount transferred on a nuclear time scale may, however, still be of order 0.5 $M_\odot$, and this phase, in which the system resembles Cyg X-2 (which has an F-subgiant companion) may still last several tens of millions of years (see the Appendix).

4.3.2 The P_{spin} vs. P_{orb} diagrams and B vs. P_{orb} diagrams for LMBP: evidence for accretion-induced magnetic field decay and for the occurrence of neutron star formation by accretion induced collapse?

Figures 13a,b show plots of $P_{\rm spin}$ vs. $P_{\rm orb}$, and, for those cases where P has been measured, of B vs. $P_{\rm orb}$, for the 23 LMBP systems for which data are available in the literature (Van den Heuvel & Bitzaraki 1994). Table II lists the relevant observational data on these systems. Filled circles indicate systems in the galactic disk, open circles are systems in globular clusters. The figures show that, with the exception of only one globular cluster system (PSR 1718–19) and one disk-system (PSR 1831–00), the LMBP show a clear correlation between $P_{\rm spin}$ and $P_{\rm orb}$, between B and $P_{\rm orb}$, respectively, as tentatively outlined by the solid curves in the diagrams. At the top of the figure we have indicated the theoretically estimated amounts of mass accreted by the neutron stars in these systems. These amounts were calculated by assuming: (i) that the donor stars started out with a mass of 1.0 $M_\odot$, (ii) that the neutron stars were present in the systems from the onset of the mass transfer (i.e., that they were not formed during the mass transfer process itself, by the accretion-induced collapse of a white dwarf), and (iii) the neutron stars could never accrete more than the Eddington-limiting rate of 1.5×10^{-8} $M_\odot$ y^{-1}; in phases were the mass-transfer rate was higher than this value, the excess amount of transferred mass was assumed to have been lost from the systems.

We now only consider the systems in the galactic disk, since the evolution and the mass transfer of the globular-cluster systems may have been strongly affected by dynamical effects (encounters) in the clusters.

If one ignores, for the moment, the one discordant disk system PSR 1831–00 (see below), one observes that there is a very clear correlation between magnetic field strength and amount of matter accreted onto the neutron star: all disk neutron stars that accreted more than about 0.1 $M_\odot$ have field strengths below 10^9 G. The amazing thing is, that for accreted amounts above about 0.45 $M_\odot$ the field strengths reach apparently a 'bottom' value of a few times 10^8 G, that does not decrease any further with increasing amounts of matter accreted, up to about 0.7

$M_{\odot}$. On the other hand, in the range of accreted amounts between zero and 0.45 $M_{\odot}$, there is a sharp decrease in field strength with amount of matter accreted.

It will be clear that the relation between B and P_{orb} is the more fundamental one of the two: once B is low ($< 10^9$ G), and the accreted amount is more than 0.03 $M_{\odot}$, the neutron star will have been spun-up to a period shorter than 10 ms. So, the relation between P_{spin} and P_{orb} in Fig. 13a is a consequence of the relation between B and P_{orb} in Fig. 13b.

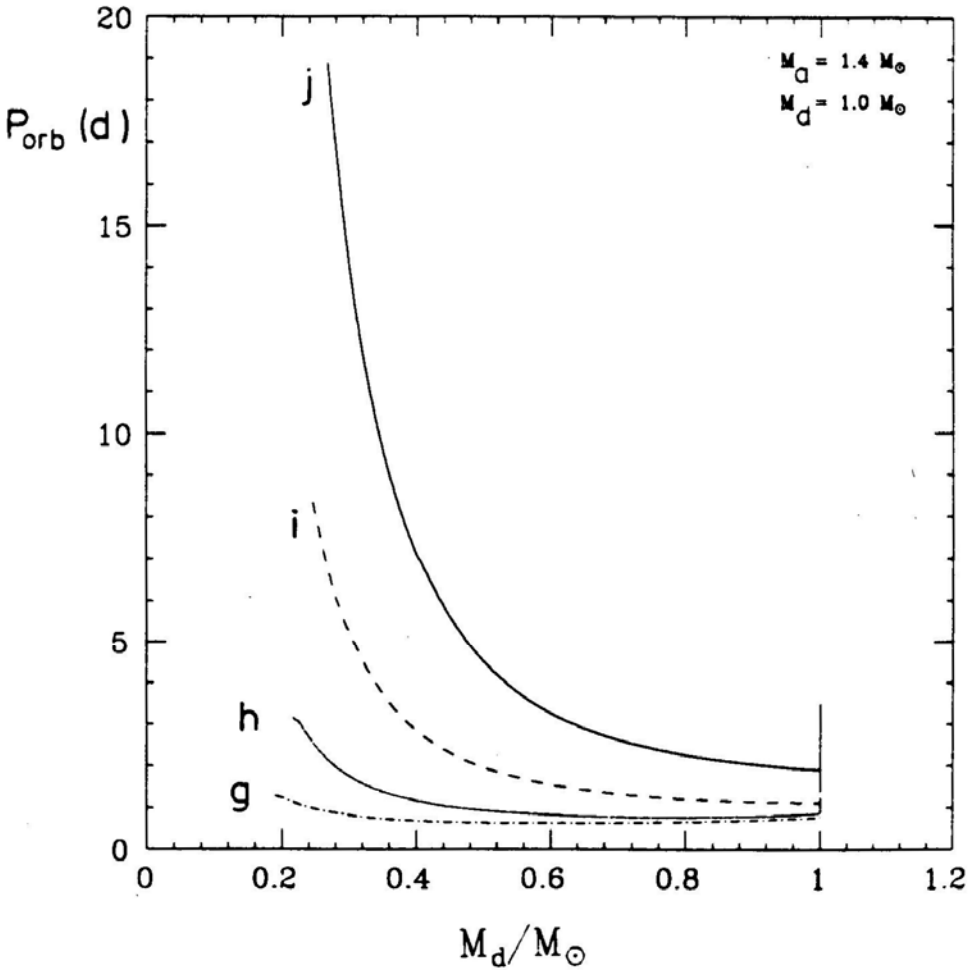

Figure 12: The evolution of the orbital periods of the systems of figure 11.

Concerning the two discordant systems in Fig. 13b: because of the capture processes that occur in globular clusters, the globular-cluster system PSR 1718–19 might have been produced by a recent capture event, i.e., here the star may not have accreted the amount that we calculated under the abovementioned assumptions. On the other hand, for the system PSR 183–100 there is no way out, it seems: in view of its short orbital, period, the mass transfer rate in this system

must always have been below the Eddington-limit rate (assuming the companion to have started out with a mass below about 1.3 $M_\odot$). So, if the neutron star was present in the system throughout the mass transfer phase, it must have accreted more than 0.7 $M_\odot$, and it seems very difficult to understand why its field has not decayed to below 10^9 G.

We see only two possible ways out of this dilemma, which we will now briefly discuss: (i) The accretion of a large amount of matter does not *always* result in substantial decay of the magnetic dipole moment of the star; this is the case, for example in the 'plate tectonics' models for the decay of the dipole moment suggested by Ruderman (Chen & Ruderman 1993). In these models the final dipole moment depends on the initial field configuration with respect to rotation axis and, if the two magnetic poles were located initially in different rotational hemispheres of the star the dipole moment does not decay much, even if much accretion took place.

(ii) The neutron star was not present throughout the entire mass transfer phase, but was formed only near the end of the mass transfer phase, by the accretion-induced collapse of a white dwarf; the newly formed neutron star had a strong field, and after its formation the mass transfer phase was already almost over, such that subsequently it did not accrete enough to induce substantial field decay. (There is no physical reason why accretion-induced collapse would lead to the formation of a weakly-magnetized neutron star, as suggested on an ad-hoc basis by, e.g., Baylin & Grindlay 1990).

(One might also think as a third possibility that the donor star started out witha mass of 2 $M_\odot$ or larger, and that this would have led to a such short-lasting mass transfer phase that the neutron star would hardly have accreted anything. However, this solution does not work, since, as pointed out above, the thermal time scale mass-transfer phase will be followed by a nuclear time scale phase, in which still several tenths of a solar mass are slowly transferred, which may all be accreted by the neutron star; see Appendix).

In our opinion the second possibility is the most likely one here. This is because -in terms of the plate-tectonics model - it would seem quite amazing that in only one out of the more than a dozen neutron stars (depicted in Fig. 13b) the initial field configuration would be such that upon accretion the field would not decay. If the plate tectonics model would be the right explanation for the decay of the dipole moments of a fraction of the accreting neutron stars, then one would, statistically, expect a higher fraction (for geometrical reasons, of order fifty percent) of neutron stars to have retained a strong dipole moment. It seems to us hard to understand why in that case only one out of a dozen accreting neutron stars has retained a strong field.

Therefore, in our opinion, the very strong magnetic field of PSR 1831–00 is a strong indication that this neutron star was formed during the mass-transfer phase by the accretion-induced collapse of a massive white dwarf. (In fact, the nova-like system GK Persei seems like an excellent progenitor for this system. Its orbital period is more than a day and its white dwarf is quite massive.) This is – to our knowledge - so far the strongest indication for the occurrence of neutron-star formation by accretion-induced collapse.

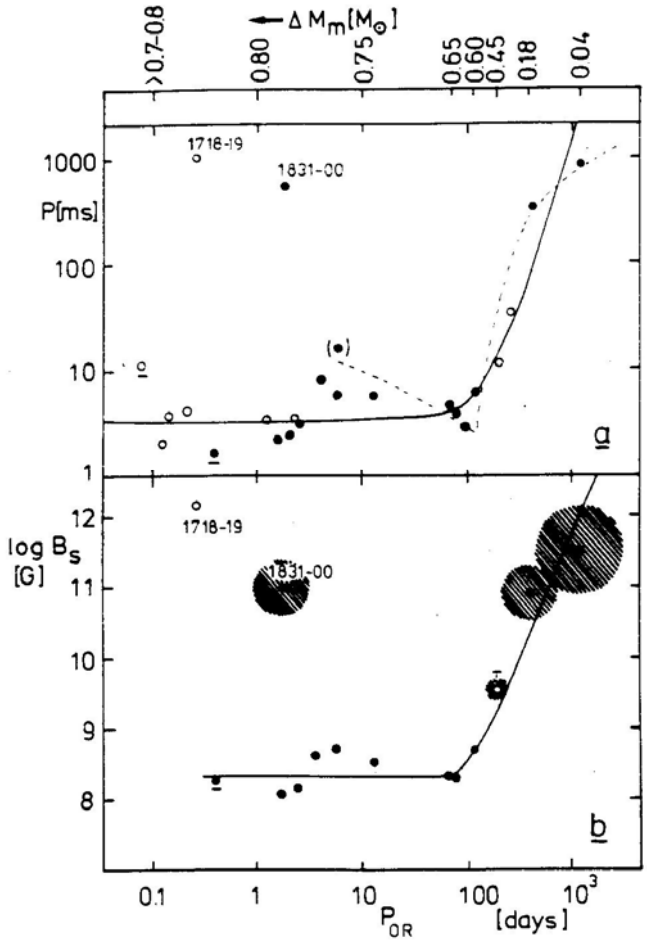

Figure 13: (a) The spin period vs. orbital period diagram for binary radio pulsars with circular orbits and low-mass companions. Pulsars in globular clusters are indicated by open circles, those in the galactic disk by filled circles. Systems with evaporating companions are underlined. (b) The magnetic field strength vs. orbital period diagram for those systems where the field strength is known (for 1620–26 an upper limit to the field is given derived from the spin up line). In both diagrams the solid curves indicate the best-fit to the observations, if the systems 1830–00 and 1718–19 are excluded. At the top of the figure the amounts of mass acccreted by the neutron star during the preceding LMXB phase is indicated, assuming that the neutron star was present from the onset of the mass-transfer phase, and never accreted more than the Eddington-limit rate (after Van den Heuvel & Bitzaraki 1994). The hatched circles around four strong-field pulsars indicate their individual birth rates ((:)B), relative to that of a pulsar with B = 2.10^8G (the circle-radius is taken proportional to the one-third power of the birth rate, with circles of $B = 2 \times 10^8$ G as unity; further explanation in the text).

4.3.3 The birth rates of the various types of LMBP

The B vs. P_{orb} diagram in Fig. 13b contains important information on the birth rates of the various types of LMBP systems. All presently available evidence indicates that without accretion the magnetic fields of pulsars do not decay (see Bhattacharya, this volume). It is then simple to show that if radio pulsars are born with an arbitrarily short spin period the time they need to reach the death line (the position of which in the B vs. P diagram is given by the equation: B/P^2 = constant) is inversely proportional to the magnetic field strength:

$$T_{to} = \frac{\text{constant}}{B} \tag{7}$$

For millisecond pulsars, with $B \simeq 3 \times 10^8$ G, this implies $T_{to} = 3 \times 10^{10}$ yrs, whereas a pulsar with a canonical field strength $B = 2 \times 10^{12}$ G turns off in 5×10^6 yrs. Thus, the birth rates of the strong-field LMBP (which we will abbreviate as SF-LMBP) in the diagram shown in Fig. 13b must be much higher than those of the millisecond pulsars in this diagram. The two systems PSR 1831–00 ($B = 0.87 \times 10^{11}$ G) and PSR 0820+02 ($B = 3 \times 10^{11}$ G) have turn-off lifetimes of 10^8 yrs and 3×10^7 yrs, respectively, whereas the turnoff times of the 14 ms pulsars are 3×10^{10} yrs. So the ratio of the birth rates of these two types of LMBP is given by

$$\frac{r_{SF-LMBP}}{r_{ms-LMBP}} = \left(\sum_i N_{SF-LMBP(i)} / T_{SF-LMBP(i)} \right) / \left(N_{ms-LMBP} / T_{ms-LMBP} \right) \tag{8}$$

where i stands for each of the 3 SFLMBP (in view of their slightly different lifetimes this sum has to be made). This results into:

$$\frac{r_{SF-LMBP}}{r_{ms-LMBP}} = 190$$

Thus, the 3 SF-LMBP have an about two hundred times higher birth rate than the 14 millisecond LMBP systems. We thus see that, although there are only three of these systems known, in terms of birth rate they vastly outnumber the millisecond pulsars in low-mass binaries.

4.3.4 The relation between the ms-LMBP and the 'classical' LMXB

The birth rate of the millisecond LMBP can be estimated from the finding by Stokes *et al.* (1986) that in an unbiased complete Arecibo survey of a part of the sky, some ten per cent of the pulsars detected turned out to be ms pulsars (3 pulsars, of which 2 in binaries, out of a total of 24 detected pulsars). With an estimated total number of 3×10^5 active pulsars in the Galaxy, this leads to a number of approximately 3×10^4 ms pulsars in the Galaxy. Since their turn-off time exceeds the Hubble time, we can estimate their birth rate by dividing this number by the Hubble time. Assuming the latter to be 1.5×10^{10} yrs, one obtains a millisecond pulsar birth rate of 2×10^{-6} y^{-1}.

This is remarkably close to the estimated birth rate of the LMXBs, which with an estimated active lifetime of about 10^8 yrs and a galactic number of 130, have a

birth rate of 1.3×10^{-6} yr^{-1}. However, not more than one third of the LMXB that we know have orbital periods long enough (> 0.7 d) to produce an LMBP. Thus, the LMBP birth rate expected from these LMXB-systems is 0.4×10^{-6} yr^{-1}, i.e., about one fifth only of the observed LMBP birth rate. As we argued above in Section 4.3.1., the birth rate of Her X-l type systems (i.e., systems with donors in the mass range 1.4 – 2.3 $M_\odot$) is some three times higher than that of the classical LMXBs, and also the neutron stars in these systems will have enough accretion to be turned into millisecond pulsars (see section 4.3.1.). Combined with the 'classical' LMXB birth rate this provides a total ms-LMBP birth rate of just about 2×10^{-6} yr^{-1}!

We thus come to the remarkable conclusion that only about one fifth of the LMBP come from the 'classical' LMXB and eighty per cent from Her X-l type systems.

As to the SF-LMBP, their surprisingly large birth rate of 4×10^{-4} yr^{-1} in the galactic disk shows that for these systems a category of progenitors different from the LMXB is required, with an about 100 times larger birth rate.

4.3.5 The birth rate and possible progenitors of the SF-LMBP: a high fraction of all Supernovae

We will consider this problem in two different ways, as follows: (a) by deriving some general statements about the birth rates of the progenitors of the SF-LMBP; (b) by searching to identify specific types of progenitor systems.

As to (a): The Supernovae that gave rise to the progenitors of the SF-LMBP took place in binaries in which the companion of the supernova was of relatively low mass (< 2.3 $M_\odot$) while the orbital period was of order of a day or longer. Taking into account the mean random kick velocity of 450 ± 90 km/s that neutron stars appear to receive at birth (Lyne &· Lorimer 1994), only a small fraction of these systems, of order 10^{-1} will have remained bound after the explosion, if these kicks are indeed randomly directed. This then leads to the quite amazing conclusion that the birth rate of these progenitor systems, consisting of a collapsing star and a low-mass star (< 2.3 $M_\odot$) in the Galaxy must be of the order of 4×10^{-3} yr^{-1}, in order to obtain a birth rate of 4×10^{-4} yr^{-1} for the SF-LMBP. Thus, the birth rate of the progenitors of the SF-LMBP is almost of the same order as the total galactic supernova rate! This then leads to the conclusion that a sizeable fraction of all galactic Supernovae (of order > 20 percent) must be taking place in close binaries in which the companion to the supernova is a low-mass star.

Note that this conclusion is derived purely from the observations of SF-LMBP, in combination with the observed fact that high kick velocities are imparted to neutron stars at birth.

On purely theoretical grounds, and on the basis of entirely different reasoning we had reached quite similar conclusions in the past (Van den Heuvel 1981ab): these supernovae with close low-mass companions are the post-spiral-in remnants of relatively wide high-mass binary systems in which the companion was a low-mass main-sequence star. They are the high-mass analogues of the CV-binaries. From the observed distributions of mass ratios and separations of unevolved massive binaries we argued that a considerable fraction of all supernovae must take place

in such post-spiral-in systems. This seems now to be confirmed.

The above inferred high birth rate of the progenitors of the SFLMBP provides important and independent evidence that among the massive stars (> 8 – 10 $M_\odot$) low-mass companions (< 2.3 $M_\odot$) in relatively wide orbits (up to 10 AU) must be common. To have > 20 percent of all Supernovae occur in the post-spiral-in remnants of such systems, some > 20 per cent of the massive stars must have such companions. This is indeed in accordance with all present observational evidence (cf. Tout, 1991; Hogeveen 1991, 1992). Furthermore, a considerable fraction (30%) of the early-type stars have close *massive* companions, which will lead to more-or-less conservative mass exchange and the production of HMXBs. Later on these also spiral in to form systems like Cyg X-3, and, subsequently, double neutron stars or two runaway neutron stars. It, therefore, seems likely that many neutron stars (> 50%) result from ultra-close binaries, either with a low-mass main-sequence star or a neutron star as a companion. Also this idea is not new (Van den Heuvel 1981ab; Meurs & Van den Heuvel 1989), but the above information derived from the SF-LMBP now seems to provide strong independent supporting evidence for it.

5. Possible reasons for the occurrence of 'Bottom Field Strength'

Figure 13b shows that for accreted amounts of matter in excess of about 0.45 $M_\odot$ the field-strengths of the neutron stars do not seem to decay any further, even not if as much-as 0.7 $M_\odot$ has been accreted. The bottom field strength where this 'leveling-off' of the field decay occurs is a few times 10^8 G. This is exactly the field strength where the value of the Alfvén-radius (for accretion rates of order of the Eddington-limiting rate) becomes of the same order as the radius of the neutron star, i.e., about 10-20 km. This means: at this polar strength of the - assumedly dipolar - field the accreted matter will no longer feel much influence of the field, and will no longer be guided in a systematic way by the field to accrete only in two patches near the magnetic poles: at these field strengths the matter will now accrete all over the surface, in a more or less random way.

This suggests that as long as the matter accreted in a systematic way towards patches near the magnetic poles, the accretion causes the field to decay, while for accretion all over the surface, in a more or less random way, the field is no longer induced to decay. The only model for field decay by accretion in the literature that naturally predicts such a difference in field decay between 'ordered polar accretion' and 'random accretion' is the model proposed by Romani (1990). Here the accretion on the two polar patches (that occurs as long as the field is sufficiently strong) pushes the field lines aside and thus dilutes the polar field strengths, and the equatorwards flowing crustal matter pushes the field under in the equatorial regions. This systmatic 'decay' due to the flow of crustal matter away from the poles will stop once the field has reached a strength of a few times 10^8 G, and the accretion begins to occur all over the surface.

We propose here an alternative model for the field decay that will have the same effect, *i.e.* where the decay is due to the channeling of the accreted matter

towards the magnetic poles, and stops once the accretion begins to take place all over the surface. The accretion in LMXB always takes place through a disk. Due to the differential rotation in the disk the fields in the disk will be wound up and increase to their equipartition field strength, such that anywhere in the disk the following expression will hold:

$$\rho\, v^2 = \frac{B^2}{2} \tag{9}$$

The location of the Alfvén surface is given by exactly the same equation, where now B is the strength of dipole field of the neutron star at that place in the disk. This means that at the location of the Alfvén radius, the field in the disk has the same strength as the dipolar field of the neutron star. Blobs of disk matter with fields oriented in the same direction as that of the neutron star at that place will be repelled by the neutron star field, but blobs with oppositely directed fields will be attracted and fall in to the respective magnetic pole. Thus, the poles will preferentially accrete matter with a field direction that is opposite to the field direction of the poles themselves, and at the Alfvén surface has about the same strength as the field of the neutron star. During the infall the surface area of the blob shrinks in such a way that its field strength remains roughly similar to that of the neutron star, all the way down to the surface, where the accreting matter joins the crust. Because of its high electrical conductivity, it will carry with it the currents which generate its field. These currents will be directed opposite to the crustal currents that generate the polar fields of the neutron star. Therefore these polar currents will be gradually neutralized by the accreting matter, causing the polar fields to decay. Clearly, this decay of the polar fields will stop once the guiding of the accreting matter by the polar fields will stop, i.e., when the fields have decayed so far that the Alfvén radius also has become roughly equal to the neutron star radius. Clearly, this model predicts that the field decay will stop once a field strength of order a few times 10^8 G has been reached (the precise value where it stops will depend on the precise value of the accretion rate, which may vary slightly from system to system).

6. Summary and Conclusions

A. *High Mass Binary Pulsar systems*

- With the identification of Cyg X-3 as a Wolf-Rayet binary an important missing link between the HMXB and the double neutron star binaries has been identified.

- Cyg X-3 may well be the 'tip of an iceberg' of some 10^3 to 10^4 helium star plus neutron star systems in the galaxy; those with $M_{\rm He} < 6\ M_\odot$ (59/60 of all) do not have the strong winds required to make them show up as WR stars and to produce an X-ray source. Another 90 per cent of those that have strong enough winds may have neutron stars that spin too fast (due to the preceding spiral-in phase with very large accretion), to presently allow the accretion of matter.

- Similarly, PSR 1913+16 and PSR 1534+12, with their abnormally weak magnetic fields - and, consequently, very long spindown lifetimes - are likely to be the 'tip of an iceberg' of a much larger population of close double neutron stars that

either have (i) strong magnetic fields (> 10^{12} G), and therefore remain observable as pulsars only for < 5 x 10^6 yr before reaching the death line, or: (ii) ultra-short orbital periods (of order a few tens of minutes), as a result of a second spiral-in phase during helium-shell burning. These systems will coalesce due to emission of gravitational waves within a few million years after they were born.

The existence of these theoretically expected systems allows a birth rate of double neutron star systems in the Galaxy of order 10^{-4} yr^{-1} (0.2×10^{-4} yr^{-1} if the observable number of radiopulsars is five times lower than we estimated, see section 3.2.3), without any of the strong-field and/or ultra-short- period systems having been detected so far. With this predicted birth rate, however, one expects systems of these types to be detected in future pulsar surveys rather soon, as their steady-state galactic numbers are expected to be of order 500 (100, in case of a five times lower number of observable pulsars).

B. *Low Mass Binary Pulsar systems*

- The progenitors of the LMBP systems are the neutron star binaries which were born with orbital periods (after tidal circularization) of > 0.7 d and companions less massive than $2.3M_{\odot}$.

- A subset of these, i.e., those with $M_d < M_{ns} = 1.4$ M¤ and $P_{orb} < 15$ d, shows up as long-lived (10^8 yr) accreting LMXB. These are the progenitors of a fraction (roughly 20 %) of the observed millisecond LMBP. The remaining 80% of the ms-LMBP are expected to be the remnants of systems in which the donor had a mass in the range 1.4 to 2.3 $M_{\odot}$ ('Her X-1 type systems'). These systems are expected, after an 10^7 yr phase of highly supercritical accretion, to show up as LMXB for a few times 10^7 yr (see Appendix). The resulting galactic birth rate of ms-LMBP is 2 x 10^{-6} yr^{-1}.

- The strong-field LMBP (SF-LMBP) have a galactic birth rate of about 4×10^{-4} yr^{-1}. With the exception of PSR 1831–00 they started out with orbital periods > 20 d. Assuming that all neutron stars receive a random kick of order 450 km/s at birth, the bulk ($\simeq$ 90%) of the progenitor binaries of such systems were disrupted in the supernova, which implies a birth rate of these progenitor systems of order 4×10^{-3} yr^{-1} in the Galaxy, i.e., almost of the same order as the supernova rate. From this together with the rate of second supernovae in HMXB-descendants we conclude that over 50 percent of the supernovae in the Galaxy take place in post-spiral-in binaries, either with a low-mass main-sequence (<2.3 $M_{\odot}$) companion, or a compact companion (neutron star or black hole).

C. *Field decay*

- Simple models in which the crustal field decays due to ordered accretion onto the magnetic poles, and stops to decay once the ordered accretion stops - i.e., when the Alfvén radius has become roughly equal to the neutron star radius - can successfully explain the existence of a 'bottom' field strength of a few times 10^8 G for accreting neutron stars.

acknowledgements

We are grateful to Mr Hanno Spreeuw for many discussions on the origins of double neutron stars, and to Dr M. Ruderman for a remark on the birth rate of the strong-field LMBP.

7. Appendix: The Evolution of Her X-1 type X-ray Binaries

We assume these to consist of a donor star of mass $m_1 = 2M_\odot$, and an accretor of mass $m_2 = M_\odot$ (a neutron star). Also for slightly different (m_1, m_2) combinations the evolution will proceed similarly to what we will now describe.

As mentioned in Section 4, the mass transfer stage by beginning Roche lobe overflow with $\dot{M} < \dot{M}_{\rm Edd}$ lasts some $(2 - 5) \times 10^5$ yr (Savonije 1983), which is followed by a phase of thermal-timescale mass transfer lasting for about

$$t_{\rm th} = \frac{3 \times 10^7 {\rm yrs}}{(M/M_\odot)^2} = 7.25 \times 10^6 {\rm yr} \tag{10}$$

during which about one solar mass is transferred, with $\dot{M} = 1.4 \times 10^{-7}$ $M_\odot$ yr^{-1} ($= 10$ $\dot{M}_{\rm Edd}$). The neutron star will be unable to accept most of this matter, and over 90 per cent of it is expected to be expelled from the system by the large radiation pressure. Since the matter will first flow to the neutron star before it is expelled, we expect it to be expelled (blown away) with the specific orbital angular momentum of the neutron star. As one can easily derive (e.g., see Bhattacharya & Van den Heuvel 1991) that when the neutron star accretes nothing (a good approximation here) the orbit will change according to the equation:

$$\frac{a}{a_0} = \left(\frac{m_{10}}{m_1}\right)^2 \times \left(\frac{m_{10}+m_2}{m_1+m_2}\right) \times \exp[2(m_1 - m_{10})/m_2] \tag{11}$$

and the orbital period according to the equation:

$$\frac{P}{P_0} = \left(\frac{m_{10}}{m_1}\right)^3 \times \left(\frac{m_{10}+m_2}{m_1+m_2}\right)^2 \times \exp[3(m_1 - m_{10})/m_2] \tag{12}$$

and the Roche lobe radius changes according to:

$$\frac{R_{\rm L}}{R_{\rm L0}} = \left(\frac{m_{10}}{m_1}\right)^{5/3} \left(\frac{m_{10}+m_2}{m_1+m_2}\right)^{4/3} \times \exp[2(m_1 - m_{10})/m_2] \tag{13}$$

Here subscripts zero denote the initial situation.

From these equations one can easily derive that the minimum orbital period reached during the exchange occurs for

$$m_1 = \frac{m_2}{3}\left(\sqrt{10}+1\right) \approx 1.39 m_2 \tag{14}$$

and the minimum Roche-lobe radius for

$$m_1 = \frac{m_2}{4}\left(1+\sqrt{\frac{43}{3}}\right) \approx 1.20 m_2 \tag{15}$$

Now, the stabilization of $\dot{M}$ to a nuclear timescale mass-transfer rate occurs only once m_1 has reached again the same Roche-lobe radius as it had at the onset of the mass transfer (because of the core-mass-radius relation of stars with degenerate helium cores). This occurs in the case we study here for $m_1 = 0.63\ M_\odot$.

Hence, 1.37 $M_\odot$ is transferred on a thermal timescale, and the remaining about 0.35 $M_\odot$ of hydrogen-rich envelope matter of the 0.63 $M_\odot$ remnant is transferred on a nuclear time scale. Adopting the transfer rate of $1.4 \times 10^{-8}\ M_\odot\ yr^{-1}$ of the ($2M_\odot$ +1 $M_\odot$) system of Kippenhahn *et al.* (1967) to also apply here during this phase, the duration of this slow phase is about 2.4×10^7 yrs. Hence, during this phase, Her X-l is expected to have become a 'standard' LMXB with an evolved (subgiant) companion of mass < 0.7 $M_\odot$, resembling a system like Cygnus X-2 (P_{orb} = 9.8 d). Adopting the orbit to change according to Eq. (10) until m_1 = 0.63 $M_\odot$, and conservatively afterwards, one obtains that the ratio of final orbital period P_f to initial orbital period P_0 is about 9.8. Hence, with Po = 1.7 d, as in the case of Her X-l, one obtains P_f = 16.7 d. If the initial period were 1.0 d, the final period, similarly, would be about 9.8 d, etc. (Because of the core-mass vs. period relation, the final orbital period is not exactly given by the above P_f/P_0 value, but it will not differ much from it.) It should be noticed that in this way, even without invoking magnetic braking, short final orbital periods can be obtained for these systems.

References

Abbott, D.C. and Conti, P.S. 1987, *Ann. Rev. Astron. Astrophys.*, **25**, 113.

Alpar, M.A., Cheng, A.F., Ruderman, M. and Shaham, J. 1982, *Nature*, **300**, 728

Bailes, M., Harrison, P.A., Lorimer, D.R., Johnston, S., Lyne, A.G., Manchester, R.N., D'Amico, N., Nicastro, L., Tauris, T. and Robinson, C. 1994, *Astrophys. J.*, **425**, L41.

Baylin, C D. and Grindlay, J.E. 1990, *Astrophys. J*, 353, 159.

Bhattacharya, D. and Van den Heuvel, E.P.J. 1991, *Phys. Reports*, **203**, 1.

Bisnovatyi-Kogan, G.S. and Komberg, B.V. 1974, *Astron. Zh.*, **51**, 373(Soviet Astron. 18, 217)

Canal, R., Isern, J. and Labay, J. 1990, *Ann. Rev. Astron. Astrophys.* **28**, 183.

Chen, K. and Ruderman, M. 1993, *Astrophys. J.*, **408**, 179.

Delgado, A.J. and Thomas, H.C. 1981, *Astron. Astrophys.* **96**, 142.

De Loore, C, De Grève, J.P. and De Cuyper, J.P. 1975, *Astrophys. & Space Sci* **36**, 219.

Flannery, B.P. and Van den Heuvel, E.P.J. 1975, *Astron. Astrophys.*, **39**, 61.

Foster, R.S., Wolszczan, A. and Camilo, F. 1993, Astrophys. J., **410**, L91

Habets, G.M.H.J. 1985, *Advanced Evolution of Helium Stars and Massive Close Binaries*, Ph.D. Thesis, Univ. Amsterdam.

Habets, H.GJ.M. 1986, *Astron. Astrophys.*, **187**, 209.

Hameury, J.-M., King, A.R., Lasota, J.P. and Raison, F. 1993, *Astron. Astrophys.*, **277**, 81.

Harpaz, A. and Rappaport, S. 1991, *Astrophys. J.*, **383**, 739.

Hogeveen, S. 1991, *The Mass Ratio Distribution of Binary Stars*, Ph.D. Thesis, Univ. Amsterdam.

Hogeveen, S. 1992, *Astrophys. & Space Sci*., **196**, 299.

Joss, P.C. and Rappaport, S. 1983, *Nature*, **304**, 419.

Joss, P.C., Rappaport, S. and Lewis, W. 1987, *Astrophys. J.*, **319**, 180.

Kippenhahn, R., Kohl, K. and Weigert, A. 1967, *Zeitschr. f. Astrophysik*, **66**, 58.

Lipunov, A. 1992, *Astrophysics of Neutron Stars* (Springer).

Lipunov, A. 1992, in *Evolutionary Relations in the Zoo of Interacting Binaries*, Ed. F. d'Antona, *Mem. Soc. Astron. Ital.*, (in press).

Lyne, A. and Lorimer, D. 1994, *Nature*, **369**, 127.

Meurs, E.M. and Van den Heuvel, E.P.J. 1989, *Astron. Astrophys.*, **226**, 88.

Narayan, R., Piran, T. and Shemi, A. 1991, *Astrophys. J*., **379**, L17.

Nice, D.J., Taylor, J.H. and Fruchter, A.S. 1993, *Astrophys . J.*, **402**, L49

Paczynski, B. 1971, *Ann. Rev. Astron. Astrophys.*, **9**, 183.

Paczunski, B. 1983, *Nature* , **304**, 421

Phinney, E.S. 1991, *Astrophys. J* ., **380**, L17.

Podsiadlowski, P. 1991, *Nature*, **350**, 136.

Pylyser, E. and Savonije, G.J. 1988, *Astron. & Astrophys.,* **191**, 57.

Pylyser, E. and Savonije, G.J. 1989, *Astron. & Astrophys.,* **208**, 52.

Radhakrishnan, V. and Srinivasan, G. 1982, *Curr. Sci*., **51**, 1096

Radhakrishnan, V. and Srinivasan, G. 1984, Proc. 2nd Asian-Pacific Regional Meeting of the IAU (eds. B. Hidayat and M.W. Feast), Jakarta, Tira Pustaka, p. 423.

Refsdal, S. and Weigert, A. 1971, *Astron. & Astrophys.*, **6**, 426.

Romani, R. 1990, *Nature*, **347**, 741.

Savonije, G.J. 1983, *Nature*, **304**, 422

Savonije, G.J. 1983, in *Accretion Driven Stellar X-ray Sources*, Eds, W.H.G. Lewin and E.P.J, van den Heuvel, (Cambridge Univ. Press), p. 343.

Smarr, L.L. and Blandford, R.D. 1976, *Astrophys.* J., **207**, 574

Srinivasan, G. and Van den Heuvel, E.P.J. 1982, *Astron. & Astrophys*., **108**, 143

Stokes, G.H., Segelstein, D.J., Taylor, J.H. and Dewey, R.J. 1986, *Astrophys. J.*, **311**, 694.

Taam, R.E. 1983, *Astrophys. J*., **270**, 694.

Taam, R.E. and Bodenheimer, P. 1992, in *X-ray Binaries and Recycled Pulsars*, Eds. E.P.J. van den Heuvel and S.A. Rappaport (Kluwer), p. 281.

Taam, R.E., Bodenheimer, P. and Ostriker, J.P. 1978, *Astrophys. J*., **222**, 269.

Taylor, J.H., Manchester, R.N. and Lyne, A.G. 1993, *Astrophys. J. Supp*., **88**, 529.

Tout, C. 1991, *Monthly Notices Roy. Astron. Soc*, **250**, 701.

Tutukov, A.V. and Yungelson, L.R. 1993, *Monthly Notices Roy. Astron. Soc*, **260**, 675.

Van den Heuvel, E.P.J. 1981a, in *Fundamental Problems in the Theory of Stellar Evolution,* Ed. J. Sugimoto *et al.,* (Reidel), p. 155.

Van den Heuvel, E.P.J. 1981b, in *Pulsars*, Eds. W. Sieber and R. Wielebinski, (Reidel), p. 379.

Van den Heuvel, E.P.J. 1983, in *Accretion Driven Stellar X-ray Sources*, Eds. W.H.G. Lewin and E.P.J. van den Heuvel, (Cambridge Univ. Press), p. 303.

Van den Heuvel, E.P.J. 1992, in *X-ray Binaries and Recycled Pulsars*, Eds. E.P.J. van den Heuvel and S.A. Rappaport (Kluwer), p. 233.

Van den Heuvel, E.P.J. 1994, in *Interacting Binaries*, Lecture Notes Saas Fee Advanced Course 22, (Springer), p. 263.

Van den Heuvel, E.P.J. and Bitzaraki, O. 1994, in *Evolutionary Relations in the Zoo of Interacting Binaries*, Ed. F. d'Antona, Mem. Soc. Astron. Ital. (in press).

Van den Heuvel, E.P.J. and De Loore, C. 1973, *Astron. & Astrophys.*, **25**, 387

Van den Heuvel, E.P.J. and Taam, R.E. 1984, *Nature*, **309,** 235.

Van der Hucht, K.A. 1992, *Astron. Astrophys. Rev*., **4**, 123.

Van Kerkwijk, M.H. 1993, *The Mass of VelaX-l, the Nature of Cygnus X-3, the Character of Be Stars*, Ph.D. Thesis Univ. Amsterdam.

Van Paradijs, J. 1994, in *X-ray Binaries*, Eds W.H.G. Lewin, J. van Paradijs and E.P.J. van den Heuvel, (Cambridge Univ. Press), in press.

Verbunt, F. 1990, in *Neutron Stars and their Birth Events*, Ed. W. Kundt, (Kluwer), p. 179.

Verbunt, F. 1993, *Ann. Rev. Astron. Astrophys*., **31,** 93.

Verbunt, F. and Zwaan, C. 1981, *Astron. Astrophys*., **100,** L7.

Webbink, R.F., Rappaport, S.A. and Savonije, G.J. 1983, *Astrophys. J*., **270**, 678.

Diamond Jubilee Symposium on Pulsars
14–17 March 1994
Raman Research Institute, Bangalore

J. Astrophys. Astr. (1995) **16,** 289–305

Spin Evolution of Neutron Stars in Binary Systems

Pranab Ghosh *Tata Institute of Fundamental Research, Bombay 400005, INDIA. e-mail : pranab@tifrvax.tifr.res.in*

Abstract. I review our understanding of the evolution of the spin periods of neutron stars in binary stellar systems, from their birth as fast, spin-powered pulsars, through their middle life as accretion-powered pulsars, upto their recycling or "rebirth" as spin-powered pulsars with relatively low magnetic fields and fast rotation. I discuss how the newborn neutron star is spun down by electromagnetic and "propeller" torques, until accretion of matter from the companion star begins, and the neutron star becomes an accretion- powered X-ray pulsar. Detailed observations of massive radio pulsar binaries like PSR 1259-63 will yield valuable information about this phase of initial spindown. I indicate how the spin of the neutron star then evolves under accretion torques during the subsequent phase as an accretion-powered pulsar. Finally, I describe how the neutron star is spun up to short periods again during the subsequent phase of recycling, with the accompanying reduction in the stellar magnetic field, the origins of which are still not completely understood.

1. Introduction

We are primarily discussing spin-powered pulsars in this symposium: according to our current understanding of the origin and evolution of neutron stars in binary systems (see van den Heuvel 1992, hereafter vdH92), such a neutron star can have two distinct phases as a spin-powered pulsar. The first phase is that of the newborn, fast-spinning neutron star with rather high magnetic field ($\sim 10^{11} - 10^{13}$ G), while the second one is that of the recycled, very fast-spinning neutron star with rather low magnetic field ($\sim 10^{8} - 10^{11}$ G). Connecting these phases is that part of the life of the neutron star during which it appears as an accretion-powered pulsar.

This paper is a brief review of the processes that determine the evolution of the spin-rate of the neutron star as it passes from the first spin-powered phase to the accretion-powered phase, and then on to the second spin-powered phase through recycling (see Ghosh 1994, hereafter G94). The passage from the first

Spin-powered phase to the accretion-powered phase occurs through a process of spindown of the neutron star by electromagnetic and plasma torques which I call "initial spindown" throughout this paper. In the accretion-powered phase of pulsed X-ray emission, the neutron star shows both spin-up and spindown under the action of accretion torques. Finally, the passage from accretion-powered phase to the second spin-powered phase, *i.e*., recyclings, occurs through a process of massive (~ Eddington-rate) accretion, during which there is spin-up by accretion torques-called "final spinup" throughout this paper, followed by a termination of accretion. These processes are discussed in turn in the subsequent sections of this paper.

Spin evolution, and the above processes that cause it, are best studied on a Magnetic Field-Period ($B - P$) diagram of neutron stars, as shown in Fig.1. In addition to the "pulsar island" (which contains the bulk of those single neutron stars which are in a state analogous to that which I named "first spin-powered phase" above for neutron stars in binaries), the figure shows (a) the recycled pulsars at the bottom left of the diagram, *i.e*., the second spin-powered phase of pulsars, (b) the X-ray pulsars at the top right of the diagram, *i.e*.., the accretion-powered phase of pulsars (only those X-ray pulsars for which a direct measurement of the magnetic field from the cyclotron line is available [see Nagase 1992] have been used here), and, (c) the two examples of binary neutron stars known at the present time which are in their first spin-powered phase, namely, PSR B1259-63 and PSR J0045-73 (Johnston *et al.* 1994, hereafter J94; Kaspi *et al.* 1994): we nave heard about these two massive radio binary pulsars in detail from Dr. Manchester in this symposium. Note that recycled neutron stars can be either binary or single: the processes that may disrupt the binary before the second spin-powered phase begins are. indicated in §4.

2. Initial Spindown

During this process, the neutron star moves to the right on the $B - P$ diagram on an approximately horizontal track. I consider the braking torques in turn.

2.1 *Electromagnetic Torque*

Electromagnetic braking torques are usually expressed in the form $N \propto \mu^2 (\Omega_s /c)^3$, in analogy with the expression for magnetic dipole radiation in vacuum. Here, μ is the magnetic dipole moment of the star, and Ω_s is its angular velocity. This torque, which spins the pulsar down to a period P in $\sim 3.10^4 (P/50\ ms)^2 I_{45} \mu_{30}^{-2}$ yr, can brake the stellar spin to the critical point where plasma effects first dominate the torque. The critical period depends on the properties of the plasma flow from the companion to the neutron star: for mass capture at rates $\sim 10^{-11}\ M_\odot$ yr^{-1} from winds of speed $\sim 10^3$ km s^{-1} from the companion, this period is $\sim 100 \mu_{30}^{1/2}$ ms (Illarionov & Sunyaev 1975, hereafter IS). Here, I_{45} is the moment of inertia of the neutron star in units of 10^{45} gm cm^2, and μ_{30} is μ in units of 10^{30} G cm^3.

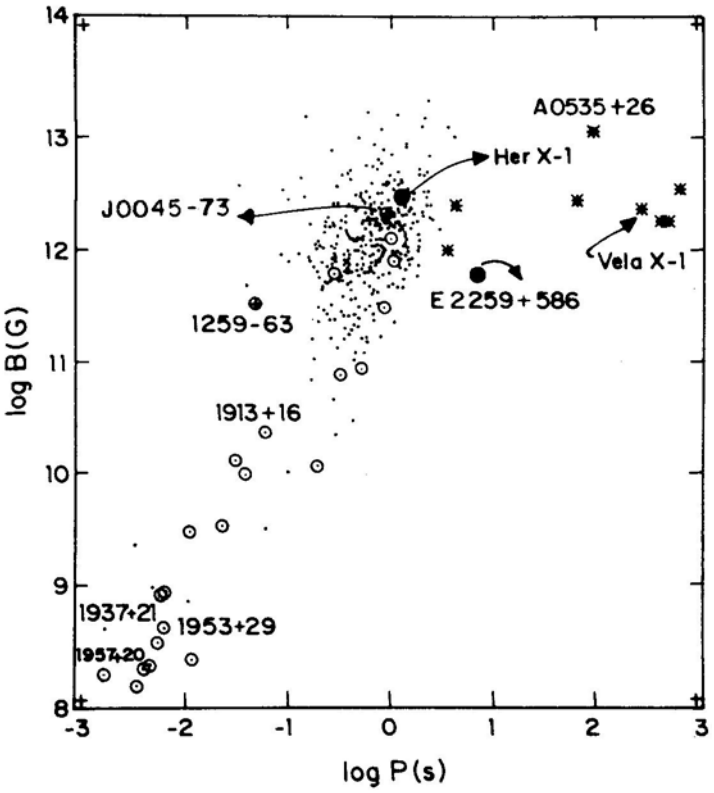

Figure 1: Spin and accretion-powerd pulsars on the B-P diagram. Dots indicate spin-powered pulsars, and stars, accretion-powered ones. Those spin-powered ones which are in binaries are encircled, and the two recently discovered massive radio pulsar binaries (PSRs B1259-63 and J0045-73) have an additional cross on their symbols. Some well-known pulsars are marked individually: these include (a) recycled pulsars, (b) PSR B1259-63, (c) two accretion-powered pulsars with relatively low-mass companions (Her X-1 and E 2259+586), and (d) one accretion-powered pulsar with a massive companion (Vela X-1).

2.2 *Propeller & Related Torques*

When the spin of the neutron star becomes slower than the above critical value, the dominant braking torques are those due to the deposition of energy and momentum into the matter (coming from the companion star) by the stresses associated with the magnetic field of the neutron star: these are the propeller-type torques. The scaling of the propeller torque was given in the original formulation (IS) as $N \propto (\mu^2/r_A^3)(\Omega_K(r_A)/\Omega_s)$, where r_A is the Alfvén radius and Ω_K is the Keplerian velocity. More detailed work (Mineshige *et al.* 1991; Davies & Pringle 1981; see

Henrichs 1983 for a review) on the plasma torques has shown since then that the most effective braking obtains at subsonic spin rates ($r_A\Omega_s < c_s$, c_s being the sound speed). This is the so-called subsonic propeller, the torque due to which scales as $\mu^2\Omega_s^2/GM$, independent of r_A. For supersonic propellers, the torque is smaller by a factor $\sim (c_s/\Omega_s r_A)$, and reduces to the original IS scaling if $c_s \sim v_{ff}$ at r_A. Here, v_{ff} is the free-fall velocity. These braking torques, as well as some others described below, are listed in Table 1.

Table 1: Spindown Torques

Spindown Mechanism	Torque Scaling
Electromagnetic	$N \sim \mu^2(\Omega_s/c)^3$
Propeller: Original (IS)	$N \sim (\mu^2/r_A^3)(\Omega_K(r_A)/\Omega_s)$
Propeller: Subsonic	$N \sim \mu^2\Omega_s^2/GM$
Propeller: Supersonic	$N \sim (\mu^2\Omega_s^2/GM)(c_s/\Omega_s r_A)$
"Frictional" (Aligned Rotator)	$N \sim p\, r_A^3$
Compton-Heated Wind	$N \sim \dot{M}_{out}\, \Omega_s r_A^2$

I now mention two other types of braking torques that may be relevant in the initial spindown phase. First, note that the propeller effect, as originally concieved, requires a misalignment between the spin and magnetic axes of the neutron star. However, even when the two axes are aligned, there may be a significant "frictional" braking torque (Mineshige *et al.* 1991) on the star, which is expected to scale as $N \propto p\, r_A^3$, where p is the total pressure at r_A. This torque is therefore expected to operate simultaneously with all propeller-type torques. Second, it has been suggested recently (Illarionov & Kompaneets 1990) that the propeller mechanism "switches off" when the condition $\Omega_s > \Omega_K\ (r_A)$ is no longer satisfied. There is, instead; accretion to the star over some parts of the total cross-section, and outflow of a Compton-heated wind over the other parts, the resultant braking torque scaling as $\dot{M}_{out}\Omega_s r_A^2$. Here, $\dot{M}_{out}$ is the mass outflow, rate.

For typical values of stellar and binary parameters, the plasma torques described above give timescales for spindown which are comparable to or shorter than that given above for the electromagnetic torque. It was therefore argued (Henrichs 1983) that the total duration of the initial spindown phase is essentially determined by the "bottleneck" of the elctromagnetic torque. However, this is true only if the different torques act *consecutively*. As I indicate below, this need not be the case in a highly eccentric binary system, such as PSR B1259 – 63, since, during each orbital cycle, elctromagnetic torques may dominate over those parts of the orbit where the plasma density is small, while plasma torques may dominate over those parts where the density is high, particularly near periastron. Then spindown would occur on a timescale which is an appropriate average of those due to the various torques acting over the orbital cycle, and which can be considerably shorter than that for electromagnetic braking alone.

2.3 *Spindown of PSR B1259-63*

Studies of the spindown history of PSR B125963, a neutron star-Be star binary with a highly eccentric ($e \simeq 0.87$) 3.4 yr orbit (J94), will map out the details of the processes of initial spindown. Far away from the periastron, the 47 ms pulsar undergoes spindown with a characteristic age of $3.3.10^5$ yr, predominantly by electromagnetic torques, which implies a magnetic field $\sim 3.3.10^{11} G$ for the neutron star (J94). Close to periastron, plasma torques associated with the wind and the disk of the Be star contribute appreciably to spindown, and may even dominate it, depending on the relative dispositions of the orbital plane and the plane of the disk around the Be star. It is easy to show from Table 1 and the parameters given above that the timescales for spindown of this pulsar by the subsonic propeller torque and the supersonic (in the original IS formulation) propeller torque are approximately the same, and each is $\sim 3.10^4$ yr. The *instantaneous* spindown rate is, therefore, expected to go up by ~ an order of magnitude as the pulsar passes through the Be star's disk. How much enhancement this causes of the total spindown during periastron passage (*i.e.*, between the radio disappearance of the pulsar before periastron and its reappearance after periastron), which is the quantity actually observed, depends on the relative orientation referred to above (Ghosh 1994, in preparation). Naively, one expects the Be-star disk to be in the orbital plane, but this need not always be so, particularly for a young system such as PSR B1259-63. In fact, there are indications already that this is *not* the case here. First, there is little perturbation to the *Hα* emission during periastron passage (Manchester 1994): this emission, which is thought to originate in the Be-star disk, is expected to be grossly perturbed by the tidal torques of the neutron star during periastron passage if the disk is coplanar with the orbit, as the detailed simulations of Kochanek (1993) have shown. Second, a coplanar disk would produce an orbital-phase-dependent perturbation in the spindown even relatively far away from periastron, for which there is little evidence at this point. Analysis of the radio observations of this system during the periastron passage of January 9, 1994, described by Dr. Manchester in an exciting talk in this symposium, will soon clarify this point.

2.4 *Braking by Onset of Disk Accretion*

At the onset of accretion to the neutron star from disks, or from stellar winds, the star is spun down further by the accretion torque. Here, I indicate how the braking torque acting at the onset of disk accretion is particularly effective in spinning down the star to $P \sim 100$ s (Elsner, Ghosh, & Lamb 1980, hereafter EGL).

The principal features of the accretion torque for disk accretion by magnetic neutron stars are summarized in §3.2. The torque spins the star down if the stellar spin rate, as measured by the dimensionless fastness parameter ω_s, exceeds a critical value ω_c, *i.e.*, the spin period is shorter than the critical value P_c which corresponds to the point $\omega_s = \omega_c$ where the accretion torque vanishes. Under the action of the braking torque, the star spins down from an initial period P_i to a final period $P_f \approx P_c$ in a time $\simeq 2.10^6 \mu_{30}^{-2} (P_f / 100_s)^2 (P_i / 1_s)^{-1}$ yr, if the accretion rate

is a constant (EGL). If $\dot{M}$ goes through outbursts or flares, spindown can occur even more rapidly, as the braking torque can then continue to be very effective as the star spins down. In this way, the star can be spun down to a final period P_f from an initial period $P_i \ll P_f$ in a time as short as $1.5.10^5\ \mu_{30}^{-2}\ (P_f\ /100_s)$ yr. Hence, this mechanism is clearly capable of producing the initial spindown to the long ($\gtrsim 100$ s) periods, which ~ 45% of the known accretion-powered pulsars have, in a time which is short compared to the main-sequence lifetime of their companions(EGL).

3. Spin Evolution During the Accretion-Powered Pulsar Phase

For about half of the known (~ 35) accretion-powered pulsars, long-term period histories have been compiled from data collected over ~ 2 decades of satellite observation (for a review, see Ghosh 1994). From these compilations, the following (approximate) categories of secular trends in spin evolution have sometime been identified. First, there are those pulsars which have shown secular spin-up over essentially the entire stretch of observation (except possibly for a brief episode of standstill or slight spin-down), *e.g.*, Her X-l. Second, there are those which have, similarly, shown essentially secular spin-down, *e.g.*, 1E 1048.1-5937. Third are those which have shown considerable stretches of both spin-up and spindown, *e.g.,* A 0535+26, GX 1+4. Finally, there are those that seem to show "erratic" variation on these timescales, *e.g.,* X Per. It is quite possible, and indeed, rather likely, that such "different" categories are really manifestations of the same phenomenon, which is that all accretion-powered pulsars show intervals of spin-up and spindown when observed over sufficiently long periods of time. This is strongly suggested by the fact that one after another of these pulsars with a so called "pure" trend of either spin-up or spindown has shown a reversal of sign as the extent of the period history has become longer. One of the most recent examples of this is 4U 1626-67 (a 7.7 s pulsar with a very low-mass companion), which had been observed to spin up at almost a constant rate since its discovery in 1977, but is now observed by BATSE (see below) to be spinning down at a roughly comparable rate.

Recent observations by the Burst & Transient source Experiment (BATSE) on board the Compton Gamma-Ray Observatory have produced detailed period histories (see Ghosh 1994, and the individual references to BATSE work therein) of accretion-powered pulsars, accurately documenting changes on timescales which can be as short as ~ hours to days. This is to be contrasted with earlier X-ray satellite observations, which typically documented changes on timescales ~ months to years. BATSE observations have now provided detailed records of a phenomenon seen in earlier work, namely that spin-up/spin-down reversals on short timescales can occur even during a so-called "secular" phase of monotonic spin change on longer timescales.

These trends of spin evolution are interpreted in terms of accretion torques, whose characteristics are summarized below.

3.1 *Disk Accretion*

When well-developed accretion disks form (as in Low Mass X-ray Binaries, due to Roche lobe overflow, and as is expected in Be-star binaries due to accretion from the Be-star disk) around the neutron star, the interaction between the rotating plasma in the accretion disk and the magnetic field of the rotating neutron star determines the rate of angular momentum transport and so the accretion torque.

3.1.1 Disk-Magnetosphere Interaction

The stellar magnetic field has a tendency to penetrate into the disk plasma due to a variety of processes, *e.g.*, Kelvin-Helmholz instability, turbulent diffusion, and reconection to small-scale fields in the disk (Ghosh and Lamb 1979a,b, 1991; hereafter GL). Penetration is actually expected to occur over a considerable part of the disk because the rate of inward radial drift at which the ionized disk plasma can "sweep" the field inward is much slower than the rates of the above processes. Thus, the diamagnetic disk picture, in which the disk is completely excluded from stellar magnetic field (Aly 1980; Kundt & Robnik 1980), is not a self-consistent description of the physical situation.

The precise extent and structure of the disk-magnetosphere interaction region is still a matter of some debate. GL originally described the region in terms of its two conceptually different components: (a) a broad outer transition zone, where magnetic stresses participate in the angular momentum transport, but are not strong enough to cause deviation from Keplerian flow, and, (b) a narrow boundary layer at the inner edge of the disk, where strong magnetic stresses dominate the angular momentum transport, terminate the disk, and channel the accretion flow along the stellar field lines. The location of the inner edge of the disk, r_0, is given by the conservation of angular momentum in the boundary layer,

$$\frac{B_p B_\phi}{4\pi} 4\pi r^2 \delta \simeq \dot{M} r v_K \,. \tag{1}$$

Here, B_p and B_ϕ are respectively the poloidal and toroidal components of the magnetic field, δ is the width of the boundary layer, and v_K is the Keplerian velocity. The value of r_0 obtained in this way, and its scaling with the essential variables $\dot{M}$, μ, and M, depends on the model of the boundary layer, which, in turn, depends on the model of accretion disk appropriate at such radii. For accretion rates and magnetic fields typical of accretion-powered pulsars, the so-called "middle" region of the Shakura-Sunyaev (1973) disk model is appropriate, and the inner radius is given (GL) by

$$r_0 \simeq 1.3 \times 10^8 \dot{M}_{17}^{-46/187} \mu_{30}^{108/187} (M/M_\odot)^{-41/187}$$

Here, $\dot{M}_{17}$ is $\dot{M}$ in units of 10^{17}gs^{-1}. Note that the above scalings are close, but not identical, to those of the Alfvén radius for spherical accretion, $r_A = \dot{M}^{-2/7} \mu^{4/7} (2GM)^{-1/7}$.

While GL treated the two above regions separately by semi-analytic or numerical methods, it should be possible to treat the entire region numerically in a unified scheme. Preliminary results of such calculations (Daumerie *et al.* 1993) show that

the full region does, indeed, have an outer part where the physical variables change on a lengthscale ~ r, and an inner, boundary-layer like, part where the variables change on a lengthscale ~ $\delta \ll r$. However, the width of the boundary layer is larger than that calculated by GL.

Possible structures of the disk-magnetosphere interaction region which are related to the GL structure, but differ from it in detail, have been discussed qualitatively in recent years. Arons (1987) and coauthors have suggested, for example, that some stellar field lines in the outer parts of the interaction region may become open if the disk plasma loaded on them can be spun up to super- Keplerian rotation. A centrifugal wind would then be driven along these field lines. In the picture of Aly and Kuijpers (1990), on the other hand, the interaction region is confined to a thin annular zone where the strength of the stellar magnetic field is ≈ that of the small-scale magnetic fields in the disk (so that reconnection between the two proceeds the most efficiently), and a highly pinched version of the disk extends far into the magnetosphere.

Understanding the electrodynamics of the interaction region is a complicated and challenging task. The stellar magnetic field is wound up in the azimuthal direction and pinched inward in the radial direction by the differential motion between the disk and the star. While it is reasonable to suppose that these distortions are ultimately limited by a variety of processes, *e.g.,* reconnection (GL), flux escape (Wang 1987), and current-driven instabilities, the expected saturation value of the magnetic pitch B_ϕ / B_p in a steady state, and the dominant process that determines this value, are still uncertain. Indeed, the process of buildup and release of magnetic energy is inherently episodic, and the adequacy of a time-averaged description of it in terms of steady-state models may be in question. GL focused on reconnection-limited pitch, and showed that steady-state electrodynamics can then be formulated in terms of an effective elctrical conductivity, assumed isotropic for simplicity. The idea is generally valid, of course, and Campbell (1987) turned it around to calculate the pitches corresponding to simple, mathematically tractable, models of disk conductivity.

3.1.2 Accretion Torque

The accretion torque on the neutron star consists of two parts. The first comes from stresses associated with matter accreting from the inner edge of the disk, and is given by (GL)

$$N_0 \equiv \dot{M}(GMr_0)^{1/2}. \tag{3}$$

The second comes from the stresses associated with the magnetic field coupling the star with the disk. The total torque N can be conveniently expressed in terms of N and the dimensionless torque, $n \equiv N/N_0$, depends only on the fastness parameter (GL; EGL),

$$\omega_s \equiv \Omega_s/\Omega_K(r_0) \simeq P^{-1}\dot{M}_{17}^{-3/7}\mu_{30}^{6/7}, \tag{4}$$

of the star. Slow rotators ($\omega_s < \omega_c$) are spun up ($n > 0$), while fast rotators ($\omega_s > \omega_c$) are spun down ($n < 0$), by this accretion torque. For $\omega_s > 1$, steady accretion is of course not possible. Here, ω_c is the critical fastness at which the

torque changes direction, whose value was found to be ~ 0.3–0.5 in the original GL calculations. A simple analytic approximation to the torque calculated numerically by GL is

$$n(\omega_s) \simeq 1.4 \left(\frac{1 - \omega_s/\omega_c}{1 - \omega_s} \right) . \tag{5}$$

It was suggested by EGL that, due to the balance between stretches of spinup and spindown, the period of a pulsar can be maintained in a range around its critical period, if its luminosity goes through alternate high and low states. This would explain the observability of long-period sources like GX 1+4 and A 0535+26, despite their short spinup timescales in high states. Extensive stretches of spinup and spindown seen in these and other sources since then have borne out this conclusion (also see below).

While the results of subsequent torque calculations using GL-type models (Campbell 1987; Wang 1987; Daumerie *et al.* 1993) have been qualitatively similar, a major issue has been the value of the critical fastness. This parameter depends on the magnetic spindown torque, and so on the magnetic pitch (see above) in the outer parts of the interaction region. GL undoubtedly overestimated the pitch in their approximate treatment of the electrodynamics, so that a more exact calculation should lead to smaller pitches and therefore to larger values of ω_c . However, the extreme value of $\omega_c \simeq 0.97$ obtained by Wang (1987) seems untenable on both theoretical and observational grounds. Wang (a) made an incorrect algebraic approximation, as a result of which the torque diverges as $\omega_s \rightarrow 0$, and, (b) neglected screening of the poloidal field. Observationally (see below), there is little evidence for such a large value of ω_c. Indeed, $\omega_c \simeq 0.97$ would imply a tiny range of accretion rates for each pulsar over which spindown could occur (see eq.[4]), making it a rare phenomenon. This is clearly not the case, as most pulsars show spindown, and many of them have long and repeated intervals of it (see above).

3.1.3 Comparison With Observation

Predictions from, accretion torque theories were compared (GL and references therein) with the observed spinup rates of pulsars in the 1970s, as few episodes of spindown were known at the time. The rich structure of spinup/spindown patterns revealed by further observations (see above) makes these comparisons more interesting and complex, and provides more stringent tests of accretion torque models. Observation of spinup and spindown during an outburst of the transient Be-star binary source EXO 2030+375 (Parmar *et al.* 1989) with a pulse period ~ 42 s provided the first opportunity to study the spinup-spindown transition in detail as the luminosity declines and a slow rotator turns into a fast one.

If, as outlined above, both spinup and spindown can be described in terms of a dimensionless torque n which is a function of a dimensionless stellar spin rate ω, alone, this universal scaling (GL) can be demonstrated in the following way. Since $n \propto - \dot{P} P^{-2} L^{-6/7} \mu^{-2/7}$ roughly (as can be shown by combining eqns.[2] and [3]), and $\omega_s \propto P^{-1} L^{-3/7} \mu^{6/7}$, the n vs. ω_s curve can be mapped out from period-luminosity data. Here, L is luminosity of the pulsar. With data on one individual pulsar (μ = constant), we need only plot $- \dot{P} P^{-2} L^{-6/7}$ vs. $P^{-1} L^{-3/7}$. Data on a collection of pulsars can be combined if we have a knowledge of the relative values

of μ of these from, say, cyclotron line energies (Nagase 1992; Mihara 1993). I show below the results for two well-studied pulsars.

The ~ 120 s pulsar GX 1+4 with an M6 III giant companion was observed to spin up at a rate $\dot{P}/P \approx -3.10^{-2}$ yr^{-1} in its high-luminosity state in the 1970s (Nagase 1989). It entered an extended low state in the 1980s, from which it reappeared in 1987 in a low-luminosity spindown state (Makishima *et al.* 1988), and has continued to spin down at a rate $P/P \approx 2.10^{-2}$ yr^{-1} upto the BATSE observations. Observations of this source first resolved the dilemma of the short spinup timescales of long-period pulsars (EGL). Shown in Fig. 2a is the observed torque curve for GX 1+4, using a compilation of the long-term period history. A theoretical torque curve given by eqn. (5) with $\omega_c = 0.3$ accounts well for the observations, except perhaps for the highest-fastness point, as Fig.2a shows.

For Her X-l, one of the best-studied pulsars ($P = 1.24$ s), BATSE data with $\dot{P}$ measured ~ every month (Wilson *et al.* 1993) has been used in Fig. 2b to map out the torque curve for this source from shorter-term period variations, which show spinups and spindowns of comparable maximum strength $|\dot{P}/P| \approx 2.10^{-5}$ yr^{-1} In this case, an additional assumption about the relation between the pulsed, flux (which is what BATSE normally sees) and the total flux is necessary, and I have used a direct proportionality, guided by observations of those sources (*e.g.,* GS 0834-430; C. A. Wilson *et al.*1993) where the latter flux is also available from Earth occultation measurements. The same theoretical curve as in Fig.2a fits these observations, as shown, although other choices of ω_c (see below) are also possible.

These examples are thus consistent with the idea of universal scaling, which implies the same ω_c for both sources. For the two sources above, this yields a relation between their stellar magnetic moments. Using the Her X-1 magnetic field inferred from cyclotron-feature observations (Nagase 1992), this indicates a surface magnetic field ~ 10^{14} G for GX 1+4, in agreement with recent suggestions (Mony *et al.* 1991); proposals have been made for the observation of the corresponding cyclotron feature at ~ 1 MeV with OSSE on CGRO (Prince 1993) or archival HEAO data (Ghosh & Gruber 1994). Finally, note that, although the normalization constant for the observed ω_s is unspecified in these examples, an *upper bound* on it is implied by the requirement that the maximum observed value of fastness must not exceed unity (see above). The use of this requirement for GX 1+4 leads to $\omega_c \lesssim 0.3$ (Fig.2a). Similar arguments for Her Xl lead to $\omega_c \lesssim 0.6$ (Fig.2b). Thus, spinup/spindown observations suggest a critical fastness of $\omega_c \sim 0.3 - 0.6$.

3.2 *Wind Accretion*

In massive X-ray binaries, if the companion is a supergiant, it drives a strong stellar wind, gravitational capture from which produces accretion on to the neutron star. If the companion is a Be star, the accretion in the quiescent state may be from a similar, weaker wind, and, even during flares due to accretion at a much higher rate from equatorial disks around the Be star, this weak wind may continue to blow from the polar regions of the Be star (Waters & van Kerkwijk 1989, hereafter WK).

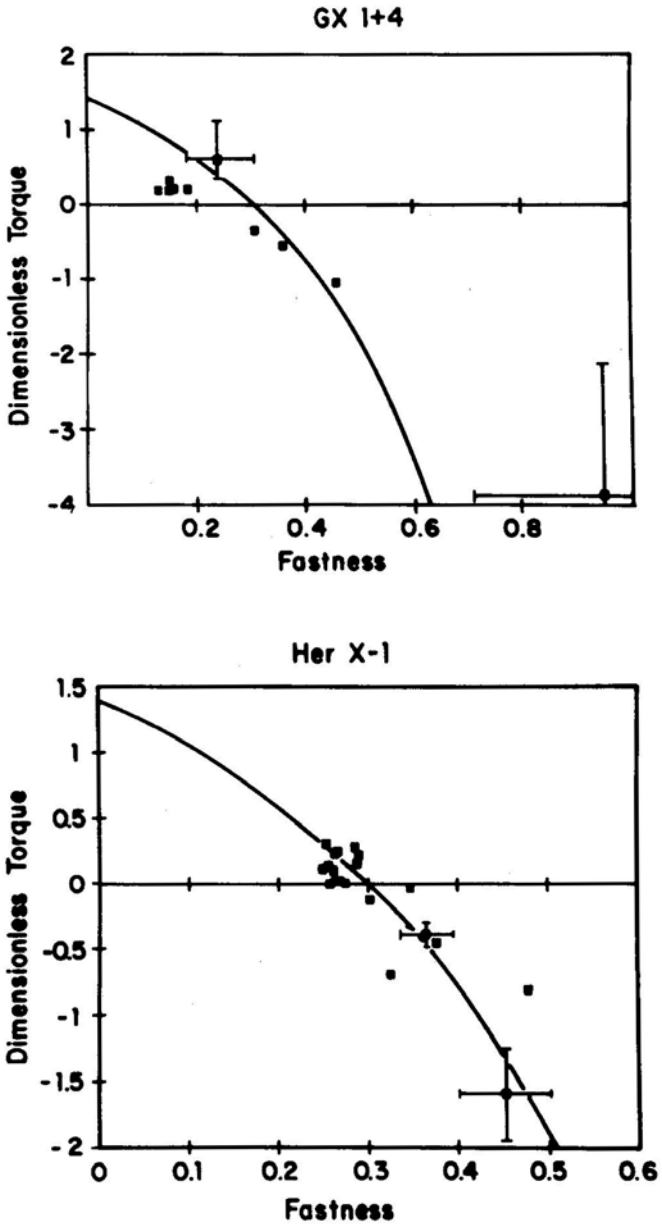

Figure 2: Torque curves for (a) GX 1+4, and, (b) Her Xl. Shown are the dimensionless torque (n) vs. fastness (ω_s) data, superposed on the curve given by eqn.[5] with ω_c = 0.3. Also shown are the typical uncertainties in the observed values, dominated by luminosity variations (see text) during each observation. Such examples support the idea of universal scaling.

3.2.1 Supergiant Systems

The angular momentum transferred to the neutron star per unit mass captured from the wind is usually parameterized in the form $l_\omega = \eta r_a^2 \ \Omega_{orb,}$ where $r_a \equiv 2GM/v_0^2$ is the accretion radius, Ω_{orb} is the orbital angular velocity, and η is a dimensionless number. The value of η, which depends on the density and velocity-gradient in the wind, has generally been calculated to be of order unity and both signs by various authors (Shapiro & Lightman 1976; Wang 1981; Anzer *et al.* 1987; Ho 1988). Alternatively, l_ω can be expressed in terms of $r_a v_0$.

Numerical studies of mass capture from stellar winds carried out in recent years (Matsuda *et al.* 1987; Taam & Fryxell 1989; Blondin *et al.* 1990; Matsuda *et al.* 1991, Livio 1993) have shown that the flow patterns often do not approach a steady state; rather, the shock cone oscillates from side to side, producing circulation that reverses quasi-periodically. The origins of this "flip-flop" behavior, which occurs in 2D simulations, but sometimes appears in 3D calculations and sometimes does not, are not fully understood (Livio 1993), even apart from the question of whether numerical artifacts of the simulations, *e.g.,* dimensionality and zoning, are responsible for it. Attempts to attribute it to asymmetries in the upstream flow (Blondin *et al.* 1990) have been in conflict with the result that uniform upstream flows can also develop this behavior when the size of the accreting body is relatively small (Matsuda *et al.* 1991).

The instantaneous magnitude of the specific angular momentum, l_ω, given by these simulations can be $\sim 0.15 r_a v_O$ when a circulating "disk" develops, but its long-term average value is much smaller, as the flow has reversals, accompanied by outbursts of mass flux to the star (Taam & Fryxell 1989). This behavior may be related to the pulse period history of wind-fed HMXBs like Vela X-1, which do indeed show torque reversals on timescales of at least a few days (Deeter *et al.* 1989). However, the typical timescales of reversal given by the current simulations are ~ 1 hr.

3.2.2 Be Star Systems

Accretion from the matter expelled episodically from the Be star in the form of equatorial disks is thought to cause outbursts in these systems. Although more work needs to be done on the formation of accretion disks in such systems, the strong spinup torques observed during outbursts (*e.g.,* in EXO 2030+375) are indirect indications that well-developed accretion disks do form in them.

A useful probe into the spin evolution of these systems is the correlation, $P_{spin} \sim P_{orb}^2$, observed between their spin and orbital periods (Corbet 1986). This has been explained (WK) in terms of the concept of the critical spin period ($\Omega_s = \Omega_c \propto \Omega_K (r_m)$, where r_m is the outer radius of the magnetosphere), at which the net torque on the star vanishes, in analogy with what is done in disk accretion theory (see above). When one uses this concept, radial stellar winds give the (weaker) correlation, $P_{spin} \sim P_{orb}^{4/7}$, observed in wind-fed supergiant systems (WK). However, the observed relation for Be-star systems given above can only be reproduced by dense, equatorial, disk-like flows with a much more gradual velocity law (WK) than the standard radial stellar wind; such winds are now being studied

in detail (Bjorkman & Cassinelli 1993).

4. Final Spinup

4.1 *Evolutionary Scenarios*

The final evolution of massive neutron-star binaries (HMXBs) can go in two ways when the common-envelope (CE) phase begins (see vdH92 and references therein). An initially wide binary (*e.g.,* a Be star system) can eject the entire envelope and produce a neutron star with a helium core companion. The system then evolves either (a) by a supernova explosion of the companion, or, (b) by evolution of the companion into a massive white dwarf. In the former case, the chances are high that the system remains bound, producing a double neutron star system like PSR 19134+ 16; if it does become unbound, it produces two single, runaway neutron stars, one recycled and the other newborn. In the latter case, a system like PSR 0655+64 is thought to be produced. On the other hand, an initially narrow binary undergoes a complete spiral-in in the CE phase, producing a Thorne-Zytkow object (vdH92): the envelope is ejected susequently by the flux of energy generated by accretion, leaving behind a single, recycled, neutron star.

The final evolution of low-mass neutron-star binaries (LMXBs) proceeds very differently (see Webbink 1992, 1994 and references therein), in a rather straightforward way. Nuclear evolution of the low-mass companion drives the mass-transfer, ending up with a low-mass helium white dwarf companion to the neutron star, a system like PSR 1953+29.

4.2 *Spin Evolution*

The spin evolution HMXBs is straightforward in principle. In an initially wide system, the neutron star is spun up to short periods (~ 50 – 1000 ms, say) determined by the strength of the full-scale Roche lobe overflow (that initiates the CE phase) and the magnetic field of the neutron star. On the other hand, an initially narrow binary undergoes a complete spiral-in in the CE phase, producing a Thorne-Zytkow object (vdH92) with a disk-accreting neutron star in its core. The end product in this case is a recycled, spun up, single radio pulsar. However, not much work has been done so far on the details of the spin evolution in these cases.

Recent research has mainly focussed instead on the spinup of neutron stars to millisecond periods in LMXBs. Here, the accretion rate is very large (near or at the Eddington rate), and the magnetic field of the neutron star is thought to have become much less (~ 10^8 – 10^9 G), perhaps by the same accretion process (see below, and also Verbunt 1994). A straightforward application of the principles of accretion torques sketched above shows then that recycled pulsars are expected to have spin periods in the observed range of 1 – 100 ms: this was one of the major triumphs of accretion torque theory in the 1980's. The concept can be displayed pictorially as in Fig.3, which shows the period distribution of recycled spin-powered pulsars superposed on that of the accretion-powered pulsars: *the*

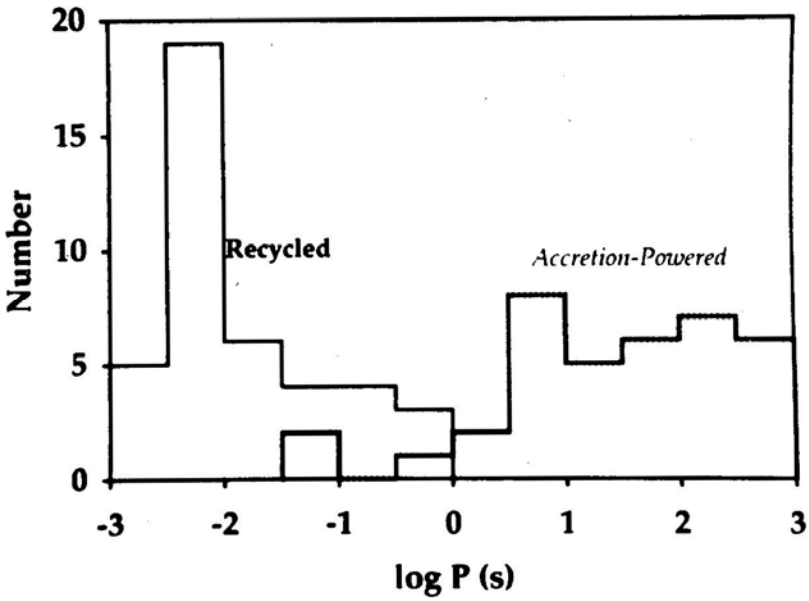

Figure 3: Period distributions of (a) recycled spin-powered pulsars (solid line) and (b) accretion-powered pulsars (shaded line). Included here are all 37 pulsars of the latter category known as of July 1994.

process that moves the latter distribution to the former is the accretion torque that operates during the stage of high mass transfer described above.

4.3 *Magnetic Field Evolution*

A glance at Fig. 1 reveals recycled pulsars are not sacttered all over the bottom left corner of the $B - P$ diagram; rather, they are distributed roughly on a linear band. This agrees very well with the ideas of recycling (see, *e.g.,* White & Stella 1988; Ghosh & Lamb 1992). Indeed, the upper edge of this band is called the "spinup line" (see Bhattacharya & van den Heuvel 1992 for a review), and it represents the shortest period achieved by a pulsar with a given magnetic field during the final spinup process described above. The position of the spinup line gives an excellent diagnostic of the final spinup process, particularly of the state of the inner parts of the accretion disk around the neutron star during this process. It has been shown that this diagnostic can place severe constraints on suggested models of the inner accretion disks in LMXBs (Ghosh & Lamb 1992). Possible models for such disks include the class of cool, one-temperature, optically thick models constructed by Shakura & Sunyaev (1973), and the class of hot, two-temperature, optically thin models constructed by Shapiro *et al.* that the latter class of models is not consistent with observation, although the matter needs to be investigated further (Ghosh & Lamb 1992).

It is also clear from Fig.l that magnetic fields of neutron stars are reduced

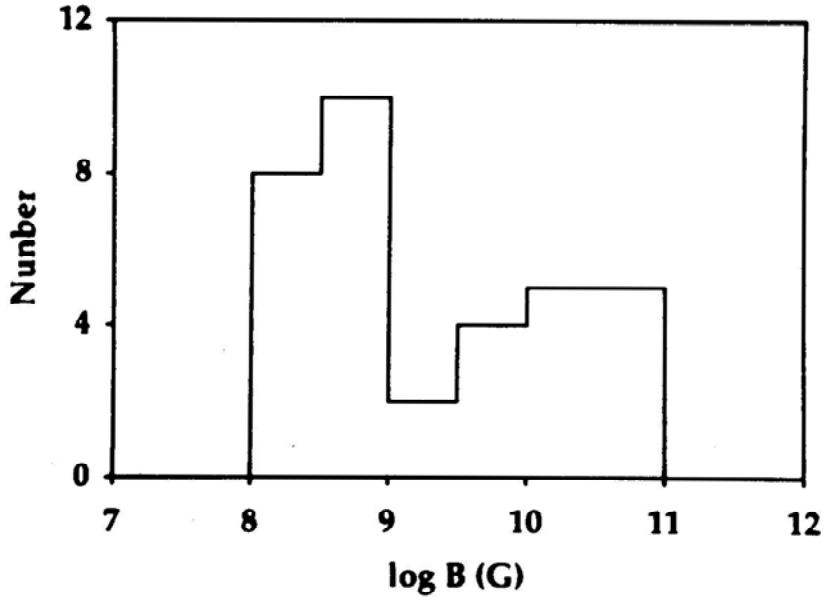

Figure 4: Magnetic field distribution of recycled pulsars. Included are 34 pulsars whose spindown rates have been reliably measured as of July 1994.

considerably during the passage from the accretion-powered phase to the second spin-powered phase. A connection between this magnetic field decay and the accretion during the final spinup phase is obviously possible, and this has been a subject of much study recently (for a review, see Verbunt 1994). I show in Fig.4 the magnetic field distribution of recycled pulsars. (Note that these are uncorrected for the so-called Shklovskii effect described by Camillo *et a*. Fig.4: inclusion of this effect does not change any of the conclusions described here.) A bimodal distribution is strongly hinted at (Kulkarni 1992). The pulsars with the lower magnetic fields have low-mass companions in wide, circular orbits (*i.e*., pulsars of the "1953+29 Class", vdH92), and are thought to have descended from LMXBs. By contrast, the pulsars with the higher magnetic fields have either neutron star companions in narrow and eccentric orbits, or massive white dwarf companions in narrow orbits (*e.g*., PSR 0665+64): these are collectively called pulsars of the "1913+16 Class" (vdH92) and are thought to have descended from HMXBs. Why is this so? From the point of view of accretion-induced field decay, an obvious explanation is, of course, that the $\sim 10^3$ -10^4 yr timescale for the final evolution of HMXBs (vdH92) implies that only a tiny amount of matter has been accreted by the neutron star, while the much longer, $\sim 8.10^7$ yr, timescale for the final evolution of LMXBs implies a significant amount of accreted matter, typically a few tenths of a solar mass. This has immediate, and quantitative, consequences for the systematics of accretion-induced field decay, which are being keenly pursued at present.

References

Aly, J.-J. 1980, *Astron. & Astrophys.,* **86**, 192
Aly, J.-J., & Kuijpers, J. 1990, *Astron. & Astrophys.,* **227**, 473
Angelini, L., *et al.* 1989, *Astrophys. J.* **346**, 906
Anzer, U., *et al*. 1987, *Astron. Astrophys*., **176,** 235
Arons, J. 1987, in The Origin & Evolution of Neutron Stars, ed. D. J. Helfand & J.-H. Huang (Dordrecht: Reidel), 207
Bhattacharya, D., & van den Heuvel, E. P. J. 1991, *Phys. Rep.,* **203**, 1
Bildsten, L. 1993, Proc. Second Compton Symposium, in press
Bjorkman, J. E., & Cassinelli, J. P. 1993, *Astrophys. J.* **409**, 429
Blondin, J. M., *et al.* 1990, *Astrophys. J.* **356**, 591
Camilo, F., *et al.* 1994, *Astrophys. J.* **421**, L37
Campbell, C. G. 1987, *Mon. Not. R. astr. Soc.* **229**, 405
Cominsky, L. 1994, in The Evolution of X-ray Binaries, ed. S. S. Holt & C. S. Day New York: American Institute of Physics), 291
Corbet, R. H. D. 1986, *Mon. Not. R.astr. Soc.* **220**, 1047
Corbet, R. H. D., & Day, C. S. R. 1990, *Mon. Not. R.astr. Soc.* **243**, 553
Daumerie, P., Ghosh, P.,& Lamb, F. K. 1993, in preparation
Davies, R. E., & Pringle, J. E. 1981, *Mon. Not. R. astr. Soc.* **196**, 209
Deeter, J. E., *et al.* 1989, *Astrophys. J.* **336**, 376
Eisner, R. F., Ghosh, P., & Lamb, F. K. 1980, *Astrophys. J.* **241**, L155 (EGL)
Finger, M. H., *et al.* 1993, Proc. Second Compton Symposium, in press
Ghosh, P. 1994, in The Evolution of X-ray Binaries, ed. S. S. Holt & C. S. Day (New York: American Institute of Physics), 439
Ghosh, P., & Gruber, D. E. 1994, in preparation
Ghosh, P., & Lamb, F. K. 1979a, *Astrophys. J.* **232**, 259 (GL)
Ghosh, P., & Lamb, F. K. 1979b, *Astrophys. J.* 234, 296 (GL)
Ghosh, P., &Lamb, F. K. 1991, in Neutron Stars: Theory & Observation, ed. J. Ventura & D. Pines (Dordrecht: Reidel), 363 (GL)
Ghosh, P., & Lamb, F. K. 1992, in X-ray Binaries & Recycled Pulsars, ed. E. P. J. van den Heuvel & S. Rappaport (Dordrecht: Kluwer), 487
Henrichs, H. 1983, in Accretion-Driven Stellar X-ray Sources, ed. W. H. G. Lewin & E. P. J. van den Heuvel (Cambridge: Cambridge Univ. Press), 393
Ho, C. 1988, *Mon. Not. R. astr. Soc.* **232**, 91
Illarionov, A., F. & Kompaneets, D. A. 1990, *Mon. Not. R. astr. Soc.* **247**, 219
Illarionov, A., F. & Sunyaev, R. A. 1975, *Astron. & Astrophys.,* **39**, 185 (IS)
Johnston, S., *et al.* 1994, *Mon. Not. R. astr. Soc.* **268**, 430 (J94)
Kaspi, V. M., *et al.* 1994, *Astrophys. J.* **423**, L43
Kochanek, C. 1993, *Astrophys. J.* **406**, 638
Kulkarni, S. R. 1992, *Phil. Trans. Roy. Soc. London A* **341**, 77
Kundt, W., &Robnik, M. 1980, *Astron. & Astrophys.,* **91**, 305
Livio, M. 1993, private communication

Makishima, K., *et al.* 1988, *Nature*, **333**, 746
Manchester, R. N. 1994, private communication
Matsuda, T., *et al.* 1987, *Mon. Not. R. astr. Soc.* **226**, 785
Matsuda, T., *et al.* 1991, *Astron. & Astrophys.,* **248**, 301
Mihara, T. 1993, this volume
Mineshige, S., Rees, M. J., & Fabian, A. C. 1991, *Mon. Not. R. astr. Soc.* **251**, 555
Mony, B., *et al.* 1991, *Astron. & Astrophys.,* 247, 405
Nagase, F. 1989, *Proc. Astr. Soc. Japan* 41, 1
Nagase, F. 1992, in Proc. Ginga Memorial Symposium, ed. F. Makino & F. Nagase (Tokyo: ISAS), 1
Parmar, A. N., *et al.* 1989, *Astrophys. J.* 338, 359
Prince, T. A. 1993, Proc. Second Compton Symposium, in press
Shakura, N. L, & Sunyaev, R. A. 1973, *Astron .& Astrophys.,* 24, 337
Shapiro, S. L., & Lightman, A. P. 1976, *Astrophys. J.* 204, 555
Shapiro, S. L., *et al.* 1976, *Astrophys. J.* 204, 187
Stollberg, M. T., *et al.* 1993, IAU Circ. 5836
Taam, R. E., & Fryxell, B. A. 1989, *Astrophys. J.* 339, 297
van den Heuvel, E. P. J. 1992, in X-ray Binaries & Recycled Pulsars, ed. E. P. J. van den Heuvel & S. Rappaport (Dordrecht: Kluwer), 233 (vdH92)
van Paradijs, J. 1993, in X-ray Binaries, ed. W. H. G. Lewin *et al.,* (Cambridge: Cambridge Univ. Press), in press
Verbunt, F. 1994, in The Evolution of X-ray Binaries, ed. S. S. Holt & C. S. Day (New York: American Institute of Physics), 351
Wang, Y.-M. 1981, *Astron. & Astrophys.,* 102, 36
Wang, Y.-M. 1987, *Astron. & Astrophys.,* 183, 257
Waters, L.B. F. M., & van karkwijk, M. H. 1989, *Astron & Astrophys.,* 223, 196 (WK)
Webbink, R. F. 1992, in X-ray Binaries & Recycled pulsars, ed. E. P. J. van den Heuvel & S. Rappaport (Dordrecht: Kluwer), 269
Whit, N. E. & Stella, L. 1988, *Nature,* 332, 416
Wilson, C. A. *et al.*1993, Proc. Second Compton Symposium, in press
Wilson, R. B., *et al.* 1994, in The Evolution of X-ray Binaries, ed. S. S. Holt & C. S, Day (New York: American Institute of Physics), 475

Diamond Jubilee Symposium on Pulsars
14–17 March 1994
Raman Research Institute, Bangalore

J. Astrophys. Astr. (1995) **16,** 307–325

Reprinted with permission from
Reviews of Modern Physics, **66** No. 3, 711–719, 1994

Binary Pulsars and Relativistic Gravity*

Joseph H. Taylor, Jr. *Princeton University, Princeton, New Jersey 08544*

1. Search and Discovery

Work leading to the discovery of the first pulsar in a binary system began more than twenty years ago, so it seems reasonable to begin with a bit of history. Pulsars burst onto the scene (Hewish *et al*., 1968) in February 1968, about a month after I. completed my Ph.D. at Harvard University. Having accepted an offer to remain there on a post-doctoral fellowship, I was looking for an interesting new project in radio astronomy. When *Nature* announced the discovery of a strange new rapidly pulsating radio source, I immediately drafted a proposal, together with Harvard colleagues, to observe it with the 92 m radio telescope of the National Radio Astronomy Observatory. By late spring we had detected and studied all four of the pulsars which by then had been discovered by the Cambridge group, and I began thinking about how to find further examples of these fascinating objects, which were already thought likely to be neutron stars. Pulsar signals are generally quite weak, but have some unique characteristics that suggest effective search strategies. Their otherwise noise-like signals are modulated by periodic, impulsive waveforms; as a consequence, dispersive propagation through the interstellar medium makes the narrow pulses appear to sweep rapidly downward in frequency. I devised a computer algorithm for recognizing such periodic, dispersed signals in the inevitable background noise, and in June 1968 we used it to discover the fifth known pulsar (Huguenin *et al*., 1968).

Since pulsar emissions exhibited a wide variety of new and unexpected phenomena, we observers put considerable effort into recording and studying their details and peculiarities. A pulsar model based on strongly magnetized, rapidly spinning neutron stars was soon established as consistent with most of the known facts (Gold, 1968). The model was strongly supported by the discovery of pulsars inside the glowing, gaseous remnants of two supernova explosions, where neutron stars should be created (Large, *et al*., 1968; Staelin and Reifenstein, 1968), and also

*Nobel Lecture, presented to the Royal Swedish Academy of Sciences on 8 December 1993.

by an observed gradual lengthening of pulsar periods (Richards and Comella, 1969) and polarization measurements that clearly suggested a rotating source (Radhakrishnan and Cooke, 1969). The electrodynamical properties of a spinning, magnetized neutron star were studied theoretically (Goldreich and Julian, 1969) and shown to be plausibly capable of generating broadband radio noise detectable over interstellar distances. However, the rich diversity of the observed radio pulses suggested magnetospheric complexities far beyond those readily incorporated in theoretical models. Many of us suspected that detailed understanding of the pulsar emission mechanism might be a long time coming – and that, in any case, the details might not turn out to be fundamentally illuminating.

In September 1969 I joined the faculty at the University of Massachusetts, where a small group of us planned to build a large, cheap radio telescope especially for observing pulsars. Our telescope took several years to build, and during this time it became clear that whatever the significance of their magnetospheric physics, pulsars were interesting and potentially important to study for quite different reasons. As the collapsed remnants of supernova explosions, they could provide unique experimental data on the final stages of stellar evolution, as well as an opportunity to study the properties of nuclear matter in bulk. Moreover, many pulsars had been shown to be remarkably stable natural clocks (Manchester and Peters, 1972), thus providing an alluring challenge to the experimenter, with consequences and applications about which we could only speculate at the time. For such reasons as these, by the summer of 1972 I was devoting a large portion of my research time to the pursuit of accurate timing measurements of known pulsars, using our new telescope in western Massachusetts, and to planning a large-scale pulsar search that would use bigger telescopes at the national facilities.

I suspect it is not unusual for an experiment's motivation to depend, at least in part, on private thoughts quite unrelated to avowed scientific goals. The challenge of a good intellectual puzzle, and the quiet satisfaction of finding a clever solution, must certainly rank highly among my own incentives and rewards. If an experiment seems difficult to do, but plausibly has interesting consequences, one feels compelled to give it a try. Pulsar searching is the perfect example: it's clear that there must be lots of pulsars out there, and, once identified, they are not so very hard to observe. But finding each one for the first time is a formidable task, one that can become a sort of detective game. To play the game you invent an efficient way of gathering clues, sorting, and assessing them, hoping to discover the identities and celestial locations of all the guilty parties.

Most of the several dozen pulsars known in early 1972 were discovered by examination of strip-chart records, without benefit of further signal processing. Nevertheless, it was clear that digital computer techniques would be essential parts of more sensitive surveys. Detecting new pulsars is necessarily a multidimensional process; in addition to the usual variables of two spatial coordinates, one must also search thoroughly over wide ranges of period and dispersion measure. Our first pulsar survey, in 1968, sought evidence of pulsar signals by computing the discrete Fourier transforms of long sequences of intensity samples, allowing for the expected narrow pulse shapes by summing the amplitudes of a dozen or more harmonically related frequency components. I first described this basic algorithm (Burns and Clark, 1969) as part of a discussion of pulsar search techniques, in 1969. An

efficient dispersion-compensating algorithm was conceived and implemented soon afterward (Manchester *et al*., 1972; Taylor, 1974), permitting extension of the method to two dimensions. Computerized searches over period and dispersion measure, using these basic algorithms, have by now accounted for discovery of the vast majority of nearly 600 known pulsars, including forty in binary systems (Taylor *et al*., 1993; Camilo, 1994).

In addition to private stimuli related to "the thrill of the chase", my outwardly expressed scientific motivation for planning an extensive pulsar survey in 1972 was a desire to double or triple the number of known pulsars. I had in mind the need for a more solid statistical basis for drawing conclusions about the total number of pulsars in the Galaxy, their spatial distribution, how they fit into the scheme of stellar evolution, and so on. I also realized (Taylor, 1972) that it would be highly desirable "... to find even *one* example of a pulsar in a binary system, for measurement of its parameters could yield the pulsar mass, an extremely important number." Little did I suspect that just such a discovery would be made, or that it would have much greater significance that anyone had foreseen! In addition to its own importance, the binary pulsar PSR 1913+16 is now recognized as the harbinger of a new class of unusually short-period pulsars with numerous important applications.

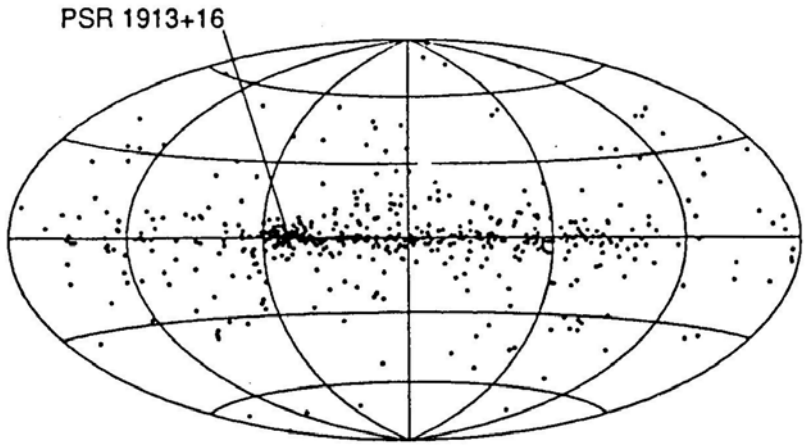

Figure 1: Distribution of 558 pulsars in Galactic coordinates. The Galactic center is in the middle, and longitude increases to the left.

An up-to-date map of known pulsars on the celestial sphere is shown in Fig. 1. The binary pulsar PSR 1913+16 is found in a clump of objects close to the Galactic plane around longitude 50°, a part of the sky that passes directly overhead at the latitude of the Arecibo Observatory in Puerto Rico. Forty of these pulsars, including PSR 1913+16, were discovered in the survey that Russell Hulse and I

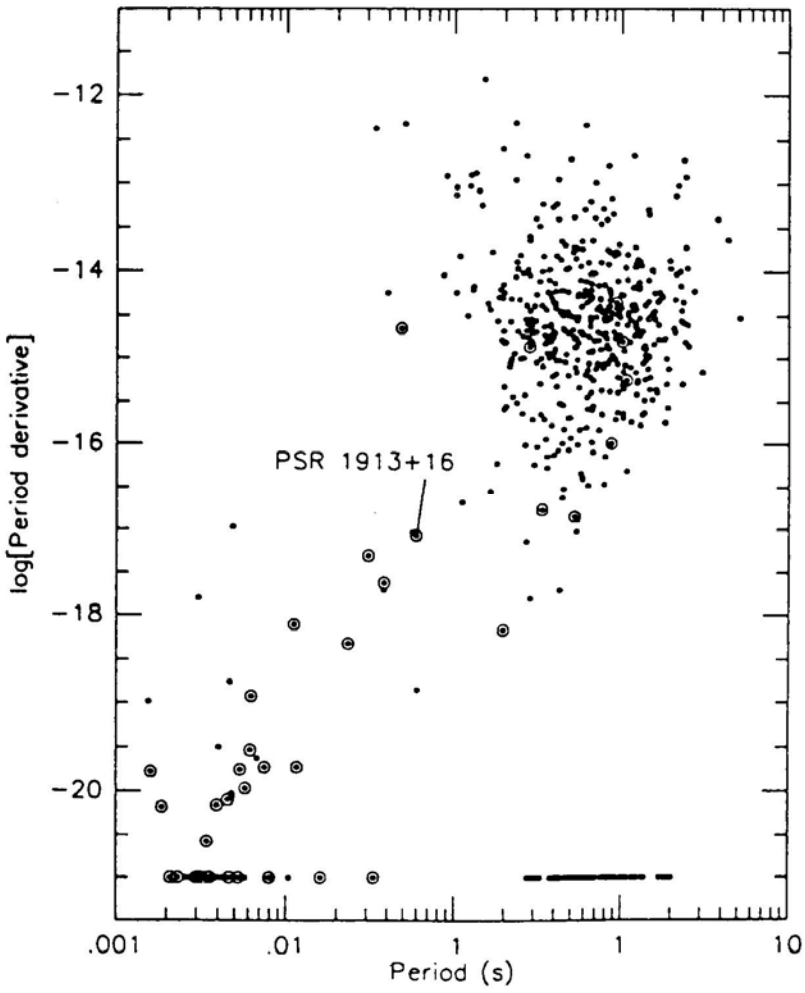

Figuie 2: Periods and period derivatives of known pulsars. Binary pulsars, denoted by large circles around the dots, generally have short periods and small derivatives. Symbols aligned near the bottom represent pulsars for which the slow-down rate has not yet been measured.

carried out with the 305 m Arecibo telescope (Hulse and Taylor, 1974, 1975a, 1975b). Figure 2 illustrates the periods and spin-down rates of known pulsars, with those in binary systems marked by larger circles around the dots. All radio pulsars slow down gradually in their own rest frames, but the slow-down rates vary over nine orders of magnitude. Figure 2 makes it clear that binary pulsars are special in this regard. With few exceptions, they have unusually small values of both period and period derivative—an important factor which helps to make

them especially suitable for high-precision timing measurements.

Much of the detailed implementation and execution of our 1973–74 Arecibo survey was carried out by Russell Hulse. He describes that work, and particularly the discovery of PSR 1913+16, in his accompanying lecture (Hulse, 1994). The significant consequences of our discovery have required accurate timing measurements extending over many years, and since 1974–76 I have pursued these with a number of other collaborators. I shall now turn to a description of these observations.

2. Clock-Comparison Experiments

Pulsar timing experiments are straightforward in concept: one measures pulse times of arrival (TOAs) at the telescope, and compares them with time kept by a stable reference clock. A remarkable wealth of information about a pulsar's spin, location in space, and orbital motion can be obtained from such simple measurements. For binary pulsars, especially, the task of analyzing a sequence of TOAs often assumes the guise of another intricate detective game. Principal

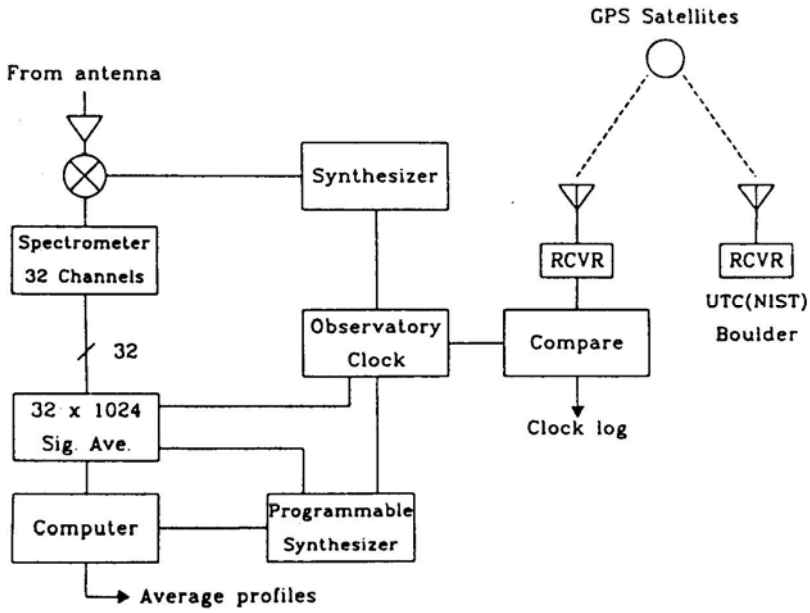

Figure 3: Simplified block diagram of equipment used for timing pulsars at Arecibo.

clues in this game are the recorded TOAs. The first and most difficult objective is the assignment of unambiguous pulse numbers to each TOA, despite the fact that some of the observations may be separated by months or even years from their nearest neighbors. During such inevitable gaps in the data, a pulsar may have

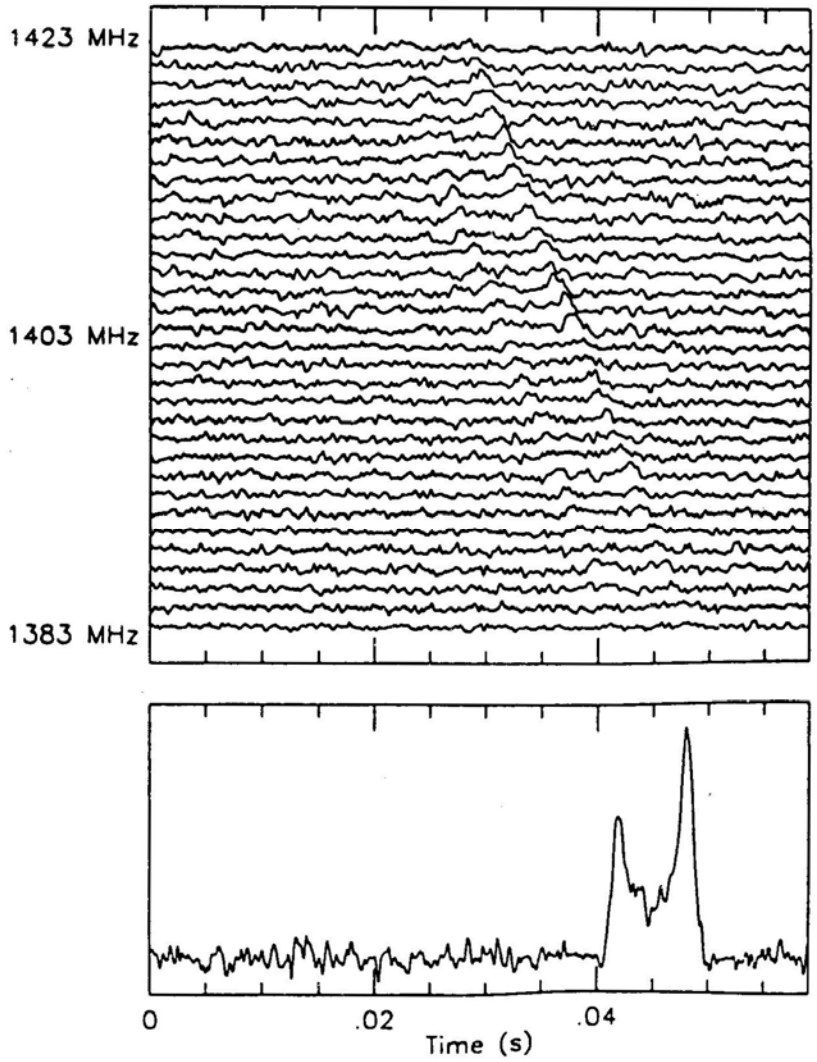

Figure 4: Pulse profiles obtained on April 24, 1992 during a five-minute observation of PSR 1913+16. The characteristic double-peaked shape, clearly seen in the de-dispersed profile at the bottom, is also discernible in the 32 individual spectral channels.

rotated through as many as 10^7–10^{10} turns, and in order to extract the maximum information content from the data, these integers must be recovered *exactly*. Fortunately, the correct sequence of pulse numbers is easily recognized, once attained, so you can tell when the game has been "won".

A block diagram of equipment used for recent pulsar timing observations (Taylor, 1991) at Arecibo is shown in Fig. 3. Incoming radio-frequency signals from the antenna are amplified, converted to intermediate frequency, and passed through

a multichannel spectrometer equipped with square-law detectors. A bank of digital signal averages accumulates estimates of a pulsar's periodic wave form in each spectral channel, using a precomputed digital ephemeris and circuitry synchronized with the observatory's master clock. A programmable synthesizer, its output frequency adjusted once a second in a phase-continuous manner, compensates for changing Doppler shifts caused by accelerations of the pulsar and the telescope. Average profiles are recorded once every few minutes, together with appropriate time tags. A log is kept of small measured offsets (typically of order 1 μs) between the observatory clock and the best available standards at national time-keeping laboratories, with time transfer accomplished via satellites in the Global Positioning System.

An example of pulse profiles recorded during timing observations of PSR 1913+16 is presented in Fig. 4, which shows intensity profiles for 32 spectral channels spanning the frequency range 1383–1423 MHz, followed by a "de-dispersed" profile at the bottom. In a five-minute observation such as this, the signal-to-noise ratio is just high enough for the double-peaked pulse shape of PSR 1913+16 to be evident in the individual channels. Pulse arrival times are determined by measuring the phase offset between each observed profile and a long-term average with much higher signal-to-noise ratio. Differential dispersive delays are removed, the adjusted offsets are averaged over all channels, and the resulting mean value is added to the time tag to obtain an equivalent TOA. Nearly 5000 such five-minute measurements have been obtained for PSR 1913+16 since 1974, using essentially this technique. Through a number of improvements in the data-taking systems (Taylor *et al*., 1976; McCulloch *et al*., 1979; Taylor *et al*., 1979; Taylor and Weisberg, 1982, 1989; Stinebring *et al*., 1992), the typical uncertainties have been reduced from around 300 μs in 1974 to 15–20 μs since 1981.

3. Model Fitting

In the process of data analysis, each measured topocentric TOA, say $t_{\rm obs}$, must be transformed to a corresponding proper time of emission T in the pulsar frame. Under the assumption of a deterministic spin-down law, the rotational phase of the pulsar is given by

$$\phi(T) = \nu T + \frac{1}{2}\,\dot{\nu}\,T^2, \tag{1}$$

where ϕ is measured in cycles, $\nu \equiv 1/P$ is the rotation frequency, P the period, and $\dot{\nu}$ the slowdown rate. Since a topocentric TOA is a relativistic space-time event, it must be transformed as a four-vector. The telescope's location at the time of a measurement is obtained from a numerically integrated solar-system model, together with published data on the Earth's unpredictable rotational variations. As a first step one normally transforms to the solar-system barycenter, using the weak-field, slow-motion limit of general relativity. The necessary equations include terms depending on the positions, velocities, and masses of all significant solar-system bodies. Next, one accounts for propagation effects in the interstellar medium; and finally, for the orbital motion of the pulsar itself.

With presently achievable accuracies, all significant terms in the relativistic

transformation can be summarized in the single equation

$$\begin{aligned} T &= t_{\rm obs} - t_0 + \Delta_C - D/f^2 + \Delta_{R\odot}(\alpha, \delta, \mu_\alpha, \mu_\delta, \pi) \\ &\quad + \Delta_{E\odot} - \Delta_{S\odot}(\alpha, \delta) \\ &\quad - \Delta_R(x, e, P_b, T_0, \omega, \dot{\omega}, \dot{P}_b) - \Delta_E(\gamma) - \Delta_S(r, s). \end{aligned} \tag{2}$$

Here t_0 is a nominal equivalent TOA at the solar-system barycenter; Δ_C represents measured clock offsets; D/f^2 is the dispersive delay for propagation at frequency f through the interstellar medium; $\Delta_{R\odot}$, $\Delta_{E\odot}$, and $\Delta_{S\odot}$ are propagation delays and relativistic time adjustments within the solar system; and Δ_R, Δ_E, and Δs are similar terms for effects within a binary pulsar's orbit. Subscripts on the various Δ's indicate the nature of the time-dependent delays, which include "Römer", "Einstein", and "Shapiro" delays in the solar system and in the pulsar orbit. The Römer terms have amplitudes comparable to the orbital periods times $v/2\pi c$, where v is the orbital velocity and c the speed of light. The Einstein terms, representing the integrated effects of gravitational redshift and time dilation, are

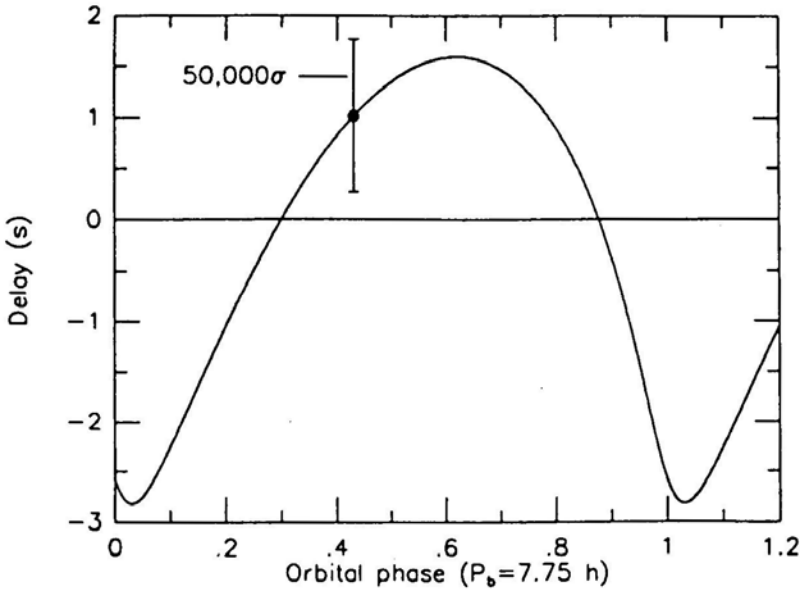

Figure 5: Orbital delays observed for PSR 1913+16 during July, 1988. The uncertainty of an individual five-minute measurement is typically 50 000 times smaller than the error bar shown.

smaller by another factor ev/c, where e is the orbital eccentricity. The Shapiro time delay is a result of reduced velocities that accompany the well-known bending of light rays propagating close to a massive object. The delay amounts to about 120 μs for one-way lines of sight grazing the Sun, and the magnitude depends logarithmically on the angular impact parameter. The corresponding delay within

a binary pulsar orbit depends on the companion star's mass, the orbital phase, and the inclination i between the orbital angular momentum and the line of sight.

Figure 5 illustrates the combined orbital delay $\Delta_R + \Delta_E + \Delta s$ for PSR 1913+16, plotted as a function of orbital phase. Despite the fact that the Einstein and Shapiro effects are orders of magnitude smaller than the Römer delay, they can still be measured separately if the precision of available TOAs is high enough. In fact, the available precision is very high indeed, as one can see from the lone data point shown in Fig. 5 with 50 000σ error bars.

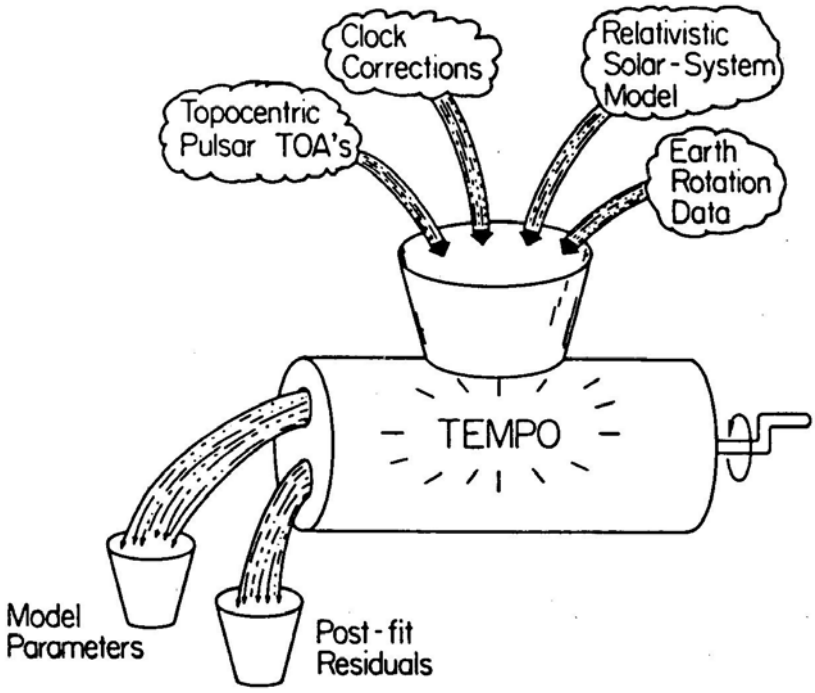

Figure 6: Schematic diagram of the analysis of pulsar timing measurements carried out by the computer program TEMPO. The essential functions are all described in the text.

Equations (1) and (2) have been written to show explicitly the most significant dependences of pulsar phase on as many as nineteen *a priori* unknowns. In addition to the rotational frequency ν and spin-down rate $\dot{\nu}$, these phenomenological parameters include a reference arrival time t_0, the dispersion constant D, celestial coordinates α and δ, proper-motion terms μ_α and μ_δ, and annual paralax π. For binary pulsars the terms on the third line of Eq. (2), with as many as ten signify-cant orbital parameters, are also required. The additional parameters include five that would be necessary even in a purely Keplerian analysis of orbital motion: the projected semimajor axis $x \equiv a_1 \sin i/c$, eccentricity e, binary period P_b, longitude of periastron ω, and time of periastron T_0. If the experimental precision is high

enough, relativistic effects can yield the values of five further "post-Keplerian" parameters: the secular derivatives $\dot{\omega}$ and $\dot{P}_b$, the Einstein parameter γ, and the range and shape of the orbital Shapiro delay, r and $s \equiv \sin i$. Several earlier versions of this formalism for treating timing measurements of binary pulsars exist (Blandford and Teukolsky, 1976; Epstein, 1977; Haugan, 1985), and have been historically important to our progress with the PSR 1913+16 experiment. The elegant framework outlined here was derived during 1985–86 by Damour and Deruelle (1985, 1986).

Model parameters are extracted from a set of TOAs by calculating the pulsar phases $\phi(T)$ from Eq. (1) and minimizing the weighted sum of squared residuals,

$$\chi^2 = \sum_{i=1}^{N} \left[\frac{\phi(T_i) - n_i}{\sigma_i / P} \right]^2 , \tag{3}$$

with respect to each parameter to be determined. In this equation, n_i is the closest integer to $\phi(T_i)$, and σ_i is the estimated uncertainty of the ith TOA. In a valid and reliable solution the value of χ^2 will be close to the number of degrees of freedom, i.e., the number of measurements N minus the number of adjustable parameters. Parameter errors so large that the closest integer to $\phi(T_i)$ may not be the correct pulse number are invariably accompanied by huge increases in χ^2; this is the reason for my earlier statement that correct pulse numbering is easily recognizable, once attained. In addition to providing a list of fitted parameter values and their estimated uncertainties, the least-squares solution produces a set of post-fit residuals, or differences between measured TOAs and those predicted by the model (see Fig. 6). The post-fit residuals are carefully examined for evidence of systematic trends that might suggest experimental errors, or some inadequacy in the astrophysical model, or perhaps deep physical truths about the nature of gravity.

Necessarily some model parameters will be easier to measure than others. When many TOAs are available, spaced over many months or years, it generally follows that at least the pulsar's celestial coordinates, spin parameters, and Keplerian orbital elements will be measurable with high precision, often as many as 6–14 significant digits. As we will see, the relativistic parameters of binary pulsar orbits are generally much more difficult to measure—but the potential rewards for doing so are substantial.

4. The Newtonian Limit

Thirty-five binary pulsar systems have now been studied well enough to determine their basic parameters, including the Keplerian orbital elements, with good accuracy. For each system the orbital period P_b and projected semimajor axis x can be combined to give the mass function.

$$f_1(m_1, m_2, s) = \frac{(m_2 s)^3}{(m_1 + m_2)^2} = \frac{x^3}{T_\odot (P_b/2\pi)^2} . \tag{4}$$

Here m_1 and m_2 are the masses of the pulsar and companion in units of the Sun's mass, $M_\odot$; I use the shorthand notations $s \equiv \sin i$, $T_\odot \equiv GM_\odot / c^3 = 4.925490947 \times$

10^{-6} s, where G is the Newtonian constant of gravity. In the absence of other information, the mass function cannot provide unique solutions for m_1, m_2, or s. Nevertheless, likely values of m_2 can be estimated by assuming a pulsar mass close to $1.4M_\odot$ (the Chandrasekhar limit for white dwarfs) and the median value $\cos i = 0.5$, which implies $s = 0.87$. With this approach one can distinguish three categories of binary pulsars, which I shall discuss by reference to Fig. 7: a plot of binary pulsar companion masses versus orbital eccentricities.

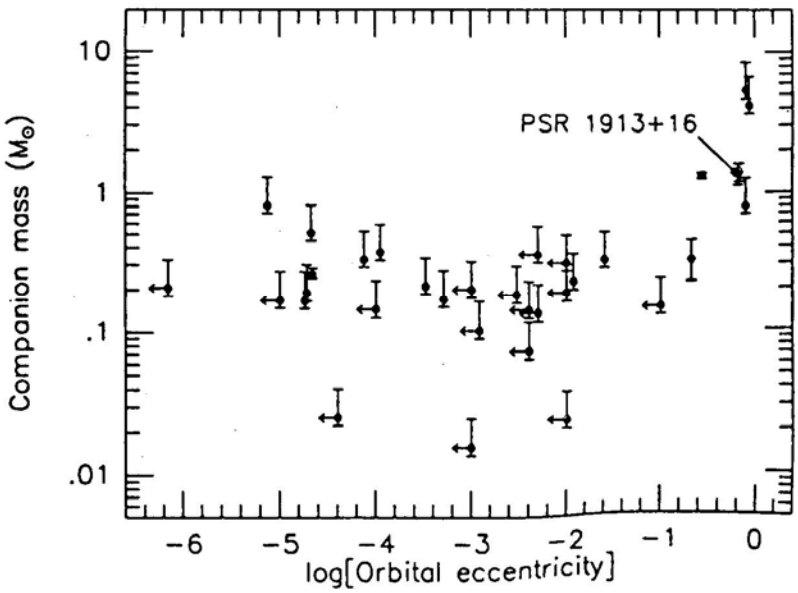

Figure 7: Masses of the companions of binary pulsars, plotted as a function or orbital eccentricity. Near the marked location of PSR 1913+16, three distinct symbols have merged into one; these three binary systems, as well as their two nearest neighbors in the graph, are thought to be pairs of neutron stars. The two pulsars at the upper right are accompanied by high-mass main-sequence stars, while the remainder are believed to have white-dwarf companions.

Twenty-eight of the binary systems in Fig. 7 have orbital eccentricities $e < 0.25$ and low-mass companions likely to be degenerate dwarfs. Most of these have nearly circular orbits; indeed, the only ones with eccentricities more than a few percent are located in globular clusters, and their orbits have probably been perturbed by near collisions with other stars. Five of the binaries have much larger eccentricities and likely companion masses of 0.8 $M_\odot$ or more; these systems are thought to be pairs of neutron stars, one of which is the detectable pulsar. The large orbital eccentricities are almost certainly the result of rapid ejection of mass in the supernova explosion creating the second neutron star. Finally, at the upper right of Fig. 7 we find two binary pulsars that move in eccentric orbits around high-mass main-sequence stars. These systems have not yet evolved to the stage of a second supernova

explosion. Unlike the binary pulsars with compact companions, these two systems have orbits that could be significantly modified by complications such as tidal forces or mass loss.

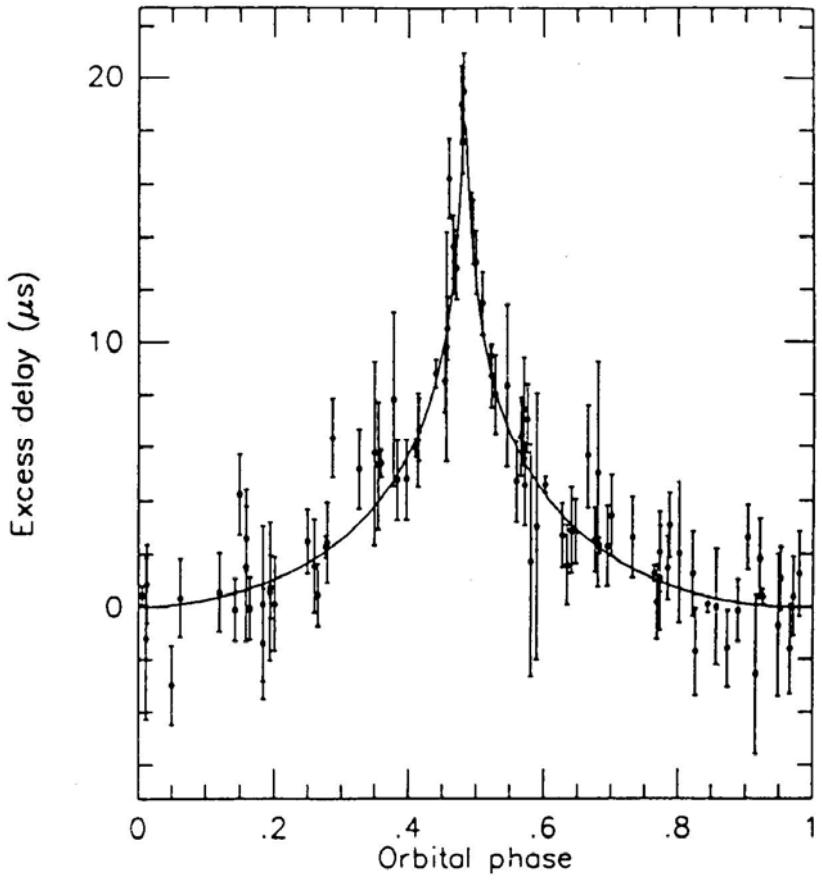

Figure 8: Measurements of the Shapiro time delay in the PSR 1855+09 system. The theoretical curve corresponds to Eq. (10), and the fitted values of r and s can be used to determine the masses of the pulsar and companion star.

5. General Relativity as a Tool

As Russell Hulse and I suggested in the discovery paper for PSR 1913+16 (Hulse and Taylor, 1975a), it should be possible to combine measurements of relativistic orbital parameters with the mass function, thereby determining masses of both stars and the orbital inclination. In the post-Keplerian (PK) framework outlined above, each measured PK parameter defines a unique curve in the (m_1 , m_2) plane, valid within a specified theory of gravity. Experimental values for any two PK parameters (say, $\dot{\omega}$ and γ, or perhaps r and s) establish the values of m_1, m_2 , and

s unambiguously. In general relativity the equations for the five most significant PK parameters are as follows (Damour and Deruelle, 1986; Taylor and Weisberg, 1989; Damour and Taylor, 1992):

$$\dot{\omega} = 3\left[\frac{P_b}{2\pi}\right]^{-5/3}(T_\odot M)^{2/3}\left(1-e^2\right)^{-1}\,, \tag{5}$$

$$\gamma = e\left[\frac{P_b}{2\pi}\right]^{1/3}T_\odot^{2/3}M^{-4/3}m_2(m_1+2m_2)\,, \tag{6}$$

$$\dot{P}_b = -\frac{192\pi}{5}\left[\frac{P_b}{2\pi}\right]^{-5/3}\left[1+\frac{73}{24}e^2+\frac{37}{96}e^4\right] \times(1-e^2)^{-7/2}T_\odot^{5/3}m_1m_2M^{-1/3}\,, \tag{7}$$

$$r = T_\odot m_2\,, \tag{8}$$

$$s = x\left[\frac{P_b}{2\pi}\right]^{-2/3}T_\odot^{-2/3}M^{2/3}m_2^{-1}\,. \tag{9}$$

Again the masses m_1, m_2 , and $M \equiv m_1 + m_2$ are expressed in solar units. I emphasize that the left-hand sides of Eqs. (5) through (9) represent directly measurable quantities, at least in principle. Any two such measurements, together with the well-determined values of e and P_b, will yield solutions for m_1 and m_2, as well as explicit predictions for the remaining PK parameters.

The binary systems most likely to yield measurable PK parameters are those with large masses and high eccentricities and which are astrophysically "clean", so that their orbits are overwhelmingly dominated by the gravitational interactions between two compact masses. The five pulsars clustered near PSR 1913+16 in Fig. 7 would seem to be especially good candidates, and this has been borne out in practice. In the most favourable circumstances, even binary pulsars with low-mass companions and nearly circular orbitals can yield significant post-Keplerian measurements. The best present example is PSR 1855+09: its orbital plane is nearly parallel to the line of sight, greatly magnifying the orbital Shapiro delay. The relevant measurements (Rawley *et al*., 1988; Ryba and Taylor, 1991; Kaspi *et al*., 1994) are illustrated in Fig. 8, together with the fitted function $\Delta s(r, s)$, in this case closely approximated by

$$\Delta_S = -2r\log(1 - s\cos[2\pi(\phi-\phi_0)])\,, \tag{10}$$

where ϕ is the orbital phase in cycles and $\phi_0 = 0.4823$ the phase of superior conjunction. The fitted values of r and s yield the masses $m_1 = 1.50^{+0.26}_{-0.14}$, $m_2 = +0.0258^{+0.028}_{-0.016}$. In a similar way, all binary pulsars with two measurable PK parameters yield solutions for their component masses. At present, most of the experimental data on the masses of neutron stars (see Fig. 9) come from such timing analyses of binary pulsar systems (Taylor and Dewey, 1988; Thorsett *et al.,* 1993, and references therein).

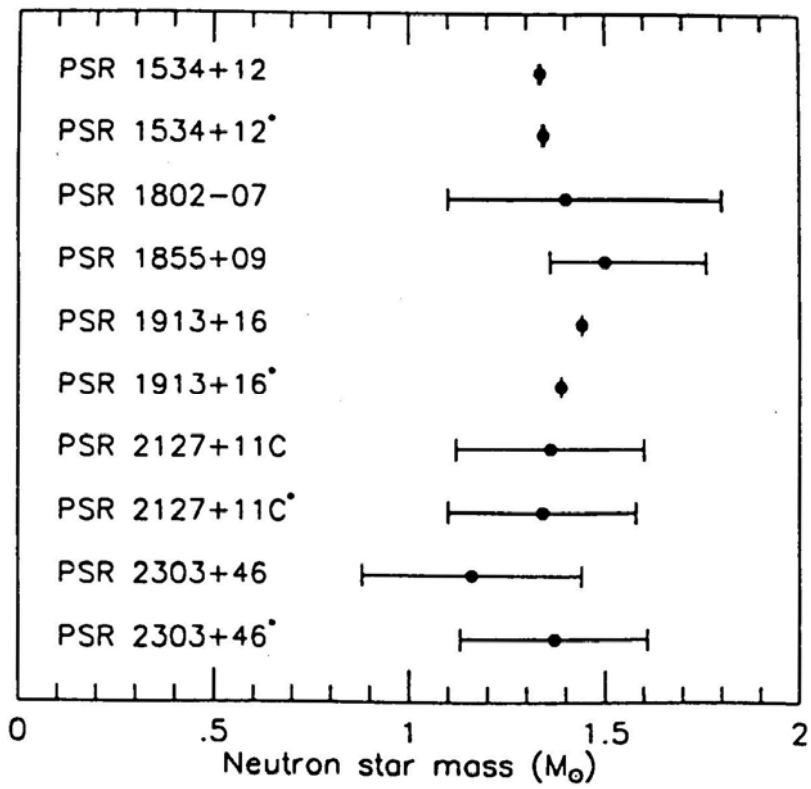

Figure 9: The masses of 10 neutron stars, measured by observing relativistic effects in binary pulsar orbits. Asterisks after pulsar names denote companions to the observed pulsars.

6. Testing for Gravitational Waves

If three or more post-Keplerian parameters can be measured for a particular pulsar, the system becomes over-determined, and the extra experimental degrees of freedom transform it into a calibrated laboratory for testing relativistic gravity. Each measurable PK parameter beyond the first two provides an explicit, quantitative test. Because the velocities and gravitational energies in a high-mass binary pulsar system can be significantly relativistic, strong-field and radiative effects come into play. Two binary pulsars, PSRs 1913+16 and 1534+12, have now been timed well enough and long enough to yield three or more PK parameters. Each one provides significant tests of gravitation beyond the weak-field, slow-motion limit (Damour and Taylor, 1982; Taylor *et al*., 1992).

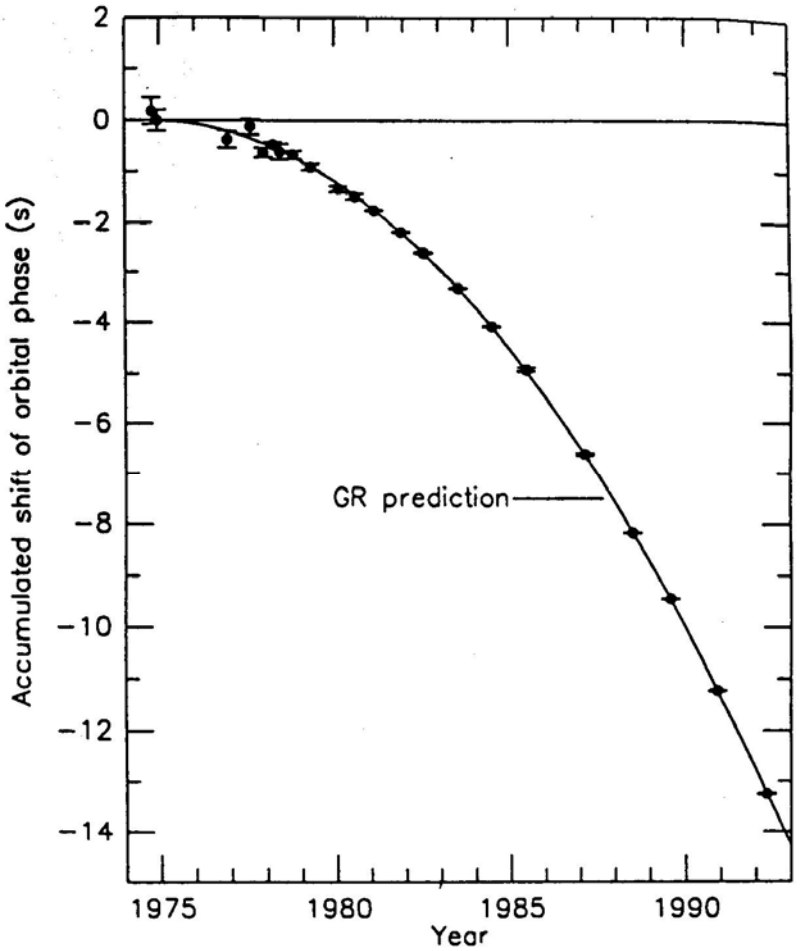

Figure 10: Accumulated shift of the time of periastron in the PSR 1913+16 system, relative to an assumed orbit with constant period. The parabolic curve represents the general relativistic prediction for energy losses from gravitational radiation.

PSR 1913+16 has an orbital period $P_b \approx 7.8$ h, eccentricity $e \approx 0.62$, and mass function $f_1 \approx 0.13 M_\odot$. With the available data quality and time span, the Keplerian orbital parameters are actually determined with fractional accuracies of a few parts per million, or better. In addition, the PK parameters $\dot{\omega}$, γ, and $\dot{P}_b$ are determined with fractional accuracies better than 3×10^{-6}, 5×10^{-4}, and 4×10^{-3}, respectively (Taylor and Weisberg, 1989; Taylor, 1993). Within any viable relativistic theory of gravity, the values of $\dot{\omega}$ and γ, yield the values of m_1 and m_2 and a corresponding prediction for $\dot{P}_b$ arising from the damping effects of gravitational radiation. At present levels of accuracy, a small kinematic correction (approximately 0.5% of the observed $\dot{P}_b$) must be included to account for accelerations of the solar system and the binary pulsar system in the Galactic gravitational

field (Damour and Taylor, 1991). After doing so, we find that Einstein's theory passes this extraordinarily stringent test with a fractional accuracy better than 0.4% (see Figs. 10 and 11). The clock-comparison experiment for PSR 1913+16 thus provides direct experimental proof that changes in gravity propagate at the speed of light, thereby creating a dissipative mechanism in an orbiting system. It necessarily follows that gravitational radiation exists and has a quadrupolar nature.

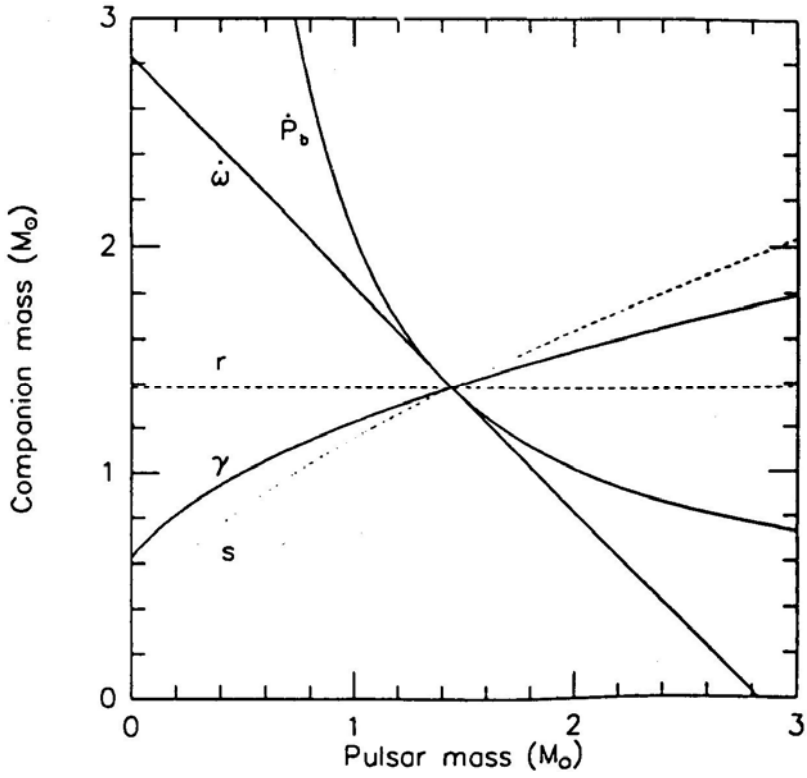

Figure. 11: Solid curves correspond to Eqs. (5)–(7) together with the measured values of $\dot{\omega}$, γ, and $\dot{P}_b$. Their intersection at a single point (within the experimental uncertainty of about 0.35% in $\dot{P}_b$), establishes the existence of gravitational waves. Dashed curves correspond to the *predicted* values of parameters r and s; these quantities should become measurable with a modest improvement in data quality.

PSR 1534+12 was discovered just three years ago, in a survey by Aleksander Wolszczan (1991) that again used the huge Arecibo telescope to good advantage. This pulsar promises eventually to surpass the results now available from PSR 1913+16. It has orbital period $\dot{P}_b \approx 10.1$ h, eccentricity $e \approx 0.27$, and mass function $f_1 \approx 0.31 M_\odot$. Moreover, with a stronger signal and narrower pulse than PSR 1913+16, its TOAs have considerably smaller measurement uncertainties, around 3 μs for five-minute observations. Results based on 15 months of data (Taylor *et al.,* 1992) have already produced significant measurements of four PK

parameters: $\dot{\omega}$, γ, r, and s. In recent work not yet published, Wolszczan and I have measured the orbital decay rate, P_b, and found it to be in accord with general relativity at about 20% level. In fact, *all* measured parameters of the PSR 1534+12 system are consistent within general relativity, and it appears that when the full experimental analysis is complete, Einstein's theory will have passed three more very stringent tests under strong-field and radiative conditions.

I do not believe that general relativity necessarily contains the last valid words to be written about the nature of gravity. The theory is not, of course, a quantum theory, and at its most fundamental level the universe appears to obey quantum-mechanical rules. Nevertheless, our experiments with binary pulsars show that, whatever the precise directions of future theoretical work may be, the correct theory of gravity must make predictions that are asymptotically close to those of general relativity over a vast range of classical circumstances.

Acknowledgements

Russell Hulse and I have many individuals to thank for their important work, both experimental and theoretical, without which our discovery of PSR 1913+16 could not have borne fruit so quickly or so fully. Most notable among these are Roger Blandford, Thibault Damour, Lee Fowler, Peter McCulloch, Joel Weisberg, and the skilled and dedicated technical staff of the Arecibo Observatory.

References

Blandford, R., and S.A. Teukolsky, 1976, "Arrival-time analysis for a pulsar in a binary system", *Astrophys. J.* **205,** 580–591.

Burns, W.R., and B.G. Clark, 1969, "Pulsar search techniques", *Astron. Astrophys.* **2,** 280–287

Camilo, F., 1994, "Millisecond pulsar searches", in *Lives of the Neutron Stars*, *NATO ASI Series*, edited by A. Alpar (Kluwer, Dordrecht).

Damour, T., and N. Deruelle, 1985, "General relativistic celestial mechanics of binary systems. I. The post-Newtonian motion", Ann. Inst. Henri Poincare Phys. Theor. **43,** 107–132.

Damour, T., and N. Deruelle, 1986, "General relativistic celestial mechanics of binary systems. II. The post-Newtonian timing formula", Ann. Inst. Henri Poincare Phys. Theor. **44,** 263–292.

Damour, T., and J.H. Taylor, 1991, "On the orbital period change of the binary pulsar PSR 1913+16", *Astrophys. J.* **366,** 501–511.

Damour, T., and J.H. Taylor, 1992, "Strong-field tests of relativistic gravity and binary pulsars", *Phys. Rev. D.* **45,** 1840–1868.

Epstein, R., 1977, "The binary pulsar: Post Newtonian timing effects", *Astrophys. J.* **216,** 92–100.

Gold,T., 1968, "Rotating neutron stars as the origin of the pulsating radio sources", *Nature* **218,** 731–732.

Goldreich, P., and W.H. Julian, 1969, "Pulsar electrodynamics", *Astrophys. J.* **157,** 869–880.

Haugan, M.P., 1985, "Post-Newtonian arrival-time analysis for a pulsar in a binary system", *Astrophys. J.* **296,** 1–12

Hewish, A., S.J. Bell, J.D.H. Pilkington, P.F. Scott, and R.A. Collins, 1968, "Observations of a rapidly pulsating radio source", *Nature* **217,** 709–713.

Huguenin, G.R., J.H. Taylor, L.E. Goad, A. Hartai, G.S.F. Orsten, and A.K. Rodman, 1968, "New pulsating radio source", *Nature* **219,** 576.

Hulse, R.A., 1994, "The discovery of the binary pulsar", in Les Prix Nobel (The Nobel Foundation).

Hulse, R.A., and J.H. Taylor, 1974, "A high sensitivity pulsar survey", *Astrophys. J.* **191,** L59–L61.

Hulse, R.A., and J.H. Taylor, 1975a, "Discovery of a pulsar in a binary system", *Astrophys. J.* **195,** L51–L53.

Hulse, R.A., and J.H. Taylor, 1975b, "A deep sample of new pulsars and their spatial extent in the galaxy", *Astrophys. J.* **201,** L55–L59.

Kaspi, V.M., J.H. Taylor, and M. Ryba, 1994, "High-precision timing of millisecond pulsars. III. Long term monitoring of PSRs B1855+09 and B1937+21", *Astrophys. J.* (in press)

Large M.I., A.E. Vaughan, and B.Y. Mills, 1968, "A pulsar supernova association", *Nature* **220,** 340–341.

Manchester, R.N., and W.L. Peters, 1972, "Pulsar parameters from timing observations", *Astrophys. J.* **173,** 221–226.

Manchester, R.N., J.H. Taylor, and G.R. Huguenin, 1972, "New and improved parameters for twenty-two pulsars", *Nature Phys. Sci.* **240,** 74.

McCulloch, P.M., J.H. Taylor, and J.M. Weisberg, 1979, "Tests of a new dispersion-removing radiometer on binary pulsar PSR 1913+16", *Astrophys. J.* **227,** L133–L137.

Radhakrishnan, V., and D.J. Cooke, 1969, "Magnetic poles and the polarization structure of pulsar radiation", *Astrophys. Lett.* **3,** 225–229.

Rawley, L.A., J.H. Taylor, and M.M. Davis, 1988, "Fundamental astronomy and millisecond pulsars", *Astrophys. J.* **326,** 947–953.

Richards, D.W., and J.M. Comella, 1969, "The period of pulsar NP 0532", *Nature* **222,** 551–552.

Ryba, M.F., and J.H. Taylor, 1991, "High precision timing of millisecond pulsars. I. Astrometry and masses of the PSR 1855+09 system", *Astrophys. J.* **371,** 739–748.

Staelin, D.H., and E.C. Reifenstein, III, 1968, "Pulsating radio sources near the Crab Nebula", *Science* **162,** 1481–1483.

Stinebring, D.R., V.M. Kaspi, D.J. Nice, M.F. Ryba, J.H. Taylor, S.E. Thorsett, and T.H. Hankins, 1992, "A flexible data acquisition system for timing pulsars", *Rev. Sci. Instrum.* **63,** 3551–3555.

Taylor, J.H., 1972, "A high sensitivity survey to detect new pulsars", research proposal submitted to the US National Science Foundation, September, 1972.

Taylor, J.H., 1974, "A sensitive method for detecting dispersed radio emission", *Astron. Asirophya. Suppl. Ser*. **15,** 367.

Taylor, J.H., 1991, "Millisecond pulsars: Nature's most stable clocks", Proc. IEEE **79,** 1054–1062.

Taylor, J.H., 1993, "Testing relativistic gravity with binary and millisecond pulsars", in *General Relativity and Gravitation 1992*, edited by R.J. Gleiser, C.N. Kozameh, and O.M. Moreschi (Institute of Physics, Bristol), pp 287–294.

Taylor, J.H., and R.J. Dewey, 1988, "Improved parameters for four binary systems", *Astrophys. J*. **332,** 770–776.

Taylor, J.H., L.A. Fowler, and P.M. McCulloch, 1979, "Measurements of general relativistic effects in the binary pulsar PSR 1913+16", *Nature* **277,** 437.

Taylor, J.H., R.A. Hulse, L.A. Fowler, G.W. Gullahorn, and J.M. Rankin, 1976, "Further observations of the binary pulsar PSR 1913+16", *Astrophys. J*, **206,** L53–L58.

Taylor, J.H., R.N. Manchester, and A.G. Lyne, 1993, "Catalog of 558 pulsars", *Astrophys. J. Suppl. Ser*. **88,** 529–568.

Taylor, J.H., and J.M. Weisberg, 1982, "A new test of general relativity: Gravitational radiation and the binary pulsar PSR 1913+16", *Astrophys. J*. **253,** 908–920.

Taylor J.H., and J.M. Weiberg,1989, "Further experimental tests of relativistic gravity using the binary pulsar PSR 1913+16", *Astrophys. J*. **345,** 434–450.

Taylor, J.H., A. Wolszczan, T. Damour, and J.M. Weisberg, 1992, "Experimental constraints on strong-field relativitic gravity", *Nature* **355,** 132–136.

Thorsett, S.E., Z. Arzoumanian, M.M. McKinnon, and J.H. Taylor, 1993, "The masses of two binary neutron star systems", *Astrophys. J*, **405,** L29–L32.

Wolszczan, A., 1991, "A nearby 37.9 ma radio pulsar in a relativistic binary system", *Nature* **350,** 688–690.

Preface

The Indian Academy of Sciences was founded by C. V. Raman in 1934. Last year an international symposium on Pulsars was organized at the Raman Research Institute, Bangalore to mark the **Diamond Jubilee** of the Academy. This symposium held during 14-17 March 1994 brought together most of the leading experts in the field. The format of the meeting was in the spirit of a relaxed “discussion meeting”, with ample time for discussions. Each talk was followed by a question period of approximately 30 minutes. In addition, one hour was reserved for extended discussion after every group of talks. This plus the fact that most of the speakers concentrated on ‘what is not understood' led to a very lively and memorable meeting. On behalf of my colleagues at the Raman Research Institute I would like to express our gratitude to the participants. During the symposium there was a public lecture by Joseph Taylor on *Binary Pulsars and Relativistic Gravity* under the auspices of the Indian Academy of Sciences. Instead of transcribing that lecture we have reproduced his *Nobel Lecture* with his kind permission, and with the formal approval of Reviews of Modern Physics (we felt that this is one way of making this magnificent lecture available to our college students who may not have access to RMP).

I wish to take this opportunity to express my sincere thanks to several of my colleagues at the Raman Research Institute, in particular V. Radhakrishnan, for their generous help in organizing this symposium. I also wish to thank Prof. R. Narasimha, the past President of the Academy, for his encouragement and support in planning this meeting. Finally, I would like to acknowledge the untiring efforts of R. Ramachandran, S.R. Ramasubramaniyan and D. Bhattacharya which made the publication of this proceedings possible.

G. Srinivasan

J. Astrophys. Astr. (1995) **16,** 327–355

Polarization-Mode Separation and the Emission Geometry of Pulsar 0823 + 26: A New Pattern of Pulsar Emission?

Joanna M. Rankin *Physics Department, University of Vermont, Burlington, Vermont 05405 USA*
N. Rathnasree *Raman Research Institute, Bangalore 560080 India*

Received 1995 August 29; accepted 1995 November 17

Abstract. We explore the detailed polarization behaviour of pulsar 0823 + 26 using the technique of constructing partial 'mode-separated' profiles corresponding to the primary and secondary polarization modes. The characteristics of the two polarization modes in this pulsar are particularly interesting, both because they are anything but orthogonal and because the secondary mode exhibits a structure seen neither in the primary mode nor in the total profile. The new leading and trailing features in the secondary mode, which appear to represent a conal component pair, are interpreted geometrically on the basis of their width and the associated polarization-angle traverse as an outer cone.

If the secondary-mode features are, indeed, an outer cone, then questions about the significance of the pulsar's postcursor component become more pressing. It seems that 0823 + 26 has a very nearly equatorial geometry, in that both magnetic poles and the sightline all fall close to the rotational equator of the star. We thus associate the postcursor component with emission along those bundles of field lines which are also equatorial and which continue to have a tangent in the direction of our sight line for a significant portion of the star's rotation cycle. It seems that in all pulsars with postcursor components, this emission follows the core component, and all may thus have equatorial emission geometries. No pulsars with precursors in this sense – including the Crab pulsar – are known.

The distribution of power between the primary and secondary modes is very similar at both 430 and 1400 MHz. Our analysis shows that in this pulsar considerable depolarization must be occurring on time scales that are short compared to the time resolution of our observations, which is here some 0.5–1.0 milliseconds. One of the most interesting features of the mode-separated partial profiles is a phase offset between the primary and secondary modes. The secondary-mode 'main pulse' arrives some 1.5 ± 0.1° before the primary-mode one at 430 MHz and some 1.3 + 0.1 ° at 21 cm. Given that the polar cap has an angular diameter of 3.36°, we consider whether this is a geometric effect or an effect of differential propagation of the two modes in the inner magnetosphere of the pulsar.

Key words: Pulsars—polarization—PSR B0823 + 26.

1. Introduction

Pulsar B0823 + 26 is one of the oldest known pulsars, being the first or second pulsar discovered at the Arecibo Observatory (Craft, Lovelace & Sutton 1968). With a period of 531 ms and a spindown of 1.72×10^{-15} sec/sec-yielding a B_{12}/P^2 value of 3.44 – its timing properties could not be more ordinary. However, Backer *et al*. (1973) discovered that the pulsar has both an interpulse (IP) and a postcursor (PC) component. The pulsar is also relatively close (DM ~ 19.5pc/cm^3), bright, and exhibits a turnover in its radio-frequency spectrum only below about 50 MHz (Sieber 1973; Izvekova *et al*. 1981). For all of these reasons, it has been possible to study it over a remarkably wide interval of frequency. On the high end it has been detected at Bonn by Bartel *et al*. (1978) at 14.8 GHz, and observations on the low end have been reported at 26 MHz (Phillips & Wolszczan 1992).

Over this enormous frequency range the form of the pulsar's profile changes remarkably little [see Hankins & Rickett (1986) for a series of profiles spanning 135 to 2380 MHz]. The M P exhibits a nearly Gaussian-shaped profile at both the very highest and lowest frequencies, only distorted by what is probably interstellar scattering at 26 MHz. Its width does change, however, from being practically constant above 1 GHz, to growing with an asymptotic dependence of about $f^{-0\,58}$ below about 300 MHz (Rankin 1983b; hereafter Paper II). The half-power width of the MP, interpolated to 1 GHz, was determined in Rankin (1990; hereafter Paper IV) to be 3.38°, very close to the $2.45°/P^{1/2}$ angular diameter of the pulsar's polar cap at the surface of the star.

The MP-IP spacing is very close to 180° and could be independent of frequency, although a slight decrease with frequency is also compatible with the observations (Hankins & Fowler 1986). The MPPC separation, however, *increases* monotonically with frequency between about 400 and 2400MHz as $f^{0\cdot08}$ (Hankins & Fowler 1986), and Arecibo 130-MHz observations further confirm this behaviour (Hankins & Rankin 1994). The relative intensity of the IP is strongest at 400 MHz, with a peak intensity of just under 1 per cent that of the MP, and decreases steadily at both higher and lower frequencies. The PC, in turn, is somewhat stronger than the IP, being about 3 per cent of the MP at 400 MHz. At frequencies above about 400 MHz the relative intensities of the PC and IP fall off at about the same rate ($f^{\sim-1}$). Below 400 MHz, the relative intensity of the IP decreases very rapidly, whereas that of the PC increases, at least to about 100 MHz, though far less steeply than at higher frequencies (Hankins & Rankin 1994).

Full period, average polarimetry has been published for pulsar 0823 + 26 at 430 MHz (Rankin & Benson 1981), 1400 MHz (Rankin *et al*. 1989; Blaskiewicz *et al*. 1991), and 10.55 GHz (Xilouris *et al*. 1995), all but the last of which also includes some information about the PC and/or the IP. Individual-pulse polarimetric studies have been carried out at 430MHz (Rankin *et al*. 1974; Backer & Rankin 1980) and 1400MHz (Stinebring *et al*. 1984). The aggregate linear polarization is also Gaussian in form, occupies the central portion of the profile, and is never large—going from perhaps 35% at 430 MHz, to 25% at 1400 MHz, and 5% at 10.55 GHz. The edges of the profile are thus almost completely depolarized, but slightly more so on the leading than the trailing edge so that the residual linear 'component' looks a little delayed relative to the total-power profile.

A small amount of circular polarization is also observed in this pulsar's average profile, usually less than 5%. The published profiles often show a little left-hand (positive) circular on the leading edge, changing to a little more right-hand (negative) on the trailing. However, other unpublished observations suggest considerable variation around this general configuration.

With not only an MP, but an IP and PC as well, the linear polarization angle (PA) can be measured over a large part of the star's rotation cycle. Backer & Rankin (1980), however, found the linear PA behaviour of this pulsar to be unusually complex, apparently requiring two different angle systems. Using the information in Rankin & Benson (and correcting for '90° flips' at about – 8 and + 12°), Lyne & Manchester (1988) have obtained a value of 80° for α, the angle between the magnetic and rotation axes of the star, by fitting the single-vector model (Radhakrishnan & Cooke 1969; Komesaroff 1970) to the PA data. Better resolved observations are to be found in Rankin *et al*. (1989) and Blaskiewicz *et al*. (1991), and the rapid traverse of the PA near the peak of the profile can be seen clearly. The latter study (also correcting for a '90° flip' at about 170° in the 430-MHz observation) obtained values of 79° ± 1° and 91° ± 600° at 430 and 1418 MHz, respectively.

Fluctuation-spectral analysis yields a 'weak, broad feature in the range of 0.05 to $0.23c/P_1$ with a constant strength of 0.35….. The measured center frequency is $0.14\ c/P_1$' (Backer 1973). In other studies (Taylor & Huguenin 1969; Lang 1969), the feature appeared stronger and at a frequency of 0.18 to 0.20 c/P_1. We note here [and Rankin (1986; hereafter Paper III) did not!] that there is considerable fluctuation power at frequencies below $0.10\ c/P_1$, suggesting in the terms of Paper III both core and conal-associated fluctuations. Finally, there is no published evidence for null pulses, although the limit of $\leqslant$5% (Ritchings 1976) is not a very strong one.

As regards classification, pulsar 0823 + 26 has had a chequered history. In Paper III it was seen as a conal double (*D*) pulsar in an attempt to make sense of the MP and PC as a conal component pair. The spacing between the two components was uncomfortably large, and there was some antisymmetric MP circular polarization, but the lack of MP conal 'outriders' at high frequency tilted toward the conal side. The growing weight of evidence regarding core-component geometry in Paper IV shifted 0823 + 26 into the core-single (S_t) class. Its MP width was exactly what would be expected for a core component in a pulsar with a nearly orthogonal magnetic geometry, a geometry which seemed highly compatible with its observed interpulse. Its rather high B_{12}/P^2 also seemed to suggest that it is not a cone-dominated pulsar. And viewing the M P as primarily a core component was more compatible with its polarization characteristics. This classification left only two nagging questions: **a**) In a pulsar which can be observed to such high frequencies, where are the high frequency conal 'Outriders'? And **b**) If the MP is a core component, how are we now to interpret the PC?

These questions are the starting point for this paper. In the next section we introduce the observations considered in our analysis, and §3 begins our discussion of the polarization structure of pulsar 0823 + 26's profile. In § 4 we consider mode-separation techniques and their application to pulsar 0823 + 26, § 5–§ 7 explore the pulsar's main-pulse, postcursor, and interpulse emission geometry, respectively, § 8 then returns to the polarization-modal structure of the main-pulse emission, §9 assesses the significance of the displaced modal emission, and § 10 provides a summary and the conclusions of the paper.

2. Observations

The single-pulse observations used in our analysis below come from three programs carried out at the Arecibo Observatory over a long period of time. The older 430-MHz

observations were carried out in January 1974 with a single-channel adding polarimeter of 500-kHz bandwidth and 1.0-ms integration time, giving a nominal time resolution of about 0.7° longitude. The polarimetry scheme is described in Rankin *et al*. (1975); no attempt was made to correct the Stokes parameters for the known 0.25% cross-coupling in the feed, which can produce spurious circular polarization at a nominal level of about 10% of the linear.

The older 1400-MHz observations were carried out in October 1981, again with a single-channel, adding polarimeter. Here the bandwidth was 10 MHz and time constant 0.66 ms, giving an effective resolution of about 0.5°. A serious effort was made for the first time to correct the measured Stokes parameters for instrumental distortion using the 'orthogonal' approximation described by Stinebring *et al*. (1984).

The newer observations at 430 and 1404 MHz were made in a single observing session in October 1992, the 430 MHz on the morning of the 20th and the 21 cm on the morning of the 15th. Both used a special program to gate the 40-MHz correlator, and the basic data recorded at the telescope were the ACFs and CCFs of the right- and left-hand channel voltages. The higher frequency observations used a 20-MHz BW and the lower a 10-MHz BW, and the retention of 32 lags in both cases reduced dispersion delay across the bandpass to negligible levels. The resolution was then essentially the correlator dump time, which was 506 μs or 0.34°. The Arecibo 40-MHz correlator is described by Hagan (1987) and the observing software by Perillat (1988, 1992). The measured correlation functions were scaled, 3-level sampling corrected, and Fourier transformed to produce raw Stokes parameters, which were in turn corrected (channel by channel) for dispersion, Faraday rotation, instrumental delays, and all of the known feed imperfections as determined by full-sky tracks of pulsar 1929 +10 and other sources. During the course of our analysis, we discovered that the instrumental polarization is highly frequency dependent, particularly at 430 MHz; therefore, the most recent observations represent some of the best calibrated ever made at the Arecibo Observatory. The instrumental details will be described in a forthcoming paper (Rankin, Rathnasree & Xilouris 1996).

3. The polarization structure of pulsar 0823 + 26's profile

Figures 1a–c give a collection of profile and polarization-angle density plots for both 430 and 1404 MHz. Notice the difference in the longitude scales; at 430 MHz the entire MP-PC portion of the rotation cycle of the pulsar is included, whereas at 1404 MHz only the MP region is plotted. We should say that the lower panels are not really grey-scale plots; each point represents the polarization of an actual measured sample falling above a threshold of a few standard deviations in the off-pulse noise. The regions of greatest primary-mode power are thus 'over exposed' in the process of plotting enough individual pulses to explore the overall space represented by the diagram.

These plots are interesting and remarkably complex. Let us first consider the simpler 1404-MHz diagram (Fig. 1c), wherein it is clear that there are two distinct modes and that these have very different PA traverses. One can also see this, both in Stinebring *et al*.'s Fig. 5 and in Gil *et al*.'s Fig. 2 – we are dealing here with the same data – but considerably less clearly owing to the details of plotting or analysis. The darker primary mode has a slope of 14–15°/°, and the less prominent secondary mode a slope just about twice this. What is most striking is that the two modes are anything but orthogonal, and

near the trailing edge of the profile (near + 3° longitude) appear to be separated by barely 45°. Lest anyone wish to attribute this to instrumental causes, we have another, shorter 1404-MHz sequence from our 1992 October observations which shows an identical behaviour. Other than this it is interesting to again note the minor peak in the linear power as well as the larger one, which trails the profile center. Also one can see, both how narrow the longitude interval over which the PA can be traced is and how poorly it often traces the PA of the primary-mode power.

We see a good deal more in the 430-MHz figures (Figs. 1a and b), and it is noteworthy how much more similar the PA density plots are than the average position-angle behaviour. The primary and secondary modes are again prominent in the center of the profile, and their measured slopes are nearly the same as at 21 cm.

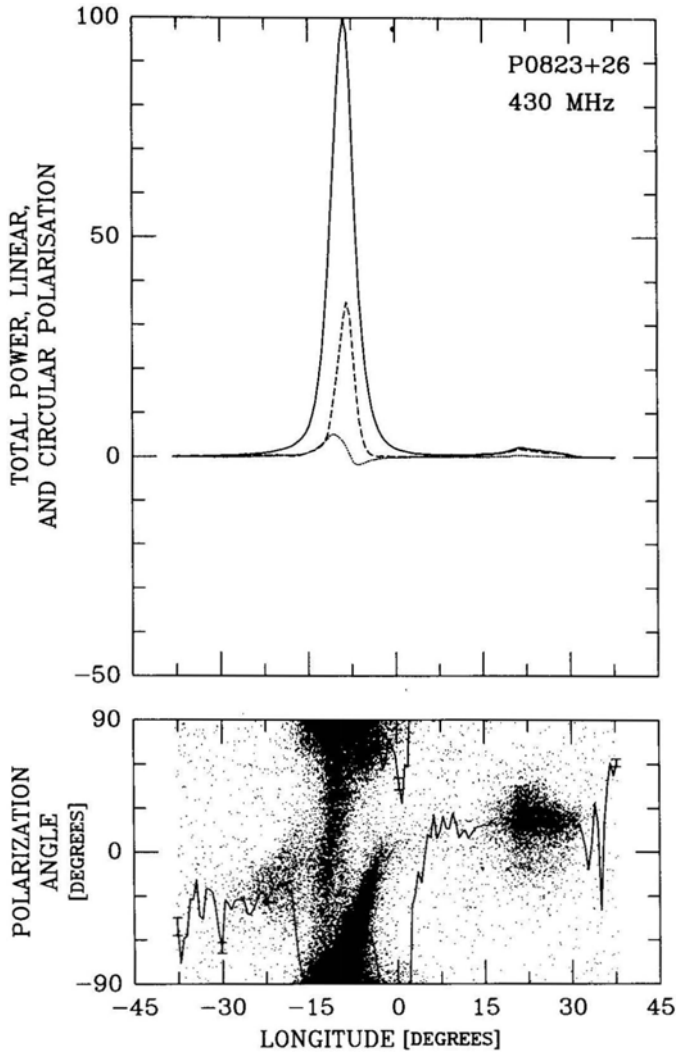

Figure l (a).

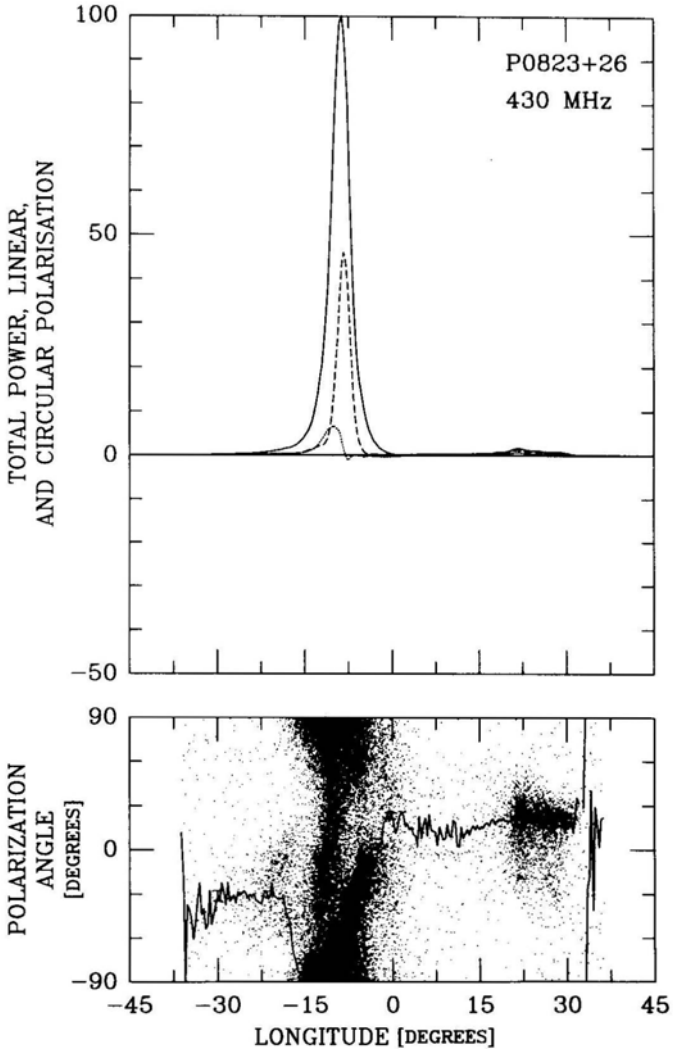

Figure 1 (b).

Again there is rather little aggregate linearly polarized power outside the MP center, but owing to the greater intensity of the pulsar at 430 MHz, individual samples with sufficient power to define the PA can be found over nearly a quarter of the rotation cycle of the pulsar. The principal primary-mode 'blotch' begins at about – 12° longitude and ± 90° PA and rotates positively through about 90°, also making the largest contribution to the overall linearly polarized power, *L*. Several other ''patches' of significant linear polarization can also be seen: Note the area associated with the postcursor, another on the extreme leading edge of the profile (which can also be seen in *L*), and a third, secondary-mode 'blotch' which begins at about – 14° longitude and – 45° PA, again rotating positively through 90°. At this point this last traverse appears to flatten off adjacent to the principle primary-mode 'blotch', and its power is conflated with the main primary-mode 'blotch' in *L*.

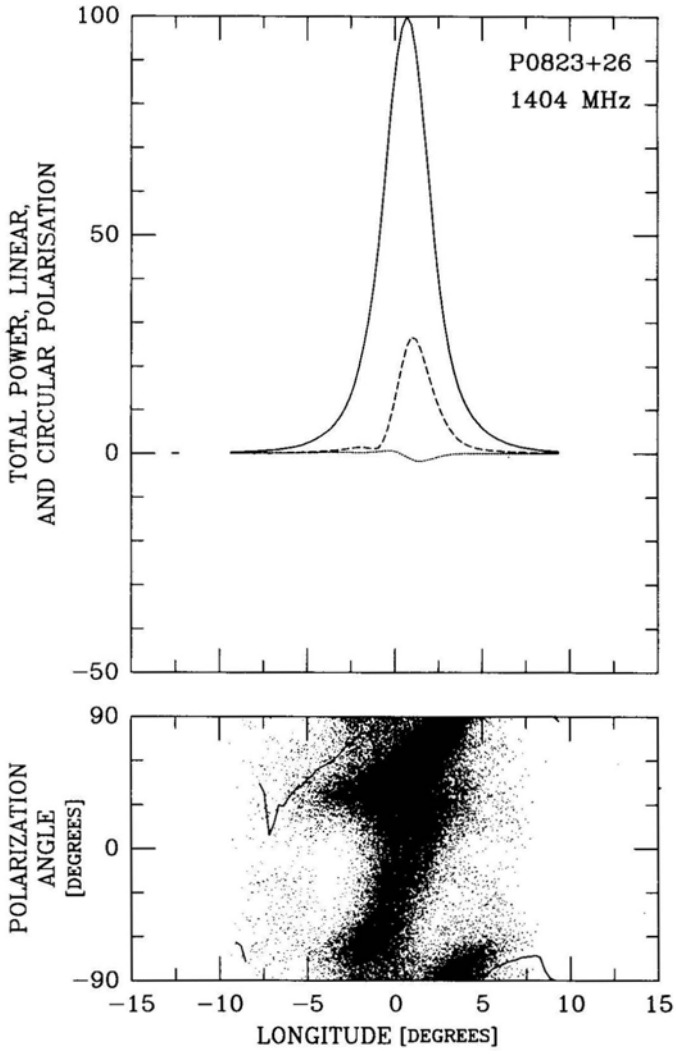

Figure l (c).

Figure 1 (a–c). Average profiles and polarization-angle density plots for pulsar 0823 + 26 at 430 MHz (**a**, **b**), and 1404 MHz (c). The upper panel plots Stokes parameter I, the total power (solid curve), $L = (Q^2 + U^2)^{1/2}$, the total linear polarization (dashed curve), and V, the circular polarization (dotted curve). The lower panel gives the polarization position angle of each sample falling above some threshold (see text), and the average position angle is also plotted, where defined, as a solid curve. The 430-MHz observations were recorded on 6th January 1974 and 20th October 1992 and represent 3194 and 1800 pulses, respectively. The 1404-MHz observation was made on 9th October 1982 and represents 6200 pulses.

Again it is interesting to consider how different the overall linear PA traverse is in the two 430-MHz observations, given the striking similarity of their modal-power distributions. It does appear that the polarization of this pulsar shows significant time variability; the differences in fractional linear polarization, PA traverse, and the entirely different form of the circular are quite typical of other (not shown) observations in our

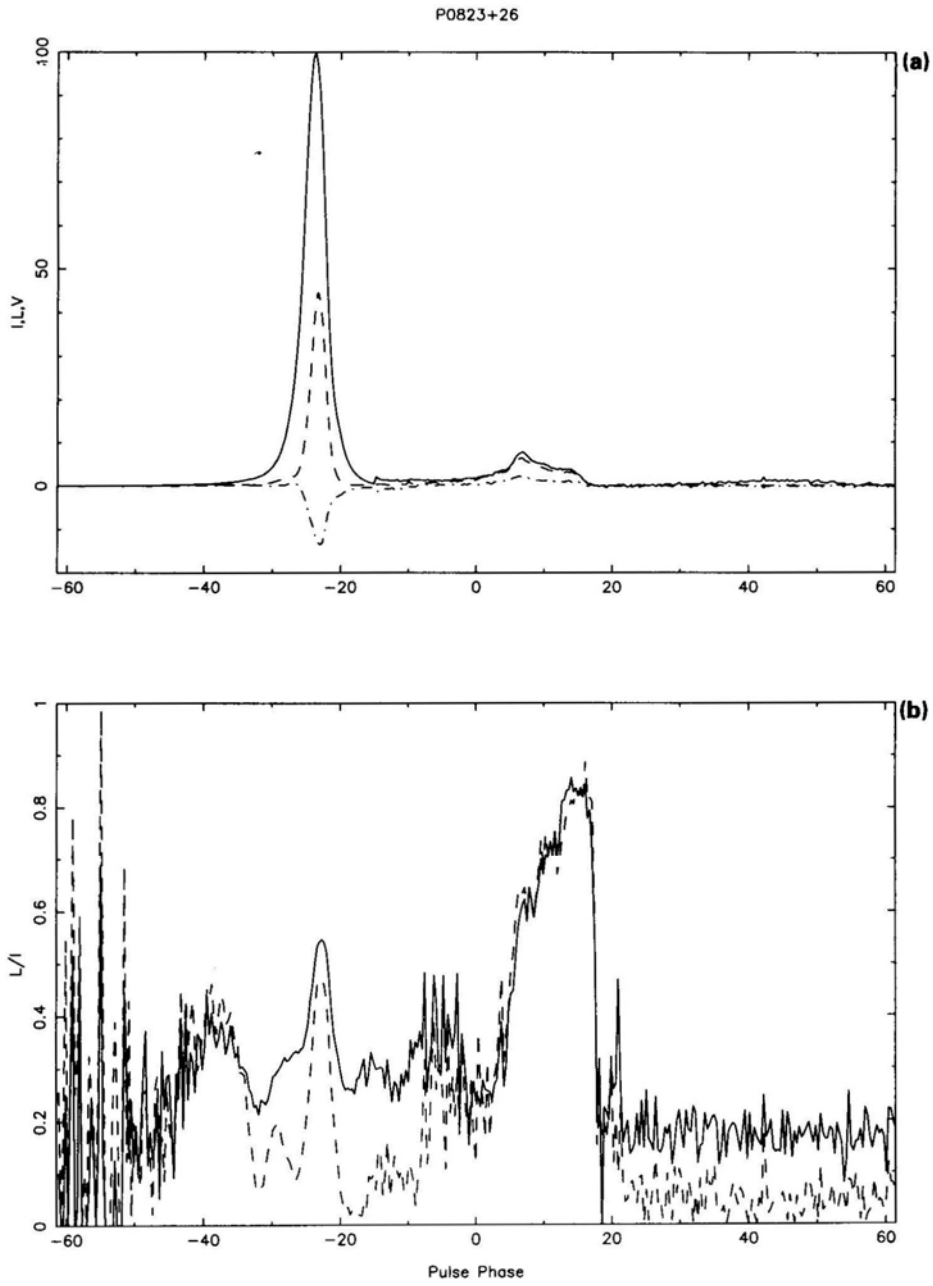

Figure 2. (**a**) Average profile of pulsar 0823 +26 at 430 MHz as in Fig. 1b.At longitudes larger than – 15° all the quantities I, L and V have been multiplied by a factor of 5 to show the region of the postcursor more clearly. (**b**) The fractional linear polarization, $\langle L/I \rangle$ (solid curve) and $\langle L \rangle / \langle I \rangle$ (dashed curve). In both the curves the averages have been corrected for statistical polarization. In regions of low intensity, the degree of polarization could be quite undefined and oscillating between high and low values as in the left hand portion of the figure.

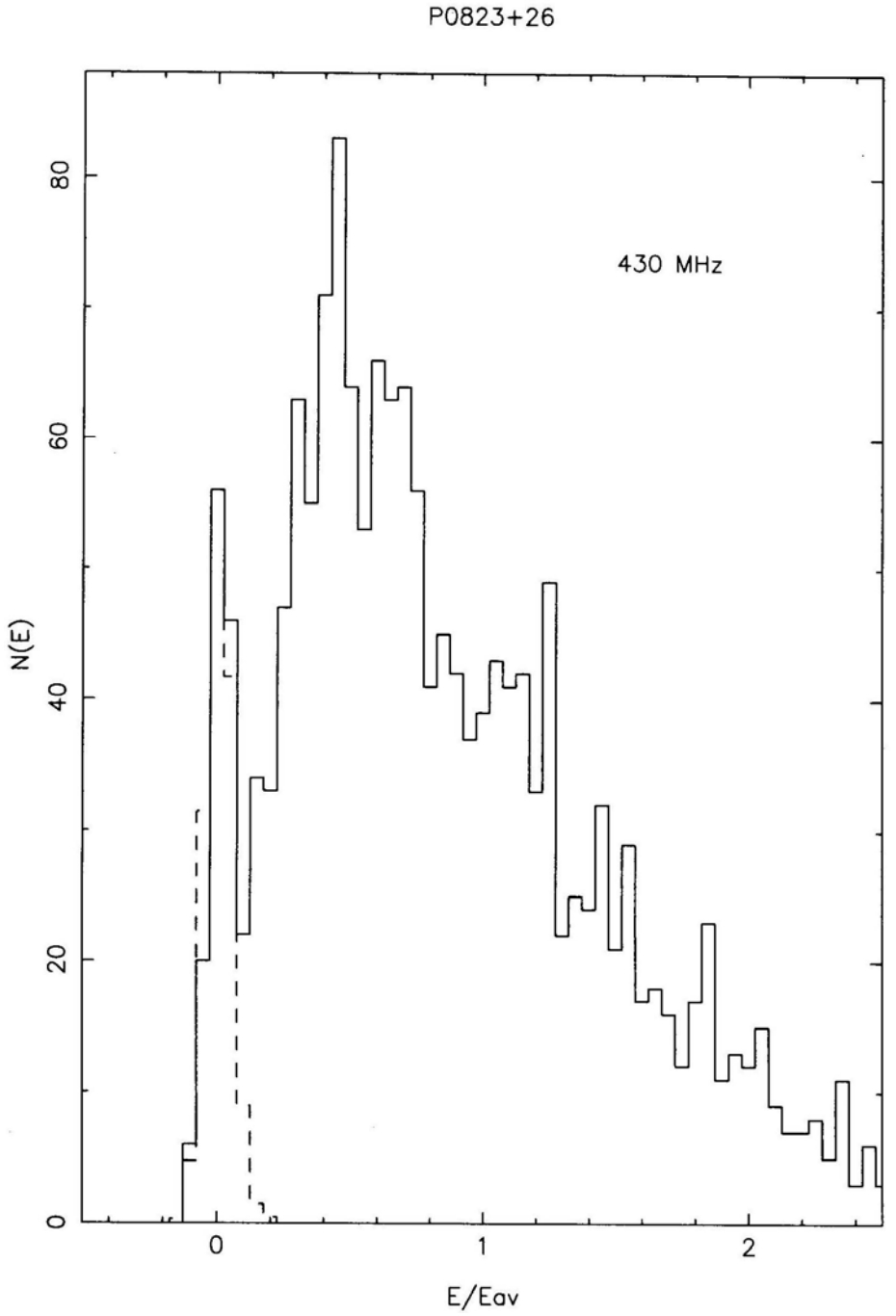

Figure 3. Pulse intensity histogram (solid line) for pulsar 0823 + 26 at 430 MHz corresponding to the October 1992 observations in Fig. 1b. The dashed line shows the intensity histogram obtained from the noise window, which is normalized to 142 pulses.

possession. It is quite conceivable that this pulsar exhibits some yet unrecognized mode-switching phenomenon (and of course this would be particularly difficult to identify in a pulsar with a single profile).

Turning now to Fig. 2, we again see the 430-MHz profile although displayed in a slightly different manner than in Fig. 1b. In the top panel, at all longitudes later than – 15°, I, L and V have been multiplied by a factor of 5, so that the postcursor and interpulse windows can be seen more clearly. The information in the bottom panel has been obtained after rejecting sample by sample all data points with I < twice the σ in the noise window. Here, we plot the fractional linear polarization, first in the usual manner by averaging Stokes parameters Q and U (dashed curve) and, second, by aggregating the linearly polarized power irrespective of the PA (solid curve). Under the MP peak the latter is larger than the former as expected, but generally only by some 10% or so, arguing that most of the depolarization is occurring on time scales short compared to the 500-μs resolution of the observation. However, the amount of depolarization taking place over time-scales larger than a period (which amounts to the difference between the two curves in the bottom panel) is considerably greater in the wings of the MP profile. This suggests that different processes and time scales of depolarization are operative in the MP wings, and overall, that the MP has a composite character. We will return to this issue below. Finally, note that exactly the opposite is true for the PC; the two linear polarization measures are identical within the noise, indicating that virtually no depolarization is occurring on time scales shorter than the sampling interval.

Finally, Fig. 3 gives a 430-MHz, pulse-intensity histogram, scaled to the average-profile intensity to show the range of fluctuation (solid line). A similar histogram (dashed line) for the noise window has been normalized so that the zero-intensity bins coincide. Interestingly, the pulse-intensity histogram is bi-modal, and the distinct zero-energy peak has a width almost exactly equal to that of the noise distribution. The fraction of null pulses from this analysis is 6.4 ± 0.8% as compared with the upper limit of 5% from Ritchings' (1976) study.

4. Polarization-mode separation

Several efforts have been made to separate the polarization modes and to reconstruct the two modal pulse profiles. Cordes *et al*. (1978) first carried out this analysis for PSR 2020 + 28, and Rankin *et al*. (1988) and Rankin (1988) then applied it to pulsars 1737 + 13 and 1604–00, respectively. About this time Gil *et al*. (1991) developed a different polarization-mode fitting technique and applied it first to 0823 + 26 observations at 1404 MHz and then to observations of a small group of other pulsars at the same frequency (Gil *et al*. 1992). The first technique relies on a model of the polarization angle as a function of longitude, usually the 'single-vector' model given by Radhakrishnan & Cooke (1969) and extended by Komesaroff (1970), whereas the second uses an algorithm which partitions the aggregate polarization angles into two groups statistically, longitude by longitude.

The two techniques are complementary in that, both have their strengths and weaknesses. The first technique is more sensitive and 'stable', but risks giving the false appearance that the modal PAs follow the model in regions of longitude where the modal power is negligible. Gil's technique, on the other hand, has the advantage of

being model-independent, but requires significant power in both modes at each longitude and easily loses track of the identity of the modes when they are discontinueous. Our study of 0823 + 26 uses only the first technique, because we were unable to obtain sensible results using Gil's technique on the 430-MHz observations.

The question then immediately arises regarding how this overall polarization PA behaviour should be interpreted. At 430 MHz, beginning with the primary mode, we see a positive, about 120°rotation of the PA which seems to terminate at around the PA of the PC; by this interpretation, however, there is no appreciable primary-mode power at longitudes earlier than that of the primary-mode 'blob'—a circumstance which is also largely true, we note, at 21 cm. What power there is at earlier longitudes is reasonably associated with the secondary mode, although the leading-edge patch seems somewhat disconnected from the main area where the secondary mode rotates

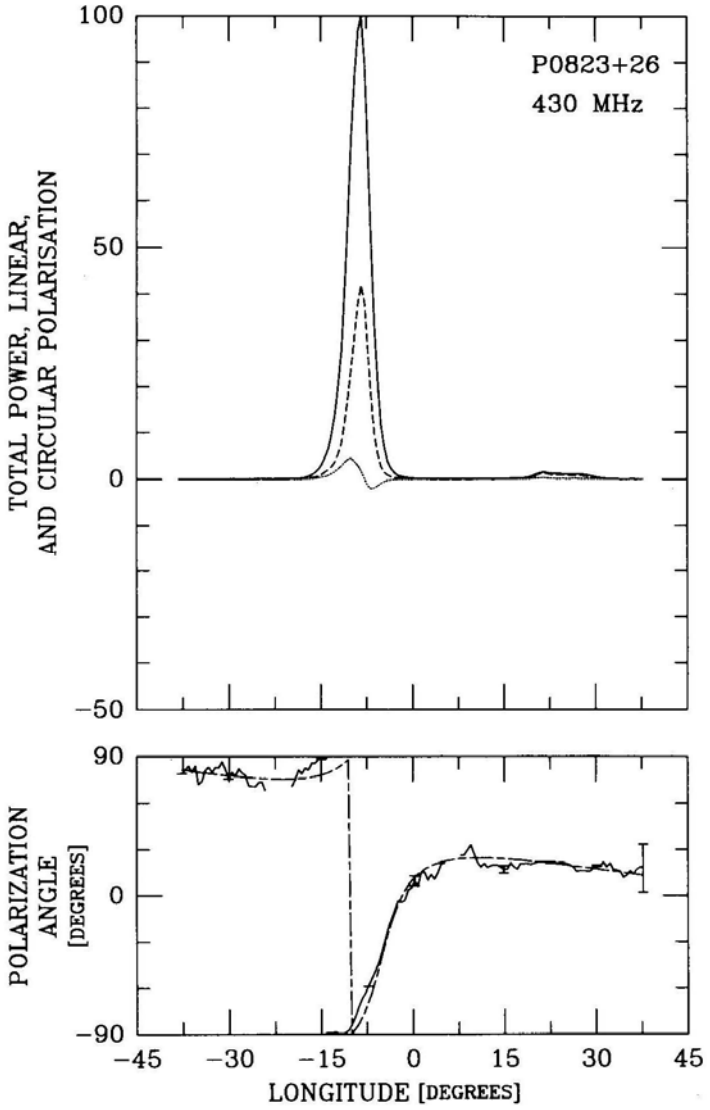

Figure 4 (a).

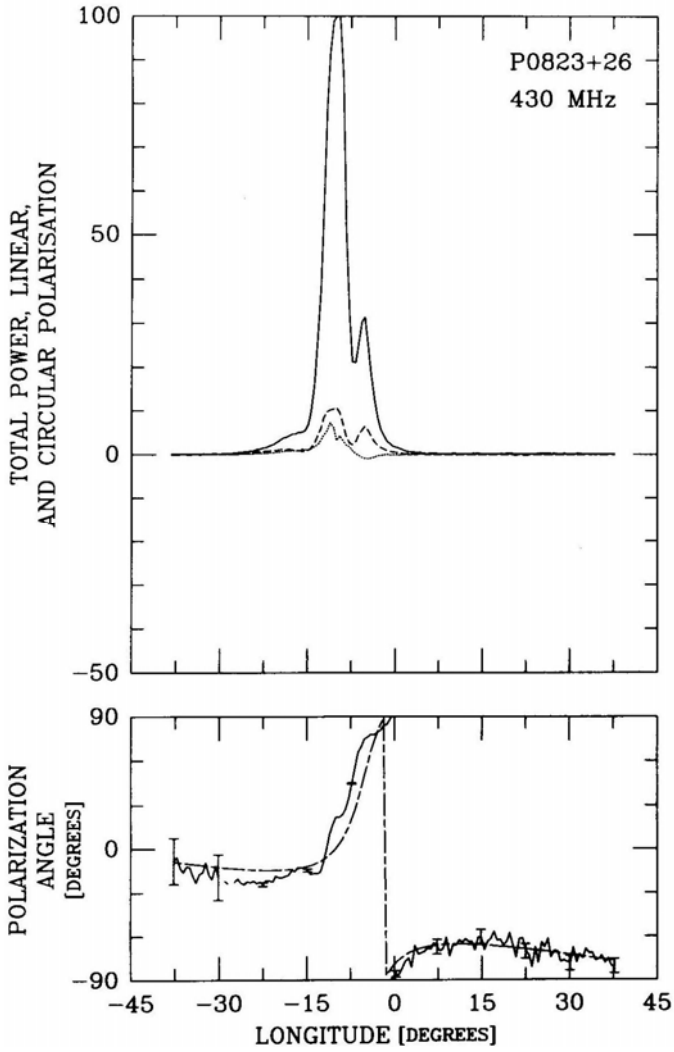

Figure 4 (b).

most rapidly. It furthermore seems that the primary and secondary mode power are barely distinguishable in the 'patch' near – 5 to – 10° longitude and + 75° PA. Conveniently – despite the uncorrected ionospheric Faraday rotation – both 430-MHz observations have nearly the same PA origin.

Using this interpretation of the polarization-mode behaviour, we can begin to separate the composite profiles into their constituent polarization-modal partial profiles. In Rankin *et al*. (1988) we found a convenient representation of the single-vector model

$$\chi = \chi_0 + \tan^{-1} \frac{\sin(\phi - \phi_0)}{A - \left(A - \frac{1}{R} \right) \cos(\phi - \phi_0)}, \qquad (1)$$

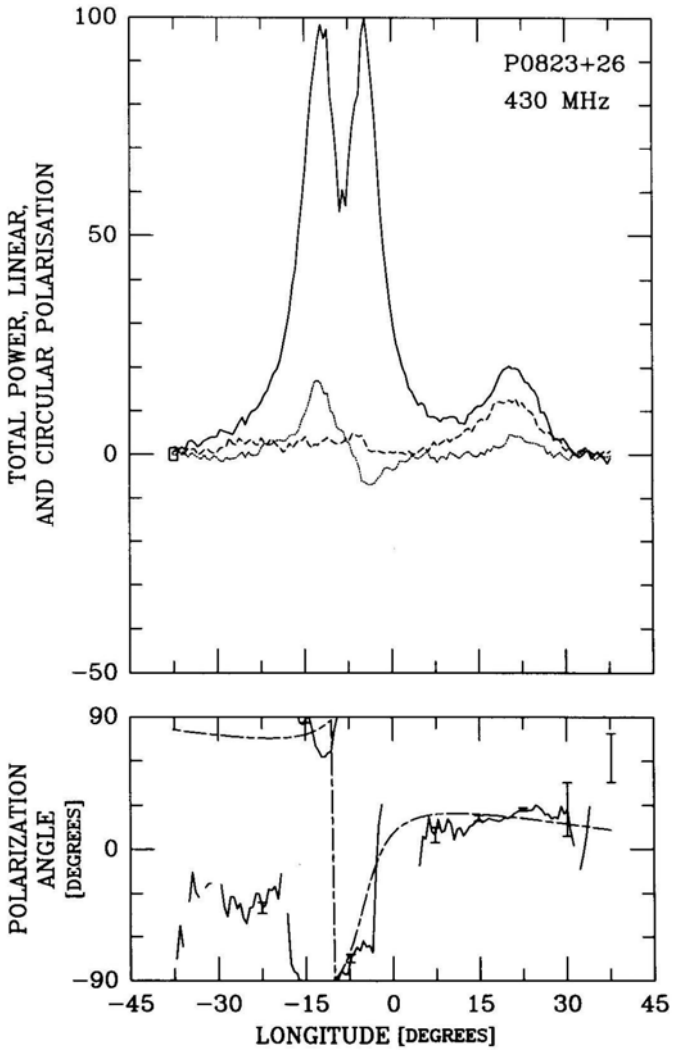

Figure 4 (c).

Figure 4 (a–c). Partial, 'modeseparated' profiles for pulsar 0823 + 26 at 430-MHz on 6th January 1974, (**a**) primary-mode,(**b**) secondary-mode, and (**c**) residual profiles. The lower panels in these figures give the PA traverses corresponding to the two modes, and the model PA is overplotted as a dashed curve.

where χ is the polarization angle, ϕ the longitude, $R = \left|\frac{d\chi}{d\phi}\right|_{max} = \sin\alpha/\sin\beta$ the maximum PA rate, and A a constant which can be computed from the total PA traverse χ_c between reference longitudes $\pm\phi_c$ as

$$A = \frac{\sin\phi_c/\tan\frac{1}{2}\chi_c - \cos\phi_c/|R|}{1-\cos\phi_c}$$

and which is formally equal to $\sin\zeta/\tan\alpha$,where α and ζ are the angles that the magnetic axis and the sight line make with the rotation axis, respectively.

Now taking the center ofthe primary-mode PA traverse at about – 4°longitude and a PA of – 40°, R as about + 15°/°, and computing A from a total traverse χ_c of 120° at ± 30° longitude, we proceed to construct partial ('modeseparated') profiles corresponding to the primary and secondary modes of 0823 + 26. The stream of samples of the individual pulses is compared with a threshold – the criteria being **a**) whether the total linear polarization exceeds twice the off-pulse baseline noise level, an d **b**) whether the computed PA falls within ± 45° of the model PA – andaccumulated in one of three partial profile 'bins' accordingly. The first, 'primary-mode' partial profile, consists of those samples which both exceeded the noise threshold and had PAs lying on that half of the Poincaré sphere closest to the Stokes vector representing the model PA, the second those in the other hemisphere, and the third those which did not meet the noise

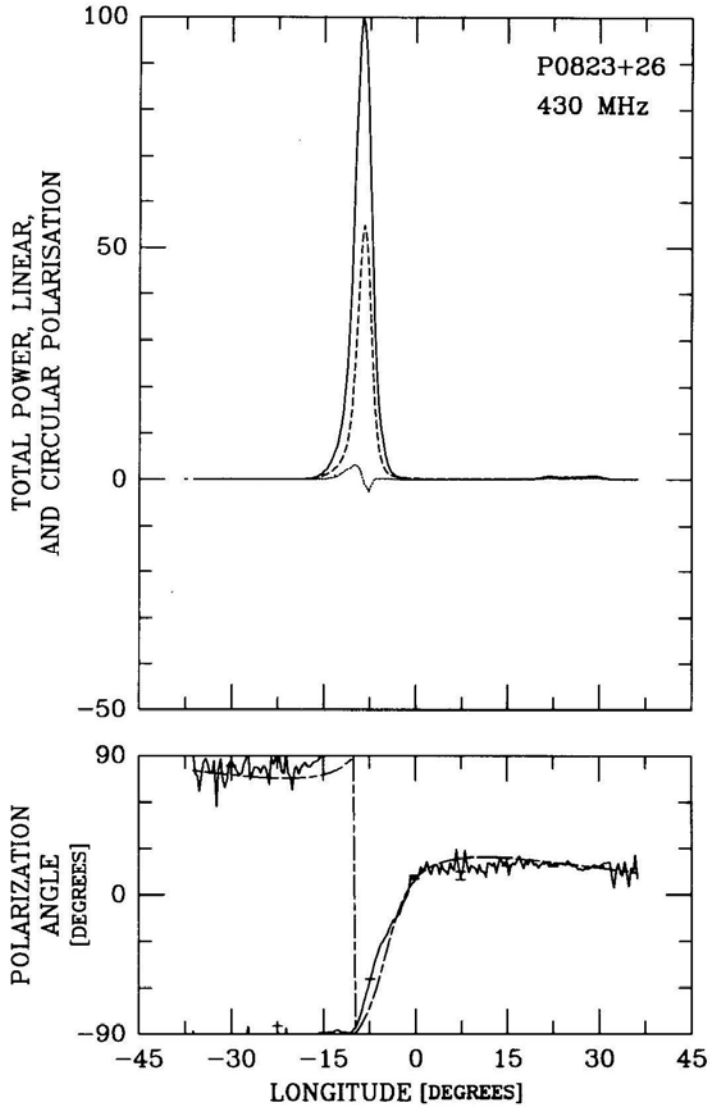

Figure 5 (a).

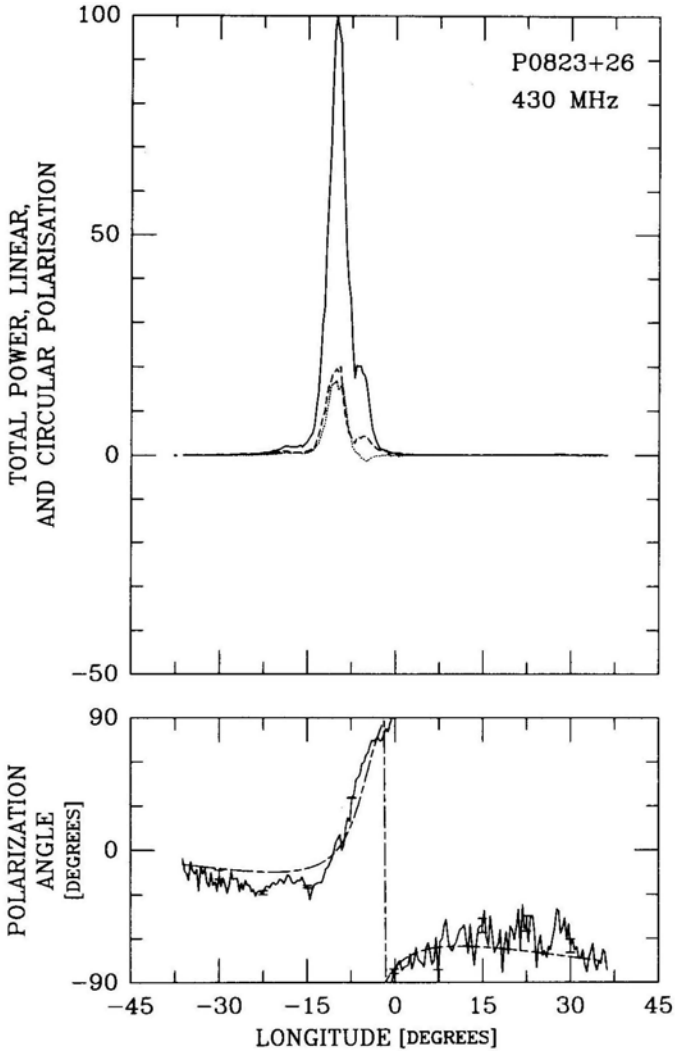

Figure 5 (b).

threshold. The 'mode-separated' profiles at 430 MHz computed from the earlier 1974 and the later 1992 observations are given in Figs. 4 and 5, respectively.

Turning first to the earlier observations in Fig. 4, we see that the primary-mode partial profile (Fig. 4a) greatly resembles the total profile in Fig. 1a. The linear polarization is only a little greater, the circular polarization almost identical, only we now have an MP which is slightly narrower with its linear polarization more symmetrically positioned in its center. With a noise threshold of about 2-σ[†] only about 9.9% of

[†] The precise off-pulse noise level is difficult to determine in the older observations as the noise-window data is no longer readily available; comparison with the 1992 observations – where the noise levels were accurately determined – however, shows that our estimate of σ is not far in error.

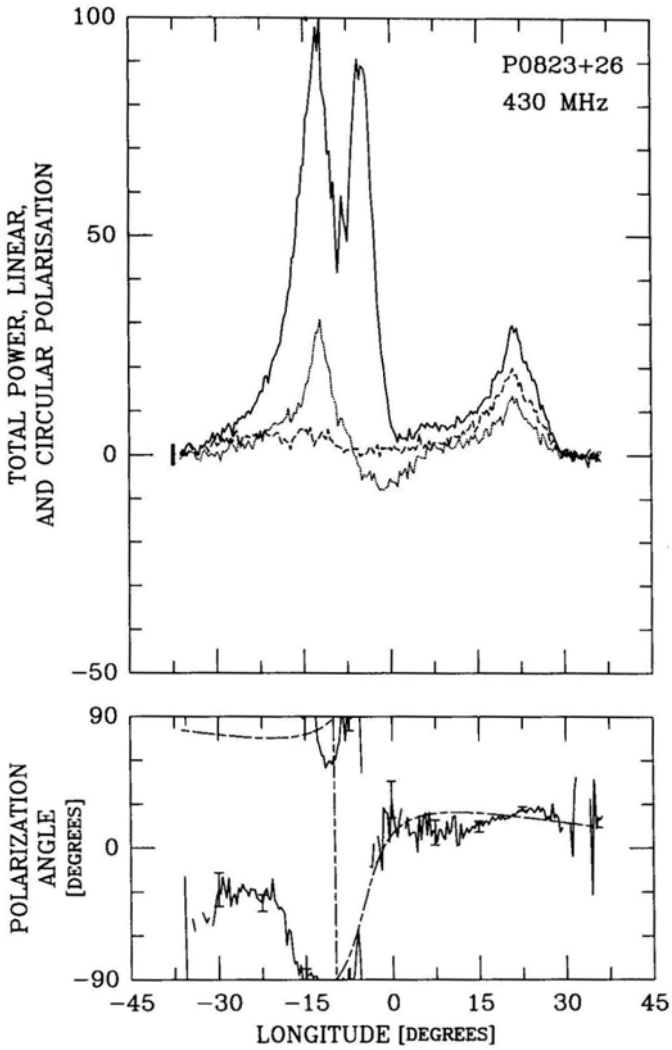

Figure 5 (c).

Figure 5 (a–c). Partial, 'modeseparated' profiles for pulsar 0823 + 26 at 430-MHz on 20th October 1992 as in Fig. 4.

the samples accrue to the primary-mode partial profile, but these carry nearly 67.9% of the total power. The only big change is in the PA traverse, which now more nearly conforms to what is expected on the basis of the single-vector model. Part of this is an artefact of the 'mode-separation' procedure; in regions of longitude where primary-mode L is small compared to the noise level – such as the 'baseline' region on the MP – the precise value of the model PA does affect the PA of the modal partial profile. However, in regions where any significant linear power is present, the partial profile PAs are only very weakly dependent upon the PA model. We also note that the PC is most prominent in the primary mode, and its linear polarization appears more complete because weakly polarized samples have not reached the noise threshold level.

It is the secondary-mode profile in Fig. 4b which holds the surprises, though it consists of only 4.1 % of the samples and 17.7% of the power. This profile shows a more complex structure, both in L and in total power. Were it a complete profile, we would immediately say it had a triple form. The polarization is low, but not insignificant, throughout its entire extent; here we see much less severely depolarized 'wings' as compared with the primary-mode profile. Part of this is again an artefact of the separation in that, weakly polarized samples in the wings will have a much reduced chance of meeting the threshold in L; however, as we shall see below, this is not the whole story. Again, the PA traverse is 'rationalized', but it is also well defined over most of its extent by 'patches' of modal power. Note that here we see a flattening of the steep traverse after about – 15° longitude as compared to the density plot in Fig. 1 because the PA model cannot track both the primary- and secondary mode traverses in this region simultaneously.

Returning now to the form of the secondary-mode profile, let us begin to ask what interpretation should be made of it. The first thing to point out is that the primary- and secondary-mode profiles are not coincident in time. The two partial profiles have virtually identical half widths (fwhm) at 4.1°, however, the secondary-mode one arrives earlier by about 1.5°. Then there is the question of the 'outriders'! The leading feature can be traced to the isolated 'patch' at about – 23° longitude and – 30° PA in Fig. 1b which we pointed out earlier. The trailing feature is more difficult to see as it is below and to the right of – but immediately adjacent to – the principle primary-mode 'patch' at – 9 to – 14° longitude and $\leqslant 90°$ PA. Note the asymmetry of the primary-mode feature, and the additional emission to the bottom right of it. Note also that the minimum between the 'MP' and the trailing feature in the secondary-mode partial profile falls just after – 7.5° longitude—and that there is a slight 'cusp' in the density distribution in Fig. 1b which apparently corresponds to it. Here the PA model used in the mode separation is sensitive to the position of the modal boundary, so that it effectively discriminates between the above primary-mode 'patch' and the secondary-mode power immediately adjacent to it. This criticality stems from the close separation in angle of the two modes in this region.

Readers may also question whether the secondary-mode features are in some manner generated by the mode-separation procedure. After all, most of the samples (86.0%) and a significant amount of the power (14.4%) in the original pulse sequence are not represented in Figs. 4(a and b) and accrue to the residual profile in Fig. 4c. In order to explore this possibility, partial profiles were computed holding the model PA parameters constant, but progressively reducing the noise threshold from 2σ to 1σ, 0σ, and even -1σ. Eventually, with the latter, the noise threshold becomes moot and all samples accrue to either one or the other modal partial profiles. The meaningless division of ever more noise-dominated samples into one or the other 'modal profiles' produces statistical travesties (total linear polarization $L > I$), but the form, boundaries, and relative amplitudes of the secondary-mode 'MP' and its 'outriders' remain intact. Therefore, we cannot trace their origin to an artefact of the partial-profile construction process. If there is an error, it must be in the interpretation of the primary- and secondary-mode related 'patches' in Fig. 1.

Turning now to the more recent 1992 observations, we see a very similar story overall. The pulsar appears to have been about 4 times weaker on the latter occasion, but 5 times the bandwidth and much better receivers were also being used in 1992. It is worth returning to Fig. 1 and again carefully comparing the two 430-MHz observations. The

MP in the 1992 observation is significantly narrower than that in the earlier one (3.7° versus 4.5°), owing perhaps to improved resolution. This seems to accentuate the asymmetry of L within the overall I envelope, and probably accounts in part for its larger relative amplitude as well. Very different, however, is the circular polarization; while the 1974 observation shows a small amount (< 5%) which varies antisymmetrically across the MP, the 1992 profile has nearly 15% RCP with only a hint of a sense reversal.

The primary-mode, secondary-mode, and residual partial profiles are given in Figs. 5(a–c), respectively. Little needs be said about the former except to note its narrowness (now about 3.2° fwhm), its increased linear symmetry as compared with the totalprofile, its nearly identical circularpolarization, and ofcourse its more orderly PA

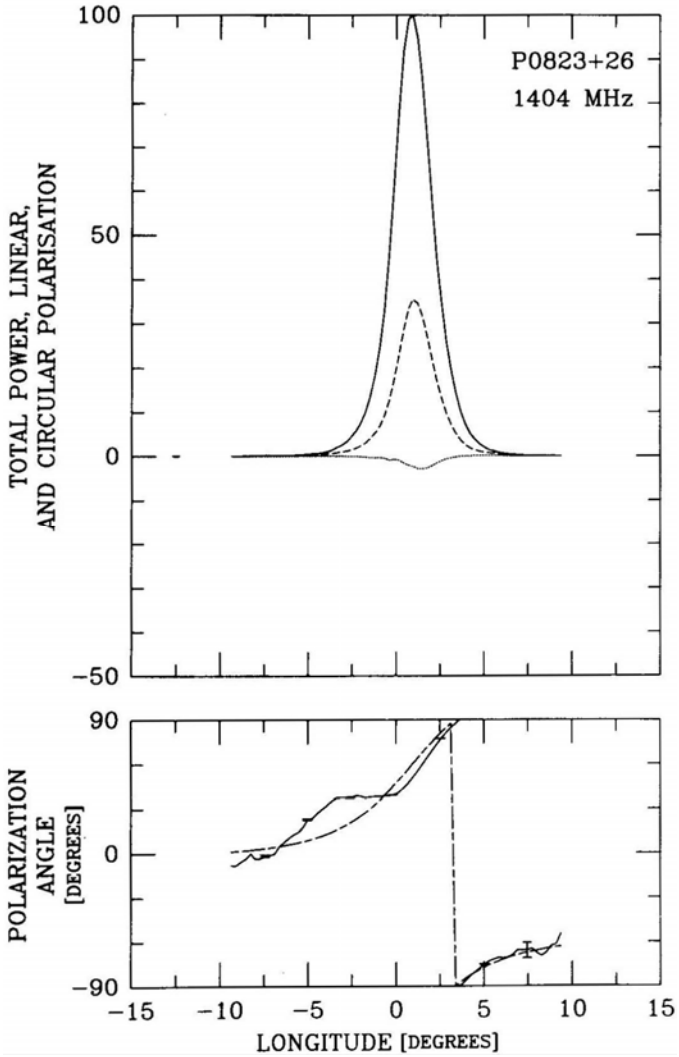

Figure 6 (a).

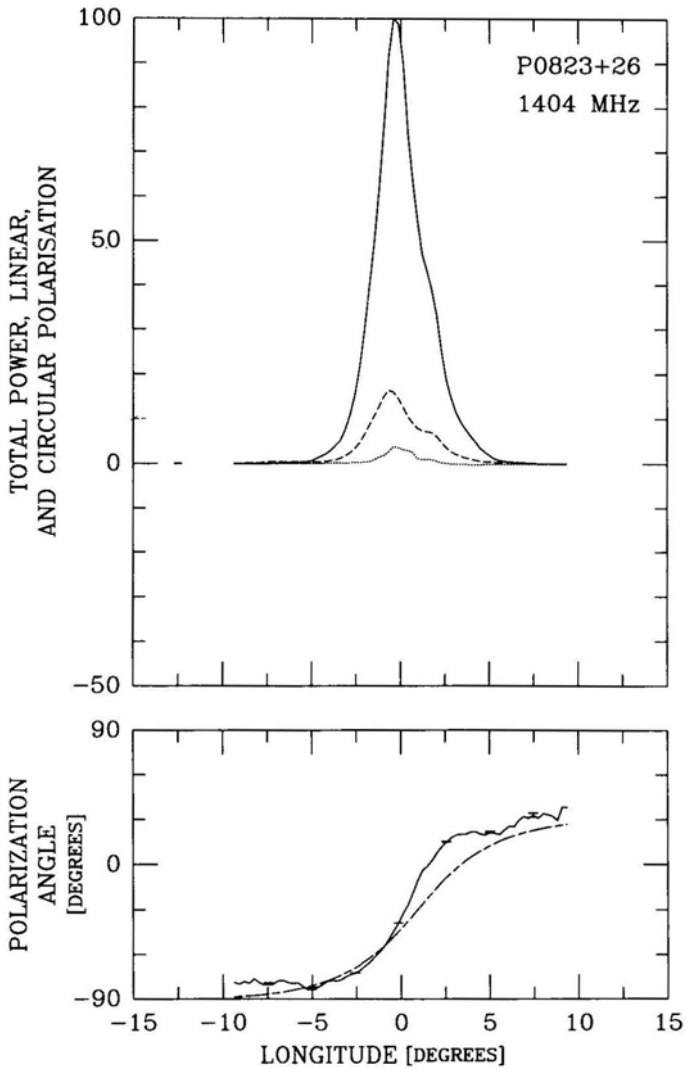

Figure 6 (b).

traverse. With a 2-σ threshold, it here represents 10.1 % of the samples and 68.9 % of the total power in the individual-pulse sequence.

The secondary-mode profile in Fig. 5 (b) again has a tripartite form, both in *I* and in total linear, *L*—although the minimum between the middle and trailing features is less well resolved. The fractional linear polarization seems to be a little larger than in the earlier observation. However, please note that the secondary-mode circular is very comparable, notwithstanding the very different primary-mode circular (again suggesting that a 'mode-changing' phenomenon is active in the pulsar which changes, over time, the relative proportions of the two polarization modes or their overall polarization states). The fwhm of the 'MP' is here about 3.3°, and it again leads the primary-mode one by almost exactly 1.5°. Here the secondary-mode

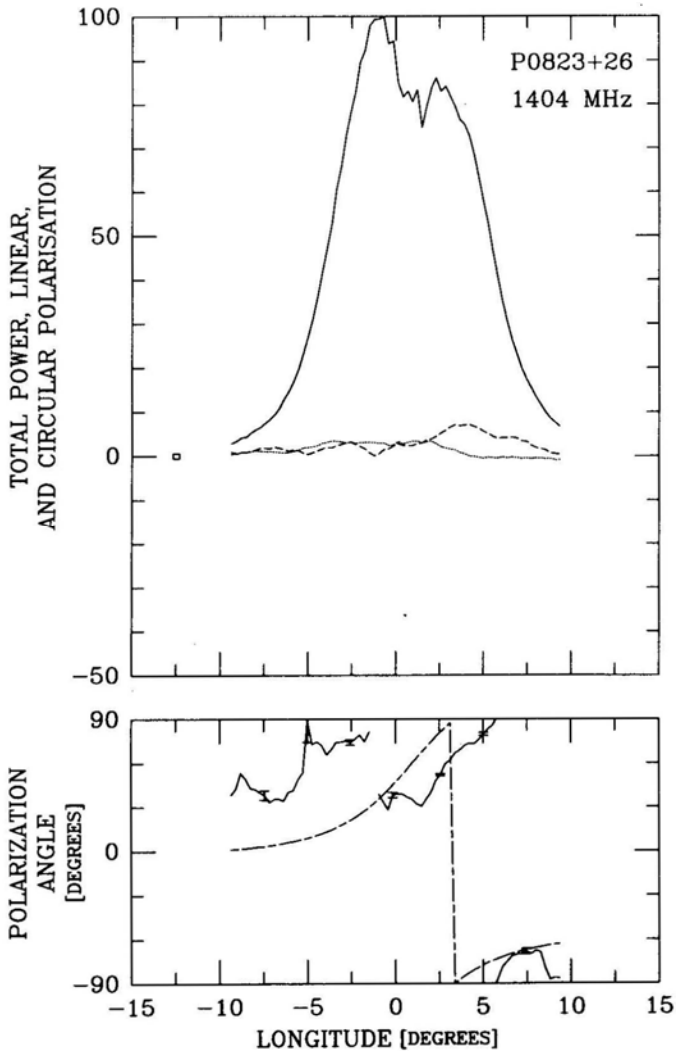

Figure 6 (c).

Figure 6 (a–c). Partial, 'modeseparated' profiles for pulsar 0823 + 26 at 1404-MHz on 9th October 1981 as in Fig. 4.

profile represents 4.0% of the samples and 19.0% of the power of the total individual-pulse sequence at an *L*-threshold value of 2σ. And, again, lowering the *L* threshold to irrelevance produces no qualitative change in the form of the secondary-mode profile.

'Mode-separated' profiles corresponding to the 1404-MHz observation in Fig. l(c) are given in Figs. 6 (a–c). Only a limited longitude range around the MP was available in these observations. The PA-model parameters used were similar to those given above. At this frequency 60.1 % (16.5 %) and 24.1 % (8.4 %) of the power (samples) accrued to the primary (Fig. 6a) and secondary (Fig. 6b) modes, respectively, and 15.8 % (75.1 %) to the residual (Fig. 6c) profile.

5. Main-pulse emission geometry

Rather few 'mode-separated' partial profiles, computed from well resolved and calibrated observations, are available in the literature; it is thus far too early to attempt any generalizetions regarding them. In particular, the question of what constitutes a 'component' in total-average profiles has been a subject fraught with controversy (and is perhaps only now beginning to clarify); therefore we certainly have no wish to hastily attribute this status to every discernible minor feature in mode-separated partial profiles. Nevertheless, the appearance of the additional features in pulsar 0823 + 26's secondary-mode profile is so extraordinary that we are emboldened to attempt some speculative analysis.

Therefore, let us proceed by entertaining the hypothesis that the two new, minor features on the leading and trailing edges of the main one are indeed correctly interpreted as a conal-component pair, which was too weak to detect in the total profile at any frequency. We noted above—and reiterate here – that 0823 + 26, though almost certainly correctly classified as a core-single (S_t) pulsar, produces no identifiable conal 'outriders' even at the highest frequencies of observation. Thus, were we to interpret the secondary-mode features as 'outriders', we would encounter no conflict with our existing knowledge of this star.

A way to assess whether this interpretation makes sense is that of exploring its geometrical consequences. The basic magnetic geometry of this pulsar seems well established: Paper IV argued that core-component widths can be used to determine the latitude of the magnetic axis α, and pulsar 0823 + 26 was discussed not only as an example of a pulsar whose interpolated 1-GHz core width implies that $\alpha \simeq 90°$, but one whose overall PA traverse supports this, and whose interpulse (0823 + 26 is almost certainly a two-pole interpulsar) leaves virtually no doubt.

More questionable then is its emission geometry in relation to our sightline. Referring again to Fig. 1, recall that the maximum PA sweep rate R is about + 15°/° for the primary mode and about + 30°/° for the secondary one. Using the definition of R following equation (1), we see that this results in β values of + 3.8° and + 1.9°, respectively, where the '+' sign has been added to indicate that these are outside (positive) traverses on the basis of their flattened wings (see Narayan & Vivekanand 1982).

The significance of the β value associated with the primary mode is not yet clear, but we are immediately at liberty to use the secondary-mode β value, along with α and the (outside, half-power) width of the conal component pair to calculate the conal emission radius which would be expected. This latter value, scaled from the older and newer secondary-mode profiles in Figs. 4 and 5 are 16.7° and 16.3°, respectively. Now using equation (4) of Rankin (1993a; hereafter Paper VIa), this implies a conal radius ρ of just less than 8.5° (if we 'round' down to 16° in an effort to 'extrapolate' to 1 GHz, ρ is 8.2°; please see Rankin (1993b); hereafter Paper VIb, Table 4). In either case, 0823 + 26's secondary-mode ρ value is clearly just what one would expect for an outer cone, as can be seen by referring to equation (5) of Paper VIa.

It would then seem that the most economical interpretation of the 'outriders' in the secondary-mode profile of pulsar 0823 + 26 is that they indeed represent an outside conal component pair, which is so weak that it can be detected only by removing the dominant primary-mode power from the profile. This line of interpretation is entirely consistent quantitatively with the known geometry of the pulsar and further an answer to the question – for 0823 + 26, certainly, but also in general – of why some core-single pulsars have no discernible conal outriders.

6. Postcursor emission geometry

First, several different lines of argument now give similar conclusions regarding the basic geometry of pulsar 0823 + 26. Its interpulse (Hankins & Fowler 1986; Paper IV), analysis of its PA traverse (Lyne & Manchester 1988; Blaskiewicz *et al*. 1991), and the width of its MP core component (Paper IV) all indicate that its magnetic axis is nearly orthogonal to its rotational axis. Moreover, two somewhat different analyses, Lyne & Manchester (see especially, their table 2) and that in both this paper and Paper VIb, find that our sight line passes within a mere 1 or 2° of the magnetic axis.

Second, the identification above of the secondary-mode 'outriders' as an outer conal component pair marks these components as falling at the extreme boundary of conal emission in this pulsar, in terms both of angle from the magnetic axis and of distance from the star. We now have overwhelming evidence that conal emission is highly consistent in its angular beaming properties (Paper VIa & b; Gil *et al*. 1993; Gil & Kijak 1993); the outer conal emission radius is $5.75° \; P^{-1/2}$, or, as we saw in the previous section, about 8°.

In this geometric context it is now much more interesting to consider the significance of the postcursor component inpulsar 0823 +26, and the first point tomake is that we now have no possible option of viewing the PC component as some kind of weak, widely separated portion of a conal double profile as was attempted in Paper III. The PC lies much too far from the magnetic axis – some 30° – for it to be of conal origin in any usual sense; furthermore, there is *only* a PC, no precursor!

While we cannot say how it is that the PC is emitted, it would seem that 0823 + 26's geometry offers a particularly good opportunity to identify unusual types of emission. As noted above, not only is this pulsar's magnetic moment nearly parallel to its equator, but so is our sight line! Only in this geometry is there a bundle of field lines (also parallel to the star's rotational equator) which remains in view as the star rotates and has tangent points in the observer's direction for an unusually large fraction of the star's rotation period. One such bundle trails the magnetic axis, and it is worth noting that any 'field-line sweepback' at high altitude will increase the curvature of this bundle. Another bundle leads the magnetic axis, and (with enough sweepback) it could also have tangents in the observer's direction, but only at great altitude and for a shorter interval.

If the PC component is emitted along this trailing bundle of peripheral, equatorial field lines at a height at which the field remains essentially dipolar, then it is possible to estimate the emission height of the PC, again using equation (2) in Paper VIa. For an angular separation between the PC and the magnetic axis (taken to be the MP peak) of about 32° (Hankins & Fowler 1986), we find an emission height of about 4×10^3 km – that is, about 400 stellar radii or some 4% of the light-cylinder radius – as compared to the nominal 210-km emission height of the outer cone. Any poloidal distortion of the field would increase the curvature of the trailing bundle of equatorial field lines and decrease the emission height. Interestingly, it would also decrease that of the leading bundle, perhaps explaining why we more generally see postcursors rather than precursors. Both height and sweepback will tend to increase the curvature of the trailing bundle, which may favour emission by particles with quite different energies than those responsible for the MP. Theories of pair-production discharge above pulsar polar caps, seem to produce a broad distribution of particle energies (Daugherty and Harding 1986). Finally, we note that the MP-PC separation *increases*

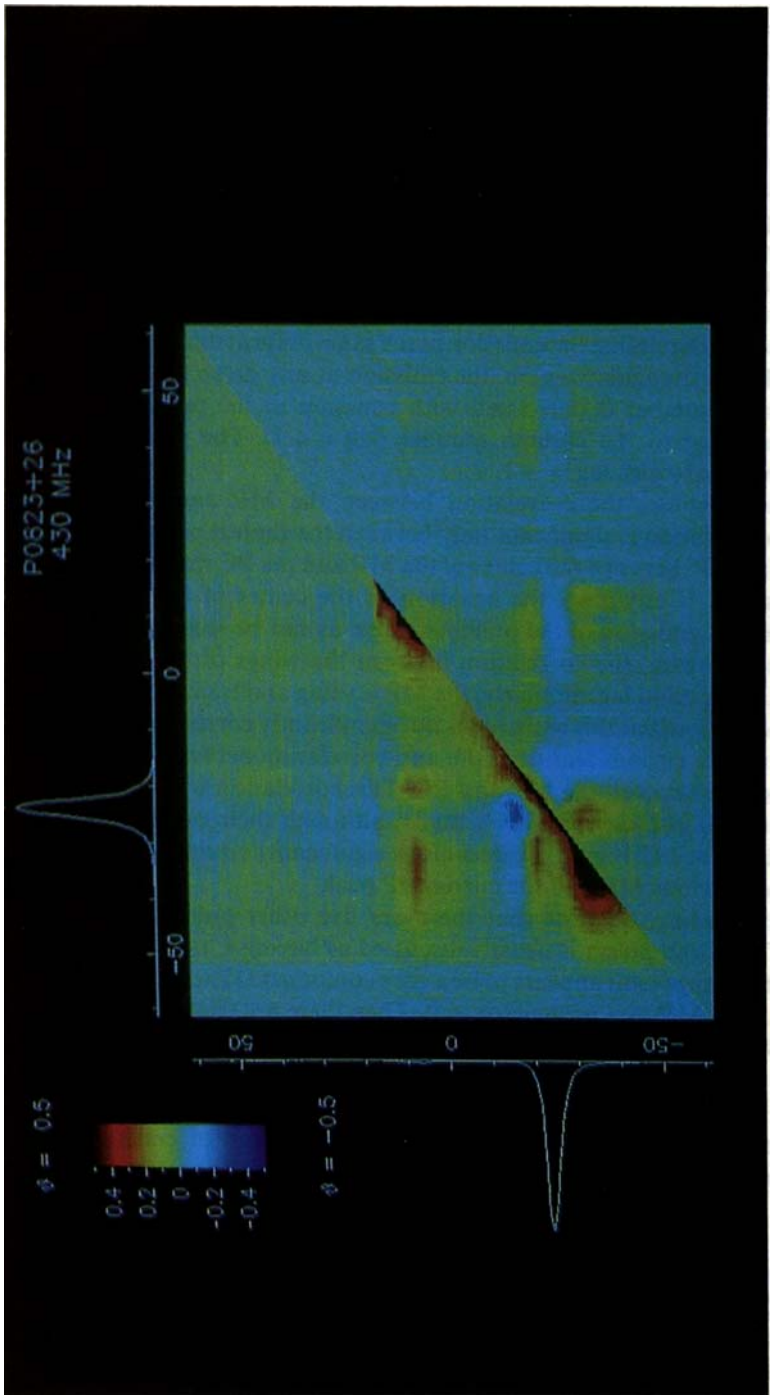

Figure 7. Longitude-to-longitude intensity correlation plot corresponding to the 430-MHz observations in Fig. 1b. Average profiles comprising the noise, the MP-PC, and IP windows have been plotted on both axes for convenience, and at longitudes larger than −15° the quantities I, L and V have been multiplied by a factor of 5 to show the postcursor and interpulse regions more clearly. The correlation is indicated by a coloured rectangle at the intersection of the two longitudes, and the colour scale in the upper left hand corner of the figure gives the magnitude of the correlation coefficient. The figure is divided into two triangular regions, the upper left one (row number > column number), gives the correlation of the current pulse with itself at different longitudes (zero lag); whereas, the lower right one gives the correlation between the current pulse and the previous pulse (lag = − 1).

weakly with frequency, suggesting that the higher frequency PC emission is emitted at greater heights than the low frequency emission; if so, this would be a 'radius-to-frequency mapping' of the opposite sense to that usually encountered.

If this is the correct interpretation for the geometry of the PC component, then we note that both the PC and the latter conal outrider are emitted along the same bundle of trailing equatorial field lines. It is then possible that the two components will exhibit some correlation in theintensities oftheir constituent individual pulses. The longitude-to-longitude correlation of the total power, corresponding to the 430-MHz observations in Fig. 1b, is given in Fig. 7. The longitude, of course, labels both axes, and average profiles comprising the noise, the MP-PC, and IP windows have been plotted for convenience. A colour scale indicating the degree of correlation is given at the upper left of the figure. The upper triangular region shows that the longitude-longitude correlations are calculated by correlating the emission in the same pulse at different longitudes (zero lag). In the lower triangular region, the emission at any given longitude corresponding to the row number is correlated with emission in the previous pulse at longitude corresponding to the column number (lag = +1). The diagonal line is included in the lower part with lag = + 1.

This figure clearly shows the correlation between the MP and PC emission. Interestingly, the correlation is significant only between the central portion of the PC and the wings of the MP; between the center of the MP and the PC there is hardly any significant correlation. If anything, the emission in the center of the MP is anti-correlated with the PC emission of the previous pulse, as can be seen from the lower part of the figure. However, the correlation between the wings of the MP and PC persists even for a one-period lag. Similarly, the MP leading and trailing wings exhibit highly correlated emission, but this emission is not significantly correlated with that of the MP center. Another curious feature is the anti-correlation between the MP peak and the 'bridge' region between the MP and PC. This correlation was also noted by Popov & Sieber (1990) in their 1700-MHz study, although their observations were restricted narrowly to the MP region. There is also a significant correlation between the leading part of the previous MP and the current IP peak.

All this notwithstanding, we note that there are five other pulsars with known PC components: The Crab pulsar is usually discussed as having a 'precursor' component, but in that this component appears to be a core component (Paper IV), one might better regard the star's MP as a postcursor to it. Then there are 0940 +16, 1530 + 27 (Rankin *et al*. 1989), probably 1530 – 53 (McCulloch *et al*. 1978; Manchester *et al*. 1980; McCulloch *et al*. 1982), 1929 + 10 (Perry & Lyne 1985; Rankin & Rathnasree 1996), and more recently 2217 + 47 (Suleymanova & Shitov 1994). We know of no pulsar with a true precursor – that is, one with a weak patch of emission which leads a core component. Apart from the Crab pulsar and 1929 + 10 – which are almost certainly orthogonal rotators – we know very little about the geometry of these other stars; most have not even been adequately classified, in part because of their odd 'postcursor' emission. Somewhat more is known about 2217 + 47; it was classified as an S_t pulsar in Paper VIb with an α of only 42°. This value could easily increase, however, as the profiles available in the literature are mostly poor (the only ~ 400-MHz profile available is from LSG in 1971!) and thus probably not well resolved.

We note that pulsars 0823 + 26 and 2217 + 47 have very similar periods and period derivatives, and the completely equatorial model used above to discuss the emission

geometry of the former also provides an attractive scenario for understanding Suleymanova & Shitov's observations of the latter. Perhaps the most surprising feature of the 2217 + 47 postcursor is that it slowly varied in amplitude and position over time, possibly correlated with changes in the torque on the star. Indeed, if the PC emission is occurring high on this bundle of trailing, equatorial field lines, torque changes might change the curvature and thus the height of the radiation, which would in turn change its phase within the profile relative to the core component. But we do not yet know whether 2217+ 47 – or really any of the other 'postcursor' pulsars apart from the Crab – have orthogonal geometries. We are guessing that they probably do, but additional observations and analysis are required to answer this question. If so, some – 2217 + 47 to be sure – may prove highly useful as a means of exploring other regions of the pulsar magnetosphere. Pulsars with PC components may also be good candidates in which to search for new interpulses.

7. Interpulse emission geometry

Little can be said with confidence about pulsar 0823 + 26's interpulse geometry. No quality observation of this feature exists in the literature, and, given its weakness, none may be possible in the foreseeable future. Nonetheless, the 430-MHz profile (Rankin & Benson 1981) appears more single, and the 1400-MHz profile (Rankin *et al.* 1989) has a flat top which might indicate incipient conal outriders (as per the usual triple or possibly conal-single evolution). Both IP profiles have a full width at half maximum of about 16 or 17°, and the PA sweep rate is about – 6°/°. These values do not make any immediate sense in terms of the geometrical arguments of Paper VIa & b. If the above width corresponds to an outer cone, either the IP sweep rate needs to be steeper or the width smaller. One possibility is that here we are cutting an outer cone on its extreme edge, so that the sightline comes nowhere near the high-intensity 'shoulder' of the conal beam.

8. Polarization-modal structure of PSR 0823 + 26's emission

We have seen above that the primary mode at 430 MHz represents about 68–69% and the secondary-mode about 18–19% of the total power in the sequence of pulses when the threshold is set at a level such that L must exceed about two σ in the off-pulse noise; that is, the primary mode is about 3.5 times stronger than the secondary one. Of course, these numbers will change somewhat if **a**) the mode-separation algorithm is not accurately segregating the modal power in the PA-longitude diagram, **b**) if the L threshold level is changed, or **c**) if the emitted modal power varies in time. We have done our best to assure that the modal separation is correct, although given the proximity of the two modes near the primary-mode 'blotch' in Fig. 1, some ambiguity is unavoidable. As for the second condition, a 2-σ threshold gives a sample uncertainty in the PA of ± 30°, and any lower threshold will increase the number of unpolarized or noise-dominated samples which are spuriously assigned to one mode or the other. We re-emphasize that only for those samples with adequate residual linear polarization can we make a choice about their mode. For the others, all such information has been lost through depolarization on time scales short compared to the sampling interval, and we

can only speculate about the significance of this depolarized portion of the pulsar's emission. Observations suggest either that these are relatively stable or that we have found the pulsar in the same 'modal' state.

We can then ask whether this is the 'true' power ratio of the two modes. Some 12–14% of the power fell below the threshold in *L*, and the average of these 'residual' samples shows virtually no linear polarization. It might then be **a**) that most of this power is associated with the secondary mode, which is only some 10% polarized, in which case the modal ratio is about 70/30%, **b**) that the power is about equally divided between the two modes (and, indeed, the residual PA falls near the primary mode before the MP peak and near the secondary mode thereafter) in which case the modal ratio is about 75/25%, or **c**) that most of the residual power is associated with the primary mode in view of its greater intensity, in which case the modal ratios are about 80/20%. At 21 cm about 60% of the power was found in the primary mode to about 24% and 16% for the secondary mode and residual categories; see Fig. 6. If the polarization-mode switching phenomenon is broad band – as, indeed, it appears to be – these latter numbers might be squared with any of the three alternatives.

It is also useful to consider the fractional linear polarization, and comparing the total average profiles in Fig. 1 with the modal partial profiles in Figs. 4–6 we see that the mode separation did not dramatically increase the fractional linear polarization, either at 430 or 1400 MHz. The earlier 430-MHz observation has a peak fractional linear polarization of about 35%, whereas the primary mode's is only about 42%. Similarly, that of the later 430-MHz run goes from about 45% to 52% and the 1400-MHz one from about 28% to 36%. The later data are better resolved than the earlier at both 430 and 1404 MHz, and this may be responsible, in part, for their somewhat larger amounts of aggregate linear polarization.

In all cases the secondary-mode fractional linear is lower. We then apparently have a situation in pulsar 0823 + 26 wherein very significant amounts of depolarization are occurring on time scales shorter than the inherent time resolution of the observations – here in all cases some part of 1° longitude. This also largely explains the fact that the secondary mode is more depolarized than the primary one, because secondary-mode samples will typically contain more primary-mode power than primary ones will secondary-mode power, by simple reason of their relative intensities. Only those unusual samples in which the secondary mode dominates the primary will be recognized as 'secondary-mode' samples—and accumulate in the 'secondary-mode' profile. Generally the secondary mode will just exceed the primary, and these are the conditions which are most depolarizing. These factors are especially complicated in 0823 + 26, however, owing to the spectacular non-orthogonality of the two modes throughout the duration of the MP.

9. Displaced modal emission in the main pulse

A very interesting feature of the modal partial profiles in Figs. 4–6 is the displacement in phase between the primary and secondary modes. Reference to these figures shows that the secondary mode 'MP' always leads the primary-mode feature, at 430 MHz by 1.5 ± 0.1° and at 1404 MHz by some 1.3 ± 0.1°. Displacement in rotational phase has been seen before in the components of mode-separated profiles – the first component of

1737 + 13, for instance, shows a dramatic offset (Rankin *et al*. 1988) – however, this effect has not, before to our knowledge, been identified in a core component[@].

The question is what interpretation to make of this phase delay, and at this point two possibilities seem open. The first is that the offset is a geometrical phenomenon. We saw above that the observed offset was somewhat greater at 430 as compared to 1400 MHz – but just so within the errors – and just over 1° of longitude is quite comparable to the 3.36° diameter of the pulsar's polar cap. Another possibility is that we are here seeing an effect of birefringent propagation in the pulsar's inner magnetosphere as suggested, for instance, by Barnard & Arons (1986). If this is the case we might expect the effect to become more pronounced at lower frequencies—and furthermore this 'double' nature of the core component might be connected with such well known, but entirely unexplained phenomena such as 'absorption' and the observed broadening of some core components at lower frequencies (see Paper II).

10. Summary and conclusions

The polarization structure of the radiation which comprises pulsar 0823 + 26's average profile at both 430 and 1400 MHz has been studied. Two polarization modes are identified in the emission over a substantial range of longitudes around the MP and PC. In some intervals they are roughly orthogonal; however, just underthe MP the two modes are more conspicuously non-orthogonal – and thus difficult to distinguish – than in any other pulsar we know of. We have attempted to construct partial profiles in which the power in the two polarization modes is largely separated and have identified two (mostly) continuous, non-orthogonal PA trajectories which seem to correspond to these modes. The primary mode in 0823 + 26 is three to perhaps five times stronger than the secondary mode overall and thus dominates the emission and the PA at most longitudes. It is then not surprising that the primary-mode MP closely resembles the total profile MP.

The secondary-mode profile consists of three MP features, which appear to be a central core component and a surrounding pair of conal outriders. The (outside half-power) width of the outriders together with the secondary-mode PA traverse appear compatible with the interpretation that these conal features represent an outer emission cone.

This technique could lead to the discovery of covert emission features in the profiles of other pulsars with single profiles but complicated PA histograms. In this context, it is interesting to speculate about the emission geometry of the PC feature, which follows the MP by some 30°. Having now identified a pair of much more closely spaced components, which appear to represent anouter cone of emission, it is clear that the PC cannot be a conal component in any usual sense.

Overall, 0823 + 26 seems to have a nearly equatorial geometry—that is, both the magnetic axis and the sight line appear to lie close to the rotational equator of this pulsar. We then note that in this situation there is a bundle of trailing field lines which has a tangent in our direction for a substantial portion of the rotation cycle of the

[@]Pulsar 1737 + 13's core component is also misaligned in the mode-separated profiles, but given the greater complexity ofboth partial profiles,it is not at all clear what interpretation to make of this circumstance.

pulsar. Perhaps it is emission along this bundle – at a height of some 4×10^3 km or about 4% of the light cylinder – that the PC emission occurs.

If the PC component and the trailing conal outrider are both emitted along this trailing bundle of equatorial field lines, then it is possible that their emission is correlated. Indeed, we find that there is significant correlation between the PC and the longitude ranges of the trailing conal outriders, and furthermore that this correlation becomes negligible between the PC and the core-emission region.

Finally, it seems that the pulsar does exhibit some $6.4 \pm 0.8\%$ null pulses, which is somewhat more than the 5% limit of Ritchings (1976).

Acknowledgements

We thank Amy Carlow, Vera Izvekova, Svetlana Suleymanova, and Kyriaki Xilouris for help with the October 1992 observing and Dan Stinebring for making the Arecibo P-467 observations available. We also acknowledge Mark McKinnon for helpful discussions. One of us (JMR) also wishes to acknowledge the support of the U.S. Educational Foundation in India and the hospitality of the Raman Research Institute, where part of this work was carried out while she was in residence on a Fulbright Fellowship. This work was supported in part by a grant from the U.S. National Science Foundation (AST 89-17722). Arecibo Observatory is operated by Cornell University under contract to the U.S. National Science Foundation.

References

Backer, D. C, Boriakoff, V., Manchester, R. N. 1973, *Nat. Phys. Sci*., **243**, 77.
Backer, D. C. 1973, *Astrophys. J*., **182,** 245.
Backer, D. C, Rankin, J. M. 1980, *Astrophys. J. Suppl*, **42,** 143.
Barnard, J. J., Arons, J. 1986, *Astrophys. J*., **302,** 138.
Bartel, N., Sieber, W., Wielebinski, R. 1978, *A & A*., **68,** 361.
Blaskiewicz, M., Cordes, J. M., Wasserman, I. 1991, *Astrophys.J*., **370,** 643.
Cordes, J. M., Rankin, J. M., Backer, D. C. 1978, *Astrophys. J*., **223,** 961.
Craft, H. D., Lovelace, R. V. E., Sutton, J. M. 1968, *I.A.U. Circ. No. 2100*.
Daugherty, J. K., Harding, A. K. 1986, *Astrophys. J*., **309,** 362.
Gil, J. A., Snakowski, J. K., Stinebring, D. R. 1991, *Astrophys. J*., **242,** 119.
Gil, J. A, Lyne, A. G., Rankin, J. M., Snakowski, J. K., Stinebring, D. R. 1992, *A&A*, **255,** 181.
Gil, J. A., Kijak, J. 1993, *A&A*, **273,** 563.
Gil, J. A., Kijak, J., Seiradakis, J. H. 1993, *A&A*, **272,** 268.
Hagan, J. 1987, *NAIC Electronics Department Manual No. 8319.*
Hankins, T. H., Fowler, L. A. 1986, *Astrophys.J*., **304,** 256.
Hankins, T. H., Rickett, B. J. 1986, *Astrophys.J*., **311,** 684.
Hankins, T. H., Rankin, J. M. 1994, private communication.
Izvekova, V.A., Kuz'min, A. D., Malofeev, V.M., Shitov, Yu. P. 1981, *Astrophys. Space Sci*, **78,** 45.
Komesaroff, M. M. 1970, *Nature*, **225,** 612.
Kramer, M., Wielebinski, R., Gil, J. A., Seiradakis, J. H., Jessner, A. 1994, *A&A*, **107,** 527.
Lang, K. R. 1969, *Astrophys. J. Lett*., **158,** L175.
Lyne, A. G., Manchester, R. N. 1988, *Mon. Not. R. astr. Soc.*, **234,** 477.
Manchester, R. N., Hamilton, P. A., McCulloch, P. M. 1980, *Mon. Not. R. astr. Soc*., **192,** 153.
McCulloch, P.M., Hamilton, P. A., Manchester, R.N., Ables, J.G.1978, *Mon. Not. R. astr. Soc*., **183,** 645.
McCulloch, P. M., Hamilton, P. A., Manchester, R. N. 1982, private communication.

Narayan, R., Vivekanand, M. 1982, *A&A*, **113,** L3.
Perillat, P. 1988, *NAIC Computer Department Report* # 23.
Perillat, P. 1992, private communication.
Perry, T. E., Lyne, A. G. 1985, *Mon. Not. R. astr. Soc.*, **212,** 489.
Phillips, J. A., Wolszczan, A. 1992, *Astrophys. J.*, **385,** 273.
Popov, M. V., Sieber, W. 1990, *Sov. Astr.*, **34,** 382.
Radhakrishnan, V., Cooke, D. J. 1969, *Astrophys. J. Lett.*, **3,** 225.
Rankin, J. M. 1983b, *Astrophys. J.*, **274,** 359. (Paper II)
Rankin, J. M. 1986, *Astrophys. J.*, **301,** 901. (Paper III)
Rankin, J. M. 1988, *Astrophys. J.*, **325,** 314.
Rankin, J. M. 1990, *Astrophys. J.*, **352,** 247. (Paper IV)
Rankin, J. M. 1993a, *Astrophys. J.*, **405,** 285. (Paper VIa)
Rankin, J. M. 1993b, *Astrophys. J.* (*Suppl.*), **85,** 145. (Paper VIb)
Rankin, J. M., Benson, J. M. 1981, *Astr. J.*, **86,** 418.
Rankin, J. M., Campbell, D. B., Backer, D. C. 1974, *Astrophys. J.*, **188,** 609.
Rankin, J. M., Campbell, D. B., Spangler, S. 1975, *NAIC Report* # 46.
Rankin, J. M., Rathnasree, N. 1996, in preparation.
Rankin, J. M., Stinebring, D. R., Weisberg, J. M. 1989, *Astrophys. J.*, **346,** 869.
Rankin, J. M., Wolszczan, A., Stinebring, D. R. 1988, *Astrophys. J.*, **324,** 1048.
Ritchings, R. T. 1976, *Mon. Not. R. astr. Soc*, **176,** 249.
Sieber, W. 1973, *A&A*, **28,** 237.
Stinebring, D. R., Cordes, J. M., Rankin, J. M., Weisberg, J. M., Boriakoff, V. 1984, *Astrophys. J.* (*Suppl*), **55,** 247.
Suleymanova, S. A., Shitov, Yu. P. 1994, *Astrophys. J. Lett.*, **422,** L17.
Taylor, J. H., Huguenin, G. R. 1969, Symposium on Pulsars and High Energy Activity in Supernova Remnants, Academia Nationale dei Lincei, Rome, 1969 December 18.
Xilouris, K. M., Seiradakis, J. M., Gil. J., Sieber, W., Wielebinski, R. 1995 *A&A*, **293,** 153.

J. Astrophys. Astr. (1995) **16,** 357–374

Disk Luminosity and Angular Momentum for Accreting, Weak Field Neutron Stars in the 'Slow' Rotation Approximation

Bhaskar Datta[1], Arun V. Thampan & Paul J. Wiita[2] *Indian institute of Astrophysics, Bangalore 560034, India.*
[1]*Visiting Professor: Raman Research Institute, Bangalore 560 080 India.*
[2]*Permanent address: Department of Physics & Astronomy, Georgia State University, Atlanta, GA 30303–3083, USA.*

Received 1995 June 29; accepted 1995 August 22

Abstract. For accretion on to neutron stars possessing weak surface magnetic fields and substantial rotation rates (corresponding to the secular instability limit), we calculate the disk and surface layer luminosities general relativistically using the Hartle & Thorne formalism, and illustrate these quantities for a set of representative neutron star equations of state. We also discuss the related problem of the angular momentum evolution of such neutron stars and give a quantitative estimate for this accretion driven change in angular momentum. Rotation always increases the disk luminosity and reduces the rate of angular momentum evolution. These effects have relevance for observations of low-mass X-ray binaries.

Key words: Stars: accretion—stars: accretion disks—stars: neutron—stars: rotation.

1. Introduction

Disk accretion on to a neutron star possessing a weak surface magnetic field ($B \lesssim 10^8\ G$) provides interesting X-ray emission scenarios, and is relevant for understanding X-ray bursters and low-mass X-ray binaries (e.g. van Paradijs 1991). Such weak-field neutron stars can rotate very rapidly and are also seen as millisecond pulsars (Radhakrishnan & Srinivasan 1982; Alpar *et al*. 1982; Bhattacharya & van den Heuvel 1991) and may be relevant for quasi-periodic oscillators (QPOs) (Priedhorsky 1986; Paczynski 1987). The equation of state of neutron star matter as well as general relativity play essential roles in such a scenario. This is in contrast to the strongly magnetic ($B \gtrsim 10^{12}\ G$) accreting neutron stars, where plasma processes dominate (e.g., Ghosh & Lamb 1991). For the weak-field case, the radius of the innermost stable circular orbit ($r_{\rm orb}$) plays a central role, deciding quantities of observational interest such as the disk luminosity. The relevance of this parameter ($r_{\rm orb}$) was emphasized by Kluzniak & Wagoner (1985, hereafter KW), who pointed out that for weak-field accreting neutron stars it is incorrect to always make the usual assumption that the accretion disk extends very close to the surface of the star, and is separated from it by a thin boundary layer. Using Schwarzschild geometry, Syunyaev & Shakura (1986, hereafter SS) concluded that the boundary layer brushing the neutron star surface will be substantially more X-ray luminous than the extended accretion disk. If the star's radius (R) is less than $r_{\rm orb}$, the

boundary layer is likely to be characterized by poorly collimated tangential motion of the infalling matter and a comparatively soft emission spectrum. Whether or not R exceeds $r_{\rm orb}$ (and consequently the detailed features of the accretion scenario) depends on the geometry of the spacetime and also the equation of state of neutron star matter.

An important aspect of disk accretion on to weak-field neutron star is the possibility that the neutron star will get spun up to very short rotation periods ($\lesssim$ millisecond) over a time of the order of hundreds of millions of years. For such rapid rates of rotation, the relativistic effect of dragging of inertial frames in the vicinity of the neutron star will be important. This effect will alter the trajectories of infalling particles as compared to the non-rotational case. Therefore, for a quantitative description of the accretion features, one must take into account the relativistic effects of rotation upon the spacetime geometry. Although the possible importance of such effects was stressed by KW and SS, the details were not worked out by them.

In this paper we address this question and calculate the disk and surface layer luminosities incorporating the rotational effects in a general relativistic framework. We take the spun up neutron star to be rotating at a particular value, namely, the secular instability limit so as to illustrate the maximal reasonable effects of rotation. This corresponds to the late stages of accretion. We use the Hartle & Thorne (1968; hereafter HT) formalism, for our purpose; this formalism describes a rotationally perturbed Schwarzschild space-time. The HT formalism is valid for strong gravitational fields but only in the limit of uniform rotation with a rate that is 'slow' compared to the critical speed for centrifugal break-up. Neutron star models rotating at the secular instability limit (assuming the star to be homogeneous), relevant in the context of accretion induced spun up neutron stars, are within this limit (Datta & Ray 1983), so this approximation will usually be adequate. Recently Cook *et al*. (1994a & b) calculated last stable orbits of rotating neutron stars incorporating higher order rotational terms that go beyond the HT approximation. However, these authors did not use their results to estimate the disk luminosity and angular momentum evolution involved in the accretion scenario. Although the Hartle & Thorne prescription assumes rotationally perturbed geometry, the use of this prescription provides a first estimate, which is amenable to a straightforward numerical treatment, of the luminosity values and angular momentum evolution for an accreting weak-field neutron star. This can be quite useful in observational applications such as low-mass X-ray binaries. Our calculations are done for a range of stable neutron star configurations computed using a representative sample of the proposed equations of state of neutron star matter. We also consider the accretion driven evolution of the angular momentum of the neutron star in a more accurate fashion than was done by KW.

2. Accretion on to a rotating neutron star

To describe the spacetime around a rotating neutron star we use the metric suggested by Hartle & Thorne (1968). This metric describes a rotationally perturbed Schwarzschild geometry to order Ω^2, where Ω is the angular velocity of the star as seen by a distant observer. The general form of the metric is (signature: $+---$)

$$\begin{aligned} {\rm d}s^2 &= g_{\alpha\beta}{\rm d}x^\alpha {\rm d}x^\beta,\ (a,\beta = 0, 1, 2, 3) \\ &= e^{2\Phi}\,{\rm d}t^2 - e^{2\psi}\,({\rm d}\phi - \omega {\rm d}t)^2 - e^{2\mu}\,{\rm d}\theta^2 - e^{2\mu\lambda}\,{\rm d}r^2 + \mathcal{O}(\Omega^3/\Omega_{\rm c}{}^3). \end{aligned} \tag{1}$$

Here ω is the angular velocity of the cumulative dragging of inertial frames and $\Omega_c = (GM/R^3)^{1/2}$, the critical angular velocity for equatorial mass shedding, where M and R are the mass and radius of the non-rotating neutron star. For simplicity, we use the geometric units: $c = 1 = G$. The metric components correspond to an interior with the identification:

$$e^{2\Phi} = e^{2\nu}\{1+2(h_0+h_2 P_2)\}, \tag{2}$$

$$e^{2\psi} = r^2 \sin^2\theta\{1+2(v_2-h_2)P_2\}, \tag{3}$$

$$e^{2\mu} = r^2\{1+2(v_2-h_2)P_2\}, \tag{4}$$

$$e^{2\lambda} = \frac{1+2(m_0+m_2P_2)/(r-2m)}{1-2m/r}, \tag{5}$$

(where 2ν is the gravitational potential function for the non-rotating star and m is the gravitational mass contained within a volume of radius r) and to an exterior with the identification:

$$e^{2\Phi} = e^{-2\lambda} = 1-2\frac{M'}{r}+2\frac{J^2}{r^4}, \tag{6}$$

$$e^{2\psi} = e^2 \sin^2\theta, \tag{7}$$

$$e^{2\mu} = r^2. \tag{8}$$

Here M' and J are respectively the mass and angular momentum of the rotating configuration of the star. The quantity P_2 is the Legendre polynomial of order 2, and h_0, h_2, m_0, m_2, v_2 are all functions of r that are proportional to Ω^2 (see HT).The metric has the desirable property that the internal and external forms match at the surface of the star. For our purpose here, we shall retain only the spherical deformation terms (characterized by subscript 0) and neglect the quadrupole deformation terms (characterized by subscript 2). The latter are necessary for computing stellar quadrupole deformation, but average out in calculating the rotation induced changes to M and R. The applicability of the metric (1) is valid for Ω small in comparison to Ω_c, and to go beyond that approximation requires a treatment similar to that of Cook *et al*. (1994a, b).

A relativistic effect of rotation, important for the astrophysical scenario that we consider here, is the dragging of inertial frames, which implies

$$\bar{\omega}(r) \neq \Omega, \tag{9}$$

where $\bar{\omega}(r)$ is the angular velocity of the stellar fluid relative to the local inertial frame, and is given by (HT)

$$\frac{\mathrm{d}}{\mathrm{d}r}\left(r^4 j\frac{\mathrm{d}\bar{\omega}}{\mathrm{d}r}\right)+4r^3\bar{\omega}\frac{\mathrm{d}j}{\mathrm{d}r}=0, \tag{10}$$

where

$$j(r) = e^{-\nu}(1-2m/r)^{1/2}, \tag{11}$$

with the boundary conditions

$$\left(\frac{\mathrm{d}\bar{\omega}}{\mathrm{d}r}\right)_{r=0}=0; \quad \bar{\omega}(r=\infty)=\Omega. \tag{12}$$

For $r > R$ (i.e., outside the star),

$$\bar{\omega}(r) = \Omega - 2J/r^3, \tag{13}$$

where J is the angular momentum of the star:

$$J = \frac{R^4}{6}\left(\frac{\mathrm{d}\bar{\omega}}{\mathrm{d}r}\right)_{r=R}. \tag{14}$$

The equations of motion are derived from the Lagrangian corresponding to the metric (1):

$$\mathcal{L} = \tfrac{1}{2}\{e^{2\Phi}\dot{t}^2 - e^{2\lambda}\dot{r}^2 - e^{2\mu}\dot{\theta}^2 - e^{2\psi}(\dot{\phi} - \omega\dot{t})^2\}, \tag{15}$$

where a dot represents a derivative with respect to proper time. We shall, for purpose of illustration, take the polar angle (θ) to be fixed and equal to $\pi/2$, which corresponds to the equatorial plane.

The metric (1) and the equations of motion provide three equations in the three variables $\dot{\phi}$, $\dot{t}$, and $\dot{r}$. From these, we can get (see KW)

$$\dot{r}^2 = \tilde{E}^2 - 2\omega\tilde{E}\tilde{l} - h^2(1 + \tilde{l}^2/r^2), \tag{16}$$

where

$$\tilde{E} = h^2\dot{t} + \omega r^2\dot{\phi}, \tag{17}$$

and

$$\tilde{l} = r^2(\dot{\phi} - \omega\dot{t}), \tag{18}$$

stand respectively for the energy and angular momentum per unit rest mass (denoted by m_B) and

$$h = (1 - 2M'/\mathrm{r})^{1/2} \tag{19}$$

The conditions for the turning point of the motion, the extremum of the energy, and the minimum of the energy are respectively given by (see Misner, Thorne & Wheeler 1974)

$$\tilde{E}^2 = V^2, \tag{20}$$

$$\frac{\mathrm{d}\tilde{E}}{\mathrm{d}r} = 0 = \frac{\mathrm{d}V}{\mathrm{d}r}, \tag{21}$$

and

$$\frac{\mathrm{d}^2\tilde{E}}{\mathrm{d}r^2} > 0, \tag{22}$$

where V is the effective potential, given by

$$V^2 = 2\omega\tilde{E}\tilde{l} + h^2(1 + \tilde{l}^2/r^2). \tag{23}$$

For marginally stable orbits we can use the condition

$$\frac{\mathrm{d}^2\tilde{E}}{\mathrm{d}r^2} = 0 = \frac{\mathrm{d}^2V}{\mathrm{d}r^2}. \tag{24}$$

Written explicitly, equations (20), (21), and (24) respectively become

$$\tilde{E}^2 - \frac{\tilde{j}a\tilde{E}}{x^3} - \left(1 - \frac{1}{x}\right)\left(1 + \frac{a^2}{x^2}\right) = 0, \tag{25}$$

$$a^2 + \frac{3\tilde{j}a\tilde{E}}{(2x-3)} - \frac{x^2}{(2x-3)} = 0, \tag{26}$$

$$x^2 - 3a^2 x + 6(a^2 - \tilde{j}a\tilde{E}) = 0, \tag{27}$$

where $x = r/2M'$, the dimensionless radial co-ordinate; $\tilde{j} = J/M'^2$ and $a = \tilde{l}/2M'$ are the dimensionless angular momenta for the star and the infalling matter respectively. Solving equations (25)–(27) simultaneously gives the values for the energy ($E_{\rm orb}$) and the specific angular momentum ($a_{\rm orb}$) of the accreted particle in the innermost stable orbit having a radius $x = x_{\rm orb}$.

Using Schwarzschild geometry, it was shown by SS that an accretion disk whose luminosity is small compared to the Eddington limit can exist only for R greater than the radius of the last stable circular orbit, $3r_{\rm g}$, where $r_{\rm g} = 2M$ = the Schwarzschild radius. For $R < 3r_{\rm g}$, the accreting matter falling on to the neutron star will follow the trajectory of a free particle in this geometry, with an energy equal to $m_B\sqrt{8/9}$. These authors also gave estimates of the energy released in the disk and in the boundary layer for $R/r_{\rm g}$ ranging from 1·5 to 10 without reference to any specific equation of state model. In the case where the neutron star has a high spin rate, the innermost stable orbit was calculated by KW using the HT metric to describe rotating spacetime. These authors, however, did not estimate the luminosity, and they neglected the rotational corrections to M and R in computing the evolution of angular momentum.

For a low-field, accreting neutron star possessing substantial rotation, the luminosity from the disk accretion can be calculated using equations (25)–(27). We use here the notation $x^* = R'/2M'$, where M' and R' correspond to the neutron star mass and radius that include corrections due to the rotation. The following distinct cases are possible:

2.1 *Case* (*a*): *Radius of the star is greater than* $r'_{\rm orb}$

If an accretion disk were to form around a relatively large neutron star (i.e., $x^* > x_{\rm orb}$), the ingress of a particle of rest mass m_B from infinity to the inner disk boundary will release an amount of energy given by

$$E'_D = m_B\,\{1 - \tilde{E}_k(x^*)\}, \tag{28}$$

where $\tilde{E}_k(x^*)$ stands for the specific energy of the particle in the stable orbit just above the surface, obtained by solving equations (25) and (26) numerically for $x = x^*$. The energy loss in the boundary layer will be

$$E'_s = m_B\,\{\tilde{E}_k(x^*) - \tilde{E}_0(x^*)\}, \tag{29}$$

where $\tilde{E}_0(x^*)$ isthe energy of the particle at rest on the surface of the neutron star, which can be calculated from equation (25) for $x = x^*$ and the specific angular momentum at the star's surface.

2.2 *Case* (*b*): *Radius of the star is smaller than* $r'_{\rm orb}$

In this case, $x^* < x_{\rm orb}$ and the accretion disk will extend inward to a radius corresponding to $x = x_{\rm orb}$. Now the energy released in the disk as the particle comes in from infinity to the innermost stable orbit will be

$$E'_D = m_B \{1 - \widetilde{E}_{\rm orb}\}, \tag{30}$$

and the energy released in the boundary layer will be

$$E'_s = m_B \{\widetilde{E}_{\rm orb} - \widetilde{E}_0(x^*)\}. \tag{31}$$

A remark about the boundary layer luminosity formula that we use, is in order here. Although this formula gives a plausible estimate for the boundary layer luminosity, strictly speaking, it is an overestimate as it does not take into account the subtraction of the energy that goes into spinning up of the neutron star. The need for such a correction was pointed out by Kluzniak (1987) and quantitative estimates for this were suggested by Ghosh, Lamb & Pethick (1977), Papaloizou & Stanley (1986), and Kley (1991). A fairly simple and general way to estimate the same was given recently by Popham & Narayan (1995) who considered the accretion disk boundary layer problem in cataclysmic variables. Significantly, these authors have stressed that most of the decrease in the boundary layer luminosity will occur in the early stages of spin-up, when the star is rotating slowly, *rather* than the late stages when it is approaching limiting break up rotation rates. The scenario that we consider in this paper corresponds to the latter stage. Therefore, for our purpose, the formula for the boundary layer luminosity that we have used is expected to be adequate. This point is elaborated in § 4.

3. Equation of state and rotation-induced changes in structure

The structure of neutron stars depends sensitively on the equation of state at high densities, especially for density regions $\gtrsim 10^{14}$ g cm^{-3}. There is no general consensus on the exact behaviour of the equation of state at these high densities. For our purpose here we choose the following six equations of state: (1) Pandharipande (N) (neutron matter) model, based on the lowest order constrained variational method using Reid potentials (Pandharipande 1971a); (2) Pandharipande (Y) (1971b) hyperonic matter; (3) Bethe-Johnson model V (N) for neutron matter (Bethe & Johnson 1974) which uses improved phenomenological potentials; (4) Walecka (1974) model for neutron matter, using scalar-vector interactions in a field theoretical framework; (5) Wiringa UV14 + UVII model for neutron-rich matter in beta equilibrium – a variational calculation incorporating the three-body interactions (Wiringa, Fiks & Fabrocini 1988); and (6) neutron-rich matter in beta equilibrium, based on the chiral sigma model (Sahu, Basu & Datta 1993). Of these, models (1) and (2) are 'soft' equations of state and and (6) are rather 'stiff' ones, while the models (3) and (5) are roughly intermediate in 'stiffness'.

The composite equation of state to determine the neutron star structure was constructed by joining the selected high density equation of state to that of Negele & Vautherin (1973) for the density range (10^{14} – 5×10^{10})g cm^{-3}, Baym, Pethick & Sutherland (1971) for densities down to $\sim 10^3$ g cm $^{-3}$ and Feynman, Metropolis & Teller (1949) for densities less than 10^3g cm $^{-3}$.

For a fixed central density (and a chosen equation of state model), the fractional changes in the gravitational mass ($\Delta M/M$) and radius ($\Delta R/R$) of the neutron star due to the rotation induced spherical deformation are proportional to Ω^2 is the angular velocity of the star as seen by a distant observer), and can be (numerically) obtained from a knowledge of the radial distributions of the mass and pressure perturbation terms, m_0 (r) and $p_0(r)$ (HT; Datta & Ray 1983; Datta 1988). The non-rotating mass (M) and radius (R) are obtained by numerically integrating the relativistic equations for hydrostatic equilibrium (see e.g. Arnett & Bowers 1977). The changes ΔM and ΔR are given by

$$\Delta M = m_0\,(R) + J^2/R^3, \tag{32}$$

$$\Delta R = -\left.\frac{p_0\,(\rho + p)}{\mathrm{d}p/\mathrm{d}r}\right|_{r=R}, \tag{33}$$

where $p(r)$ and $\rho(r)$ are the pressure and the total mass-energy density at the radial distance r from the center of the star.

For purpose of estimating the angular momentum evolution of the accreting neutron star (discussed in the next section), we need to know the baryonic mass of the rotating neutron star. The rotation induced change in the baryonic mass (denoted by ΔM_B) is conveniently written as

$$\Delta M_B = \Delta E_B + \Delta M, \tag{34}$$

where ΔE_B is the rotation induced change in the binding energy of the star (HT):

$$\Delta E_B = -J^2/R^3 + \int_0^R 4\pi r^2\, B(r)\,\mathrm{d}r\,, \tag{35}$$

where

$$\begin{aligned} B(r) = (\rho + p)\,p_0 & \left\{\frac{\mathrm{d}\rho}{\mathrm{d}p}\left[\left(1-\frac{2m}{r}\right)^{-1/2} - 1\right] - \frac{\mathrm{d}\varepsilon}{\mathrm{d}p}\left(1-\frac{2m}{r}\right)^{-1/2}\right\} \\ & + (\rho - \varepsilon)\left(1-\frac{2m}{r}\right)^{-3/2}\left[\frac{m_0}{r} + \frac{1}{3}\,j^2 r^2 \bar{\omega}^2\right] \\ & - \frac{1}{4\pi r^2}\left[\frac{1}{12}\,j^2 r^4\left(\frac{\mathrm{d}\bar{\omega}}{\mathrm{d}r}\right)^2 - \frac{1}{3}\frac{\mathrm{d}j^2}{\mathrm{d}r}\,r^3\bar{\omega}^2\right], \end{aligned} \tag{36}$$

and $\varepsilon = \rho - m_B n$ is the density of internal energy, with $n(r)$ and m_B denoting respectively, the baryonic density and rest mass.

Density profiles of neutron stars are remarkably flat out to r = (0·8–0·85) R (Datta *et al*. 1995). Therefore, the concept of rotational secular instability in the context of Maclaurin spheroids (Chandrasekhar 1969) is a relevant approximation when considering the rotational stability of neutron stars. For a uniformly rotating homogeneous spheroid, this instability corresponds to an angular velocity $\Omega = \Omega_s$, given by

$$\frac{\Omega_s^2}{2\pi\, G\bar{\rho}} = 0.18, \tag{37}$$

where ρ is the average density of the star. The quantity Ω_s sets a rough limit up to which the neutron star can be spun up, before the onset of rotational instabilities.

Table 1. Changes in Neutron Star Properties due to Rotation.

EOS Model (1)	ρ_c (g cm^{-3}) (2)	$M/M_\odot$ (3)	R (km) (4)	Ω_s ($rad\ s^{-1}$) (5)	$\Delta M/M$ (6)	$\Delta R/R$ (7)	r_{orb} (km) (8)	r'_{orb} (km) (9)
Pandharipande (N)	1.24E15	1.062	10.390	5.82E3	0.085	0.033	9.408	7.936
	1.50E15	1.241	10.150	6.52E3	0.080	0.029	10.990	9.244
	1.75E15	1.367	9.936	7.07E3	0.076	0.025	12.110	10.140
	1.83E15	1.400	9.867	7.23E3	0.074	0.024	12.400	10.360
	3.88E15	1.658	8.585	9.69E3	0.054	0.011	14.690	11.860
Pandharipande (Y)	2.18E15	1.045	8.767	7.45E3	0.073	0.029	9.257	7.817
	3.26E15	1.289	8.096	9.33E3	0.064	0.019	11.420	9.477
	3.88E15	1.354	7.796	1.01E4	0.059	0.016	11.990	9.855
	4.79E15	1.400	7.437	1.10E4	0.054	0.012	12.400	10.070
	5.74E15	1.414	7.153	1.18E4	0.050	0.010	12.530	10.080
Bethe–Johnson V (N)	9.50E14	1.003	11.100	5.12E3	0.089	0.035	8.885	7.470
	1.24E15	1.292	10.830	6.04E3	0.084	0.029	11.450	9.627
	1.25E15	1.303	10.820	6.08E3	0.084	0.029	11.540	9.712
	1.37E15	1.400	10.690	6.41E3	0.081	0.027	12.400	10.410
	2.18E15	1.683	10.020	7.75E3	0.067	0.018	14.910	12.280
	3.26E15	1.757	9.304	8.84E3	0.057	0.012	15.560	12.620

Table 1. (continued).

EOS Model (1)	ρ_c (g cm^{-3}) (2)	$M/M_\odot$ (3)	R (km) (4)	Ω_s ($rad\ s^{-1}$) (5)	$\Delta M/M$ (6)	$\Delta R/R$ (7)	r_{orb} (km) (8)	r'_{orb} (km) (9)
Walecka	6.50E14	1.035	12.200	4.52E3	0.098	0.037	9.168	7.682
	7.48E14	1.279	12.240	5.00E3	0.095	0.033	11.330	9.522
	7.75E14	1.342	12.240	5.12E3	0.094	0.032	11.890	9.994
	8.02E14	1.400	12.240	5.23E3	0.094	0.031	12.400	10.430
	2.18E15	2.243	11.060	7.71E3	0.059	0.009	19.870	15.850
Wiringa UV14 + UVII	8.50E14	1.053	11.110	5.25E3	0.095	0.035	9.328	7.837
	9.72E14	1.282	11.120	5.78E3	0.092	0.031	11.360	9.550
	1.00E15	1.330	11.120	5.88E3	0.091	0.031	11.780	9.899
	1.04E15	1.400	11.120	6.04E3	0.090	0.028	12.400	10.410
	2.70E15	2.188	9.875	9.02E3	0.053	0.004	19.380	15.120
Chiral Sigma Model	3.50E14	1.017	14.320	3.52E3	0.109	0.041	9.009	7.463
	3.85E14	1.261	14.620	3.80E3	0.110	0.038	11.170	9.345
	4.00E14	1.360	14.740	3.90E3	0.110	0.037	12.050	10.110
	4.06E14	1.400	14.780	3.94E3	0.109	0.037	12.400	10.400
	1.26E15	2.592	14.220	5.68E3	0.069	0.015	22.960	18.670

Table 2. Disk and Boundary Layer Luminosities.

EOS Model (1)	$M/M_\odot$ (2)	$M'/M_\odot$ (3)	E_D (m_0c^2) (4)	E'_D (m_0c^2) (5)	$\Delta E/E$ (6)	E_S (m_0c^2) (7)	E'_S (m_0c^2) (8)	$\Delta E/E$ (9)
Pandharipande (N)	1.062	1.152	0.056	0.066	0.1687	0.108	0.105	−0.0259
	1.298	1.400	0.057	0.073	0.2841	0.156	0.148	−0.0523
	1.400	1.504	0.057	0.074	0.2969	0.181	0.172	−0.0473
	1.642	1.738	0.057	0.075	0.3126	0.269	0.259	−0.0378
	1.658	1.748	0.057	0.075	0.3174	0.287	0.276	−0.0391
Pandharipande (Y)	1.045	1.121	0.057	0.071	0.2379	0.138	0.130	−0.0534
	1.289	1.371	0.057	0.074	0.2926	0.215	0.206	−0.0431
	1.319	1.400	0.057	0.074	0.2957	0.228	0.218	−0.0423
	1.400	1.476	0.057	0.075	0.3099	0.276	0.266	−0.0395
	1.414	1.485	0.057	0.075	0.3176	0.298	0.285	−0.0409
Bethe–Johnson V (N)	1.003	1.092	0.053	0.060	0.1347	0.090	0.089	−0.0112
	1.292	1.400	0.057	0.072	0.2542	0.138	0.132	−0.0461
	1.400	1.513	0.057	0.074	0.2919	0.160	0.152	−0.0511
	1.576	1.691	0.057	0.075	0.3030	0.200	0.191	−0.0427
	1.757	1.857	0.057	0.075	0.3155	0.278	0.267	−0.0381

Table 2. (continued).

EOS Model (1)	$M/M_\odot$ (2)	$M'/M_\odot$ (3)	E_D (m_0c^2) (4)	E'_D (m_0c^2) (5)	$\Delta E/E$ (6)	E_S (m_0c^2) (7)	E'_S (m_0c^2) (8)	$\Delta E/E$ (9)
Walecka	1.035	1.136	0.051	0.058	0.1298	0.083	0.083	0.0001
	1.279	1.400	0.057	0.067	0.1905	0.112	0.109	−0.0218
	1.400	1.531	0.057	0.071	0.2399	0.129	0.124	−0.0352
	1.680	1.825	0.057	0.075	0.3123	0.173	0.165	−0.0441
	2.243	2.375	0.057	0.077	0.3405	0.309	0.299	−0.0342
Wiringa UV14 + UVII	1.053	1.153	0.055	0.063	0.1541	0.097	0.096	−0.0114
	1.282	1.400	0.057	0.071	0.2430	0.131	0.126	−0.0384
	1.400	1.526	0.057	0.074	0.2896	0.150	0.144	−0.0439
	1.680	1.817	0.057	0.075	0.3148	0.201	0.194	−0.0359
	2.188	2.305	0.057	0.078	0.3653	0.355	0.342	−0.0369
Chiral Sigma Model	1.017	1.128	0.045	0.051	0.1140	0.066	0.067	0.0189
	1.261	1.400	0.052	0.059	0.1455	0.085	0.085	0.0075
	1.400	1.553	0.055	0.064	0.1686	0.097	0.097	−0.0010
	1.644	1.817	0.057	0.070	0.2260	0.120	0.118	−0.0224
	2.592	2.771	0.057	0.076	0.3274	0.263	0.255	−0.0324

The prescription mentioned earlier to calculate the mass and radius of a rotating relativistic star is valid only for rotation rates that are 'slow' in comparison to Ω_c Hartle & Thorne (1968) constructed 'slowly' rotating neutron star models all the way up to $\Omega = \Omega_c$ for the Harrison-Wheeler and Tsuruta-Cameron equations of state. Here we shall only consider rotating neutron stars with $\Omega = \Omega_s$ because of the secular instability consideration, and will employ the newer equation of state models mentioned earlier; these models will then illustrate the maximal reasonable effects of rotation. Since $\Omega_s = (0{\cdot}27)^{1/2}\ \Omega_c$, the models constructed by us are adequately treated in the limit of 'slow' rotation. To treat the maximal *possible* effects of rotation, one has to go beyond this limit, and use a technique similar to that employed by Cook *et al*. (1994a, b) for very rapidly (but still uniformly) rotating neutron stars; they determined that spin-up to the millisecond pulsar regime is possible for a wide range of equations of state.

4. Results and conclusions

In Table 1 we give the neutron star properties calculated for the various equations of state as a function of the central density (ρ_c). Columns (3) and (4) list the non-rotating mass and radius. Column (5) gives the corresponding value of Ω_s and columns (6) and (7) give the differences between the rotating and non-rotating neutron star mass and radius. Column (8) gives the non-rotating values of $r_{\rm orb}$ while column (9) shows how $r_{\rm orb}$ decreases due to rotation. Typical increases in mass are (5–11) %, in radius $\leqslant 4\%$, while $r_{\rm orb}$ decreases between 15% and 25%.

In the second and third columns of Table 2 we give values of the non-rotating mass M and the rotationally enhanced mass M' for a maximal reasonable rotation rate ($\Omega = \Omega_s$). Columns (4) and (7) show the disk and boundary layer luminosities for non-rotating configurations (E_D and E_s respectively). The values of E'_D and E'_S, including rotational effects treated consistently within the HT framework, are given in columns (5) and (8). All values of luminosity listed in the table are in units of the baryonic rest mass. The boundary layer luminosity values listed in Table 2 do not include corrections for the energy that goes into spinning up the neutron star. We have made estimate of this correction following the prescription of Popham & Narayan (1995) for the case of $1{\cdot}4M_\odot$ neutron star corresponding to the EOS model by Wiringa *et al*. (1988).This is shown in Fig. 1 which is a plot of the rotational energy correction $E_{\rm rot}$ in units of the particle rest mass vs. the stellar rotation rate Ω. It is clear from this figure that the rotational energy correction to the boundary layer luminosity tends to become unimportant as the angular velocity approaches very high values. For $\Omega = \Omega_s$, $E_{\rm rot} \sim 0{\cdot}048$; this is an order of magnitude less than the boundary layer luminosity given in Table2.Therefore the neglect of rotational energy correction to calculate E'_s for the neutron star rotating at the limiting Ω as considered by us does not result in a gross overestimate.

We find that as M' increases, the luminosity in the boundary layer increases monotonically. The disk luminosity increases in the rotational case as compared to the static case; the increase, illustrated in column (6), is most significant ($\gtrsim 30\%$) for high M' values. The fractional changes $\Delta E_s/E_s$ values (column (9)), however, exhibit a non-monotonic behaviour with increasing M', though they typically decrease by a few per cent. Further, as is well known, we see that the radius of the innermost stable orbit is less than the static case (where $r_{\rm orb} = 6M$) for all equations of state considered.

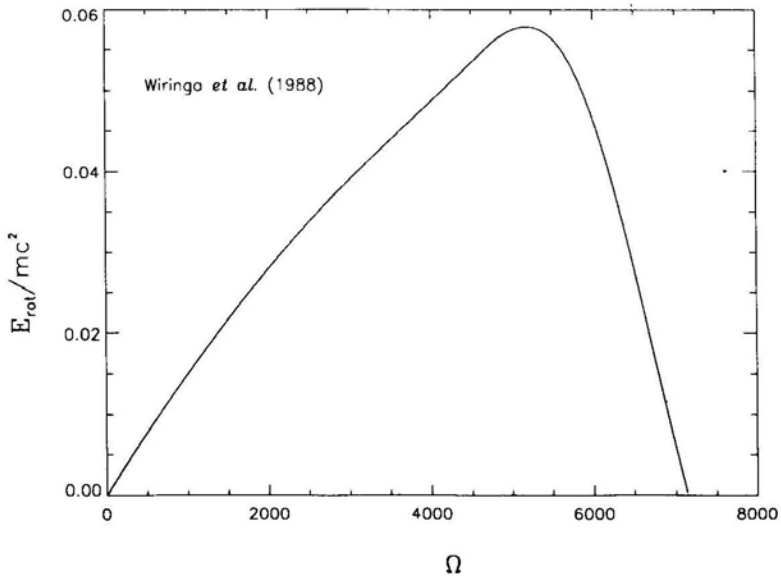

Figure 1. Rotational energy correction $E_{\rm rot}/mc^2$ to the boundary layer luminosity as a function of the stellar rotation rate Ω.

We now make a few remarks about the angular momentum evolution of the accreting neutron star. In performing the angular momentum evolution calculations, we have made the following additional assumptions:

- The central density of the neutron star does not change with mass accretion. This is a reasonable assumption to make because for a static, stable neutron star, while the central density increases with increasing mass, the rotation tends to 'decrease' the central density. Thus if the total accreted mass is not large, the effect of rotation will nearly compensate for the effect of accretion on the central density;
- The mass accretion rate is equal to $dM_B/{\rm d}t$ as in KW, but with the difference that rotational effects have been taken into account, that is, $M_{\rm acc} = dM'_B/{\rm d}t$;
- The maximum angular momentum for a particular neutron star configuration is determined by the secular instability limit:

$$\Omega = \Omega_s = (0.27)^{1/2}\,\Omega_c.$$

KW derived the evolution equation

$$\frac{{\rm d}J}{{\rm d}M'} = \tilde{I}\,(r(M'))\,\frac{{\rm d}M'_B}{{\rm d}M'} = 2M'\,a\,\frac{{\rm d}M'_B}{{\rm d}M}, \tag{38}$$

and solved it under the simplifying assumptions

$$M' \simeq M;\ \frac{{\rm d}M'_B}{{\rm d}M'} \simeq \frac{{\rm d}M_B}{{\rm d}M}.$$

For ${\rm d}M_B/{\rm d}M$, KW used a fit to the values of M and R taken from Arnett & Bowers (1977). Here, we solve equation (38) numerically, incorporating the effect of rotation as

Table 3. Gravitational and Baryonic Masses as Functions of Angular Momentum.

EOS Model (1)	ρ_c (g cm^{-3}) (2)	$M/M_\odot$ (3)	$M'/M_\odot$ (4)	$M'_B/M_\odot$ (5)	J (g cm^2 s^{-1}) (6)
Pandharipande (N)	1.83*E*15	1.400	1.400	1.567	0.000*E*00
			1.413	1.578	2.526*E*48
			1.426	1.589	3.648*E*48
			1.438	1.599	4.420*E*48
			1.467	1.623	5.823*E*48
Pandharipande (Y)	4.79*E*15	1.400	1.400	1.615	0.000*E*00
			1.416	1.627	3.269*E*48
			1.432	1.639	4.660*E*48
			1.448	1.652	5.772*E*48
			1.466	1.665	6.746*E*48
Bethe–Johnson V (N)	1.37*E*15	1.400	1.400	1.556	0.000*E*00
			1.420	1.572	3.139*E*48
			1.440	1.589	4.424*E*48
			1.460	1.606	5.422*E*48
			1.500	1.639	6.992*E*48
Walecka	8.02*E*14	1.400	1.400	1.671	0.000*E*00
			1.430	1.699	3.760*E*48
			1.486	1.750	6.318*E*48
			1.500	1.764	6.844*E*48
			1.516	1.779	7.370*E*48
Wiringa UV14 + UVII	1.04*E*15	1.400	1.400	1.562	0.000*E*00
			1.420	1.578	3.050*E*48
			1.443	1.598	4.538*E*48
			1.467	1.618	5.655*E*48
			1.512	1.656	7.291*E*48
Chiral Sigma Model	4.06*E*14	1.400	1.400	1.521	0.000*E*00
			1.434	1.549	3.975*E*48
			1.472	1.581	5.760*E*48
			1.505	1.609	6.976*E*48
			1.539	1.638	8.031*E*48

outlined above. We assume that for a central density that gives a gravitational mass of $1{\cdot}4M_\odot$ in the non-rotating case, $J = \Omega = 0$, and we then vary Ω from zero to Ω_s. The results are presented in Table 3; these should be compared with Table 1 of KW.

From Table 3, we see that for each equation of state, a plot of M'_B vs M' gives an almost constant slope. We solve equation (38) using the boundary condition $J = 0$ for

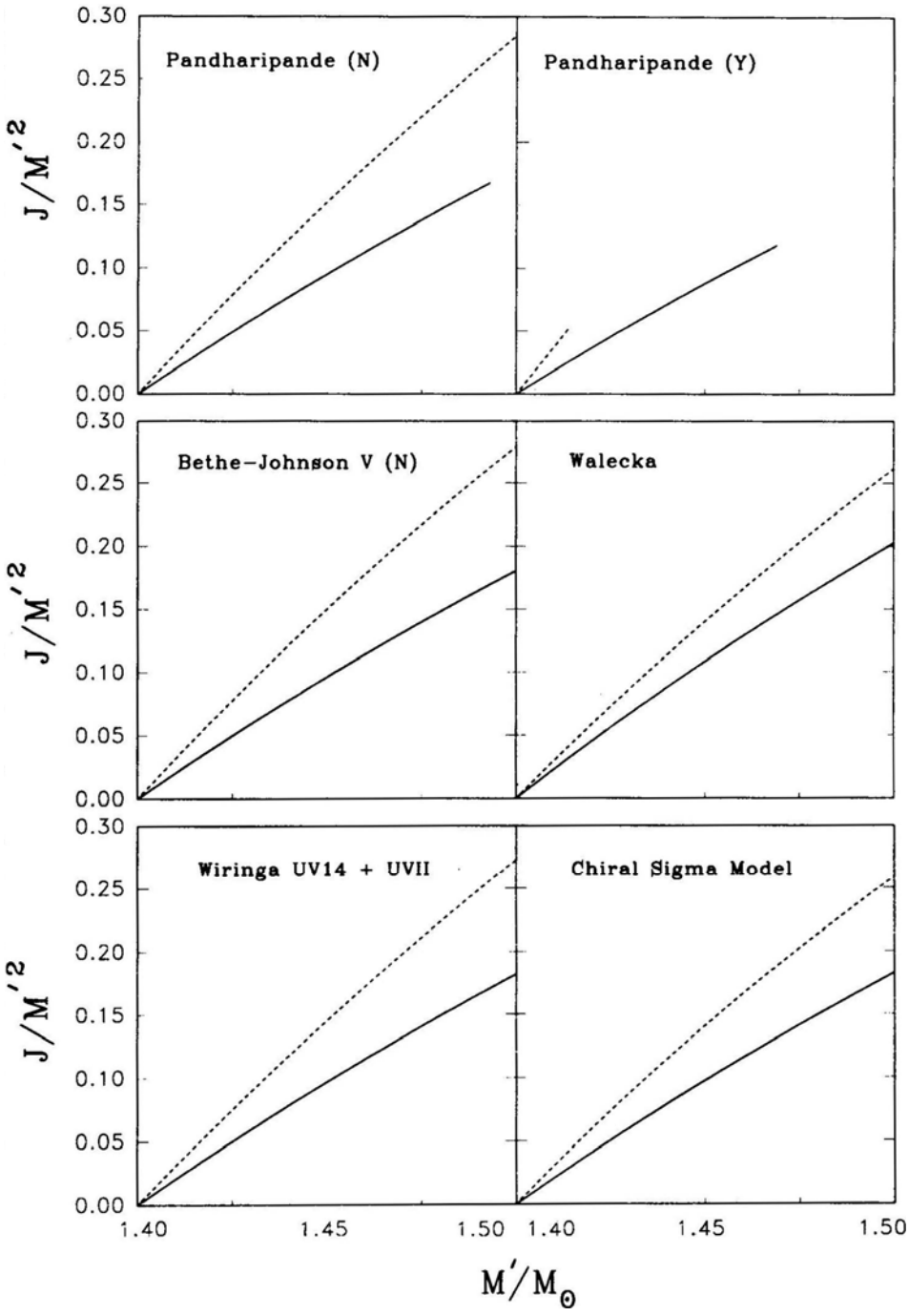

Figure 2. Evolution of the dimensionless angular momentum, $\tilde{j} = J/M^2$, of a neutron star with the accretion of mass, for six representative equations of state. The dashed curves correspond to the approach of KW, and the solid curves to our more self-consistent approach.

M' =1·4 $M_\odot$ configuration. We integrate it either until $M' = M'_{\max}$, where $M'_{\max}$ is the mass corresponding to $J_{\max}$ or until $J = J_{\max}$ (the last entry for J in Table 3) whichever comes first.

The results of our computations for the angular momentum are illustrated in Fig. 2. The x-axis corresponds to $M'/M_\odot$ and the y-axis to J/M^2. The dashed curves correspond to the angular momentum evolution computed in the fashion of KW, while the solid curves represent the results of the more self-consistent (numerical) estimates made by us as described above. The graphs indicate a slower rate of evolution of the accreting neutron star's angular momentum in the rotational case as compared to the case where rotational effects are not treated.

There are two factors contributing to the slower evolution of the angular momentum that we obtain. The less significant one is a comparatively smaller value of dM'_B/dM'. The more significant factor is that the angular momentum $\tilde{l}$ of the accreted particle is systematically less in the rotational case. Our calculations include the fact that infalling material co-rotating with the neutron star has a smaller cross-section for accretion than does counter-rotating infalling matter, so that the effective angular momentum is reduced (e.g., Misner, Thorne, & Wheeler 1974). Within the realm of overlap of our approximations, the results we find agree reasonably well with those of Cook *et al*. (1994a, b) for accretion induced changes of angular momentum.

5. Discussion

In presenting the results in the previous section, we have made the implicit assumption that the magnetic field of the neutron star is too small to affect accretion. Clearly, a quantitative estimate of this limit is in order. The Alfvén radius (r_A), is defined by the relationship (see Lamb, Pethick & Pines 1973)

$$\frac{B^2(r_A)}{8\pi} = \rho(r_A)\, v^2(r_A), \tag{39}$$

where ρ and v are respectively the density and radial velocity in the accretion disk, determines the location at which magnetic pressure channels the flow from a disk into an accretion column structure above the magnetic poles. Lamb, Pethick & Pines (1973) show that

$$r_A \lesssim 2{\cdot}6 \times 10^8 \left[\frac{\mu_{30}^{4/7}\, (M/M_\odot)^{1/7}}{L_{37}^{2/7}\, R_6^{2/7}} \right] \text{cm}, \tag{40}$$

where $\mu_{30} = B_0\, R^3/10^{30}$ G cm^3, L_{37} is the total luminosity in units of 10^{37} ergs $^{-1}$, $R_6 = R/10^6$ cm and B_0 is the magnetic field on the surface of the neutron star in gauss. The condition that $r_A < R$ implies that (taking M =1·4 $M_\odot$ and $R_6 = 1$):

$$B_0 < 5{\cdot}5 \times 10^7\ L_{37}^{1/2}\ , \tag{41}$$

and is necessary for the scenario we have discussed to be fully self-consistent, but fields somewhat higher than this value will not greatly modify our conclusions.

In our notation, $L = (E'_D + E'_s)\, Mc^2$, with M the accretion rate. According to our calculations, typical values for $(E'_D + E'_s)$ are of the order of 0·2.Theluminosity $L_{37} = 1$

would then correspond to an accretion rate $\sim 5{\cdot}6 \times 10^{16}$ gs^{-1}. Such accretion rates are close to the ones estimated in X-ray binaries (Ghosh & Lamb 1991), so that our computations are relevant for systems with significant accretion on to old neutron stars whose surface magnetic fields have undergone substantial decay (to about 10^8 *G*).

Under these circumstances of weak neutron star magnetic fields, we have shown that an incorporation of rotational effects always increases the disk luminosity, usually decreases the boundary layer luminosity, and always reduces the rate at which the neutron star's angular momentum rises with accreted mass. These effects are large enough to merit their consideration in analyses of observations of low-mass X-ray binaries.

Acknowledgement

The authors thank Professor Ramesh Narayan for pointing out the role of spin-up energy correction in calculating the boundary layer luminosity. P. J. W. thanks the Director, Indian Institute of Astrophysics, for the hospitality extended to him. P. J. W.'s research in India is supported by the Smithsonian Institution through grant FR 10263600. This work was supported in part by NSF grant AST 91-02106 and by the Chancellor's Initiative Fund at Georgia State University. B. D. thanks the Director, Raman Research Institute for the kind hospitality.

References

Alpar M. A., Cheng, A. F., Ruderman, M. A., Shaham, J. 1982, *Nature*, **300** 728.
Arnett, W. D., Bowers, R. L. 1977, *Astrophys. J.Suppl*, **33,** 415.
Baym, G., Pethick, C. J., Sutherland, P. G. 1971, *Astrophys. J.*, **170,** 299.
Bethe, H. A., Johnson, M. B. 1974, *Nucl. Phys.* **A230,** 1.
Bhattacharya, D., van den Heuvel, E. P. J. 1991, *Phys. Rep*., **203** 1.
Chandrasekhar, S.1969, *Ellipsoidal Figures of Equilibrium* (New Haven: Yale University Press).
Cook, G. B., Shapiro, S. L., Teukolsky, S. A. 1994a, *Astrophys. J*., **423,** L117.
Cook, G. B., Shapiro, S. L., Teukolsky, S. A. 1994b, *Astrophys. J*., **424,** 823.
Datta, B., Ray, A. 1983, *Mon. Not. R. astr. Soc.*, **204,** 75.
Datta, B.1988, *Fund. Cosmic Phys*., **12,** 151.
Datta, B., Thampan, A. V., Bhattacharya, D. 1995, *J.Astrophys. Astr*., **16,** 375.
Feynman, R. P., Metropolis, N., Teller, E., 1949, *Phys. Rev*., **75,** 1561.
Ghosh, P., Lamb, F. K., Pethick, C. J. 1977, *Astrophys. J*., **217,** 578.
Ghosh, P., Lamb, F. K. 1991 in *Neutron Stars: Theory and Observations*, eds. J. Ventura & D. Pines, (Dordrecht: Kluwer Acad. Publ.) p. 363.
Hartle, J. B., Thorne, K. S. 1968, *Astrophys. J*., **153,** 807 (HT).
Kley, W.1991, *Astr. Astrophys*., **247,** 95.
Kluzniak, W, Wagoner, R. V. 1985, *Astrophys. J*., **297,** 548 (KW).
Kluzniak, W. 1987, *Ph. D. Thesis*, Stanford Univ.
Lamb, F. K., Pethick, C. J., Pines, D. 1973, *Astrophys. J*., **184,** 271.
Misner, C. W., Thorne, K. S., Wheeler, J. A. 1974, *Gravitation* (San Francisco: Freeman).
Negele, J. W., Vautherin, D. 1973, *Nucl. Phys*., **A207,** 298.
Paczyński, B. 1987, *Nature*, **327** 303.
Pandharipande, V.R.1971a, *Nucl, Phys*., **A174,** 641.
Pandharipande, V.R.1971b, *Nucl. Phys*., **A178,** 123.
Papaloizou, J. C. B., Stanley, G. Q. G. 1986, *Mon. Not. R.astr. Soc*., **220,** 593.
Popham, R., Narayan, R. 1995, *Astrophys. J*., **442,** 337.

Priedhorsky, W. 1986, *Astrophys. J*., **306,** L97.
Radhakrishnan, V., Srinivasan, G. 1982, *Current Sci*., **51,** 1096.
Sahu, P. K., Basu, R., Datta, B. 1993, *Astrophys. J* **416,** 267.
Syunyaev, R. A., Shakura, N. I. 1986, *Sov. Astr. Lett*., **12,** 117 (SS).
van Paradijs, J. 1991 in *Neutron Stars: Theory and Observations*, Eds.J.Ventura & D. pines, (Dordrecht :Kluwer Acad.Publ.),p.245.
Walecka, J. D. 1974, *Ann. Phys*., **83,** 491.
Wiringa, R. B., Fiks, V., Fabrocini, A. 1988, *Phys. Rev. C*, **38,** 1010.

J. Astrophys. Astr. (1995) **16,** 375–391

A Numerical Survey of Neutron Star Crustal Density Profiles

B. Datta[1,3], A. V. Thampan[1] & D. Bhattacharya[2]
[1]*Indian Institute of Astrophysics, Bangalore 560034, India.*
[2]*Raman Research Institute, Bangalore 560 080 India.*
[3]*Visiting Professor: Raman Research Institute, Bangalore 560 080 India.*

Received 1995 June 17; accepted 1995 August 14

Abstract. An accurate numerical survey of the density profiles corresponding to the crusts of neutron stars for representative equation of state models is presented. This will find application in calculations of thermal and magnetic evolution of neutron stars.

Key words: Stars: neutron—crusts: neutron star.

1. Introduction

The crust of a neutron star refers to a region, near the surface, that is composed of mainly neutron-rich bare nuclei which interact electrostatically and are arranged in a lattice. The outer crust has small admixtures of free electrons and the inner crust has, in addition to electrons, 'drip' neutrons populating continuum states and permeating the nuclear lattice space. With increasing depth from the surface, and hence with increasing density, the neutron-to-proton ratio of the nuclei increases till a point is reached where the nuclei 'dissolve' and the composition is largely a homogeneous sea of neutrons. This point is characterized as the crust bottom. Although the crusts comprise a relatively small fraction of the total radius of the neutron star (usually about 10%), their importance derives from the fact that these possess interesting transport properties, and are believed to play a central role in a variety of directly and indirectly observable properties of neutron stars. The former include glitches, X-ray emission, and the latter concern the evolution of neutron star magnetic fields (and hence the evolution of pulsars) and possible changes in the neutron star structure and composition due to long-term accretion from a binary companion star. In order to understand all these and related phenomena quantitatively, it is imperative to have accurate knowledge of the radial distribution of the density in the crust.

Calculations suggest that neutron stars possess a more or less flat density profile from the centre to the crust bottom (Arnett & Bowers 1977; Datta 1988), and that the crust contains negligible mass in comparison to the mass in the rest of the star. The crust bottom (which is the boundary layer between the inner crust and the interior region) according to realistic calculations, is roughly equal to the equilibrium nuclear matter density, $\simeq 2.4 \times 10^{14}$ g cm^{-3}. This is about an order of magnitude less than the central densities obtained in neutron stars. Across, the crust, however, the density drop is extremely sharp – about fourteen orders of magnitude. Clearly, an accurate knowledge of the crustal density profile needs an accurate numerical treatment while integrating the equilibrium structure equations in this region of extremely rapid density

variation. The equation of state (EOS) of neutron star matter is the key input parameter in all these calculations, the crustal properties depending sensitively on which particular EOS model is adopted to describe the neutron star interior. In general, the stiffer the EOS, the more the extent of the crust. In this paper, we present a numerical survey of crustal density profiles for several neutron star configurations, and for a representative choice of the EOS models.

2. Equations of state

The structure of neutron star depends sensitively on the EOS at high densities. Although the main composition of degenerate matter at densities $\gtrsim 2.4 \times 10^{14}$ g cm^{-3}, that characterize neutron star interiors, is expected to be dominated by neutrons, significant admixtures of other elementary particles (such as pions, muons and hyperons) are not ruled out. A persistent problem in determining the EOS (namely, pressure as a function of density) of such high density matter is what to choose for the interaction among the various particles, for which reliable experimental information is not available. All calculations involve either extrapolations from known nuclear matter properties or field theoretical approaches. Another unresolved problem is: what many-body technique is adequate for the purpose of evaluating the higher order correlation terms for the pressure. In this paper we do not address these problems, but choose for our purpose, eight EOS models based on representative neutron star matter interaction models. A brief description of these is given below.

***A. Pandharipande (neutron matter)*:** Pandharipande (1971a) studied behaviour of dense neutron matter using a many-body theory based upon the variational approach suggested by Jastrow (1955). The two-body wave function was taken as satisfying a simplified form of the Bethe-Goldstone equation, in which, terms representing the Pauli exclusion principle were omitted but simulated by imposing a 'healing' constraint on the wave function. Instead of a state-dependent correlation function, an average was used with spin dependence. To describe the nuclear interaction, the Reid nucleon-nucleon potential was used (Reid 1968). This potential model is now considered to be inadequate as it does not fully describe known nuclear matter properties.

***B. Pandharipande (hyperonic matter)*:** At high densities that prevail in neutron star interiors, it is possible that elementary particles heavier than neutrons, such as hyperons, may also be present. The suggestion that hyperons may be additional baryonic constituents of neutron star interiors was first made by Ambartsumyan & Saakyan (1960) based on energetic arguments. Although our knowledge of hyperonic interactions is meagre (primarily because of Jack of experimental data), there have been several theoretical attempts aimed at deriving the EOS of baryonic liquid made up of neutrons, protons, hyperons (Λ, $\Sigma^{\pm 0}$). One of the early such attempts is due to Pandharipande (1971b), who assumed the hyperonic potentials to be similar to the nucleon-nucleon potentials, but altered suitably to represent the different isospin states. The many-body method adopted to derive the EOS was similar as in the case A. Several EOS models of hyperonic matter have since been proposed by different authors. However, this still remains an open problem because our knowledge of hyperon-nucleon and hyperon-hyperon interactions and their coupling constants have large uncertainties.

***C. Bethe-Johnson*:** Bethe & Johnson (1974) devised phenomenological potentials for nucleon-nucleon interaction that have more realistic short-range behaviour than the Reid potentials. These authors then used the lowest order constrained variational method as given by Pandharipande (1971a) to calculate the EOS of neutron star matter. The work of Bethe & Johnson (1974) consists of two different parts: (1) determination of the EOS for a pure neutron gas and (2) derivation of a hyperonic equation of state. For purpose of illustration here, we have chosen their EOS model V (neutron matter).

***D. Walecka*:** The exchange of vector and scalar mesons among nucleons is known to provide the short-range repulsion and intermediate-range attraction in the nucleon-nucleon potential. The effective interaction will be characterized by the meson parameters, such as their masses and coupling constants. If these parameters are specified, the meson wave functions can be easily solved as a function of density (assuming the wave functions to be space-time independent). From this, one can evaluate the stress tensor, which then provides the EOS. Walecka (1974) chose the meson parameters so as to reproduce the binding energy of nuclear matter (assumed to be – 15.75 MeV/nucleon) at a saturation density of 0.193 nucleons fm^{-3}. More recent analysis of experimental data suggests the nuclear matter binding energy to be – 16.3 MeV/nucleon and a saturation density of 0.153 nucleons fm^{-3} (Möller *et al.* 1988). The EOS model of Walecka corresponds to pure neutron matter. Both the scalar and vector mesons are assumed to have zero isospin by Walecka, so the model does not give the right asymmetry energy for nuclear matter.

***E. Friedman-Pandharipande (neutrons)*:** This model (Friedman & Pandharipande 1981), is also based on the lowest order constrained variational method. However, instead of the Reid potentials, the authors have made use of an improved phenomenological nucleon-nucleon potential containing a two-body part as well as three-body correlations. This interaction fits the nucleon-nucleon scattering cross-section data, deuteron properties, and also the nuclear matter properties rather well.

***F. Wiringa, Fiks & Fabrocini (1988)*:** These authors gave a model of EOS for dense nuclear and neutron matter which includes three-nucleon interactions. This is a non-relativistic approach based on the variational method. The three-body potential considered by the authors includes long-range repulsive parts that are adjusted to give light nuclei binding energies and nuclear matter saturation properties. This work represents an improvement over the calculation of Friedman & Pandharipande (1981) regarding the long-range attraction term in the Hamiltonian. The authors have given three models. We consider here their model for beta stable case: UV14 + UVII (neutrons, protons, electrons and muons).

G. Prakash, Ainsworth & Lattimer (1988) proposed EOS models for neutron stars, based on an extrapolation of the energy per particle of symmetric nuclear matter. The approach is empirical, and involves several parameters. The total energies are obtained by inclusion of the nucleon kinetic energy and the effect of finite forces between nucleons. Four models have been suggested by the authors; we use model 1 for our purpose.

H. Sahu, Basu & Datta (1993) gave a field theoretical EOS for neutron-rich matter in beta equilibrium based on the chiral sigma model. The model includes an isoscalar vector

field generated dynamically and reproduces the empirical values of the nuclear matter saturation density and binding energy and also the isospin symmetry coefficient for asymmetric nuclear matter. The energy per nucleon of nuclear matter according to Sahu, Basu & Datta (1993) is in very good agreement, up to about four times the equilibrium nuclear matter density, with estimates inferred from heavy-ion collision experimental data.

Models A, B and G are relatively soft EOS, models E, C and F are roughly intermediate in their stiffness whereas models D and H are very stiff EOS. The composite EOS for the entire span of neutron star densities was constructed by joining the selected high density EOS to that of Negele & Vautherin (1973) for the density range ($10^{14} - 5 \times 10^{10}$) g cm^{-3}, Baym, Pethick & Sutherland (1971) for densities down to $\sim 10^3$ g cm^{-3} and Feynman, Metropolis & Teller(1949) for densities less than 10^3 g cm^{-3}.

3. Calculations

The Tolman-Oppenheimer-Volkoff (Oppenheimer & Volkoff 1939) equations that must be integrated numerically to obtain stable, non-rotating neutron star structure are:

$$\frac{\mathrm{d}m}{\mathrm{d}r} = 4\pi r^2 \rho \tag{1}$$

$$\frac{\mathrm{d}p}{\mathrm{d}r} = -\frac{G(m + 4\pi r^3 P/c^2)(\rho + P/c^2)}{r(r - 2Gm/c^2)}, \tag{2}$$

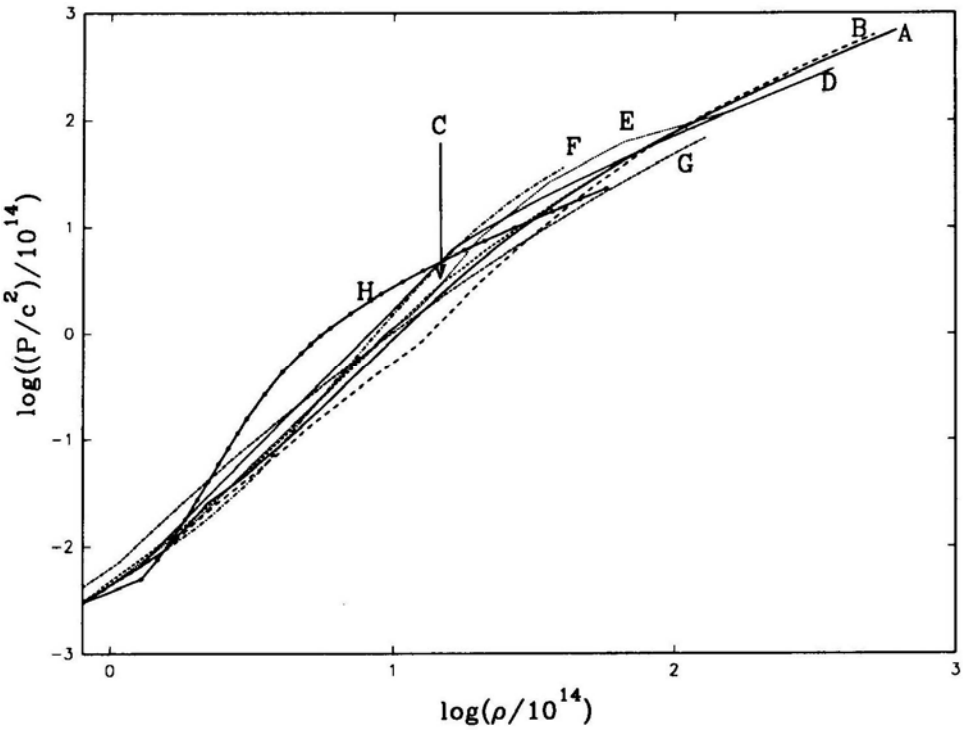

Figure 1. Pressure as a function of density for the EOS models (A–H).

Table 1. Neutron star structure parameters for the EOS Models (A–H).

EOS	$M/M_\odot$	R (km)	ρ_c (g cm^{-3})	Δ (km)	M_{cr}/M
Pandharipande	1.330	10.006	$1.669E+15$	0.963	$3.024E-02$
(neutrons)	1.400	09.867	$1.830E+15$	0.858	$2.537E-02$
	1.658	08.492	$4.100E+15$	0.404	$8.031E-03$
Pandharipande	1.330	07.921	$3.606E+15$	0.484	$9.189E-03$
(hyperons)	1.400	07.437	$4.795E+15$	0.361	$5.863E-03$
	1.414	07.082	$6.017E+15$	0.300	$4.426E-03$
Bethe-Johnson	1.330	10.782	$1.283E+15$	1.149	$3.945E-02$
Model V (neutrons)	1.400	10.691	$1.373E+15$	1.044	$3.411E-02$
	1.758	09.200	$3.466E+15$	0.454	$9.565E-03$
Walecka	1.330	12.252	$7.158E+14$	1.442	$5.482E-02$
	1.400	12.280	$7.415E+14$	1.387	$5.415E-02$
	2.285	11.216	$2.174E+15$	0.452	$1.040E-02$
Friedman-Pandharipande	1.330	10.824	1.332E+15	1.134	3.859E-02
(neutrons)	1.400	10.701	1.413E+15	1.023	3.297E-02
	1.986	09.028	3.450E+15	0.307	5.531E-03
Wiringa *et al.*	1.330	11.122	$1.000E+15$	1.120	$3.543E-02$
(UV14 + UVII)	1.400	11.115	$1.043E+15$	1.039	$3.167E-02$
	2.189	09.800	$2.830E+15$	0.294	$4.946E-03$
Prakash, Ainsworth	1.330	11.384	$1.507E+15$	1.702	$7.376E-02$
& Lattimer Model 1	1.400	10.987	$1.808E+15$	1.456	$5.781E-02$
	1.510	09.483	$3.590E+15$	0.901	$2.744E-02$
Sahu, Basu	1.330	14.685	$3.952E+14$	3.128	$2.518E-01$
& Datta	1.400	14.761	$4.063E+14$	2.970	$2.342E-01$
	2.593	14.096	$1.345E+15$	0.975	$4.588E-02$

NOTE: In Tables 1–9, the numbers following the letter E represent powers of ten.

where P and ρ stand for pressure and density and m is the gravitational mass contained within a sphere of radius r. The integration of equations (1) and (2) is done for a given EOS which specifies $P(\rho)$, and with initial condition $\rho = \rho_c$, a chosen value for the central density. The numerical integration started from the centre of the star is terminated at the radius of the star, defined as the point where the density $\lesssim 7.86$ g cm^{-3}, expected to correspond to the neutron star surface. The total gravitational mass is then given by $M = m(R)$.

We integrate equations (1) and (2) simultaneously using Runge-Kutta fourth order method, having an adaptive step size control. The step size is adjusted for the required accuracy from a calculation of the local truncation error (Antia 1991). We find that this provides an extremely accurate method to integrate equations (1) and (2) for neutron

Table 2. Crustal density profiles: Pandharipande (neutrons).

$M = 1.330\ M_\odot$ $R = 10.006$ (km)		$M = 1.400\ M_\odot$ $R = 9.867$ (km)		$M = 1.658\ M_\odot$ $R = 8.492$ (km)	
$(1 - r/R)$	ρ (g cm^{-3})	$(1 - r/R)$	ρ (g cm^{-3})	$(1 - r/R)$	ρ (g cm^{-3})
$0.00000E+00$	$7.866E+00$	$0.00000E+00$	$7.863E+00$	$0.00000E+00$	$7.866E+00$
$1.13773E-09$	$1.319E+01$	$1.28891E-09$	$1.360E+01$	$9.91795E-10$	$1.447E+01$
$2.39423E-08$	$4.972E+01$	$2.23090E-08$	$5.120E+01$	$1.27579E-08$	$5.428E+01$
$1.41172E-07$	$1.874E+02$	$1.31095E-07$	$1.927E+02$	$7.44405E-08$	$2.037E+02$
$6.75515E-07$	$7.066E+02$	$6.21865E-07$	$7.252E+02$	$3.46816E-07$	$7.642E+02$
$2.35836E-06$	$2.664E+03$	$2.17080E-06$	$2.730E+03$	$1.19743E-06$	$2.867E+03$
$6.95373E-06$	$1.004E+04$	$6.34094E-06$	$1.027E+04$	$3.47397E-06$	$1.076E+04$
$1.94642E-05$	$3.786E+04$	$1.77038E-05$	$3.866E+04$	$9.73952E-06$	$4.037E+04$
$5.14517E-05$	$1.427E+05$	$4.67151E-05$	$1.455E+05$	$2.53765E-05$	$1.515E+05$
$1.26075E-04$	$5.382E+05$	$1.14160E-04$	$5.477E+05$	$6.23815E-05$	$5.683E+05$
$2.88548E-04$	$2.029E+06$	$2.60880E-04$	$2.061E+06$	$1.40445E-04$	$2.132E+06$
$6.06912E-04$	$7.649E+06$	$5.47153E-04$	$7.758E+06$	$2.93273E-04$	$8.001E+06$
$1.14403E-03$	$2.884E+07$	$1.03012E-03$	$2.920E+07$	$5.56213E-04$	$3.002E+07$
$2.05310E-03$	$1.087E+08$	$1.84738E-03$	$1.099E+08$	$9.86545E-04$	$1.126E+08$
$3.46132E-03$	$4.099E+08$	$3.11233E-03$	$4.136E+08$	$1.65994E-03$	$4.226E+08$
$5.44170E-03$	$1.545E+09$	$4.89128E-03$	$1.557E+09$	$2.61038E-03$	$1.586E+09$
$8.57267E-03$	$5.826E+09$	$7.70080E-03$	$5.859E+09$	$4.10792E-03$	$5.950E+09$
$1.28894E-02$	$2.196E+10$	$1.15691E-02$	$2.205E+10$	$6.20721E-03$	$2.233E+10$
$1.89605E-02$	$8.280E+10$	$1.70260E-02$	$8.299E+10$	$9.14044E-03$	$8.377E+10$
$2.54733E-02$	$3.122E+11$	$2.28786E-02$	$3.124E+11$	$1.22832E-02$	$3.143E+11$
$3.04385E-02$	$1.177E+12$	$2.73482E-02$	$1.176E+12$	$1.47004E-02$	$1.179E+12$
$3.39494E-02$	$4.437E+12$	$3.05103E-02$	$4.425E+12$	$1.64164E-02$	$4.425E+12$
$4.02999E-02$	$1.673E+13$	$3.62239E-02$	$1.665E+13$	$1.94675E-02$	$1.660E+13$
$5.34854E-02$	$6.306E+13$	$4.81026E-02$	$6.268E+13$	$2.59768E-02$	$6.230E+13$
$9.62614E-02$	$2.400E+14$	$8.69610E-02$	$2.400E+14$	$4.75309E-02$	$2.400E+14$

Note: In the crustal density profiles presented here and in the subsequent tables, the third mass column corresponds to that of the maximum stable mass.

star configurations varying widely in their density profiles. The method, of course, gives bulk properties such as masses, radii and moments of inertia that agree with the values already reported in the literature.

Table 3. Crustal density profiles: Pandharipande (hyperons).

$M = 1.330\ M_\odot$ $R = 7.921$ (km)		$M = 1.400\ M_\odot$ $R = 7.437$ (km)		$M = 1.658\ M_\odot$ $R = 7.082$ (km)	
$(1 - r/R)$	ρ (g cm^{-3})	$(1 - r/R)$	ρ (g cm^{-3})	$(1 - r/R)$	ρ (g cm^{-3})
$0.00000E+00$	$7.869E+00$	$0.00000E+00$	$7.873E+00$	$0.00000E+00$	$7.872E+00$
$1.07340E-09$	$1.386E+01$	$5.54109E-10$	$1.310E+01$	$7.30479E-10$	$1.386E+01$
$1.67489E-08$	$5.212E+01$	$1.22270E-08$	$4.937E+01$	$1.14305E-08$	$5.206E+01$
$9.81838E-08$	$1.959E+02$	$7.20507E-08$	$1.861E+02$	$6.69361E-08$	$1.956E+02$
$4.63059E-07$	$7.366E+02$	$3.44856E-07$	$7.013E+02$	$3.15345E-07$	$7.349E+02$
$1.61124E-06$	$2.769E+03$	$1.21581E-06$	$2.643E+03$	$1.09890E-06$	$2.761E+03$
$4.69519E-06$	$1.041E+04$	$3.55792E-06$	$9.961E+03$	$3.19785E-06$	$1.037E+04$
$1.31881E-05$	$3.914E+04$	$1.00363E-05$	$3.754E+04$	$8.98933E-06$	$3.898E+04$
$3.44931E-05$	$1.471E+05$	$2.63282E-05$	$1.415E+05$	$2.34770E-05$	$1.464E+05$
$8.49483E-05$	$5.531E+05$	$6.51209E-05$	$5.333E+05$	$5.78740E-05$	$5.502E+05$
$1.92058E-04$	$2.079E+06$	$1.47600E-04$	$2.010E+06$	$1.30595E-04$	$2.067E+06$
$4.02430E-04$	$7.817E+06$	$3.11479E-04$	$7.575E+06$	$2.74208E-04$	$7.767E+06$
$7.63318E-04$	$2.939E+07$	$5.91571E-04$	$2.855E+07$	$5.20308E-04$	$2.918E+07$
$1.35630E-03$	$1.105E+08$	$1.05199E-03$	$1.076E+08$	$9.30193E-04$	$1.096E+08$
$2.28591E-03$	$4.153E+08$	$1.77814E-03$	$4.056E+08$	$1.55724E-03$	$4.120E+08$
$3.59396E-03$	$1.561E+09$	$2.80054E-03$	$1.529E+09$	$2.45039E-03$	$1.548E+09$
$5.66066E-03$	$5.870E+09$	$4.42319E-03$	$5.761E+09$	$3.86507E-03$	$5.815E+09$
$8.55549E-03$	$2.207E+10$	$6.70178E-03$	$2.171E+10$	$5.85049E-03$	$2.185E+10$
$1.25852E-02$	$8.296E+10$	$9.87052E-03$	$8.183E+10$	$8.61429E-03$	$8.209E+10$
$1.70822E-02$	$3.119E+11$	$1.34460E-02$	$3.084E+11$	$1.17295E-02$	$3.084E+11$
$2.03323E-02$	$1.173E+12$	$1.60261E-02$	$1.162E+12$	$1.39806E-02$	$1.159E+12$
$2.26843E-02$	$4.408E+12$	$1.78947E-02$	$4.381E+12$	$1.56106E-02$	$4.354E+12$
$2.68735E-02$	$1.657E+13$	$2.12047E-02$	$1.651E+13$	$1.84789E-02$	$1.636E+13$
$3.57424E-02$	$6.230E+13$	$2.82703E-02$	$6.223E+13$	$2.46211E-02$	$6.146E+13$
$6.11192E-02$	$2.400E+14$	$4.84971E-02$	$2.400E+14$	$4.24178E-02$	$2.400E+14$

4. Results and discussions

The EOS models (A–H) are illustrated in Fig. 1 (which is a plot of pressure versus density). This plot refers to the high density region corresponding to the neutron star interior. We have already mentioned in section 2 the EOS that is used for the crustal region. It is important to note that because of substantial variation in the various EOS

models (A–H), the crustal thicknesses and density profiles are expected to exhibit variation even though the crustal EOS is assumed to be the same for all cases.

In Table 1, we have summarized the results for the mass (M), radius (R), central density (ρ_c), the crustal thickness (Δ) and the mass contained in the crust as a fraction of the total gravitational mass (M_{cr}/M). We have done this for three configurations of the

Table 4. Crustal density profiles: Bethe-Johnson Model V (neutrons).

$M = 1.330\ M_\odot$ $R = 10.782$ (km)		$M = 1.400\ M_\odot$ $R = 10.691$ (km)		$M = 1.658\ M_\odot$ $R = 9.200$ (km)	
$(1 - r/R)$	ρ (g cm^{-3})	$(1 - r/R)$	ρ (g cm^{-3})	$(1 - r/R)$	ρ (g cm^{-3})
$0.00000E+00$	$7.865E+00$	$0.00000E+00$	$7.865E+00$	$0.00000E+00$	$7.870E+00$
$9.62517E-10$	$1.274E+01$	$5.12115E-10$	$1.193E+01$	$1.18152E-09$	$1.483E+01$
$2.58471E-08$	$4.811E+01$	$2.15850E-08$	$4.517E+01$	$1.38593E-08$	$5.561E+01$
$1.52912E-07$	$1.817E+02$	$1.28431E-07$	$1.711E+02$	$8.06756E-08$	$2.084E+02$
$7.38784E-07$	$6.859E+02$	$6.31512E-07$	$6.479E+02$	$3.73427E-07$	$7.814E+02$
$2.60124E-06$	$2.590E+03$	$2.25472E-06$	$2.454E+03$	$1.28236E-06$	$2.929E+03$
$7.68367E-06$	$9.780E+03$	$6.70487E-06$	$9.292E+03$	$3.71389E-06$	$1.098E+04$
$2.15801E-05$	$3.693E+04$	$1.88968E-05$	$3.519E+04$	$1.03945E-05$	$4.116E+04$
$5.71082E-05$	$1.394E+05$	$5.02536E-05$	$1.333E+05$	$2.70460E-05$	$1.543E+05$
$1.40477E-04$	$5.265E+05$	$1.24064E-04$	$5.047E+05$	$6.63716E-05$	$5.784E+05$
$3.21795E-04$	$1.988E+06$	$2.85596E-04$	$1.911E+06$	$1.49243E-04$	$2.168E+06$
$6.78933E-04$	$7.507E+06$	$6.06957E-04$	$7.238E+06$	$3.10676E-04$	$8.129E+06$
$1.28251E-03$	$2.835E+07$	$1.14719E-03$	$2.741E+07$	$5.88968E-04$	$3.047E+07$
$2.30214E-03$	$1.070E+08$	$2.06531E-03$	$1.038E+08$	$1.04251E-03$	$1.142E+08$
$3.88311E-03$	$4.041E+08$	$3.49272E-03$	$3.931E+08$	$1.75488E-03$	$4.282E+08$
$6.10597E-03$	$1.526E+09$	$5.50294E-03$	$1.489E+09$	$2.75858E-03$	$1.605E+09$
$9.57620E-03$	$5.762E+09$	$8.64390E-03$	$5.638E+09$	$4.33485E-03$	$6.017E+09$
$1.44965E-02$	$2.176E+10$	$1.31203E-02$	$2.135E+10$	$6.54368E-03$	$2.256E+10$
$2.12980E-02$	$8.215E+10$	$1.92967E-02$	$8.086E+10$	$9.63627E-03$	$8.456E+10$
$2.81867E-02$	$3.102E+11$	$2.56295E-02$	$3.062E+11$	$1.27252E-02$	$3.170E+11$
$3.38868E-02$	$1.171E+12$	$3.08582E-02$	$1.160E+12$	$1.53170E-02$	$1.188E+12$
$3.78217E-02$	$4.423E+12$	$3.44667E-02$	$4.392E+12$	$1.71185E-02$	$4.454E+12$
$4.49199E-02$	$1.670E+13$	$4.09600E-02$	$1.663E+13$	$2.03358E-02$	$1.670E+13$
$5.92713E-02$	$6.306E+13$	$5.41059E-02$	$6.299E+13$	$2.71825E-02$	$6.259E+13$
$1.06539E-01$	$2.400E+14$	$9.76166E-02$	$2.400E+14$	$4.93717E-02$	$2.400E+14$

Table 5. Crustal density profiles: Walecka.

$M = 1.330\ M_\odot$ $R = 12.252$ (km)		$M = 1.400\ M_\odot$ $R = 12.280$ (km)		$M = 1.658\ M_\odot$ $R = 11.216$ (km)	
$(1 - r/R)$	ρ (g cm^{-3})	$(1 - r/R)$	ρ (g cm^{-3})	$(1 - r/R)$	ρ (g cm^{-3})
$0.00000E+00$	$7.861E+00$	$0.00000E+00$	$7.863E+00$	$0.00000E+00$	$7.873E+00$
$1.23191E-09$	$1.285E+01$	$8.38888E-10$	$1.236E+01$	$8.18035E-12$	$8.104E+00$
$3.16611E-08$	$4.842E+01$	$2.80625E-08$	$4.672E+01$	$5.39587E-09$	$3.119E+01$
$1.86840E-07$	$1.825E+02$	$1.66453E-07$	$1.766E+02$	$3.34822E-08$	$1.200E+02$
$9.00051E-07$	$6.877E+02$	$8.10853E-07$	$6.679E+02$	$1.81747E-07$	$4.621E+02$
$3.16390E-06$	$2.592E+03$	$2.87465E-06$	$2.525E+03$	$7.10899E-07$	$1.778E+03$
$9.32544E-06$	$9.767E+03$	$8.51191E-06$	$9.546E+03$	$2.18496E-06$	$6.845E+03$
$2.61696E-05$	$3.681E+04$	$2.39565E-05$	$3.609E+04$	$6.34256E-06$	$2.635E+04$
$6.91322E-05$	$1.387E+05$	$6.35046E-05$	$1.364E+05$	$1.71650E-05$	$1.014E+05$
$1.70007E-04$	$5.228E+05$	$1.56575E-04$	$5.158E+05$	$4.38472E-05$	$3.903E+05$
$3.88916E-04$	$1.970E+06$	$3.59261E-04$	$1.950E+06$	$1.03477E-04$	$1.502E+06$
$8.20653E-04$	$7.426E+06$	$7.60393E-04$	$7.373E+06$	$2.27039E-04$	$5.782E+06$
$1.54960E-03$	$2.799E+07$	$1.43749E-03$	$2.788E+07$	$4.36443E-04$	$2.225E+07$
$2.77895E-03$	$1.055E+08$	$2.58236E-03$	$1.054E+08$	$7.97867E-04$	$8.565E+07$
$4.68399E-03$	$3.975E+08$	$4.35895E-03$	$3.984E+08$	$1.36479E-03$	$3.297E+08$
$7.30487E-03$	$1.498E+09$	$6.83400E-03$	$1.506E+09$	$2.19964E-03$	$1.269E+09$
$1.15413E-02$	$5.646E+09$	$1.07640E-02$	$5.695E+09$	$3.46460E-03$	$4.884E+09$
$1.74576E-02$	$2.128E+10$	$1.62969E-02$	$2.153E+10$	$5.32332E-03$	$1.880E+10$
$2.55827E-02$	$8.019E+10$	$2.39257E-02$	$8.140E+10$	$7.89448E-03$	$7.235E+10$
$3.44452E-02$	$3.022E+11$	$3.21742E-02$	$3.078E+11$	$1.09013E-02$	$2.785E+11$
$4.11286E-02$	$1.139E+12$	$3.84200E-02$	$1.164E+12$	$1.31475E-02$	$1.072E+12$
$4.58221E-02$	$4.292E+12$	$4.28220E-02$	$4.399E+12$	$1.47359E-02$	$4.125E+12$
$5.41156E-02$	$1.618E+13$	$5.07298E-02$	$1.663E+13$	$1.74490E-02$	$1.588E+13$
$7.09277E-02$	$6.097E+13$	$6.67522E-02$	$6.287E+13$	$2.33665E-02$	$6.111E+13$
$1.17734E-01$	$2.400E+14$	$1.12973E-01$	$2.400E+14$	$4.03436E-02$	$2.400E+14$

gravitational mass, namely, 1.33 $M_\odot$, 1.4 $M_\odot$ and the maximum stable mass. A look at Table 1 shows that, for the EOS models considered here, the maximum neutron star mass (M) and their corresponding radii (R) lie in the range (1.414–2.593) $M_\odot$, and (7.082–14.096) km respectively, with the lower value of each of the quantities corresponding to the Pandharipande hyperonic matter EOS (a very soft one) and the higher

to the EOS due to Sahu, Basu & Datta (a very stiff EOS). The values of the crust thickness (Δ) for maximum mass configurations lie in the range (0.2940–0.975) km. Clearly, the crust thickness, and therefore the crustal density profile, depend sensitively on the EOS model chosen to describe neutron star matter. Of the three mass configurations listed in Table 1, the 1.4 $M_{\odot}$ neutron star models are of particular interest because analysis of available binary pulsar data suggests the pulsar masses in

Table 6. Crustal density profiles: Friedman-Pandharipande (neutrons).

$M = 1.330\ M_{\odot}$ $R = 10.824$ (km)		$M = 1.400\ M_{\odot}$ $R = 10.701$ (km)		$M = 1.658\ M_{\odot}$ $R = 9.028$ (km)	
$(1 - r/R)$	ρ (g cm^{-3})	$(1 - r/R)$	ρ (g cm^{-3})	$(1 - r/R)$	ρ (g cm^{-3})
$0.00000E+00$	$7.860E+00$	$0.00000E+00$	$7.863E+00$	$0.00000E+00$	$7.861E+00$
$8.52656E-10$	$1.255E+01$	$1.37922E-09$	$1.350E+01$	$1.29813E-09$	$1.673E+01$
$2.55103E-08$	$4.744E+01$	$2.53386E-08$	$5.086E+01$	$1.12913E-08$	$6.237E+01$
$1.51130E-07$	$1.793E+02$	$1.49079E-07$	$1.915E+02$	$6.47614E-08$	$2.325E+02$
$7.33104E-07$	$6.773E+02$	$7.08975E-07$	$7.213E+02$	$2.89898E-07$	$8.667E+02$
$2.58950E-06$	$2.559E+03$	$2.46504E-06$	$2.716E+03$	$9.72901E-07$	$3.231E+03$
$7.65971E-06$	$9.671E+03$	$7.24485E-06$	$1.023E+04$	$2.78838E-06$	$1.204E+04$
$2.15325E-05$	$3.654E+04$	$2.02704E-05$	$3.852E+04$	$7.74926E-06$	$4.490E+04$
$5.70408E-05$	$1.381E+05$	$5.34425E-05$	$1.451E+05$	$1.99766E-05$	$1.674E+05$
$1.40445E-04$	$5.217E+05$	$1.30935E-04$	$5.463E+05$	$4.87008E-05$	$6.239E+05$
$3.22040E-04$	$1.971E+06$	$2.98868E-04$	$2.057E+06$	$1.09401E-04$	$2.326E+06$
$6.80500E-04$	$7.449E+06$	$6.26729E-04$	$7.748E+06$	$2.23341E-04$	$8.670E+06$
$1.28579E-03$	$2.815E+07$	$1.18248E-03$	$2.918E+07$	$4.22660E-04$	$3.232E+07$
$2.30933E-03$	$1.064E+08$	$2.11855E-03$	$1.099E+08$	$7.50797E-04$	$1.205E+08$
$3.89716E-03$	$4.019E+08$	$3.56727E-03$	$4.138E+08$	$1.24788E-03$	$4.491E+08$
$6.13009E-03$	$1.519E+09$	$5.60437E-03$	$1.558E+09$	$1.95988E-03$	$1.674E+09$
$9.61827E-03$	$5.738E+09$	$8.77043E-03$	$5.869E+09$	$3.06589E-03$	$6.241E+09$
$1.45658E-02$	$2.168E+10$	$1.32620E-02$	$2.210E+10$	$4.61747E-03$	$2.326E+10$
$2.14052E-02$	$8.193E+10$	$1.94955E-02$	$8.324E+10$	$6.80311E-03$	$8.673E+10$
$2.87813E-02$	$3.096E+11$	$2.61564E-02$	$3.135E+11$	$9.09191E-03$	$3.233E+11$
$3.43830E-02$	$1.170E+12$	$3.12389E-02$	$1.180E+12$	$1.08689E-02$	$1.205E+12$
$3.83380E-02$	$4.420E+12$	$3.48329E-02$	$4.446E+12$	$1.21344E-02$	$4.492E+12$
$4.54710E-02$	$1.670E+13$	$4.13380E-02$	$1.674E+13$	$1.43877E-02$	$1.675E+13$
$5.99013E-02$	$6.311E+13$	$5.44597E-02$	$6.305E+13$	$1.92192E-02$	$6.243E+13$
$1.04735E-01$	$2.400E+14$	$9.55692E-02$	$2.400E+14$	$3.40162E-02$	$2.400E+14$

Table 7. Crustal density profiles: Wiringa *et al*. (UV14 + UVII).

$M = 1.330\ M_\odot$ $R = 11.122$ (km)		$M = 1.400\ M_\odot$ $R = 11.115$ (km)		$M = 1.658\ M_\odot$ $R = 9.800$ (km)	
$(1 - r/R)$	ρ (g cm^{-3})	$(1 - r/R)$	ρ (g cm^{-3})	$(1 - r/R)$	ρ (g cm^{-3})
$0.00000E+00$	$7.865E+00$	$0.00000E+00$	$7.863E+00$	$0.00000E+00$	$7.862E+00$
$4.79318E-10$	$9.545E+00$	$3.12246E-11$	$8.123E+00$	$1.33983E-09$	$1.684E+01$
$1.84269E-08$	$3.649E+01$	$1.35178E-08$	$3.127E+01$	$1.10568E-08$	$6.274E+01$
$1.14890E-07$	$1.395E+02$	$8.71834E-08$	$1.204E+02$	$6.25945E-08$	$2.338E+02$
$5.88007E-07$	$5.332E+02$	$4.62922E-07$	$4.636E+02$	$2.78294E-07$	$8.710E+02$
$2.21576E-06$	$2.038E+03$	$1.81126E-06$	$1.785E+03$	$9.35252E-07$	$3.246E+03$
$6.74056E-06$	$7.792E+03$	$5.62199E-06$	$6.872E+03$	$2.67672E-06$	$1.209E+04$
$1.92271E-05$	$2.979E+04$	$1.61628E-05$	$2.646E+04$	$7.43546E-06$	$4.506E+04$
$5.19015E-05$	$1.139E+05$	$4.41569E-05$	$1.019E+05$	$1.91534E-05$	$1.679E+05$
$1.29966E-04$	$4.353E+05$	$1.11643E-04$	$3.922E+05$	$4.66804E-05$	$6.256E+05$
$3.03771E-04$	$1.664E+06$	$2.64122E-04$	$1.510E+06$	$1.04872E-04$	$2.331E+06$
$6.60309E-04$	$6.361E+06$	$5.82289E-04$	$5.813E+06$	$2.13857E-04$	$8.686E+06$
$1.25384E-03$	$2.432E+07$	$1.11103E-03$	$2.238E+07$	$4.04672E-04$	$3.236E+07$
$2.27729E-03$	$9.295E+07$	$2.03311E-03$	$8.617E+07$	$7.18723E-04$	$1.206E+08$
$3.88460E-03$	$3.553E+08$	$3.49593E-03$	$3.318E+08$	$1.20173E-03$	$4.493E+08$
$6.17831E-03$	$1.358E+09$	$5.61392E-03$	$1.277E+09$	$1.87529E-03$	$1.674E+09$
$9.70251E-03$	$5.193E+09$	$8.77612E-03$	$4.918E+09$	$2.93350E-03$	$6.238E+09$
$1.48127E-02$	$1.985E+10$	$1.34625E-02$	$1.893E+10$	$4.41814E-03$	$2.324E+10$
$2.18186E-02$	$7.588E+10$	$1.99008E-02$	$7.290E+10$	$6.50913E-03$	$8.661E+10$
$2.97300E-02$	$2.901E+11$	$2.73359E-02$	$2.807E+11$	$8.70128E-03$	$3.227E+11$
$3.56409E-02$	$1.109E+12$	$3.28536E-02$	$1.081E+12$	$1.04031E-02$	$1.203E+12$
$3.97973E-02$	$4.239E+12$	$3.67344E-02$	$4.160E+12$	$1.16147E-02$	$4.481E+12$
$4.71200E-02$	$1.620E+13$	$4.35051E-02$	$1.602E+13$	$1.37662E-02$	$1.670E+13$
$6.18097E-02$	$6.195E+13$	$5.71556E-02$	$6.167E+13$	$1.83039E-02$	$6.221E+13$
$1.00741E-01$	$2.400E+14$	$9.34953E-02$	$2.400E+14$	$2.99743E-02$	$2.400E+14$

these binaries to be close to this value. For the 1.4 $M_\odot$ models, the Δ is in the range (0.361–2.970) km, a much wider range than for the maximum mass cases. In Tables 2–9, we give the crustal density variation with the depth in normalized units with respect to the radius $(1 - r/R)$, (where r is the radial distance from the centre of the star) from the surface of the neutron star for the three mass configurations. These tables will be of direct application in calculations of magnetic field evolution of pulsars. The same thing,

namely, the crustal density variations, is graphically illustrated in Figs. 2 and 3 for 1.4 $M_{\odot}$ configurations for the various EOS models. The dashed lines in these figures represent the core-inner crust boundary (which corresponds to $r = R - \Delta$) and the dot-cum-dashed lines represent the surface of the neutron star ($r = R$). The variation is sharpest for the softest EOS considered here (Pandharipande hyperonic matter) and gets to be comparatively less sharp as the EOS gets to be more stiff. The dependences on

Table 8. Crustal density profiles: Prakash, Ainsworth & Lattimer Model 1.

$M = 1.330\ M_{\odot}$ $R = 11.384$ (km)		$M = 1.400\ M_{\odot}$ $R = 10.987$ (km)		$M = 1.658\ M_{\odot}$ $R = 9.483$ (km)	
$(1 - r/R)$	ρ (g cm^{-3})	$(1 - r/R)$	ρ (g cm^{-3})	$(1 - r/R)$	ρ (g cm^{-3})
$0.00000E+00$	$7.864E+00$	$0.00000E+00$	$7.861E+00$	$0.00000E+00$	$7.868E+00$
$1.23204E-09$	$1.299E+01$	$5.64384E-10$	$1.202E+01$	$7.20466E-10$	$1.297E+01$
$2.87558E-08$	$4.893E+01$	$2.26968E-08$	$4.539E+01$	$1.70600E-08$	$4.893E+01$
$1.69510E-07$	$1.843E+02$	$1.34550E-07$	$1.714E+02$	$1.00739E-07$	$1.846E+02$
$8.13995E-07$	$6.945E+02$	$6.59261E-07$	$6.476E+02$	$4.84015E-07$	$6.966E+02$
$2.85212E-06$	$2.616E+03$	$2.34711E-06$	$2.446E+03$	$1.70821E-06$	$2.628E+03$
$8.40799E-06$	$9.857E+03$	$6.97231E-06$	$9.238E+03$	$5.00958E-06$	$9.917E+03$
$2.35563E-05$	$3.713E+04$	$1.95999E-05$	$3.489E+04$	$1.41327E-05$	$3.742E+04$
$6.22494E-05$	$1.399E+05$	$5.20863E-05$	$1.318E+05$	$3.71474E-05$	$1.412E+05$
$1.52771E-04$	$5.270E+05$	$1.28304E-04$	$4.978E+05$	$9.18752E-05$	$5.327E+05$
$3.49639E-04$	$1.986E+06$	$2.95396E-04$	$1.880E+06$	$2.08710E-04$	$2.010E+06$
$7.37203E-04$	$7.480E+06$	$6.28698E-04$	$7.102E+06$	$4.40124E-04$	$7.585E+06$
$1.39012E-03$	$2.818E+07$	$1.18548E-03$	$2.683E+07$	$8.35840E-04$	$2.862E+07$
$2.49418E-03$	$1.062E+08$	$2.13488E-03$	$1.013E+08$	$1.48947E-03$	$1.080E+08$
$4.20487E-03$	$4.000E+08$	$3.61133E-03$	$3.827E+08$	$2.51514E-03$	$4.074E+08$
$6.60710E-03$	$1.507E+09$	$5.69228E-03$	$1.446E+09$	$3.95905E-03$	$1.537E+09$
$1.04093E-02$	$5.677E+09$	$8.98241E-03$	$5.460E+09$	$6.24693E-03$	$5.801E+09$
$1.56800E-02$	$2.139E+10$	$1.35685E-02$	$2.062E+10$	$9.43094E-03$	$2.189E+10$
$2.29656E-02$	$8.057E+10$	$1.99082E-02$	$7.790E+10$	$1.38631E-02$	$8.258E+10$
$3.27849E-02$	$3.036E+11$	$2.85376E-02$	$2.942E+11$	$1.98362E-02$	$3.116E+11$
$3.71907E-02$	$1.144E+12$	$3.26160E-02$	$1.111E+12$	$2.24955E-02$	$1.176E+12$
$4.15513E-02$	$4.308E+12$	$3.63684E-02$	$4.198E+12$	$2.51423E-02$	$4.436E+12$
$4.96169E-02$	$1.623E+13$	$4.34154E-02$	$1.586E+13$	$3.01974E-02$	$1.674E+13$
$6.63662E-02$	$6.115E+13$	$5.79696E-02$	$5.989E+13$	$4.11830E-02$	$6.316E+13$
$1.49536E-01$	$2.400E+14$	$1.32527E-01$	$2.400E+14$	$9.50182E-02$	$2.400E+14$

Table 9. Crustal density profiles: Sahu, Basu & Datta.

$M = 1.330\ M_\odot$ $R = 14.685$ (km)		$M = 1.400\ M_\odot$ $R = 14.761$ (km)		$M = 1.658\ M_\odot$ $R = 14.096$ (km)	
$(1 - r/R)$	ρ (g cm^{-3})	$(1 - r/R)$	ρ (g cm^{-3})	$(1 - r/R)$	ρ (g cm^{-3})
$0.00000E+00$	$7.861E+00$	$0.00000E+00$	$7.861E+00$	$0.00000E+00$	$7.863E+00$
$1.68177E-10$	$8.839E+00$	$6.18207E-10$	$1.139E+01$	$1.28531E-09$	$1.483E+01$
$2.51686E-08$	$3.391E+01$	$3.29844E-08$	$4.323E+01$	$1.50712E-08$	$5.553E+01$
$1.54202E-07$	$1.301E+02$	$1.96946E-07$	$1.640E+02$	$8.76310E-08$	$2.080E+02$
$8.19531E-07$	$4.990E+02$	$9.80469E-07$	$6.220E+02$	$4.05511E-07$	$7.789E+02$
$3.13725E-06$	$1.914E+03$	$3.54032E-06$	$2.360E+03$	$1.39181E-06$	$2.917E+03$
$9.61781E-06$	$7.344E+03$	$1.05575E-05$	$8.951E+03$	$4.02961E-06$	$1.092E+04$
$2.75907E-05$	$2.817E+04$	$2.98693E-05$	$3.396E+04$	$1.12695E-05$	$4.091E+04$
$7.48055E-05$	$1.081E+05$	$7.95623E-05$	$1.288E+05$	$2.93190E-05$	$1.532E+05$
$1.88519E-04$	$4.146E+05$	$1.97315E-04$	$4.886E+05$	$7.19116E-05$	$5.737E+05$
$4.42469E-04$	$1.591E+06$	$4.54910E-04$	$1.854E+06$	$1.61745E-04$	$2.149E+06$
$9.61559E-04$	$6.102E+06$	$9.64816E-04$	$7.032E+06$	$3.36900E-04$	$8.046E+06$
$1.84383E-03$	$2.341E+07$	$1.83881E-03$	$2.667E+07$	$6.38253E-04$	$3.013E+07$
$3.35559E-03$	$8.979E+07$	$3.31124E-03$	$1.012E+08$	$1.13022E-03$	$1.128E+08$
$5.73697E-03$	$3.445E+08$	$5.60155E-03$	$3.839E+08$	$1.90195E-03$	$4.226E+08$
$9.15009E-03$	$1.321E+09$	$8.77845E-03$	$1.456E+09$	$2.98755E-03$	$1.583E+09$
$1.43445E-02$	$5.069E+09$	$1.38724E-02$	$5.524E+09$	$4.69758E-03$	$5.927E+09$
$2.18743E-02$	$1.945E+10$	$2.10140E-02$	$2.095E+10$	$7.09328E-03$	$2.220E+10$
$3.21388E-02$	$7.460E+10$	$3.07877E-02$	$7.949E+10$	$1.04322E-02$	$8.313E+10$
$4.41761E-02$	$2.862E+11$	$4.18584E-02$	$3.015E+11$	$1.41597E-02$	$3.113E+11$
$5.25674E-02$	$1.098E+12$	$4.96901E-02$	$1.144E+12$	$1.68582E-02$	$1.166E+12$
$5.85730E-02$	$4.212E+12$	$5.53066E-02$	$4.339E+12$	$1.88106E-02$	$4.366E+12$
$6.90648E-02$	$1.616E+13$	$6.52886E-02$	$1.646E+13$	$2.22586E-02$	$1.635E+13$
$9.05533E-02$	$6.198E+13$	$8.55960E-02$	$6.245E+13$	$2.95893E-02$	$6.123E+13$
$2.13000E-01$	$2.400E+14$	$2.01202E-01$	$2.400E+14$	$6.91727E-02$	$2.400E+14$

neutron star mass of the radius and of the crustal thickness respectively are illustrated in Figs. 4 and 5. From Fig. 4, it can be seen that for the EOS models Walecka (1974), and Sahu, Basu & Datta (1993), i.e. curves D and H, the slope for the lower values of the stable mass is noticeably positive. This is because of the substantial contribution of attractive force brought on by the scalar σ-meson interaction present in these equations of state. It may be mentioned here that the σ-interaction plays an important role at

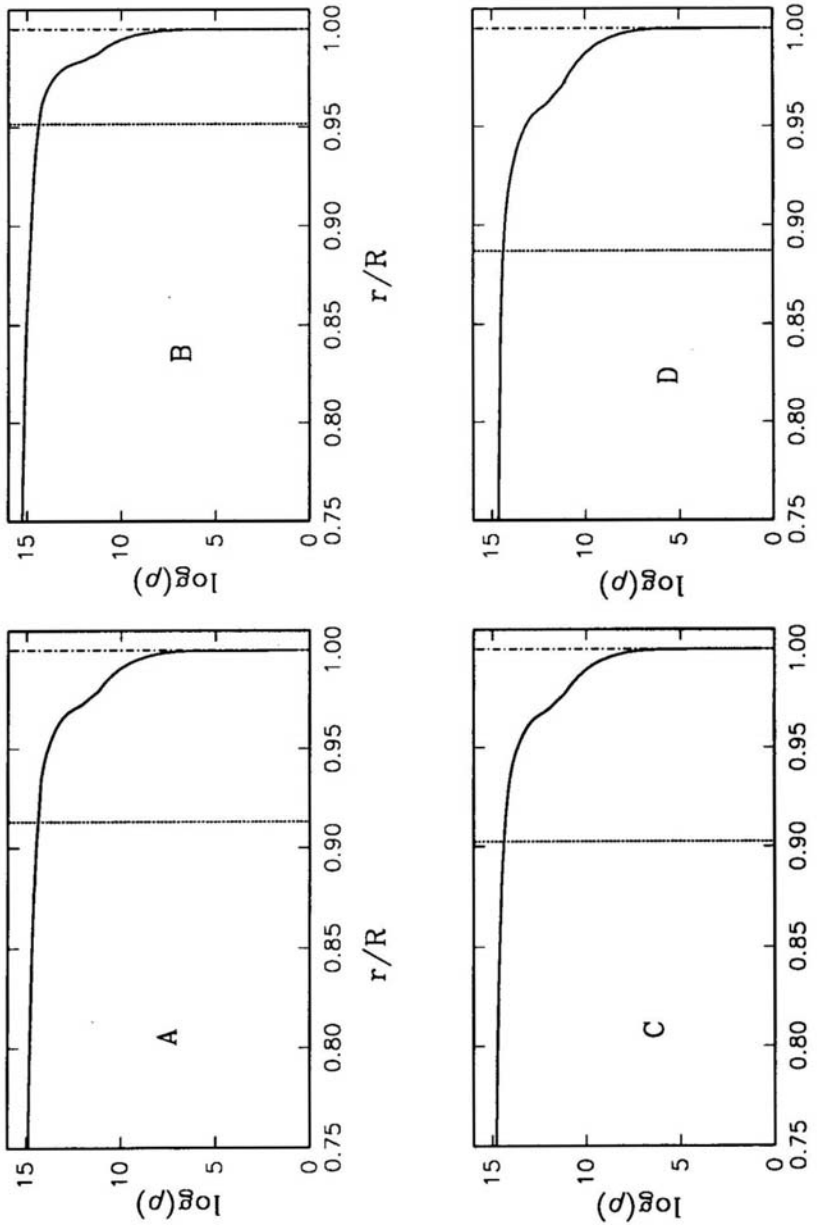

Figure 2. Neutron star density profiles for 1.4 $M_{\odot}$: EOS models (A–D).

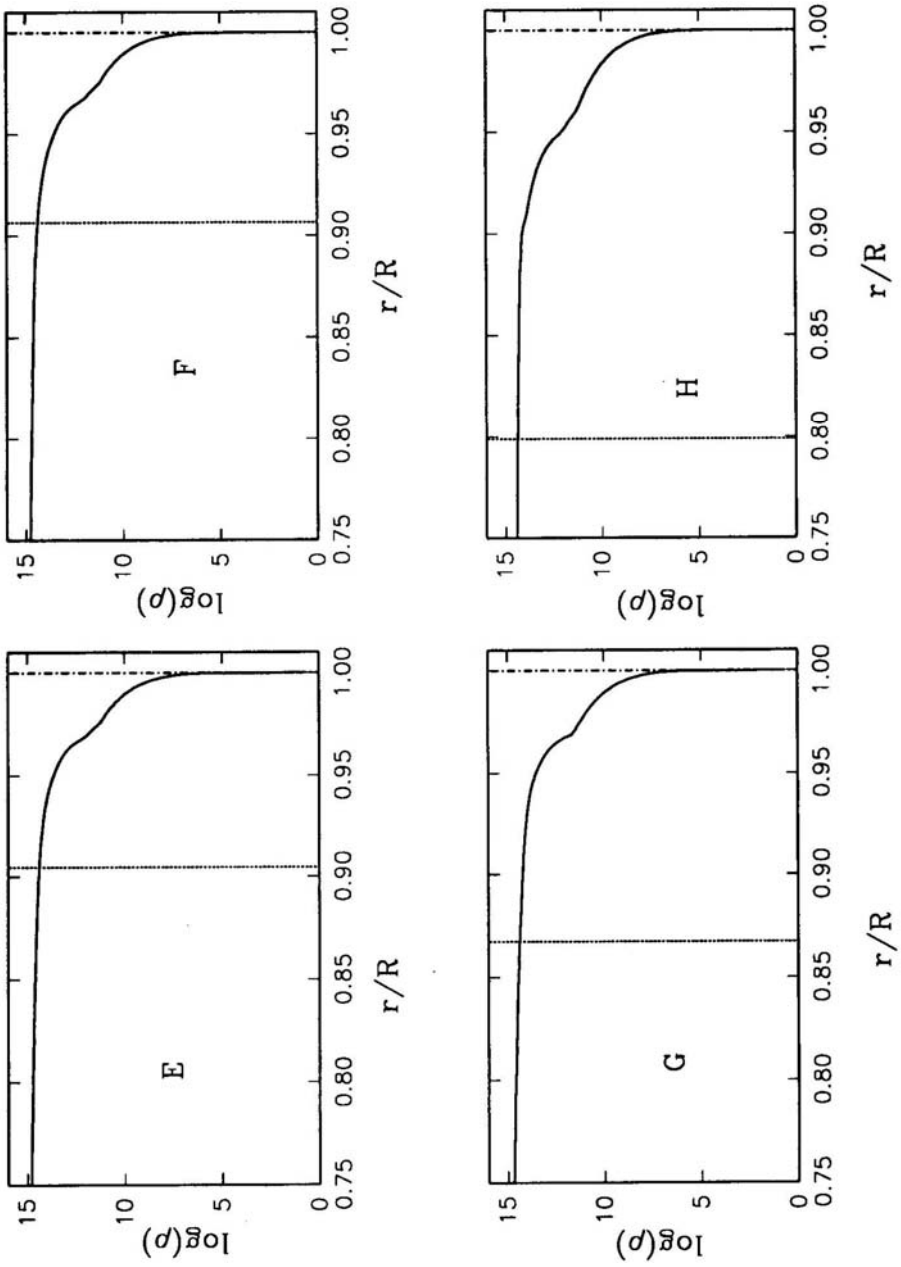

Figure 3. Neutron star density profiles for 1.4 $M_{\odot}$: EOS models (E–H).

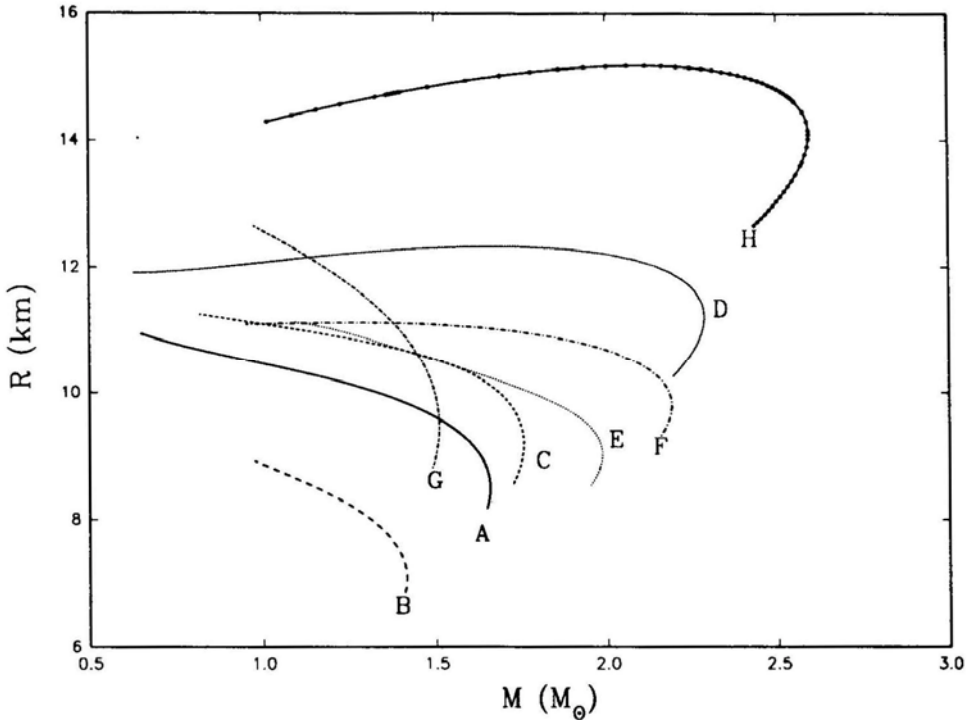

Figure 4. Neutron star mass-radius dependences for the EOS models (A–H).

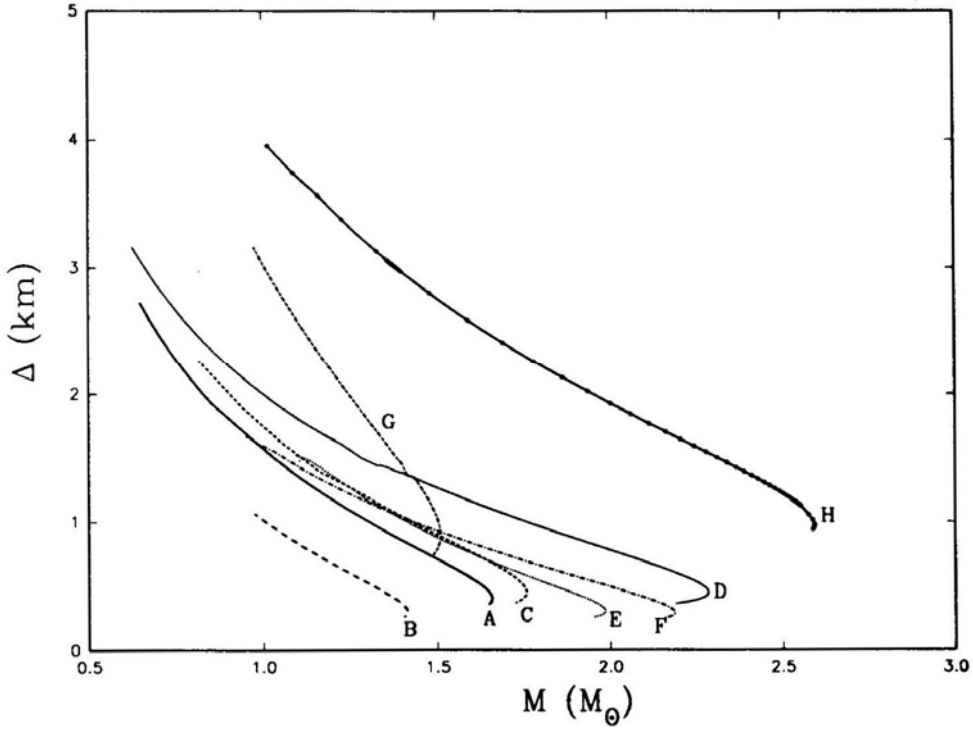

Figure 5. Neutron star crustal thickness (Δ) as a function of the gravitational mass (*M*) for the EOS models (A–H).

intermediate densities providing nuclear saturation, and must be included in any field theoretical EOS model. At high densities the contribution of the vector meson (ω) interaction, which provides repulsive force dominates, and the slope becomes negative. The crustal thickness (Δ) is decided by how much mass is contained in the core and interior regions of the neutron star, so that, in general, the more the mass of the neutron star, the less the value of Δ for any EOS.

As already emphasized, the crustal density profile of neutron stars is a key input in the proper understanding of a variety of important features associated with pulsars, such as the cooling rate. Another important application, that is of much current interest in astrophysics, relates to the evolution of magnetic fields of pulsars. However, several calculations reported in the literature on the problem of magnetic field evolution have considered cooling models for a specific EOS model while using the crustal model that corresponds to a different EOS model. This is mainly because of non-availability of detailed, numerical crustal density profiles. The survey presented here is a preliminary step towards a uniform and consistent investigation of the problem of evolution of neutron star magnetic fields, which will be reported in a forthcoming paper (Bhattacharya & Datta 1995).

Acknowledgement

B. Datta thanks the Director, Raman Research Institute for the kind hospitality.

References

Ambartsumyan, V.A., Saakyan, G.S.1960, *Soviet Astr.*, **4,** 187.
Antia, H. M. 1991, *Numerical Methods for Scientists & Engineers* (New Delhi:Tata McGraw Hill Publ.) 895.
Arnett, W.D., Bowers, R. L. 1977, *Astrophys. J. Suppl.*, **33,** 415.
Baym, G., Pethick, C. J., Sutherland, P. G.1971, *Astrophys. J.*, **170,** 299.
Bethe, H. A., Johnson, M. B. 1974, *Nucl. Phys.*, **A230,** 1.
Bhattacharya, D., Datta, B. 1995, preprint.
Datta, B. 1988, *Fund. Cosmic Phys.*, **12,** 151.
Feynman, R. P., Metropolis, N., Teller, E. 1949, *Phys. Rev.*, **75,** 1561.
Friedman, B., Pandharipande, V. R. 1981, *Nucl. Phys.*, **A361,** 502.
Jastrow, R. 1955, *Phys. Rev.*, **98,** 1479.
Möller, P., Myers, W. D., Swiatecki, M. J., Treiner, J. 1988, *Atomic Data Nucl. Data Tables* **39,** 225.
Negele, J. W., Vautherin, D. 1973, *Nucl. Phys.*, **A207,** 298.
Oppenheimer, J. R., Volkoff, G. M. 1939, *Phys. Rev.*, **55,** 374.
Pandharipande, V. R. 1971a, *Nucl. Phys.*, **A174,** 641.
Pandharipande, V. R. 1971b, *Nucl. Phys.*, **A178,** 123.
Prakash, M., Ainsworth, T. L., Lattimer, J. M. 1988, *Phys. Rev. Lett.*, **61,** 2518.
Reid, R. V., Jr. 1968, *Ann. Phys.*, **50,** 411.
Sahu, P. K., Basu, R., Datta, B. 1993, *Astrophys. J.*, **416,** 267.
Walecka, J. D. 1974, *Ann. Phys.*, **83,** 491.
Wiringa, R. B., Fiks, V., Fabrocini, A, 1988, *Phys. Rev. C*, **38,** 1010.

J. Astrophys. Astr. (1995) **16,** 393–398

Flux Monitoring at 327 MHz during SL9-Jupiter Collision

Rakesh K. Malik*, Pradeep Gothoskar*, P. K. Manohran[@], G. Swarup*, K. Subramanian* & V. Balasubramanian[@]
**National Centre for Radio Astrophysics, TIFR, Post Box 3, Pune 411 007.*
[@]Radio Astronomy Centre, TIFR, Ooty 643001.

Received 1995 July 31; accepted 1995 August 25.

Abstract. Jupiter flux at 327 MHz was monitored using the Ooty radio telescope from July 12th to July 29th during the collision of comet Shoemaker-Levi 9 with Jupiter. Flux was found to increase steadily from July 17th to July 26th by ~ 2·5 Jy, after which it declined to its pre-event value. The comparison of 327 MHz observations with those at 840 MHz and 2240 MHz indicates that the enhancement was mainly due to the increased synchrotron emission and the contribution of thermal emission was very small at metric-decimetric frequencies. The enhancement in radio emission was found to be more at 840 MHz than at 327 or 2240 MHz. The steepening of the spectrum between 327 and 840 MHz as well as between 2240 and 840 MHz was also noted.

Key words: SL9-Jupiter collision—radio flux monitoring—Jupiter radio emission.

1. Introduction

Radio emission from Jupiter spans a wide frequency range from 0·01 MHz to 300 GHz. This radio spectrum consists of three distinct components. Thermal radiation from the cloud layer dominates at millimeter and centimeter wavelengths. At metric-decimetric wavelengths, the dominant component is the synchrotron emission by relativistic electrons trapped in the Jupiter's magnetic field. At the low frequency end, below 40 MHz, the emission consists of sporadic bursts due to plasma instabilities in the inner magnetosphere that generate the emission at frequencies slightly above the local electron cyclotron frequency.

In the metric-decimetric band of interest to us, the emission is due to synchrotron process powered by electrons accelerated to 10–100s of MeV by radial diffusion from the outer magnetosphere into ~ 2 R_j. These high energy electrons are then trapped in a shell of ~ 2 R_j above the cloud top level and centered on the magnetic equator which is tilted by about 10° with respect to the spin equator. The mirror points of most of these trapped electrons are within ~ 1 R_j above and below the magnetic equatorial plane. The observed synchrotron source therefore is the projection of a toroidal source surrounding the planet. The width and height of this projection are approximately 6 R_j and 2 R_j respectively. The spectrum in the metric-decimetric band is nearly flat with the peak at around 1000 MHz. At higher frequencies, the thermal component dominates the synchrotron emission as shown in Fig. 1.

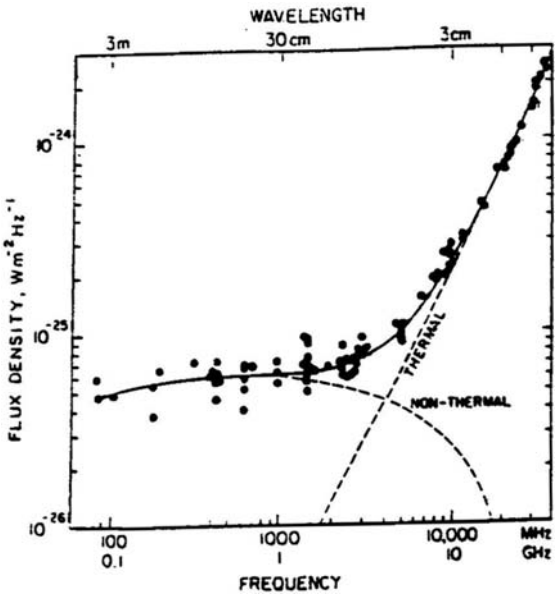

Figure 1. Radio spectrum of Jupiter observed over metric and decimetric frequency bands. The observed spectrum (solid line) is composed of emission due to thermal and non-thermal components (dashed lines), (Carr, T. D. *et al*. 1986, *Physics of Jovian Magnetosphere*, pp 235).

The passage of cometary fragments through the Jovian magnetosphere and the subsequent collisions were expected to affect Jupiter's metric-decimetric emission. Various scenarios for the change in the Jovian radio emission were thought of and are mentioned below.

- It was expected that the energy released in the impact could ionize the cometary material resulting in an enhancement in the electron density. These electrons could be accelerated to high energies in the shock waves that would have resulted from the, impact. The resulting increase in the number of relativistic electrons would enhance the emission.
- The emission could also be enhanced, if instead of producing new relativistic electrons in the impact, low energy electrons already existing in the synchrotron radiation belts were accelerated to sufficiently high energies thus resulting in a net enhancement in the density of high energy electrons.
- Enhanced thermal emission due to the heating up of the Jovian atmosphere by the impacts was also a possibility. Enhancement due to thermal emission was however expected to be seen for short durations after the impact because of short cooling time scales.
- On the other hand, increase in the dust grains and larger-sized material in the magnetosphere with the entry of the comet was expected to slow down the high energy electrons. As a result, the intensity was expected to decrease immediately after the cometary material entered the radiation belts. Inward diffusion of electrons through a dusty magnetosphere was therefore expected to result in a drop in emission for many months after the comet had entered the magnetosphere (de Pater 1994).

We briefly describe our observational results in section 2. Results are discussed in section 3, and section 4 concludes the paper.

2. Observational results

The observations were carried out using the Ooty Radio Telescope (ORT). The ORT consists of a 500 m long cylindrical parabolic antenna with an effective collecting area of about 8000 sqm situated in southern India at a latitude of + 12°. The telescope operates at 327 MHz. The telescope can be steered around its equatorial axis from – 4·5 to + 4·5 hours which allows one to monitor a single source for a stretch of 9 hours. In declination, the telescope can be pointed electronically from + 35 to – 35° by phasing the array of dipoles (Swarup *et al* 1971). The telescope can be operated

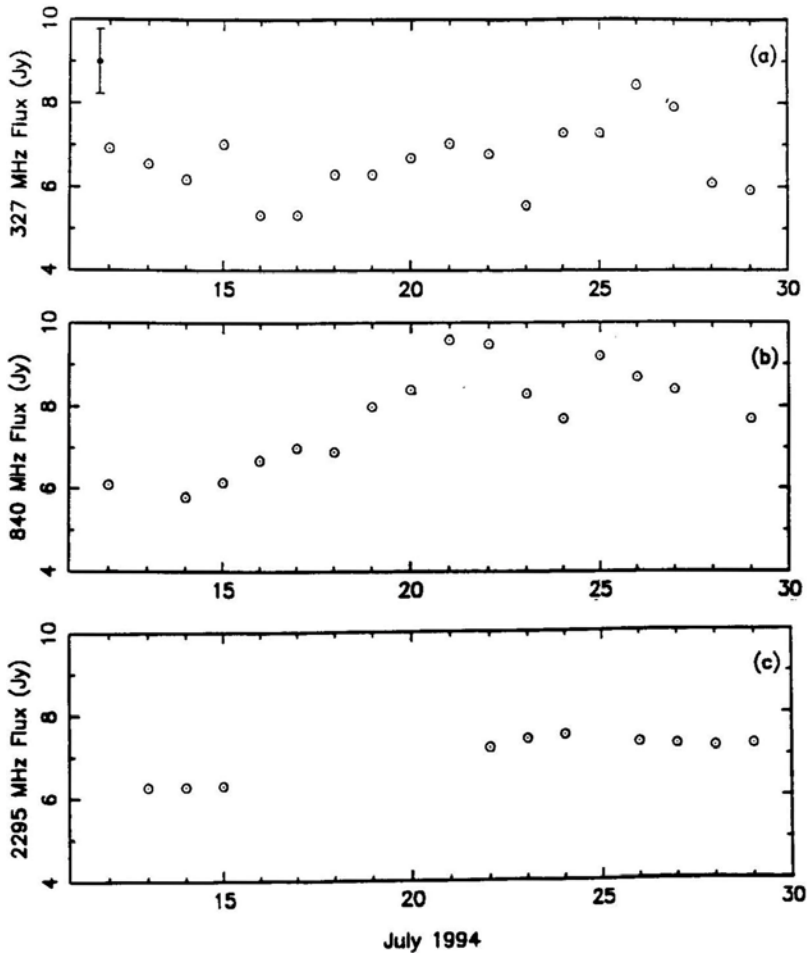

Figure 2. Radio flux measurements carried out between 12th July and 29th July 1994. Measurements at 327 MHz (**a**) were done using the Ooty radio telescope which we have compared with the reported observations at 840 MHz (**b**) and 2295 MHz (**c**) from Molonglo and J P L observatories, respectively. All the flux values were normalized to a distance of 4AU.

either in total power mode, where contribution from all the dipoles is added, or in phase-switched mode, where the signals from the north and south half of the telescope are correlated. In the phase-switched mode the ORT beam is 2·0° in the right ascension and 3′·5 sec (δ) in declination.

The observations for the Jupiter-Comet collision were started on July 12th and continued till July 29th, 1994, well after the collision had taken place. Jupiter observations were interspersed with observations of calibrators. A total of five calibration sources were used during the course of these observations, and at least three of them were observed on a given day (except for July 16th and 17th when the number was 2 and 1 respectively). The data found contaminated with interference were rejected. Observations were corrected for the effect of ORT beamshape as Jupiter drifted in the beam. For any Jupiter observation, confusion sources in the ORT beam down to 10 milli Jansky (1 Jansky = 10^{-26} Wm^{-2} Hz^{-1}) were subtracted. After calibrating it against the calibration sources observed that day, a daily average of the Jupiter flux was obtained. The daily variation of the Jupiter flux thus obtained is shown in Fig. 2(a).

As can be seen in Fig. 2(a) there was a systematic increase of about 2·5 Jy (after normalizing it to a distance of 4 AU) observed between 17th and 26th July which was greater than the limit of flux measurement for ORT. This is indicated by the vertical error bar in Fig. 2(a). This increase in flux started after the impact of the first cometary fragment. The maximum flux was observed on 26th July after which the flux steadily declined over the next 4 days of observations. The data from July 12th to July 16th, when the cometary fragments had entered the Jovian magnetosphere and were approaching Jupiter, show a gradual decrease in flux.

We have compared our results with the observations at 840 MHz (Huntstead & Campbell-Wilson 1994) and 2240 MHz (Klein *et al*. 1994) (Fig. 2b–c). The enhanced emission was more at 840 MHz than at the other two frequencies. There is evidence of progressive steepening of the radio spectrum between 327 and 840 MHz, and between 840 and 2240 MHz as a result of the impacts. As the radio emission declined after July 22nd (at 840 MHz) the spectra in these two frequency ranges also became less steep.

3. Discussion

The initial decrease in the emission level (July 12th to July 16th) could have resulted from the absorption of high energy synchrotron electrons by the dust added to the atmosphere by the comet. For the later enhanced radio emission we now explore two possible explanations – both enhanced thermal as well as non-thermal emission.

3.1 *Thermal emission*

The data show a day-to-day increase in the flux with a peak on July 26th (i.e. 4 days after the last impact). The impacts therefore seemed to have had a cumulative effect on the radio emission rather than just a transitory enhancement at the time of the impact. The optical depth τ for free-free absorption is (e.g. Benz 1993):

$$\tau \sim 0{\cdot}11\ n_e^2\ \nu^{-2}\ T^{-1{\cdot}5}\ \delta L, \tag{1}$$

where n_e is in number of electrons per cm^3, ν is in Hz, T in degree Kelvin and δL is measured in cm.

In order to explain the enhanced emission at 327 MHz in terms of optically thick thermal emission, an enhanced electron density of the order of 10^8 cm^{-3} would be required, assuming $T \sim 5000$ K (since there is evidence that the temperature of the plumes resulting from the impact reached several thousand degrees, see Chapman 1994) and $\delta L \sim 1000$ km. (Note that we cannot account for the observations by assuming optically thin thermal emission since the increase in flux at 840 MHz is more than that at 327 MHz). However gas with density as high as indicated above, will cool very fast. For example, taking an analogy with HI or HII regions since the dominant component of the Jovian atmosphere is hydrogen, the cooling rate can be roughly estimated by (Spitzer 1978) $\Lambda/n_h^2 \sim 7 \times 10^{-26}$ erg cm^3 s^{-1} (assuming fraction of the H atoms ionized to be 10^{-2}).

The cooling time scale therefore would be $t_c \sim (3/2n_h\, kT)/\Lambda$. Taking $n_h \sim 10^{10}$ (for fraction of ionized H atoms $\sim 10^{-2}$) and $T \sim 5000$ K, we find that the cooling time would be $\sim$ 1/2 hr. Even if the cooling time derived above is off by an order of magnitude compared to what may hold for the Jovian atmosphere, we find that it is still difficult to understand the slow and sustained rise in the emission seen at the metric-decimetric band. The thermal model however is more plausible for understanding the rapid variation in the emission reported at millimeter wavelengths.

Another difficulty with the thermal emission is that the electron density of $\sim 10^8$ cm^{-3} is required across the Jupiter disk in a shell of thickness $\sim$ 1000 km. This is possible only if ALL the electrons from a typical cometary fragment spread out across the disk, which seems difficult to justify.

We can however use the shape of the frequency spectrum to constrain the thermal contribution to the observed enhanced emission. Assuming the thermal contribution to be optically thick at 2240 MHz, and further assuming that the increase of flux of $\sim$ 1·56 Jy at 2240 MHz was purely due to thermal emission, in order to derive an upper limit on the thermal part of the enhanced emission, we find that the thermal contribution at 327 MHz would be $\leqslant$ 50 mJy while at 840 MHz it would be smaller than 300 mJy because the thermal emission scales as l/λ^2 for optically thick emission.

3.2 *Synchrotron emission*

The peak of the Jovian synchrotron spectrum is determined by $\nu_{\max}$ (MHz) $\sim 4{\cdot}8\ (E)^2\ (B)$ sin (α), where energy and magnetic field is in MeV and Gauss respectively (Carr *et al*. 1986). Taking $\nu_{\max} \sim 1$ GHz, $\sin(\alpha) \sim 1$ and $B \sim 3$ Gauss we find that the energies to which electrons need to be accelerated are $\sim$ 8 MeV to explain the enhanced emission. The power emitted by one electron is (Carr *et al*. 1986):

$$p \approx 6{\cdot}10^{-22} \left(\frac{E}{\text{MeV}}\right)^2 \left(\frac{B}{\text{Gauss}}\right)^2 \sin^2 \alpha \sim 3{\cdot}10^{-19}\ \text{W}. \tag{2}$$

Assuming that the enhanced emission comes from a volume of scale size $\sim$ 1000 km, we find that an excess electron density of the order of $2{\cdot}5 \times 10^2$ cm^{-3} accelerated to energies $\sim$ 10 MeV is sufficient to explain the enhanced emission.

Considering the moderate increase in the number density, compared to that for thermal emission, of relativistic electrons required to explain it, the synchrotron process seems to be the source of enhanced emission. The requirement of electrons accelerated to relativistic speeds could be met by a variety of processes:

- Shock waves generated by the impact could have accelerated the low energy electrons existing in the inner regions of the Jovian magnetosphere.
- There is an evidence of production of new electrons as inferred from the increase in auroras seen in ultraviolet images obtained by HST soon after the impact. Therefore there is also a possibility that these newly generated electrons were accelerated and deposited in the inner regions of the magnetosphere.
- A third possibility would be the reconnection of magnetic field taking place behind the blob of ionized material as it arose after the impact and stretched the field lines.

All three of these scenarios would also explain the inward movement of the synchrotron belts.

4. Conclusion

We have observed the radio emission from Jupiter at the time of collision with comet Shoemaker-Levy at 327 MHz using the Ooty radio telescope. A careful analysis of the data indicates that there was a systematic but marginal increase of ~ 2·5 Jy in the Jovian radio emission at 327 MHz due to the cometary impacts. The flux continued to increase till July 26th after which it declined.

Comparison with observations carried out at 840 MHz and 2240 MHz indicates that the enhanced radio emission from Jupiter due to the cometary impacts was due to synchrotron emission. Acceleration of electrons in the inner regions of the magnetosphere either due to shock waves emanating as an after effect of the impact or due to magnetic reconnection could be the cause of the increase in emission.

Though the thermal emission cannot explain the sustained rise in the radio emission at meter-decimeter wavelengths, it is more plausible for 'bursts' seen at the time of impacts as e.g. in milli-metric wavelengths.

References

Benz, A. O. 1993, *Plasma Astrophysics*, (Dordrecht, Boston, London: Kluwer Academic Publishers.) pp.263.

Carr, T.D., Desch, M. D., Alexander, J. K. 1986, *Physics of Jovian Magnetosphere*, Cambridge Planetary Science Series, pp. 235.

Chapman, C. R. 1994, *Nature*, **370,** 245.

de Pater, I.1994, *Geophys. Res. Lett*., **21,** 1071.

Huntstead, R., Campbell-Wilson, D. 1994, (private communication).

Klein, M. J., Gulkis, S., Bolton, S. J. 1994, *Symposium on the Magnetospheres of the Outer Planets* (private communication).

Spitzer, Jr., L. 1978, *Physical Processes in the Interstellar Medium* (New York, Chichester, Brisbane, Toronto: Wiley-Interscience Publication) p. 143

Swarup, G., Sharma, N. V. G., Joshi, M. N., Kapahi, V. K., Bagri, D. S., Damle, S. M., Ananthakrishnan, S., Balasubramanian, V., Sinha, R. P. 1971, *Nat. Phys. Sci*., **230,** 185.

J. Astrophys. Astr. (1995) **16,** 399–405

Effect of Strong Magnetic Field on Cosmic Quark-Hadron Phase Transition and Baryon Inhomogeneity

Somenath Chakrabarty †*Department of Physics, University of Kalyani, West Bengal, India 741 235, and Inter-University Centre for Astronomy and Astrophysics, Post Bag 4, Ganeshkhind, Pune, India 411 007.*

Received 1995 July 4; accepted 1995 December 1

Abstract. The effect of intense magnetic field on the cosmic quark-hadron phase transition and also on the baryon number inhomogeneity has been investigated using phenomenological MIT bag model for the quark sector. For the sake of simplicity an ideal gas equation of state has been considered for the hadronic phase.

Key words: Cosmic quark-hadron phase transition—Baryon number inhomogeneity—equation of state—Landau levels—quark nuggets.

1. Introduction

In the past few years a lot of work has been done on the effect of strong magnetic field on various properties of dense astrophysical and cosmological matter. These works are mainly related to the emissions from magnetized neutron matter (Kaminker *et al*. 1991, 1992), electron-induced electromagnetic and weak processes (Shul'man 1991), and the Landau diamagnetism and Pauli paramagnetism of dense nuclear matter (Shul'man 1991; Fushiki *et al*. 1992). Very recently the effects of such intense magnetic field on the primordial nucleo-synthesis and also on the expansion rate of the universe micro-second after the Big Bang have been studied by Schramm *et al*. (Cheng *et al*. 1993, 1994) and Grasso & Rubinstein (1994). In recent years some interesting work has also been done on quantum electrodynamics in the presence of strong external magnetic field (Persson & Zeitlin 1994; Zeitlin 1994; Danielsson & Grasso 1995) and also on the stability of matter in the presence of strong magnetic field (Vshivtsev & Serebryakova 1994; Elliott *et al*. 1995). In a series of publications we have also reported some new results on the effect of strong magnetic field on first order quark-hadron phase transition at the core of a neutron star. In particular, we have studied the stability of strange quark matter, equation of state of such stable phase and also the nucleation of quark bubbles in metastable neutron matter in the presence of strong magnetic field. We have seen that strange quark matter becomes more stable in the presence of strong magnetic field and the equation of state of magnetized strange quark matter differs significantly from that of a non-magnetized one. The most interesting observation was that there cannot be any quark droplet nucleation in metastable neutron matter if the strength of the magnetic field is strong enough to make the quarks populate the Landau levels (Chakrabarty & Goyal 1994; Chakrabarty 1994, 1995a, b).

†Permanent address.

In all these reported results, mentioned above, the possible effects of strong magnetic fields on cosmic QCD phase transition have not been considered. Initially the universe is at a high temperature and in the quark-gluon plasma phase. The net baryon number of the universe resides entirely in the primordial quark soup. Due to cosmic expansion the temperature of the quark soup decreases and near the critical temperature, T_c, a transition to colour singlet hadronic phase takes place. During phase separation the baryon number is transported to the hadronic phase mainly by the formation of nucleons which are the lightest baryons. The other possible hadrons are mostly light mesons, which do not carry the baryon number. Now, the quarks in the quark gluon plasma are almost massless and carry 1/3 baryon number, whereas the mass of the lightest baryon, the nucleon, is ~ 940 MeV. A simple thermodynamic calculation shows that the baryon number solubility of primordial quark soup is much higher than that of hadronic matter at the critical temperature T_c. This gives rise to inhomogeneity in the baryon number distribution. This particular aspect has also not been studied in the presence of strong magnetic field. The aim of this paper is to investigate the effect of strong magnetic field on both cosmic quark-hadron phase transition and baryon inhomogeneity.

In § 2 we give the basic thermodynamic formalism of quark matter in the presence of strong magnetic field. In sections 3 and 4 we study the effect of strong magnetic field on the cosmic QCD phase transition and on the baryon inhomogeneity. Section 5 contains the conclusion of this work.

2. Formalism

As is well known, the energy of a charged particle changes significantly in the quantum limit if the magnetic field strength is equal to or greater than some critical value $B_m^{(c)} = m_i^2\ c^3/\ (q_i\ h)$ in Gauss; where m_i and q_i are respectively the mass and charge (absolute value) of the particle (e.g., $q_i = 2e/3$ for u-quark, $e/3$ for d and s quarks, here $e = |e|$ is the absolute value of electronic charge), h and c are respectively the reduced Planck constant and velocity of light, both of which along with the Boltzmann constant k_B are taken to be unity in our choice of units. For an electron of mass 0·5 MeV, the strength of this critical field as mentioned above is $B_m^{(c)(e)} = 4{\cdot}4 \times 10^{13}\ G$, whereas for a light quark of current mass 5 MeV, this particular value becomes ~ $10^2 \times B_m^{(c)(e)}$, arise for s-quark of current mass 150 MeV, it is ~ $10^{20}\ G$, which is too high to realize at the core of a neutron star. But the possibility of such high magnetic field cannot be discarded in the case of the early universe (Vachaspati 1991). The critical magnetic field as defined above is the typical strength at which the cyclotron lines begin to occur, and in this limit the cyclotron quantum is of the order of or greater than the corresponding rest energy. This is also equivalent to the requirement that the de-Broglie wavelength is of the order of or greater than the Larmor radius of the particle in the magnetic field.

To study the cosmic QCD transition in the early universe in the presence of a strong magnetic field, we have considered the conventional MIT bag model. For the sake of simplicity we assume that quarks move freely within the system. The current masses of both u and d-quarks are assumed to be extremely low (in our actual calculation we have taken the current mass for both of them to be 5 MeV, whereas for s-quark, the current mass is taken to be 150 MeV).

For a constant magnetic field along the z-axis ($\vec{B}_m$ $B_m = B_{m,(z)} = B_m$ = constant), the single particle energy eigen value is given by

$$\varepsilon_{k,n,s}^{(i)} = [k^2 + m_i^2 + q_i B_m (2n + s + 1)]^{1/2}, \tag{1}$$

where n = 0, 1, 2,...., being the principal quantum numbers for allowed Landau levels, $s = \pm 1$ refers to spin up (+) or down (–) states and k is the component of particle momentum along the direction of external magnetic field. Setting $2v = 2n + s + 1$, where v = 0, 1, 2,..., we can rewrite the single particle energy eigen value in the following form

$$\varepsilon_v^{(i)} = [k^2 + m_i^2 + q_i B_m 2v]^{1/2}. \tag{2}$$

Now it is very easy to show that the $v = 0$ state is singly degenerate while all other states with $\nu \neq 0$ are doubly degenerate.

The general expression for the thermodynamic potential of the system at temperature $T = \beta^{-1}$ is given by

$$\Omega = -T \ln Z = \sum_i \Omega_i V + BV, \tag{3}$$

where Z is the grant-partition function and the explicit form of the thermodynamic potential density for the ith species is given by

$$\Omega_i = -\frac{Tg_i}{(2\pi)^3} \int d^3 k \ln (1 + \exp (\beta (\mu_i - \varepsilon_i))), \tag{4}$$

where g_i is the degeneracy of the ith species (= 6 for a quark or an antiquark), B is the bag pressure and V is the volume occupied by the system. The sum in equation (3) is over u, d, s-quarks and their antiparticles. We assume that for antiparticles the chemical potential $\bar{\mu}_i = -\mu_i$ i.e. they are in chemical equilibrium with respect to annihilation processes.

Now let us consider the necessary changes to be made in equation (4) if a strong external magnetic field is present in the system. Here we shall investigate the magnetism arising from quantization of orbital motion of charged particles in the presence of a strong magnetic field. We know that if the magnetic field is along z-axis, the path of the charged particle will be a regular helix whose axis lies along the z-axis and whose projection on an x-y plane is a circle. If the magnetic field is uniform, both the linear velocity along the field direction and the angular velocity in the x-y plane will be constant, the latter arises from the constant Lorentz force experienced by the particle. Quantum mechanically the energy associated with the circular motion in the x-y plane is quantized in units of $2q_i B_m$. The energy associated with the linear motion along the z-axis is also quantized; but in view of the smallness of the energy intervals, they may be taken as continuous variables. We thus have equation (1) or (2) as single particle energy eigen value. Now, these magnetized energy levels are degenerate because they result from an almost continuous set of zero field levels. All those levels for which the values of the quantity $k_x^2 + k_y^2$ lie between $2q_i B_m v$ and $2q_i B_m (v + 1)$ now coalesce into a single level characterized by the quantum number v. The number of these levels is given by

$$\frac{S}{(2\pi)^2} \iint dk_x \, dk_y = \frac{Sq_i B_m}{2\pi}, \tag{5}$$

here S is the area of the orbit in the x-y plane. This expression is independent of v. Then, in the integral of the form $\int d^3\, kf\,(k)$, we can replace $\iint dk_x\, dk_y$ by the expression given above, whereas the limit of k_z, which is a continuous variable, ranges from $-\infty$ to $+\infty$. Then we can rewrite equation (4) for the thermodynamic potential density in the presence of a strong magnetic field in the form

$$\Omega_i = -\, T \frac{q_i g_i B_m}{2\pi^2} \sum_{v=0}^{\infty} \int_0^{\infty} dk_z \ln\left(1 + \exp(\beta(\mu_i - \varepsilon_v^{(i)}))\right). \tag{6}$$

We have used equation (4) for s and $\bar{s}$ if $B_m < 10^{20}$ G and equation (6) for u, d-quarks and their anti-particles. Whereas for $B_m > 10^{20}$ G, equation (6) has been used for all the constituents. In equation (4), $\varepsilon_i = (k^2 + m_i^2)^{1/2}$, whereas in equation (6), it is given by equation (2).

The expression for kinetic pressure of the system is given by

$$P = -\sum_i \Omega_i, \tag{7}$$

and the number density of the ith species is given by

$$n_i = \left(\frac{\partial \Omega_i}{\partial \mu_i}\right)_T. \tag{8}$$

3. Cosmic quark-hadron phase transition

Assuming for the sake of simplicity that only nucleons and pions are present in the hadronic phase and that they obey the free hadronic gas equation of state, the conditions to be satisfied by the coexisting phases are

$$\mu_p = \mu_d + 2\mu_u, \tag{9}$$

$$\mu_n = \mu_u + 2\mu_d, \tag{10}$$

$$\mu_\pi = 0, \tag{11}$$

$$P_h = P_q, \tag{12}$$

and

$$T_h = T_q = T_c. \tag{13}$$

The chemical equilibrium conditions are also valid for anti-quarks and anti-hadrons i.e. we can write down equations similar to equations (9) and (10) for $\bar{q}$, $\bar{n}$ and $\bar{p}$ (where $q = u$ or d). We also assume that the condition of β-equilibrium is satisfied in both the quark-gluon and hadronic phases. For the anti-particles, the chemical potential $\bar{\mu}_i = -\mu_i$. The expressions for kinetic pressures are then obtained from equation (7) by replacing Ω_i either by equation (4) or (6), depending on whether $B_m < B_m^{(c)(i)}$ or $> B_m^{(c)(i)}$, respectively.

In Fig. 1 we have shown the phase diagram (n_B vs T diagram) for such a mixed phase of quark-gluon plasma and hadronic matter. The dotted curve is for $B_m = 0$, whereas the solid curve is for $B_m = 10^3 \times B_m^{(c)(e)}$. This figure shows that the phase diagram changes significantly in the presence of a strong magnetic field.

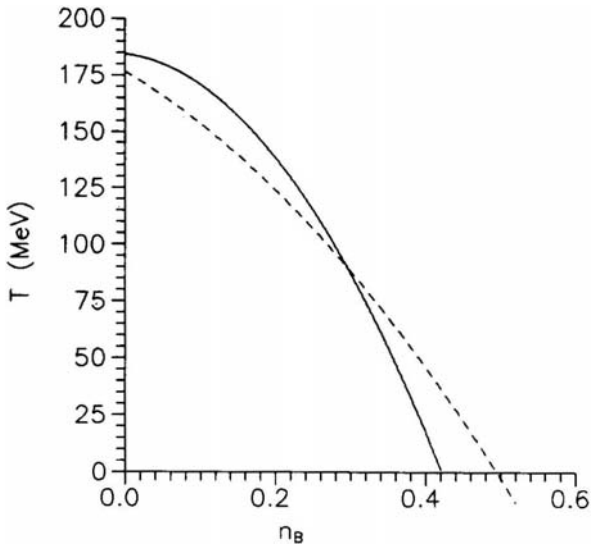

Figure 1. Phase diagram ($T - n_B$ plot) for a mixture of QGP and hadronic matter. The dotted curve is for $B_m = 0$ and the solid one is for $B_m = 10^3 \times B_m^{(c)(e)}$.

4. Baryon inhomogeneity

Before the quark-hadron phase transition in the early universe, the quark gluon plasma had almost an equal number of quarks and anti-quarks, since the baryon number of the universe is so small,

$$\frac{n_B}{n_\gamma} \sim 10^{-9}, \tag{14}$$

where n_B ad n_y are respectively the net baryon number and photon number densities in the early universe. This ratio is too small to affect the dynamics or the evolution of the early universe. Since the present universe is matter dominated, all the anti-baryons must have been annihilated with their counterparts.

Now in the quark gluon phase, the baryon number is carried by the quarks, which are almost massless (except *s*-quark, whose mass is ~ 150 MeV). On the other hand, in the hadronic sector, the lightest baryons are nucleons of mass ~ 940 MeV. Therefore the baryon number prefers to reside in the quark gluon phase during phase transition (Witten 1984), or in other words, the baryon number solubility of primordial quark soup is much higher than that of hadronic phase at T_c. We can estimate the ratio of baryon number densities in these two phases at T_c, given by

$$R = \frac{n_q^{(B)}}{n_h^{(B)}}, \tag{15}$$

A simple non-relativistic thermodynamic calculation (Witten 1984) shows that $R \sim \exp(M_h/T_c)$, where M_h is the hadronic mass $\gg T_c$. Therefore the ratio R is a large

Table 1.

$B_m/B_m^{(c)(e)}$	T_c(MeV)	$n_q^{(B)}/n_h^{(B)}$
0·0	100	455·4
	150	33·4
	180	14·7
	200	9·9
10^2	100	2732·69
	150	200·66
	180	88·49
	200	59·21
10^3	100	2783·01
	150	201·39
	180	89·03
	200	61·35
10^5	100	51908·2
	150	1695·85
	180	520·75
	200	285·51

number. It has been shown that $R \approx 6$ or 100 for $T_c = 200$ or 100 MeV respectively (Kurki-Suonio 1988, 1991; Fuller *et al*. 1988; Kapusta & Olive 1988).

Since the net baryon number of the universe is small, $\mu_B = 3\mu_q \rightarrow 0$. Then the ratio R is given by

$$R = \lim_{\mu_q \rightarrow 0,\, \mu_B \rightarrow 0} \frac{1}{3} \frac{(\partial \Omega_q / \partial \mu_q)_{T=T_c}}{(\partial \Omega_B / \partial \mu_B)_{T=T_c}}. \tag{16}$$

Using the explicit form of Ω_i ($i = q$ or B), it is very easy to show that in the limiting condition $n_B \rightarrow 0$, the ratio R reduces to 0/0 form. Then by L'Hospital's theorem, we have

$$R = \lim_{\mu_q \rightarrow 0, \mu_B \rightarrow 0} \frac{1}{3} \frac{(\partial^2 \Omega_q / \partial \mu_q^2)_{T=T_c}}{(\partial^2 \Omega_B / \partial \mu_B^2)_{T=T_c}}, \tag{17}$$

which is not in the 0/0 form.Using the explicit form of the second derivatives as written above we have calculated R for four different values of T_c (= 100, 150, 180 and 200 MeV) and for $B_m = 0$, $10^2 \times B_m^{(c)(e)}$ $10^3 \times B_m^{(c)(e)}$ and $10^5\, B_m^{(c)(e)}$. In Table 1 we have shown the variation of R with T_c and B_m. The variation of R with T_c has already been reported and the results presented here are consistent with those of old published data. The variation of R with B_m has not been done before. If $B_m > 10^2 \times B_m^{(c)(e)}$, R changes significantly from zero field values. If this is true for the early universe, this could possibly lead to a very high baryon number inhomogeneity, which could modify the picture at the end of the quark-hadron phase transition. It is also obvious that the presence of a strong magnetic field favours the formation of quark nuggets during the early universe quark-hadron phase transition, which is expected to be one of the natural candidates for baryonic dark matter.

5. Conclusions

We have seen that in the presence of a strong magnetic field greater than the corresponding critical field, the phase diagram for a mixture of quark gluon plasma and hadronic matter differs significantly from that for zero magnetic field case.

The other interesting observation is that the baryon number inhomogeneity in the early universe increases by a few orders of magnitude if the magnetic field strength becomes greater than $10^2 \times B_m^{(c)(e)}$.

If this theoretical prediction is correct, then it may have some effect on the primordial nuclear abundances and also on the formation of quark nuggets during the first order quark hadron phase transition in the early universe, which in turn affects the Big Bang nucleo-synthesis.

Here we have given a very simplified picture of the baryon number transport during the first order cosmic quark hadron phase transition in the presence of a strong magnetic field. Such calculations should only be used to indicate the order of magnitude of the baryon number penetrability and a rough comparison with zero magnetic field case.

References

Chakrabarty, S. 1994, *Astr. Space Sci*., **213,** 121.
Chakrabarty, S., Goyal, A. 1994, *Mod. Phys. Lett*., **A9,** 3611.
Chakrabarty, S. 1995a, *Phys. Rev*., **D51,** 4591.
Chakrabarty, S. 1995b, *Ann. Phys*. (submitted).
Cheng, B., Schramm, D. N., Truran, J. W. 1993, *Phys. Lett*, **B316,** 521.
Cheng, B., Schramm, D. N., Truran, J. W. 1994, *Phys. Rev*., **D49,** 5006.
Danielsson, Ulf, H., Grasso, D. 1995, Preprint UUITP-2/95.
Elliot, Lieb, Michael, Loss, Jan Philip, Solovej 1995, GATECH, Preprint.
Fuller, G. M., Mathews, G. J., Alcock, C. R. 1988, *Phys. Rev*., **D37,** 1380.
Fushiki, I. *et al.* 1992, *Ann. Phys*., **216,** 29.
Grasso, D., Rubinstein, H. R. 1994, Preprint Uppsala-UUITP 14/1994 (to appear in *Astro-particle Phys*.).
Kaminker, A. D. *et al*. 1991, *Soviet Astr. Lett*., **17,** 450.
Kaminker, A. D. *et al*. 1992, *Phys. Rev*., **D46,** 3256.
Kapusta, J. I., Olive, K. A. 1988, *Phys. Lett.*, **209B,** 295.
Kurki-Suonio, H. 1988, *Phys. Rev*., **D37,** 2104.
Kurki-Suonio, H. 1991, *Nucl. Phys*., **B24,** 67.
Persson, D., Zeitlin, V. 1994, Preprint FIAN/TD/94-01.
Shul'man, G. A. 1991, *Soviet Astr*., **35,** 50, 492.
Vachaspati, T. 1991, *Phys. Lett*., **B265,** 258.
Vshivtsev, A. S., Serebryakova, D. V. 1994, *JETP*, **79,** 17.
Witten, E. 1984, *Phys. Rev*., **D30,** 272.
Zeitlin, V. 1994, Preprint FIAN/TD/94-10.

J. Astrophys. Astr. (1995) **16,** 407–424

VV Orionis – Improved Elements

M. B. K. Sarma & P. Vivekananda Rao *Centre for Advanced Study in Astronomy, Osmania University, Hyderabad 500 007, India*

Received 1995 April 3; accepted 1995 August 1.

Abstract. The *UBV* light curves obtained by Duerbeck (1975) and *Hα* (wide) and H*α* (narrow) light curves obtained by Chambliss & Davan (1987) of the detached eclipsing binary VV Orionis (VV Ori) were analysed using the Wilson-Devinney method fixing the two parameters T_h (25,000 K) and q(0.4172), resulting in the following absolute elements: A = 13.605 ± 0.031$R_\odot$, R_h = 5.03 ± 0.03$R_\odot$, , R_c = 2.43 ± 0.02$R_\odot$, $M_{\mathrm{bol},h}$ = – 5.18 ± 0.11, $M_{\mathrm{bol},c}$ = – 1.54 ± 0.06, m_h = 10.81 ± 0.42$m_\odot$ and m_c = 4.51 ± 0.41$m_\odot$. The de-reddened colours obtained from applying the reddening corrections of $E(B\text{-}V)$ = $0^m.05$ and $E(U\text{-}B)$ = $0^m.04$, and the derived temperatures of the components, gave spectral types of *B*1.5*V* for the primary and *B*4-5*V* with an *UV* excess of $0^m.3$ for the secondary component. A comparison of the log L and log T_e of the components with the observed ZAMS shows the primary component to be a little above and the secondary component to be a little below/or on the ZAMS. A comparison of the properties of the components of VV Ori and a few other detached systems with the normal stars in the log L, log R and log T_e versus log m planes, indicated a need for either a readjustment of the scales of the above parameters or modifications in the theoretical models. From the position of the components on the evolutionary tracks of Pop I composition computed by Schaller et al. (1992) it is noticed that while the primary component of VV Ori had slightly evolved along the main-sequence, its secondary is still unevolved. The age of VV Ori is found to be 10 ± 1 million years and it is at a distance of 368 ± 10 pc.

Key words: Eclipsing binaries—detached—VV Ori—elements—individual.

1. Introduction

VV Orionis (HR 1868 = HD 36695, $P = I^{d}.4854$) was first found to be a light variable by Barr in 1903 (Barr 1905). It is an eclipsing binary of type *E B* with both the components belonging to the main sequence of spectral type *B*. There were many spectroscopic and photometric investigations of this system. The spectroscopic studies of Struve & Luyten (1949) showed this system to be single-lined and they suggested a mass ratio of unity for the components. From their spectral studies, Beltrani & Galeotti (1970) estimated the mass ratio to be about 0.5. Using high dispersion spectra, Duerbeck (1975) could locate a few lines of the secondary component and was thus able to get an improved mass ratio of 0.45. However, the detection of the secondary lines had been questioned (Andersen 1976, Popper 1981) and the value of the mass-ratio remained ambiguous.

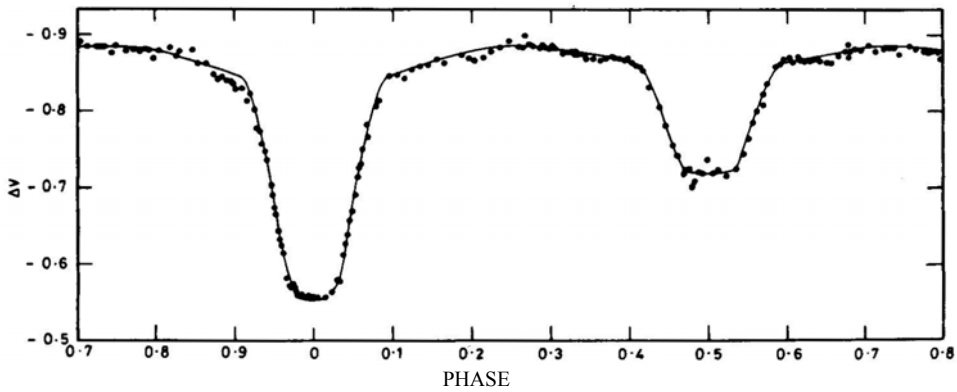

Figure 1a. VV Ori: Light curve in yellow. Filled circles represent observations (normals) and the solid line represents the theoretical curve obtained from the elements obtained from the combined *V, B,Hα*(*n*) solution (Table 2, col. 2).

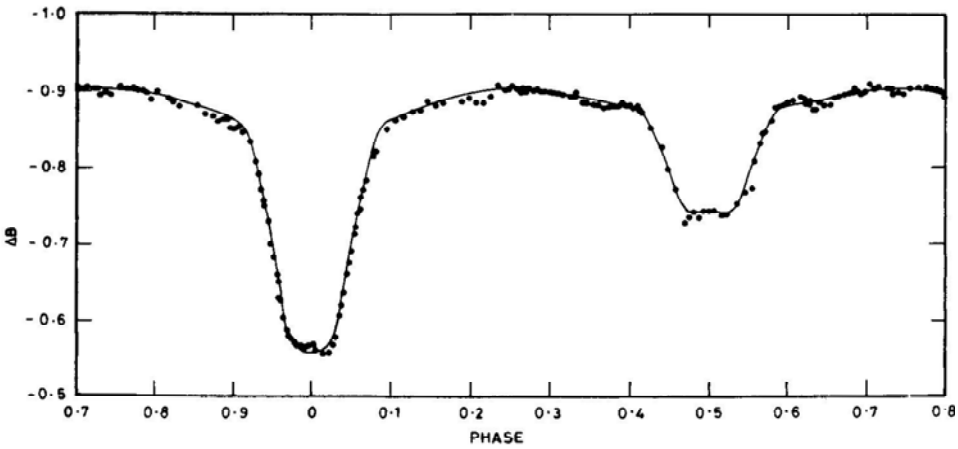

Figure 1b. VV Ori: Same as in Fig. 1a, for blue.

Popper (1993) reported the detection of the lines of the secondary component of VV Ori. His radial velocity curves of the two components yielded a mass-ratio of 0.4172. Even though the variation of the center of mass velocity V_o is poorly determined, Popper (1993) suggests that "One can derive fundamental properties of VV Ori,making use of the results in (his) Table 3, that should be improvements over previously published work". Hence we felt it useful to re-analyse the published photometric data with the newly derived mass-ratio of 0.4172 and obtain reliable photometric elements for VV Ori. The results of the analysis of a few published light curves of this system is given below.

2. Earlier analysis of the light curves of VV Ori

Of all the published light curves of VV Ori, the *UBV* data of Duerbeck (1975) is the most extensive. Duerbeck himself had analysed his data using the Russell-Merrill method (1952). Eaton (1975) analysed a series of OAO-2 light curves of this system

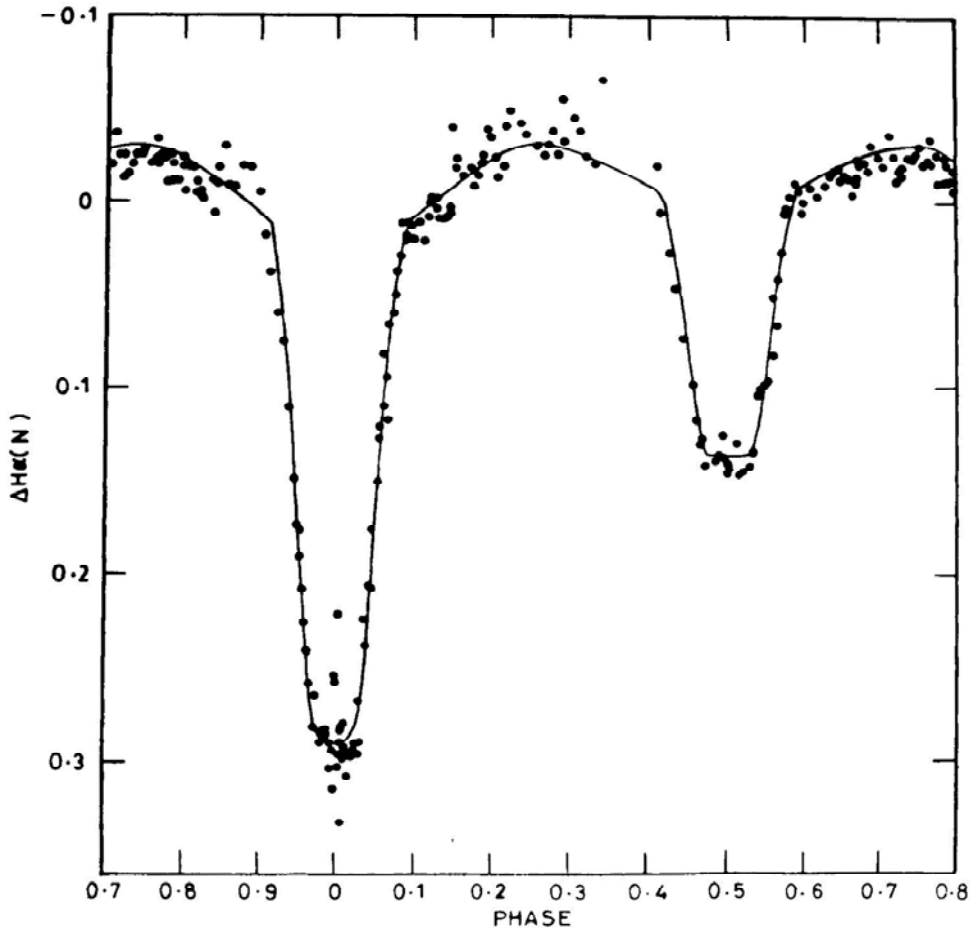

Figure 1c. VV Ori: Same as in Fig. 1a, for *Hα*. (*n*).

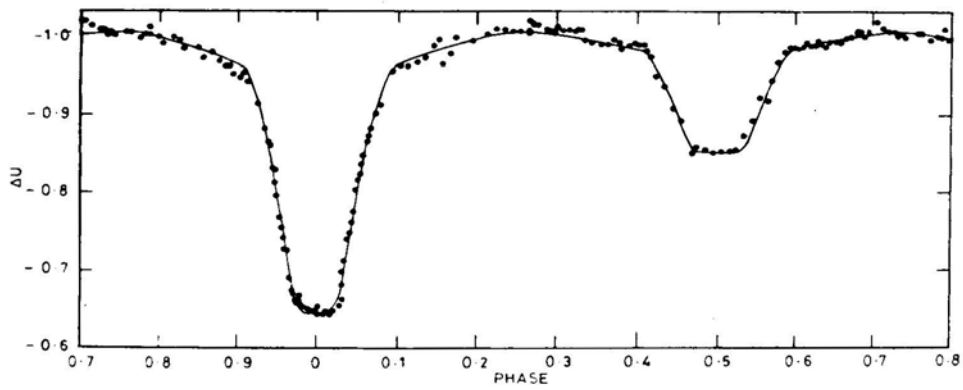

Figure 1d. VV Ori: Same as in Fig. 1 a, for ultraviolet. Here, the theoretical curve is calculated using the elements given in (Table 2, col. 3).

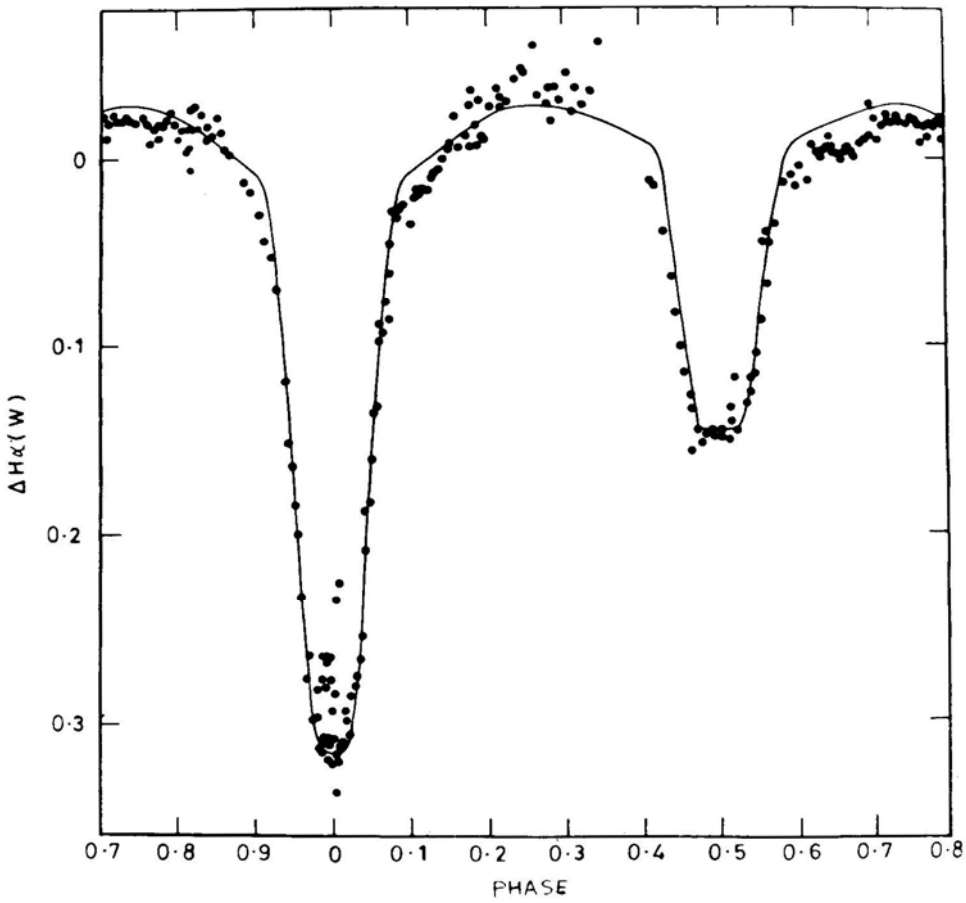

Figure 1e . VV Ori: Same as in Fig. 1a for *Hα*(*w*). Here, the theoretical curve is calculated using the elements given in (Table 2, col. 4).

which covered the wavelength range of 1300–4300Å , using a computational model developed by Lucy (1968). Cester et al. (1978) analysed Duerbecks's data using Wood's WINK method. Budding & Najim (1980) analysed Eaton's (1975) data with Kopal's Frequency Domain method. Chambliss & Leung (1982) solved their own *UBVuvby* light curves with the Wilson-Devinney method. Giuricin et al. (1983) and Chambliss (1983) analysed the data of Chambliss & Leung (1982) with Wood's WINK pro–gramme. Chambliss & Davan (1987) analysed their H*α* (wide) and H*α* (narrow) band observations of this system using the WINK programme. All the above analyses, wherever needed, used a mass–ratio of 0.45.

3. Present study

3.1 *Data*

Since an improved mass-ratio for VV Ori (Popper 1993) is now available and as Wilson-Devinney (1971)synthetic right curve method(W-D) is regarded as the most reliable among

Table 1. VV Ori: Elements obtained from the solution of individual light curves using W-D method.

Element		Initial parameter	*U*	*B*	*V*	*Hα* (*w*)	*Hα* (*n*)
1		2	3	4	5	6	7
$*T_{e,h}K$		25,000	25,000	25,000	25,000	25,000	25,000
$T_{e,c}K$		15,550	15,667	15,544	15,544	15,560	15,571
$*q$		0.4172	0.4172	0.4172	0.4172	0.4172	0.4172
$i°$		86.0	86.050	86.108	86.128	86.078	86.108
r_h	pole point	0.368	0.3700	0.3630	0.3640	0.3572	0.3612
	side back		0.4100	0.3989	0.4006	0.3901	0.3962
			0.3846	0.3765	0.3777	0.3698	0.3744
			0.3971	0.3879	0.3893	0.3804	0.3855
r_c	pole point	0.182	0.1859	0.1774	0.1774	0.1822	0.1774
	side back		0.1936	0.1837	0.1837	0.1893	0.1837
			0.1879	0.1791	0.1791	0.1841	0.1792
			0.1922	0.1826	0.1826	0.1881	0.1827
	U	0.894	0.9194	0.9149	0.9082	0.8934	0.9010
	B	0.886					
$L_h/L_h + L_c$	*V*	0.878					
	Hα (*w*)	0.901					
	Hα (*n*)	0.903					
	U	0.106	0.0806	0.0851	0.0918	0.1066	0.0990
	B	0.114					
$L_c/L_h + L_c$	*V*	0.122					
	Hα (*w*)	0.099					
	Hα (*n*)	0.097					
l_3		0.0	0.0	0.0	0.0	0.0	0.0
$*x_h$	*U*	0.320					
	B	0.390					
	V	0.325					
	Hα (*w*)	0.240					
	Hα (*n*)	0.240					
$*x_c$	*U*	0.390					
	B	0.470					
	V	0.370					
	Hα (*w*)	0.250					
	Hα (*n*)	0.240					
$*A_h = A_c$		1.0					
$*G_h = G_c$		0.25					

*Fixed parameters

all the available synthetic curve methods, we re-analysed the *UBV* light curves of Duerbeck (1975) and H*α* (*w*) and H*α* (*n*) light curves of Chambliss & Davan (1987) with this method using Popper's mass-ratio of 0.4172. The data published by Duerbeck (1975) contains 655*U,* 675*B* and 668*V* observations of VV Ori. As the memory of the computer available with the department is limited, to save computer time, we formed 163 *U*, 167*B* and 171*V* normal points from these observations During the phases of the primary eclipse, observations within a phase range of about 0.003 (1°) and at the

Table 2. VV Ori: Elements obtained from the combined solution of *B*, *V* & *Hα* (*n*) light curves.

Element		Combined solution for *B*, *V* & *Hα* (*n*)	Parameters used for fitting the *U* & *Hα* (*w*) light curves	
			U	*Hα* (*w*)
1		2	3	4
$*T_{e,h}K$		25,000	25,000	25,000
$T_{e,c}K$		15,579 ± 28	15,579	15,579
$*q$		0.4172	0.4172	0.4172
$i°$		86.09 ± 0.05	86.09	86.09
r_h	pole point	0.3582 ± 0.0013	0.3633 ± 0.0016	0.3554 ± 0.0033
	side back	0.3916 ± 0.0012	0.3994 ± 0.0017	0.3875 ± 0.0034
		0.3709 ± 0.0013	0.3768 ± 0.0016	0.3677 ± 0.0034
		0.3816 ± 0.0012	0.3883 ± 0.0017	0.3781 ± 0.0034
r_c	pole point	0.1762 ± 0.0012	0.1838 ± 0.0018	0.1807 ± 0.0034
	side back	0.1823 ± 0.0013	0.1912 ± 0.0018	0.1875 ± 0.0035
		0.1778 ± 0.0012	0.1858 ± 0.0018	0.1826 ± 0.0036
		0.1813 ± 0.0013	0.1899 ± 0.0019	0.1864 ± 0.0035
	B	0.9077 ± 0.0015	0.9147 ± 0.0017	0.8938 ± 0.0284
$L_h/L_h + L_c$	*V*	0.9023 ± 0.0015		
	Hα (*n*)	0.9005 ± 0.0270		
	B	0.0923	0.0853	0.1062
$L_c/L_h + L_c$	*V*	0.0977		
	Hα (*n*)	0.0995		
l_3		0.0	0.0	0.0

*Fixed parameters.

remaining portions of the light curve points within a phase range of 0.01 (4°) were combined to form one normal point. By using the normal points instead of the actual observations, the distortions in the light curve, if any, might have been obliterated, but the final results will not be affected (Chambliss 1983). The *Hα* (*w*) and *Hα* (*n*) data of Chambliss & Davan (1987) contain 692 *Hα* (*w*) and 686 *Hα* (*n*) observations. All these observations were also formed into 209 *Hα* (*w*) and 213 *Hα* (*n*) normal points. For our analysis these normal points were used and the number of points in each normal was taken as its weight. These normal points are shown as filled circles in Fig. 1 (a–e).

3.2 *Methodology*

As already mentioned, the Wilson-Devinney (1971) method was used for solving the |above light curves. For initiating the W-D method, one needs reliable preliminary elements. For this purpose we used the values of the inclination, *i*, fractional radii, r_h and r_e and the luminosities, L_h and L_c for the *UBV* pass bands given by Duerbeck (1975). The luminosities for *Hα* (*w*) and *Hα* (*n*) pass bands were taken from Chambliss & Davan (1987). The values of temperatures $T_{e,h}$ and $T_{e,c}$ and the mass-ratio are from Popper (1993). The limb-darkening coefficients for *UBV* pass bands were from Gryger (1972) and for *Ha* (*w*) and *Hα* (*n*) were from Chambliss & Davan (1987). These preliminary elements are given in Table 1, col. 2.

Table 3a. VV Ori: Elements obtained from the *UBV* data of Duerbeck (1975).

Element Method		Duerbeck (1975) R-M	Cester *et al.* (1978) WINK	Present studies W-D
$*T_{e,h}K$		—	25,000	25,000
$T_{e,c}K$		—	16,190	15,580
$*q$		0.450 ± 0.014	0.45	0.417
i°		86.1 ± 0.2	86.3 ± 0.5	86.09 ± 0.05
r_h		0.368 ± 0.002	0.364 ± 0.003	0.3702 ± 0.0012
r_c		0.182 ± 0.002	0.177 ± 0.002	0.1784 ± 0.0012
L_h	*U*	0.894	0.952	0.915
	B	0.886	0.968	0.908
	V	0.878	0.965	0.902
L_c	*U*	0.106	0.048	0.085
	B	0.114	0.032	0.092
	V	0.122	0.035	0.098
$m_h/m_\odot$		7.60	7.6	10.81
$m_c/m_\odot$		3.42	3.4	4.51
$R_h/R_\odot$		4.47	4.44	5.03
$R_c/R_\odot$		2.21	2.13	2.43
$M_{h,v}$		−2.58	—	−2.59
$r(pc)$		372	—	368

* Assumed parameter.

Table 3b. VV Ori: Elements obtained from the *Hα*(*w*) & *Hα*(*n*) data of Chambliss & Davan (1987).

Element Method Wavelength	Chambliss & Davan (1987) WINK		Present studies (individual solutions) W-D	
	Hα (*w*)	*Hα* (*n*)	*Hα* (*w*)	*Hα* (*n*)
$*T_{e,h}K$	25,000	25,000	25,000	25,000
$T_{e,c}K$	$15,690 \pm 150$	$15,760 \pm 170$	$15,560 \pm 50$	$15,571 \pm 54$
$*q$	0.45	0.45	0.4172	0.4172
i°	83.6 ± 0.5	85.5 ± 0.8	86.078 ± 0.140	86.108 ± 0.150
r_h	0.367 ± 0.003	0.361 ± 0.004	0.3691 ± 0.0035	0.3737 ± 0.0036
r_c	0.179 ± 0.003	0.173 ± 0.004	0.1848 ± 0.0036	0.1798 ± 0.0038
L_h	0.901	0.903	0.893	0.901
L_c	0.099	0.097	0.107	0.099
l_3	0.0	0.0	0.0	0.0

* Assumed parameter.

According to the principles of the WD method we adjusted the following parameters: the inclination i, the surface potentials Ω_h and Ω_c, the relative monochromatic luminosity L_h, the temperature of the secondary $T_{e,c}$ and the third light l_3. The temperature of the primary component, $T_{e,h}$ (25,000 K) and the mass-ratio q(0.4172)

Table 3c. VV Ori: Elements obtained from the *UBVubvy* data of Chambliss & Leung (1982).

Element Method		Chambliss & Leung (1982) W-D	Giuricin *et al.* (1983) WINK	Chambliss (1983) WINK
$*T_{e,h}K$		21,000	26,000	25,000
$T_{e,c}K$		12,835	17,017	15,957
$*q$		0.4568 ± 0.0012	0.40	0.45
i°		90 ± 0.49	86.3	85.60 ± 0.17
r_h		0.3530 ± 0.0004	0.362 ± 0.003	0.3627 ± 0.0017
r_c		0.1709 ± 0.0004	0.177 ± 0.004	0.1764 ± 0.0014
L_h	*U*	0.9446	0.924	0.925
	B	0.9115	0.907	0.895
	V	0.9026	0.904	0.891
L_c	*U*	0.0554	0.076	0.075
	B	0.0885	0.093	0.105
	V	0.0974	0.096	0.109
l_3		0.0	0.0	0.0

*Assumed parameter.

Table 3d. VV Ori: Elements obtained from the OAO-2 data.

Element Method	Eaton (1975) Computational method of Lucy (1968)	Budding & Najim (1980) Kopal's frequency domain
$*T_{e,h}K$	21,000	—
$T_{e,c}K$	$11,800 \pm 500$	—
$*q$	0.458 ± 0.050	—
i°	84.5 ± 0.5	87.5 ± 1.3
r_h	0.3790 ± 0.0040	0.3708 ± 0.0026
r_c	0.1745 ± 0.0040	0.1748 ± 0.0080

* Assumed parameters.

were treated as fixed parameters. It is expected that analysis of the light curves with fixed T_h and q at known values should yield most reliable elements. The limb darkening coefficients x_h and x_c, the albedos A_h and A_c and the gravity darkening coefficients G_h and G_c were also kept constant. From our earlier studies we noticed that the choice of these coefficients had negligible effect on the derived elements. As it is now well established that VV Ori is a detached system, we used code-2 of the WD method meant for detached systems. A sufficient number of runs of the DC programme was made till the sum of the residuals $\Sigma\omega\,(0\text{-}C)^2$ showed a minimum and the corrections to the parameters became smaller than their probable errors. In order to check the internal consistency of the results (Popper 1984) separate solutions for each of the *UBVHα* (*w*) and *H* (*n*) light curves were made. These results are given in cols. 3, 4, 5, 6 and 7 of Table 1.In none of the solutions was the third light l_3 present.

From the results of the above analysis, it is noticed that the relative fractional sizes r_h and r_c derived from the U solution, are slightly larger than those derived from *B*, *V* and *Hα* (*n*) pass bands. Since only a small discrepancy exists between the r_h and r_c values derived from the *Hα* (*w*) and *Hα*(*n*) pass bands, and that the r_h and r_c values of *Hα*(*n*) solution are almost identical with those of *B* and *V* solutions and in order not to combine many light curves and complicate the analysis, it was decided to get a combined solution only for *B*, *V* and *Hα*. (*n*) and as before, keeping $T_{e,h}$ and as fixed parameters, another solution was made for the combined *B*, *V* and *Hα* (*n*) light curves. These results are given in Table 2, col. 2. The third light l_3 is absent in this solution also. Using these elements, we have fitted the *U* and *Hα* (*w*) light curves. In doing so we had kept all the parameters except L_h as fixed parameters. The final parameters used for fitting the *U* and *Hα* (*w*) light curves are given in Table 2, cols. 3 and 4. For calculating the absolute elements, we used the elements obtained from the combined solution only. However for obtaining the (*UB*) colours of the components, we used the $L_{h,u}$ and $L_{c,u}$ values given in Table 2, col. 3.

The theoretical curves obtained from the elements given in Table 2 for the *UBVHα* (*w*) and *Hα* (*n*) light curves are shown as solid lines in Fig. 1 (a–e). The fit of the theoretical curves to the observed normals is quite satisfactory. In Table 3a we have given for comparison the elements derived from the *UBV* data of Duerbeck (1975). Table 3b gives the elements obtained by Chambliss & Davan (1987) from the analysis of their *Hα* (*w*) and *Hα* (*n*) data. In Tables 3c and 3d we have compiled the elements obtained by various investigators using the same data but different methods of solution. It can be noticed that the values of the derived parameters depend only on the method of analysis and not on the underlying data. In such analysis the most significant differences exist between the parameter *i* and *L*. The high value of 90° obtained for *i* from the *UBVubvy* data using the W-D method by Chambliss & Leung (1982) (Table 3c) may be attributed to their combining many light curves which might have complicated the solution.

4. Spectral types

From the derived luminosities of *V* and *B* pass bands for the combined solution (Table 2, col. 2) and *U* pass band (Table 2, col. 3) and using the corresponding differential magnitudes for unit luminosity at the quadrature [$\Delta V = -0^m..885$, $\Delta B = -0^m..902$, $\Delta U = -1^m..006$] and the standard magnitudes and colours of $V = 6^m..24$, $(B\text{-}V) = -0^m..18$ and $(U\text{-}B) = -0^m..81$ for the comparison, C_1, (Duerbeck 1975) we obtained the following magnitudes and colours for the individual components of VV Ori:

	Hot component	Cool component
V	5.46	7.88
(*B-V*)	− 0.21	− 0.14
(*U-B*)	− 0.92	− 0.82

According to Eaton (1975) an interstellar reddening correction of $E(B\text{-}V) = 0^m..05$ is applicable to VV Ori. Assuming the law of interstellar reddening (Allen 1976) to be

holding good, this reddening in $E(B\text{-}V)$ corresponds to a reddening of $E(U\text{-}B) = 0^m.04$ and $A_V A_V = 0^m.16$. Correcting the above derived magnitudes and colours for the reddening, one gets

	Hot component	Cool component
V_0	5.30	7.72
$(B\text{-}V)_0$	− 0.26	− 0.19
$(U\text{-}B)_0$	− 0.96	− 0.86

The above corrected $(B\text{-}V)_0$ of the primary component corresponds to a spectral type of either *B*2 *V* (Allen 1976) or *B*1 *V* (Popper 1980), giving it an average spectral type *B*1.5 *V*. For such a star the $(U\text{-}B))_0$ would be — 0.96 (Allen 1976; Schmidt-Kaler 1982) which is the same as that obtained above. Hence both the derived $(B\text{-}V))_0$ and $(U\text{-}B))_0$ colours give a consistent spectral type of *B1.5 V* to the primary component. The average temperature of a *B*1.5 *V* star would be 25,500 ± 800 K (Allen 1976; Popper 1980; Schmidt-Kaler 1982), which is the same as the fixed parameter, $T_{e,h}$(25,000 K) used for solving the light curves. This confirms that our analysis with fixed T_h(25,000 K) and (0.4172) yielded results akin to the reddening free data.

The derived $(B\text{-}V)_o$ of $-0^m.19$ of the secondary component corresponds to a spectral type of *B*4 *V* (Allen 1976), and its derived temperature of 15,580 K suggests a spectral type of *B*5 *V* (Allen 1976, Popper 1980). Thus both the $(B\text{-}V)_0$ colour and temperature give a consistent spectral type of *B*4-5*V* to the secondary component. However, for such a star, the $(U\text{-}B)_0$ should be $-0^m.60$ (Allen 1976; Schmidt-Kaler 1982), but its derived $(U\text{-}B)_0 = -0^m.86$. Hence the secondary component appears to be a *B*4-5*V* star with a *UV* excess of about $0^m.3$. In view of their small sizes and low luminosities (section 5) the possibility of the colours of these components corresponding to those of supergiants is not considered. According to Popper (1993) the properties of the components of VV Ori correspond well with those of the main-sequence stars of types *B*1 and *B*5. Eaton (1975) classified the primary as *B*0 *V* to *B*1.5 *V* while the secondary in the middle *B* range and concludes that VV Ori seems to be a reasonably normal main-sequence pair'. Chambliss (1983) suggested that VV OriA is a *B*1 *V* star. Duerbeck (1975) derived a spectral type of *B*1 *V* for the primary and *B*5-9 *V* for the secondary components. Hence our derived spectral types of the components (*B*1.5 *V* + *B*4-5 *V*) agree quite well with those of other investigators except that the secondary appears to have a *UV* excess of $0^m.3$. Since the standard magnitudes and colours of the comparison star used by Chambliss & Davan (1987) are not available, we could not get the magnitudes and colours of the components of VV Ori in *Hα* pass bands.

5. Absolute elements

Taking the amplitudes of the radial velocity curves as $K_{11} = 136 \pm 6$ and $K_2 = 326 \pm 7$ km/sec from Popper (1993) and $i\ i = 86.09°$ from the present study (Table 2, col. 2) one gets the masses of the individual components of VV Ori as $m_h/m_\odot = 10.81 \pm 0.42$ and

$m_c / m_\odot = 4.51 \pm 0.41$ and $A/R_\odot = 13.605 \pm 0.031$. Combining these values with those of r_h, r_c, T_h and T_c, we obtained the following sizes, luminosities, bolometric and visual magnitudes.

	Hot component	Cool component
$R/R_\odot$	5.03 ± 0.03	2.43 ± 0.02
$\log L/L_\odot$	3.948 ± 0.044	2.493 ± 0.023
M_{bol}	-5.18 ± 0.11	-1.54 ± 0.06
M_v	-2.59 ± 0.11	-0.10 ± 0.06

In calculating M_v, we used the bolometric correction of $-2^m..59$ and $-1^m..44$for the hot and cool components respectively (Popper 1980). Applying the interstellar absorption of $A_v = 0^m..16$, the distance of VV Ori was found to be 368 ± 10 pc.

6. Component properties and comparison with other similar systems

From a plot of the positions of the two components on observed ZAMS in Fig. 2(Morton & Adams 1968) it is noticed that the primary component lies slightly above and the secondary component slightly below or on the ZAMS. Chambliss (1984) found the larger component (primary) to be normal for a spectral type of *B*1 *V* and found it to be fairly close to the ZAMS. Eaton (1975) concludes that VV Ori seems to be a reasonably normal main-sequence pair and when plotted on the observational ZAMS the primary lies a little above the main-sequence and the secondary lies slightly below.

In order to compare the above properties of VV Ori with other detached systems having *B* type components, we plotted in Fig. 2 the positions of a few systems as given in tables 2 and 4 of Popper (1980). From this we notice that except a few primaries, notably no. 14 (χ^2 Hya), all the other components lie either on the ZAMS or very near to it. A little adjustment in the scale of either the derived parameters or the observed ZAMS in the log T_e range of 4.3 to 4.05 may make most of the systems to fall on the ZAMS. For ready reference, the list of systems given by Popper (1980) and used in this study are given in Table 4.

In Figs. 3,4 and 5 (solid lines) we have plotted the relations of log *LL*, log *R* and log T_e with respect to log mass of the normal main-sequence stars (Allen 1976). In these figures, in addition to the positions of the components of VV Ori, we have also plotted the positions of other detached systems given in Table 4. From these plots one can see that the primary component of VV Ori is overluminous, hotter and a little undersized for its mass. In the case of the secondary component it is seen that while its luminosity is consistent with its mass, its radius is smaller and the temperature is higher for its mass. However from a comparison of the positions of the other detached systems in these plots, it is apparent that in addition to getting more accurate elements, there is a need for either refixing the scales of the observed log *L*, log *R* and log T_e or modifying the models and getting new theoretical relations. Unless this is done, one cannot come to any conclusion regarding the properties of the components of VV Ori and compare them with other detached systems.

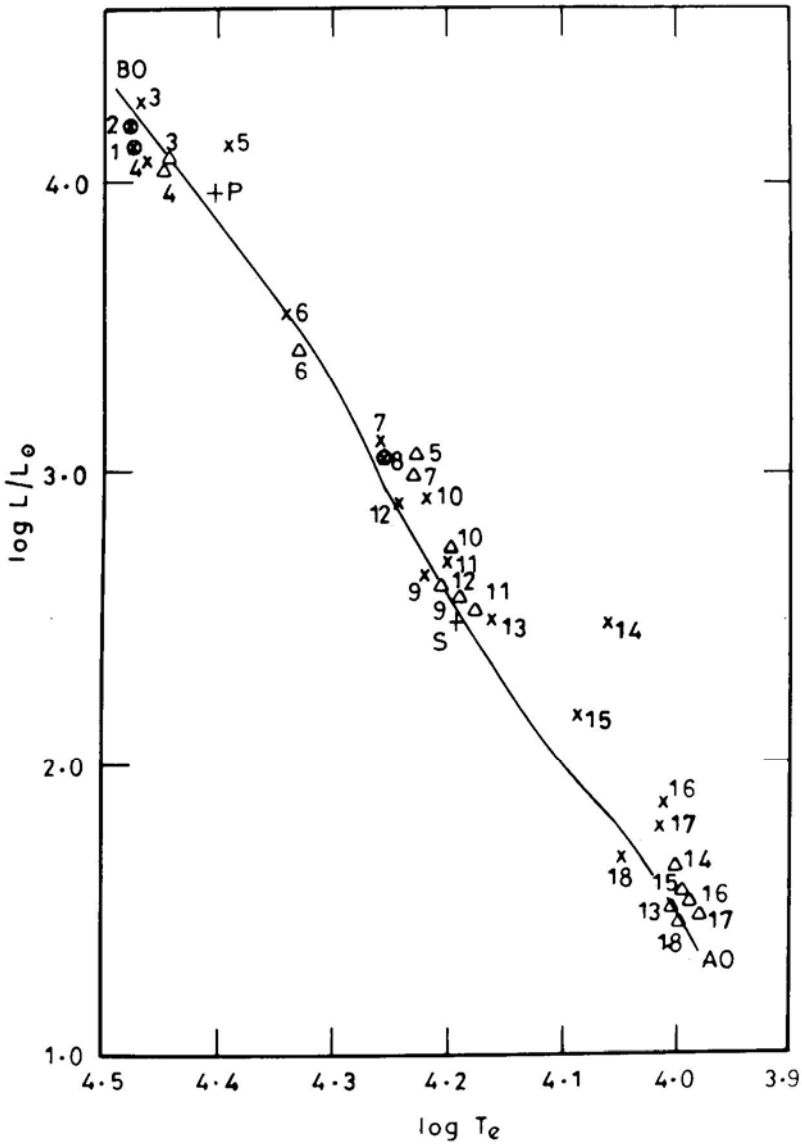

Figure 2. VV Ori: Plot of log $L/L_{\odot}$ versus log T_e. The solid line represents the observed ZAMS (Morton & Adams 1968). The primary (P)and secondary(5) components of VV Ori are indicated as ' + '. Components of other detached systems are shown as '×' (*P*) and 'Δ' (*S*). Numbers represent the names of the systems given in Table 4. '⊗' represent both the primary and secondary components of a system.

7. Evolution

With a view to study the evolutionary status of the components of VV Ori, we used the evolutionary tracks computed by Schaller et al. (1992) for stars of Pop I composition. These evolutionary tracks for stars of initial masses of 10.8 and 4.5 in solar units are

Table 4. VV Ori: List of detached systems used in Fig. 2.

No.	Name	$\log m_1$	$\log L_1$	$\log R_1$	$\log T_1$	$\log m_2$	$\log L_2$	$\log R_2$	$\log T_2$
1	Y Cyg	1.220	4.45	0.780	4.485	1.220	4.45	0.780	4.485
2	V478 Cyg	1.190	4.62	0.860	4.485	1.190	4.62	0.860	4.485
3	V453 Cyg	1.160	4.69	0.930	4.470	1.050	4.20	0.730	4.445
4	CW Cep	1.070	4.28	0.730	4.470	1.040	4.13	0.700	4.445
5	α Vir	1.030	4.33	0.910	4.390	0.830	3.16	0.640	4.230
6	QX Car	0.960	3.59	0.630	4.340	0.930	3.48	0.600	4.330
7	V539 Ara	0.790	3.26	0.640	4.255	0.720	3.02	0.570	4.230
8	CV Vel	0.780	3.19	0.610	4.255	0.780	3.19	0.610	4.255
9	DI Her	0.720	2.65	0.410	4.220	0.660	2.52	0.410	4.190
10	U Oph	0.710	2.90	0.540	4.220	0.660	2.74	0.490	4.200
11	V760 Sco	0.700	2.71	0.480	4.200	0.670	2.53	0.430	4.18
12	AG Per	0.660	2.89	0.480	4.245	0.610	2.62	0.410	4.210
13	ξ Phe	0.593	2.50	0.455	4.160	0.405	1.51	0.267	4.005
14	χ^2 Hya	0.558	2.49	0.642	4.063	0.422	1.64	0.334	4.005
15	AS Cam	0.520	2.17	0.431	4.088	0.400	1.56	0.301	4.001
16	V451 Oph	0.444	1.86	0.423	4.015	0.373	1.54	0.326	3.985
17	RX Her	0.439	1.79	0.387	4.015	0.367	1.48	0.292	3.985
18	AR Aur	0.394	1.67	0.262	4.048	0.360	1.46	0.262	3.997

shown in Fig. 6, which is a plot of $\log L / L_{\odot}$ versus T_e. In the same diagram, the isochrone for an age of 10 million years is also shown. This isochrone was obtained by interpolation between the evolutionary tracks of Schaller et al. (1992) based on points of corresponding evolutionary status. One can see from this figure that the primary has evolved from its initial position along the $10.8 m_{\odot}$ track. The secondary component is still unevolved and lies at the foot of the track of a $4.5 m_{\odot}$ star with a slightly lower luminosity. Both the components satisfactorily fit the isochrone of 10 million years and hence we conclude that the age of VV Ori is 10 ± 1 million years.

8. Discussion

The *UV* excess of about $0^m.3$ found for the secondary component may be explained as due to hot gases surrounding this component, the source of which might be the gases expelled by the primary during its present evolution. Comparing the observed fractional radii of 0.370 and 0.178 of the primary and secondary components with their critical Roche lobes of 0.457 and 0.299 respectively, (for a mass-ratio of 0.42) (Plavec & Kratochvil 1964), it is found that these components are filling 80% and 60% of their respective Roche lobes. Even though any stellar activity like gas streams etc., are not generally expected in detached systems, a slightly bigger fractional radius (of about 0.01) obtained for *U* pass band in our analysis suggests some form of gases or gaseous streams in the system. From their studies of VV Ori light curves, Duerbeck (1975) and Giuricin et al. (1983) had also arrived at similar conclusions.

Even though the geometrical and absolute elements of VV Ori are now well established, a few peculiarities are still left unexplained. The influence of mutual interactions on the evolution of the system should be carefully estimated.

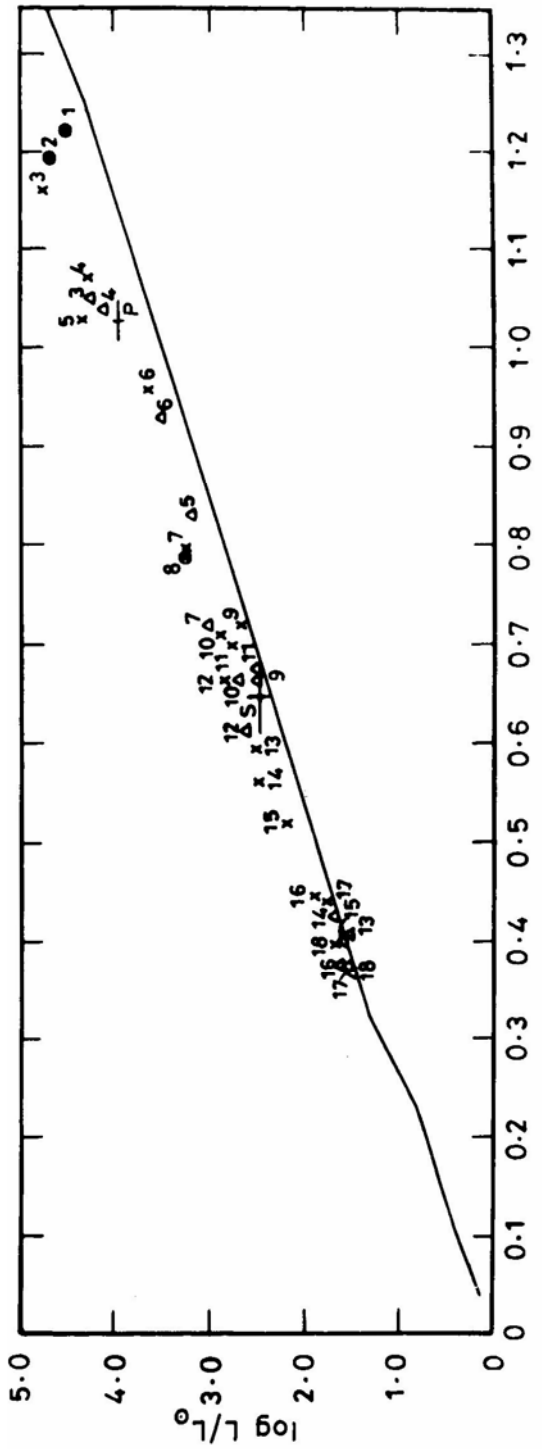

Figure 3. VV Ori: Plot of $\log L/L_{\odot}$ versus $\log m/m_{\odot}$. The solid line represents the relation for normal stars (Allen 1976). The primary (P) and secondary (S) components of VV Ori are shown in the figure with error bars. Other details are the same as for Fig. 2.

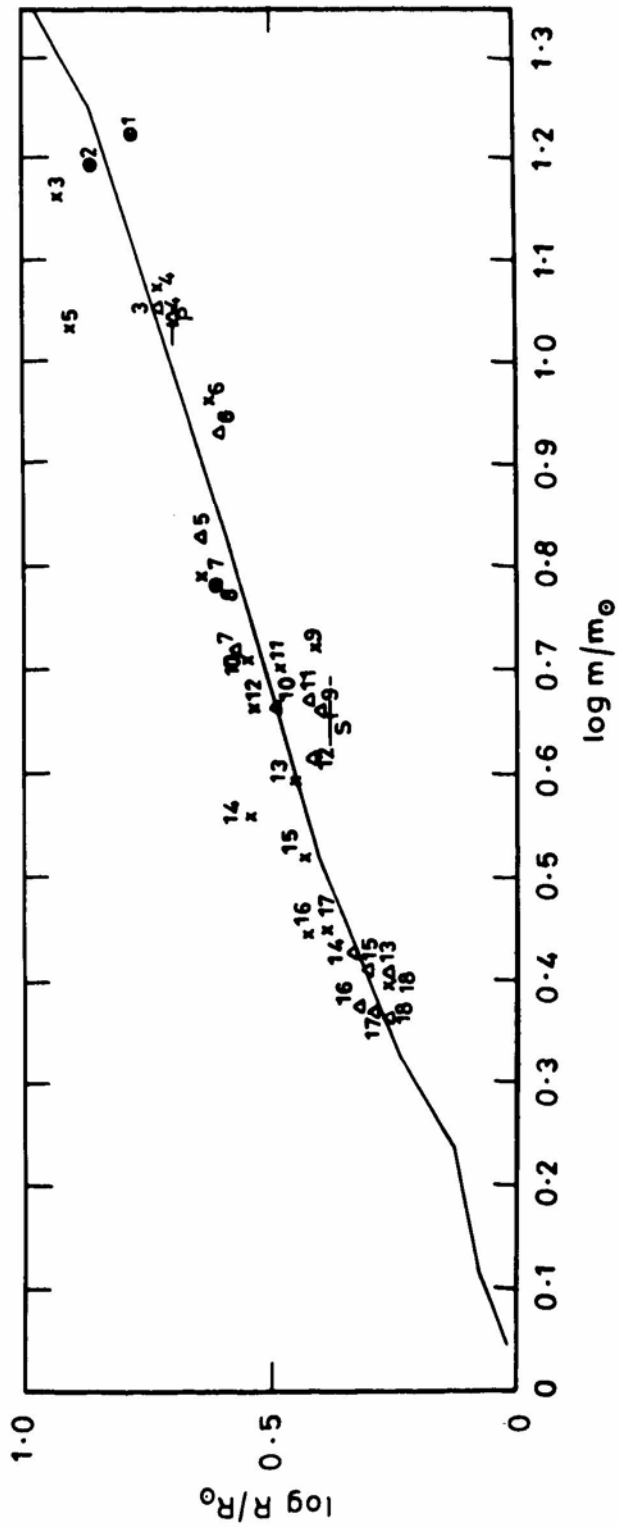

Figure 4. VV Ori: Plot of $\log R/R_\odot$ versus $\log m/m_\odot$. Details are the same as for Fig. 3.

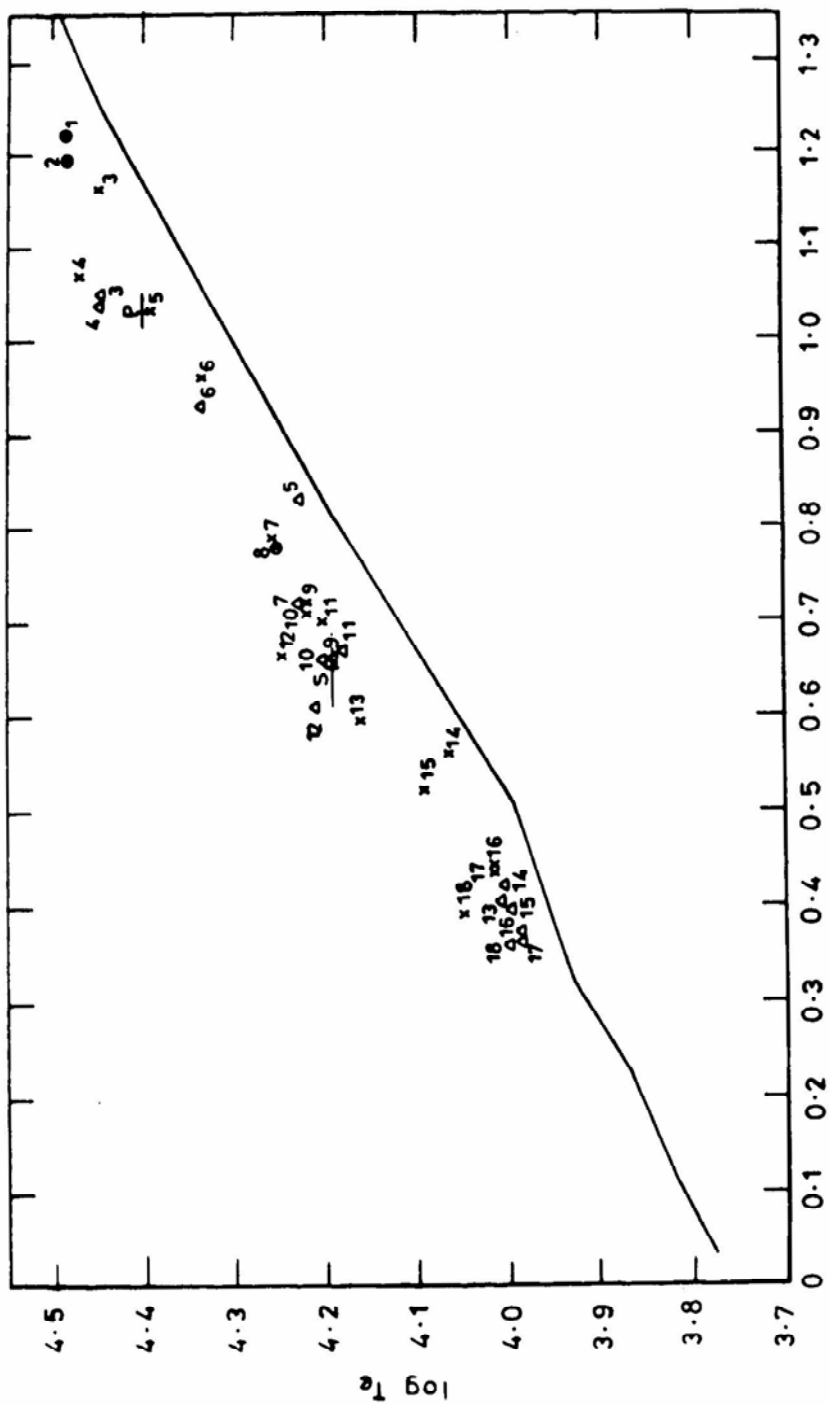

Figure 5. VV Ori: Plot of log T_e versus log $m/m_\odot$. Details are the same as for Fig. 3.

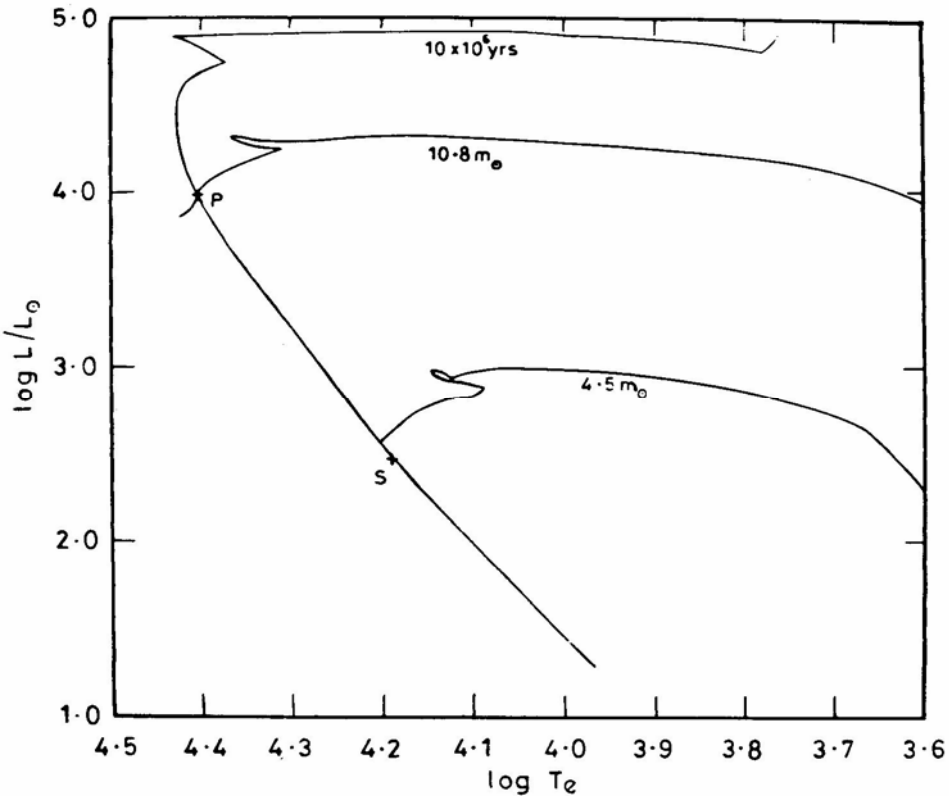

Figure 6. VV Ori: Evolutionary tracks of stars of initial masses 10.8 and 4.5 in solar units. These tracks were computed by Schaller et al. (1992) for stars of Pop I composition. The isochrone for 10×10^6 yrs is also shown in the diagram, the positions of the primary (*P*) and secondary (*S*) components of VV Ori are shown as '+'.

Acknowledgements

The authors are thankful to Professor K. D. Abhyankar for many helpful discussions. M. B. K. S.gratefully acknowledges the financial support given to him by the Council of Scientific and Industrial Research (CSIR), Government of India, New Delhi, under the emeritus scientists scheme.

References

Allen, C. W. 1976, *Astrophysical Quantities*, 3rd edn., (London: The Athlone Press)
Andersen, J. 1976, *Astr. Astrophys*., **47**,467.
Barr, J. M. 1905, *Selected papers*, *Proc. R. Astron. Soc. Canada, 1904*, 42.
Beltrani, G.,Galeotti, P.1970, *Mem. Soc. Astron. Ita* ., **41**,167.
Budding, E., Najim, N. N. 1980, *Astrophys. Space Sci.*, **72**, 369.
Cester, B.,Fedel, B.,Giuricin, G., Mardirossian, F., Mezzetti, M.1978, *Astr. Astrophys. Suppl.*, **33**, 91.
Chambliss, C. R., Leung, K. C. 1982, *Astrophys. J. Suppl.*, **49**, 531.

Chambliss, C. R. 1983, *Astrophys. Space Sci*., **89**, 15.
Chambliss, C. R. 1984, *Astrophys. Space Sci.*, **99**, 163.
Chambliss, C. R., Davan, B. M. 1987, *Astr. J*., **93**,950.
Duerbeck, H. W. 1975, *Astr. Astrophys. Suppl*., **22**,19.
Eaton, J. A. 1975, *Astrophys.* ., **197**, 379.
Giuricin, G., Mardirossian, F., Mezzetti, M., Chambliss, C. R. 1983, *Astr. Astrophys. Suppl.*, **51**, 111.
Gryger, J. 1972, *Bull. astr. Inst. Cs* ., **23**, 157.
Lucy, L. B. 1968, *Astrophys. J*., 1**53**, 877.
Morton, D. C, Adams, T. F. 1968, *Astrophys. J*., **151**, 611.
Plavec, M., Kratochvil, P. 1964, *Bull. astr. Inst. Csl*., **15**,165.
Popper, D. M. 1980, *A. Rev. Astr. Astrophys*., **18**, 115.
Popper, D. M. 1981, *Astrophys. J. Suppl.*, **47**, 339.
Popper, D. M. 1984, *Astr. J.,* **89**,132.
Popper, D. M. 1993, *Publ. Astr. Soc. Pacific,* **105**, 721.
Russell, H. N., Merrill, J. E. 1952, *Contr. Princeton Univ. Obs., No*. 26.
Schaller, G., Schearer, D., Meynet, G., Maeder, A. 1992, *Astr. Astrophys. Suppl.*, **96** ,269.
SchmidtKaler, Th. 1982, *in Landolt/'Bornstein, Numerical data and functional relationship in Science and Technology*, Eds. K. Scaifers & H. H. Voigt, (Berlin: SpringerVerlag), New Series, Group VI, Volume 2(b), p. 453.
Struve, O., Luyten, W. J. 1949, *Astrophys. J*., **110**,160.
Wilson, R. E., Devinney, E. J. 1971, *Astrophys. J*., **166**, 605.